Dual-Responsive Spin-Crossover Cages

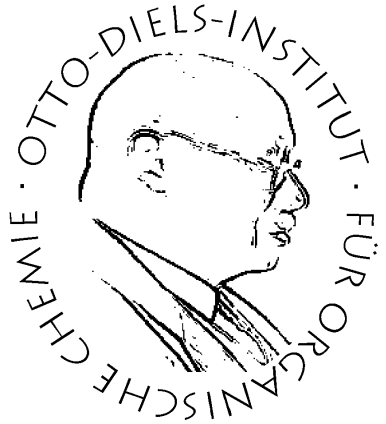

Dissertation

zur Erlangung des Doktorgrades

der Mathematisch-Naturwissenschaftlichen Fakultät

der Christian-Albrechts-Universität zu Kiel

vorgelegt von

Tobias Paschelke

Otto-Diels-Institut für Organische Chemie

Hamburg, 2023

Erste Gutachterin: Prof. Dr. Anna J. McConnell

Zweite Gutachterin: Prof. Dr. Thisbe K. Lindhorst

Tag der mündlichen Prüfung: 10.11.2023

Zum Druck genehmigt: 10.11.2023

Die vorliegende Arbeit wurde in der Forschungsgruppe McConnell
unter Anleitung von
Prof. Dr. Anna J. McConnell
in der Zeit von Dezember 2019 bis August 2023
am Otto-Diels-Institut für Organische Chemie der
Christian-Albrechts-Universität zu Kiel angefertigt.

Teile dieser Dissertation wurden veröffentlicht:

i) Marc Lehr, Tobias Paschelke, Eicke Trumpf, Anna-Marlene Vogt, Christian Näther, Frank D. Sönnichsen, Anna J. McConnell, *Angew. Chem. Int. Ed.* **2020**, *59*, 19344-19351. | *Angew. Chem.* **2020**, *59*, 19344-19351. (doi.org/10.1002/anie.202008439 | doi.org/10.1002/ange.202008439)
ii) Marc Lehr[‡], Tobias Paschelke,[‡] Victoria Bendt, André Petersen, Lorenz Pietsch, Patrick Harders, Anna J. McConnell, *Eur. J. Org. Chem.* **2021**, 2728-2735. [‡] = The authors contributed equally (doi.org/10.1002/ejoc.202100275)
iii) Tobias Paschelke, Eicke Trumpf, David Grantz, Malte Pankau, Niclas Grocholski, Christian Näther, Frank D. Sönnichsen, Anna J. McConnell, *Dalton Trans.* **2023**, *52*, 12789-12795. (doi.org/10.1039/d3dt01569f)

Eidesstattliche Erklärung

Hiermit erkläre ich, Tobias Paschelke, an Eides statt, dass ich die vorliegende Dissertation nach Inhalt und Form eigenständig und nur mit den angegebenen Hilfsmitteln verfasst habe, abgesehen von der Beratung durch meine Betreuerin Prof. Dr. Anna J. McConnell. Diese Arbeit und Teile davon wurden nicht an einer anderen Stelle im Rahmen eines Prüfungsverfahrens vorgelegt, veröffentlicht oder zur Veröffentlichung eingereicht. Diese Arbeit ist unter Einhaltung der Regeln guter wissenschaftlicher Praxis der Deutschen Forschungsgemeinschaft entstanden. Mir, Tobias Paschelke, wurde kein akademischer Grad entzogen.

Hamburg, den November 24, 2023

Tobias Paschelke

Danksagung

Hiermit möchte ich meinen ersten Dank für die vielen Jahre der intensiven Betreuung an meine Professorin, Anna J. McConnell, richten. Ohne die vielen hilfreichen Meetings, Tipps und Tricks in der Promotion, das spannende Forschungsthema und die exzellente Betreuung wäre diese Dissertation in dieser Form nicht möglich gewesen. Danke dafür!

Auch geht ein großer Dank an Prof. Dr. Lindhorst für die Übernahme der Zweitkorrektur.

Ebenso bedanke ich mich bei meinen Laborpartnern Marc und Eicke, welche mir die Laborzeit sehr versüßt haben. Auch geht ein großer Dank an Patrick, Tjorge und Rene für die schöne Laborzeit.

Auch möchte ich meinen Dank an das Team um Prof. F. Sönnichsen richten, welches für mich unzählbar viele Spezialmessungen rund um mein Thema durchgeführt hat und mich in vielen Fragestellungen unterstützt hat.

Ich danke auch Ragnar, Niclas und Beshr für ihre Mitarbeit an verschiedensten Themen.

Ich danke zusätzlich Eicke, Friederike und Dr. Brigitte Muntermann für das Durcharbeiten meiner Arbeit um Fehler zu finden.

Mein letzter Dank widmet sich meiner Familie, die während meiner Promotionszeit stets ein offenes Ohr für mich hatte und mir den Rücken gestärkt hat. Vielen Dank, dass es euch gibt.

Kurzzusammenfassung

Als supramolekulare Strukturen können metallorganischen Käfige durch Selbstorganisation zwischen labilen Metallionen und organischen Liganden erhalten werden. In den letzten Jahren zeigten metallorganische Käfige ihre Anwendbarkeit als stimuliresponsive Spin-Crossover Materialien. Jedoch ist die Anzahl der publizierten Beispiele bisher auf eine geringe Anzahl von thermisch-und lichtresponsiven Spin-Crossover Käfigen limitiert. Diese Doktorarbeit beschäftigt sich mit der Entwicklung von neuartigen metallorganischen Käfigen, deren Spinzustand sich mittels Temperatur und Licht in Lösung schalten lässt. Dabei soll für die Lichtresponsivität der LD-LISC ("ligand-driven light-induced spin-state change") Effekt ausgenutzt werden.

Die Untersuchung von metallorganischen Käfigen mit thermischer Spinzustandsänderung wurde durch die Implementierung einer Charakterisierungsmethodik und optimierten Ligandensynthese ermöglicht. Zunächst wurden paramagnetische NMR Methoden an paramagnetische Substanzen angepasst und optimiert, welche die vollständige Strukturaufklärung von high-spin Fe^{II}-basierten Käfigen ermöglichen. Durch anschließende Optimierung einer Sonogashira-Kreuzkupplung wurden Diarylalkinliganden für Käfige synthetisch zugänglich. Mit Hilfe beider Methoden wurde folgend eine Bibliothek von Fe^{II}-basierten Käfigen mit 2-(2'-Pyridyl)-benzimidazol- und -imidazolbindungsmotiven synthetisiert und charakterisiert und die Spin-Crossover Eigenschaften der Käfige in Abhängigkeit von sterischen und elektronischen Ligandenmodifikationen quantifiziert.

Für mononukleare Komplexe als Modellsysteme für lichtresponsive Käfige wurden drei Azobenzolderivate und ein Dithienylethen über teilweise neuartige Syntheserouten hergestellt und ihre photochemischen Eigenschaften untersucht. Während keine Isomerisierung für das Dithienylethen festgestellt werden konnte, zeigten die drei Azobenzolderivate vergleichbare photostationäre Gleichgewichte und lange Halbwertszeiten von bis zu 180.4 h. Diese Ergebnisse stellen eine vielversprechende Basis für die Untersuchung der entsprechenden Fe^{II}-basierten mononuklearen Komplexe dar, welche zunächst charakterisiert und anschließend auf den LD-LISC Effekt untersucht werden müssen.

Abschließend wurde die erste Generation eines photoschaltbaren Liganden durch ein verbessertes Dithienylethen-System für metallorganische Käfige synthetisiert, welcher eine fast quantitative Isomerisierung und Cycloreversion zeigt. Die Anwendung des Liganden in der Selbstorganisation mit verschiedenen Metallsalzen (Zn^{II}, Co^{II}, Fe^{II}) konnte anschaulich dargelegt und die potentielle Nutzung als Ein-Weg-Photoschalter näher untersucht werden. Die Ergebnisse dieser Arbeit bieten erste Erkenntnisse auf dem Weg zum gezielten Design von dualresponsiven metallorganischen Spin-Crossover Käfigen.

Abstract

Metal-organic cages can be self-assembled as supramolecular architectures from labile metal ions and organic ligands. In the past years metal-organic cages have shown great potential as stimuli-responsive spin-crossover materials. However, the number of known thermal- and light-responsive spin-crossover cage examples is limited. This dissertation is concerned with the development of novel metal-organic cages, whose spin-state can be switched in solution by temperature and light. The LD-LISC effect ("ligand-driven light-induced spin-state change") will be utilised for the introduction of light-responsiveness.

The investigation of metal-organic cages with thermal spin-state transitions was made possible through the development of a characterisation method and an optimised ligand synthesis. Initially, paramagnetic NMR spectroscopic methods were adapted and optimised for paramagnetic substances. The methods enable the complete characterisation of high-spin Fe^{II}-based cages. Afterwards, an optimised Sonogashira cross-coupling reaction gave synthetic access to diarylalkyne ligands for cages. In combination with both methods, a library of Fe^{II}-based cages with 2-(2'-pyridyl)-benzimidazole- und -imidazole binding motifs was synthesised, characterised and the spin-crossover properties of the cages were quantified based on steric and electronic ligand modifications.

For mononuclear complexes as model systems for light-responsive cages three azobenzene derivatives and one dithienylethene were synthesised using in part novel synthetic routes and their photochemical properties were investigated. While a isomerisation of the dithienylethene was not observed, the three azobenzene derivatives had similar photostationary states and long half-life times up to 180.4 h. These results are a promising basis for investigation of the corresponding Fe^{II}-based mononuclear complexes, which in future studies will be characterised and afterwards for the properties with regard to the LD-LISC effect.

Finally, a first generation light-responsive ligand for metal-organic cages was synthesised with an optimised dithienylethene design and it showed almost quantitative isomerisation and cycloreversion. The self-assembly of the ligand with multiple metal salts (Zn^{II}, Co^{II}, Fe^{II}) was investigated as well as the potential use of the self-assemblies as a one-way switch. The results of this dissertation provide first insights into the rational design of dual-responsive spin-crossover metal-organic cages.

Contents

Chapter 1

1 Introduction

1.1 Inspired by Nature: Supramolecular Chemistry

The origins of synthetic supramolecular chemistry are difficult to date. One of the first examples in the supramolecular field were gas clathrates that were investigated by Sir Humphry Davy in 1810. They persist of frozen water molecules providing cavities ideal for gas binding such as chlorine or oxymuriatic acid as it was known back then.[31] This encapsulation can also be defined as one of the first reported host-guest interactions.[31–33] Over the course of the next 150 years the term supramolecular chemistry was still unknown until Jean-Marie Lehn defined it as "chemistry beyond the molecule".[34–36] Compounds that are not only bound by covalent bonds, but naturally assemble as aggregates by non-covalent interactions like e.g. van der Waals forces or hydrogen donor-acceptor interactions were defined as such supramolecular structures.[35–38] Until today the importance of this research topic has been demonstrated by the award of Nobel Prizes in 1987 and 2016[39,40] and its broad range of applications including as chemical sensors,[41,42] in tumor therapy as drug delivery agents,[43] in polymer science[44,45] or in catalysis.[46,47]

Modern supramolecular chemistry, such as the previous examples,[41–47] is inspired by aggregates found in nature itself. Very prominent examples are the double helix of deoxyribonucleic acid, also known as DNA, where both strands are held together by hydrogen donor-acceptor interactions between the pyrimidine and purine derivatives (adenine/thymine and guanine/cytosine)[48] or the tobacco mosaic virus, a highly ordered aggregate self-assembled from proteins and ribonucleic acid.[49–51] The term self-assembly is used for a process where organised aggregation of multiple building blocks into larger supramolecular structures spontaneously occurs, promoted by energetically favoured non-covalent interactions.[51–54] Due to an equilibrium between the starting materials, potential intermediates and the thermodynamically favored products, assembling errors can be corrected.[55] Simultaneously, the used starting materials may be able to discriminate molecules from each other to find the most compatible partner or building block, also known as molecular recognition.[56]

Although the field of supramolecular chemistry is relatively new, a variety of supramolecular structures

with diverse functionalities has emerged such as e.g. crown ethers,[57,58] rotaxanes[59–61] or metal-organic cages,[62–64] the latter being the research topic of the McConnell research group.

1.2 Metal-Organic Cages as Supramolecular Aggregates

As the first metal-organic cage, Saalfrank *et al.* investigated in 1988 the first magnesium-based tetrahedral cage.[65,66] Since then metal-organic cages are of great interest within the supramolecular chemistry field for their potential applications,[67–69] for example in the field of catalysis.[70,71] Cages self-assemble from simple building blocks such as metal ions and organic ligands that coordinate to the metal ion.[72,73] In general, labile metal ions (e.g. Fe^{II}[74,75] or Zn^{II}[76,77]) are used in the self-assemblies to ensure reversibility.[55,78] Multiple cage structures are feasible such as tetrahedra,[79–82] helicates,[83–85] spheres[86] or a twisted cube.[87] Even very large cages such as rhombicuboctahedra ($M_{24}L_{48}$)[88] and icosidodecahedron ($M_{30}L_{60}$)[89] were already self-assembled by other research groups (Figure 1.1). The obtained architectures lead to cavities with well-defined sizes.[73]

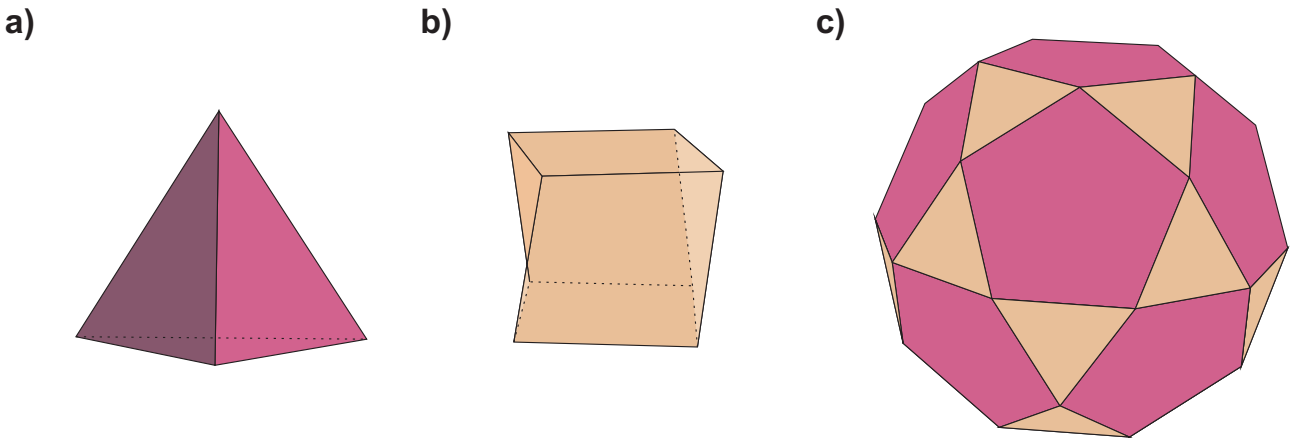

Figure 1.1: Different Platonic or Archimedean solids as observed for metal-organic cages: a) a tetrahedron,[80] b) a twisted cube-shaped structure[87] and c) an icosidodecahedron.[89] Design was adapted from Seidel *et al.*[90]

As an example, similar cube-shaped architectures can be self-assembled by eight metal ions and using either twelve linear ligands resulting in edge-bridged metal-organic cages or six four-fold symmetric ligands leading to face-capped structures (Figure 1.2).[91–94] As four-fold symmetric ligands a porphyrin backbone is typically used.[93,94]

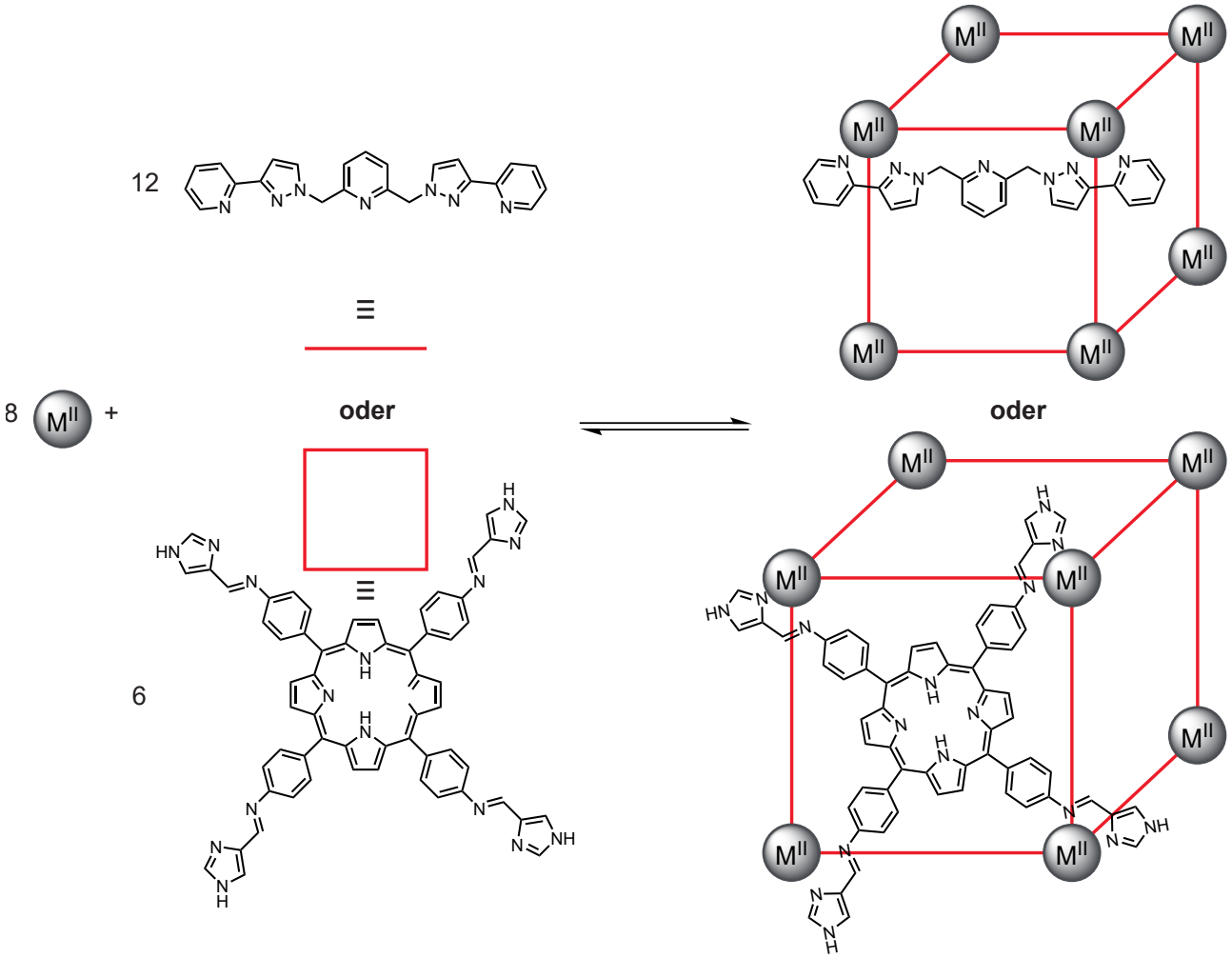

Figure 1.2: The self-assembly of cube-shaped metal-organic cages based on linear or four-fold symmetric ligands.[92–94]

The resulting architecture of a metal-organic cage depends on many different influencing factors such as the used solvent,[95–97] the concentration and temperature,[98] anion templation,[99,100] but also the used organic ligands and metal ions. As an example, Kieffer *et al.* investigated sterically differing ligands and the effect of steric bulk on the self-assembly process (Scheme 1.1). X-ray crystallography data of the respective mononuclear complexes indicated that substitution with sterically bulkier groups (F vs. H) leads to lower symmetry metal-organic cages since additional steric bulk around the coordination sites of the metal ions alters the preferred ligand coordination in order to avoid steric clashes. As the result, substitution of F vs. H led to the cubic lower symmetry cage **6** in comparison to the highly symmetrical tetrahedron **5**.[87] This study also indicated that mononuclear complexes can provide information to predict the structural arrangement in metal-organic cages (Scheme 1.1).[87] In addition to steric bulk,[87] also other ligand modifications may influence the self-assembly process such as the ligand's geometry. The design of bent ligands may result in more spherical structures.[88,101,102]

Also the choice of the metal ion is important due to its preferred coordination such as octahedrally coordinated Fe^{II} may result in tetrahedral[103,104] or cubic[105,106] structures or Pd^{II} being coordinated in a square planar arrangement leading to the self-assembly of Pd_2L_4 cages.[107,108] Further transition metals such as Co^{II},[109] Zn^{II},[105,106,110] Cu^{II}[111] or Rh^{II}[112] are also known to form cages, but also other larger cations as Ce^{III}[113] or Eu^{III}[114] are used.

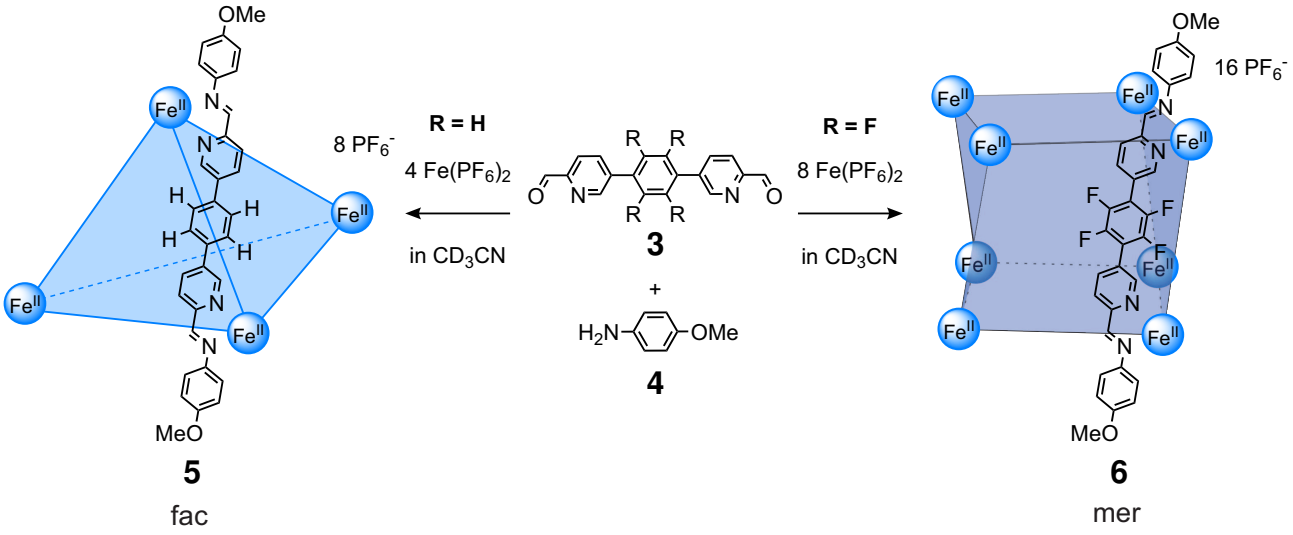

Scheme 1.1: The two different cage structures that were designed by Kieffer *et al.* to obtain either cage **5** or cage **6**. Figure design is adapted from Kieffer *et al.*[87]

In general, two approaches for the self-assembly process based on the ligand design are known: i) subcomponent self-assembly based on dynamic covalent bonds[115–119] and ii) the use of pre-synthesised ligands (Figure 1.3).[120–123] In approach i) subcomponents of the desired ligand, usually a carbonyl compound and an amine, are synthesised and the ligand self-assembles in solution by imine condensation.[115–119] The metal-organic cage self-assembles from the formed imine ligand and the respective metal ions.[119] In comparison, approach ii) uses pre-synthesised ligands for the self-assembly with metal ions.[120–122] The majority of reported metal-organic cages have been designed and self-assembled based on approach i) since the subcomponents are more soluble than pre-synthesised ligands in organic solvents and due to a greater variability since the small building blocks as the carbonyl compounds or amines can be flexibly exchanged.[123,124] In a few experiments whole libraries of different ligands can be prepared by using different building blocks and subcomponent exchange.[123,124] An example for approach i) is shown in Figure 1.3, a). Amine **7** and aldehyde **8** were used as subcomponents and self-assembled into ligand **9** in solution.[123] Upon ligand formation, cage **10** was self-assembled with iron(II) triflate.[123] By pursuing approach ii) pre-synthesised ligands can be directly used for the self-assembly process without the need for a potentially sensitive[125] pre-equilibrium between the carbonyl and amine building blocks. However, in approach ii) the insolubility

of the ligand in the used solvent can be a challenging problem. A few examples for cages based on approach ii) are reported.[121,126,127] Borsley *et al.* prepared symmetrical 2,2'-bipyridine ligands that were self-assembled with Fe(II) or Co(III) salts (Figure 1.3, b)).[122] In this thesis approach ii) will be focused on in order to enable the characterisation of the photochemical properties of the ligands such as the half-life times.

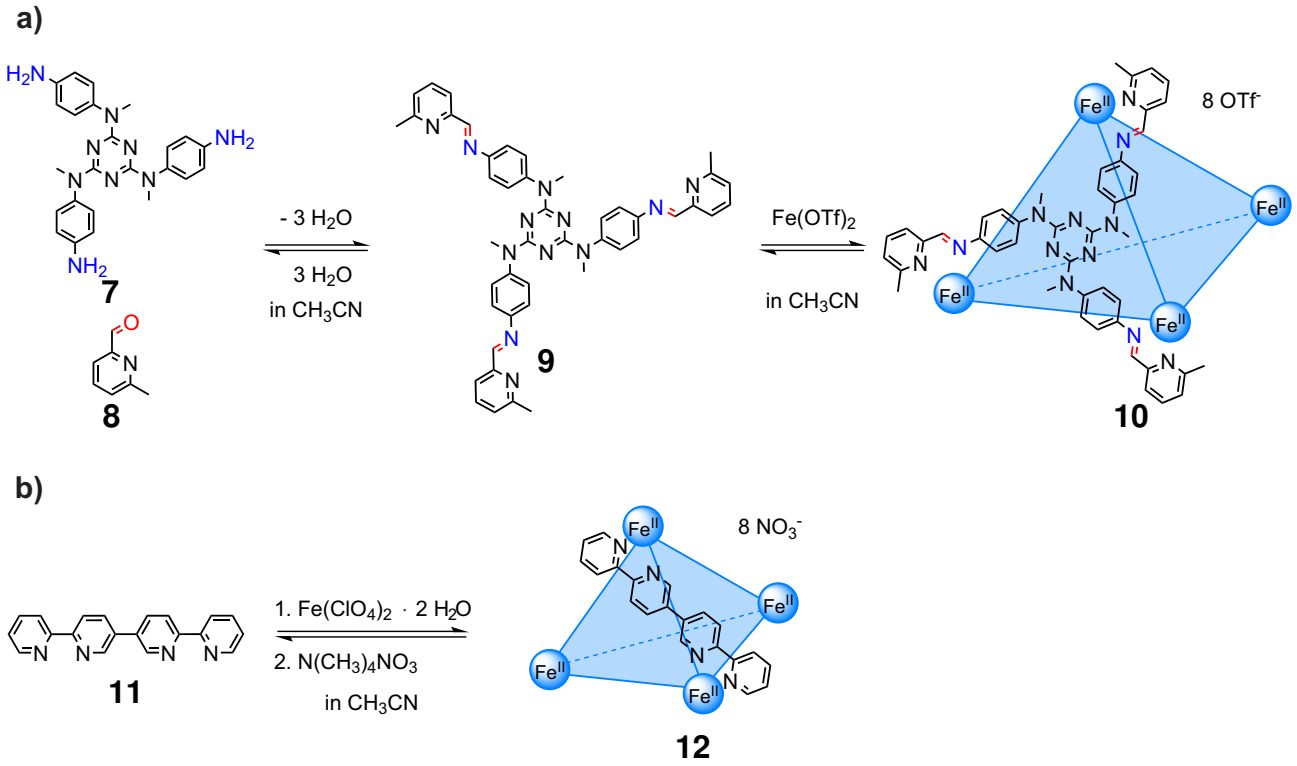

Figure 1.3: For the self-assembly of metal-organic cages two approaches are in use: a) subcomponent self-assembly with an amine and aldehyde (blue and red)[123] and b) use of pre-synthesised ligands.[122]

In general, metal-organic cages are structured as mononuclear complexes, except that additional spacer units on the ligand moieties are connecting the metal centers (Figure 1.4). For octahedrally coordinated metal ions such as Fe^{II} [128,129] or Zn^{II},[130–132] the structure of one vertex of the cage can be simplified as ML_3 (M = metal, L = bidentate ligand). The octahedral structure can be observed as a facial (*fac*) or a meridional (*mer*) isomer if bidentate ligands with distinguishable donor atoms (A and B) are used.[133] In the meridional isomer different donor atoms span two triangular surfaces that are orthogonal to each other. The surfaces are connected via an intersection point being the metal center. This results in C_1 symmetry for the meridional isomer resulting in three different ligand environments.[133–135] In comparison, in the facial isomer two triangular planes are parallel to each other leading to C_3 symmetry and just one ligand environment.[133–135] Based on this stereoisomerism a statistical mixture of both isomers is expected (*mer*:*fac* 3:1).[133,136] However, deviations from the statistical ratio[137,138] can be observed due to e.g. the influence of steric bulk[133,139] or the solvent.[140] This stereoisomerism can

also be observed in metal-organic cages such as e.g. *fac*[87,141] or *mer*[87] coordinated cages or even mixed ones.[98]

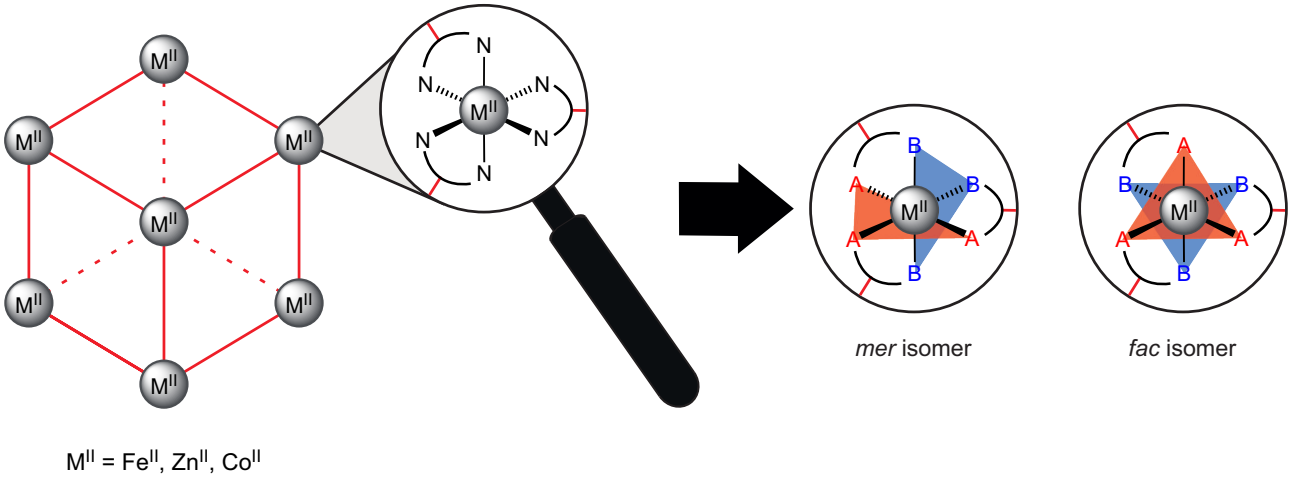

Figure 1.4: Representation of the *fac*/*mer* isomerism that occurs in mononuclear complexes and other coordination compounds as metal-organic cages. M^{II} equals a metal center with an oxidation number of two as Fe^{II} and is illustrated as a general metal vertex. The design is adapted from Carrillo *et al.*[133]

Metal-organic cages have been used in different applications including as photosensitizers[142] or catalysts[70,71] for cycloadditions, as polymers[143,144] or as detection agents for antibiotics or ions.[145,146] To date, a variety of metal-organic cages were used as molecular containers (hosts) encapsulating e.g. the poorly water soluble greenhouse gas SF_6 in an hydrophobic cavity in water[147] or organic molecules as adamantane derivatives,[123] ferrocene,[123] anions[141] or even elements as white phosphorus[148,149] due to complementary cavity and guest sizes. A prominent study for a catalytic process was reported by Chen *et al.* about the hydrogen production by cage **14** (Figure 1.5, a)).[150] By mixing $Pd(BF_4)_2(CH_3CN)_4$ with a pre-formed ruthenium precursor (Ru**13**$_3$), an octahedral $[Pd_6(Ru\mathbf{13}_3)_8](BF_4)_{28}$ heteronuclear cage (**14**) was obtained. In the presence of a reductant (TEOA) and a proton source (H_2O), cage **14** was able to produce H_2 under visible light irradiation following an electron transfer mechanism.[150]

Likewise, Pd^{II} and Pt^{II} capsules **16** and **17** self-assembled from ligand **15**, were investigated in a biomedical application by Ahmedova *et al.* (Figure 1.5, b)).[151] In comparison to cisplatin, the capsules **16** and **17** with and without encapsulated caffeine or pyrene were tested for their cytotoxicity against different tumor cell lines. The empty capsules **16** and **17** had significantly higher cytotoxicity towards four out of five cell lines. In addition, the effect of guest encapsulation led in most of the studied cell lines to decreased cytotoxicity and increased IC_{50} values in comparison to the empty capsules **16** and **17** due to more stable host-guest complexes.[151]

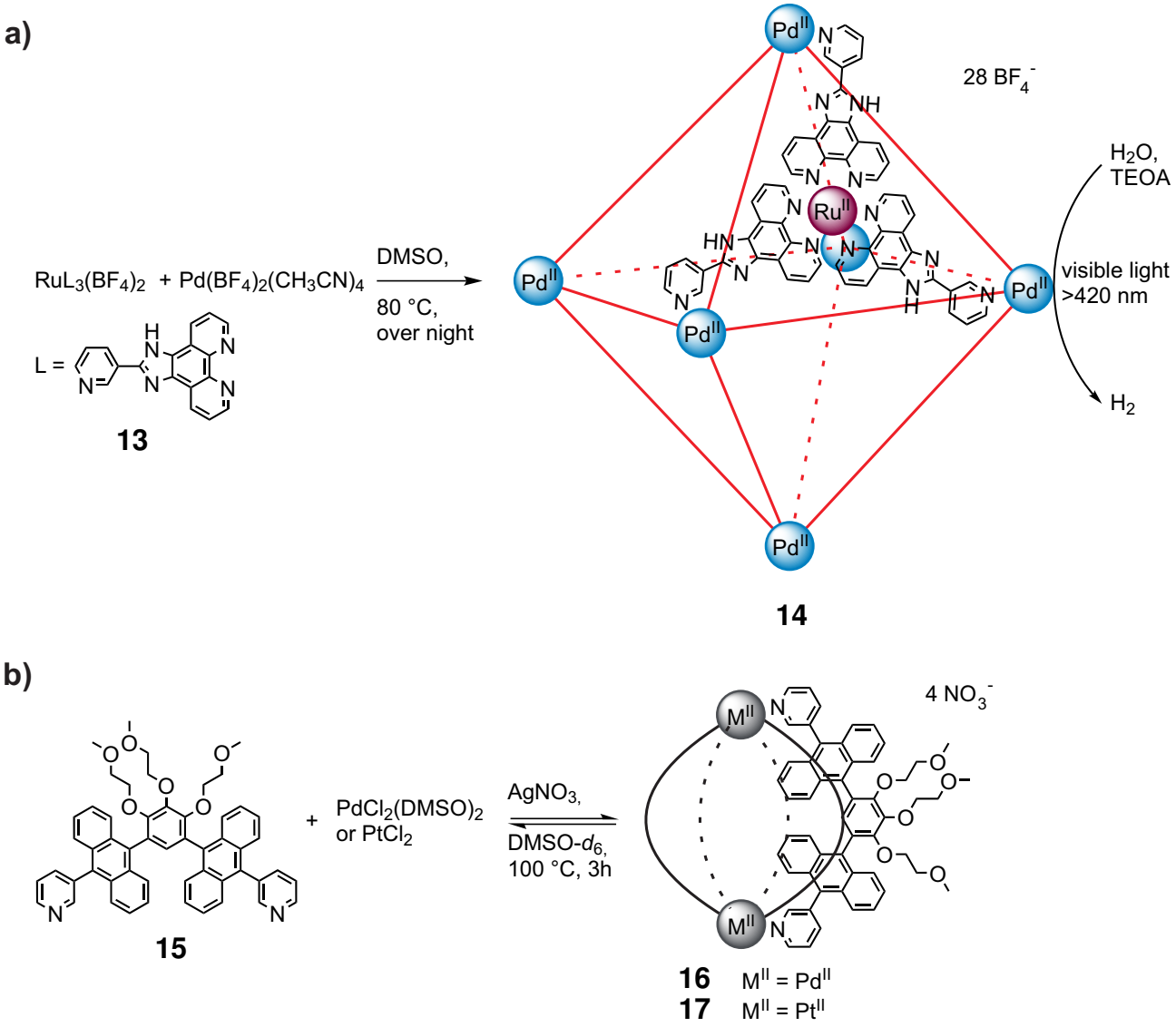

Figure 1.5: Self-assembly of a) a heterometallic metal-organic cages based on Pd^{II} and Ru^{II} and its hydrogen producing activity[150] and b) two capsules based on Pd^{II} and Pt^{II} for a biomedical application.[151]

In the recent years stimuli-responsive metal-organic cages attracted great attention since the structure and properties of cages can be selectively modified by external stimuli such as light,[83,84,152,153], guests[154,155] or concentration.[156] An emerging application of stimuli-responsivity are spin-crossover Fe^{II}-based metal-organic cages, whose spin-state can be selectively changed by e.g. temperature.[105,106,157,158]

1.3 Spin-Crossover Phenomena in Fe^{II}-based Complexes and Cages

For octahedrally coordinated transition metal ions such as those found in mononuclear complexes and metal-organic cages, energetically unequal d-orbitals are observed, which can be divided into two groups: t_{2g} and e_g.[159–161] The energetic state of the orbitals depends on repulsive electronic interactions between the ligand and transition metal ion and can be illustrated in a three-dimensional coordinate system with the ligands placed on the axes and the expected quantum mechanical orbital shapes for the d-orbitals (Figure 1.6).[159,160,162] Orbitals aligned on the axes ($d_{x^2-y^2}$ and d_{z^2}) have strong repulsive interactions with the electrons of the ligands, leading to an increase of its energetic state. Based on their symmetry they are classified as the e_g set. In comparison, the orbitals (d_{xy}, d_{xz}, d_{yz}) are positioned between the axes experiencing less repulsive interactions. Therefore, they are energetically favored and known as the t_{2g} set.[159–161] The energy gap between both groups is defined as the ligand field splitting (Δ).[160]

Electronic occupation of the orbitals depends on the electronic configuration of the used transition metals. Based on Hund's rule, transition metal ions with an electronic configuration of d^1 to d^3 occupy the t_{2g} orbitals unpaired with parallel spins being the energetically favored state of the complex.[160,161,163] A similar phenomenon is observed for electronic configurations of d^8 to d^{10}, where six paired electrons are located in the t_{2g} orbitals and the remaining ones in the e_g group.[160] In contrast, for d^4 to d^7 electronic configurations two spin states can occur: the high-spin (HS) and low-spin state (LS). In the low-spin state the maximum number of paired electrons is observed and the high-spin state leads to the complete occupation of all d-orbitals with electrons of parallel spin before spin-pairing occurs.[160,164] The spin-state depends on the ligand field splitting as well as the spin-pairing energy.[160,161,165] The energetically favored spin-state depends on the interaction between the used metal ion as well as the ligands, which both influence the ligand field splitting.[160,166,167] In 1938 Tsuchida analysed absorption bands of mononuclear complexes and developed a spectrochemical series that indicates how strongly certain ligands influence the ligand field splitting. At that time only simple ligands were included in the series such as nitrite as a very strong ligand able to induce a high ligand field splitting and likely leading to low-spin complexes or bromide as the contrary.[166]

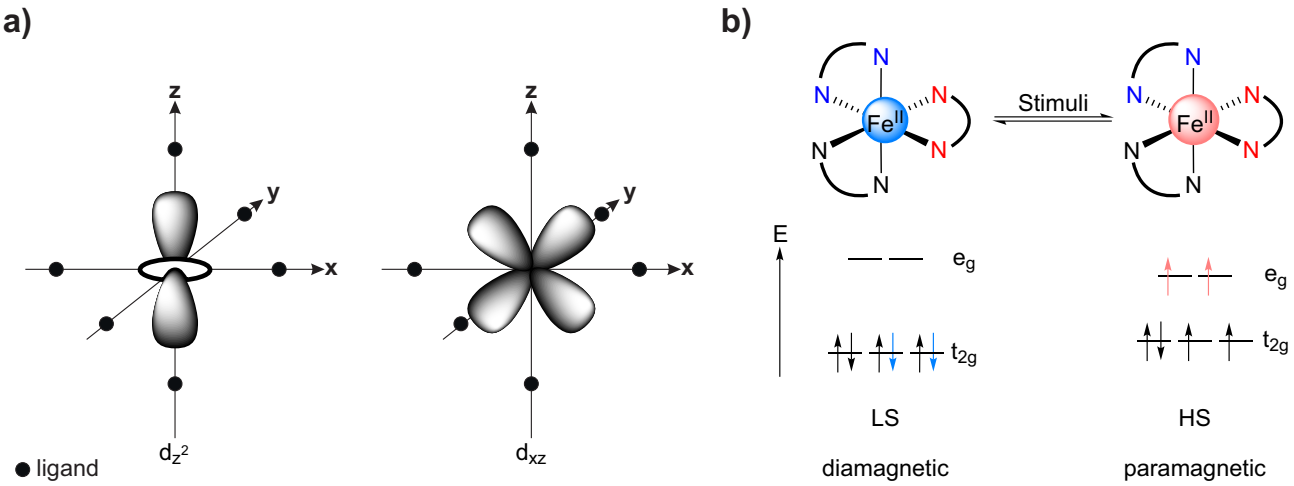

Figure 1.6: a) Exemplified representation of the d_{z^2}-orbital as an energetically disfavored orbital (e_g set) and the d_{xz}-orbital out of the energetically favored t_{2g} set. b) Simplified illustration of the low-spin and high-spin states for a d^6 Fe^{II} center with the potentially exposure to external stimuli inducing spin-crossover. Adapted from ref.[159,160,162]

The possible spin-states result in different properties such as the magnetism of a Fe^{II}-based complex in its d^6-configuration being either diamagnetic or paramagnetic.[160] External factors such as temperature,[157,168] pH-value changes[169] or light[170–173] can induce a spin-crossover leading to spin-state transitions between the low-spin and the high-spin state (Figure 1.7). Similar ligand field splitting and spin-pairing energies are the requirement for spin-crossover.[165] This phenomenon is observed when the energetic difference of both energies (ΔE) is equal to the thermal energy k_BT.[174,175] The spin-transition also leads to other property changes of both compounds, next to the magnetic change of the molar magnetic susceptibility.[160,165] The ionic radius of the coordination center increases and metal-ligand bonds (M-L, Δd = d(HS) - d(LS)) are lengthened, which is a result of newly occupied e_g orbitals that lead to repulsive interactions with the ligands on the axes. Optical differences like colour changes are observable due to changed ligand field splitting.[16,160,174,176,177]

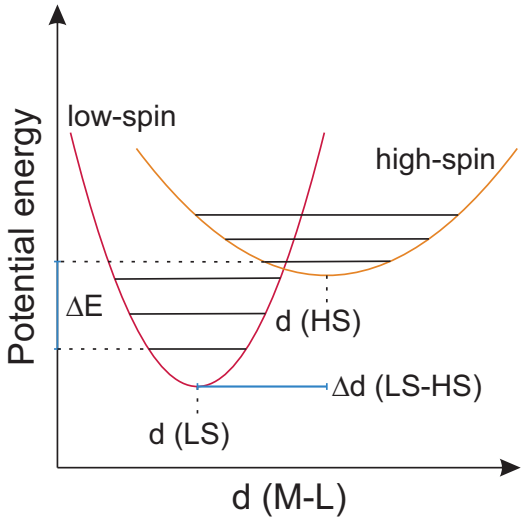

Figure 1.7: Potential energy of the low-spin and high-spin state as a function of the distance of the coordination center (M) to the coordinating heteroatom (L). Adapted from ref.[174,178]

During the spin-state transition, the temperature at which equimolar quantities of a complex are in the low-spin and high-spin state is known as the spin-crossover temperature ($T_{1/2}$).[179] The determination of $T_{1/2}$ depends on the state of aggregation, i.e. in the solid-state normally magnetometers are used,[165] while for studies in solution the Evans method from 1959 is a well-used approach.[180] While solid-state measurements can be performed up to 400 K as seen by reported solid-state studies,[158,181,182] the Evans method[180] is more restricted to the solvent range between its freezing and boiling point. In addition, the solid-state requires consideration of additional intermolecular interactions.[183–185] For the determination of $T_{1/2}$ (spin-crossover temperature) the product of the molar magnetic susceptibility and the temperature ($\chi_M T$) is plotted against the temperature. $T_{1/2}$ is derived at 50% of $\chi_M T$ of the completely high-spin complex.[165,182] Alternatively, the molar high-spin fraction based on thermodynamic data (ΔS and ΔS)[157,186] can be plotted against the temperature (Figure 1.8) with $T_{1/2}$ displayed at 50% high-spin fraction.[182,187,188]

Spin-crossover curves can be classified into five different groups based on their form.[188] Complete spin-state transitions from 100% low-spin to 100% high-spin state exhibit abrupt or gradual curve shapes, however, step-wise spin-transitions with plateaus or hysteretic behaviour are also possible (Figure 1.8). In addition, incomplete transitions can occur leading to metal centers with a mixed spin-state population.[185,189] The prediction of spin-crossover curves is challenging since they depend on different factors such as intermolecular interactions[185,189–191] and cooperative effects,[190,192] sample preparation[193] or crystal solvent.[194]

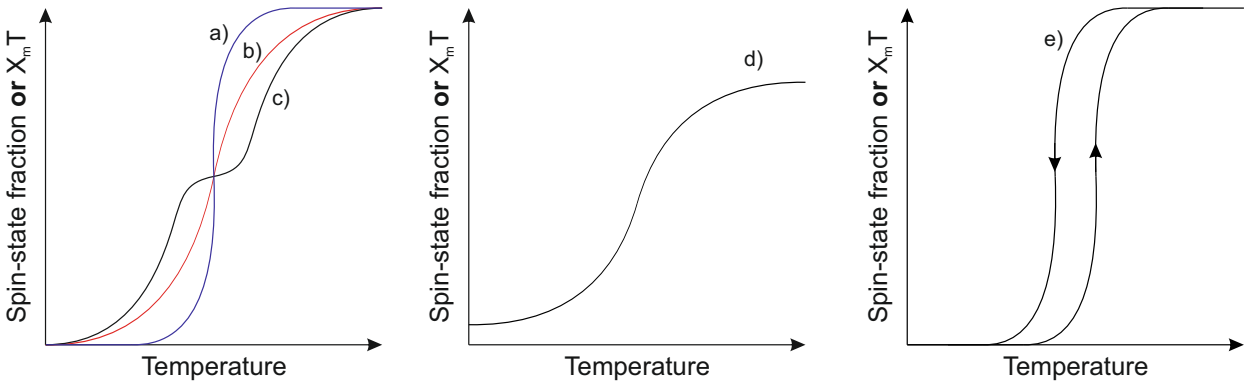

Figure 1.8: For spin-crossover materials five different curve shapes can appear, including relative simple ones like a) an abrupt b) a gradual or c) a curve with plateaus. In addition, d) incomplete spin-crossover behaviour can occur leading to not completely populated spin-states or e) hysteresis with different spin-crossover temperatures in heating/cooling mode.[182] Adapted from Martinho *et al.*[188]

In the last years multiple methods have been developed to tune spin-crossover properties by exploiting light-sensitive materials. One of the most prominent methods was published by Decurtins *et al.* in 1984 about the so-called light-induced excited spin-state trapping (LIESST) effect.[175] Decurtins *et al.* demonstrated the effect below 50 K by using the low-spin complex $[Fe(ptz)_6](BF_4)_2$ (**18**) (ptz = 1-propyl-1*H*-tetrazole) in its $^1A_1$ state (Figure 1.9, a)). Suitable irradiation with a xenon arc lamp led to excitation into the unstable $^1T_2$ state which relaxed by intersystem crossing into the metastable high-spin $^5T_2$ state. The complex **18** persists trapped in this occupied $^5T_2$ state if the requirement $\Delta E > T$ (thermal energy) is fulfilled.[175,195,196] Furthermore, in 1996 Sato *et al.*[197] investigated spin-state transitions (5-150 K) based on charge transfer (Figure 1.9, b)). Irradiation of the heterodinuclear complex $K_{0.2}Co_{1.4}[Fe(CN)_6]\cdot 6.9H_2O$ (**19**) led to a measurable increase of the magnetization being a thermally reversible electron transfer from the Fe^{II} to the Co^{III} center.[197] Although spin-state transitions occured in both phenomena, they are restricted to low temperature.[175,197] The restricted temperature range might not be suitable for applications, especially in solution.

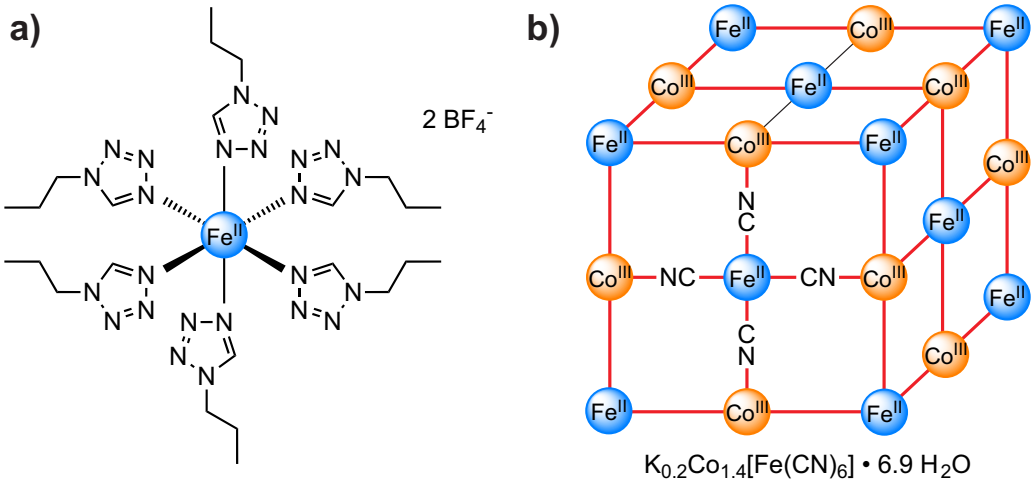

18 19

Figure 1.9: The spin-crossover complex a) **18** by Decurtins *et al.*[175] and a representation of the unit cell of complex **19** ($K_{0.2}Co_{1.4}[Fe(CN)_6]\cdot 6.9H_2O$) with the red lines being CN ligands. Only the surface of the cell is shown for reduced complexity.[197]

For improving the accessible temperature range two alternative methods have been developed allowing in-solution studies: light-driven coordination-induced spin-state switching (LD-CISSS)[198] and ligand-driven light-induced spin-state change (LD-LISC).[199,200] Both methods offer spin-transitions at ambient conditions, where light-responsive ligands are used to change the coordination number of the central atom (LD-CISSS) or the ligand field strength (LD-LISC) (Scheme 1.2, a)).[198,200] Venkataramani *et al.*[198] first introduced the LD-CISSS approach by synthesising a Ni^{II}-based porphyrin attached with a photo-responsive azobenzene unit. Upon irradiation a reversible spin-change between the square planar diamagnetic and the square pyramidal paramagnetic Ni^{II} porphyrins **20** and **21** were observed induced by azobenzene isomerisation.[198]

In comparison, LD-LISC-based systems have been known for almost 30 years.[199,200] In 2009 Hasegawa *et al.*[16] reported a novel LD-LISC system based on a 2-(2'-pyridyl)-1*H*-benzimidazole ligand functionalised with an azobenzene as a T-type photoswitch[201,202] (Scheme 1.2, b)). The Fe^{II}-based complex was irradiated with 365 nm to induce a change of the ligand field strength by *trans* to *cis* isomerisation. As a result, a more populated high-spin state was observed. Following the Evans method,[180] the spin-crossover temperature of the 100% *trans* complex **22** was calculated to be 279 K in deuterated acetone.[16] Unfortunately, the photoefficiency of the investigated complex **23** was not ideal since only 33% of the azobenzenes responded to external irradiation with 365 nm (PSS (365 nm): 67:33)). Furthermore, upon repeated irradiation cycles (365 nm/436 nm) the fatigue resistance decreased indicated by a degrading magnetic susceptibility.[16]

In addition, also other promising photoswitchable groups such as dithienylethenes are feasible ligands for LD-LISC complexes.[203] Dithienylethenes are known as P-type photoswitches with a high

stability towards thermal energy with fast response to light.[201,202] In 2013 Milek *et al.* reported the LD-LISC heteroleptic mononuclear complex **24** (100% high-spin at room temperature) bearing one 1,10-phenanthroline-based dithienylethene ligand (Scheme 1.2, c)).[203] The opened-ring complex **24** undergoes a thermal spin-state transition at 164 K in toluene, determined by the Evans method.[180] Upon irradiation with 254 nm at room temperature an incomplete photocyclisation is observed with a low-spin fraction of 40%.[203]

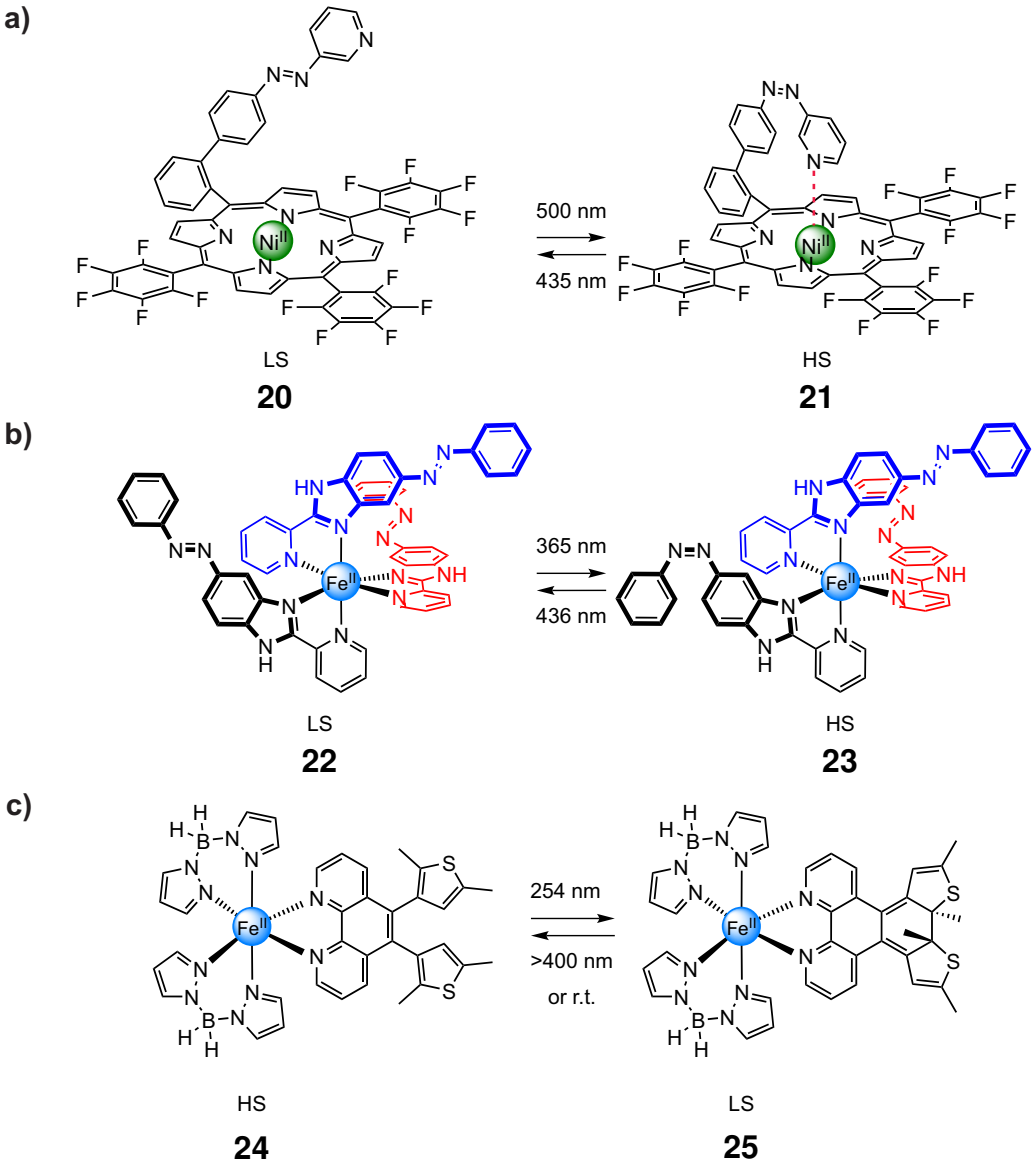

Scheme 1.2: Spin-crossover examples for light-responsive materials based on a) LD-CISSS by Venkataramani *et al.*[198] and LD-LISC by b) Hasegawa *et al.*[16] and c) Milek *et al.*[203]

The use of light as a stimuli to induce spin-state transitions is frequently used for mononuclear complexes,[16,198,203] however, light-responsive spin-crossover cages are rarely reported[204] and underexplored since the majority of reported light-responsive cages do not exhibit spin-state transitions as they are based on other metal ions such as Pd^{II},[152,153,205,206] Co^{II}[83,84] or Zn^{II} metal ions.[207] The design of photoswitchable ligands for Fe^{II}-based metal-organic cages may offer the possibility to induce spin-state transitions due to photocyclisation of the respective ligands resulting in ligand field strength changes (LD-LISC).[200]

As an alternative external stimulus, thermal energy is frequently used to induce spin-state transitions in metal-organic cages over the past ten years.[93,94,105,106,157,158,208–210] Usually, reported thermal spin-crossover cages are based on subcomponent self-assembly using imine-based ligands such as imidazolimines[158,208,211,212] or thiazolimines,[209] whereas the use of pre-synthesised ligands for thermal spin-crossover cages is underexplored. In addition, the spin-crossover properties are often reported in the solid state[158,208,209,211,212] with limited examples of in solution studies.[105,106,157] For the design of thermal spin-crossover cages many different factors need to be investigated since prediction of the spin-transition properties is more challenging than for mononuclear complexes due to the complexity of the system or cooperative effects[213] that need to be considered. In general, spin-state transitions are preferred close to room temperature for potential applications.[105,106] As a starting point, a ligand scaffold with a ligand field strength similar to the spin-pairing energy should be chosen to access both spin-states by temperature changes.[165] Although the number of reported Fe^{II}-based spin-crossover cages and studies is limited,[93,94,105,106,157,158,208,209,211] additional mononuclear complex data may provide information about potential suitable ligand motifs and modifications to tune the spin-crossover properties. In 2021 Hardy *et al.*[105,106] reported a first study about the spin-crossover properties of several azole scaffolds in cubic-like metal-organic cages (Figure 1.10). The cages **26**-**28** were prepared by subcomponent self-assembly. Cage **26** based on 4-imidazolecarbaldehyde was observed to have the lowest spin-transition temperature of 215 K, followed by cage **27** with *N*-methyl-2-imidazolecarbaldehyde as the subcomponent ($T_{1/2}$ = 281 K). The highest spin-crossover temperature of 324 K was observed for cage **28** that is based on the 4-thiazolecarbaldehyde component. In this study the differences were attributed to the different ligand field strengths of the respective azole units.[105,106] Depending on the desired spin-crossover temperature this study provides first information about three suitable ligand scaffolds for metal-organic cages.

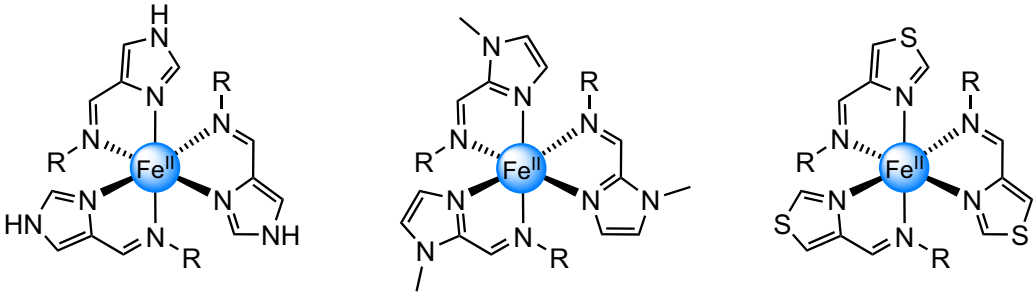

26 **27** **28**

$T_{1/2}$ = 215 K $T_{1/2}$ = 281 K $T_{1/2}$ = 324 K

Figure 1.10: Three different cube-shaped thermal spin-crossover cages **26**-**28** by Hardy *et al.*[105,106] For reduced complexity only one Fe^{II} vertex is shown.

Alternatively, for mononuclear complexes the pyridylbenzimidazole motif that has been well-studied for mononuclear complexes and shows also suitable ligand field strengths for compounds exhibiting spin-transitions close to room temperature.[16,214,215] Further fine-tuning of the spin-crossover properties can be facilitated by the use of ligand modifications such as the introduction of substituents. Based on systematic studies of mononuclear complexes,[216–218] the low-spin state can be destabilised and $T_{1/2}$ decreased by introducing sterically bulkier groups such as methyl groups close to the coordination center.[216] The same phenomenon is observed by introducing electron-donating substituents in the *p*-pyridine position.[217,218] The observed tendencies may be applicable for the design of metal-organic cages, but systematic studies about the spin-crossover property changes of metal-organic cages remain. The porous structure of metal-organic cages offers more tunable properties. Bilbeisi *et al.* showed that guest binding influences the spin-crossover temperature (Figure 1.11).[157] The empty cage **30** undergoes a spin-transition at 336 K, however, upon guest encapsulation, the spin-crossover temperature decreases by 9 K (Br^-) or 15 K (CS_2) depending on the used guest. Also other factors as the chosen solvent[219] or cooperative effects[213] can have an influence on the spin-crossover properties and need to be investigated to obtain the targeted spin-crossover properties. Due to the novely of stimuli-responsive metal-organic cages as a research field further investigations about the influence of cage modifications are required in order to design predictable spin-crossover metal-organic cages.

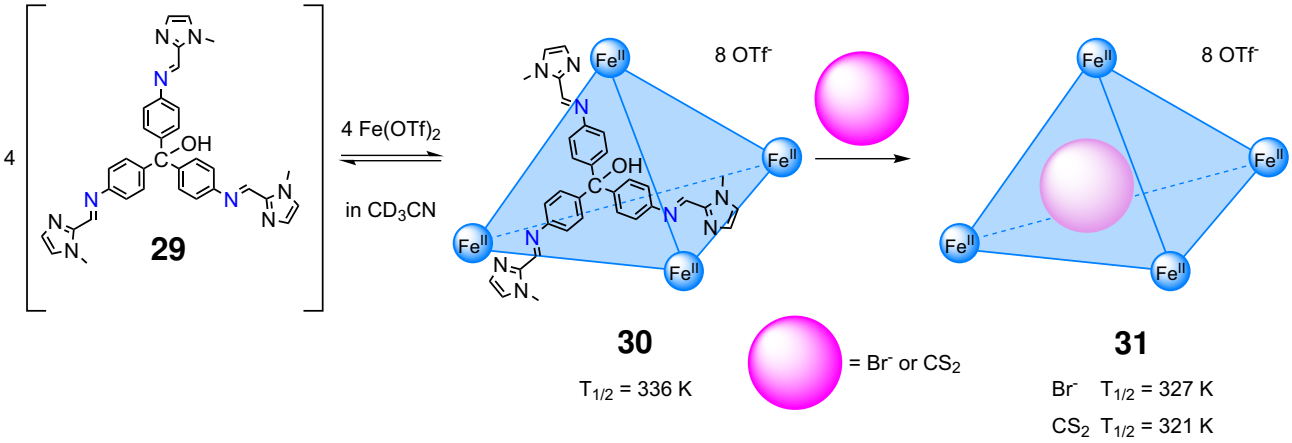

Figure 1.11: Guest encapsulation effect on the thermal spin-crossover properties of metal-organic cage **30**. A $T_{1/2}$ decrease of 9 K was observed for binding bromide in the cavity and 15 K for methanedithione.[157]

Chapter 2
2 Thesis Aim

Thermal induced spin-state transitions of Fe^{II}-based metal-organic cages have been studied over the past 10 years.[93,94,105,106,157,158,208,209] The use of light as an alternative external factor could be advantageous due to fast populating spin-state transitions.[220] Although light-responsive metal-organic cages and helicates are known,[83,84,152,153,205–207] the number of light induced spin-crossover cages is limited.[204] This doctoral thesis is about the incorporation of thermal- and light-responsivity into metal-organic cages as dual-responsive spin-crossover materials. Since the synthesis of ligands can be challenging and the reported examples of stimuli-responsive spin-crossover metal-organic cages are limited,[93,94,105,106,157,158,204,208,209] the aim of this thesis is divided into three chapters. For that, different ligand scaffolds need to be investigated to identify ligand motifs with suitable ligand field strengths to exhibit thermal spin-crossover properties close to room temperature (Figure 2.1). Furthermore, light-induced spin-state transitions can be induced by the introduction of additional photoswitchable groups with a high photoefficiency (Figure 2.1, blue spheres and purple squares). Upon irradiation with light a isomerisation/backisomerisation process could change the ligand field strength[200] and induce a spin-state transition of an Fe^{II}-based metal-organic cage.

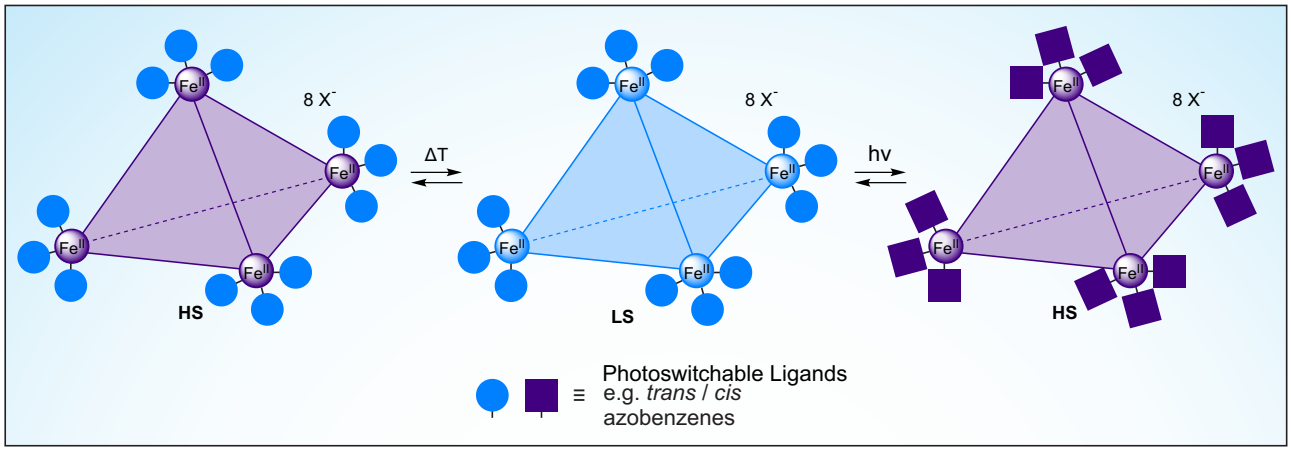

Figure 2.1: Illustration of dual-responsive spin-crossover cages with photoswitchable groups (blue spheres and purple squares). Upon temperature changes or irradiation with light spin-state transitions of Fe^{II}-based cages can be induced.

Chapter 3 concentrates on the design of thermal spin-crossover Fe^{II} cages with mainly 2-(2'-pyridyl)-benzimidazole, -imidazole and benzothiazole binding motifs due to their well-known spin-crossover properties (Figure 2.2).[105,106,214,215,221–225] Firstly, methods will be developed for the characterisation of paramagnetic Fe^{II}-based cages and ligand synthesis. The methods will be used to facilitate the spin-crossover investigations. Electronic[217,218] and steric effects[216,226] are known to fine-tune the spin-crossover properties of Fe^{II}-based mononuclear complexes, however, systematic studies about the spin-crossover properties of metal-organic cages are poorly reported.[105,106] Therefore, the effect of ligand modifications such as substituents, steric effects or linker groups on the spin-crossover properties of metal-organic cages will be examined.

In Chapter 4 light-responsive Fe^{II}-based mononuclear complexes utilising the LD-LISC effect will be investigated as model complexes for metal-organic cages (Figure 2.2). For an efficient LD-LISC effect the designed Fe^{II}-complexes with incorporated photoswitchable groups should have an efficient isomerisation process and long half-life times in order to stabilise both spin-states.[200] Based on the results of Hasegawa *et al.*[16] (Scheme 1.2) 2-(2'-pyridyl)benzimidazole-based azobenzenes have been chosen as the first photoswitches. The ligands will be modified by *N*-substitution (see Scheme 1.2) to i) suppress the tautomerism of the imidazole moiety and identify if the tautomerism causes the poor reported photoefficiency[16] and ii) increase the spin-crossover temperature closer to room temperature by methylation.[215] As a second class, dithienylethenes are known as LD-LISC model systems[203] and will be investigated due to the excellent photochemical properties reported for other dithienylethenes.[201,202,227,228]

In chapter 5 the knowledge about optimised thermal spin-crossover properties (chapter 3) will be combined with the results of the model complexes from chapter 4 in order to design and investigate the first generation of dual-responsive spin-crossover metal-organic cages.

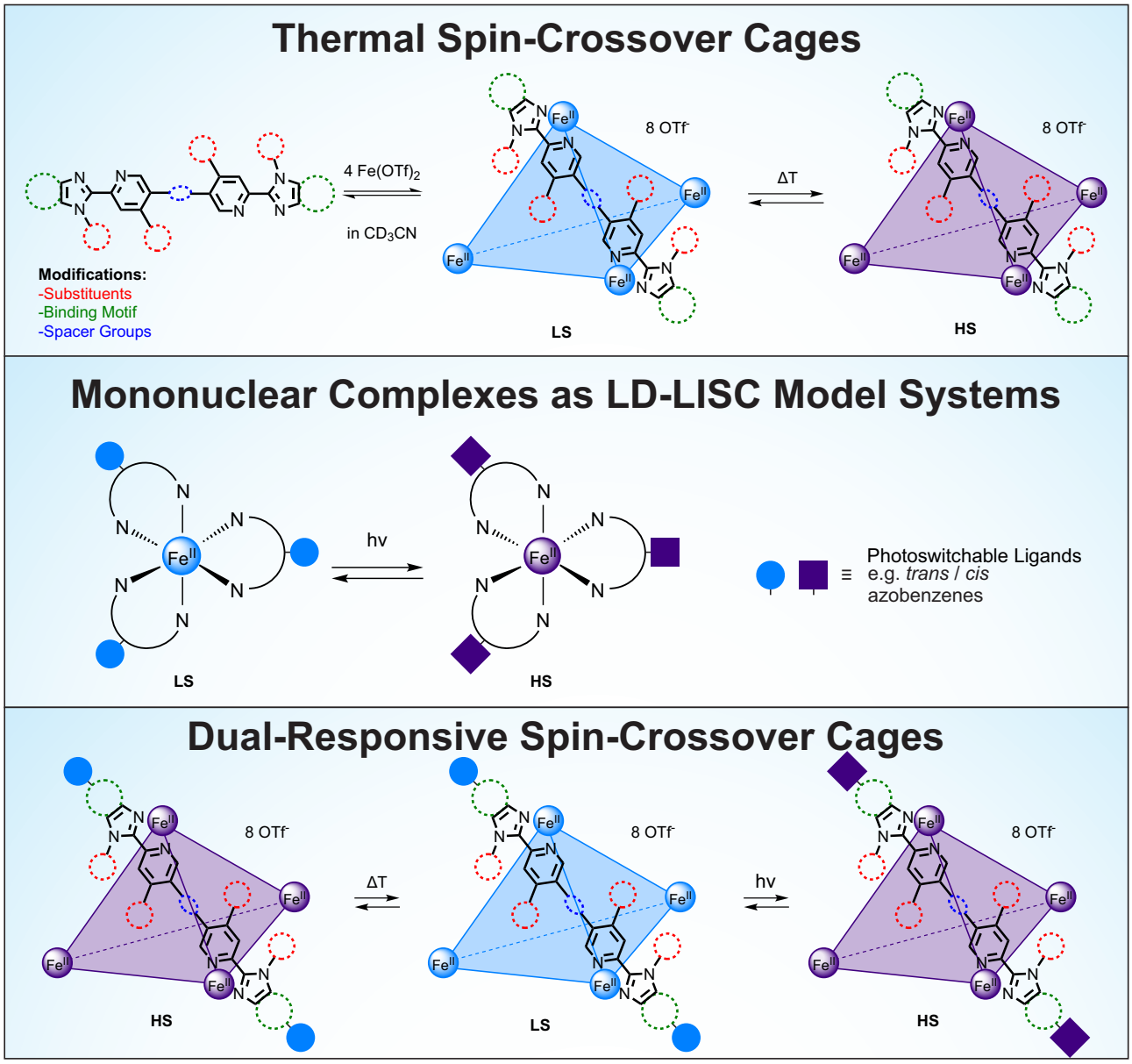

Figure 2.2: The thesis is divided into three chapters: i) thermal spin-crossover cages, ii) mononuclear complexes as LD-LISC model systems and iii) dual-responsive spin-crossover cages. The imidazole scaffold is exemplarily shown as a potential, modifiable ligand.

Chapter 3

3 Thermal Spin-Crossover Cages

This chapter focuses on the development of thermal spin-crossover cages with spin-state transition temperatures close to room temperature. For this aim, three azole scaffolds were chosen and investigated based on related well-studied compounds[16,105,106,214,215,221–225,229] (Figure 3.1): i) 2-(2'-pyridyl)imidazole (**32**), ii) 2-(2'-pyridyl)benzimidazole (**33**) and iii) 2-(2'-pyridyl)benzothiazole (**34**). Data for related mononuclear complexes based on 2-(2'-pyridyl)benzimidazole ligands indicated ligand field strengths suitable to induce spin-state transitions around room temperature.[16,222,229] Due to these results, scaffold ii) will be the main focus. In comparison, the low-spin state is expected to be more stabilised of ligand scaffolds i) and iii) due to stronger ligand fields.[105,106,224,225] Ligand scaffold i) will be investigated in section 3.1, ii) in sections 3.1 and 3.2 and scaffold iii) in section 3.2.

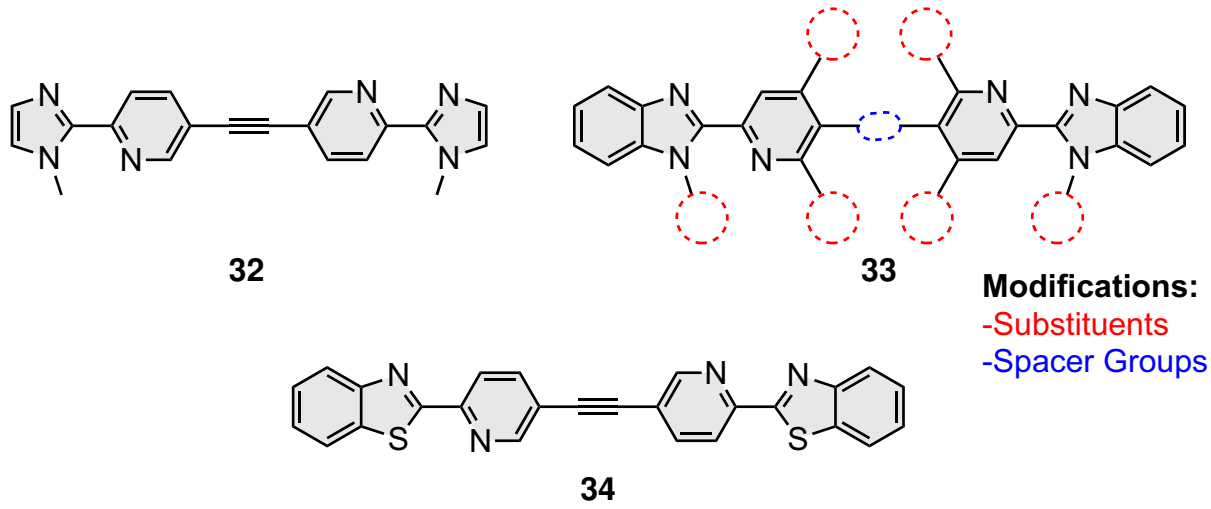

Scheme 3.1: The depicted ligands and scaffolds will be investigated in this chapter. 2-(2'-Pyridyl)-1*H*-benzimidazole-based ligands will be modified by spacer and functional groups.

3.1 Publication List

In this section the main focus was the investigation of the spin-crossover properties of thermal spin-crossover cages based on a 2-(2'-pyridyl)-1*H*-benzimidazole motif. For studying the thermal spin-crossover cages, multiple methods have been investigated and optimised: i) a paramagnetic NMR toolbox that enabled the characterisation of paramagnetic mononuclear complexes and metal-organic cages (Section 3.1.1) and ii) a one-pot Sonogashira cross-coupling reaction for synthesising in an efficient way the desired di(2-(2'-pyridyl)-1*H*-benzimidazole)alkyne ligands for Fe^{II}-based metal-organic cages (Section 3.1.2). Afterwards, these methods have been used to systematically study the spin-crossover properties of eleven Fe^{II}-based metal-organic cages bearing 2-(2'-pyridyl)-1*H*-benzimidazole/imidazole coordination units with different electronic and steric properties (iii, Section 3.1.3). Overall, the author, Tobias Paschelke, contributed to these publications (i-iii). A summary, the contribution of Tobias Paschelke (author's contribution) as well as the manuscript are given in the respective sections for each publication (Manuscript: sections 3.1.1, 3.1.2 and 3.1.3. The supporting information are provided on an external storage device. The numbering of the substances mentioned in the abstracts is identical to the numbering within the publication for consistency and ease of reading.

3.1.1 Article: A Paramagnetic NMR Spectroscopy Toolbox for the Characterisation of Paramagnetic/Spin-Crossover Coordination Complexes and Metal-Organic Cages

Marc Lehr, Tobias Paschelke, Eicke Trumpf, Anna-Marlene Vogt, Christian Näther, Frank D. Sönnichsen, Anna J. McConnell

Angew. Chem. Int. Ed. **2020**, *59*, 19344-19351. | *Angew. Chem.* **2020**, *59*, 19344-19351.

doi.org/10.1002/anie.202008439 | doi.org/10.1002/ange.202008439

This publication is about the optimisation and development of suitable NMR spectroscopic techniques to facilitate the characterisation of paramagnetic materials. For the initial optimisation studies model complex **1a** was chosen, which was prepared from three 2-pyridylquinoline ligands and $Co(BF_4)_2 \cdot 6H_2O$ in CD_3CN. *mer*-Complex **1a** was obtained as indicated by three different ligand environments in the ^{1}H NMR spectrum and its crystal structure. For proton assignments ^{1}H-^{1}H COSY pulse programs were optimised and cross-peaks were observable to assign the ligand's protons in complex **1a**. Broad proton signals without observable cross-peaks were assigned based on steady-state NOE experiments. EXSY instead of NOE cross-peaks were observed in the optimised ^{1}H-^{1}H NOESY spectrum and were used to group protons according to the three different ligand environments in the *mer* complex **1a**.

For the carbon assignment ^{1}H-coupled ^{13}C NMR spectra were measured to identify multiplicities and to discriminate quaternary and tertiary carbons. Tertiary carbons were assigned by optimising a ^{1}H-^{13}C HMQC pulse program, which gave ^1J cross-peaks. The results were validated by comparison to the previously performed selective ^{1}H-decoupling ^{13}C NMR experiments. Reference complexes were used for the assignment of quaternary carbons due to missing cross-coupling information within ^{1}H-^{13}C HMBC experiments.

The applicability of the optimised NMR parameters was further demonstrated by the complete characterisation of a further six Co^{II}-based complexes (**2a**-**7a**) and the Fe^{II}-based high-spin complex **1b** based on the 2-pyridylquinoline motif, and the Co^{II}-based metal-organic cage **8** bearing 2,2'-bipyridine type ligands. Multiple complex species (e.g. the *fac* and *mer* isomers) were differentiable using the NMR spectroscopic techniques. In the special case of Fe^{II}-based complex **1b**, the proton and carbon spectra were assigned at 248 K due to line broadening at 298 K, which sharpened upon cooling.

Contribution from own Master thesis:[230] Synthesis of 2-(2-pyridyl)quinoline; synthesis development for 1-(5-bromopyridin-2-yl)ethanone, 2-(5'-bromopyridin-2'-yl)quinoline (large scale); self-assembly and characterisation of cage **8**
Contribution in this dissertation: Preparation and proofreading of the supporting information; proofreading of the manuscript

How to cite: *Angew. Chem. Int. Ed.* **2020**, *59*, 19344 – 19351
International Edition: doi.org/10.1002/anie.202008439
German Edition: doi.org/10.1002/ange.202008439

Metal–Organic Cages

A Paramagnetic NMR Spectroscopy Toolbox for the Characterisation of Paramagnetic/Spin-Crossover Coordination Complexes and Metal–Organic Cages

*Marc Lehr, Tobias Paschelke, Eicke Trumpf, Anna-Marlene Vogt, Christian Näther, Frank D. Sönnichsen, and Anna J. McConnell**

Abstract: *The large paramagnetic shifts and short relaxation times resulting from the presence of a paramagnetic centre complicate NMR data acquisition and interpretation in solution. As a result, NMR analysis of paramagnetic complexes is limited in comparison to diamagnetic compounds and often relies on theoretical models. We report a toolbox of 1D (^{1}H, proton-coupled ^{13}C, selective ^{1}H-decoupling ^{13}C, steady-state NOE) and 2D (COSY, NOESY, HMQC) paramagnetic NMR methods that enables unprecedented structural characterisation and in some cases, provides more structural information than would be observable for a diamagnetic analogue. We demonstrate the toolbox's broad versatility for fields from coordination chemistry and spin-crossover complexes to supramolecular chemistry through the characterisation of Co^{II} and high-spin Fe^{II} mononuclear complexes as well as a Co_4L_6 cage.*

Introduction

NMR spectroscopy is indispensable for the solution structural characterisation of macromolecules from proteins[1] to supramolecular architectures,[2] including interlocked structures,[3] metal-organic cages[4] and topologically complex molecules.[5] With the standard suite of 1D and 2D NMR methods, structural assignment of diamagnetic compounds and complexes is straightforward but NMR spectroscopy in the presence of paramagnetic centres is more difficult.

Paramagnetic NMR spectroscopy[6] is central to many fields from chemical and structural biology for studying the structure, dynamics and interactions of proteins[1b,c,7] to probing spin-state populations in spin-crossover compounds[8] and the structural characterisation of paramagnetic complexes[9] and supramolecular architectures.[4b,10] However, NMR data acquisition and interpretation in the presence of a paramagnetic centre presents a number of challenges due to the large paramagnetic shifts, short relaxation times and broad linewidths: pulse programs with long or multiple pulses are not suitable since relaxation can occur before data acquisition takes place;[6b] uniform excitation is more difficult over the larger spectral range; some signals may be lost completely in the case of very short relaxation times and broad linewidths;[6e] structural information usually extracted from the chemical shift and *J*-coupling is lost.[6e,9a,10a] Furthermore, there are limitations to current methods for spectral assignment; they often rely on the availability of accurate theoretical models[6b,9b,11] or single crystal X-ray structures for correlation of T_1 relaxation times to metal-proton distances using the Solomon equation.[4b,10b,d] As a result, solution characterisation is, in many cases, limited to a ^{1}H NMR spectrum only where complete and unambiguous assignment may not be possible.

Nevertheless, paramagnetic NMR spectroscopy also has advantages compared to diamagnetic NMR spectroscopy: the large paramagnetic shifts result in reduced likelihood of signal overlap from dispersion of the NMR signals over a wider chemical shift range;[10c] the fast relaxation times in comparison to diamagnetic compounds enables reduction of the acquisition times and recycle delays, thereby significantly reducing the demand on instrument time.[4b,6b,12] Alternatively, this can be exploited for a greater sensitivity of detection through extensive scan averaging. In supramolecular chemistry this has allowed detection of guest binding within paramagnetic cages,[4b,10c] even when the guest is present as a trace impurity.[4b]

Despite these advantages, the full potential of paramagnetic NMR spectroscopy is still to be realised; in comparison to the wealth of 1D and 2D NMR methods for diamagnetic compounds, the number of methods suitable for paramagnetic complexes is limited by fast relaxation although paramagnetic DOSY has been recently reported.[6e,13] Furthermore, the data acquisition/interpretation difficulties[6c] still need to be overcome to enable straightforward structural characterisation by paramagnetic NMR spectroscopy.

We report a toolbox of 1D (^{1}H, proton-coupled ^{13}C, selective ^{1}H-decoupling ^{13}C, steady-state NOE) and 2D (COSY, NOESY, HMQC) paramagnetic NMR methods that have proven particularly robust towards fast relaxation and enable unprecedented in-depth structural analysis of para-

[*] M. Lehr, T. Paschelke, E. Trumpf, A.-M. Vogt, Prof. Dr. F. D. Sönnichsen, Prof. Dr. A. J. McConnell
Otto Diels Institute of Organic Chemistry
Christian-Albrechts-Universität zu Kiel
Otto-Hahn-Platz 4, Kiel 24098 (Germany)
E-mail: amcconnell@oc.uni-kiel.de
Prof. Dr. C. Näther
Institute of Inorganic Chemistry
Christian-Albrechts-Universität zu Kiel
Max-Eyth-Straße 2, Kiel 24118 (Germany)
Supporting information and the ORCID identification number(s) for the author(s) of this article can be found under https://doi.org/10.1002/anie.202008439.

magnetic complexes in solution. We demonstrate the general applicability of this selection of robust experiments by characterising paramagnetic complexes from various fields of chemistry: Co^{II} mononuclear complexes **1a**–**7a** (Figure 1a) as representative examples of paramagnetic coordination complexes; Fe^{II} mononuclear complex **1b** (Figure 1a), whose perchlorate and tetrafluoroborate salts are known to undergo spin-crossover in the solid state,[14] to represent the high-spin state of a spin-crossover complex; and metal-organic cage **8** (Figure 1b) as an example of a paramagnetic supramolecular architecture.

a)

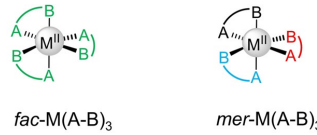

1a $Co(pq)_3$ **2a** $Co(pq\text{-}5'\text{-}Br)_3$ **5a** $Co(pq\text{-}6\text{-}Br)_3$
1b $Fe(pq)_3$ **3a** $Co(pq\text{-}5'\text{-}CCH)_3$ **6a** $Co(pq\text{-}6\text{-}CCH)_3$
4a $Co(pq\text{-}5'\text{-}Ph)_3$ **7a** $Co(pq\text{-}6\text{-}Ph)_3$

A-B =

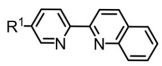

R^1 = H, pq
R^1 = Br, pq-5'-Br
R^1 = CCH, pq-5'-CCH
R^1 = Ph, pq-5'-Ph

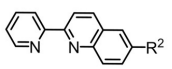

R^2 = Br, pq-6-Br
R^2 = CCH, pq-6-CCH
R^2 = Ph, pq-6-Ph

b)

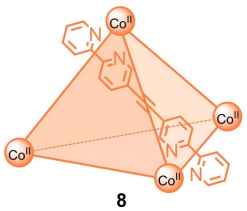

8

Figure 1. Paramagnetic a) mononuclear Co^{II} and Fe^{II} complexes based on sterically bulky 2-pyridylquinoline (pq) motifs and b) Co_4L_6 cage for characterisation by the toolbox of paramagnetic NMR techniques.

Results and Discussion

We initially investigated the mononuclear complexes to optimise the toolbox and test its limits for spectral assignment. Since the mononuclear complexes could form a mixture of meridional (*mer*) and facial (*fac*) isomers, up to four sets of NMR signals could, in principle, be observed based on symmetry considerations: 1 set for the *fac* isomer (represented as green ligands in Figure 1a) and 3 sets for the ligand in the three different environments in the *mer* isomer (represented as black, red and blue ligands, Figure 1a). The 2-pyridylquinoline (pq) coordination motif was chosen to investigate the influence of steric bulk on the *fac/mer* ratio since its coordination chemistry with labile octahedral metal ions has been underexplored in solution.[11b]

Co^{II} complex **1a** with the parent pq[15] ligand (SI, Section 2.1) was studied first rather than the literature-known Fe^{II} complex **1b**,[14] which could undergo spin-crossover complicating NMR analysis. Complex **1a** was prepared either in situ or as crystals by mixing $Co(BF_4)_2{\cdot}6H_2O$ and three equivalents of the ligand in CD_3CN or EtOH, respectively. Single crystal X-ray analysis revealed *mer*-**1a** crystallised (Figure 2 and SI, Section 3.1.1.1).[18] Like the analogous crystal structure of $[Fe(pq)_3](BF_4)_2$ (**1b**),[14a] adoption of the *mer* configuration is attributed to the ligands' steric bulk and π-π stacking interactions are observed between two of the ligands (black and red ligand environments in Figure 1a) causing distortion of the N-Co^{II}-N angles from the ideal 90° octahedral geometry (Table S3).

In solution, the ^1H NMR spectra of the complex prepared in situ and by redissolving the crystals in CD_3CN were similar (Figure S32). The ^1H signals were spread over a 250 ppm range with 24 relatively sharp signals of equal intensity (linewidths up to 70 Hz, Table S5) and 4 broader signals (Figure S34). This suggests that the *mer* isomer is not only the solid-state structure but also the only structure in solution; the deviation from the expected 30 signals is attributed to either overlapping or broad signals.

Assignment of the ^1H spectrum was initially attempted using the Solomon equation, which has been successfully applied to assign the spectra of highly symmetric cages by correlating T_1 relaxation times to the metal-proton distances from the single crystal X-ray structure.[4b,10b,d] For complex **1a** the T_1 relaxation times varied from 0.7 to 80 ms (Table S4) but a limitation of this currently available assignment method was highlighted during analysis; only partial assignment was possible since not only protons *d* and *g* (Figure 3a) but also, and more importantly, the three different ligand environments cannot be distinguished on the basis of T_1 relaxation times/Co^{II}-proton distances alone. Ward also encountered this limitation in the assignment of a lower symmetry metal-organic cage.[10c] Therefore, we sought to remove the reliance of assignment on the Solomon equation by optimising a toolbox of paramagnetic NMR experiments with broad applicability for the straightforward characterisation of a variety of

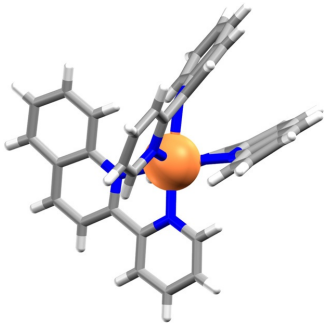

Figure 2. Single crystal X-ray structure of $[Co(pq)_3](BF_4)_2$ (**1a**) with counteranions omitted for clarity.

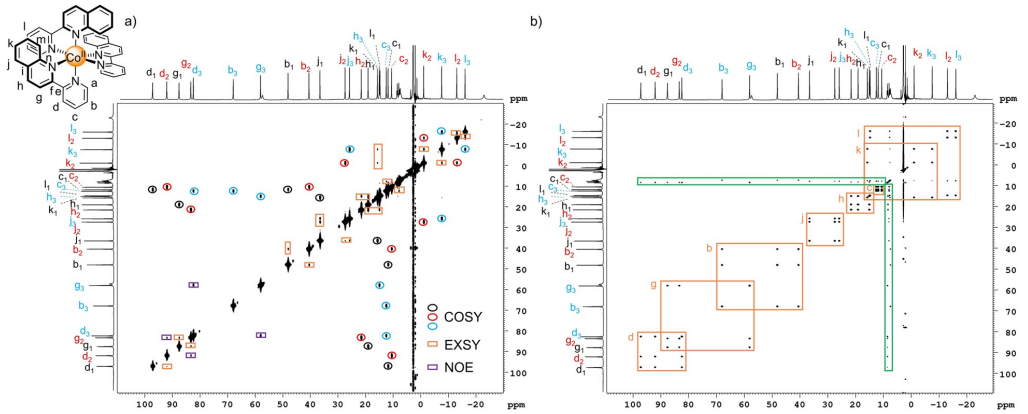

Figure 3. a) ^{1}H-^{1}H COSY NMR spectrum (600 MHz, CD_3CN, 298 K) of *mer*-$[Co(pq)_3](BF_4)_2$ (**1a**) where through-bond (COSY) cross-peaks within the three ligand environments are represented by the red, black and blue circles, respectively. Additional structural information in the form of exchange (EXSY) cross-peaks (orange boxes) and through-space (NOE) cross-peaks (purple boxes) is present due to chemical exchange and cross-correlation,[16] respectively. Note: the numbers 1, 2, 3 on the proton labels represent the three sets of coupled protons within a single spin system (i.e. protons *b-d*). The absence of NOE cross-peaks between protons *h* and *j* prevented assignment of these spin systems to a particular ligand environment and therefore, spin system *j-l* was arbitrarily labelled with black, red and blue labels in decreasing chemical shift order of proton *j* to represent the three ligand environments. b) ^{1}H-^{1}H NOESY NMR spectrum (600 MHz, CD_3CN, 298 K) of *mer*-$[Co(pq)_3](BF_4)_2$ (**1a**). Exchange (EXSY) cross-peaks are represented by the orange boxes and exchange cross-peaks between the complex and excess ligand are shown by the green boxes.

paramagnetic complexes. The following description of the structural assignment of complex **1a** and related mononuclear complexes is used to illustrate how the paramagnetic NMR toolbox was optimised to overcome commonly encountered data acquisition and interpretation difficulties. An instruction manual for application of the toolbox to the characterisation of other paramagnetic complexes and cages is provided in Section 1.1.1 of the SI.

We initially turned our attention to COSY since this would allow grouping of the resonances within the different ligand environments. Encouraged by the observation of cross-peaks in the COSY spectra of several paramagnetic complexes[9a] and supramolecular architectures[4b,10a,b] despite the broad linewidths and short relaxation times, we tested and optimised several COSY variants (SI, Section 1.1.1.2). Reduction of the recycle delays and acquisition times due to the fast relaxation times enabled the acquisition of more data in a shorter amount of time using these optimised paramagnetic COSY parameters (typically 5.5 mins for 4 scans, Table S1) compared to the standard COSY parameters (8 min for 1 scan, Table S1).

Cross-peaks were observed in spectra recorded using the pulse programs cosygpqf (Figure 3a), cosyqf90 and cosygpmfqf (Figure S35), although intense diagonal peaks[6b] and commonly observed artefacts, such as T_1 noise streaks and anti-diagonal peaks, were present to varying degrees dependent on the pulse program. The availability of three suitable paramagnetic COSY pulse programs will enable broad applicability to a variety of paramagnetic complexes and facilitate the implementation of paramagnetic COSY as a standard characterisation method.

The three COSY spectra of complex **1a** display a large number of cross-peaks (Figure 3a, Figure S35). Notably, COSY[19] cross-peaks expected on the basis of ^{3}J coupling were observable facilitating identification of neighbouring protons and thus, grouping of the proton resonances to one of the three ligand environments (black, red and blue circles, Figure 3a). Unexpectedly, additional cross-peaks were observed (orange and purple boxes in Figure 3a, Figure S35), although the COSY spectrum of $[Co(bpy)_3](BF_4)_2$ as a reference complex showed only the two expected cross-peaks arising from ^{3}J coupling (Figure S96). The origin of these additional cross-peaks was investigated using NOESY since Wimperis and Bodenhausen[16c,d] as well as Bertini[16a,b] have reported the presence of additional relaxation-allowed cross-peaks in the COSY spectra of paramagnetic complexes that result not from through-bond coupling but rather cross-correlation from through-space (NOE) coupling between the nuclei as well as between the nuclei and the paramagnetic centre.

The standard NOESY pulse program was modified for application to paramagnetic complexes (SI, Section 1.1.1.3). For an initial experiment, a mixing time of 20 ms was chosen as a compromise between the short relaxation times and comparatively long NOE cross-relaxation rates. Pleasingly, cross-peaks for the sharp signals (linewidth <70 Hz) were observed (Figure 3b). Given the range of T_1 relaxation times within the complex, optimisation of the mixing time was investigated. A series of NOESY spectra were measured varying the mixing time from 1 ms to 20 ms and the cross-peaks were integrated (Figure S36). For protons with T_1 relaxation times significantly longer than the mixing time, the exchange integral approached a maximum as the mixing

time increased. However, for protons with shorter T_1 relaxation times (e.g. protons *d* and *g*), the exchange integral reached a maximum before decreasing as relaxation began competing with exchange when the mixing time increased. A mixing time of 10 ms was found to be a good compromise for maximising the exchange cross-peak of all protons despite their differing T_1 relaxation times.

Analysis of the NOESY spectrum revealed groups of three cross-peaks (orange boxes, Figure 3b), corresponding to chemical exchange between the three different ligand environments of the *mer* isomer. Thus, the spectrum has no NOE cross-peaks but is an EXSY spectrum since the mixing time was so short. Furthermore, EXSY cross-peak intensities can be close to 100%,[6c] whereas NOE intensities are, in general, small for small molecules and reduced even further by the fast relaxation from coupling to the paramagnetic center.[6d] Since some excess ligand was also present in the complex solution, exchange cross-peaks were also observed between the excess ligand and ligand in the complex (green boxes, Figure 3b), enabling assignment of protons *b-l* in the complex using the free ligand assignments (Table S6) despite broadening and small shifts between free and excess ligand signals due to the presence of Co^{II}.

The COSY spectrum (Figure 3a) was then reanalysed with the proton assignments to determine the origin of the additional cross-peaks beyond the expected COSY cross-peaks (black, red and blue circles). These additional cross-peaks correspond to structural information that is not typically observable in the COSY spectra of diamagnetic compounds; relaxation-allowed through-space (NOE) cross-peaks between protons *d* and *g* (purple squares) were observed due to cross-correlation[16] and EXSY cross-peaks (orange boxes) were observed due to exchange between the three ligand environments, as confirmed by the exchange cross-peaks in the NOESY spectrum (Figure 3b).

Thus, almost complete assignment of the ^{1}H spectrum of **1a** was possible using COSY and NOESY with the exceptions of the assignment of: i) spin systems *g-h* and *j-l* to a particular ligand environment since relaxation-allowed (NOE) cross-peaks were not observed between protons *h* and *j* in the COSY spectrum; ii) the broad signals, which are proposed to be protons *a* and *m* due to their close proximity to the paramagnetic Co^{II} centre. TOCSY (Figure S37) and steady-state NOE experiments (Figures S38, S39) were carried out but exchange cross-peaks rather than long-range coupling and NOE cross-peaks, respectively, dominated these experiments. Therefore, the unambiguous assignment of spin-system containing protons *j-l* to a particular ligand environment was not possible and the spin system was arbitrarily labelled with black, red and blue labels according to decreasing chemical shift of proton *j* to represent the three different ligand environments. Steady-state NOE experiments, however, did allow assignment of the broad signals above and below −22 ppm as protons *a* and *m*, respectively (Figure S40). The complete proton assignment of complex **1a** was independently corroborated by T_1 relaxation measurements (Table S4) as well as exchange cross-peaks between the excess ligand present in the sample and the complex.

Having successfully assigned the ^{1}H NMR spectrum of **1a**, we investigated assignment of the ^{13}C NMR spectrum using paramagnetic analogues of heteronuclear 1D and 2D techniques (e.g. HSQC and HMBC). The proton-coupled ^{13}C spectrum contained signals over almost a 900 ppm range (Figure S41), making uniform excitation over this very wide spectral range difficult. Therefore, overlapping spectra of smaller spectral widths were acquired to cover the entire range. The quaternary carbons could be distinguished from the tertiary carbons on the basis of the multiplicity and initially, the tertiary carbons were assigned using selective ^{1}H-decoupling ^{13}C experiments where one after another, each proton signal was selectively irradiated during repeated acquisitions of the ^{13}C NMR data (Figures S42–S46). However, this method is time-consuming due to the number of signals and the sensitivity of ^{13}C NMR measurements and therefore, we instead chose to investigate 2D heteronuclear experiments.

We focused on the HMQC pulse program as an alternative to HSQC because of its simple four pulse sequence and pleasingly, cross-peaks were observed for the sharp ^{1}H signals (linewidth <70 Hz, Figures S47–S49). However, the acquisition of two HMQC spectra was necessary to cover the large spectral range in both dimensions as non-uniform excitation resulted in a decrease in the intensity or complete loss of cross-peaks at the extremes of the spectral range (Figure 4). Nevertheless, an overlay of the two HMQC spectra confirmed the assignments made using the selective ^{1}H-decoupling ^{13}C experiments (Figures S42–S46). HMBC spectra were also acquired in an attempt to assign the quaternary carbons and the three spin systems within a particular ligand environment; however, no cross-peaks were observed due to the long delays resulting from the small magnitude of ^3J coupling constants in contrast to the large ^1J coupling constants utilised in the HMQC experiments. Therefore, the quaternary carbons and carbon *a* were tentatively assigned through comparison to the reference complex $[Co(bpy)_3](BF_4)_2$ (Figures S97–S99).

Thus, we successfully assigned the ^{1}H and ^{13}C NMR spectra of complex *mer*-**1a** using a combination of 1D (^{1}H, proton-coupled ^{13}C, selective ^{1}H-decoupling ^{13}C, steady-state NOE) and 2D (COSY, NOESY, HMQC) NMR paramagnetic experiments. We then sought to test the limits of this paramagnetic NMR toolbox in complexes where proton coupling within a spin system is interrupted by substitution as well as complexes with broader linewidths. We prepared a series of 2-pyridylquinoline ligands substituted in the 5′- or 6-positions (Figure 1a) and their corresponding Co^{II} complexes **2a**–**7a** in situ by mixing $Co(BF_4)_2{\cdot}6H_2O$ and three equivalents of the ligand in CD_3CN.

These complexes fulfil both criteria, as revealed by their NMR spectra (Figures S93–S94, Table S5), and they also allowed investigation of the influence of substitution on the *fac/mer* isomerism. Based on comparison to the ^{1}H NMR spectrum of the parent complex **1a**, it appeared that the *mer* isomer also predominated for complexes **3a**–**7a** but additional species were also present (Figures S93–S94). In the case of the complex with pq-5′-Br, a set of broader signals consistent with only one ligand environment was also a significant species within the mixture (Figure S51).

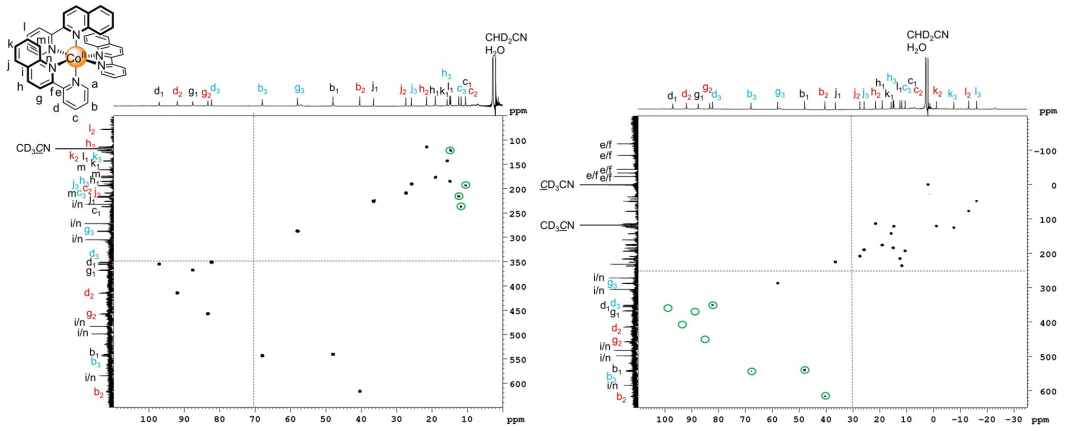

Figure 4. ^{1}H-^{13}C HMQC NMR spectra (600 MHz/151 MHz, CD_3CN, 298 K) of *mer*-$[Co(pq)_3](BF_4)_2$ (**1a**). Two spectra with differing offsets (represented by the dashed lines) were recorded since uniform excitation could not be achieved with standard square pulses over the large spectral range resulting in absent cross-peaks or cross-peaks with reduced intensities (green circles) at the extremes of the spectral range.

Initially, assignment of the proposed *mer* isomer in the ^{1}H and ^{13}C NMR spectra of complexes **2a**–**7a** was investigated. In comparison to the parent complex **1a**, the ^{1}H signals of complexes **2a**–**4a** with 5′-substituted ligands had the largest linewidths (> 90 Hz, Table S5) followed by complexes **5a**–**7a** containing 6-substituted ligands (< 130 Hz, Table S5). Nevertheless, cross-peaks were still observable in the 2D spectra (COSY, NOESY and HMQC) including exchange cross-peaks in the COSY spectra to varying degrees for complexes **3a**–**7a** (Figures S59, S66, S72, S79, S87). The ^{1}H assignments for these complexes confirmed that in each case the major species in solution is the *mer* isomer (Figures S93–S94). ^{1}H assignment of *mer*-**2a** was also possible despite the absence of many cross-peaks in the COSY spectrum since exchange cross-peaks were still observable in the NOESY spectrum. We attribute the incompleteness of cross-peaks in the COSY spectrum to the presence of broad linewidths (> 200 Hz, Table S5). Assignment of the ^{13}C NMR spectra of complexes **2a**–**7a** was not as straightforward as the ^{1}H spectra, most likely due to the lower sensitivity of ^{13}C NMR spectroscopy compared to ^{1}H NMR spectroscopy, the broadness of the signals and the presence of multiple species. Thus, in some cases only partial assignment was possible (Figures S62–S63, S68–S69, S74–S75, S81–S83, S89–S91).

A comparison of the ^{1}H assignments for *mer*-**2a**–**7a** to those of the parent complex *mer*-**1a** showed that the signals of the 2-pyridylquinoline backbone do not shift significantly upon substitution and as expected, the ^{1}H signals for the 5′- and 6-positions are not present in the spectra of complexes **2a**–**4a** and **5a**–**7a**, respectively, due to substitution (Figures S93–S94). The protons in these spin systems with substituents could be assigned by the exchange peaks in the NOESY spectra but not to a particular ligand environment, due to the disruption of proton coupling by substitution in the COSY spectrum and absence of suitable TOCSY and HMBC pulse programs for paramagnetic complexes.

We then investigated the assignment of the species other than the *mer* isomer in the spectra of **2a**–**7a**. A set of sharp signals consistent with only one ligand environment was visible in the spectra of complexes **3a** and **5a** (Figures S93–S94), and another set of broader signals, also consistent with only one ligand environment, was visible for all complexes with the exception of **6a** (Figures S93–S94). We propose these two species to be the *fac* isomer and a symmetric CoL_2-based species. While these species cannot be distinguished on the basis of the number of NMR signals, we attribute the set of broader signals to a symmetric CoL_2-based species; this set of broader signals was significant for the complex with pq-5′-Br yet decreased in intensity upon addition of a fourth equivalent of ligand while the *mer*-**2a** signals increased (Figure S51). Furthermore, in two samples of the complex with pq-6-Ph, the chemical shifts of the proposed symmetric CoL_2-based species were sensitive to the differing water content of the samples whereas those corresponding to *mer*-**7a** were not (Figure S86). We attribute the observation of a symmetric CoL_2-based species as well as *mer*-**2a** to the steric bulk of pq-5′-Br from not only the quinoline ring but also the bromine substituent since this could reduce the efficiency of π-π stacking interactions between two of the ligands. In contrast, the predominance of *mer*-**5a** based on the pq-6-Br ligand is likely due to the reduced steric influence of the bromine substituent in the 6-position compared with the 5′-position in complex **2a**.

Assignment of these species was more difficult than the *mer* isomer since cross-peaks for these species were not typically observable in the COSY spectra, most likely due to the broadness of the signals in the case of the CoL_2-based species and low concentration in the case of the *fac* isomer (estimated to constitute less than 1% of the complex mixture). However, NOESY appears to be less sensitive to signal broadness than COSY since exchange cross-peaks between the CoL_2-based species and the *mer* complex were still observed (Figures S54, S60, S67, S73). Furthermore, these

cross-peaks were even visible when the CoL_2-based species was not detectable in the ^{1}H NMR spectrum due to signal broadness and/or the low concentration of this species as seen in the spectrum of complex **6a** (Figures S78, S80).

To further investigate the applicability of the paramagnetic NMR toolbox we extended our studies to the characterisation of a high spin/spin-crossover Fe^{II} complex. Complex **1b** was prepared in a glovebox by mixing $Fe(OTf)_2$ and three equivalents of the pq ligand in dry CD_3CN. At room temperature the ^{1}H NMR spectra of the complex contained broad signals for the complex and therefore, detailed analysis was not possible. We attributed the broad signals to fast ligand exchange processes and therefore, variable temperature experiments were carried at lower temperatures where ligand exchange would be slower.

Upon cooling the solutions from 298 K to 248 K, the signals sharpened and displayed Curie–Weiss behaviour (Figure S106–S109).[17] There was no evidence of spin-crossover over this temperature range, consistent with previous studies on the tetrafluoroborate salt of complex **1b** in acetone.[14b] At 248 K almost complete assignment of the ^{1}H and ^{13}C NMR spectra was possible for *mer*-**1b** since the signals were relatively sharp and cross-peaks were observable in the COSY, NOESY and HMQC spectra (Figures S101–S105). However, the carbon signals for *d* and *g* could not be assigned on the basis of the HMQC spectrum since the cross-peaks were absent or very weak, attributed to the increased influence of the paramagnetic Fe^{II} ion on the relaxation times at lower temperature. In addition, at least one other species was present at equilibrium as broader signals were also seen in the ^{1}H NMR spectrum but they could not be assigned in the absence of cross-peaks in the 2D NMR spectra.

Given the large change in the linewidth of the ^{1}H NMR signals between 248 K and 298 K (Table S7), we carried out temperature-dependent COSY, NOESY and HMQC experiments to investigate whether cross-peaks were also observable at higher temperatures (Figures S110–112). HMQC and COSY appeared to be more sensitive to temperature than NOESY since by 266 K most cross-peaks were no longer observable (Figures S110, S112). Nevertheless, assignment of the ^{1}H signals was still possible exploiting the exchange cross-peaks in the NOESY spectra (Figure S111) and the assignments from lower temperatures to assign coupled protons within a single spin system when COSY cross-peaks were not observable at that temperature (Figures S110).

Finally, we applied the paramagnetic NMR toolbox to the characterisation of paramagnetic metal-organic cages. The rational design of lower symmetry metal-organic cages is challenging and therefore, we prepared and characterised instead the highly symmetric tetrahedral $Co^{II}{}_4L_6$ cage **8** as proof-of-principle for paramagnetic cage characterisation (Figures S113–S117). A solution of four equivalents of $Co(NTf_2)_2$ and six equivalents of ligand was heated at 50 °C in acetonitrile and the cage was isolated by precipitation with diethyl ether.

The ^{1}H NMR spectrum of the redissolved cage in CD_3CN contained 5 sharp and 2 broad signals, reflecting the presence of one ligand environment due to *fac* coordination around the metal centres. Only the expected through-bond cross-peaks were observed in the COSY spectrum (Figure S114). Full and unambiguous assignment of the ^{1}H and ^{13}C NMR spectra was possible using the paramagnetic NMR toolbox, with the exception of the quaternary carbons and the broad signals corresponding to *a* and *j* (Figures S113, S115).

Following the characterisation of mononuclear complexes **1a**–**7a**, **1b** and cage **8**, we propose a workflow including troubleshooting experiments for the application of the paramagnetic NMR toolbox to the structural characterisation of other paramagnetic complexes and cages (Figure 5). A more detailed instruction manual for each toolbox experiment is provided in the SI (Section 1.1.1). The workflow begins with the acquisition of a ^{1}H NMR spectrum to establish the spectral width as well as the linewidths of the signals since large spectral widths often necessitate the acquisition of several 2D spectra with smaller spectral widths and the observation of cross-peaks in 2D spectra is, in many cases, dependent on the linewidth. With broad linewidths (typically >100 Hz), variation and optimisation of the temperature is recommended in an attempt to reduce the linewidths and increase the likelihood of cross-peak observation in 2D experiments.

COSY is recommended as the second toolbox experiment to identify coupled protons within each spin system. However, additional relaxation-allowed exchange and NOE cross-peaks may be observable complicating assignment and therefore, either NOESY (toolbox experiment 3a) or steady-state NOE (toolbox experiment 3b) experiments are recommended to complete the ^{1}H NMR spectrum assignment. These two experiments provide similar structural information but NOESY has the advantage that the exchange and NOE cross-peaks can be observed in a single 2D spectrum compared with multiple 1D spectra for steady-state NOE experiments. For

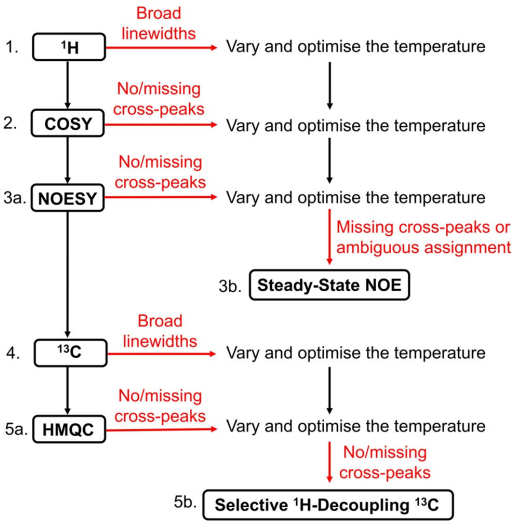

Figure 5. Proposed workflow including troubleshooting experiments (red arrows) for the application of the paramagnetic NMR toolbox to the structural characterisation of paramagnetic complexes and cages.

this reason, steady-state NOE experiments may only be necessary in the case of troubleshooting (Sections 1.1.1.3 and 1.1.1.4).

The assignment of the ^{13}C NMR spectrum has a similar workflow beginning with acquisition of the ^{13}C NMR spectrum (toolbox experiment 4) followed by HMQC (toolbox experiment 5a) and/or selective ^{1}H-decoupling ^{13}C experiments (toolbox experiment 5b) to identify the $^{1}J_{CH}$ coupling. Again, the 2D HMQC experiment is preferable to a series of selective ^{1}H-decoupling ^{13}C experiments but these 1D experiments may be useful in troubleshooting (Sections 1.1.1.6 and 1.1.1.7).

Conclusion

We report a toolbox of 1D (^{1}H, proton-coupled ^{13}C, selective ^{1}H-decoupling ^{13}C, steady-state NOE) and 2D (COSY, NOESY, HMQC) paramagnetic NMR methods that enables the straightforward characterisation of paramagnetic complexes. This toolbox overcomes the data acquisition challenges due to the presence of paramagnetic centres, such as large paramagnetic shifts and short relaxation times, and also removes the reliance of data interpretation on theoretical models[6b,9b,11] or the Solomon equation.[4b,10b,d] We demonstrated the general applicability of this toolbox for fields from coordination chemistry to spin-crossover complexes and supramolecular chemistry through the characterisation of Co^{II} and high-spin Fe^{II} mononuclear complexes as well as a Co_4L_6 cage. Furthermore, we demonstrated the toolbox can be successfully applied to structural characterisation in a variety of situations: the assignment of complexes with multiple ligand environments (e.g. *mer* complexes), complexes with a range of signal linewidths (including broad signals in the case of the CoL_2-based species) and mixtures of complexes (e.g. *mer*- and *fac*-CoL_3 isomers as well as CoL_2-based species).

This study also shows the advantages of paramagnetic versus diamagnetic NMR spectroscopy; the short relaxation times of paramagnetic complexes enable reduction of the repetition delays and acquisition times, thereby significantly reducing the experiment times or enabling the acquisition of more data in a similar time (Table S1). In addition to reduced signal overlap and increased sensitivity, structural information can be observed by paramagnetic NMR spectroscopy that would not be observable in the diamagnetic analogue; in the COSY spectra of the Co^{II} *mer* mononuclear complexes, relaxation-allowed through-space (NOE) cross-correlation peaks and exchange (EXSY) cross-peaks were observed in addition to the expected through-bond (COSY) cross-peaks. Furthermore, the sensitivity of the exchange NOESY technique enabled the identification of additional species present at equilibrium that were not visible in the ^{1}H NMR spectra due to broad linewidths and/or their low concentration.

While solution characterisation of paramagnetic complexes and cages was previously typically limited to a ^{1}H NMR spectrum only, we demonstrate that in-depth structural analysis comparable to that for diamagnetic compounds is now possible using the paramagnetic NMR toolbox. We are now extending the use of this toolbox to the characterisation of more complex as well as mixtures of supramolecular architectures.

Acknowledgements

We thank the Deutsche Forschungsgemeinschaft (DFG, project number 413396832 (M.L.), project number 429518153 (T.P.) and CRC677) for financial support and we also thank Prof. Dr Thisbe K. Lindhorst and Prof. Dr Rainer Herges for bridging financial support for M.L. We thank the spectroscopy department and Dr Claus Bier for NMR and mass spectral data collection. We thank Jan-Christian Carstensen, Felix Piontek, André Petersen and Tjorge Neumann for preliminary studies on the complexes and the synthesis of ligand precursors. Open access funding enabled and organized by Projekt DEAL.

Conflict of interest

The authors declare no conflict of interest.

Keywords: metal–organic cage · NMR spectroscopy · paramagnetic complex · spin-crossover · supramolecular chemistry

[1] a) G. Wang, Z.-T. Zhang, B. Jiang, X. Zhang, C. Li, M. Liu, *Anal. Bioanal. Chem.* **2014**, *406*, 2279 – 2288; b) W.-M. Liu, M. Overhand, M. Ubbink, *Coord. Chem. Rev.* **2014**, *273 – 274*, 2 – 12; c) X.-C. Su, J.-L. Chen, *Acc. Chem. Res.* **2019**, *52*, 1675 – 1686.

[2] a) A. Pastor, E. Martínez-Viviente, *Coord. Chem. Rev.* **2008**, *252*, 2314 – 2345; b) L. Avram, A. D. Wishard, B. C. Gibb, A. Bar-Shir, *Angew. Chem. Int. Ed.* **2017**, *56*, 15314 – 15318; *Angew. Chem.* **2017**, *129*, 15516 – 15520; c) L. Avram, M. A. Iron, A. Bar-Shir, *Chem. Sci.* **2016**, *7*, 6905 – 6909; d) Y. Cohen, S. Slovak, *Org. Chem. Front.* **2019**, *6*, 1705 – 1718.

[3] a) M. Dumartin, M. C. Lipke, J. F. Stoddart, *J. Am. Chem. Soc.* **2019**, *141*, 18308 – 18317; b) H. Li, H. Zhang, A. D. Lammer, M. Wang, X. Li, V. M. Lynch, J. L. Sessler, *Nat. Chem.* **2015**, *7*, 1003 – 1008; c) T. Bunchuay, A. Docker, A. J. Martinez-Martinez, P. D. Beer, *Angew. Chem. Int. Ed.* **2019**, *58*, 13823 – 13827; *Angew. Chem.* **2019**, *131*, 13961 – 13965; d) N. Pairault, H. Zhu, D. Jansen, A. Huber, C. G. Daniliuc, S. Grimme, J. Niemeyer, *Angew. Chem. Int. Ed.* **2020**, *59*, 5102 – 5107; *Angew. Chem.* **2020**, *132*, 5140 – 5145; e) Y. Xu, R. Kaur, B. Wang, M. B. Minameyer, S. Gsänger, B. Meyer, T. Drewello, D. M. Guldi, M. von Delius, *J. Am. Chem. Soc.* **2018**, *140*, 13413 – 13420.

[4] a) M. Hardy, N. Struch, J. J. Holstein, G. Schnakenburg, N. Wagner, M. Engeser, J. Beck, G. H. Clever, A. Lützen, *Angew. Chem. Int. Ed.* **2020**, *59*, 3195 – 3200; *Angew. Chem.* **2020**, *132*, 3221 – 3226; b) A. J. McConnell, C. M. Aitchison, A. B. Grommet, J. R. Nitschke, *J. Am. Chem. Soc.* **2017**, *139*, 6294 – 6297; c) R. A. S. Vasdev, J. A. Findlay, A. L. Garden, J. D. Crowley, *Chem. Commun.* **2019**, *55*, 7506 – 7509; d) A. J. Metherell, W. Cullen, N. H. Williams, M. D. Ward, *Chem. Eur. J.* **2018**, *24*, 1554 – 1560; e) S. M. Jansze, K. Severin, *J. Am. Chem. Soc.* **2019**, *141*, 815 – 819.

[5] a) J. Zhong, L. Zhang, D. P. August, G. F. S. Whitehead, D. A. Leigh, *J. Am. Chem. Soc.* **2019**, *141*, 14249 – 14256; b) Y. Inomata, T. Sawada, M. Fujita, *Chem* **2020**, *6*, 294 – 303; c) H.-

N. Zhang, W.-X. Gao, Y.-J. Lin, G.-X. Jin, *J. Am. Chem. Soc.* **2019**, *141*, 16057 – 16063.
[6] a) C. L. I. Bertini, *Coord. Chem. Rev.* **1996**, *150*, 1 – 28; b) A. J. Pell, G. Pintacuda, C. P. Grey, *Prog. Nucl. Magn. Reson. Spectrosc.* **2019**, *111*, 1 – 271; c) C. L. I. Bertini, *Coord. Chem. Rev.* **1996**, *150*, 185 – 220; d) C. L. I. Bertini, *Coord. Chem. Rev.* **1996**, *150*, 163 – 184; e) M. P. Crockett, H. Zhang, C. M. Thomas, J. A. Byers, *Chem. Commun.* **2019**, *55*, 14426 – 14429.
[7] a) B.-B. Pan, F. Yang, Y. Ye, Q. Wu, C. Li, T. Huber, X.-C. Su, *Chem. Commun.* **2016**, *52*, 10237 – 10240; b) A. Bahramzadeh, T. Huber, G. Otting, *Biochemistry* **2019**, *58*, 3243 – 3250.
[8] a) R. W. Hogue, C. P. Lepper, G. B. Jameson, S. Brooker, *Chem. Commun.* **2018**, *54*, 172 – 175; b) S. Rodríguez-Jiménez, M. Yang, I. Stewart, A. L. Garden, S. Brooker, *J. Am. Chem. Soc.* **2017**, *139*, 18392 – 18396; c) D. F. Evans, *J. Chem. Soc.* **1959**, 2003 – 2005; d) A. Ferguson, M. A. Squire, D. Siretanu, D. Mitcov, C. Mathoniere, R. Clerac, P. E. Kruger, *Chem. Commun.* **2013**, *49*, 1597 – 1599; e) R. A. Bilbeisi, S. Zarra, H. L. C. Feltham, G. N. L. Jameson, J. K. Clegg, S. Brooker, J. R. Nitschke, *Chem. Eur. J.* **2013**, *19*, 8058 – 8062; f) A. J. McConnell, *Supramol. Chem.* **2018**, *30*, 858 – 868; g) A. A. Pavlov, G. L. Denisov, M. A. Kiskin, Y. V. Nelyubina, V. V. Novikov, *Inorg. Chem.* **2017**, *56*, 14759 – 14762.
[9] a) H. S. Chow, E. C. Constable, C. E. Housecroft, K. J. Kulicke, Y. Tao, *Dalton Trans.* **2005**, 236 – 237; b) M. Kruck, D. C. Sauer, M. Enders, H. Wadepohl, L. H. Gade, *Dalton Trans.* **2011**, *40*, 10406 – 10415.
[10] a) C. Piguet, G. Bernardinelli, B. Bocquet, A. Quattropani, A. F. Williams, *J. Am. Chem. Soc.* **1992**, *114*, 7440 – 7451; b) H. Amouri, L. Mimassi, M. N. Rager, B. E. Mann, C. Guyard-Duhayon, L. Raehm, *Angew. Chem. Int. Ed.* **2005**, *44*, 4543 – 4546; *Angew. Chem.* **2005**, *117*, 4619 – 4622; c) S. Turega, M. Whitehead, B. R. Hall, A. J. H. M. Meijer, C. A. Hunter, M. D. Ward, *Inorg. Chem.* **2013**, *52*, 1122 – 1132; d) I. S. Tidmarsh, B. F. Taylor, M. J. Hardie, L. Russo, W. Clegg, M. D. Ward, *New J. Chem.* **2009**, *33*, 366 – 375; e) M. J. Burke, G. S. Nichol, P. J. Lusby, *J. Am. Chem. Soc.* **2016**, *138*, 9308 – 9315.
[11] a) W. C. Isley III, S. Zarra, R. K. Carlson, R. A. Bilbeisi, T. K. Ronson, J. R. Nitschke, L. Gagliardi, C. J. Cramer, *Phys. Chem. Chem. Phys.* **2014**, *16*, 10620 – 10628; b) T. L. J. Huang, D. G. Brewer, *Can. J. Chem.* **1981**, *59*, 1689 – 1700; c) M. L. Wicholas, R. S. Drago, *J. Am. Chem. Soc.* **1968**, *90*, 6946 – 6950.
[12] a) S. Cai, C. Seu, Z. Kovacs, A. D. Sherry, Y. Chen, *J. Am. Chem. Soc.* **2006**, *128*, 13474 – 13478; b) F. A. A. Mulder, L. Tenori, C. Luchinat, *Angew. Chem. Int. Ed.* **2019**, *58*, 15283 – 15286; *Angew. Chem.* **2019**, *131*, 15427 – 15430.
[13] S. Denis-Quanquin, F. Riobé, M.-A. Delsuc, O. Maury, N. Giraud, *Chem. Eur. J.* **2016**, *22*, 18123 – 18131.
[14] a) I. S. Jahro, D. Onggo, Ismunandar, S. I. Rahayu, M. C. Muñoz, A. B. Gaspar, M. Seredyuk, P. Gütlich, J. A. Real, *Inorg. Chim. Acta* **2008**, *361*, 4047 – 4054; b) D. Onggo, J. M. Hook, A. D. Rae, H. A. Goodwin, *Inorg. Chim. Acta* **1990**, *173*, 19 – 30; c) C. Harris, S. Kokot, H. Patil, E. Sinn, H. Wong, *Aust. J. Chem.* **1972**, *25*, 1631 – 1643.
[15] R. Wang, H. Fan, W. Zhao, F. Li, *Org. Lett.* **2016**, *18*, 3558 – 3561.
[16] a) I. Bertini, C. Luchinat, D. Tarchi, *Chem. Phys. Lett.* **1993**, *203*, 445 – 449; b) I. Bertini, M. Piccioli, D. Tarchi, C. Luchinat, *Concepts Magn. Reson.* **1994**, *6*, 307 – 335; c) S. Wimperis, G. Bodenhausen, *Mol. Phys.* **1989**, *66*, 897 – 919; d) S. Wimperis, G. Bodenhausen, *Chem. Phys. Lett.* **1987**, *140*, 41 – 45.
[17] C. P. Landee, M. M. Turnbull, *J. Coord. Chem.* **2014**, *67*, 375 – 439.
[18] Deposition number 1987819 contains the supplementary crystallographic data for this paper. These data are provided free of charge by the joint Cambridge Crystallographic Data Centre and Fachinformationszentrum Karlsruhe Access Structures service.
[19] It is likely that the cross-peaks attributed to through-bond correlations also have a contribution from through-space coupling due to cross-correlation (see ref. [16]).

Manuscript received: June 15, 2020
Accepted manuscript online: July 20, 2020
Version of record online: August 26, 2020

3.1.2 Article: Copper-Free One-Pot Sonogashira-Type Coupling for the Efficient Preparation of Symmetric Diarylalkyne Ligands for Metal-Organic Cages

Marc Lehr[‡], Tobias Paschelke,[‡] Victoria Bendt, André Petersen, Lorenz Pietsch, Patrick Harders, Anna J. McConnell

Eur. J. Org. Chem. **2021**, 2728-2735.

doi.org/10.1002/ejoc.202100275

[‡] = The authors contributed equally

Optimised Sonogashira cross-coupling reaction conditions were developed for the synthesis of linear diarylalkyne ligands with 2,2'-bipyridine or 2-(2'-pyridyl)-1*H*-benzimidazole binding motifs. Compound **5a**, prepared within one synthetic step, and trimethylsilylacetylene were chosen as the precursors to screen different Sonogashira reaction conditions to synthesise the model system ligand **1a**.
In previous studies,[231,232] ligand **1a** was prepared over multiple steps and in this study a method was developed combining these steps in one-pot. Based on TBAF-mediated Sonogashira cross-coupling reactions by Liang *et al.*[233] and Mori *et al.*,[234] initial reaction conditions were adapted for the one-pot method that relied on TBAF as an amine and copper catalyst substitute. Over the course of this one-pot method development, multiple reaction parameters such as the reaction vessel, stoichiometric amounts, reaction temperatures and times, and Pd-based catalysts were screened to yield ligand **1a** in 62% over three steps in optimised reaction conditions (N_2 atmosphere, 1 eq. TMSA, 6 eq. degassed TBAF, 5 mol% $Pd(PPh_3)_4$, 70 °C, 3 h, pressure tube). The scalability of the optimised one-pot method was demonstrated by synthesising ligand **1a** in 60% yield on a tenfold higher scale. The versatility of this one-pot method was further shown by application of the reaction conditions to two other 2,2'-bipyridine-based and two 2-(2'-pyridyl)-1*H*-benzimidazole-based precursors yielding the ligands **1b**, **1c**, **6b** and **6c** in yields up to 92%. Finally, Co^{II}-based metal-organic cages were self-assembled from the synthesised ligands and characterised using the paramagnetic NMR toolbox.[231,232]

Contribution: Synthesis of compounds **1b**, **2b**, **2c**, **3b** (re-made from own Master Thesis),[230] **4a**, **4b**, **6a**, **6b** and **6c**; synthesis development for compound **5d**; optimisation of reaction conditions (Table 1, entries 4 & 5 | Table 2, entries 1-4 | Table 3, entries 1-3); editing and proofreading of the manuscript; preparation and proofreading of the supporting information

EurJOC
European Journal of Organic Chemistry

Full Papers
doi.org/10.1002/ejoc.202100275

Chemistry Europe
European Chemical Societies Publishing

Copper-Free One-Pot Sonogashira-Type Coupling for the Efficient Preparation of Symmetric Diarylalkyne Ligands for Metal-Organic Cages**

Marc Lehr[+],[a] Tobias Paschelke[+],[a] Victoria Bendt,[a] André Petersen,[a] Lorenz Pietsch,[a] Patrick Harders,[a] and Anna J. McConnell*[a]

The often time-consuming and challenging multi-step synthesis of ligands for metal-organic cages is a limiting factor for the discovery and application of new cages. We report a highly efficient copper-free one-pot Sonogashira-type coupling for the preparation of symmetric diarylalkyne ligands on both a small and large scale; bipyridine- and benzimidazole-based ligands for the self-assembly of Co_4L_6 cages were synthesized in short reaction times and high isolated yields directly from aryl halide precursors. This one-pot method reduces the synthetic burden of ligand synthesis and will facilitate the preparation of ligands with additional functionality for applications of their corresponding cages.

Introduction

Palladium-catalyzed cross-coupling reactions are powerful synthetic methods for carbon–carbon bond formation in modern organic chemistry.[1] In particular, Sonogashira cross-coupling reactions[2] have been used extensively for the synthesis of diarylalkynes in natural products,[3] conjugated oligomers/polymers in materials science[4] and ligands/building blocks[5] in coordination chemistry and supramolecular chemistry due to their typically high yields and tolerance of a wide range of functional groups.

Symmetric diarylalkynes find application in diverse fields since they are precursors in the synthesis of hexaarylbenzene derivatives,[6] building blocks for light-emitting materials,[7] and inorganic heterocycles[8] as well as building blocks in supramolecular architectures.[5b,c,f] However, their preparation is typically a multi-step synthesis (black route, Scheme 1), often involving long reaction times and multiple purification steps, resulting in overall lower yields and making scale-up for applications difficult.[7] Glaser coupling[9] can also take place in the presence of the copper co-catalyst with traces of oxygen, leading to side-product formation[2a,10] and difficult purifications.

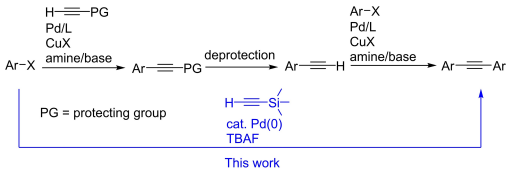

Scheme 1. Multi-step synthesis of diarylacetylenes via sequential Sonogashira cross-coupling reactions (black) and the copper-free one-pot Sonogashira method (blue) in this work.

As a result, one-pot cross-coupling methods using a variety of acetylene sources (e.g. gaseous acetylene,[11] calcium carbide,[12] propiolic acid[13] and silyl-protected alkynes[14]) as well as copper-free Sonogashira-type couplings[12–13,14b,15] (*e.g.* replacing the copper co-catalyst and amine with tetrabutylammonium fluoride (TBAF)[15a,b]) have been developed to overcome these problems, respectively.

Ligand synthesis is a bottleneck for the self-assembly and application of metal-organic cages[5g–m] due to multi-step syntheses and challenging purifications. Diarylalkyne-based ligands are appealing given their potential synthesis via a one-pot procedure and further functionalisation via the alkyne functionality, *e.g.* through post-assembly modification.[5c] However, most one-pot Sonogashira couplings have been reported for symmetric carbocyclic rather than heterocyclic diarylalkynes with limited examples including those based on thiophene[11–12,14b,c] and pyridine[12,14] derivatives.

We report the efficient synthesis of symmetric diarylalkyne ligands **1a–c** and **2b–c** for metal-organic cages **3a–c** and **4a–b** (Figure 1) via a copper-free one-pot procedure using trimethylsilylacetylene as the acetylene source and TBAF functioning as a base, activator, and deprotection reagent (blue route, Scheme 1). In addition to significantly reducing the synthetic burden from a 3 step synthesis with a long overall reaction time to a single 3-hour step, the ligands were prepared in high

[a] *M. Lehr,[+] T. Paschelke,[+] V. Bendt, A. Petersen, L. Pietsch, P. Harders, Prof. Dr. A. J. McConnell*
Otto Diels Institute of Organic Chemistry
Christian-Albrechts-Universität zu Kiel
Otto-Hahn-Platz 4, Kiel 24098, Germany
E-mail: amcconnell@oc.uni-kiel.de
https://www.otto-diels-institut.de/mcconnell

[+] *These authors contributed equally*

[**] *A previous version of this manuscript has been deposited on a preprint server (DOI: doi.org/10.26434/chemrxiv.13625783.v1)*

Supporting information for this article is available on the WWW under https://doi.org/10.1002/ejoc.202100275

Full Papers
doi.org/10.1002/ejoc.202100275

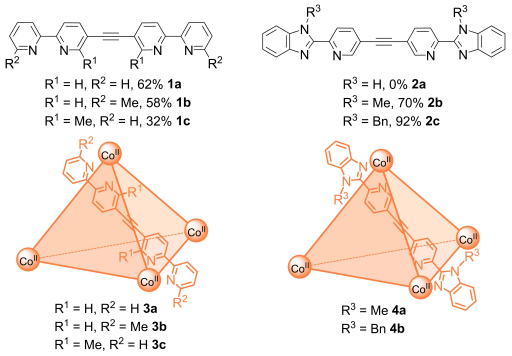

Figure 1. Symmetric heterocyclic diarylalkyne ligands synthesized using the copper-free one-pot Sonogashira-type coupling and their respective Co_4L_6 metal-organic cages.

isolated yields (32–92%) for a one-pot procedure. The proof-of-principle for large-scale ligand synthesis was also demonstrated. Thus, this method enables rapid access to ligands for metal-organic cages from suitable aryl halide building blocks and this will facilitate the discovery of new cages as well as the translation of cages to applications.

Results and Discussion

We recently reported that the synthesis of ligand **1a**[16] could be reduced from three to two steps using TBAF for the *in situ* deprotection of the TMS-protected alkyne (first step in black route, Scheme 2).[5f] However, the Glaser by-product was also obtained in the final Sonogashira coupling using copper(I) iodide in some instances. Mori[15a] and Li[15b] reported copper- and amine-free Sonogashira couplings between terminal alkynes and aryl halides, including aryl chlorides, with short reaction times and good to excellent yields using TBAF as an activator. It is proposed that the TBAF activates and stabilizes the Pd(0) species, deprotonates the alkyne, and acts as a phase-transfer catalyst.[15b] Therefore, we envisaged TBAF could play the role of not only a deprotection reagent but also an activator and base in a one-pot procedure while preventing the formation of Glaser by-products.

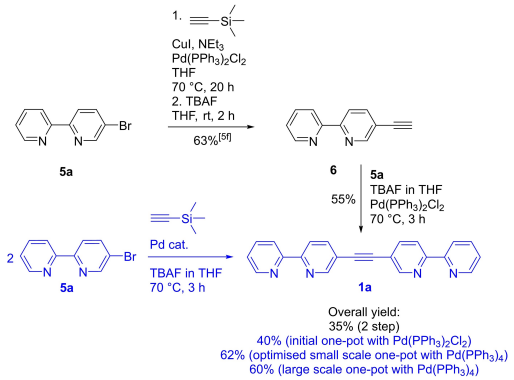

Scheme 2. Development of the copper-free one-pot synthesis of ligand **1a** from **5a**: proof-of-principle for the use of TBAF as a deprotection reagent and activator in a 2 step synthesis (black route); yield and reaction time improvements through a one-pot approach and reaction optimization (blue route).

Firstly, we investigated the applicability of the Sonogashira-type coupling using TBAF to heterocyclic diarylalkynes by reacting **5a** with **6**[5f] (second step in black route, Scheme 2). The previously reported Sonogashira coupling[5f] reaction conditions for **1a** were initially adapted replacing the copper(I) iodide and amine with a commercially available TBAF solution in THF. Since this would function as both a reagent and solvent, an excess of TBAF was used compared to the previously reported methods of Mori[15a] and Li[15b] to ensure both sufficient TBAF was present for its multiple roles in the reaction and a suitable reaction volume. Ligand **1a** was obtained with full conversion of **5a** within a shorter reaction time of 3 hours in 55% isolated yield following column chromatography. Taking into account the 63% yield for the synthesis of **6**,[5f] the overall yield of ligand **1a** from **5a** via the two sequential cross-couplings is 35% (Scheme 2).

Having demonstrated that TBAF functions in both the deprotection and Sonogashira-type steps (black route, Scheme 2), the one-pot synthesis of ligand **1a** was carried out under analogous conditions, using 1 eq. of **5a** and 0.5 eq. of TMSA (blue route, Scheme 2). Ligand **1a** was isolated in 40% yield and 12% of the starting material **5a** was also recovered (Table 1, entry 1). This with the observation of intense gas release upon addition of TBAF suggested immediate deprotection of TMSA's silyl protecting group, resulting in the release of gaseous acetylene. While no starting material was recovered upon increasing the TMSA to 1 eq., a similar yield was obtained (Table 1, entry 2).

The reaction vessel was then changed to a pressure tube to investigate if acetylene loss over the course of the reaction was significant. While the yield did not improve with a stoichiometric amount of TMSA (Table 1, entry 3), the yield could be improved to 53% by using an excess of TMSA (Table 1, entry 4). In entries 1–4 the reactions were carried out under a nitrogen

Table 1. Initial one-pot Sonogashira-type experiments for the preparation of **1a** from **5a**.[a]

Entry	TMSA (eq.)	Reaction Vessel	Yield[c] [%]
1	0.5	RBF	40
2	1	RBF	35
3	0.5	PT	40
4	1	PT	53
5[b]	1	PT	54

[a] Reaction conditions: 1 eq. **5a** (723 µmol), 5 mol% $Pd(PPh_3)_2Cl_2$, 6 eq. 1 M TBAF in THF (not degassed), N_2 atmosphere. RBF = round bottom flask, PT = pressure tube. [b] Degassed 1 M TBAF in THF. [c] Isolated yield after column chromatography.

atmosphere without degassing the TBAF solution in THF before addition to the reagents. Degassing of the TBAF solution by bubbling nitrogen was unnecessary as a similar yield was obtained when this additional step was performed (Table 1, entry 5).

In an effort to optimize the yield further, various palladium catalysts were screened (Table 2). Compared to $Pd(PPh_3)_2Cl_2$ (Table 2, entry 1), the catalysts $Pd(OAc)_2$ (Table 2, entry 2) and $Pd(dppf)Cl_2$ (Table 2, entry 3) gave lower yields. However, the reaction with $Pd(PPh_3)_4$ (Table 2, entry 4) gave the product in an improved yield of 62%. As a precaution, the TBAF solution for this reaction was degassed due to the oxygen sensitivity of the catalyst.[17]

Further experiments were carried out to investigate if the reaction parameters (time, temperature, catalytic loading, aryl halide reactivity) can be reduced without significantly impacting the yield (Table 3). With a 1 hour instead of a 3 hour reaction time, ligand **1a** was still isolated in good yield and no starting material was recovered (Table 3, entry 2). However, reducing the reaction time further to 30 min led to a significant decrease in the yield, and 40% of the starting material was recovered (Table 3, entry 3). Heating the reaction was necessary since the coupling did not take place at room temperature and 98% of the starting material was recovered, even with a longer reaction time of 20 hours (Table 3, entry 4). Although a ten-fold lower catalytic loading of 0.5 mol% still gave **1a** in 32% yield, the reaction was not complete within 3 hours since 41% of the starting material was recovered (Table 3, entry 5). Given the short reaction time with aryl bromide **1a**, the one-pot procedure was also extended to the less reactive aryl chloride **5d** (SI, Section S2.1.2) but no product was obtained (Scheme S2).

Table 2. Catalyst screening of one-pot Sonogashira-type experiments for the preparation of **1a** from **5a**.[a]

Entry	Pd catalyst	Temp. [°C]	Time [h]	Yield[c] [%]
1	$Pd(PPh_3)_2Cl_2$	70	3	53
2	$Pd(OAc)_2$	70	3	13
3	$Pd(dppf)Cl_2$	70	3	40
4[b]	$Pd(PPh_3)_4$	70	3	62

[a] Reaction conditions: 1 eq. **5a** (723 μmol), 1 eq. TMSA, 5 mol% Pd catalyst, 6 eq. non-degassed 1 M TBAF in THF, pressure tube, N_2 atmosphere. [b] Degassed 1 M TBAF in THF. [c] Isolated yield after column chromatography.

Table 3. Catalyst loading, temperature and reaction time screening of one-pot Sonogashira-type experiments for the preparation of **1a** from **5a**.[a]

Entry	Pd cat. [mol%]	Temp. [°C]	Time [h]	Yield[b] [%]
1	5	70	3	62
2	5	70	1	50
3	5	70	0.5	23 (40)[c]
4	5	rt	20	0 (98)[c]
5	0.5	70	3	32 (41)[c]

[a] Reaction conditions: 1 eq. **5a** (723 μmol), $Pd(PPh_3)_4$, 1 eq. TMSA, 6 eq. degassed 1 M TBAF in THF, pressure tube, N_2 atmosphere. [b] Isolated yield after column chromatography. [c] Recovered **5a**.

Through the development and optimization of the copper-free one-pot procedure, ligand **1a** can now be prepared both more efficiently and without the formation of Glaser by-products. Li and co-authors proposed a mechanism for TBAF promoted cross-couplings[15b] and we propose a similar mechanism for the one-pot procedure. Compared to the previous 3 step synthesis of ligand **1a** with a total reaction time over 40 hours,[16a,b,18] this one-pot procedure gives the ligand after a significantly reduced overall reaction time of 3 hours. Although a shorter reaction time is possible, 3 hours was chosen for subsequent experiments to ensure full consumption of the starting material.

Furthermore, the overall isolated ligand yield has been significantly improved from 35% for the shortened 2 step synthesis (black route, Scheme 2) and 40% yield in initial one-pot experiments to 62% yield following optimization (blue route, Scheme 2). Although no starting material was observed in the ^{1}H NMR spectra of crude reaction mixtures, the yield of each step in the one-pot procedure is not quantitative and product losses are also attributed to purification steps. The optimized yield of 62% corresponds to an average yield of 85% for each of the 3 steps (Scheme 1). Finally, the scalability of the procedure was investigated by increasing the reaction scale ten-fold to 1.7 g of **1a**. A similar isolated yield of 60% was obtained following a chromatography-free purification (Scheme 2).

Having optimized the one-pot conditions for the synthesis of **1a**, we extended the reaction scope to the related ligands **1b, 1c**, and **2a** based on 6-methyl-2,2′-bipyridine and benzimidazole coordination motifs, respectively (Figure 1). Ligand **1b** was synthesized in a comparable yield to **1a** (Table 4, entry 1), whereas **1c** was obtained in a lower yield even with a longer reaction time of 24 h (Table 4, entry 2), attributed to a steric clash of the methyl substituent in close proximity to the cross-coupling site (Scheme 3).

The synthesis of NH-benzimidazole **2a** was attempted using the same conditions (Scheme 4), however, only starting material was recovered (Table 4, entry 3). We proposed deprotonation of the imidazole under the basic conditions prevented the coupling taking place and therefore, the NH was substituted with a methyl (**6b**) or benzyl (**6c**) group (Scheme 4). Indeed, ligands **2b** (Table 4, entry 4) and **2c** (Table 4, entry 5) were isolated in good to excellent yields.[19] Finally, ligands **1b,c** and

Table 4. One-pot Sonogashira-type experiments for the preparation of **1b,c** and **2a–c** from the respective Ar–Br derivatives.[a]

Entry	Ar–Br	Ligand	Time [h]	Yield [%]
1	**5b**	**1b**	3	58[b]
2	**5c**	**1c**	24	32[b]
3	**6a**	**2a**	3	–
4	**6b**	**2b**	3	92[c]
5	**6c**	**2c**	3	70[c]

[a] Reaction conditions: 1 eq. Ar–Br (723 μmol), 5 mol% $Pd(PPh_3)_4$, 1 eq. TMSA, 6 eq. degassed 1 M TBAF in THF, 70 °C, pressure tube, N_2 atmosphere. [b] Isolated yield after column chromatography. [c] Product precipitated from the reaction mixture.

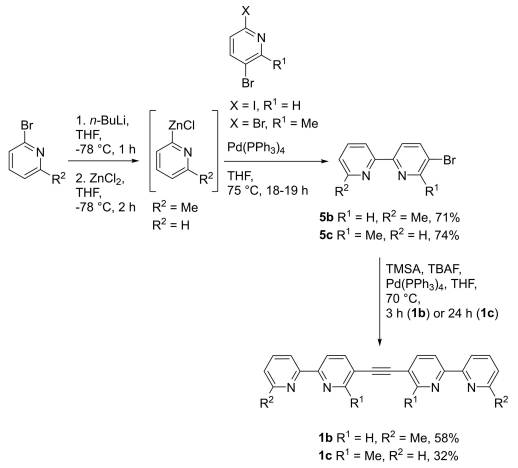

Scheme 3. Synthesis of 6-methyl-2,2′-bipyridine-based ligands **1 b** and **1 c** via the copper-free one-pot procedure.

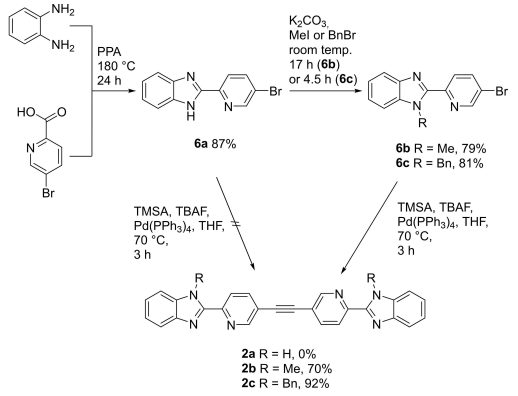

Scheme 4. Synthesis of benzimidazole-based ligands **2 b** and **2 c** via the copper-free one-pot procedure.

2 b,c synthesised from the one-pot procedure were used for the self-assembly of Co_4L_6 cages **3 b,c** and **4 a,b** (Figures S55–81).

Conclusion

In summary, we have reported a copper-free one-pot Sonogashira-type procedure for the preparation of symmetric heterocyclic diarylalkynes. We have applied this method to the synthesis of ligands **1 a–c** and **2 b–c**, which can be used to self-assemble a series of novel metal-organic cages **3 b–c** and **4 a–b**. This procedure has the following advantages: reduction of a 3 step synthesis to 1 step; good to excellent isolated yields (32–92%) for a one-pot synthesis; short reaction times of typically 3 hours; scalability; copper-free conditions preventing the formation of Glaser side-products; commonly used reagents that are commercially available and relatively inexpensive.

This one-pot procedure now enables rapid access to symmetric diarylalkynes ligands directly from aryl halide substrates both on a small and large scale. This reduces the synthetic burden for scale-up as well as incorporating additional functionality for applications. Libraries of ligands could also be generated for high-throughput screening of self-assembly conditions enabling the discovery of new cages. Given the application of symmetric diarylalkynes in numerous fields, this straightforward copper-free one-pot procedure could also be extended to other carbocyclic and heterocyclic aryl halide substrates and allow scale-up for applications.

Experimental Section

Material and Methods. Solvents and reagents were commercially obtained and used without further purification. Anhydrous tetrahydrofuran was dried using a Pure Solv MD-5 apparatus from Innovative Technologies. Tetrabutylammonium fluoride (1 M in tetrahydrofuran) for use in reactions with $Pd(PPh_3)_4$ was degassed by bubbling nitrogen through the solution for 24 h ensuring solvent evaporation did not affect the reagent's concentration. $Pd(PPh_3)_4$ was stored under a nitrogen atmosphere due to its air sensitivity. Pressure tubes (15 mL) were purchased from FengTecEx GmbH and as a precaution, the reactions using pressure tubes were performed behind a blast shield.

For thin-layer chromatography, Macherey Nagel plates (Polygram®-SIL G/UV_{254}, coating thickness 0.2 mm) equipped with a fluorescence indicator were used. Silica gel with a pore diameter of 0.040–0.063 mm was purchased from Merck. For flash chromatography Biotage® SNAP Ultra columns (10 g, 25 g, 50 g) and Biotage® Sfär Silica HC D columns (10 g, 25 g) were used on an Isolera One from Biotage®.

Synthetic Procedures. Compound **6** was prepared according to a literature procedure[5f] and the synthesis of ligands **1 a–c**, **2 b–c** and their precursors **5 a–c**, **6 a–c** are detailed below. Procedures for the preparation and characterization of metal-organic cages **3 a–c** and **4 a–b** are provided in the Supplementary Information.

5-Bromo-2,2′-bipyridine (5 a): Adapted from literature procedure.[5h] Under a nitrogen atmosphere 2-iodo-5-bromopyridine (2.00 g, 7.04 mmol) and $Pd(PPh_3)_4$ (408 mg, 5 mol%) were dissolved in a solution of 2-pyridylzinc(II) bromide (0.5 M in tetrahydrofuran, 14.0 mL, 7.00 mmol). The reaction mixture was heated at 75 °C for 20 h. After cooling to room temperature, sat. ethylenediaminetetraacetic acid (20 mL) and sat. sodium bicarbonate solution (20 mL) were added and the reaction mixture was stirred at room temperature for another 2 h. The aqueous layer was extracted with dichloromethane (3×150 mL), the organic layers were combined, dried over magnesium sulfate and filtered. The solvent was removed *in vacuo*. The crude product was purified by flash chromatography (silica gel, 5–15% ethyl acetate/cyclohexane) and the product was obtained as a yellowish solid (1.19 g, 5.06 mmol, 72%). The analytical data was consistent with literature data:[20] **^{1}H NMR** (500 MHz, $CDCl_3$, 298 K, TMS) δ (ppm): 8.72 (d, ^4J = 2.4 Hz, 1H, H_j), 8.67 (ddd, ^3J = 4.8 Hz, ^4J = 1.8 Hz, ^5J = 0.8 Hz, 1H, H_a), 8.38 (dt, ^3J = 7.8 Hz, ^4J = 1.0 Hz, 1H, H_d), 8.33 (d, ^3J = 8.5 Hz, 1H, H_g), 7.94 (dd, ^3J = 8.5 Hz, ^4J = 2.4 Hz, 1H, H_h), 7.83 (td, ^3J = 7.8 Hz, ^4J = 1.8 Hz, 1H, H_c), 7.33 (ddd, ^3J = 7.8 Hz, ^3J = 4.8 Hz, ^4J = 1.2 Hz, 1H, H_b). **^{13}C NMR** (126 MHz, $CDCl_3$, 298 K, TMS) δ (ppm): 155.1 (C_e), 154.5 (C_f), 150.2

(C_j), 149.2 (C_a), 139.5 (C_h), 137.1 (C_c), 124.0 (C_b), 122.4 (C_g), 121.2 (C_i), 121.0 (C_d). **HRMS** (EI, 70 eV) *m/z*: 233.97939 $[M]^+$ (calculated: 233.97926 for $C_{10}H_7{}^{79}Br_1N_2$), 235.97764 $[M]^+$ (calculated: 235.97721 for $C_{10}H_7{}^{81}Br_1N_2$). **FT-IR**: $\tilde{\nu}$ = 2360.2 (w), 2248.9 (w), 1586.2 (w), 1570.3 (w), 1542.1 (m), 1496.9 (w), 1458.4 (s), 1433.5 (m), 1370.6 (w), 1243.1 (w), 1145.3 (w), 1090.0 (w), 1061.1 (w), 1021.9 (m), 992.5 (w), 927.9 (w), 905.9 (w), 858.2 (m), 797.3 (s), 749.6 (s), 648.9 (w), 620.4 (w), 593.8 (w), 564.0 (w) cm^{-1}. **M. p.**: 76 °C.

Large Scale Synthesis of 5-Bromo-2,2′-bipyridine (5 a): Under a nitrogen atmosphere 2-iodo-5-bromopyridine (7.10 g, 25.0 mmol) and $Pd(PPh_3)_4$ (1.44 g, 5 mol%) were dissolved in a solution of 2-pyridylzinc(II) bromide (0.5 M in tetrahydrofuran, 50.0 mL, 25.0 mmol). The reaction mixture was heated at 75 °C for 48 h. After cooling to room temperature, sat. ethylenediaminetetraacetic acid (150 mL) and sat. sodium bicarbonate solution (150 mL) was added and the reaction mixture was stirred at room temperature for another 24 h. The aqueous layer was extracted with dichloromethane (3×150 mL), the organic layers were combined, dried over magnesium sulfate, and filtered. The solvent was removed *in vacuo*. The crude product was purified by flash chromatography (silica gel, 5–15% ethyl acetate/cyclohexane) and the product was obtained as a yellowish solid (4.19 g, 17.8 mmol, 71%).

5-Chloro-2,2′-bipyridine (5 d): Under a nitrogen atmosphere 2-bromo-5-chloropyridine (577 mg, 3.00 mmol) and $Pd(PPh_3)_4$ (173 mg, 5 mol%) were dissolved in a solution of 2-pyridylzinc(II) bromide (0.5 M in tetrahydrofuran, 6.0 mL, 3.00 mmol). The reaction mixture was heated at 75 °C for 18 h. After cooling to room temperature, sat. ethylenediaminetetraacetic acid (40 mL) and sat. sodium bicarbonate solution (40 mL) were added and the reaction mixture was stirred at room temperature for another 2 h. The aqueous layer was extracted with dichloromethane (3×100 mL), the organic layers were combined, dried over magnesium sulfate, and filtered. The solvent was removed *in vacuo*. The crude product was purified by flash chromatography (silica gel, 5–15% ethyl acetate/cyclohexane) and the product was obtained as a colourless solid (276 mg, 1.45 mmol, 48%): **^{1}H NMR** (600 MHz, $CDCl_3$, 298 K, TMS) δ (ppm): 8.66 (unres. ddd, ^3J = 4.7 Hz, 1H, H_a), 8.61 (d, ^4J = 2.2 Hz, 1H, H_j), 8.37 (d, ^3J = 8.5 Hz, 1H, H_g), 8.36 (d, ^3J = 7.8 Hz, 1H, H_d), 7.81 (td, ^3J = 7.8 Hz, ^4J = 1.7 Hz, 1H, H_c), 7.78 (dd, ^3J = 8.5 Hz, ^4J = 2.2 Hz, 1H, H_h), 7.32 (ddd, ^3J = 7.8 Hz, ^3J = 4.7 Hz, ^4J = 0.9 Hz, 1H, H_b). **^{13}C NMR** (151 MHz, $CDCl_3$, 298 K, TMS) δ (ppm): 155.1 (C_e), 154.3 (C_f), 149.2 (C_a), 148.0 (C_j), 137.0 (C_c), 136.7 (C_h), 132.4 (C_i), 124.0 (C_b), 121.9 (C_g), 121.0 (C_d). **HRMS** (ESI) *m/z*: 191.03689 $[M+H]^+$ (calculated: 191.03705 for $C_{10}H_8N_2Cl$). **M. p.**: 76 °C.

1,2-Di([2′,2″-bipyridin]-5′-yl)ethyne (1 a): The analytical data from the various reactions was consistent with literature data.[16b,c]

Procedure for the Optimised One-Pot Reaction in a Pressure Tube: 5-Bromo-2,2′-bipyridine (**5 a**) (170 mg, 723 μmol) and $Pd(PPh_3)_4$ (41.8 mg, 5 mol%) were added to a pressure tube and evacuated for five minutes. Using counterflow technique, degassed tetrabutylammonium fluoride (1 M in tetrahydrofuran, 4.30 mL, 4.30 mmol) and trimethylsilylacetylene (100 μL, 723 μmol) were added. The pressure tube was immediately closed and the reaction mixture was heated at 70 °C for 3 h. After cooling to room temperature, the mixture was washed with water (50 mL) and the aqueous layer was extracted with dichloromethane (3×33 mL). The organic layers were combined, dried over magnesium sulfate and the solvent removed *in vacuo*. The crude product was purified by flash chromatography (silica gel, 10–20% ethyl acetate/cyclohexane) to give the product as a colourless solid (74.9 mg, 224 μmol, 62%): **H NMR** (500 MHz, $CDCl_3$, 298 K, TMS) δ (ppm): 8.85 (dd, ^4J = 2.2 Hz, ^5J = 0.8 Hz, 2H, H_j), 8.71 (ddd, ^3J = 4.8, ^4J = 1.8 Hz, ^5J = 0.8 Hz, 2H, H_a), 8.47–8.45 (m, 2H, H_g), 8.45–8.43 (m, 2H, H_d), 7.99 (dd, ^3J = 8.3 Hz, ^4J = 2.2 Hz, 2H, H_h), 7.85 (td, ^3J = 7.7 Hz, ^4J = 1.8, 2H, H_c), 7.34 (ddd, ^3J = 7.7 Hz, ^3J = 4.8 Hz, ^4J = 1.2 Hz, 2H, H_b). **^{13}C NMR** (126 MHz, $CDCl_3$, 298 K, TMS) δ (ppm): 155.3 (C_e), 155.2 (C_f), 151.7 (C_j), 149.2 (C_a), 139.5 (C_h), 137.1 (C_c), 124.1 (C_b), 121.5 (C_d), 120.5 (C_g), 119.7 (C_i), 90.5 (C_k). **HRMS** (EI, 70 eV) *m/z*: 334.12117 $[M]^+$ (calculated: 334.12185 for $C_{22}H_{14}N_4$). **FT-IR**: $\tilde{\nu}$ = 2360.2 (w), 2248.9 (w), 1586.2 (w), 1570.3 (w), 1542.1 (m), 1496.9 (w), 1458.4 (s), 1433.5 (m), 1370.6 (w), 1243.1 (w), 1145.3 (w), 1090.0 (w), 1061.1 (w), 1021.9 (m), 992.5 (w), 927.9 (w), 905.9 (w), 858.2 (m), 797.3 (s), 749.6 (s), 648.9 (w), 620.4 (w), 593.8 (w), 564.0 (w) cm^{-1}. **M. p.**: 228 °C.

Large Scale Procedure for the Optimised One-Pot Reaction in a Pressure Tube: 5-Bromo-2,2′-bipyridine (**5 a**) (1.70 g, 7.23 mmol) and $Pd(PPh_3)_4$ (418 mg, 5 mol%) were added to a pressure tube and evacuated for five minutes. Using counterflow technique, degassed tetrabutylammonium fluoride (1 M in tetrahydrofuran, 43.0 mL, 43.0 mmol) and trimethylsilylacetylene (1.00 mL, 7.23 mmol) were added. The pressure tube was immediately closed and the reaction mixture was heated at 70 °C for 3 h. After cooling to room temperature, the precipitate was collected by filtration and was dissolved in dichloromethane (100 mL) and the organic layer was extracted with hydrochloric acid (3×30 mL, 6 M). The layers were separated and the pH value of the aqueous layer was adjusted to 7 with 25% ammonia solution and the precipitate was collected (720 mg, 2.15 mmol, 60%).

Procedure for the Coupling of 6 and 5 a in a Round-Bottom Flask: Under a nitrogen atmosphere 5-bromo-2,2′-bipyridine (**5 a**) (85.1 mg, 362 μmol), 5-ethynyl-2,2′-bipyridine (**6**) (65.2 mg, 362 μmol) and $Pd(PPh_3)_2Cl_2$ (25.4 mg, 10 mol%, to have the same amount of palladium catalyst as the one-pot conditions) were added to a three-neck flask. Tetrabutylammonium fluoride (1 M in tetrahydrofuran, 4.30 mL, 4.30 mmol) was added and the reaction mixture heated at 70 °C for 3 h. After cooling to room temperature water was added, the mixture was extracted with dichloromethane (3×33 mL), dried over magnesium sulfate and the solvent was removed *in vacuo*. The crude product was purified by flash chromatography (silica gel, 10–20% ethyl acetate/cyclohexane) to give **1 a** as colorless solid (66.3 mg,198 μmol, 55%).

5-Bromo-6′-methyl-2,2′-bipyridine (5 b): Under a nitrogen atmosphere 2-bromo-6-methylpyridine (1.42 g, 8.25 mmol) was suspended in anhydrous tetrahydrofuran (20 mL). The solution was degassed three times using the freeze-pump-thaw technique. Afterwards, the solution was cooled to −78 °C, *n*-butyllithium (2.5 M in hexane, 3.90 mL, 9.75 mmol) was slowly added and the mixture was stirred at −78 °C for 1 h. Zinc(II) chloride (1 M in tetrahydrofuran, 1.31 g, 9.60 mL, 9.63 mmol) was added and the solution was stirred at −78 °C for 2 h. At this temperature, 2-iodo-5-bromopyridine (1.95 g, 6.87 mmol) and $Pd(PPh_3)_4$ (398 mg, 5 mol%) were added and the reaction mixture was stirred at 75 °C for 18 h. After cooling to room temperature, sat. ethylenediaminetetraacetic acid (50 mL) and sat. sodium bicarbonate solution (50 mL) were added and the mixture was stirred for further 2 h. The layers were separated, the aqueous layer were extracted with dichloromethane (3×100 mL), the organic layers were combined, dried over magnesium sulfate and the solvent was removed *in vacuo*. The crude product was purified by flash chromatography (silica gel, 10% ethyl acetate/cyclohexane) to obtain the product as a colourless solid (1.21 g, 4.86 mmol, 71%): **^{1}H NMR** (500 MHz, $CDCl_3$, 298 K, TMS) δ (ppm): 8.70 (dd, ^4J = 2.4 Hz, ^5J = 0.6 Hz, 1H, H_k), 8.33 (dd, ^3J = 8.4 Hz, ^5J = 0.6 Hz, 1H, H_h), 8.15 (d, ^3J = 7.8 Hz, 1H, H_e), 7.92 (dd, ^3J = 8.4 Hz, ^4J = 2.4 Hz, 1H, H_i), 7.70 (t, ^3J = 7.8 Hz, 1H, H_d), 7.18 (d, ^3J = 7.8 Hz, 1H, H_c), 2.63 (s, 3H, H_a). **^{13}C NMR** (126 MHz, $CDCl_3$, 298 K, TMS) δ (ppm): 158.1 (C_b), 155.0 (C_g), 154.6 (C_f), 150.1 (C_k), 139.4 (C_i), 137.2 (C_d), 123.6 (C_c), 122.5 (C_h), 120.9 (C_j), 118.0 (C_e), 24.6 (C_a). **HRMS** (EI, 70 eV) *m/z*: 247.99469 $[M]^+$ (calculated: 247.99491 for $C_{11}H_9{}^{79}Br_1N_2$), 249.99278 $[M]^+$ (calculated: 249.99286 for $C_{11}H_9{}^{81}Br_1N_2$). **FT-IR**: $\tilde{\nu}$ = 2920.3 (w), 2307.9 (w), 1751.1 (w), 1593.9

(w), 1566.3 (m), 1547.9 (m), 1448.8 (m), 1366.0 (m), 1285.2 (w), 1247.9 (w), 1154.9 (w), 1124.8 (w), 1082.1 (m), 1003.4 (s), 927.5 (w), 870.0 (w), 848.3 (s), 789.6 (s), 752.9 (s), 738.3 (m), 696.4 (w), 656.1 (w), 631.8 (m), 595.1 (m), 540.9 (w), 513.3 (w) cm^{-1}. **M. p.**: 91 °C.

1,2-Di([6′′-methyl-2′,2′′-bipyridin]-5′-yl)ethyne (1 b): 5-Bromo-6′-methyl-2,2′-bipyridine (**5 b**) (180 mg, 723 μmol) and $Pd(PPh_3)_4$ (41.8 mg, 5 mol%) were added to a pressure tube and evacuated for five minutes. Using counterflow technique, degassed tetrabutylammonium fluoride (1 M in tetrahydrofuran, 4.30 mL, 4.30 mmol) and trimethylsilylacetylene (100 μL, 723 μmol) were added, the pressure tube was immediately closed and the reaction mixture was heated at 70 °C for 3 h. Upon cooling, the product precipitated and the precipitate was filtered and was washed with cold tetrahydrofuran (10 mL). The precipitate was dissolved in dichloromethane (10 mL) and the organic layer was extracted with hydrochloric acid (3×10 mL, 6 M). The layers were separated and the pH value of the aqueous layer was adjusted to 7 with 25% ammonia solution and the precipitate was collected (75.3 mg, 208 μmol, 58%): **^{1}H NMR** (500 MHz, $CDCl_3$, 298 K, TMS) δ (ppm): 8.84 (dd, ^4J = 2.1 Hz, ^5J = 0.8 Hz, 2H, H_k), 8.48 (d, ^3J = 8.2 Hz, 2H, H_h), 8.23 (d, ^3J = 7.8 Hz, 2H, H_e), 7.96 (dd, ^3J = 8.2 Hz, ^4J = 2.1 Hz, 2H, H_i), 7.73 (t, ^3J = 7.8 Hz, 2H, H_d), 7.19 (d, ^3J = 7.8 Hz, 2H, H_c), 2.65 (s, 6H, H_a). **^{13}C NMR** (126 MHz, $CDCl_3$, 298 K, TMS) δ (ppm): 158.1 (C_b), 155.5 (C_g), 154.7 (C_f), 151.7 (C_k), 139.4 (C_i), 137.3 (C_d), 123.7 (C_c), 120.5 (C_h), 119.5 (C_j), 118.5 (C_e), 90.4 (C_i), 24.6 (C_a). **HRMS** (EI, 70 eV) *m/z*: 362.15253 $[M]^+$ (calculated: 362.15315 for $C_{24}H_{18}N_4$). **FT-IR**: $\tilde{\nu}$ = 2920.9 (w), 2359.9 (w), 1738.9 (w), 1589.9 (m), 1568.0 (w), 1545.6 (m), 1487.1 (w), 1453.3 (m), 1372.2 (m), 1244.7 (w), 1157.0 (w), 1133.6 (w), 1082.9 (m), 1022.9 (w), 997.9 (w), 983.9 (w), 926.3 (w), 901.3 (w), 861.9 (s), 846.3 (w), 799.3 (s), 754.9 (s), 693.6 (m), 644.1 (m), 598.3 (m), 553.1 (w), 517.0 (w) cm^{-1}. **M. p.**: 227 °C.

5-Bromo-6-methyl-2,2′-bipyridine (5 c): Under a nitrogen atmosphere 2-bromopyridine (390 μL, 3.90 mmol) was suspended in anhydrous tetrahydrofuran (12 mL). The solution was degassed using the freeze-pump-thaw technique. Afterwards, the solution was cooled to −78 °C, *n*-butyllithium (2.5 M in hexane, 1.90 mL, 4.75 mmol) was slowly added and the mixture was stirred at −78 °C for 1 h. Zinc(II) chloride (1 M in tetrahydrofuran, 681 mg, 5.00 mmol) was added and the solution was further stirred at −78 °C for 2 h. At −78 °C, 3,6-dibromo-2-methylpyridine (1.00 g, 3.90 mmol) and $Pd(PPh_3)_4$ (230 mg, 5 mol%) were added and the reaction mixture was stirred at 75 °C for 19 h. After cooling to room temperature, sat. ethylenediaminetetraacetic acid (25 mL) and sat. sodium bicarbonate solution (25 mL) were added and the mixture was stirred for further 1.5 h. The layers were separated, the aqueous layer was extracted with dichloromethane (3×50 mL), the organic layers were combined, dried over magnesium sulfate and the solvent was removed *in vacuo*. The crude product was purified by flash chromatography (silica gel, 5% ethyl acetate/cyclohexane) to obtain the product as a colourless solid (714 mg, 2.87 mmol, 74%): **^{1}H NMR** (500 MHz, $CDCl_3$, 298 K, TMS) δ (ppm): 8.66 (ddd, ^3J = 4.8 Hz, ^4J = 1.8 Hz, ^5J = 0.9 Hz, 1H, H_a), 8.40 (dt, ^3J = 7.8 Hz, ^5J = 0.9 Hz, 1H, H_d), 8.10 (d, ^3J = 8.3 Hz, 1H, H_g), 7.91 (d, ^3J = 8.3 Hz, 1H, H_h), 7.81 (td, ^3J = 7.8 Hz, ^4J = 1.8 Hz, 1H, H_c), 7.31 (ddd, ^3J = 7.8 Hz, ^3J = 4.8 Hz, ^4J = 1.2 Hz, 1H, H_b), 2.74 (s, 3H, H_k). **^{13}C NMR** (126 MHz, $CDCl_3$, 298 K, TMS) δ (ppm): 156.6 (C_j), 155.5 (C_e), 154.2 (C_f), 149.1 (C_a), 140.6 (C_h), 137.0 (C_c), 123.8 (C_b), 121.8 (C_i), 121.1 (C_d), 119.9 (C_g), 25.2 (C_k). **HRMS** (EI, 70 eV) *m/z*: 247.99492 $[M]^+$ (calculated: 247.99491 for $C_{11}H_9{}^{79}Br_1N_2$), 249.99355 $[M]^+$ (calculated: 249.99286 for $C_{11}H_9{}^{81}Br_1N_2$). **FT-IR**: $\tilde{\nu}$ = 2923.9 (w), 2853.05 (w), 1571.8 (w), 1554.9 (m), 1419.5 (s), 1382.5 (w), 1246.8 (m), 1095.6 (m), 1029.7 (s), 996.0 (w), 977.6 (w), 845.7 (s), 789.8 (s), 741.6 (s), 733.0 (s), 718.3 (m), 620.2 (m) cm^{-1}. **M. p.**: 88 °C.

1,2-Di([6′-methyl-2′,2′′-bipyridin]-5′-yl)ethyne (1 c): 5-Bromo-6-methyl-2,2′-bipyridine (**5 c**) (180 mg, 723 μmol) and $Pd(PPh_3)_4$ (41.8 mg, 5 mol%) were added to a pressure tube and evacuated for five minutes. Using counterflow technique, degassed tetrabutylammonium fluoride (1 M in tetrahydrofuran, 4.3 mL, 4.30 mmol) and trimethylsilylacetylene (100 μL, 723 μmol) were added, the pressure tube immediately closed and the reaction mixture stirred at 70 °C for 24 h. After cooling to room temperature, the precipitate was collected by filtration, dissolved in tetrahydrofuran (200 mL) and the solvent removed *in vacuo*. The crude product was purified by flash chromatography (silica gel, 20–40% ethyl acetate/cyclohexane) to obtain the product as a colourless solid (42.3 mg, 117 μmol, 32%): **^{1}H NMR** (500 MHz, $CDCl_3$, 298 K, TMS) δ (ppm): 8.69 (d, ^3J = 4.9 Hz, ^4J = 1.8 Hz, ^5J = 0.9 Hz, 2H, H_a), 8.47 (ddd, ^3J = 7.9 Hz, ^4J = 1.2 Hz, ^5J = 0.9 Hz, 2H, H_d), 8.27 (d, ^3J = 8.1 Hz, 2H, H_g), 7.92 (d, ^3J = 8.1 Hz, 2H, H_h), 7.83 (td, ^3J = 7.9 Hz, ^4J = 1.8 Hz, 2H, H_c), 7.31 (ddd, ^3J = 7.9 Hz, ^3J = 4.9 Hz, ^4J = 1.2 Hz, 2H, H_b), 2.87 (s, 6H, H_k). **^{13}C NMR** (126 MHz, $CDCl_3$, 298 K) δ (ppm): 159.7 (C_i), 155.7 (C_e), 154.5 (C_f), 149.3 (C_a), 139.9 (C_h), 136.9 (C_c), 124.0 (C_b), 121.4 (C_d), 118.9 (C_j), 118.1 (C_g), 93.7 (C_i), 24.1 (C_k). **HRMS** (EI, 70 eV) *m/z*: 362.15271 $[M]^+$ (calculated: 362.15315 for $C_{24}H_{18}N_4$). **FT-IR**: $\tilde{\nu}$ = 2987.4 (w), 2252.5 (w), 1572.1 (w), 1546.4 (w), 1450.5 (m), 1433.8 (m), 1393.1 (w), 1246.0 (w), 1094.7 (w), 1044.0 (w), 993.5 (w), 848.8 (m), 794.5 (s), 747.9 (s), 718.1 (w), 615.1 (m) cm^{-1}. **M. p.**: 218 °C.

2-(5′-Bromopyridin-2′-yl)-1*H*-benzo[*d*]imidazole (6 a): In a three-neck flask polyphosphoric acid (40 mL) was added and was preheated to 140 °C. *o*-Phenylenediamine (1.34 g, 12.4 mmol) and 5-bromopicolinic acid (2.50 g, 12.4 mmol) were added and the reaction mixture was heated at 180 °C for 24 h. The mixture was cooled to 140 °C, poured into water (200 mL) and neutralised to pH 7 with ammonia solution (25%). The precipitate was collected by filtration and, after intensive drying *in vacuo*, the product was obtained as a colourless solid (2.96 g, 10.8 mmol, 87%). The analytical data was consistent with literature data:[21] **^{1}H NMR** (500 MHz, DMSO-d_6, 298 K δ (ppm): 13.2 (s, 1H, H_a), 8.86 (dd, ^4J = 2.3 Hz, ^5J = 0.8 Hz, 1H, H_m), 8.26 (dd, ^3J = 8.5 Hz, ^5J = 0.8 Hz, 1H, H_j), 8.23 (dd, ^3J = 8.5 Hz, ^4J = 2.3 Hz, 1H, H_k), 7.71 (d, ^3J = 7.8 Hz, 1H, $H_{c/f}$), 7.54 (d, ^3J = 7.8 Hz, 1H, $H_{c/f}$), 7.29–7.18 (m, 2H, $H_{d,e}$). **^{13}C NMR** (126 MHz, DMSO-d_6, 298 K) δ (ppm): 150.0 (C_m), 149.7 (C_h), 147.2 (C_i), 143.7 ($C_{b/g}$), 140.1 (C_k), 134.9 ($C_{b/g}$), 123.3 ($C_{d/e}$), 122.9 (C_j), 122.0 ($C_{d/e}$), 120.9 (C_l), 119.3 ($C_{c/f}$), 112.0 ($C_{c/f}$). **HRMS** (EI, 70 eV) *m/z*: 272.98975 $[M]^+$ (calculated: 272.99016 for $C_{12}H_8{}^{79}Br_1N_3$), 274.98788 $[M]^+$ (calculated: 274.98811 for $C_{12}H_8{}^{81}Br_1N_3$). **FT-IR**: $\tilde{\nu}$ = 3386 (m), 3049 (w), 1422 (s), 1005 (s) cm^{-1}. **M. p.**: 227 °C.

2-(5′-Bromopyridin-2′-yl)-1-methyl-1*H*-benzo[*d*]imidazole (6 b): 2-(5′-Bromopyridin-2′-yl)-1*H*-benzo[*d*]imidazole (**6 a**) (1.60 g, 5.84 mmol) and potassium carbonate (milled, 2.50 g, 18.1 mmol) were dissolved in dimethylformamide (25 mL). Methyl iodide (500 μL, 8.03 mmol) was added and the reaction mixture was stirred at room temperature for 17 h. Water (100 mL) was added and the aqueous layer extracted with ethyl acetate (3×50 mL). The organic layers were combined, washed with brine (150 mL) and sodium hydroxide solution (10%, 100 mL), dried over magnesium sulfate and the solvent was removed *in vacuo*. The product was obtained as a greyish solid (1.33 g, 4.62 mmol, 79%). The analytical data was consistent with literature data:[22] **^{1}H NMR** (600 MHz, DMSO-d_6, 298 K) δ (ppm): 8.88 (unres. dd, 1H, H_m), 8.29–8.23 (m, 2H, $H_{j,k}$), 7.73 (d, ^3J = 8.1 Hz, 1H, H_j), 7.66 (d, ^3J = 8.1 Hz, 1H, H_c), 7.35 (t, ^3J = 7.6 Hz, 1H, H_d), 7.29 (t, ^3J = 7.6 Hz, 1H, H_e), 4.21 (s, 3H, H_a). **^{13}C NMR** (151 MHz, DMSO-d_6, 298 K) δ (ppm): 149.6 (C_m), 148.8 (C_h), 148.7 (C_i), 142.0 (C_b), 140.1 (C_k), 137.2 (C_g), 126.0 (C_j), 123.4 (C_d), 122.5 (C_e), 120.9 (C_l), 119.5 (C_f), 110.9 (C_c), 32.7 (C_a). **MS** (EI, 70 eV) *m/z*: 288.01 (100) $[M]^+$. **HRMS** (ESI) *m/z*: 288.01275 $[M+H]^+$ (calculated: 288.01309 for $C_{13}H_{11}N_3Br$). **FT-IR**: $\tilde{\nu}$ = 3041 (w), 1434 (m), 1004 (m), 727 (s) cm^{-1}. **M.p.**: 137 °C.

1,2-Di(6′′-(1′-methyl-1*H*-benzo[*d*]imidazol-2′-yl)pyridin-3′′-yl) ethyne (2 b): 2-(5′-Bromopyridin-2′-yl)-1-methyl-1*H*-benzo[*d*]

imidazole (**6b**) (208 mg, 722 μmol) and $Pd(PPh_3)_4$ (41.8 mg, 5 mol%) were added to a pressure tube and evacuated for five minutes. Using counterflow technique, degassed tetrabutylammonium fluoride (1 M in tetrahydrofuran, 4.30 mL, 4.30 mmol) and trimethylsilylacetylene (100 μL, 723 μmol) were added, the tube was immediately closed and the reaction mixture was heated at 70 °C for 3 h. The product precipitated, was filtered and washed with cold tetrahydrofuran (100 mL). The product was obtained as a yellow to green solid (112 mg, 254 μmol, 70%): **^{1}H NMR** (600 MHz, $CDCl_3$, 298 K) δ (ppm): 8.87 (d, ^4J = 1.9 Hz, 2H, H_m), 8.48 (d, ^3J = 8.2 Hz, 2H, H_j), 8.00 (dd, ^3J = 8.2 Hz, ^4J = 1.9 Hz, 2H, H_k), 7.85 (d, ^3J = 7.8 Hz, 2H, H_l), 7.47 (d, ^3J = 7.8 Hz, 2H, H_c), 7.39–7.32 (m, 4H, $H_{d,\ e}$), 4.32 (s, 6H, H_a). **^{13}C NMR** (126 MHz, $CDCl_3$, 298 K) δ (ppm): 151.1 (C_m), 149.8 (C_i), 149.4 (C_j), 142.6 (C_g), 139.2 (C_k), 137.4 (C_b), 124.0 (C_j), 123.7 ($C_{d/e}$), 122.9 ($C_{d/e}$), 120.2 (C_f), 119.5 (C_h), 110.0(C_c), 90.7 (C_n), 32.9 (C_a). **HRMS** (EI, 70 eV) *m/z*: 440.17491 $[M]^+$ (calculated: 440.17494 for $C_{28}H_{20}N_6$). **FT-IR**: $\tilde{\nu}$ = 3050 (w), 1466 (m), 725 (s) cm^{-1}. **M. p.**: decomposed at > 220 °C.

2-(5′-Bromopyridin-2′-yl)-1-benzyl-1*H*-benzo[*d*]imidazole (6c): 2-(5′-Bromopyridin-2′-yl)-1*H*-benzo[*d*]imidazole (**6a**) (614 mg, 2.24 mmol) and potassium carbonate (milled, 496 mg, 3.59 mmol) were dissolved in dry dimethylformamide (5 mL). Benzyl bromide (350 μL, 2.94 mmol) was added and the reaction mixture stirred at room temperature for 4.5 h. The solvent was removed *in vacuo* (55 °C, 20 mbar). Water (50 mL) was added and the aqueous layer was extracted with ethyl acetate (1 × 50 mL). The organic layers were combined, washed with brine (2 × 125 mL) and sodium hydroxide solution (10%, 1 × 50 mL), dried over magnesium sulfate and the solvent was removed *in vacuo*. The product was obtained as a greyish solid (663 mg, 1.82 mmol, 81%): **^{1}H NMR** (600 MHz, DMSO-d_6, 298 K) δ (ppm): 8.82 (dd, ^4J = 2.3 Hz, ^5J = 0.6 Hz, 1H, H_q), 8.32 (dd, ^3J = 8.6 Hz, ^5J = 0.6 Hz, 1H, H_n), 8.25 (dd, ^3J = 8.6 Hz, ^4J = 2.3 Hz, 1H, H_o), 7.78–7.74 (m, 1H, H_j), 7.61–7.57 (m, 1H, H_h), 7.32–7.26 (m, 2H, $H_{g,j}$), 7.26–7.22 (m, 2H, H_b), 7.20–7.17 (m, 1H, H_a), 7.14–7.11 (m, 2H, H_c), 6.17 (s, 2H, H_e). **^{13}C NMR** (151 MHz, DMSO-d_6, 298 K) δ (ppm): 149.6 (C_q), 148.6 (C_l), 148.4 (C_m), 142.2 (C_c), 140.3 (C_o), 137.7 (C_d), 136.6 (C_k), 128.6 (C_b), 127.3 (C_a), 126.7 (C_c), 126.0 (C_n), 123.8 ($C_{j/g}$), 122.9 ($C_{j/g}$), 121.2 (C_p), 119.8 (C_j), 111.5 (C_h), 48.1 (C_e). **MS** (EI, 70 eV) *m/z*: 364.02 (100) $[M]^+$. **HRMS** (ESI) *m/z*: 364.04380 $[M+H]^+$ (calculated: 364.04439 for $C_{19}H_{15}N_3Br$). **FT-IR**: $\tilde{\nu}$ = 3252.9 (w), 2158.9 (w), 1572.4 (w), 1496.22 (w), 1434.8 (m), 1407.8 (m), 1328.6 (m), 1291.5 (w), 1259.3 (w), 1236.2 (m), 1157.5 (m), 1089.5 (m), 1009.8 (m), 977.5 (w), 923.7 (w), 845.9 (m), 778.1 (w), 763.1 (m), 736.7 (s), 717.9 (s), 692.8 (m), 641.8 (w) cm^{-1}. **M. p.**: 131 °C.

1,2-Di(6″-(1′-benzyl-1*H*-benzo[*d*]imidazol-2′-yl)pyridin-3″-yl) ethyne (2c): 2-(5′-Bromopyridin-2′-yl)-1-benzyl-1*H*-benzo[*d*] imidazole (6c) (263 mg, 722 μmol) and $Pd(PPh_3)_4$ (41.8 mg, 5 mol%) were added to a pressure tube and evacuated for five minutes. Using counterflow technique, degassed tetrabutylammonium fluoride (1 M in tetrahydrofuran, 4.30 mL, 4.30 mmol) and trimethylsilylacetylene (100 μL, 723 μmol) were added, the tube was immediately closed and the reaction mixture was heated at 70 °C for 3 h. The product precipitated, was filtered and washed with cold tetrahydrofuran (1 × 200 mL). The product was obtained as a neon green solid (196 mg, 331 μmol, 92%): **^{1}H NMR** (500 MHz, TFA-d_1, 298 K) δ (ppm): 9.42 (dd, ^4J = 2.0 Hz, ^5J = 0.8 Hz, 2H, H_q), 8.65 (dd, ^3J = 8.2 Hz, ^4J = 2.0 Hz, 2H, H_o), 8.41 (dd, ^3J = 8.2 Hz, ^5J = 0.8 Hz, 2H, H_n), 8.21 (d, ^3J = 7.8 Hz, 2H, H_j), 8.09–8.00 (m, 6H, $H_{g,h,j}$), 7.64–7.59 (m, 4H, $H_{a,b}$), 7.45–7.40 (m, 2H, H_c), 6.18 (s, 4H, H_e). **^{13}C NMR** (126 MHz, TFA-d_1, 298 K) δ (ppm): 154.8 (C_q), 147.1 (C_l), 145.3 (C_o), 141.6 (C_m), 135.6 (C_f), 134.5 (C_d), 132.6 (C_k), 132.0 ($C_{a/b}$), 131.9 ($C_{a/b}$), 131.7 ($C_{h/i}$), 131.2 ($C_{h/i}$), 128.8 (C_n), 128.6 (C_c), 126.8 (C_p), 117.0 (C_j), 115.6 (C_g), 93.4 (C_f), 52.8 (C_e). **HRMS** (EI, 70 eV) *m/z*: 592.23610 $[M]^+$ (calculated: 592.23754 for $C_{40}H_{28}N_6$). **FT-IR**: $\tilde{\nu}$ = 1972.9 (w), 1592.1 (w), 1519.5 (w), 1495.9 (w), 1465.8 (m), 1442.3 (m), 1405.5 (m), (w), 1368.3 (m), 1330.4 (m), 1296.8 (s), 1240.1 (w), 1166.5 (w), 1069.5 (w), 853.7 (m), 743.2 (s), 726.1 (s), 452.3 (m) cm^{-1}. **M. p.**: > 300 °C.

Acknowledgements

We thank the Deutsche Forschungsgemeinschaft (DFG, project numbers 413396832 and 429518153) for financial support. We thank the spectroscopy department and Dr. Claus Bier for NMR and mass spectral data collection. We thank Felix Piontek and Etienne Rommens for preliminary studies and Niclas Grocholski for the synthesis of additional ligand. Open access funding enabled and organized by Projekt DEAL.

Conflict of Interest

The authors declare no conflict of interest.

Keywords: Cross-coupling · Metal-organic cages · One-pot reactions · Sonogashira coupling · Supramolecular chemistry

[1] A. Biffis, P. Centomo, A. Del Zotto, M. Zecca, *Chem. Rev.* **2018**, *118*, 2249–2295.
[2] a) R. Chinchilla, C. Najera, *Chem. Rev.* **2007**, *107*, 874–922; b) R. Chinchilla, C. Najera, *Chem. Soc. Rev.* **2011**, *40*, 5084–5121; c) K. Sonogashira, Y. Tohda, N. Hagihara, *Tetrahedron Lett.* **1975**, *16*, 4467–4470.
[3] D. Wang, S. H. Gao, *Org. Chem. Front.* **2014**, *1*, 556–566.
[4] a) J. M. Tour, *Acc. Chem. Res.* **2000**, *33*, 791–804; b) U. H. F. Bunz, *Chem. Rev.* **2000**, *100*, 1605–1644.
[5] a) D. Zare, B. Doistau, H. Nozary, C. Besnard, L. Guenee, Y. Suffren, A. L. Pele, A. Hauser, C. Piguet, *Dalton Trans.* **2017**, *46*, 8992–9009; b) R. L. Greenaway, V. Santolini, M. J. Bennison, B. M. Alston, C. J. Pugh, M. A. Little, M. Miklitz, E. G. B. Eden-Rump, R. Clowes, A. Shakil, H. J. Cuthbertson, H. Armstrong, M. E. Briggs, K. E. Jelfs, A. I. Cooper, *Nat. Commun.* **2018**, *9*, 2849; c) R. J. Marshall, T. Richards, C. L. Hobday, C. F. Murphie, C. Wilson, S. A. Moggach, T. D. Bennett, R. S. Forgan, *Dalton Trans.* **2016**, *45*, 4132–4135; d) S. Ø. Scottwell, A. B. S. Elliott, K. J. Shaffer, A. Nafady, C. J. McAdam, K. C. Gordon, J. D. Crowley, *Chem. Commun.* **2015**, *51*, 8161–8164; e) S. M. Kopp, H. Gotfredsen, J.-R. Deng, T. D. W. Claridge, H. L. Anderson, *J. Am. Chem. Soc.* **2020**, *142*, 19393–19401; f) M. Lehr, T. Paschelke, E. Trumpf, A. M. Vogt, C. Näther, F. D. Sönnichsen, A. J. McConnell, *Angew. Chem. Int. Ed.* **2020**, *59*, 19344–19351; g) P. Liao, B. W. Langloss, A. M. Johnson, E. R. Knudsen, F. S. Tham, R. R. Julian, R. J. Hooley, *Chem. Commun.* **2010**, *46*, 4932–4934; h) P. Bonakdarzadeh, F. F. Pan, E. Kalenius, O. Jurcek, K. Rissanen, *Angew. Chem. Int. Ed.* **2015**, *54*, 14890–14893; *Angew. Chem.* **2015**, *127*, 15103–15106; i) S. M. Jansze, K. Severin, *J. Am. Chem. Soc.* **2019**, *141*, 815–819; j) M. Kaseborn, J. J. Holstein, G. H. Clever, A. Lutzen, *Angew. Chem. Int. Ed.* **2018**, *57*, 12171–12175; k) R. A. Bilbeisi, J. K. Clegg, N. Elgrishi, X. de Hatten, M. Devillard, B. Breiner, P. Mal, J. R. Nitschke, *J. Am. Chem. Soc.* **2012**, *134*, 5110–5119; l) Y. Domoto, M. Abe, T. Kikuchi, M. Fujita, *Angew. Chem. Int. Ed.* **2020**, *59*, 3450–3454; m) J. E. M. Lewis, A. Tarzia, A. J. P. White, K. E. Jelfs, *Chem. Sci.* **2020**, *11*, 677–683.
[6] a) V. Vij, V. Bhalla, M. Kumar, *Chem. Rev.* **2016**, *116*, 9565–9627; b) S. Suzuki, Y. Segawa, K. Itami, J. Yamaguchi, *Nat. Chem.* **2015**, *7*, 227–233.
[7] O. Shynkaruk, Y. Y. Qi, A. Cottrell-Callbeck, W. T. Delgado, R. McDonald, M. J. Ferguson, G. He, E. Rivard, *Organometallics* **2016**, *35*, 2232–2241.
[8] G. He, B. D. Wiltshire, P. Choi, A. Savin, S. Sun, A. Mohammadpour, M. J. Ferguson, R. McDonald, S. Farsinezhad, A. Brown, K. Shankar, E. Rivard, *Chem. Commun.* **2015**, *51*, 5444–5447.
[9] a) C. Glaser, *Ber. Dtsch. Chem. Ges.* **1869**, *2*, 422–424; b) A. S. Hay, *J. Org. Chem.* **1960**, *25*, 1275–1276; c) A. S. Hay, *J. Org. Chem.* **1962**, *27*, 3320–3321.
[10] A. Elangovan, Y. H. Wang, T. I. Ho, *Org. Lett.* **2003**, *5*, 1841–1844.

[11] a) C.-J. Li, D.-L. Chen, C. W. Costello, *Org. Process Res. Dev.* **1997**, *1*, 325–327; b) M. Iyoda, A. Vorasingha, Y. Kuwatani, M. Yoshida, *Tetrahedron Lett.* **1998**, *39*, 4701–4704; c) S. Krompiec, M. Filapek, I. Grudzka-Flak, A. Slodek, S. Kula, J. G. Malecki, J. Malarz, G. Szafraniec-Gorol, M. Penkala, E. Schab-Balcerzak, M. Paluch, M. Mierzwa, M. Matussek, A. Szlapa, M. Pajak, D. Blach, B. Marcol, W. Danikiewicz, B. Boharewicz, A. Iwan, *Molecules* **2015**, *20*, 4565–4593.
[12] W. Zhang, H. Wu, Z. Liu, P. Zhong, L. Zhang, X. Huang, J. Cheng, *Chem. Commun.* **2006**, 4826–4828.
[13] J. Moon, M. Jeong, H. Nam, J. Ju, J. H. Moon, H. M. Jung, S. Lee, *Org. Lett.* **2008**, *10*, 945–948.
[14] a) M. J. Mio, L. C. Kopel, J. B. Braun, T. L. Gadzikwa, K. L. Hull, R. G. Brisbois, C. J. Markworth, P. A. Grieco, *Org. Lett.* **2002**, *4*, 3199–3202; b) J. Gil-Molto, C. Najera, *Adv. Synth. Catal.* **2006**, *348*, 1874–1882; c) S. Z. Qiu, C. Y. Zhang, R. Qiu, G. D. Yin, J. K. Huang, *Adv. Synth. Catal.* **2018**, *360*, 313–321.
[15] a) A. Mori, J. Kawashima, T. Shimada, M. Suguro, K. Hirabayashi, Y. Nishihara, *Org. Lett.* **2000**, *2*, 2935–2937; b) Y. Liang, Y. X. Xie, J. H. Li, *J. Org. Chem.* **2006**, *71*, 379–381; c) G. Hamasaka, D. Roy, A. Tazawa, Y. Uozumi, *ACS Catal.* **2019**, *9*, 11640–11646; d) B. Jin, F. Gallou, J. Reilly, B. H. Lipshutz, *Chem. Sci.* **2019**, *10*, 3481–3485; e) S. Handa, J. D. Smith, Y. Zhang, B. S. Takale, F. Gallou, B. H. Lipshutz, *Org. Lett.* **2018**, *20*, 542–545; f) Q. Chen, F. Gao, H. Tang, M. Yao, Q. Zhao, Y. Shi, Y. Dang, C. Cao, *ACS Catal.* **2019**, *9*, 3730–3736.
[16] a) V. Grosshenny, R. Ziessel, *Tetrahedron Lett.* **1992**, *33*, 8075–8078; b) M. Kim, C. H. Kang, S. Hong, W. Y. Lee, B. H. Kim, *Inorg. Chim. Acta* **2013**, *395*, 145–150; c) V. Grosshenny, F. M. Romero, R. Ziessel, *J. Org. Chem.* **1997**, *62*, 1491–1500.
[17] R. W. Friesen, E. M. D. Allouche, in *Encyclopedia of Reagents for Organic Synthesis*, **2017**, pp. 1–7.
[18] a) S. Ladouceur, A. M. Soliman, E. Zysman-Colman, *Synthesis* **2011**, 3604–3611; b) A. M. Soliman, D. Fortin, P. D. Harvey, E. Zysman-Colman, *Chem. Commun.* **2012**, *48*, 1120–1122.
[19] Due to precipitation of the ligand from the reaction mixture, these ligands could be isolated without the need for purification by column chromatography.
[20] M. Kuss-Petermann, O. S. Wenger, *J. Phys. Chem. A* **2013**, *117*, 5726–5733.
[21] J. Jia, C. Jiang, X. Zhang, Y. Jiang, D. Ma, *Tetrahedron Lett.* **2011**, *52*, 5593–5595.
[22] M. Lin, Q. Tang, H. Zeng, G. Xing, Q. Ling, *Russ. J. Gen. Chem.* **2016**, *86*, 1747–1752.

Manuscript received: March 5, 2021
Revised manuscript received: March 5, 2021
Accepted manuscript online: March 9, 2021

3.1.3 Article: Tuning the Spin-Crossover Properties of $Fe^{II}_4L_6$ Cages via the Interplay of Coordination Motif and Linker Modifications

Tobias Paschelke, Eicke Trumpf, David Grantz, Malte Pankau, Niclas Grocholski, Christian Näther, Frank D. Sönnichsen, Anna J. McConnell

Dalton Trans. **2023**, *52*, 12789-12795.

doi.org/10.1039/d3dt01569f

The first systematic study about the influence of ligand modifications (coordination motif and linker) on the thermal spin-crossover properties of metal-organic cages is reported. Over the course of this study one 2-(2'-pyridyl)-1*H*-imidazole-based and ten 2-(2'-pyridyl)-1*H*-benzimidazole-based ligands modified with differing binding motifs, linker and substituents were synthesised. The ligands were self-assembled with $Fe(OTf)_2$ in CD_3CN under anhydrous and air-free conditions to yield eleven edge-bridged Fe_4L_6 cages, as confirmed by NMR spectroscopy, ESI-MS and X-ray crystallography (cages **5** & **7**). By using the ideal solution model based on the temperature-dependent chemical shift change,[186] cages **1**-**11** were studied over the range of 248 K to 348 K in solution.
The change of the 2-(2'-pyridyl)-1*H*-imidazole binding motif in low-spin cage **1** to the 2-(2'-pyridyl)-1*H*-benzimidazole backbone gave more high-spin state stabilised Fe_4L_6 cages **3** and **6**. In addition, the temperature-dependent chemical shift changes were larger for *N*-methylated cage **3** than for *N*-benzylated cage **6**. This trend was also observed by changing the alkyne linker with either no linker or a phenylene spacer, where the *N*-methylation led to more stabilised high-spin species (cages **5** & **7**) in comparison to its *N*-benzylated analogues (cages **2** & **4**). Unfortunately, no spin-crossover temperatures ($T_{1/2}$) for cages **1**-**5** were calculable due to too small chemical shift changes. The influence of the linker exchange onto $T_{1/2}$ was determined based on the *N*-methylated cages **5**-**7** (401 K (**6**) vs. 430 K (**7**) vs >430 K (**5**)).
Further optimisations focused on the decrease of $T_{1/2}$. In the first comparison, cage **6** ($T_{1/2}$ = 401 K) was modified by the introduction of electron-donating CH_3 groups onto the *p*-pyridine position. Due to the electronic effect of the CH_3 group the more high-spin stabilised cage **10** ($T_{1/2}$ = 353 K, ΔT = 48 K) was obtained. In a separate study the steric influence of substituents was analysed. F/CH_3 substituents were introduced onto the phenylene spacer of cage **7** (R = H, $T_{1/2}$ = 430 K), resulting in a $T_{1/2}$ decrease of 55 K (cage **8**, R = F, 375 K) and 91 K (cage **9**, R = CH_3, 339 K). The decrease was assumed to be mainly caused by altered dihedral angles between the aryl systems with a small electronic influence of the substituents. In the last study CH_3 groups were implemented in the *p*-pyridine positions of cage **7** (($T_{1/2}$ = 430 K)) leading to a lowered $T_{1/2}$ of 186 K for cage **11** ($T_{1/2}$ = 244 K). This study

demonstrates factors that influence the spin-crossover properties of thermal metal-organic cages to advance the development of spin-crossover cages with predictable properties.

Contribution: Synthesis and full characterisation (NMR spectroscopy + EI/ESI-MS) of compounds **1**-**5**, **6** (re-made), **7**-**11**, **15**-**19**, **20**-**23**, **25**-**32**, **34**, **36**-**40a/40b**, **43a/43b**; optimisation of reaction conditions for compounds **12**-**14**, **24**; planning and performing crystal growth experiments for cages **5** and **7**; data collection, calculations and evaluation of all spin-crossover studies (including Evans method attempt, excluding VT-NMR experiment for cage **44**); planning and performing anion binding studies; preparation & revision of the manuscript and supporting information

Dalton Transactions

ROYAL SOCIETY OF CHEMISTRY

PAPER

View Article Online
View Journal | View Issue

Cite this: *Dalton Trans.*, 2023, **52**, 12789

Tuning the spin-crossover properties of $Fe^{II}_4L_6$ cages *via* the interplay of coordination motif and linker modifications†

Tobias Paschelke,[a] Eicke Trumpf,[a] David Grantz,[a] Malte Pankau,[a] Niclas Grocholski,[a] Christian Näther,[b] Frank D. Sönnichsen[a] and Anna J. McConnell *‡[a]

Received 24th May 2023,
Accepted 27th July 2023

DOI: 10.1039/d3dt01569f

rsc.li/dalton

Despite the increasing number of spin-crossover Fe^{II}-based cages, the interplay between ligand modifications (*e.g.* coordination motif substituents and linker) is not well-understood in these multinuclear systems, limiting rational design. Here, we report a family of $Fe^{II}_4L_6$ spin-crossover cages based on 2,2′-pyridylbenzimidazoles where subtle ligand modifications lowered the spin crossover temperature in CD_3CN by up to 186 K. Comparing pairs of cages, CH_3 substituents on either the coordination motif or phenylene linker lowered the spin-crossover temperature by 48 K, 91 K or 186 K, attributed to electronic effects, steric effects and a combination of both, respectively. The understanding of the interplay between ligand modifications gained from this study could be harnessed on the path towards the improved rational design of spin-crossover cages.

Introduction

Most known spin-crossover complexes are based on Fe^{II} ions.[1–5] These complexes can be switched between paramagnetic high- and diamagnetic low-spin states by external stimuli like light,[6–12] pressure[6,13,14] or temperature[6,10,15–20] if their spin-pairing and ligand field splitting energies are similar.[2,3,21] Despite extensive studies, there are still limitations to the prediction of spin-crossover properties[22] but methods have been established for predicting the spin state[23,24] and tuning the spin-crossover properties.[9,25] For example, steric bulk proximal to the coordination site is known to stabilize the high-spin state through lengthening the metal–ligands bonds.[26,27] However, rationalisation of electronic effects on the spin-crossover temperature ($T_{1/2}$) is more difficult, especially since most studies were performed in the solid state where intermolecular interactions also need to be considered.[18,28] Halcrow's systematic solution study on 2,6-di(pyrazol-1-yl)pyridine-based complexes revealed that electron-donating *p*-pyridine substituents lower $T_{1/2}$ while *m*-pyrazole substituents raise it,[18] attributed to differing σ and π bonding contributions.[18,28]

Spin-crossover cages[29–39] consist of multiple Fe^{II} ions and organic ligands with two or more coordination motifs connected *via* linkers. They are an interesting emerging class of spin-crossover materials[2,3] since multiple avenues exist for tuning the spin-crossover properties. These include modifications to the coordination motif,[31,36] guest encapsulation,[30,33,35] linker modifications[30] and cooperative effects. Furthermore, the potential to access multiple spin-states with distinct optical and magnetic properties makes cages appealing for applications as sensors, electronic switches and in information storage.[1–5]

However, spin-crossover cage examples, especially those studied in solution,[29,30,33,36,38] are limited and they are usually comprising imidazolimine ligands that form cubic[33,35,36,38,39] or tetrahedral[29–32,38] cages. The rational design of a cage with predictable spin-crossover properties is also challenging and the effect of modifications to the coordination motif and linker has not been extensively studied in Fe^{II}-based cages.

Motivated to improve the rational design of spin-crossover cages, we studied a family of $Fe^{II}_4L_6$ cages (**1–11**, Fig. 1) and varied the coordination motif and linker to determine their influence on $T_{1/2}$. These subtle ligand modifications tuned the $T_{1/2}$ values, determined using the ideal solution model, from >430 K to 244 K in CD_3CN; $T_{1/2}$ decreased by 48 K from introducing CH_3 groups on the pyridine motifs (cage **6** *vs.* **10**), 91 K from increasing the steric bulk of the linker with CH_3

[a]*Otto Diels Institute of Organic Chemistry, Kiel University, Otto-Hahn-Platz 4, Kiel 24098, Germany*
[b]*Institute of Inorganic Chemistry, Kiel University, Max-Eyth-Straße 2, Kiel 24118, Germany*

†Electronic supplementary information (ESI) available. CCDC 2207255 (for **18**), 2207256 (for cage **5**) and 2207257 (for cage **7**). For ESI and crystallographic data in CIF or other electronic format see DOI: https://doi.org/10.1039/d3dt01569f

‡Current address: Department of Chemistry and Biology, University of Siegen, Adolf-Reichwein-Strasse 2, Siegen 57068, Germany. E-mail: anna.mcconnell@uni-siegen.de

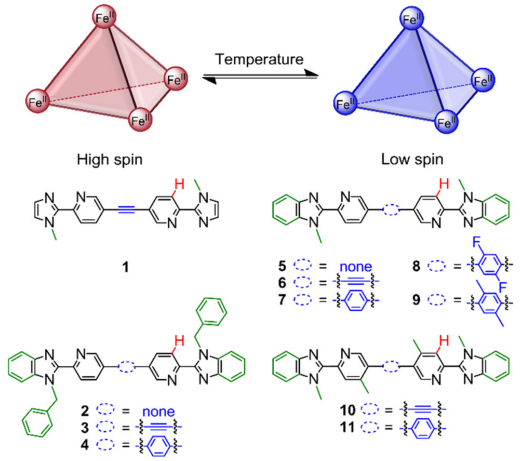

Fig. 1 $Fe^{II}_4L_6$ cages **1–11** for investigating the effect of ligand modifications within the coordination motif (represented by the changes in green) and linker (represented in blue) on the spin-crossover properties. The chemical shift changes of the proton in red were used for fitting to the ideal solution model.

groups (cage **7** *vs.* **9**) and 186 K for a combination of electronic and steric effects (cage **7** *vs.* **11**).

Results and discussion

Complexes and helicates based on 2,2′-pyridyl(benz)imidazole ligands exhibit a range of ligand field strengths, resulting in low-spin[40] complexes and those showing spin-crossover[41,42] depending on the ligand substitution. We decided to focus on $Fe^{II}_4L_6$ cages to probe the interplay of coordination site modifications and linker on $T_{1/2}$ since: (i) there are relatively few spin-crossover examples;[31,34,37] (ii) a variety of linkers can be introduced into the bis-bidentate ligand design with relative synthetic ease; (iii) the guest binding (*e.g.* solvent or counteranion) influence on $T_{1/2}$ is likely minimised by the more open faces of the cages as compared to the more enclosed faces of an $Fe^{II}_4L_4$ cage. The studies were performed in solution rather than the solid state to disentangle these intramolecular ligand field strength changes from intermolecular interactions. Furthermore, the structure and spin-state changes of individual species with temperature could be probed by NMR spectroscopy.

A family of $Fe^{II}_4L_6$ cages was designed based on four related coordination motifs with the modifications highlighted in green (Fig. 1): (i) imidazole-based **1** and benzimidazole-based (ii) **2–4** with *N*-benzyl substituents; (iii) **5–9** with *N*-methyl substituents; (iv) **10–11** with *N*-methyl substituents and CH_3 groups on the pyridine ring. Furthermore, the linker (Fig. 1, blue) was also varied from no spacer to an alkyne and phenylene derivatives. Edge-bridged $Fe^{II}_4L_6$ cages **1–11** (ESI, section 4†) were self-assembled at room temperature in anhydrous acetonitrile in a glovebox using four equivalents of $Fe(OTf)_2$ and six equivalents of the appropriate ligand (preparations in ESI, section 2† using our recently reported one-pot Sonogashira-type procedure[43] or *via* Suzuki couplings). The corresponding $Zn^{II}_4L_6$ cages were also prepared using $Zn(OTf)_2$ to serve as diamagnetic analogues. However, a discrete cage species did not form with the imidazole ligand (ESI, section 3.1†).

The formation of M_4L_6 cages was confirmed by ESI mass spectrometry, the observation of one set of signals in the NMR spectra and in the case of cages **5** and **7**, by X-ray crystallography (Fig. 2 and ESI, section 6†). Although the diffraction data were of limited quality due to poor diffraction and disorder, as is commonly observed for metallosupramolecular cages,[44] they were sufficient to establish the cages' connectivity. In both cages, an *anti* ligand conformation was adopted resulting in a *T*-symmetric cage with the same stereochemistry at each metal center (Fig. 2). Cage **5** was also observed to bind a triflate counterion in its cavity.

While the $Fe^{II}_4L_6$ cages were obtained as the only species, a second minor species was also observed in some self-assemblies with Zn^{II} (ESI, sections 3.7, 3.8 and 3.10†). Analysis by ^1H and DOSY NMR spectroscopy and ESI mass spectrometry revealed the formation of Zn_2L_3 helicates. Lusby and coworkers have reported a helicate/tetrahedron equilibrium with the Co(II) and Co(III) analogues of cage **7**.[45] We attribute the formation of Zn_2L_3 but not Fe_2L_3 helicates to a combination of the metal's ionic radius and ligand's steric bulk increasing the energy of the Fe_2L_3 relative to the Fe_4L_6 self-assembly, as has been observed in related systems.[46,47]

The spin-crossover properties of cages **1–11** were investigated in solution between 248 K and 348 K in CD_3CN. While the Evans method[48] can determine the magnetic susceptibility from variable-temperature (VT) NMR experiments, preliminary

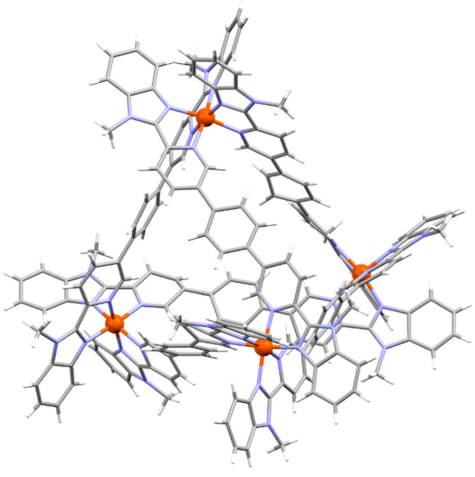

Fig. 2 X-ray crystal structure of cage **7**.

studies with cage **6** showed the NMR signals shifted upon addition of the *p*-xylene standard, suggesting possible guest binding (Fig. S239†). In addition, the magnetic susceptibility is dependent on accurate determination of the paramagnetic species concentration and influenced by the presence of other paramagnetic species, leading to large sources of error and inaccurate $T_{1/2}$ values.[49] Therefore, the ideal solution model[50] was used since the spin-crossover properties of a single species can be determined even in the presence of other paramagnetic impurities. In addition, our recent report of a paramagnetic NMR toolbox would enable the detailed characterisation of the cages in the high-spin state.[51] The chemical shift change of proton H (Fig. 1, red) was fitted using Origin (eqn (1)) to obtain ΔH, ΔS and $T_{1/2}$ values.§

$$\delta = \delta_{LS} + \frac{C}{T + T \cdot \exp\left(\frac{\Delta H - T\Delta S}{RT}\right)} \quad (1)$$

Only small chemical shift changes were observed for cages **1** and **2**, indicating that these cages are predominantly low spin over the measured temperature range (Fig. 3). For the other cages, initial fitting of all four parameters (C, ΔH, ΔS, δ_{LS}) resulted in large errors or the fitting did not converge (ESI, section 5†). Therefore, δ_{LS} was fixed to the chemical shift of the diamagnetic $Zn^{II}_4L_6$ cage analogue, yielding ΔH, ΔS and $T_{1/2}$ values for cages **6–11** (Table 1). The fitting for cages **3–5** still did not converge, likely attributable to an insufficient change in the spin-state populations within the temperature range available for the solvent CD_3CN.¶ Since cages **1–7** were predominantly low spin at 248 K, the magnitude of $\Delta\delta$ was used as a measure for $T_{1/2}$ in comparisons between cages where thermodynamic data could not be obtained.

One influence of the coordination motif on the spin-state can be delineated by comparing cages **1**, **3** and **6** (Fig. 3a). The increased $\Delta\delta$ values for benzimidazole-based cages **3** and **6** *vs.* diamagnetic imidazole-based cage **1** indicated the stabilization of the high-spin state, attributed to lengthening of the M–L bonds by the benzimidazole's steric bulk in **3** and **6** (Table 1).[40]

For benzimidazole-based cages **2–7** (Fig. 3b), the effect of *N*-benzylation was compared to *N*-methylation for three different linkers (alkyne, phenylene or no linker). Comparing cages with the same linker (*e.g.* **2** and **5**), larger $\Delta\delta$ values were observed for the *N*-methylated cages **5–7** than the *N*-benzylated analogues **2–4**, suggesting cages **5–7** have lower $T_{1/2}$ values.

§This proton was chosen to allow comparison over the family of cages and for its proximity to the paramagnetic Fe^{II} centres, resulting in large chemical shift changes without significant line broadening (relative to other protons) over the temperature range. For cages **9** and **11**, similar $T_{1/2}$ values were determined from fitting the chemical shift data for other protons close to the metal centre (ESI, sections 5.11 & 5.13†).

¶In the Evans method, it is often possible to obtain $T_{1/2}$ values from data where there is a relatively small change of the spin-state fraction within the measured temperature range. This is because the maximum $\chi_m T$ value can be fixed to values reported in the literature for Fe(II) complexes during the fitting to the regular solution model. This is not possible in fitting data to the ideal solution model since the chemical shift of the high spin state (δ_{HS}) is not known.

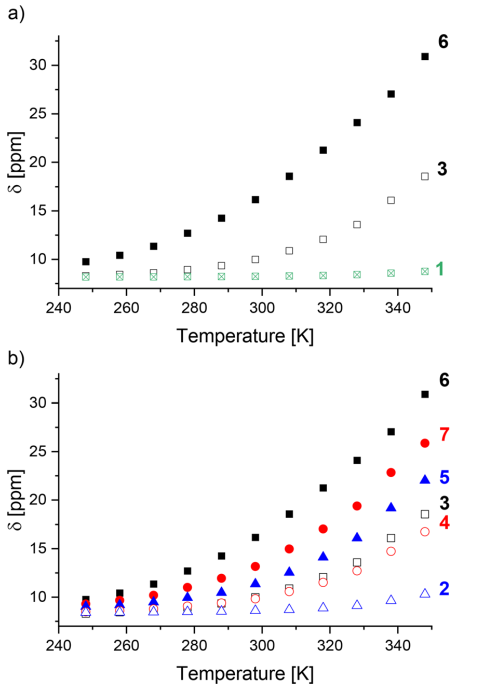

Fig. 3 Comparison of the chemical shift changes between 248 K and 348 K for cages: (a) **1**, **3** and **6**; (b) **2–7**. The symbol shading represents the change to the coordination motif: imidazole (⊠); *N*-benzylated benzimidazole (unfilled); *N*-methylated benzimidazole (filled). The symbol color and shape represent the linker: alkyne linker (black square); phenylene linker (red circle); no linker (blue triangle).

Table 1 Chemical shift changes and thermodynamic data from variable temperature NMR experiments

Cage	$\Delta\delta^a$ (ppm)	ΔH (kJ mol^{-1})	ΔS (J mol^{-1} K^{-1})	$T_{1/2}$ (K)
1	0.58	*c*	*c*	*c*
2	1.89	*b*	*b*	*d*
3	10.2	*b*	*b*	*d*
4	8.26	*b*	*b*	*d*
5	13.0	*b*	*b*	*d*
6	21.1	24.46 ± 0.58	60.94 ± 3.00	401
7	17.7	27.71 ± 0.91	64.48 ± 5.78	430
8	30.1	27.22 ± 0.93	72.61 ± 4.00	375
9	31.4	21.79 ± 0.48	64.32 ± 2.00	339
10	27.8	27.44 ± 1.12	77.65 ± 4.40	353
11	12.5	20.78 ± 0.22	85.05 ± 0.93	244

[a] Based on the chemical shift change of proton H (red, Fig. 1) between 248 K and 348 K. [b] Could not be determined since fitting did not converge. [c] Low spin cage. [d] Proposed to be >430 K.

The linker's influence on the spin-crossover properties was also investigated. For both the *N*-methylated (**5–7**) and *N*-benzylated series (**2–4**), the largest $\Delta\delta$ values were observed for an alkyne followed by the phenylene and no linker

(Table 1). This was also reflected by the increasing $T_{1/2}$ values for the *N*-methylated cages: 401 K for cage **6** (alkyne linker), 430 K for cage **7** (phenylene linker) and >430 K for cage **5** (no linker).

Different factors were considered to explain the influence of the linker on $T_{1/2}$. First, the electronic effect of the linker was estimated using the Hammett parameter σ_m for C≡CH (0.21), C_6H_5 (0.06) and 3-pyridine (0.23).[52] However, their trend does not correlate with the observed $T_{1/2}$ trend. The Hammett parameters do not take into account electronic effects from metal complexation and these will be particularly significant for the cages without a linker as the 3-pyridine is part of the coordination motif.

The ligand conformation and mechanical coupling between the Fe^{II} centers could also play a role since the linkers' steric bulk dictates twisting within the ligand in order to adopt the required *anti* ligand conformation. Dihedral angles of approx. 10–22° for the phenylene linker and 50–65° for no linker were observed in the X-ray structures of cages **5**, **7** and related cages.[45,53] No cooperativity and weaker mechanical coupling is likely in cages with alkyne and phenylene linkers (**3**–**4**, **6**–**7**) given the large Fe^{II}–Fe^{II} distances (>13 Å in cage **7**) and ligand twisting, thus making spin-crossover more favorable.[38] In contrast, cages with no linkers (**2**, **5**) likely exhibit stronger mechanical coupling and cooperative effects cannot be excluded.

Finally, the cavity size as dictated by the ligand length could also influence $T_{1/2}$ *via* host–guest chemistry. While the same counteranion OTf^- was used for all cages to minimize guest binding effects, the smallest cages **3** and **5** were observed to bind the counterion in slow exchange by ^{19}F NMR spectroscopy (Fig. S174 and S195†) and in the case of **5**, in the X-ray crystal structure (Fig. S293†).

While these different factors were considered, it was not possible to rationalize the observed $T_{1/2}$ trend as a function of the linker. Therefore, to gain further insight into coordination site and linker modifications on $T_{1/2}$, sets of cages (**6** and **10**, **7**–**9**, **7** and **11**) with the same ligand scaffold but minor modifications (*e.g.* a F or CH_3 substituent) were compared. Given the larger size of cages **7**–**11** and the observation of fast exchange of the counterion OTf^- in the ^{19}F NMR spectra at room temperature (Fig. S208, S215, S223, S230 and S236†), it was hypothesised that ligand field strength effects would dominate over solvent, guest binding and ion-pairing effects enabling the determination of trends based on steric and electronic effects.

As a control, anion binding experiments (ESI, section 7†) were carried out with cages **7** and **11** since this set of cages displayed the largest $T_{1/2}$ change within this study (Table 1). To probe guest binding within the cavity, 8 equivalents (relative to the cage) of the smaller counterion BF_4^- were added to each cage and the broad ^{19}F signals for BF_4^- indicated fast guest exchange (Fig. S296 and S299†). Small chemical shift changes ($\Delta\delta$ < 0.2 ppm) were observed in the ^1H NMR spectra and the insignificant changes of the phenylene protons ($\Delta\delta$ < 0.05 ppm) suggested counteranion binding in the cavity has a minimal effect (Fig. S295 and S297†).

Further experiments with cage **7** focused on ion-pairing. NTf_2^- was chosen as a counterion since the sharp signal in the ^{19}F NMR spectrum suggested that it is too large to fit in the cavity (Fig. S303†). Again, small ^1H chemical shift changes were observed, meaning ion-pairing likely has an insignificant effect on $T_{1/2}$. Finally, VT NMR experiments with cages **7** and **11** in the presence and absence of competing counteranions showed no evidence of a change from fast to slow counteranion exchange upon cooling to 248 K due to increased population of the low spin state with a smaller cavity (Fig. S297–S304†). Based on these control experiment results, the effect of ion-pairing or guest binding on the spin-crossover properties is proposed to be negligible for comparisons within a set of cages.

Cages **7**–**9** were compared where F or CH_3 substituents were introduced on the phenylene linker to increase the steric bulk without changing the ligand length. $T_{1/2}$ decreased from 430 K (cage **7**) to 375 K for cage **8** with F substituents and to 339 K for cage **9** with CH_3 substituents (Table 1). While the high-spin fraction of cage **7** at 298 K is 3%, increasing high-spin-state populations of 10% and 26% were obtained for cages **8**–**9**, respectively (Fig. 4). Thus, $T_{1/2}$ decreases with increasing substituent size on the linker, attributed to increased dihedral angles between the coordination motif and the linker, as observed in crystal structures of related cages.[45] However, contributions from electronic effects cannot be completely neglected since CH_3 groups are electron-donating, while F is electron-withdrawing.

Thermodynamic data analysis revealed cages **7** and **8** have similar enthalpies but cage **8** has an increased entropy (Table 1). In contrast, cage **9** had a lower enthalpy compared to cage **7**, but the entropy values were similar. Thus, the spin-transition of cage **9** is enthalpically driven, while for cage **8** it is entropically controlled. It is difficult to draw conclusions from these data since the relationship between both energies

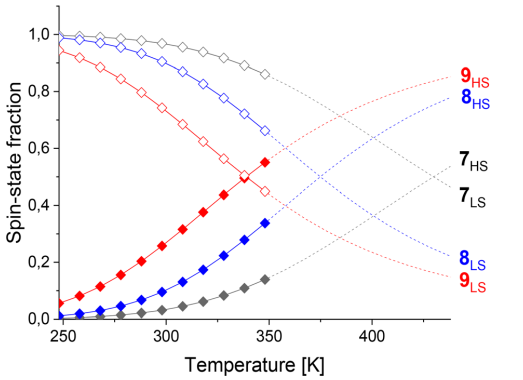

Fig. 4 High (filled diamonds) and low (unfilled diamonds) spin-state fractions of cages **7** (black), **8** (blue) and **9** (red) from VT NMR measurements between 248 K and 348 K. Data above 348 K (dashed lines) was extrapolated.

on spin-crossover properties has not been systematically studied.[54] However, we attribute stabilization of the high-spin state for cage **9** *vs.* cage **7** to the increased dihedral angles from the steric bulk of the CH_3 groups and the required adoption of an *anti*-conformation, leading to weakened M–L bonds. Thus, modifications through CH_3 substituents on the phenylene linker tuned $T_{1/2}$ by 91 K.

Further coordination site modifications were introduced to investigate the influence of interactions between these and the linker on $T_{1/2}$. For example, Halcrow and co-workers have shown that electron-donating groups on *para*-substituted pyridines in Fe^{II} mononuclear complexes based on 2,6-bis(pyrazol-1-yl)pyridines can stabilize the high-spin state.[18] Therefore, CH_3 groups were introduced on the pyridine motif in cages **10** and **11** in an attempt to decrease $T_{1/2}$ towards room temperature. Comparing cages **6** and **10**, the introduction of the CH_3 groups decreased $T_{1/2}$ from 401 K to 353 K (Table 1), resulting in an increase of the high-spin state fraction at 298 K from 7% to 15% (Fig. 5). We propose the stabilization of the high-spin state by 48 K is largely due to electronic effects since steric effects from the alkyne linker are minimized.

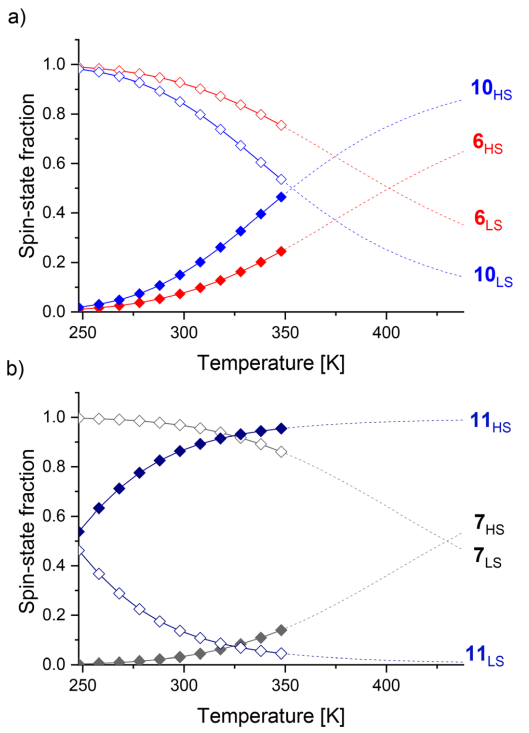

Fig. 5 High (filled diamonds) and low (unfilled diamonds) spin-state fractions of cages: (a) **6** (red) and **10** (blue); (b) **7** (grey) and **11** (blue) from VT NMR measurements between 248 K and 348 K. Data above 348 K (dashed lines) was extrapolated.

Surprisingly, $T_{1/2}$ decreased by 186 K from 430 K to 244 K for cage **7** *vs.* **11** (Table 1). The introduction of a CH_3 group in cage **11** yields a largely high-spin cage (86% high-spin state fraction) at 298 K, while cage **7** is almost completely low-spin (3% high-spin state fraction) (Fig. 5). We attribute this large change to electronic effects, and moreover, to strong steric clashes between the CH_3 substituents and the phenylene linker in cage **11**, increasing the dihedral angles between the linker and the pyridine rings as observed in crystal structures of related cages.[55] Comparing thermodynamic data (Table 1), both the enthalpy and entropy increased for cage **10** *vs.* **6**. Although the increased entropy favors the high-spin state, this is partly counteracted by the increased enthalpy stabilizing the low-spin state, resulting in a smaller $T_{1/2}$ difference. In contrast, the decrease of the enthalpy and increase of the entropy for cage **11** *vs.* **7** both favor the high-spin state, leading to the larger $T_{1/2}$ change of 186 K.

Conclusions

This study demonstrates the power of solution-based spin-crossover studies using the ideal solution model for quantifying ligand field strength modifications in the absence of intermolecular interactions, as exemplified in this family of $Fe^{II}_4L_6$ cages. Furthermore, information about the cage's structure and spin-state can be obtained from VT NMR experiments independently of other paramagnetic species.

Imidazole-based cage **1** was low-spin over the measured temperature range. However, the steric bulk of the benzimidazole motif in cages **2–11** stabilized the high-spin state.

While substitution of the coordination motif is known to influence $T_{1/2}$ in spin-crossover complexes, this systematic study reveals that the linker can also have a profound effect, despite the increased distance from the metal centers. Importantly, the interplay of coordination site and linker modification effects was quantified and minor modifications like the introduction of CH_3 groups tuned $T_{1/2}$ by up to 186 K. *p*-CH_3 substituents on the pyridine motif decreased $T_{1/2}$ by 48 K for cage **10** *vs.* **6** with alkyne linkers, attributed to predominantly electronic effects. CH_3 substituents on the phenylene linker decreased $T_{1/2}$ by 91 K for cage **9** *vs.* **7**, largely attributed to steric clashes. Finally, a combination of both effects is proposed to result in the 186 K $T_{1/2}$ decrease in cage **11** *vs.* **7** due to both electronic effects from the *p*-CH_3 substituents on the pyridine and a steric clash with the phenylene linker.

Thus, this study demonstrates how seemingly subtle modifications (*i.e.* substitution of H for CH_3) can significantly impact the spin-crossover properties of multinuclear Fe^{II}-based cages in solution, resulting in large $T_{1/2}$ changes of almost 200 K and altering the spin state from predominantly low spin to high spin at room temperature. Future work will investigate how this understanding of the interplay between ligand modifications can be applied to the design of spin-crossover cages with more predictable spin-crossover pro-

perties. This would facilitate the tailored application of spin-crossover cages, *e.g.* as sensors.

Author contributions

T. P.: conceptualisation (lead), data curation (lead), formal analysis (lead), investigation (lead), resources (lead), supervision (supporting), visualisation (lead), writing-original draft (lead), writing-review and editing (equal). E. T.: conceptualisation (lead), formal analysis (supporting), investigation (supporting), resources (supporting), visualisation (lead), writing-original draft (supporting), writing-review and editing (equal). D. G.: formal analysis (supporting), investigation (supporting), resources (supporting), writing-review and editing (supporting). M. P.: formal analysis (supporting), investigation (supporting), resources (supporting), visualisation (supporting), writing-review and editing (supporting). N. G.: formal analysis (supporting), investigation (supporting), resources (supporting), writing-review and editing (supporting). C. N.: formal analysis (supporting), investigation (supporting), resources (supporting), writing-review and editing (supporting). F. D. S.: investigation (supporting), methodology (lead), resources (supporting), writing-review and editing (equal). A. J. M.: conceptualisation (lead), formal analysis (supporting), funding acquisition (lead), project administration (lead), supervision (lead), writing-original draft (supporting), writing-review and editing (equal).

Conflicts of interest

There are no conflicts to declare.

Acknowledgements

We thank the Deutsche Forschungsgemeinschaft (DFG, project number 429518153) for financial support. We thank Etienne Rommens for preliminary studies and the spectroscopy department (including Marion Höftmann and Gitta Kohlmeyer-Yilmaz for VT NMR measurements and Johanna Baum and Dr Claus Bier for high-resolution ESI measurements) for NMR and mass spectral data collection. We also thank Prof. Dr Felix Tuczek for useful discussions.

References

1 M. A. Halcrow, *Chem. Soc. Rev.*, 2011, **40**, 4119–4142.
2 A. J. McConnell, *Supramol. Chem.*, 2018, **30**, 858–868.
3 R. W. Hogue, S. Singh and S. Brooker, *Chem. Soc. Rev.*, 2018, **47**, 7303–7338.
4 H. S. Scott, R. W. Staniland and P. E. Kruger, *Coord. Chem. Rev.*, 2018, **362**, 24–43.
5 W. Huang, X. Ma, O. Sato and D. Wu, *Chem. Soc. Rev.*, 2021, **50**, 6832–6870.
6 E. Breuning, M. Ruben, J.-M. Lehn, F. Renz, Y. Garcia, V. Ksenofontov, P. Gütlich, E. Wegelius and K. Rissanen, *Angew. Chem., Int. Ed.*, 2000, **39**, 2504–2507.
7 T. Matsumoto, G. N. Newton, T. Shiga, S. Hayami, Y. Matsui, H. Okamoto, R. Kumai, Y. Murakami and H. Oshio, *Nat. Commun.*, 2014, **5**, 3865.
8 B. Rösner, M. Milek, A. Witt, B. Gobaut, P. Torelli, R. H. Fink and M. M. Khusniyarov, *Angew. Chem., Int. Ed.*, 2015, **54**, 12976–12980.
9 M. Mörtel, A. Witt, F. W. Heinemann, S. Bochmann, J. Bachmann and M. M. Khusniyarov, *Inorg. Chem.*, 2017, **56**, 13174–13186.
10 T. Shiga, G. N. Newton and H. Oshio, *Dalton Trans.*, 2018, **47**, 7384–7394.
11 H.-Y. Sun, Y.-S. Meng and T. Liu, *Chem. Commun.*, 2019, **55**, 8359–8373.
12 M. Oppermann, F. Zinna, J. Lacour and M. Chergui, *Nat. Chem.*, 2022, **14**, 739–745.
13 D. C. Fisher and H. G. Drickamer, *J. Chem. Phys.*, 1971, **54**, 4825–4837.
14 R. J. Butcher, J. R. Ferraro and E. Sinn, *Inorg. Chem.*, 1976, **15**, 2077–2079.
15 J. Elhaïk, V. A. Money, S. A. Barrett, C. A. Kilner, I. R. Evans and M. A. Halcrow, *Dalton Trans.*, 2003, 2053–2060.
16 B. Schneider, S. Demeshko, S. Dechert and F. Meyer, *Angew. Chem., Int. Ed.*, 2010, **49**, 9274–9277.
17 S. Chorazy, R. Podgajny, K. Nakabayashi, J. Stanek, M. Rams, B. Sieklucka and S.-i. Ohkoshi, *Angew. Chem., Int. Ed.*, 2015, **54**, 5093–5097.
18 L. J. K. Cook, R. Kulmaczewski, R. Mohammed, S. Dudley, S. A. Barrett, M. A. Little, R. J. Deeth and M. A. Halcrow, *Angew. Chem., Int. Ed.*, 2016, **55**, 4327–4331.
19 A. A. Pavlov, G. L. Denisov, M. A. Kiskin, Y. V. Nelyubina and V. V. Novikov, *Inorg. Chem.*, 2017, **56**, 14759–14762.
20 S. Chorazy, J. J. Stanek, J. Kobylarczyk, S.-i. Ohkoshi, B. Sieklucka and R. Podgajny, *Dalton Trans.*, 2017, **46**, 8027–8036.
21 C.-M. Jureschi, J. Linares, A. Boulmaali, P. R. Dahoo, A. Rotaru and Y. Garcia, *Sensors*, 2016, **16**, 187.
22 N. Deorukhkar, C. Besnard, L. Guénée and C. Piguet, *Dalton Trans.*, 2021, **50**, 1206–1223.
23 H. Phan, J. J. Hrudka, D. Igimbayeva, L. M. L. Daku and M. Shatruk, *J. Am. Chem. Soc.*, 2017, **139**, 6437–6447.
24 S. Rodríguez-Jiménez, M. Yang, I. Stewart, A. L. Garden and S. Brooker, *J. Am. Chem. Soc.*, 2017, **139**, 18392–18396.
25 D. Y. Aleshin, I. Nikovskiy, V. V. Novikov, A. V. Polezhaev, E. K. Melnikova and Y. V. Nelyubina, *ACS Omega*, 2021, **6**, 33111–33121.
26 H. A. Goodwin, E. S. Kucharski and A. H. White, *Aust. J. Chem.*, 1983, **36**, 1115–1124.
27 C. Bartual-Murgui, S. Vela, M. Darawsheh, R. Diego, S. J. Teat, O. Roubeau and G. Aromí, *Inorg. Chem. Front.*, 2017, **4**, 1374–1383.
28 L. Bondì, A. L. Garden, F. Totti, P. Jerabek and S. Brooker, *Chem. – Eur. J.*, 2022, **28**, e202104314.

29 A. Ferguson, M. A. Squire, D. Siretanu, D. Mitcov, C. Mathonière, R. Clérac and P. E. Kruger, *Chem. Commun.*, 2013, **49**, 1597–1599.
30 R. A. Bilbeisi, S. Zarra, H. L. C. Feltham, D. N. L. Jameson, J. K. Clegg, S. Brooker and J. R. Nitschke, *Chem. – Eur. J.*, 2013, **19**, 8058–8062.
31 D.-H. Ren, D. Qiu, C.-Y. Pang, Z. Li and Z.-G. Gu, *Chem. Commun.*, 2015, **51**, 788–791.
32 L. Li, N. Saigo, Y. Zhang, D. J. Fanna, N. D. Shepherd, J. K. Clegg, R. Zheng, S. Hayami, L. F. Lindoy, J. R. Aldrich-Wright, C.-G. Li, J. K. Reynolds, D. G. Harman and F. Li, *J. Mater. Chem. C*, 2015, **3**, 7878–7882.
33 N. Struch, C. Bannwarth, T. K. Ronson, Y. Lorenz, B. Mienert, N. Wagner, M. Engeser, E. Bill, R. Puttreddy, K. Rissanen, J. Beck, S. Grimme, J. R. Nitschke and A. Lützen, *Angew. Chem., Int. Ed.*, 2017, **56**, 4930–4935.
34 L. Li, A. R. Craze, O. Mustonen, H. Zenno, J. J. Whittaker, S. Hayami, L. F. Lindoy, C. E. Marjo, J. K. Clegg, J. R. Aldrich-Wright and F. Li, *Dalton Trans.*, 2019, **48**, 9935–9938.
35 H.-S. Lu, W.-K. Han, X. Yan, Y.-X. Xu, H.-X. Zhang, T. Li, Y. Gong, Q.-T. Hu and Z.-G. Gu, *Dalton Trans.*, 2020, **49**, 4220–4224.
36 M. Hardy, J. Tessarolo, J. J. Holstein, N. Struch, N. Wagner, R. Weisbarth, M. Engeser, J. Beck, S. Horiuchi, G. H. Clever and A. Lützen, *Angew. Chem., Int. Ed.*, 2021, **60**, 22562–22569.
37 W. Li, C. Liu, J. Kfoury, J. Oláh, K. Robeyns, M. L. Singleton, S. Demeshko, F. Meyer and Y. Garcia, *Chem. Commun.*, 2022, **58**, 11653–11656.
38 J. Zheng, L. K. S. von Krbek, T. K. Ronson and J. R. Nitschke, *Angew. Chem., Int. Ed.*, 2022, **61**, e202212634.
39 H. Min, A. R. Craze, M. J. Wallis, R. Tokunaga, T. Taira, Y. Hirai, M. M. Bhadbhade, D. J. Fanna, C. E. Marjo, S. Hayami, L. F. Lindoy and F. Li, *Chem. – Eur. J.*, 2023, **29**, e202203742.
40 K. H. Sugiyarto and H. A. Goodwin, *Aust. J. Chem.*, 1987, **40**, 775–783.
41 S. G. Telfer, B. Bocquet and A. F. Williams, *Inorg. Chem.*, 2001, **40**, 4818–4820.
42 T. Lathion, L. Guénée, C. Besnard, A. Bousseksou and C. Piguet, *Chem. – Eur. J.*, 2018, **24**, 16873–16888.
43 M. Lehr, T. Paschelke, V. Bendt, A. Petersen, L. Pietsch, P. Harders and A. J. McConnell, *Eur. J. Org. Chem.*, 2021, 2728–2735.
44 K. Rissanen, *Chem. Soc. Rev.*, 2017, **46**, 2638–2648.
45 M. J. Burke, G. S. Nichol and P. J. Lusby, *J. Am. Chem. Soc.*, 2016, **138**, 9308–9315.
46 R. G. Siddique, K. S. A. Arachchige, H. A. Al-Fayaad, J. C. McMurtrie and J. K. Clegg, *Dalton Trans.*, 2022, **51**, 12704–12708.
47 Q. Shi, X. Zhou, W. Yuan, X. Su, A. Neniškis, X. Wei, L. Taujenis, G. Snarskis, J. S. Ward, K. Rissanen, J. de Mendoza and E. Orentas, *J. Am. Chem. Soc.*, 2020, **142**, 3658–3670.
48 D. F. Evans, *J. Chem. Soc.*, 1959, 2003–2005.
49 S. De, S. Tewary, D. Garnier, Y. Li, G. Gontard, L. Lisnard, A. Flambard, F. Breher, M.-L. Boillot, G. Rajaraman and R. Lescouëzec, *Eur. J. Inorg. Chem.*, 2018, **2018**, 414–428.
50 W. Kläui, W. Eberspach and P. Gütlich, *Inorg. Chem.*, 1987, **26**, 3977–3982.
51 M. Lehr, T. Paschelke, E. Trumpf, A.-M. Vogt, C. Näther, F. D. Sönnichsen and A. J. McConnell, *Angew. Chem., Int. Ed.*, 2020, **59**, 19344–19351.
52 C. Hansch, A. Leo and R. W. Taft, *Chem. Rev.*, 1991, **91**, 165–195.
53 N. Ousaka, J. K. Clegg and J. R. Nitschke, *Angew. Chem., Int. Ed.*, 2012, **51**, 1464–1468.
54 K. P. Kepp, *Inorg. Chem.*, 2016, **55**, 2717–2727.
55 W. Meng, J. K. Clegg, J. D. Thoburn and J. R. Nitschke, *J. Am. Chem. Soc.*, 2011, **133**, 13652–13660.

3.2 Additional 2-(2'-Pyridyl)-1*H*-benzimidazole- and 2-(2'-Pyridyl)-1*H*-benzothiazole-based Ligands

This chapter is about the synthesis of the three additional ligands **35**, **36** and **34** (Figure 3.1). The ligands are based on the 2-(2'-pyridyl)-1*H*-benzimidazole and -benzthiazole binding motif and will be used for self-assembly experiments in order to obtain the respective target edge-bridged thermal spin-crossover cages. In comparison to the previously reported 2-(2'-pyridyl)-1*H*-benzimidazole derivatives,[13,235] ligand **35** offers the possibility to fine-tune the spin-crossover properties of its potentially self-assembled Fe^{II}-based metal-organic cage by substitution of the *N*-*H* group if the investigated spin-crossover properties need to be changed.

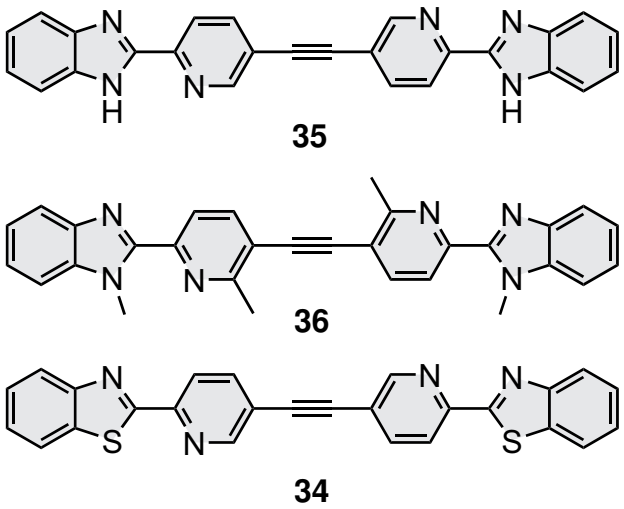

Figure 3.1: The reported spin-crossover ligands[235] are extended within this section by three additional ligands.

Additionally, the design of ligand **36** is based on a published study from Bartual-Murgui *et al.*,[216] showing that the introduction of sterically bulky groups next to coordinating heteroatoms can lead to destabilisation of the low-spin state, decreasing $T_{1/2}$. The free *N*-*H* group was methylated for synthetic ease and access via the one-pot Sonogashira cross-coupling.[13]

The final 2-(2'-pyridyl)-1*H*-benzothiazole-based ligand **34** was designed based on ligand **35** to suppress the tautomerism of the imidazole by substitution with a sulfur atom. In addition, the substitution reduces the amount of necessary synthetic steps by one since no *N*-substitution is necessary, facilitating the analysis of its properties and self-assembly with $Fe(OTf)_2$. Since thiazoles are known to have stronger ligand field strengths than imidazoles based on data of related compounds[105,106,224,225] higher spin-crossover temperatures are expected than for the imidazoles such as ligand **35** or the previously reported ligands.[235]

3.2.1 2-(2'-Pyridyl)-1*H*-benzimidazole-based Ligands 35 and 36

During the one-pot Sonogashira cross-coupling studies (Article 2, section 3.1.2) optimised reaction conditions were found for functionalised 2-(2'-pyridyl)-1*H*-benzimidazole-based ligands. However, the synthesis of ligand **35** was unsuccessful since partial amine deprotonation under the optimised reaction conditions (basic) was suggested to deactivate the reaction since *N*-protected derivatives reacted.[13] Based on this result,[13] a new synthetic approach with two reaction steps was developed for ligand **35** using 2-(5'-bromopyridin-2'-yl)-1*H*-benzo[*d*]imidazole (**37**) as the starting material (Scheme 3.2). The preparation of compound **37** was previously reported.[13] An alkyne function will be introduced using a Sonogashira reaction to yield compound **38**. Afterwards, starting material **37** will be reacted with the alkyne **38** in a second Sonogashira reaction to give the target ligand **35**.

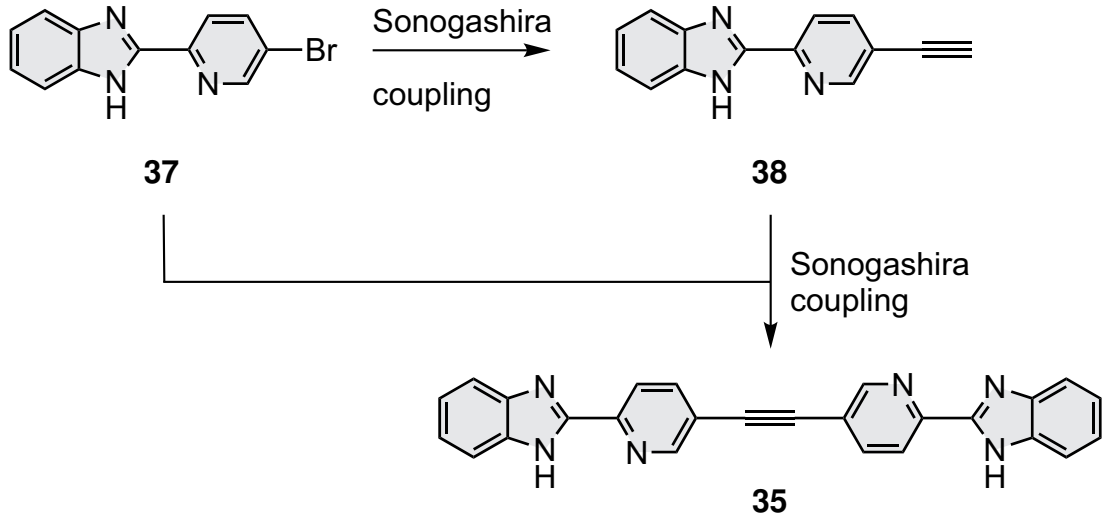

Scheme 3.2: Proposed synthesis of 1,2-bis(6"-(1*H*-benzo[*d*]imidazol-2'-yl)pyridin-3"-yl)ethyne (**35**).

Initally, product **38** was synthesised from the reaction between 2-(5'-bromopyridin-2'-yl)-1*H*-benzo[*d*]imidazole (**37**) and trimethylsilylacetylene (TMSA) with $Pd(PPh_3)_2Cl_2$ and CuI as the catalysts, triethylamine as the base and tetrahydrofuran as the solvent at 75 °C for 18 h adapting a procedure from Pietsch[1] (Scheme 3.3). Afterwards, the introduced TMS protecting group was deprotected by the addition of tetrabutylammonium fluoride. After flash chromatography the desired product **38** was isolated in a yield of 6%, being comparabily low to the reported yield of 51%.[1] The low yield might be attributed to the quality of triethylamine. This synthetic strategy was not optimised further due to the very small amount of compound **38** that was isolated (12.0 mg).

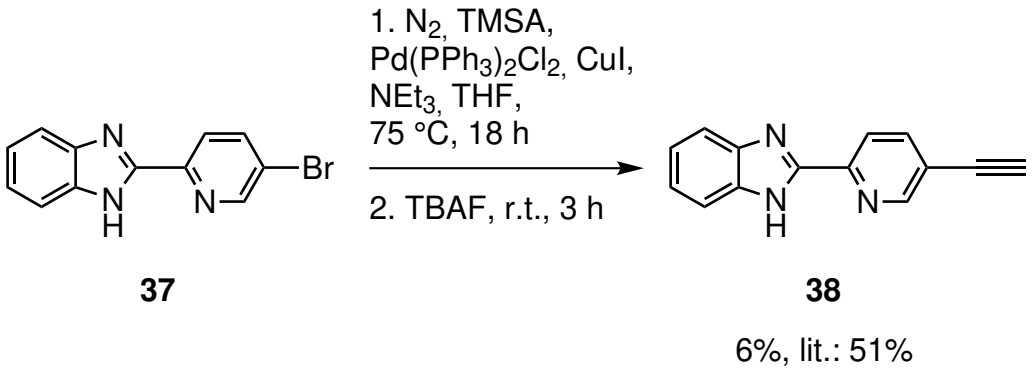

Scheme 3.3: Synthesis of 2-(5'-ethynylpyridin-2'-yl)-1*H*-benzo[*d*]imidazole (**38**).[1]

In the second attempt to synthesise ligand **35**, amine protecting groups were used to ensure that the free *N-H* groups do not interfere in the Sonogashira cross-coupling reactions. 2-(5'-Bromopyridin-2'-yl)-1*H*-benzo[*d*]imidazole (**37**) could be converted into the desired ligand **35** within three steps, including a protection, a Sonogashira reaction and a deprotection (Scheme 3.4). The *N-H* group can be protected using many different protecting groups, however, only a few are suitable due to the basic reaction conditions of the Sonogashira cross-coupling reactions. In the first attempt a Boc protecting group was introduced since it is fairly stable towards these conditions and the reaction conditions for the introduction of a Boc group are mild.[2,236] In this case, tetrabutylammonium fluoride can not be used for the Sonogashira cross-coupling reaction due to possible Boc deprotection, thus different reaction conditions need to be used.[237]

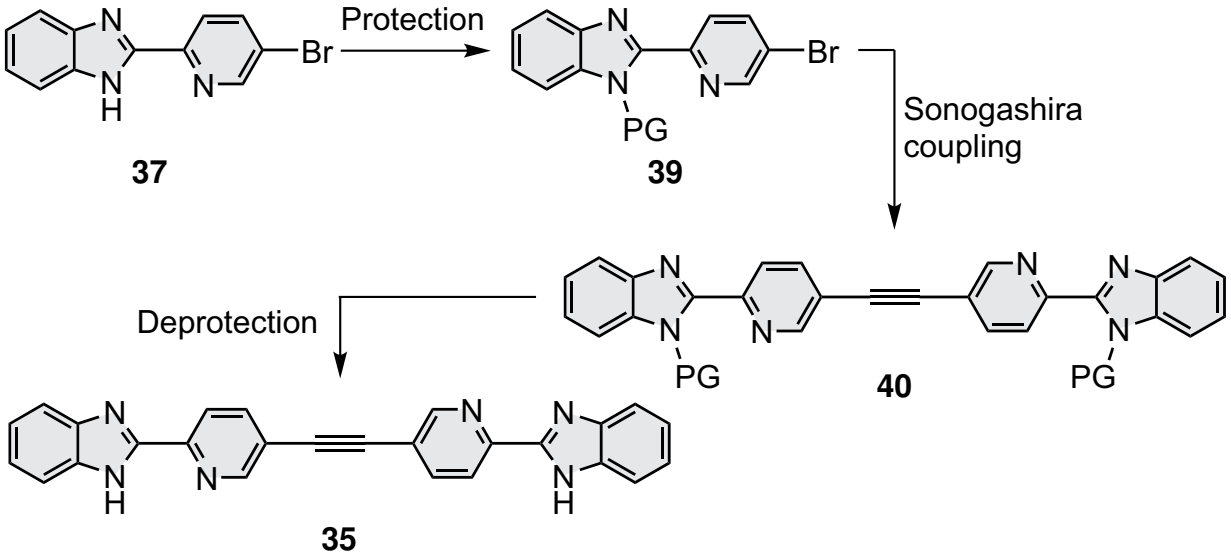

Scheme 3.4: Proposed synthesis of 1,2-bis(6"-(1*H*-benzo[*d*]imidazol-2'-yl)pyridin-3"-yl)ethyne (**35**).

Starting from compound **37** the Boc protecting group was introduced using di-*tert*-butyl dicarbonate and 4-dimethylaminopyridine in dichloromethane at room temperature for 17.5 h adapting a procedure from Taylor *et al.*.[2] The product *tert*-butyl 2'-(5"-bromopyridin-2"-yl)-1*H*-benzo[*d*]imidazole-1'-carboxylate (**41**) was isolated in an almost quantitative yield of 95% after flash chromatography.

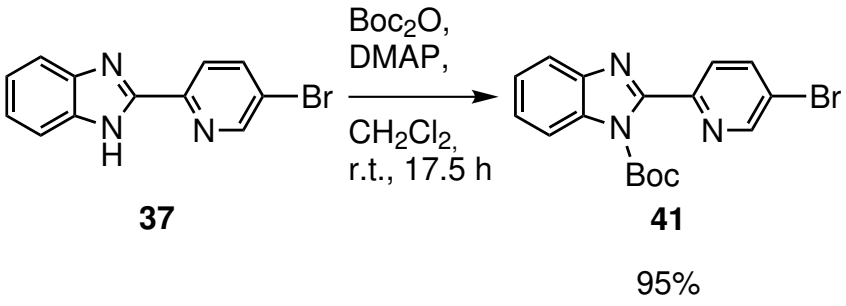

Scheme 3.5: Synthesis of *tert*-butyl 2'-(5"-bromopyridin-2"-yl)-1*H*-benzo[*d*]imidazole-1'-carboxylate (**41**).[2]

Afterwards, the synthesis of ligand precursor **40** was attempted adapting reaction conditions from Liu *et al.*[238] In 2016 Liu *et al.* published novel Sonogashira cross-coupling reaction conditions using Cu(Xantphos)I and $Pd(OAc)_2$ as the catalysts with Cs_2CO_3 as the base and obtained a library of different substrates in up to excellent yields.[238] Based on the large presented applicability of the method to 38 substrates including amines,[238] the method seemed promising for the synthesis of the desired product **42**. Thus the reaction conditions from Liu *et al.*[238] were adapted. Cu(Xantphos)I (short: Cu(X)I) was prepared according to the literature procedure.[239] Compound **41** was reacted with trimethylsilylacetylene at 60 °C for 21 h (Scheme 3.6, red). After work up, product **42** was not obtained and analysis of the ^{1}H NMR spectrum of the crude product indicated deprotection of the Boc group. Although Liu *et al.* have shown the great tolerance of their method towards functional groups, a study about the tolerance of protecting groups or the reactivity of imines was not included. Unfortunately, the reported reaction conditions[238] are not suitable for substrate **41** and this synthesis was not repeated.

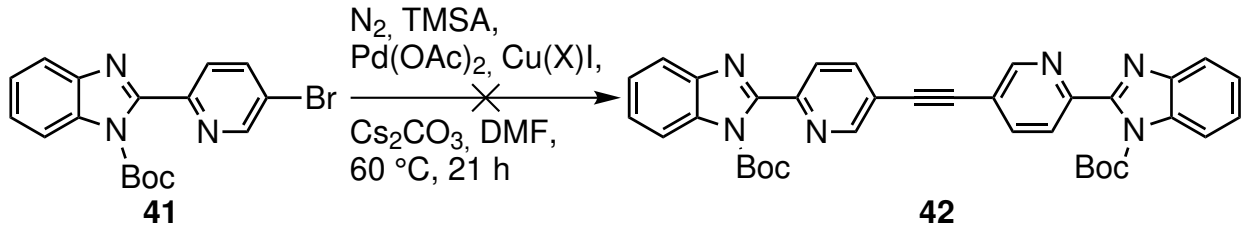

Scheme 3.6: Synthesis of precursor **42**.[13,238]

For overcoming the basic lability of the Boc protecting group three other groups were chosen: trityl (Tr), tosyl (Ts) and benzyl (Bn).[236] Firstly, the trityl group was tested (Scheme 3.7, a)). Compound **37** was reacted with trityl chloride under basic conditions in *N*,*N*-dimethylformamide at 120 °C for 22.5 h adapting a procedure from Hille *et al.*.[240] After purification by flash chromatography only starting material was recovered. In the second attempt the previously used base/solvent system from Hille *et al.*[240] was changed to triethylamine as the base and chloroform as the solvent, adapting a procedure from Aldabbagh *et al.*.[3] The reaction was performed at room temperature, but did also not lead to any product formation.
Similar results were obtained during the attempts to introduce a tosyl protecting group (Scheme 3.7, b)). Compound **37** was reacted with tosyl chloride and either triethylamine as the base adapting a procedure from Abdireimov *et al.*[241] or sodium hydride for harsher reaction conditions based on a methylation procedure from Zhegalova *et al.*.[17] In both cases only starting material was recovered leading to the assumption that trityl and tosyl protecting groups might also not be suitable since they are too sterically bulky to be introduced onto a 2-(2'-pyridyl)-1*H*-benzimidazole backbone.

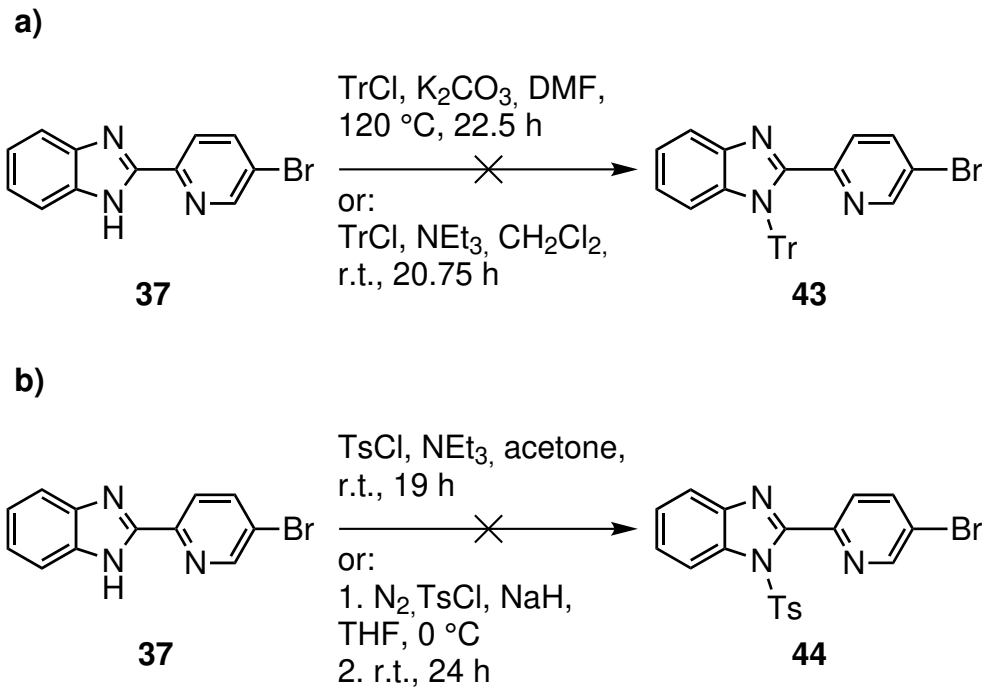

Scheme 3.7: Synthetic attempts for compound a) **43**[3,240] and b) **44**.[17,241]

Since the previously attempted protecting groups did not lead to the desired ligand **35**, the focus was changed towards the benzyl group. Starting material **45** was synthesised during the one-pot Sonogashira development[13] and can be used to target the desired ligand **35** within one step by debenzylation (Scheme 3.8). In general benzyl groups are cleaved by using hydrogen and palladium on

activated charcoal, however, in this case these conditions are not suitable since the alkyne function can also be reduced. Furthermore, ligand **45** is not soluble in organic solvents. However, according to the literature,[236] benzyl protecting groups are labile towards harsh acidic conditions (pH < 1, >100 °C). Therefore, the deprotection was performed in sulfuric acid at 120 °C for 19.75 h. After work up a solid was isolated. The solid was filtered and its ^{1}H NMR spectrum analysed. Multiple species were visible, but no assignment was possible due to broadening of the signals. Further purification by flash chromatography was not attempted since thin-layer chromatography measurements indicated streaking of multiple spots in different solvent mixtures.

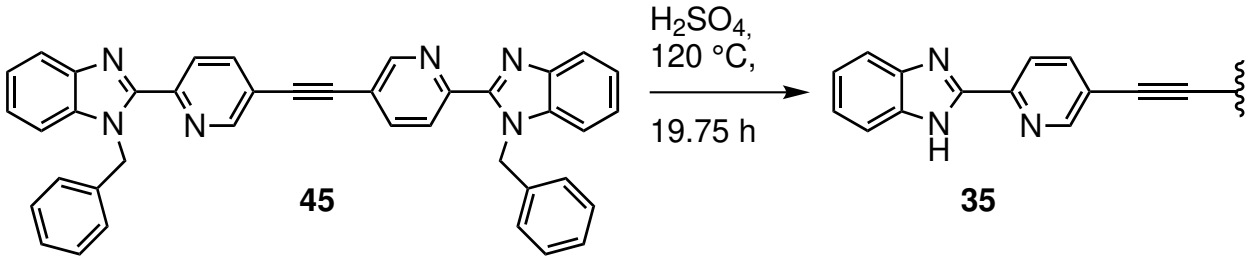

Scheme 3.8: Synthetic attempt for ligand **35** starting from the already literature-known ligand **45**.[13,236]

Although previous attempts with protecting groups did not work to synthesise target ligand **35**, a different convergent five-step synthesis for compound **35** utilising a trityl group was proposed (Scheme 3.9). The synthesis of precursor **49** is literature-known.[3,4] (**46**). Starting from compound **46**, the trityl protecting group will be introduced giving compound **47**. Afterwards, the iodide will be introduced and the trityl group will be cleaved to yield the first precursor **49**. The trityl group needs to be removed to avoid possible steric clashes as observed in a previous attempt with sterically bulky protecting groups (see Scheme 3.7). The second precursor **51** could be synthesised from 2-bromo-5-iodopyridine (**50**) in just one step in a Sonogashira cross-coupling reaction.[5] After the successful synthesis both precursors **49** and **51** will be reacted in a Negishi cross-coupling reaction.

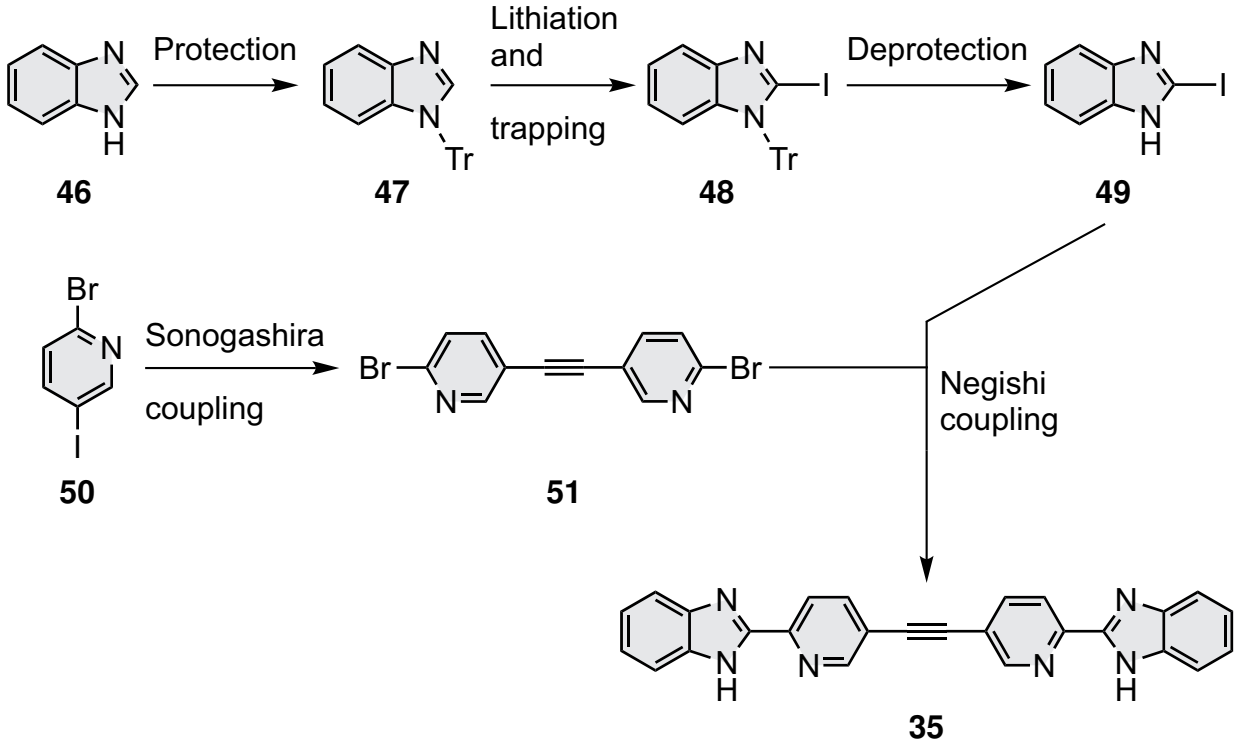

Scheme 3.9: Proposed synthesis for ligand **35** by using alternative cross-coupling reactions.[3–5]

1*H*-Benzo[*d*]imidazole (**46**) was reacted with trityl chloride using triethylamine as the base in dichloromethane at room temperature for 19.5 h following a procedure from Aldabbagh *et al.* (Scheme 3.10).[3] Purification by flash chromatography yielded the product **47** in quantitative yield (99%) without any further purification necessary. Aldabbagh *et al.* purified compound **47** by recrystallisation and obtained a lower yield (67%), likely attributed to the chosen purification method.[3]

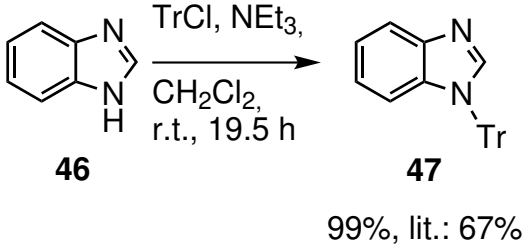

Scheme 3.10: Synthesis of 1-trityl-1*H*-benzo[*d*]imidazole (**47**).[3]

Afterwards, the iodination and deprotection were performed according to an adapted procedure from O'Connell *et al.* (Scheme 3.11).[4] Benzimidazole **47** was lithiated with *n*-butyllithium in tetrahydrofuran at -78 °C. After formation of the intermediate, the lithiated species was trapped by the addition of iodine at room temperature. After purification by flash chromatography the product **48**

was isolated in a yield of 19%, which is lower than the expected 59% reported.[4] Based on the procedure, the lithiated species is trapped at room temperature, however, such reactive species are very sensitive, thus the temperature rise to room temperature could have led to partial decomposition of the intermediate and therefore lowering the yield significantly. Although compound **47** was obtained in a low yield, enough material was obtained to perform the next step. Iodinated benzimidazole **48** was then deprotected using hydrochloric acid at 75 °C for 3 h. After work up the desired product **49** was obtained in a yield of 53%, which is slightly less than the reported yield of 75%.[4]

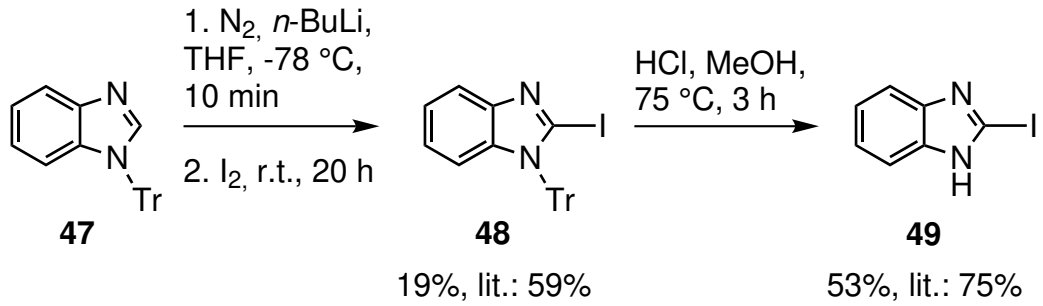

Scheme 3.11: Synthesis of 2-iodo-1-trityl-1*H*-benzo[*d*]imidazole (**48**) and 2-iodo-1*H*-benzo[*d*]imidazole (**49**).[4]

After the successful preparation of the first precursor **49**, the synthesis of pyridine **51** was attempted testing several reaction conditions (Table 3.1). In the first attempt reaction conditions from Mio *et al.* were tested since they reported the chloro analogue of precursor **51**.[5] $Pd(PPh_3)_2Cl_2$ and CuI were used as the catalysts and DBU was chosen as the base in a mixture of toluene and water. In the original procedure[5] benzene was used instead of toluene, however, benzene was substituted with toluene due to the high toxicity. After purification by flash chromatography the product **51** was obtained in a yield of 8% being only 43.5 mg. In the second attempt reaction conditions from Mori *et al.*[234] were used, being a copper-free alternative with tetrabutylammonium fluoride as the base and activator.[234] After work up the ^{1}H NMR spectrum did not indicate starting material **50** or the desired product **51**. Further analysis by ^{1}H NMR spectroscopy was not conducted. In the last attempt reaction conditions from Liu *et al.* with the Cu(Xantphos)I/$Pd(OAc)_2$ catalytic system were used. During the work up no product **51** was obtained.

Table 3.1: Reaction conditions for the synthesis of compound **51**.

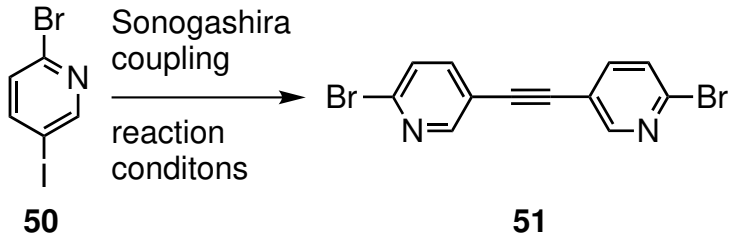

50 **51**

Attempt[1]	Catalyst	Base	solvent	Time / h	Temperature / °C	Yield **51**
1[2]	$Pd(PPh_3)_2Cl_2$, CuI	DBU	toluene, water	19.5	r.t.	8 %
2[3]	$Pd(PPh_3)_2Cl_2$	TBAF	THF	17	70	-
3[4]	Cu(X)I, $Pd(OAc)_2$	Cs_2CO_3	DMF	20	60	-

[1] All reactions were carried out with trimethylsilylacetylene as the acetylene source.
[2] Degassed. [3] Performed in a pressure tube. [4] X = Xantphos

Although compound **51** was obtained in a yield of 8% the quantity was too low to perform the last Negishi cross-coupling reaction. Therefore, a final alternative synthetic pathway was developed using the dicarboxylic acid precursor **57** (Scheme 3.12). Starting from 5-bromopicolinic acid (**52**) precursor **57** could be obtained in five steps starting with an esterification. Afterwards, a Sonogashira cross-coupling will be used to introduce a TMS protected alkyne and give compound **54**. The protecting group will be cleaved yielding precursor **55**. In a second Sonogashira cross-coupling reaction alkyne **55** and compound **53** will react to yield diester **56**. The ester group can then be deprotected and product **57** be used in a condensation reaction with *o*-phenylenediamine (**58**) yielding the target ligand **35**.

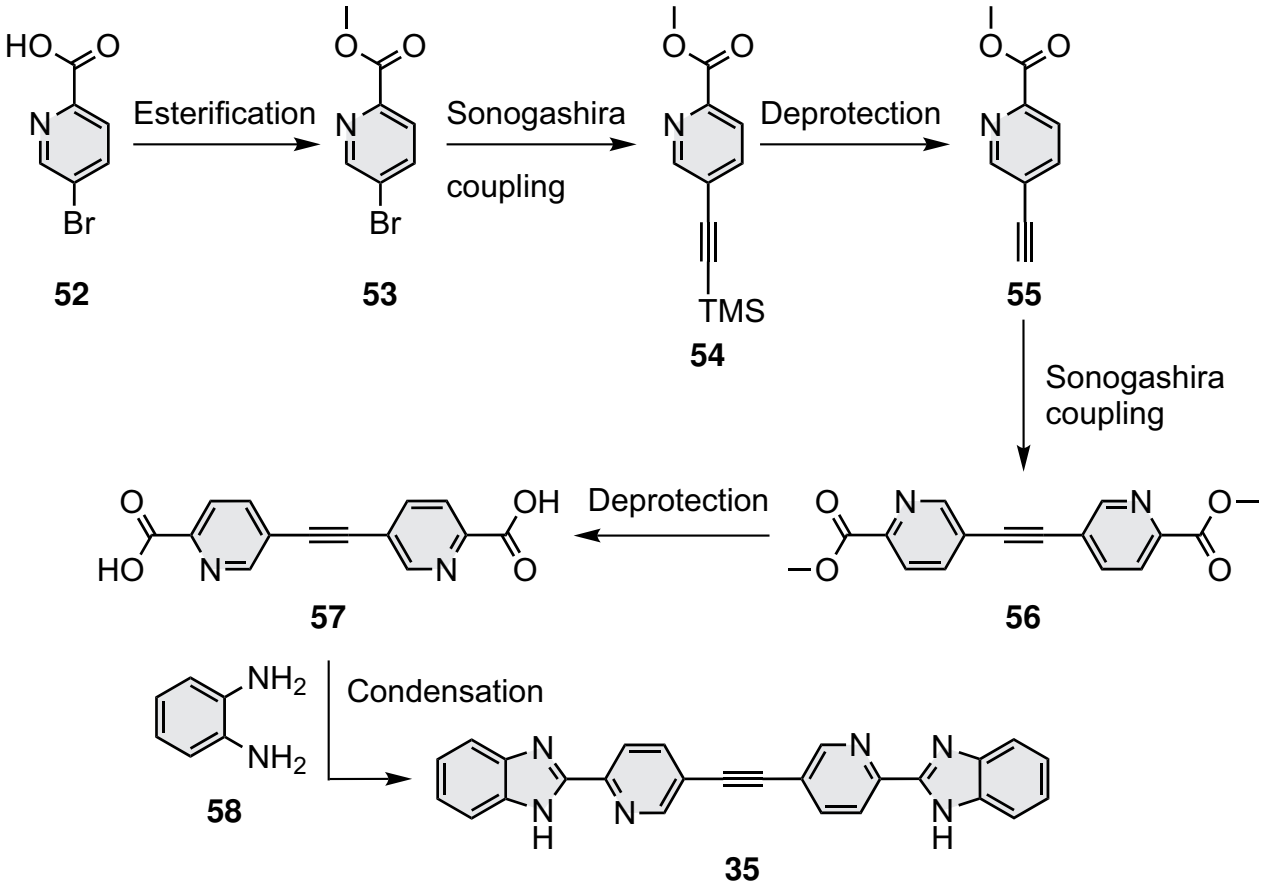

Scheme 3.12: Proposed synthesis of 1,2-bis(6'-(1''-methyl-6''-((*E*)-phenyldiazenyl)-1*H*-benzo[*d*]imidazol-2''-yl)pyridin-3'-yl)ethyne (**35**).

In the first step compound **52** was esterified with methanol in an acidic solution at 70 °C for 89 h using an adapted procedure from Andernach *et al.* (Scheme 3.13).[6] After cooling to room temperature, the product **53** was obtained by extraction of the basified aqueous solution with dichloromethane in a yield of 90% being in good agreement to the literature value of 86%.[6]

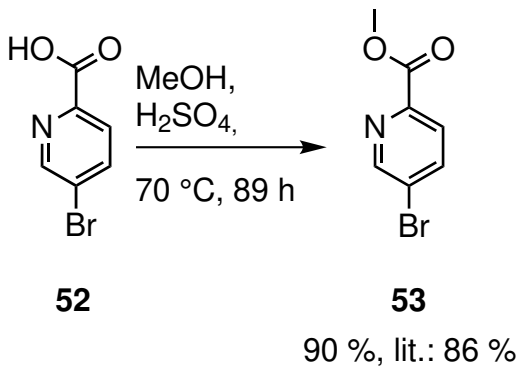

Scheme 3.13: Synthesis of methyl 5'-bromopicolinate (**53**).[6]

The introduction of an alkyne function was performed using standard Sonogashira cross-coupling reaction conditions adapting a procedure from Park *et al.* (Scheme 3.14).[7] Initially, methyl ester **53** was reacted with trimethylsilylacetylene in the presence of $Pd(PPh_3)_2Cl_2$ and CuI in a mixture of tetrahydrofuran and triethylamine at 60 °C for 22 h. The TMS protected product **54** was isolated after purification by flash chromatography in a yield of 81%. Afterwards, the TMS protecting group was cleaved with potassium carbonate in methanol at room temperature over the course of 30 min adapting a procedure from Soliman *et al.*[8] The amount of potassium carbonate was reduced to 2.3 mol% to avoid possible deprotection of the methyl ester. After work up the product **55** was obtained in a yield of 92%.

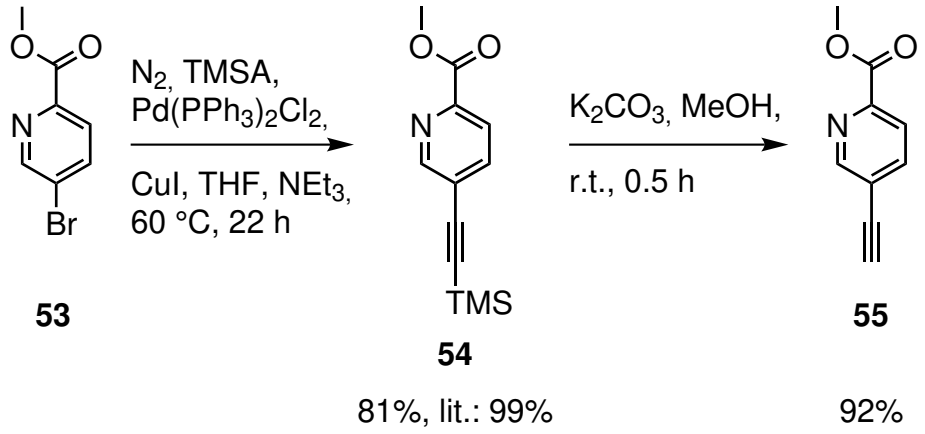

Scheme 3.14: Synthesis of methyl 5'-ethynylpicolinate over two steps (**55**).[7,8]

The synthesis of compound **57** over two steps is based on adapted procedures from Jornet-Mollá *et al.*[9] In a third Sonogashira reaction compounds **53** and **55** were reacted with $Pd(PPh_3)_4$ as the catalyst and triethylamine as the base in tetrahydrofuran as the solvent at 75 °C for 44 h (Scheme 3.15). Copper-free reaction conditions were applied to avoid possible side reactions (Glaser product). After purification by flash chromatography the product **56** was isolated in a yield of 80% and is consistent with the reported data of Jornet-Mollá *et al.*[9] The obtained methyl ester **56** was then deprotected with lithium hydroxide monohydrate in tetrahydrofuran and water at room temperature for 4 h.[9] Product **57** was obtained by precipitation with hydrochloric acid in a excellent yield of 96%.

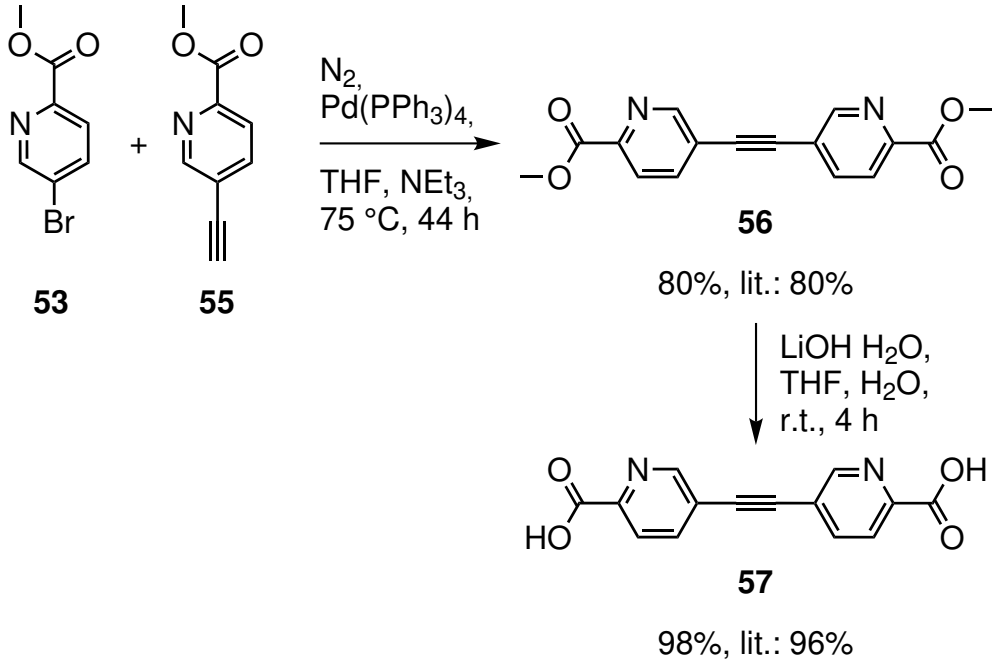

Scheme 3.15: Synthesis of dimethyl 5,5'-(ethyne-1",2"-diyl)dipicolinate (**56**) and 5,5'-(ethyne-1",2"-diyl)dipicolinic acid (**57**).[9]

Finally, dicarboxylic acid **57** was reacted with *o*-phenylenediamine at 180 °C for 22 h following a procedure from Turnbull *et al.* for related compounds.[10] (Scheme 3.16). In comparison to previous used work up procedures,[11,13] the polyphosphoric acid was dissolved in water by stirring the solution for 1 h at room temperature.[10] In the end the solution was neutralised and again stirred for 1 h to collect the precipitate.[10] After work up a yellow precipitate was obtained (see Section 7.3.12) The ^{1}H NMR spectrum of the crude product indicated multiple species, but due to line broadening and overlap of the ^{1}H signals no assignment was possible. According to thin-layer chromatography measurements a minimum of four substances were visible and flash chromatography was attemped. However, purification by column chromatography on aluminum oxide was unsuccessful due to streaking and insolubility in organic solvents. Further purification by recrystallisation with cyclohexane and/or dichloromethane was not possible due to insolubility. Based on EI-HR mass data the product **35** was obtained, but impure. The synthetic strategy for the impure ligand **35** was not further optimised. The crude product was then used for self-assembly experiments, although a stoichiometric imbalance is expected (see section 3.2.3).

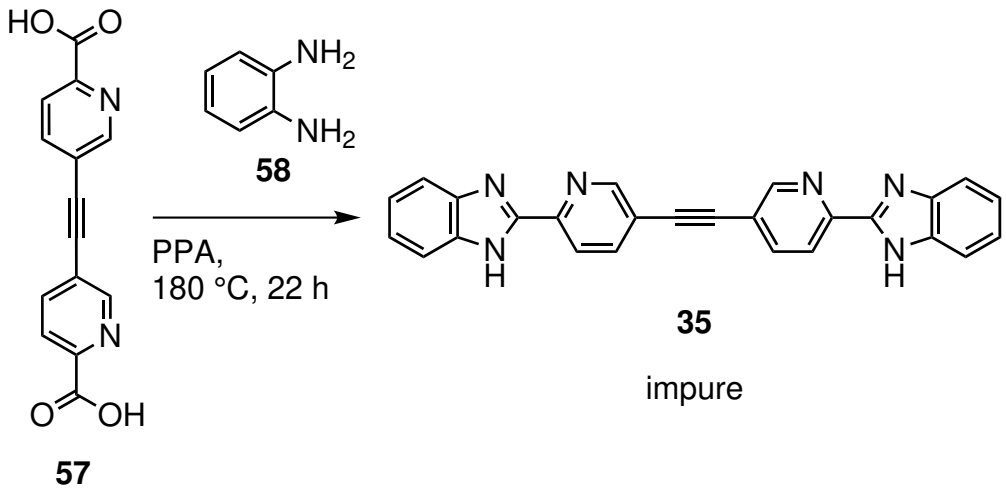

Scheme 3.16: Synthesis of 1,2-bis(6”-(1*H*-benzo[*d*]imidazol-2’-yl)pyridin-3”-yl)ethyne (**35**).[10]

In addition to ligand **35** another 2-(2’-pyridyl)-1*H*-benzimidazole based ligand (compound **36**) was synthesised bearing a methyl group next to the coordinating nitrogen atom on the pyridine ring (Scheme 3.17). Based on the reported systematic spin-crossover study,[235] a methyl group was introduced close to the coordination side to favor the high-spin state of the respective Fe_4L_6 cage.[216] This would be expected to result in a decreased spin-crossover temperature from 401 K closer to room temperature range. Starting with *o*-phenylenediamine (**58**) and 5-bromo-6-methylpicolinic acid (**59**) precursor **60** will be obtained after a condensation reaction. Afterwards, the imidazole *N-H* group will be methylated with an additional Sonogashira cross-coupling reaction[13] to yield the target ligand **36** in three steps.

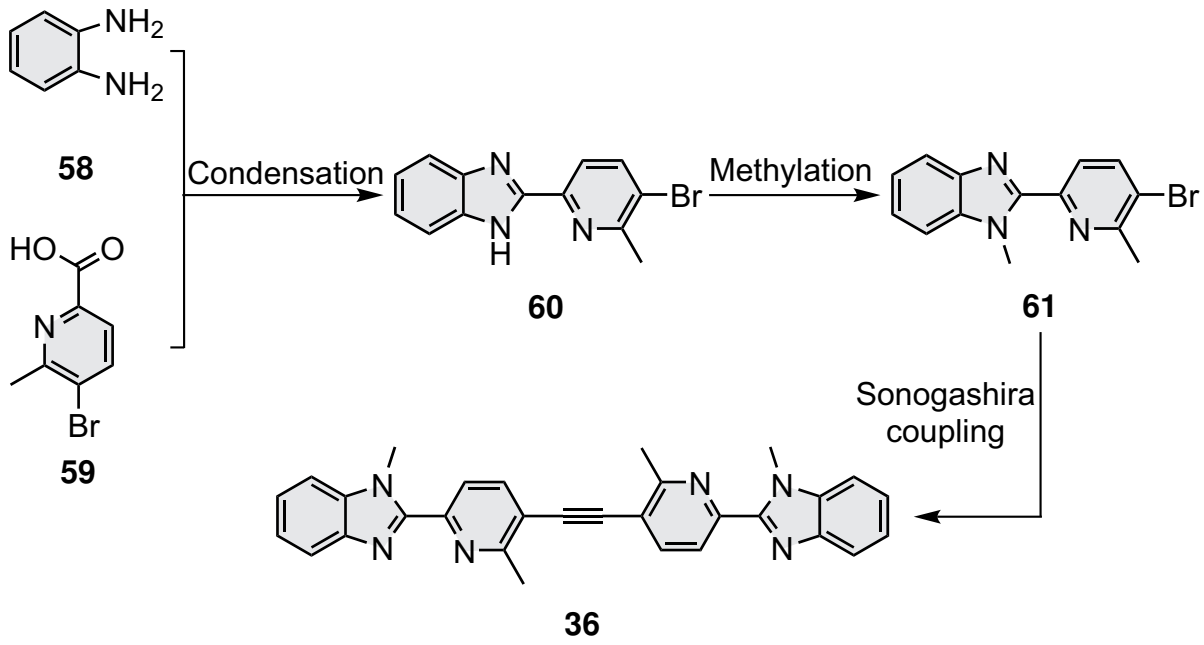

Scheme 3.17: Proposed synthesis of 1,2-bis(2''-methyl-6''-(1'-methyl-1*H*-benzo[*d*]imidazol-2'-yl)pyridin-3''-yl)ethyne (**36**).

In the first step reaction conditions from Jia *et al.* were adapted for the synthesis of precursor **60** (Scheme 3.18).[11] *o*-Phenylenediamine (**58**) and 5-bromo-6-methylpicolinic acid (**59**) were reacted in acidic conditions at 180 °C for 21.75 h. During the work up the product was collected by filtration in a yield of 74%. Although Jia *et al.* did not report compound **60**, the yield is in good agreement with the yield (60-80%) of related benzimidazoles.[11]

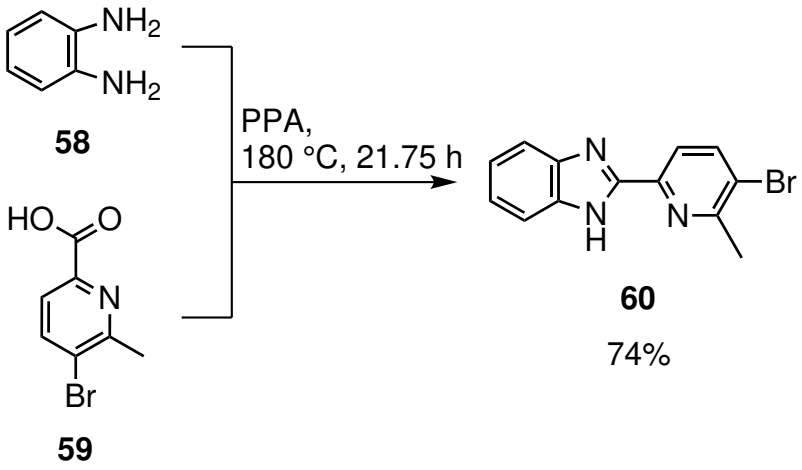

Scheme 3.18: Synthesis of 2-(5'-bromo-6'-methylpyridin-2'-yl)-1*H*-benzo[*d*]imidazole **60**.[11]

Compound **60** was then methylated using methyl iodide and potassium carbonate in *N*,*N*-dimethylformamide at room temperature for 20.5 h, adapting a procedure of Lin *et al.* (Scheme 3.19).[12] The product **61** was obtained in a yield of 75%.

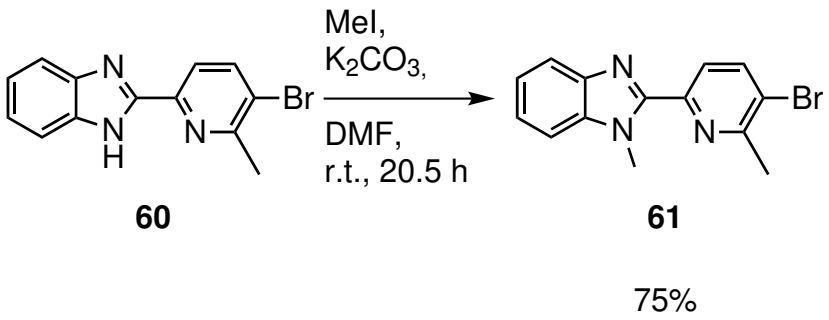

Scheme 3.19: Synthesis of 2-(5'-bromo-6'-methylpyridin-2'-yl)-1-methyl-1*H*-benzo[*d*]imidazole **61**.[12]

For the last step compound **61** was reacted with trimethylsilylacetylene and $Pd(PPh_3)_4$ as the catalyst and tetrabutylammonium fluoride at 70 °C for 19.5 h adapting the procedure by Lehr *et al.* for related compounds (Scheme 3.20).[13] Since steric bulk close to the bromide substituent is assumed to reduce the reaction rate of the Sonogashira cross-coupling reaction (see ligand **1c** in publication ii), section 3.1.2), the reaction time was lengthened to 19.5 h instead of 3 h.[13] After work up the target ligand **36** was obtained in a yield of 70%.

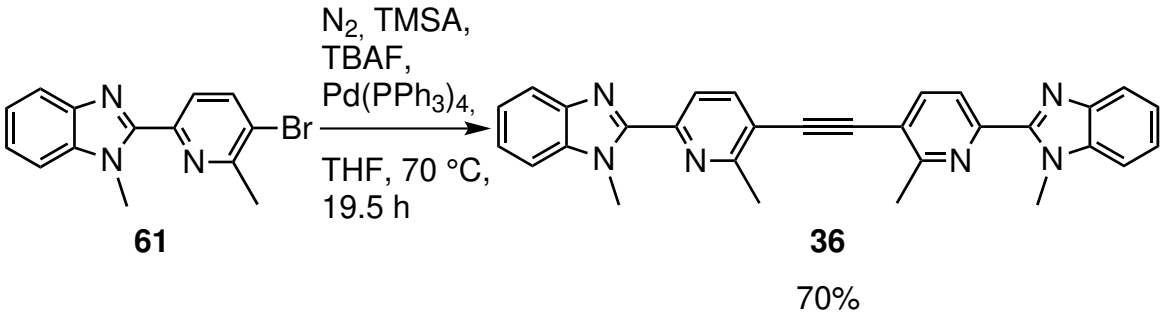

Scheme 3.20: Synthesis of 1,2-bis(2"-methyl-6"-(1'-methyl-1*H*-benzo[*d*]imidazol-2'-yl)pyridin-3"-yl)ethyne (**36**).[13]

3.2.2 2-(2'-Pyridyl)-1*H*-benzothiazole-based Ligand 34

In addition to the 2-(2'-pyridyl)-1*H*-benzimidazole-based ligands **35** and **36**, benzthiazole ligand **34** was also synthesised to i) investigate the ligand field strength and spin-crossover properties of the benzthiazole scaffold in a cage ligand since other groups only investigated the thiazole scaffold[105,106,224] and ii) to suppress the imidazole tautomerism as found in ligand **35** by substitution with a sulfur atom. Starting from 2-aminothiophenol (**62**) and 5-bromopicolinic acid (**52**) ligand **34** will be synthesised in two steps including a condensation and Sonogashira cross-coupling reaction (Scheme 3.21).

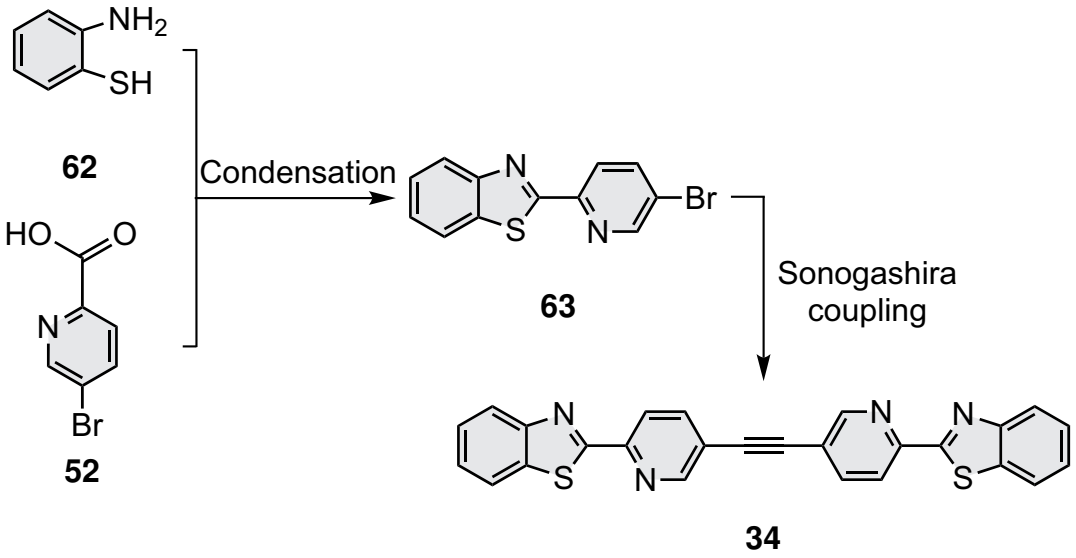

Scheme 3.21: Proposed synthesis of 1,2-bis(2'-(benzo[*d*]thiazol-2"-yl)pyridin-5'-yl)ethyne (**34**).

The condensation reaction between compounds **62** and **52** was adapted from Jia *et al.* using polyphosphoric acid as the acid and solvent at 180 h for 18.5 h (Scheme 3.22).[11] After work up further purification by flash chromatography was necessary and the product **63** was obtained in a yield of 26%. The low yield might be attributed to the additionally needed purification.

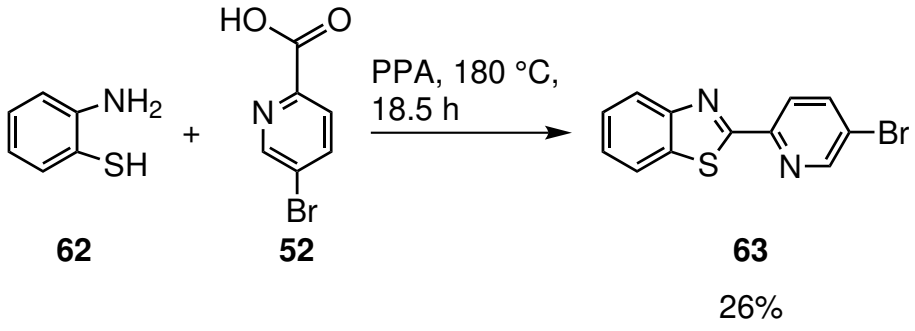

Scheme 3.22: Synthesis of 2-(5'-bromopyridin-2'-yl)benzo[*d*]thiazole (**63**).[11]

The final step was performed using standard one-pot Sonogashira cross-coupling reaction conditions from Lehr *et al.* (Scheme 3.23).[13] Ligand **34** precipitated during the course of the reaction and was after filtration obtained in a good yield of 54%.

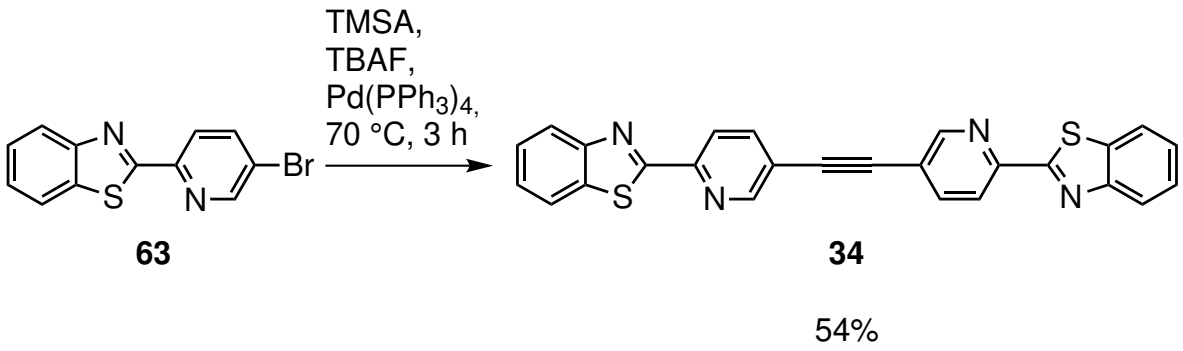

Scheme 3.23: Synthesis of 1,2-bis(2'-(benzo[*d*]thiazol-2''-yl)pyridin-5'-yl)ethyne (**34**).[13]

3.2.3 Self-Assembly of ligands 35, 36 and 34 with Fe^{II}

Previously, ligands **35** (impure), **36** and **34** were successfully synthesised. In this section self-assemblies with the respective ligands and iron(II) trifluoromethanesulfonate ($Fe(OTf)_2$) will be investigated. Based on the geometry of the used ligands an edge-bridged Fe_4L_6 metal-organic cage is expected to form for all ligands. Thus six equivalents of the appropriate ligand and four equivalents of $Fe(OTf)_2$ were dissolved in deuterated acetonitrile (Scheme 3.24). Since the purification of ligand **35** was challenging and unsuccessful, the impure ligand **35** was used for the self-assembly which could lead to a stoichiometric imbalance. The self-assemblies were analysed by NMR spectroscopy and in the case of ligand **35** also by ESI-MS.

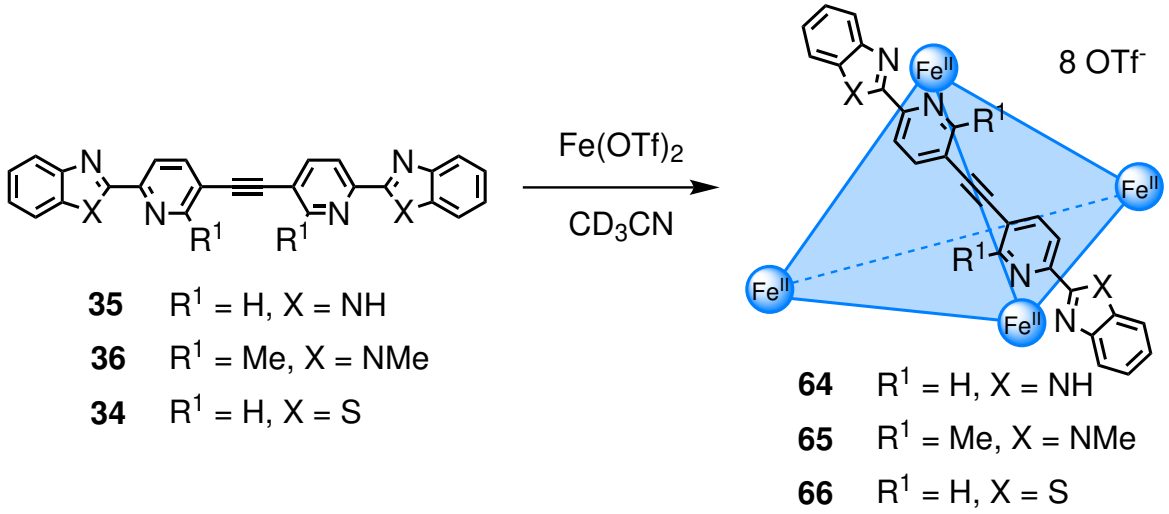

Figure 3.24: Self-assembly of $Fe(OTf)_2$ with the ligands **35**, **36** and **34** in deuterated acetonitrile with the expected Fe_4L_6 metal-organic cages **64**, **65** and **66**.

For the self-assembly with ligand **35** paramagnetic signals up to 55 ppm were visible in the ^{1}H NMR spectrum (Figure 3.2). However, proton assignment was not possible due to the observation of broad signals. The broadness of the ^{1}H NMR signals is expected to be a result of the formation of multiple species instead of one discrete cage structure. The self-assembly experiment was heated at 50 °C for 1 h to reach the thermal equilibrium, but changes within the ^{1}H NMR spectrum were not visible indicating that the equilibrium is reached (Figure 3.2, red). Since the stoichiometric imbalance was assumed to influence the self-assembly process, purification of the self-assembly was attemped by precipitation with diethyl ether (Figure 3.2, green). An ^{1}H NMR spectrum was measured, but only the intensities of the signals decreased with line broadening still observable. Further analysis by ESI-MS was conducted. Signals consistent with the expected tetrahedral structure were identified ($[Fe_4\mathbf{35}_6OTf_4]^{4+}$ (*m/z* 823.1021) and $[Fe_4\mathbf{35}_6OTf_5]^{3+}$ (*m/z* 1147.7890)), but the isotopic pattern only

matched for the $Fe_4\mathbf{35}_6OTf_5]^{3+}$ species (Figure 3.3). Unfortunately, confirmation of a tetrahedral structure was not possible since the ^{1}H NMR spectrum showed a discrete cage structure did not form and the unknown impurity of ligand **35** could lead to the formation of multiple other species due to a stoichiometry imbalance or other 2-(2'-pyridyl)-1*H*-benzimidazole-based impurities that also self-assemble structures. Overall, this study should be repeated when ligand **35** is purified in order to investigate the effect of the impurity and stoichiometric imbalance on the self-assembly results.

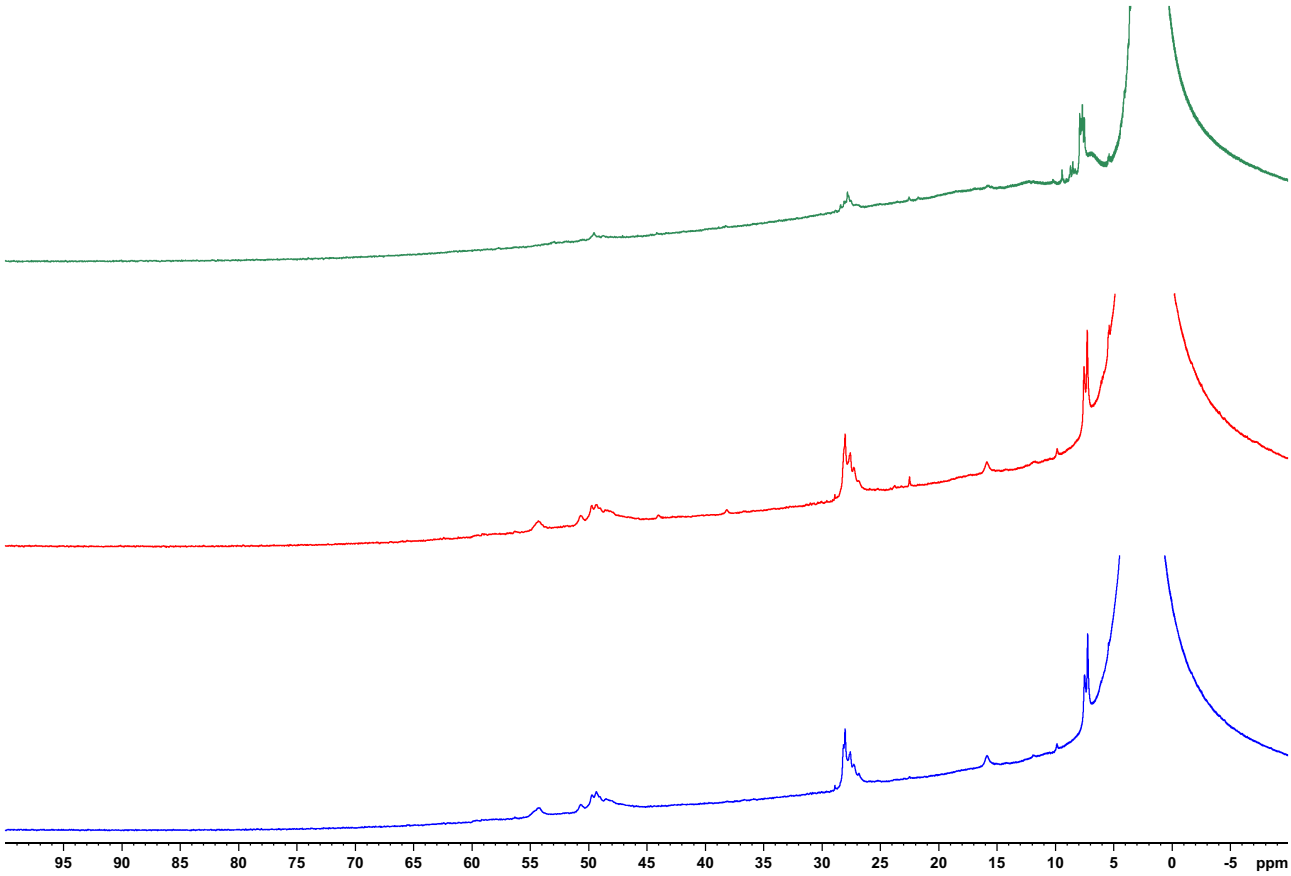

Figure 3.2: ^{1}H NMR spectra (500 MHz, CD_3CN, 298 K) of cage **64** before (blue), after heating at 50 °C for 1 h (red) and after precipitation (green).

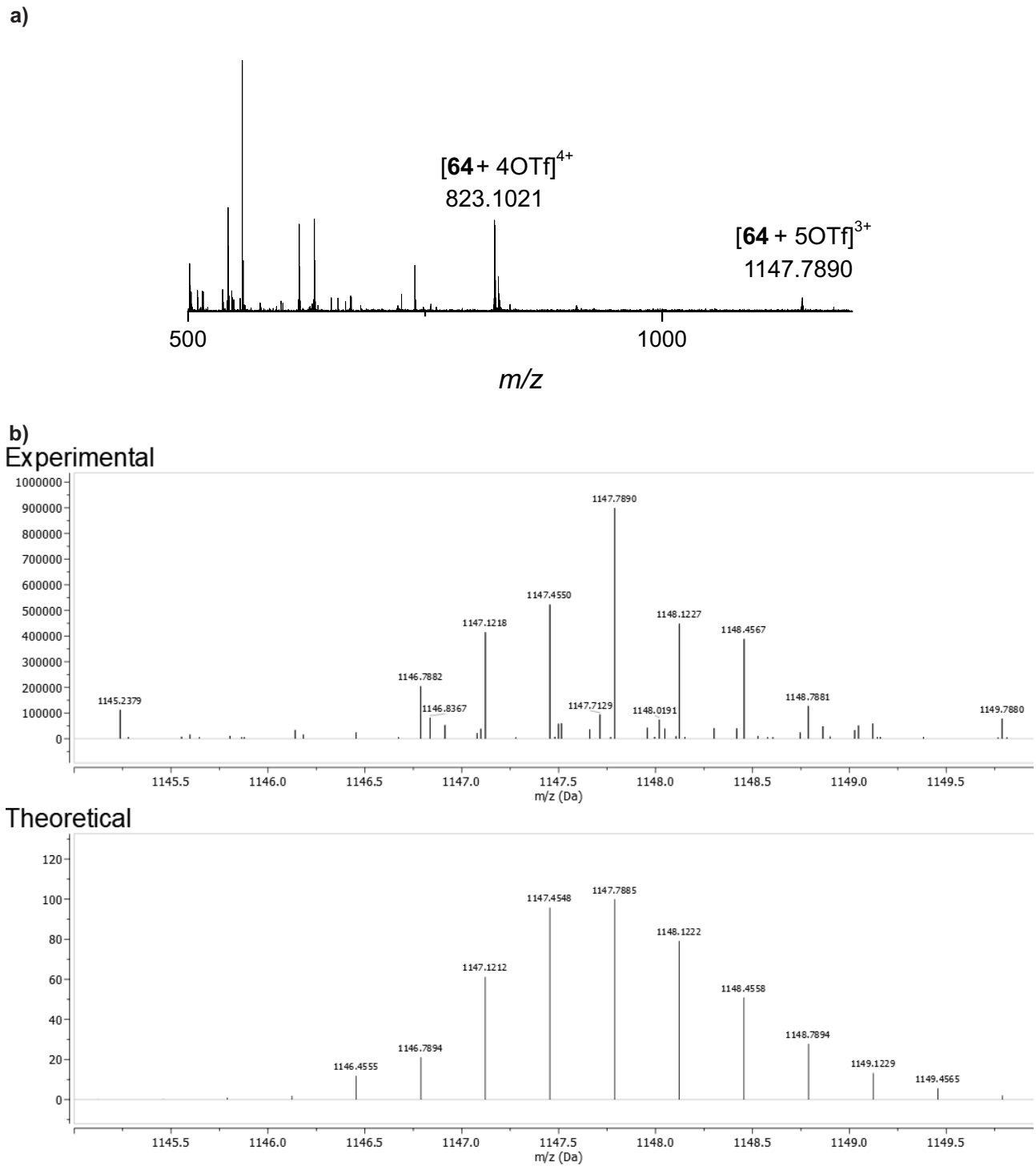

Figure 3.3: High resolution ESI mass spectrum of the self-assembly with ligand **35** a) in the range of *m/z* 500-1200 and b) the experimental and theoretical isotopic patterns.

Afterwards, self-assemblies with ligands **36** and **34** and $Fe(OTf)_2$ were investigated. In comparison to the previous self-assembly with ligand **35**, broad signals were also obtained in the ^1H NMR spectra (Figure 3.4). For the self-assembly with ligand **36** (Figure 3.4, b)) dilution experiments were further

investigated to analyse if a discrete species self-assemble upon dilution, however, only precipitation within the test tube was observed with decreasing signals in the ^{1}H NMR spectrum. Further analysis by ESI-MS did not show any of the expected cage signals, instead only free ligand was identified. Ligand **36** was designed to destabilise the low-spin state by steric bulk of a CH_3 group close to the coordination site.[216] Since a discrete species was not observed in the ^{1}H NMR spectrum, the methyl groups are proposed to lead to more sterically crowded coordination around the Fe^{II} metal center making discrete cage formation challenging. This could result in the formation of multiple species and/or broad signals.

In addition, low intensity and broad signals were only visible in the ^{1}H NMR spectrum of the self-assembly with ligand **34**. This result indicates that a discrete cage species was not formed during the self-assembly process, attributed to the bigger sulfur atom in comparison to its nitrogen analogues. The size difference leads to repulsive interactions between the benzimidazole and pyridine moiety. As a result the distance between the coordinating nitrogen atoms (*N*-*N*) could get shorter leading to distorted and unfavourable coordination to the metal center.

In conclusion, the self-assembly attempts with ligands **35**, **36** and **34** did not result in discrete cage species. Instead, only broad, unassignable ^{1}H signals were visible in the ^{1}H NMR spectra. The results indicate that ligands **36** and **34** should not be further investigated as potential spin-crossover ligands due to the discussed steric reasons. Future work needs to focus on other purification methods for ligand **35** to quantify the effect of the stoichiometric imbalance and/or impurity on the self-assembly with $Fe(OTf)_2$.

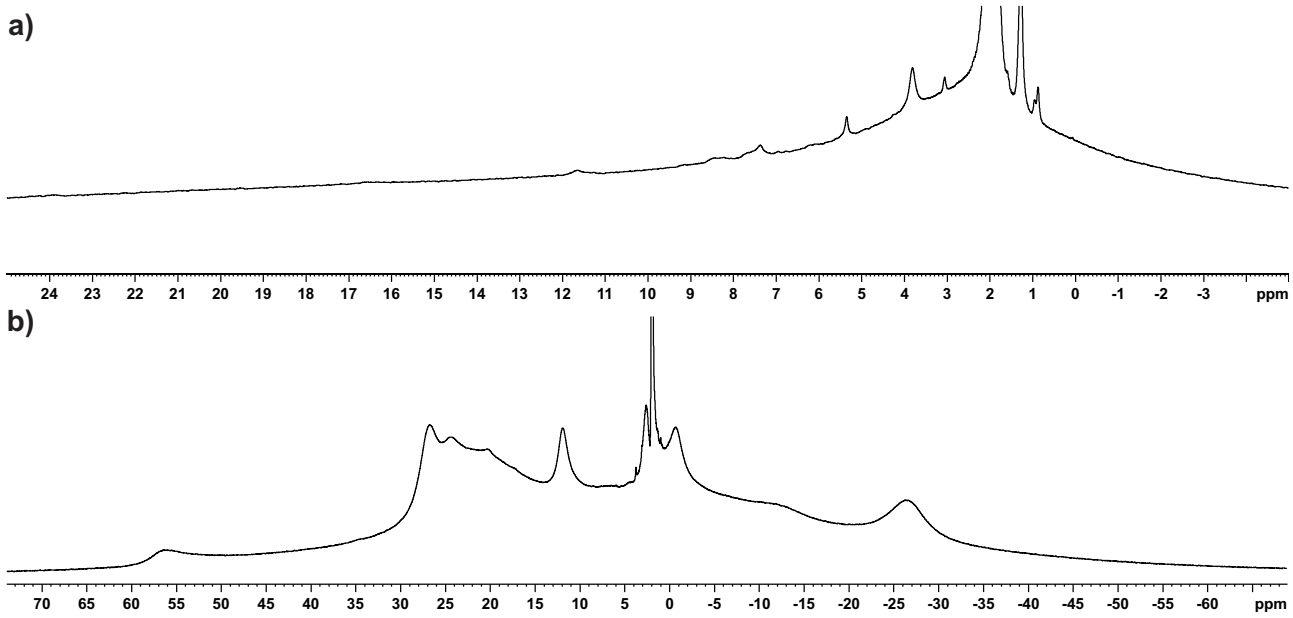

Figure 3.4: ^{1}H NMR spectra (500 MHz, CD_3CN, 298 K) of the proposed cages a) **66** and b) **65** after the self-assembly process.

Chapter 4

4 Mononuclear Complexes as LD-LISC Model Systems

This section is about the development of mononuclear complexes exhibiting the LD-LISC effect as model systems for metal-organic cages with photoswitchable ligands. Kieffer *et al.* have shown that mononuclear complexes have the potential to provide information about the properties of metal-organic cages such as the architecture or isomerism.[87] In addition other factors should be considered such as cooperativity or the complexity of the system.[213] However, in comparison to ligands for metal-organic cages, investigations of mononuclear complexes as model systems are beneficial due to the ease of synthetic accessibility of the ligands. For efficient LD-LISC model systems the ligands should stabilise both spin-states with long half-life times and provide a high photoefficiency with no switching fatigue.[200] As the photoswitchable group two different groups were investigated: i) azobenzenes based on the report of Hasegawa *et al.*[16] as a T-type photoswitch and ii) P-type dithienylethene due to its fast response to irradiation and high stability towards temperature changes[201,202] and known examples of LD-LISC complexes[203] (Figure 4.1). The depicted structures have a 2-(2'-pyridyl)-1*H*-benzimidazole backbone being a well-studied design for related thermal spin-crossover compounds.[16,214,221–223]

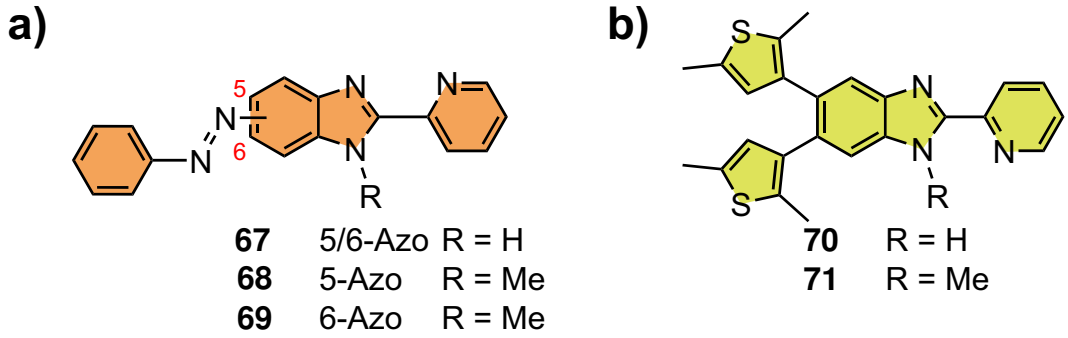

Figure 4.1: Target ligands within this section: a) azobenzenes and b) dithienylethenes.

In previous studies, Hasegawa *et al.*[16] prepared the Fe^{II}-based mononuclear complex **22** (see Chapter 1.3, Figure 1.2) and investigated its magnetic properties by irradiation with 365 nm and 436 nm. Photostationary states of 67:33 (365 nm irradiation, *trans*:*cis*) and 87:13 (436 nm irradiation, *trans*:*cis*) were observed. This means that quantitative isomerisation/back-isomerisation was not observed and that only 33% of the azobenzenes were isomerised into the *cis* configuration. Furthermore, magnetic susceptibility measurements indicated irreversible switching performance due to decreasing χ_MT values. The half-life time of azobenzene **67** and the Fe^{II}-based complex **22** were not reported.
The azobenzene design for photoswitches **68** and **69** is based on the ligand of Hasegawa *et al.*[16] (compound **67**). Since the Fe^{II}-based complex of ligand **67** exhibits a thermal spin-transition at 279 K with a poor photoeffiency, methylation of *N-H* groups of the ligands **68** and **69** will investigate i) if the imidazole tautomerism of ligand **35** (Scheme 4.1) causes the poor photoeffiency and switching fatigue and ii) if the spin-state transitions temperature increases closer to room temperature.[215] In addition, the influence of the isomerisation onto the photochemical properties and the spin-crossover behaviour of the respective Fe^{II}-based mononuclear complexes can be determined. Furthermore, the design of the dithienylethene is inspired by a related 2-(2'-pyridyl)-1*H*-imidazole compound having the photoswitchable group attached on an imidazole backbone by Lee *et al.*[242]

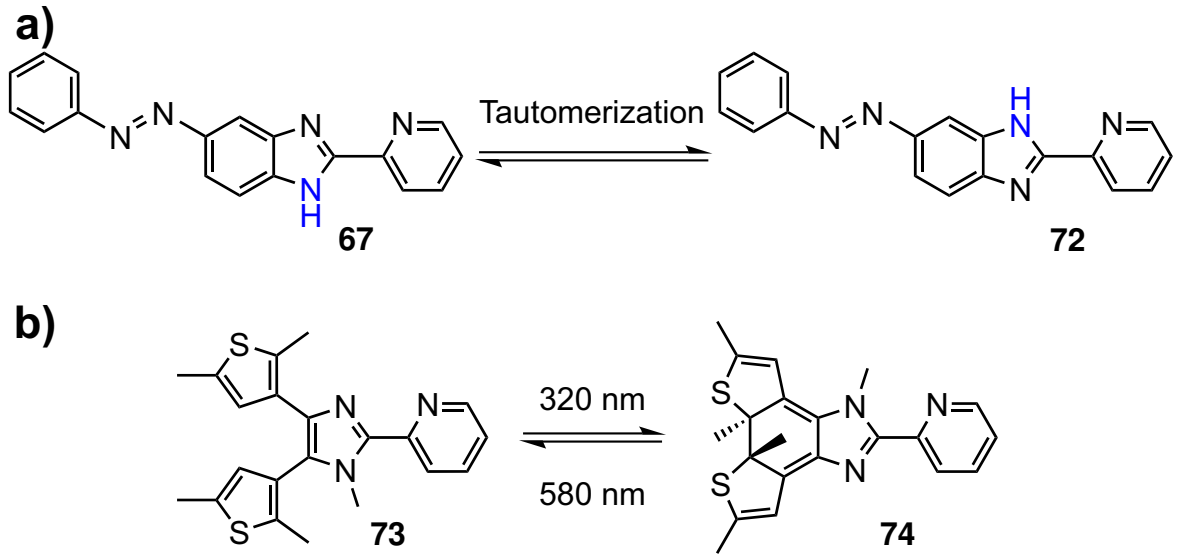

Scheme 4.1: a) Tautomerism of the *trans* isomer of azobenzene **67**. The relocated proton is highlighted in blue.[16] b) The synthesised dithienylethene **73** by Lee *et al.* as the design model for dithienylethenes in this dissertation.[242]

4.1 Azobenzene-based Model Systems

First studies focused on the reproduction of the investigations by Hasegawa *et al.* in order to gain knowledge about the synthesis and tautomerism of 2-(2'-pyridyl)-1*H*-benzimidazole derivatives. In addition, the photochemical properties such as the half-life time of azobenzene **67** will be investigated since Hasegawa *et al.* did not report the half-life time.[16] Therefore, ligand **67** was synthesised according to Scheme 4.2 in a linear four-step synthesis.[16] Hasegawa *et al.* reported the synthesis of the final product **67**,[16] whereas the other precursors are based on other known procedures.[11,14,15,243] In the first reaction a condensation reaction between *o*-phenylenediamine (**58**) and picolinic acid (**75**) will be performed to yield compound **76**. The target ligand **67** can be obtained after a nitration of **76** to compound **77**, reduction of the nitro group to the amine **78** and a Mills reaction between compound **78** and nitrosobenzene (**79**).

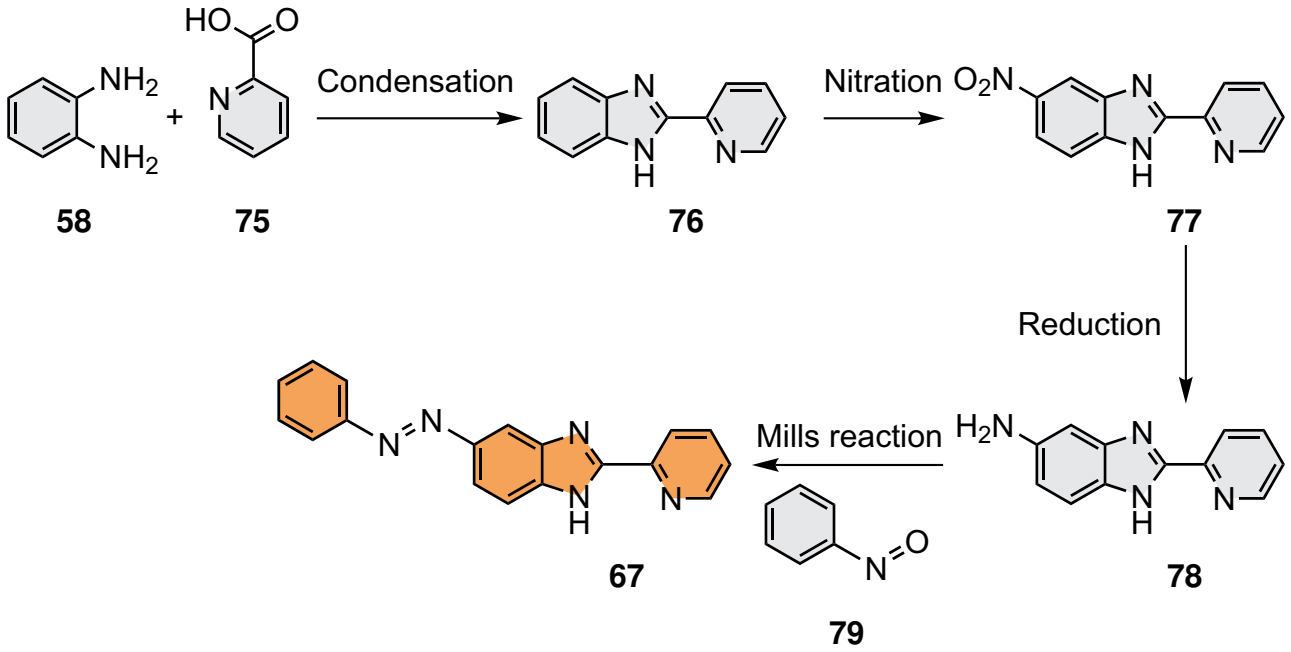

Scheme 4.2: Synthetic overview for *E*-2-(5'-bromopyridin-2'-yl)-5-(phenyldiazenyl)-1*H*-benzo[*d*]imidazole (**67**).

As the first step, *o*-phenylenediamine (**58**) and picolinic acid (**75**) were reacted in polyphosphoric acid as the catalyst and solvent at 170 °C for 20 h, adapting a procedure from Jia *et al.* (Scheme 4.3).[11] After work up the product **76** was obtained in a yield of 84% fitting to the literature value of 60-80%.[11]

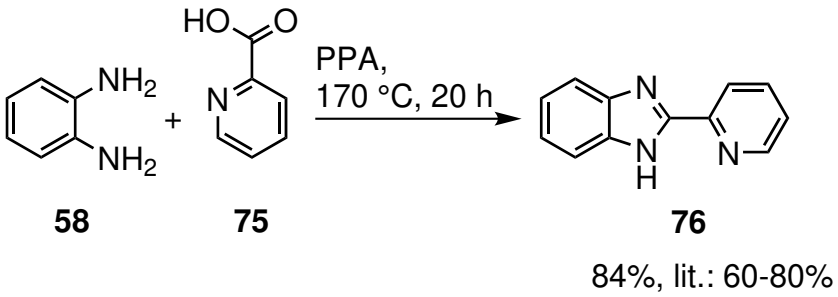

Scheme 4.3: Synthesis of 2-(pyridin-2'-yl)-1*H*-benzo[*d*]imidazole (**76**).[11]

In the first attempt the nitration was performed according to Haugwitz *et al.* using a mixture of nitric acid and sulfuric acid (1:6, v/v).[243] After cooling to 0 °C and the addition of the mixture to compound **76**, the reaction was further stirred at room temperature for 2 h. After work up, analysis by NMR spectroscopy revealed unreacted starting material **76** as well as the product **77**. Recrystallisation from methanol was performed and gave the target compound **77** in a yield of 33%, compared to the 43% reported.[243] Since unreacted starting material was observed, the ratio of nitric acid to sulfuric acid was adjusted (4:7, v/v) based on an adapted procedure from Ambacheu *et al.* (Scheme 4.4).[14] Compound **76** was dissolved in sulfuric acid, a mixture of nitric acid and sulfuric acid (4:7) was slowly added and the mixture was stirred at 0 °C and room temperature for each 1 h. Precipitation by basification gave the product **77** in quantitative yield without further purification necessary increasing the yield significantly. In addition, Ambacheu *et al.* reported a yield of 99.6%, which is in good agreement to the obtained yield.[14]

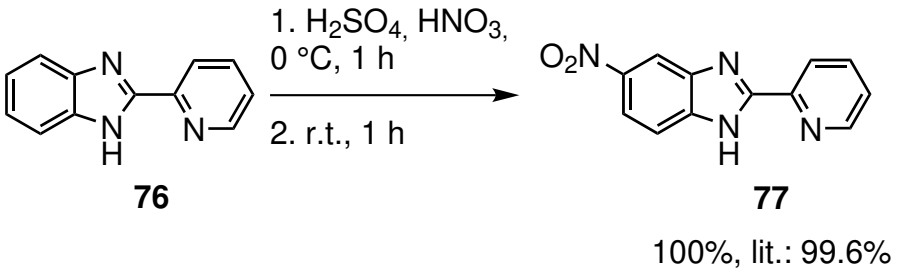

Scheme 4.4: Synthesis of 5-nitro-2-(pyridin-2'-yl)-1*H*-benzo[*d*]imidazole (**77**).[14]

In the next step the nitrated compound **77** was reduced using hydrogen and palladium on activated charcoal as the catalyst in dry ethanol (Scheme 4.5). The procedure was adapted from Schiffmann *et al.*.[15] After work up the product **78** was not obtained in pure form, therefore, purification by flash chromatography was attempted. However, unidentified impurities were still visible in the ^{1}H NMR spectrum. Further purification by recrystallisation was also not possible due to a syrup-oilish texture of the product. The crude product was used in the next step without further purification.

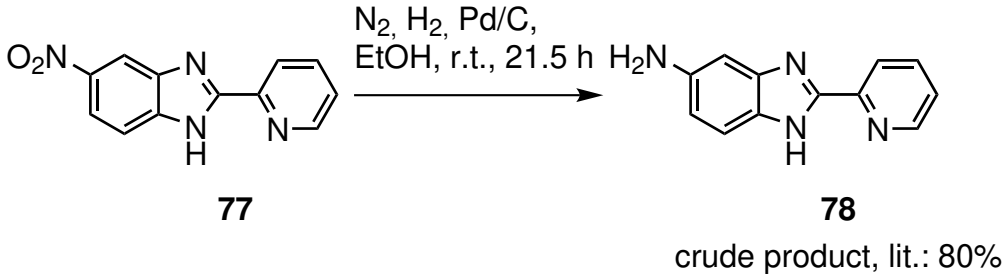

Scheme 4.5: Synthesis of 5-amino-2-(pyridin-2'-yl)-1*H*-benzo[*d*]imidazole (**78**).[15]

Compound **78** was then reacted in a Mills reaction with nitrosobenzene (**79**) in a mixture of chloroform and glacial acetic acid at room temperature for 19 h following the procedure from Hasegawa *et al.* (Scheme 4.6).[16] Multiple purifications by column chromatography on aluminum oxide gave azobenzene derivative **67** in 5% yield over two steps (equal to 22% per step). Hasegawa *et al.* reported for this reaction a higher yield of 42%. This can be explained by the difficult purification. During column chromatography the product streaked over aluminum oxide leading to losses of the product **67**. In addition, after the first flash chromatography a small impurity was visible in the ^{1}H NMR spectra leading to an additional flash chromatography being necessary to purify compound **67**.

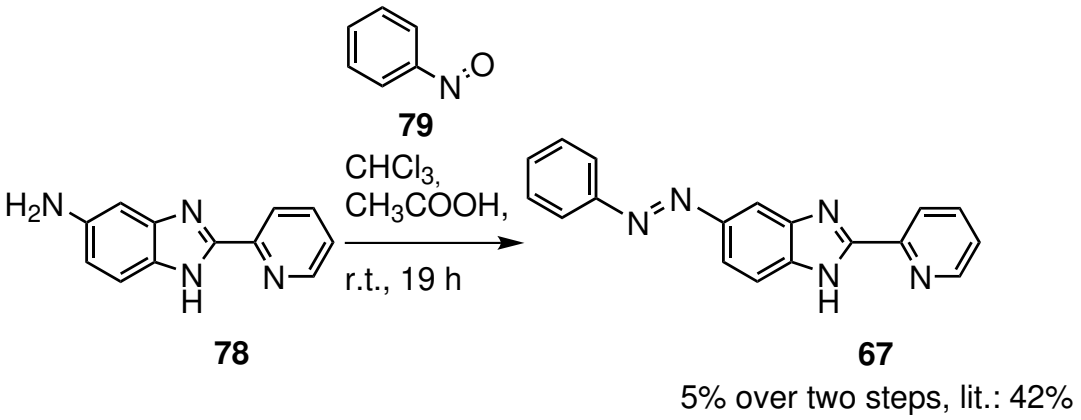

Scheme 4.6: Synthesis of *E*-2-(5'-bromopyridin-2'-yl)-5-(phenyldiazenyl)-1*H*-benzo[*d*]imidazole (**67**).[16]

Based on the reported results[16] ligands **68** and **69** were designed as two additional azobenzene derivatives (Scheme 4.7). Compound **77** will be methylated to obtain the isomers **80** and **81**. After a reduction and Mills reaction the target ligands **68** and **69** will be obtained. This synthetic strategy requires a separation of the different isomers from each other since after the different reaction steps isomeric mixtures are expected.[244]

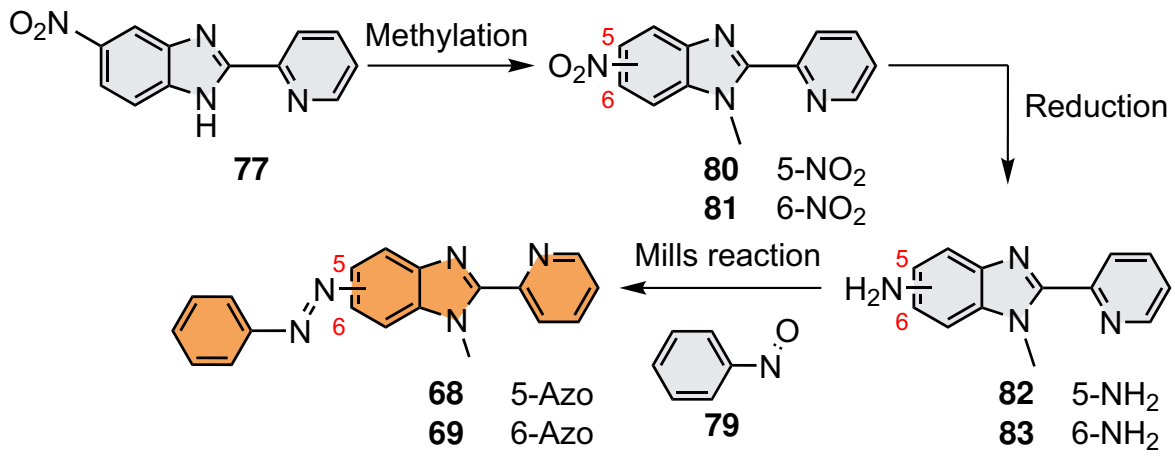

Scheme 4.7: Proposed synthesis of the methylated azobenzene derivatives **68** and **69**.

In the first attempts to synthesise isomers **68** and **69** a simple methylation of compound **77** was attempted (Scheme 4.8). Although the possible observation of an isomeric mixture is known in literature, the reaction was attempted since in some cases isomers can be separated by e.g. column chromatography.[244] Therefore, compound **77** was reacted with methyl iodide and potassium carbonate as the base in *N*,*N*-dimethylformamide at room temperature for 18 h, adapting a procedure from Lin *et al.*.[12] After work up an isomeric mixture of **80** and **81** was obtained. Thin-layer chromatography did not lead to any separation of the compounds. Due to that, the isomeric mixture was used in the next step without further purification. The isomeric mixture of **80** and **81** was reduced with hydrogen and palladium on activated charcoal as the catalyst at room temperature for 19 h.[15] After work up the separation of both isomers from each other (compound **82** and **83**) by thin-layer chromatography measurements was not possible. These results led to the conclusion that this synthetic pathway is not suitable to obtain the target ligands **68** and **69** by a simple methylation.

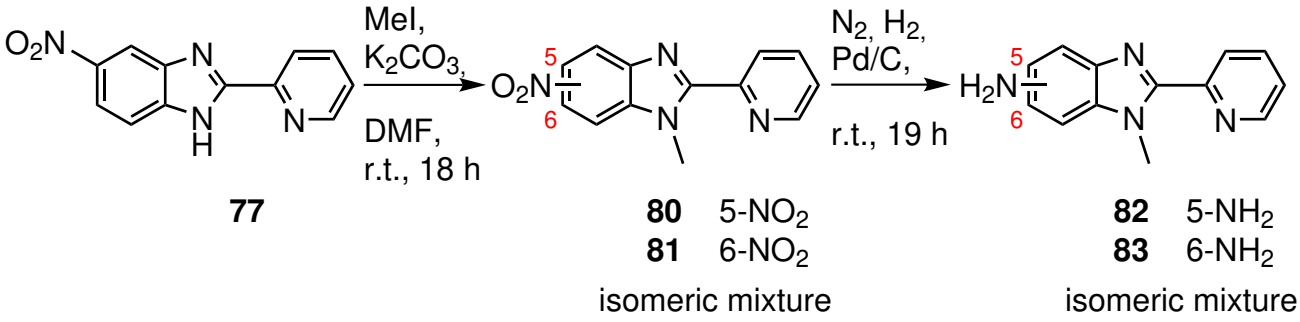

Scheme 4.8: Synthetic attempts using a methylation and reduction resulted in the isomeric mixtures **80/81** and **82/83**.

In attempt two a strategy was developed that starts with the synthesis of the isolated isomers since the separation of the isomers **80** and **81** or **82** and **83** was unsuccessful. In comparison to the previous strategy to access azobenzene **67**, this strategy uses commercially available *N*-methyl-4-nitrobenzene-1,2-diamine (**84**) as the starting material, because one amine group is regioselectively methylated to a *p*-nitro group that is required for the azo coupling. This allows the reduction of necessary synthetic steps from four to three by avoiding a nitration. The attempt was tested and designed for isomer **68** starting from compound **84** and picolinic acid (**75**) that can react in a condensation reaction to compound **85** (Scheme 4.9). After a reduction and a Mills reaction, the target ligand **68** can be obtained.

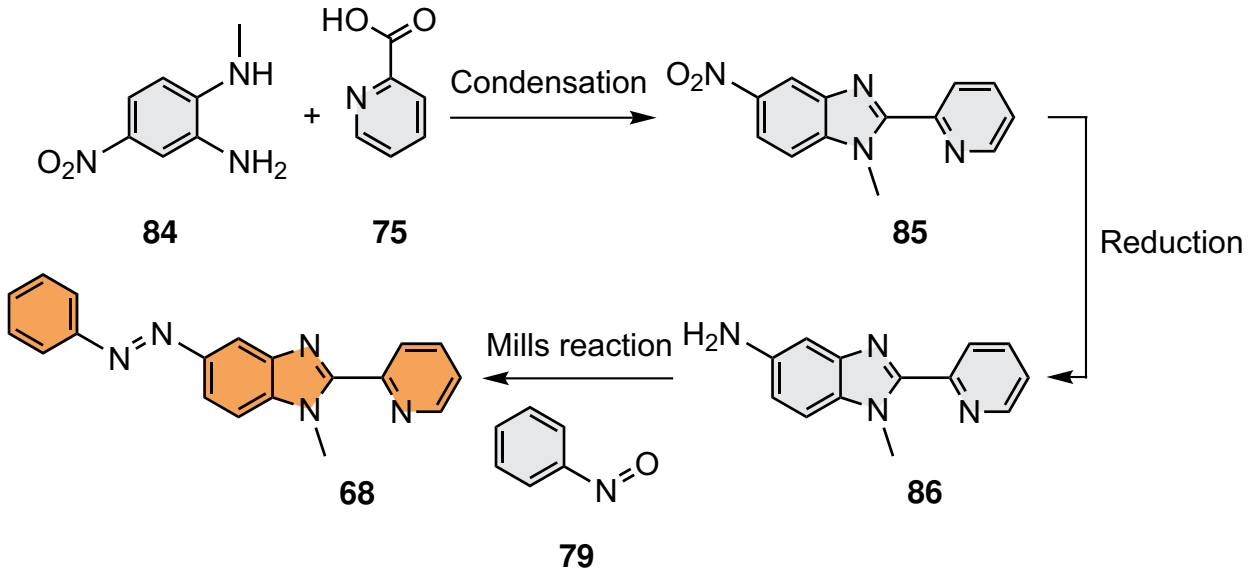

Scheme 4.9: Proposed synthesis of (*E*)-1-methyl-5-(phenyldiazenyl)-2-(pyridin-2'-yl)-1*H*-benzo[*d*]imidazole (**68**) over three steps.

N-Methyl-4-nitrobenzene-1,2-diamine (**84**) and picolinic acid (**75**) were reacted in a condensation reaction based on an adapted procedure from Jia *et al.* (Scheme 4.10).[11] In the first attempt the reaction was stirred at 180 °C for 4 h and after work up thin-layer chromatography measurements indicated the formation of the desired product **85**. Purification by flash chromatography gave the product **85** in a very low yield of 5%. The product losses might be attributed to two factors: i) streaking on silica leading to losses of product **85** during the purification and ii) incomplete conversion of the starting materials **84** and **75** after 4 h. Therefore, the reaction was repeated at 180 °C for 20 h on a smaller scale, but after the work up no product was isolated for unknown reason. Since product **85** was formed within the first reaction further optimisation reactions are necessary to increase the yield from 5%. Due to the harsh reaction conditions (180 °C in acid), reaction control by thin-layer chromatography measurements is not feasible. As a result, the focus was changed using milder reaction conditions for the condensation/cyclisation reaction for the possibility to monitor the reaction

by thin-layer chromatography.

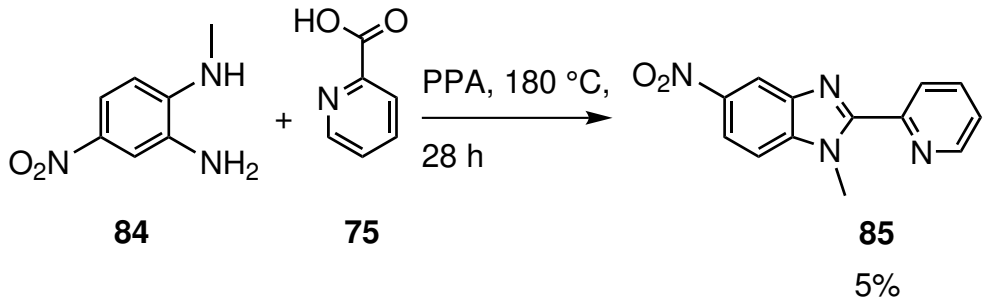

Scheme 4.10: Synthesis of 2-(pyridin-2'-yl)-1-methyl-5-nitro-1*H*-benzo[*d*]imidazole (**85**).[11]

In this approach multiple modifications to the synthetic pathway were implemented: i) the use of bromo derivatives **87** and **88** due to their lower cost in comparison to the nitro derivative in the previous attempt (compound **85**), ii) milder reaction conditions for the condensation reaction using a 2-nitro-*N*-methylamine and an aldehyde compound as the starting materials and iii) introduction of the needed amine group for the final azo-coupling by amination of the bromides. The synthetic pathway was designed in collaboration with Eicke Trumpf (Scheme 4.11).[245] Starting from the bromo derivatives **87** and **88**, the target compounds **68** and **69** can be obtained in a linear five-step synthesis. Initally, a methylation will be performed followed by a cyclisation reaction using 2-pyridinecarboxaldehyde (**91**) to give target compounds **92** and **93**. The bromo substituent will then be substituted with a protected amine group and the protecting group will be cleaved. The obtained amines **86** and **98** can be further used in the Mills reaction to obtain the desired azobenzene isomers **68** and **69**.

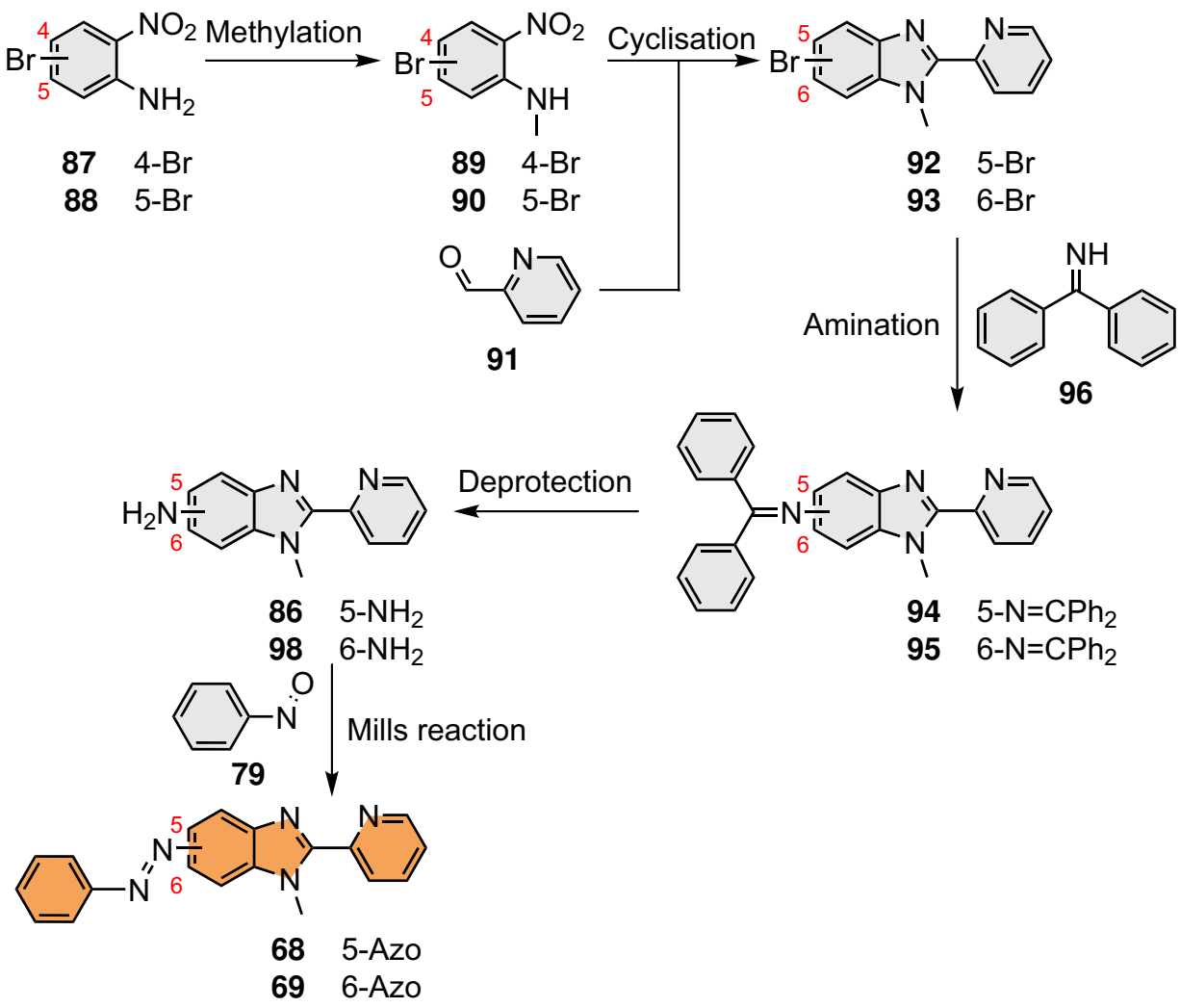

Scheme 4.11: Proposed synthesis of azobenzenes **68** and **69** following five reaction steps.

The first step was performed adapting reaction conditions from Zhegalova *et al.* (Scheme 4.12).[17] 4-Bromo-2-nitroaniline (**87**) or 5-bromo-2-nitroaniline (**88**) were reacted with sodium hydride in tetrahydrofuran at 0 °C for 5 min before methyl iodide was added for the methylation. After stirring at room temperature for 18.5 h the products **89** and **90** were obtained after a simple work up in excellent yields of 94% (compound **89**), in good agreement with the literature yield of 99%[17] and 96% (compound **90**).

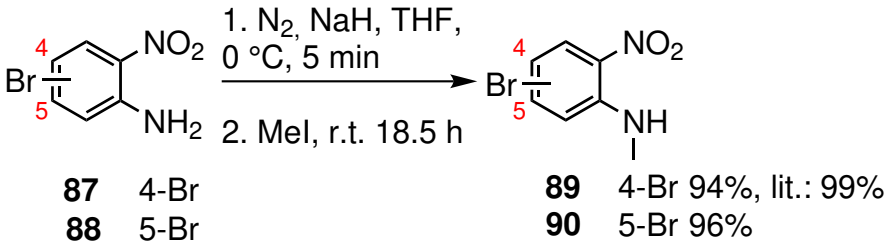

Scheme 4.12: Synthesis of 4-bromo-*N*-methyl-2-nitroaniline (**89**) and 5-bromo-*N*-methyl-2-nitroaniline (**90**).[17]

Afterwards, a milder condensation/cyclisation reaction was attempted adapting reaction conditions from Yang *et al.*.[18] Compounds **89** and **90** were reacted with 2-pyridinecarboxaldehyde (**91**) in a mixture of ethanol, *N*,*N*-dimethylformamide and water at 80 °C for 20 h in the case of compound **89** or 26 h for substance **90**. As an additive sodium dithionite was added for the *in situ* reduction of the nitro group.[18] After work up both isomers were obtained in good yields (74% for compound **92**, 72% for compound **93**) without any further purification necessary. This reaction has shown great potential as an alternative to the condensation reaction using polyphosphoric acid since milder reaction conditions can be used with the possibility to monitor the reaction by thin-layer chromatography to improve the yield, if needed.

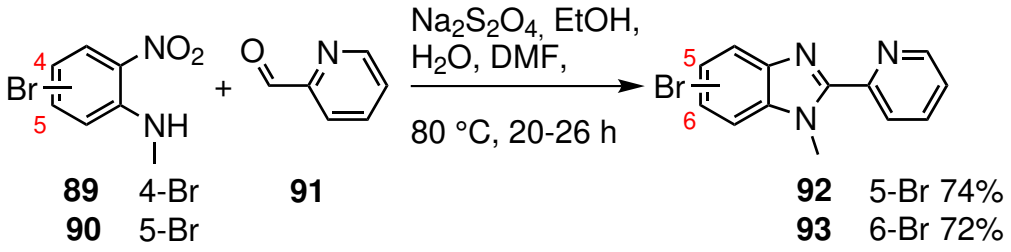

Scheme 4.13: Synthesis of 5-bromo-1-methyl-2-(pyridin-2'-yl)-1*H*-benzo[*d*]imidazole (**92**) and 6-bromo-1-methyl-2-(pyridin-2'-yl)-1*H*-benzo[*d*]imidazole (**93**).[18]

In the next step a protected amine functionality was introduced for later functionalisation with an azobenzene. Adapted reaction conditions from Wolfe *et al.* were applied.[19] The starting materials **92** or **93** were reacted with benzophenone imine (**96**) in toluene using sodium *tert*-butoxide as the base, *R*-BINAP as an additive and $Pd_2(dba)_3$ as the catalyst at 90 °C for 24 h (compound **94**) or 23 h (compound **95**). After purification by recrystallisation compound **94** was obtained in a yield of 66%, however, the recrystallisation of compound **95** was more difficult. Although some precipitate was observed it could not be filtered due to the small size of the particles. Therefore, the crude product **95** was used in the next step without further purification.

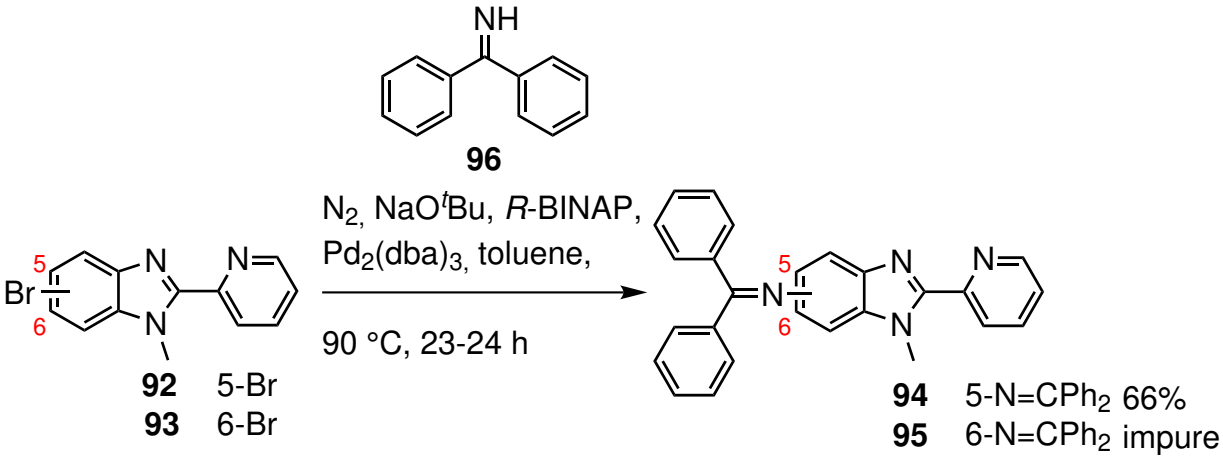

Scheme 4.14: Synthesis of *N*-(1'-methyl-2'-(pyridin-2"-yl)-1*H*-benzo[*d*]imidazol-5'-yl)-1,1-diphenylmethanimine (**94**) and *N*-(1'-methyl-2'-(pyridin-2"-yl)-1*H*-benzo[*d*]imidazol-6'-yl)-1,1-diphenylmethanimine (**95**).[19]

The benzophenone imine protecting group was then hydrolysed adapting again a procedure from Wolfe *et al.* (Scheme 4.15).[19] To a solution of compound **94** or crude product **95** was added hydrochloric acid for deprotection. After stirring at room temperature for 25 min the reaction of compound **94** was stopped, worked up and the desired product **86** was obtained in a yield of 72%. The deprotection reaction of the crude product **95** was stopped after 1.5 h and worked up in a similar manner. However, the product **98** was not obtained in pure form. Due to streaking on silica gel, the crude product **98** was used in the next step without further purification.

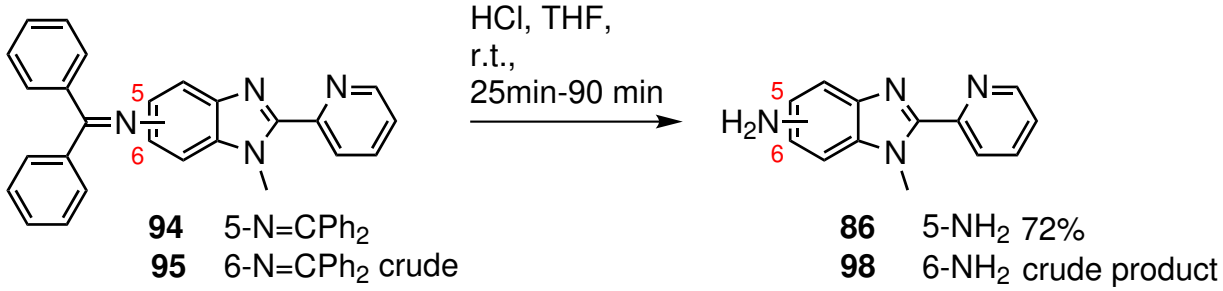

Scheme 4.15: Synthesis of 1-methyl-2-(pyridin-2'-yl)-1*H*-benzo[*d*]imidazol-5-amine (**86**) and 1-methyl-2-(pyridin-2'-yl)-1*H*-benzo[*d*]imidazol-6-amine (**98**).[19]

Since both amines were successfully synthesised the last step, a Mills reaction was attempted adapting reaction conditions from Hasegawa *et al.*.[16] The appropriate amines **86** and **98** (impure) were reacted with nitrosobenzene (**79**) in a solvent mixture of chloroform and glacial acetic acid at room temperature for 23 h (compound **68**) or 22 h (compound **69**) (Scheme 4.16). Purification by flash chromatography

with an additional recrystallisation from cyclohexane with small amounts of dichloromethane gave the desired azobenzene derivative **68** in a yield of 25% and compound **69** in a yield of 21% over three steps. In both cases single crystals suitable for X-ray crystallography were obtained, confirming the expected structures of the azobenzenes **68** and **69** (Figure 8.130).

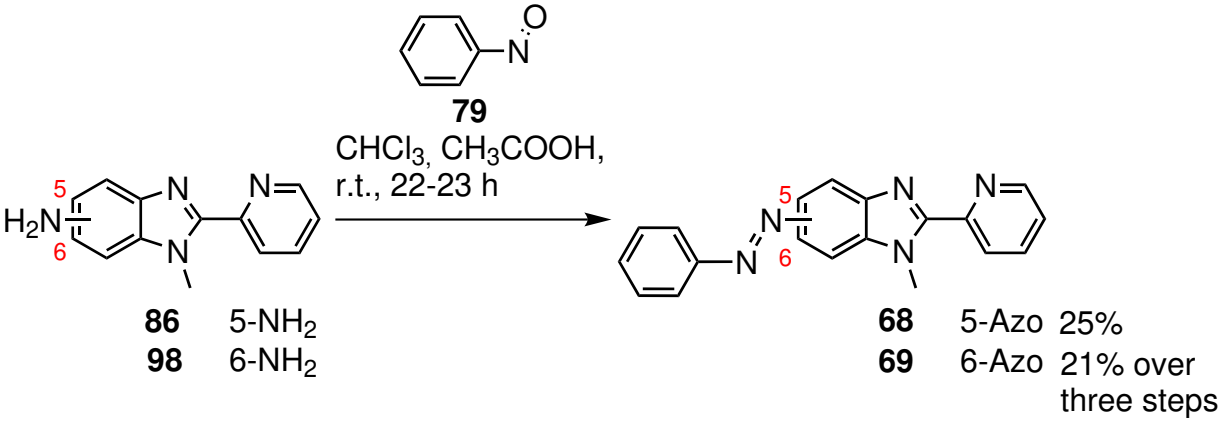

Scheme 4.16: Synthesis of (*E*)-1-methyl-5-(phenyldiazenyl)-2-(pyridin-2'-yl)-1*H*-benzo[*d*]imidazole (**68**) and (*E*)-1-methyl-6-(phenyldiazenyl)-2-(pyridin-2'-yl)-1*H*-benzo[*d*]imidazole (**69**).[16]

Since compound **98** was only obtained as an impure compound over two steps adapting the procedure from Wolfe *et al.*,[19] the work up procedure was modified (Scheme 4.17). After changing the molarity of the hydrochloric acid, pure product **98** was obtained in a yield of 68% over two steps (Experimental details see section 7.4.12).

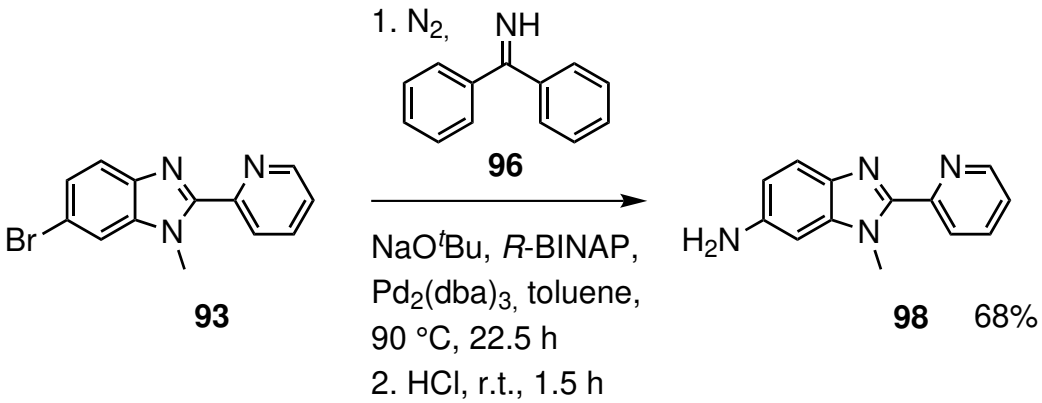

Scheme 4.17: Synthesis of 1-methyl-2-(pyridin-2'-yl)-1*H*-benzo[*d*]imidazol-6-amine (**98**).[19]

4.1.1 Tautomerism of azobenzene 67

The tautomerism of ligand **67** was investigated in deuterated acetone by irradiation with 365 nm for isomerisation and 435 nm for backisomerisation and followed by ^{1}H NMR spectroscopy (Scheme 4.18). The wavelengths for the irradiation experiments were reported by Hasegawa *et al.*[16] Before irradiation with 365 nm two sets of signals were visible in the ^{1}H NMR spectrum (Figure 4.2, blue) with similar chemical shifts. As an example, two imine proton signals were observed at 12.4 ppm. Both sets of signals were assigned to the possible *trans* tautomers **67** and **72** (Figure 4.18). Upon irradiation with 435 nm two additional signal sets were observed, attributed to the isomerisation to both *cis* tautomers **99** and **100**. However, the imine proton signals at 12.2 ppm were not distinguishable due to signal overlap. The observation of all four species made ^{1}H and ^{13}C assignment challenging, but possible (Scheme 4.18). The observation of the tautomerism was not explicitly mentioned, but is important to state for the analysis of its photochemical properties in acetone since the measured photostationary states, half-life times and absorption maxima are an average of the four possible, observable tautomers.

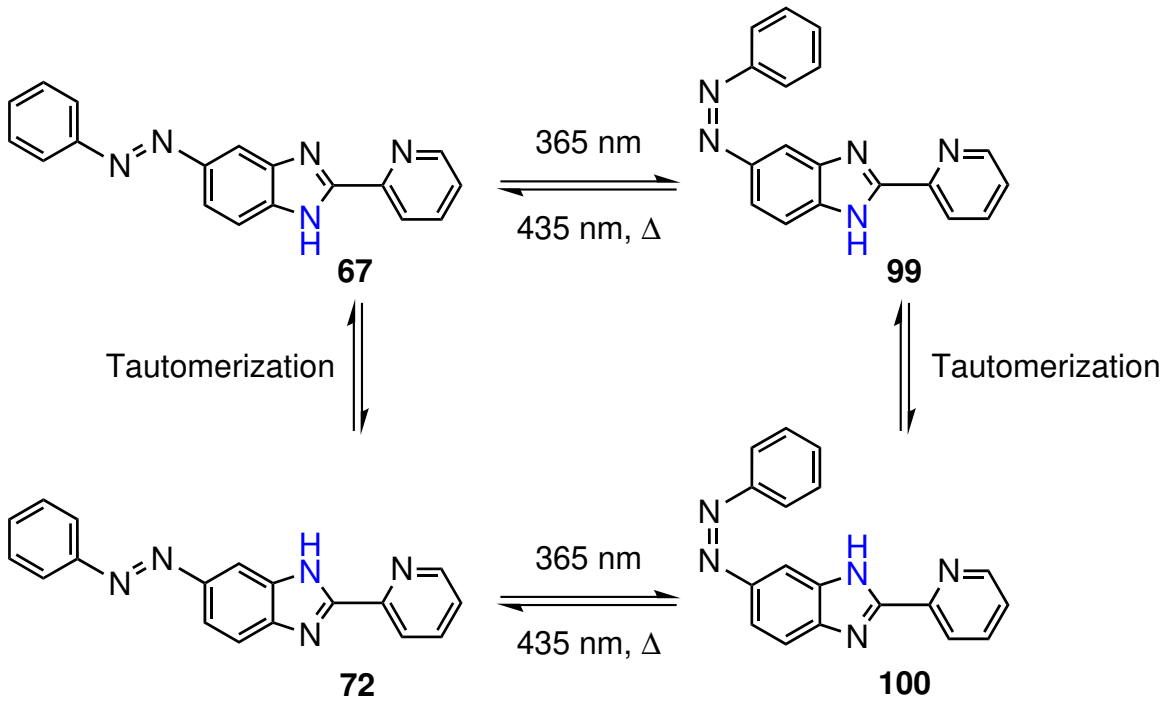

Scheme 4.18: Observed tautomerization of compound **67** and **99** in deuterated acetone. The relocated proton is highlighted in blue.

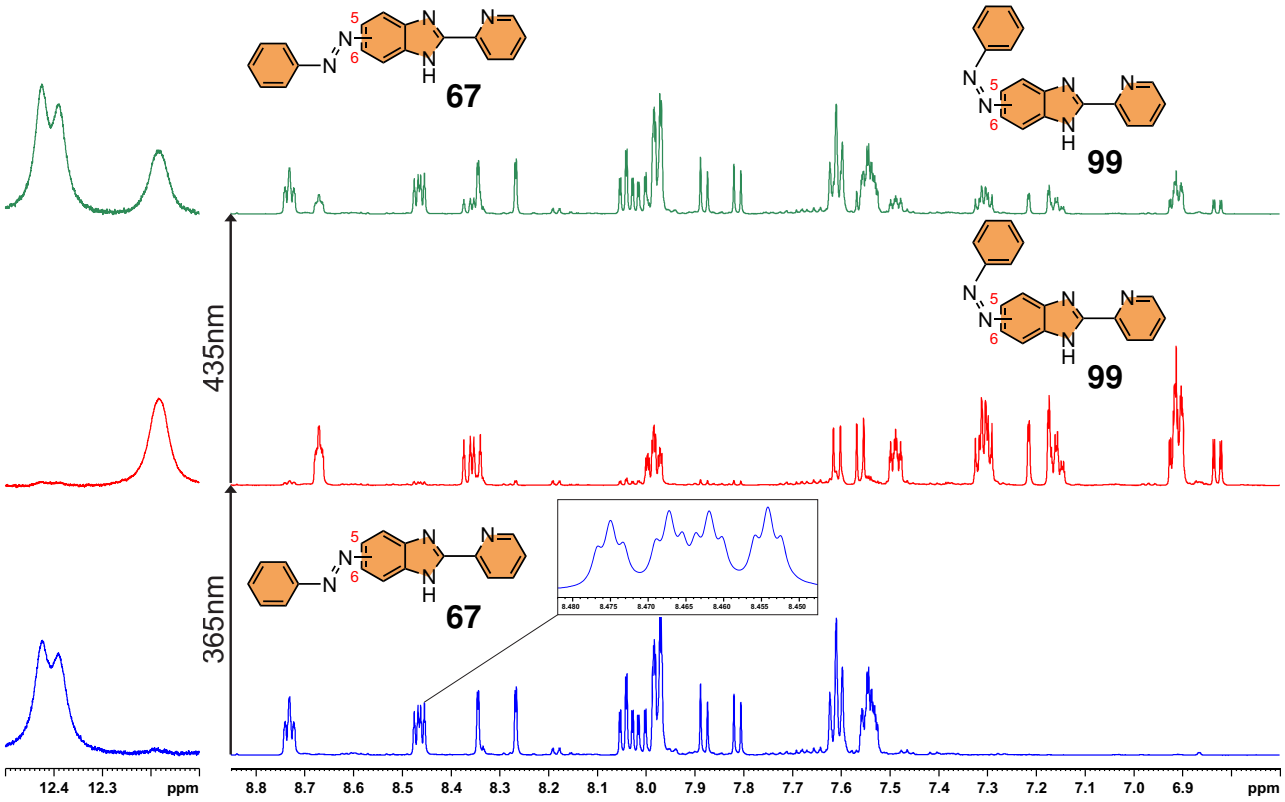

Figure 4.2: ^{1}H NMR spectra (500 MHz, acetone-d_6, 298 K) of azobenzene **67** before (blue) and after irradiation with 365 nm (red) and 435 nm (green). The N-H signal is shown in the range of 12.7 to 12.0 ppm and indicates the observation of both *trans* tautomers at room temperature.

4.1.2 Photochemical Properties

The photochemical properties of azobenzenes **67**, **68** and **69** were examined in acetone by NMR and UV/Vis spectroscopy. The switching experiments were performed using the same wavelengths as in the previous section 4.1.1 and reported by Hasegawa *et al.*[16] Based on the report of Hasegawa *et al.*, the isomerisation of compound **67** from the *trans* to the *cis* isomer or *vice versa* is not quantitative. This result was also expected for the methylated derivatives **68** and **69**.[16]

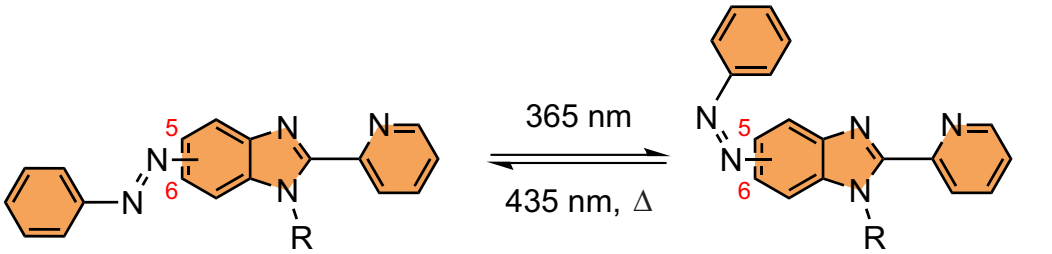

67 5/6-Azo R = H
68 5-Azo R = Me
69 6-Azo R = Me

99 5/6-Azo R = H
101 5-Azo R = Me
102 6-Azo R = Me

Scheme 4.19: The three *trans* azobenzene derivatives **67**, **68** and **69** can be switched by irradiation with 365 nm. Backisomerisation can be achieved by either irradiation with 435 nm and/or heat.

UV/Vis spectroscopy measurements were performed to calculate half-life times and assign absorption maxima for the pure *trans* isomers and in the PSS at 365 nm (Table 4.1). For the measurements stock solutions in acetone ($1 \cdot 10^{-5}$ M) of the appropriate azobenzenes were prepared and measured before and after irradiation with 365 nm/435 nm. The absorption maxima will be discussed for azobenzene **67** only since similar trends were observed for the other derivatives **68** and **69**. Initially, 100% *trans* isomer **67** shows an absorption maximum centered at 356 nm, attributed to a π-π^* band.[246] Upon irradiation with 365 nm the π-π^* band shifts hypsochromically with an decreased absorption. In addition, the rise of an additional absorption maximum at 436 nm is observed being assigned to the n-π^* band.[246] By irradiation with 435 nm the photostationary state was reached after 10 min leading to an increased π-π^* band and decreased n-π^* band.

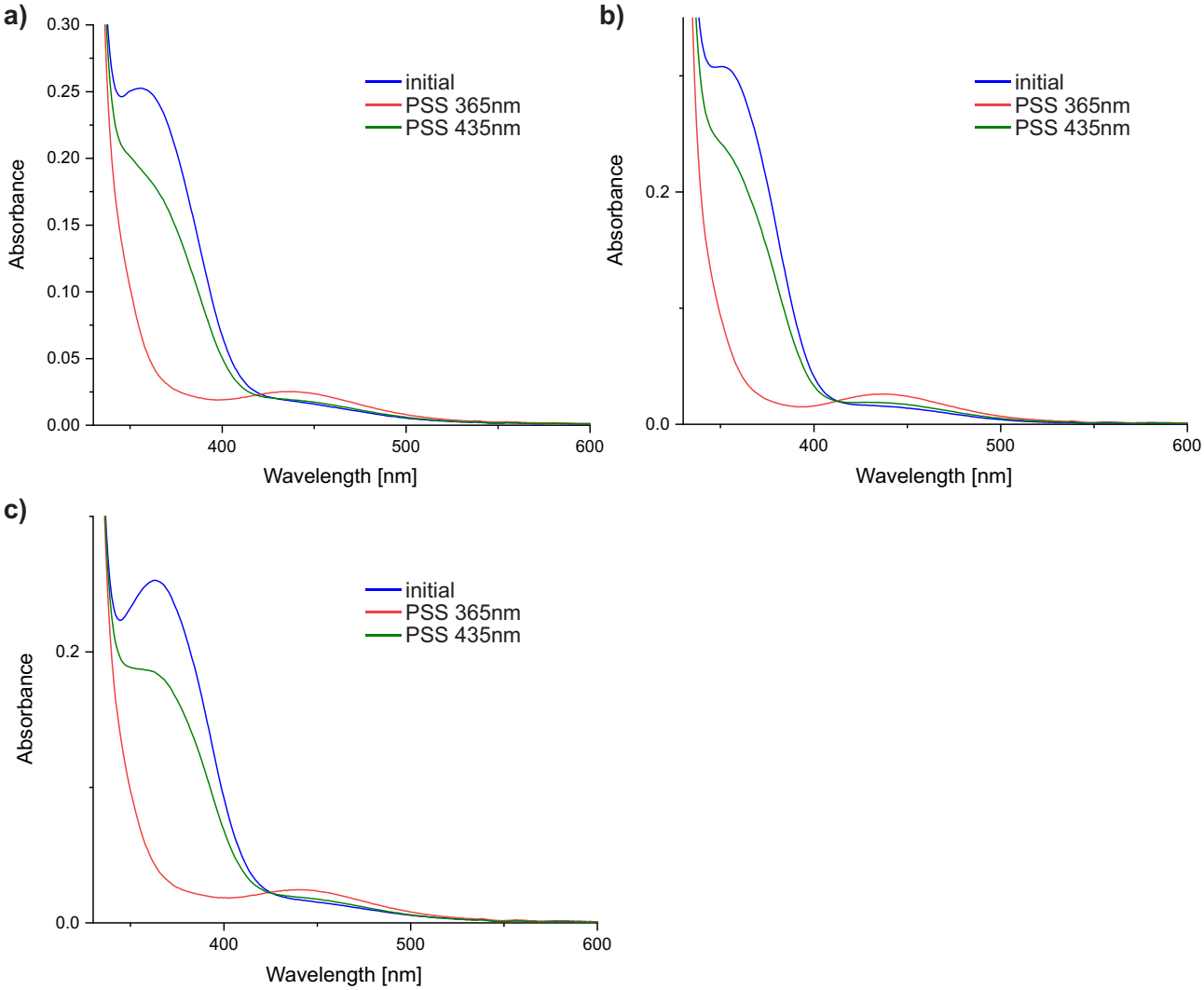

Figure 4.3: UV/Vis spectrum ($1{\cdot}10^{-5}$ M, acetone, 293 K) of azobenzenes a) **67**, b) **68** and c) **69**. Photostationary states were reached upon irradiation with 365 nm (red) and 435 nm (green).

Half-life times of azobenzenes **99**, **101** and **102** were further measured at the same stated concentrations by UV/Vis spectroscopy ($1{\cdot}10^{-5}$ M). Therefore, the azobenzenes were measured in its 100% *trans* form and the samples irradiated with 365 nm for 10 min. Afterwards, every 30 min a UV/vis spectrum was measured over the course of two days (in total 96 data points). The calculated half-life times are shown in Table 4.1. The half-life times of the methylated isomers **101** ($\tau_{1/2}$ = 180.4 h) and **102** ($\tau_{1/2}$ = 52.8 h) differ by 130 h. This result is most likely attributed to the more effective conjugation of azobenzene **69** leading to a more stabilised *trans* isomer in comparison to its *cis* form. Furthermore, the half-life time of azobenzene **99** was expected to be within the range of the other isomers, and indeed, a half-life time of 84.8 h was calculated. Based on tautomerisation this half-life time is an average of both *cis* species **99** and **100** and was not reported so far by Hasegawa *et al.*.[16] The calculated half-life

times indicate that the isomer **68** has the greatest potential as a suitable LD-LISC model compound since the respective *cis* isomer has a very long half-life time of 180.4 h.

Table 4.1: Photochemical properties of the azobenzenes **67**, **68** and **69** based on NMR and UV/Vis spectroscopy data.

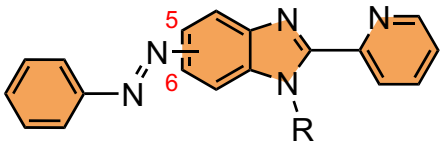

67 5/6-Azo R = H
68 5-Azo R = Me
69 6-Azo R = Me

Azobenzene	PSS 365 nm [%][1]	PSS 435 nm [%][1]	λ_{max} (E) [nm][2]	λ_{max} (Z) [nm][2]	$\tau_{1/2}$ [h][2]
67	8:92	71:29	356	436	84.8±0.1
68	5:95	71:29	351	436	180.4±0.2
69	5:95	70:30	363	440-441	52.8±0.1

[1] Data is calculated based on integrals in ^{1}H NMR spectra.

[2] Data is based on UV/Vis measurements at 293 K in acetone.

Furthermore, the photostationary states were examined by NMR spectroscopy (ratios see Table 4.1). Small amounts of the azobenzenes **67**, **68** and **69** (0.5 mg-0.7 mg/500 μmol) were dissolved in deuterated acetone and a ^{1}H NMR spectra was initally recorded. The *trans*/*cis* ratios were examined after irradiation with 365 nm by integration of the observed ^{1}H signals. The same procedure was repeated during the back-isomerisation with 435 nm.

Upon irradiation with 365 nm for 20 min the *trans* isomer **67** can be switched into the *cis* isomer **99** (Figure 4.2). Incomplete switching was observed (*trans*/*cis* ratio of 8%:92%) (Figure 8.3). This result is consistent with the reported data by Hasegawa *et al.* (*trans*/*cis* 6%:94%).[16] By irradiation with 365 nm the photostationary state of azobenzenes **68** and **69** was reached after only 10 min indicating quicker isomerisation from *trans* to *cis* (Figures 8.1 and 8.2). In both cases *trans*/*cis* ratios of 5%:95% were observed (Azobenzenes **68**:**101** and **69**:**102**) (Figures 8.4 and 8.5).

Subsequent irradiation with 435 nm for 10 min led to *trans*/*cis* ratios in the photostationary state of 71%:29% (Azobenzenes **67**:**99** and **68**:**101**) and 70%:30% (Azobenzenes **69**:**102**). These results are also in good agreement to the literature value for azobenzenes **67**:**99** of 72%:28%.[16] Complete back-isomerisation can be achieved by heating the azobenzene derivatives at 50 °C for two weeks in the dark.

4.1.3 FeL_3 Mononuclear Complexes

In section 4.1 the three azobenzene derivatives **67**, **68** and **69** were successfully synthesised and their photochemical properties were investigated by NMR and UV/Vis spectroscopy. In this section the investigations will be extended to the preparation of FeL_3 mononuclear complexes with L being either azobenzene **67**, **68** or **69**. This section will investigate whether the mononuclear complexes can be characterised using commonly used tools such as NMR spectroscopy, the paramagnetic NMR toolbox[231,232] and ESI-MS. Afterwards, the photochemical properties such as photoefficiency, half-life time and switching fatigue of the complexes would be of great interest.

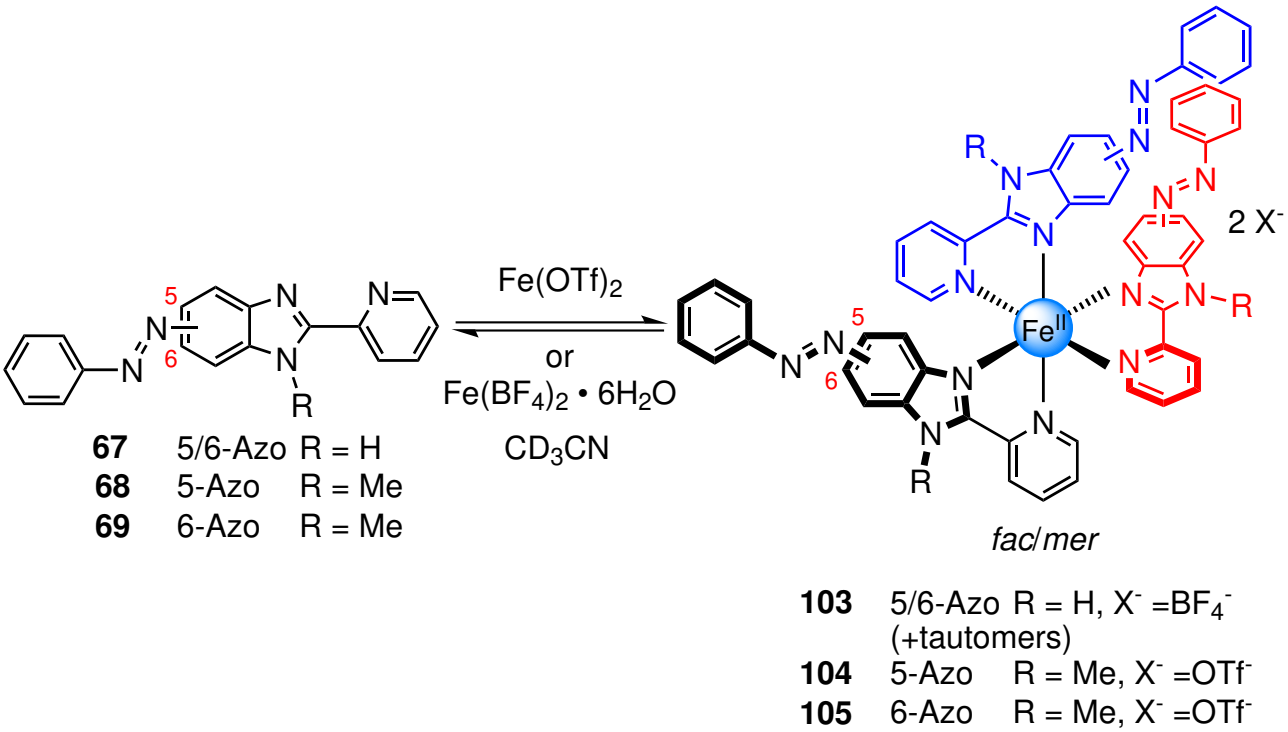

Figure 4.20: Proposed complex formation of $Fe(OTf)_2$ or $Fe(BF_4)\cdot 6H_2O$ with the respective azobenzene derivatives and the expected FeL_3 complex structures. *fac*/*mer* Isomers are expected and additional tautomers in the case of **103**.

In the previously reported study by Hasegawa *et al.* the mixture of multiple complexes **103** was prepared and their photochemical properties investigated in deuterated acetone.[16] For comparability and reproducibility of the photochemical and magnetic properties of the mixture **103** in future studies, the following characterisation attempts were also conducted in deuterated acetone. The characterisation attempts will determine whether characterisation by NMR spectroscopy of the complex mixture **103** is feasible since tautomerism is expected.

The preparation of mixture **103** was attempted adapting the procedure from Hasegawa *et al.*[16] In

two test tubes, three equivalents of azobenzene azobenzene **67** and one equivalent of $Fe(BF_4)\cdot 6H_2O$ were dissolved in acetone, the solutions were combined (c = $4.4\cdot 10^{-2}$ M) and stirred for further 20 min at 30 °C as room temperature. Afterwards, the solution was kept in the freezer over night for crystallisation. However, precipitation of the mixture **103** was not observed. In comparison, Hasegawa *et al.* reported the preparation at 20 °C as room temperature and on a larger scale.[16] Since Hasegawa *et al.* observed crystallisation[16] mixture **103** was characterised by elemental analysis instead of NMR spectroscopy. Unfortunately, in this attempt crystals were not obtained. The reason for that might be due to the high room temperature that influences the complex formation. Due to that, the solvent was removed and the residue was further investigated. As a first attempt, the solid was investigated by elemental analysis to investigate the elemental composition of the preparation attempt, but the experimental and theoretical ratios did not match to the expected FeL_3 mixture **103** and reported elemental analysis data of Hasegawa *et al.*[16] Intensive drying did not improve the results. The solid's impurity is unknown.

Therefore, further investigations were conducted using NMR spectroscopy to potentially characterise mixture **103** in solution. Eleven proton signals are expected for one ligand environment. Based on the expected statistical mixture (*mer*:*fac*, 3:1),[133,136] four ligand environments are expected making in total 44 ^{1}H signals. If tautomerism is observed an additional 44 ^{1}H signals might occur. The solid was dissolved in deuterated acetone and a ^{1}H NMR spectrum measured. The ^{1}H NMR spectrum showed more than the expected ^{1}H signals indicating the possible formation of multiple species (Figure 4.4). The large number of signals in the ^{1}H NMR spectrum is assumed to be a result of the occurance of *fac*/*mer* isomers and tautomers. ^{1}H assignment was not possible due to signal broadening and overlap. In order to clarify if mixture **103** was formed during the preparation, ESI-MS data was collected. The expected FeL_3 species (*m/z* 476.6423) was identified, but ESI-MS data also confirmed other unidentified species. Further characterisation attempts were not performed.

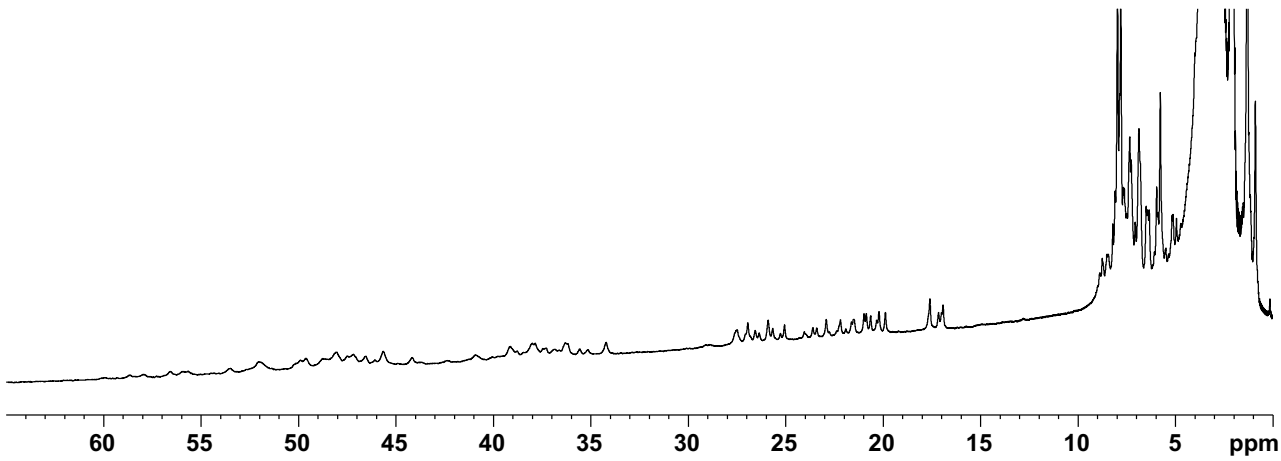

Figure 4.4: ^{1}H NMR spectra (500 MHz, acetone-d_6, 298 K) of the complex preparation with azobenzene **67** and $Fe(BF_4)_2\cdot 6H_2O$.

The focus was changed towards the methylated azobenzenes **68** and **69** as the ligand due to two reasons: i) the magnetic and photochemical properties of complex mixture **103** are already reported[16] and ii) *N*-methylation prevents tautomerism leading to a reduced number of potential species so that characterisation by NMR spectroscopy may be possible. In these attempts the preparations of the corresponding complexes were directly prepared in NMR tubes due to the unsuccessful precipitation in the previous attempt and to also investigate the complex formation on a smaller scale. Due to the hygroscopic properties of the previously used $Fe(BF_4)_2 \cdot 6H_2O$ salt, $Fe(OTf)_2$ was used as a substitute for simpler handling and for comparability since $Fe(OTf)_2$ was used in the spin-crossover studies of thermal spin-crossover cages.[235]

$Fe(OTf)_2$ and azobenzene **68** ($2.14 \cdot 10^{-2}$ M) or **69** ($2.32 \cdot 10^{-2}$ M) were dissolved in a ratio of 1:3 in deuterated acetone and were analysed by NMR spectroscopy. In the ^{1}H NMR spectra 44 ^{1}H signals are expected since the ligands **68** and **69** have 11 protons and four ligand environments are potentially observable (*fac*/*mer* isomers).[133,136] For the attempt with ligand **68** 40 signals in the range of 24.6 to 1.30 ppm were observed in the ^{1}H NMR spectrum, indicating the presence of the *fac*/*mer* isomers or free ligand with the *mer* isomer. Four ^{1}H signals are missing potentially due to signal overlap or broadening (Figure 4.5). Proton assignment was attempted using paramagnetic ^{1}H-^{1}H COSY and ^{1}H-^{1}H NOESY pulse programs.[231,232] Although some protons showed cross-peaks, assignment to a particular proton was not possible. The proton assignment was unsuccessful due to the missing cross-peaks in the ^{1}H-^{1}H COSY spectrum (Figure 4.6). Afterwards, a ^{1}H-^{1}H NOESY spectrum was measured since EXSY instead of NOE cross-peaks were observed in previous studies of paramagnetic complexes that can help to group protons according to their ligand environments.[231,232] Analysis of the ^{1}H-^{1}H NOESY spectrum showed only poorly visible exchange cross-peaks (EXSY) for 6 out of 40 signals (Figure 4.7). Based on these results proton assignment was not possible and further optimisation of the NMR parameters are needed in order to observe more cross-peaks in the 2D spectra.

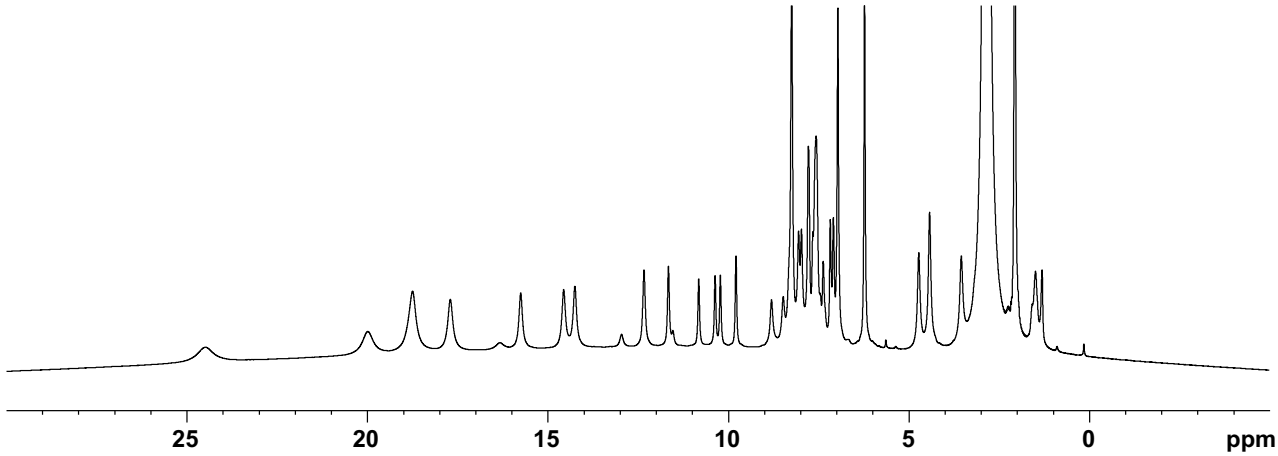

Figure 4.5: ^{1}H NMR spectrum (500 MHz, acetone-d_6, 298 K) of the expected structure of complex **104**.

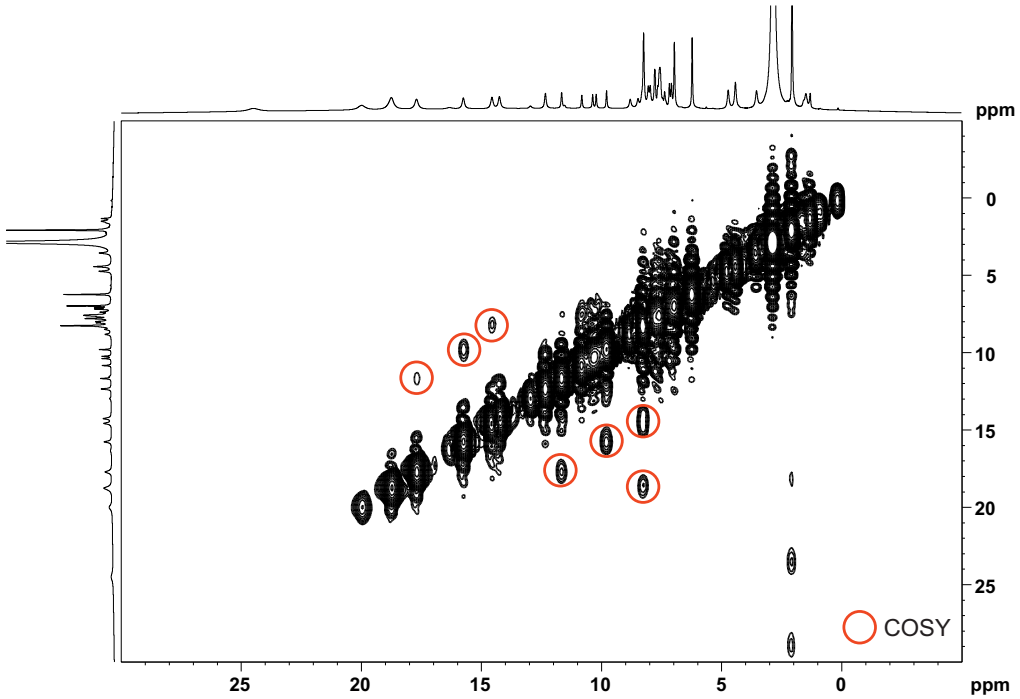

Figure 4.6: ^{1}H-^{1}H COSY spectrum (500 MHz, acetone-d_6, 298 K) of the expected structure of complex **104**. Cross-peaks are marked in red.

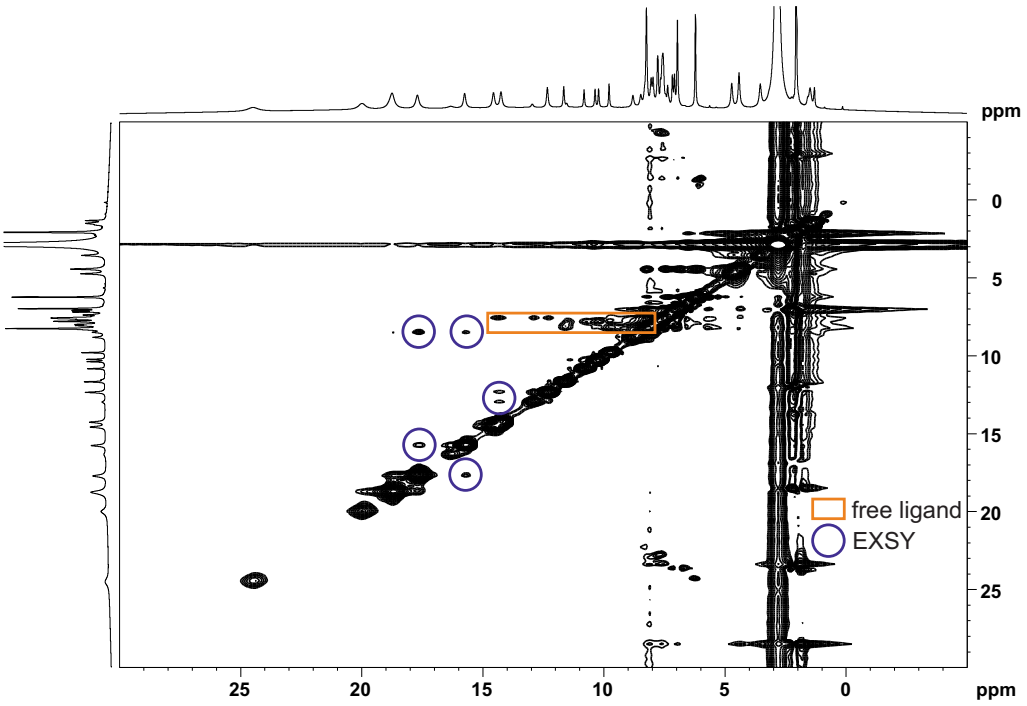

Figure 4.7: ^{1}H-^{1}H NOESY spectrum (500 MHz, acetone-d_6, 298 K) of the expected structure of complex **104**. EXSY cross-peaks are marked in blue, potential free ligand cross-peaks in orange. Protons assigned as a and b are arbitrarily grouped based on the cross-peaks.

Complex characterisation with ligand **69** appeared simpler since the observed 41 ^{1}H signals were spread over a wider range (35.0 to -1.29 ppm) making signal overlap less probable. A mixture of the *fac*/*mer* isomers or free ligand was assumed to be visible in the ^{1}H NMR spectrum (Figure 4.8). In this case the ^{1}H-^{1}H NOESY spectrum was first analysed to group the protons according to the observed EXSY cross-peaks (Figure 4.9). Overall, 7 cross-peaks were assigned as EXSY cross-peaks and the protons grouped as a, b and c. Other cross-peaks were observed, but not assigned due to intense signal overlap. Further analysis of the ^{1}H-^{1}H COSY spectrum showed cross-peaks. In combination with the grouped protons from the ^{1}H-^{1}H NOESY spectrum, the protons a^{1} to a^{3} were identified as the pyridine ring protons in three different ligand environments (see Scheme 4.20). Further assignment was not possible due to missing coupling information between other protons. ESI-MS data was not collected for both complex preparations due to time constraints.

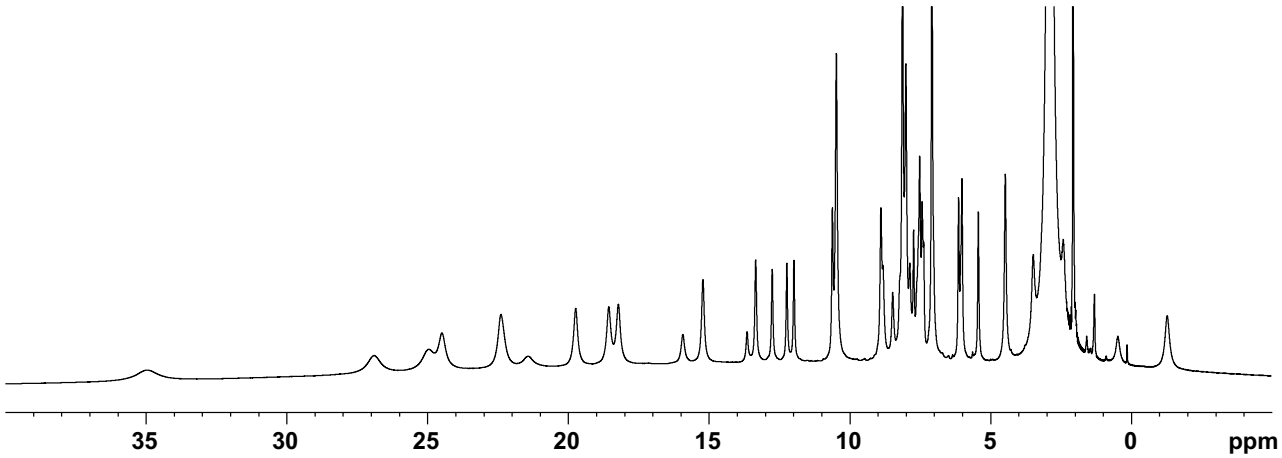

Figure 4.8: ^{1}H NMR spectrum (500 MHz, acetone-d_6, 298 K) of the expected structure of complex **105**.

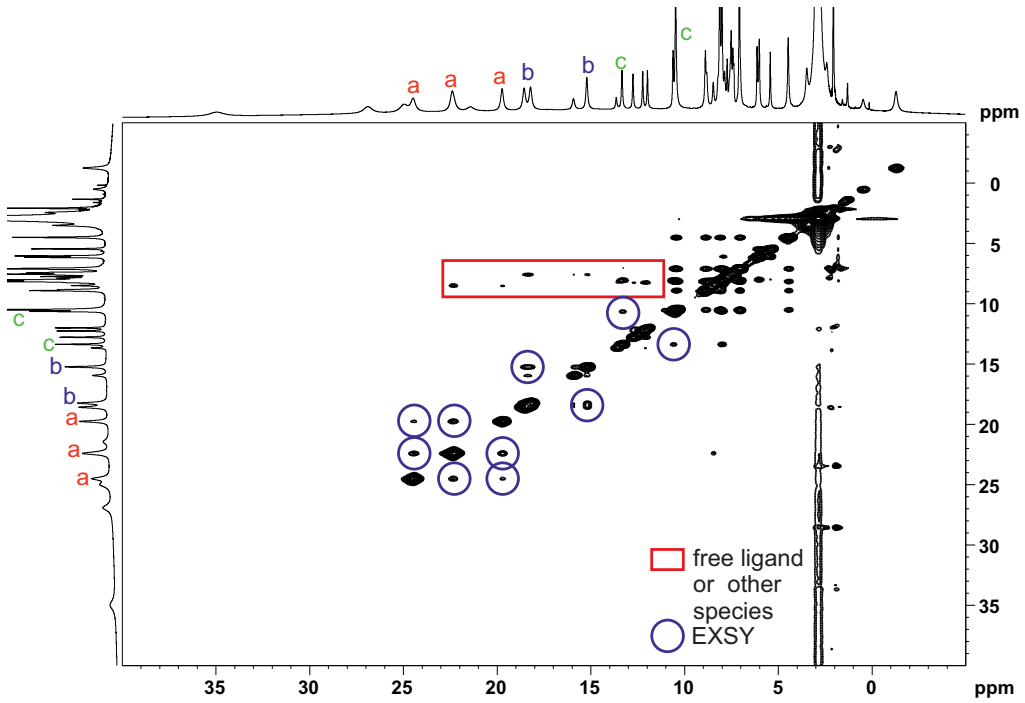

Figure 4.9: ^{1}H-^{1}H NOESY spectrum (500 MHz, acetone-d_6, 298 K) of the expected structure of complex **105**. EXSY cross-peaks are marked in blue, unidentified cross-peaks as e.g. free ligand in red. Protons assigned as a-c are arbitrarily grouped based on the cross-peaks.

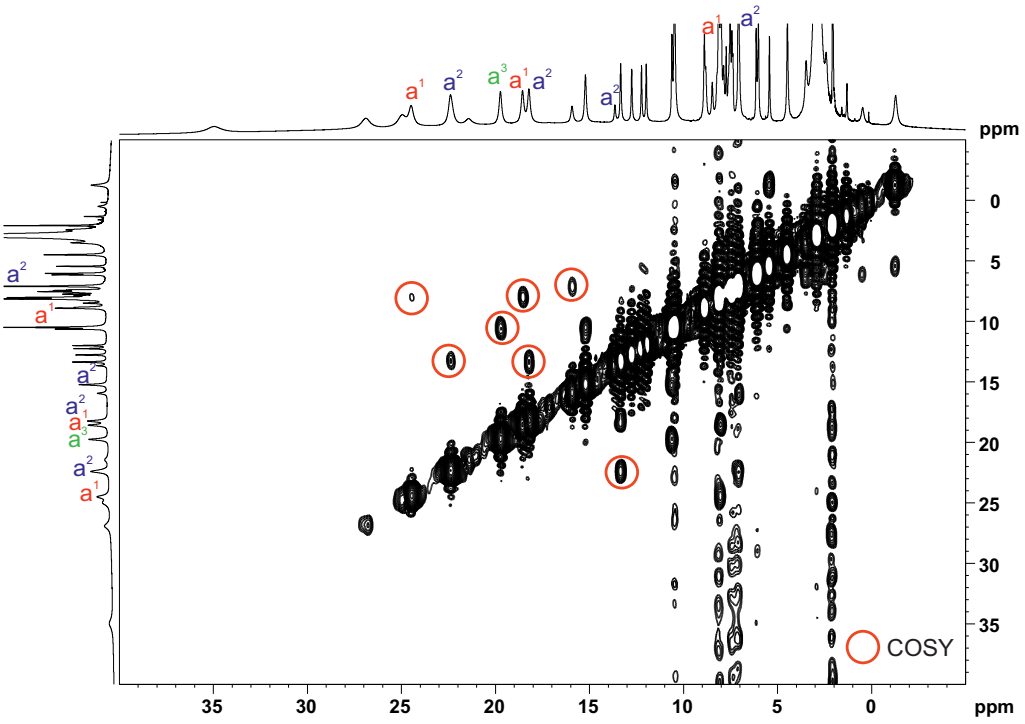

Figure 4.10: ^{1}H-^{1}H COSY spectrum (500 MHz, acetone-d_6, 298 K) of the expected structure of complex **105**. Cross-peaks are marked in red. a^1-a^3 are assigned to the pyridine ring as different ligand environments.

In conclusion, although for the preparation of complex with ligand **69** pyridine protons were partially grouped, the 2D NMR spectroscopic data did not provide sufficient information for further assignment by NMR spectroscopy. ESI-MS data confirmed the existence of the mixture **103**, while ESI-MS measurements still need to be performed for the complex preparations with the ligand **68** and **69**.
Future work should focus on the complex preparations with ligands **68** and **69** since complex **103** is already literature-known.[16] For complete assignment of the complexes optimised NMR experiments need to be developed in order to obtain the necessary coupling information in the 2D NMR techniques. As a possibility variable temperature NMR experiments could be conducted to potentially reduce signal overlap or sharpen signals as seen for the paramagnetic NMR toolbox and the thermal spin-crossover cages.[231,232,235] In order to determine the structure of the observed complexes ESI-MS measurements and crystal growth experiments are necessary.

4.2 Diarylethene-based Model Systems

In addition to the azobenzene-based model systems, dithienylethenes were investigated as a P-type photoswitch since the class of diarylethenes is well-known to undergo effective photocyclisation cycloreversion processes under irradiation with UV or visible light ideal for LD-LISC systems.[201,202] The aim of this chapter is to investigate whether dithienylethene-functionalised benzimidazoles are a suitable class of photoswitches as LD-LISC compounds with high photoefficiency. As dithienylethenes two derivatives were designed: i) compound **70** and ii) *N*-methylated compound **71** (Figure 4.21). Thiophene groups were incorporated into the benzimidazole structure of the 2-(2'-pyridyl)-1*H*-benzimidazole backbone based on a design of Lee *et al.*[242] Dithienylethene **70** was chosen since its scaffold did not require further substitution and the free *N*-*H* group can be used to tune the spin-crossover properties of the Fe^{II}-based complex, if needed. Furthermore, the modification of compound **71** is easily synthetically accessible and should increase the spin-crossover temperature by methylation.[215]

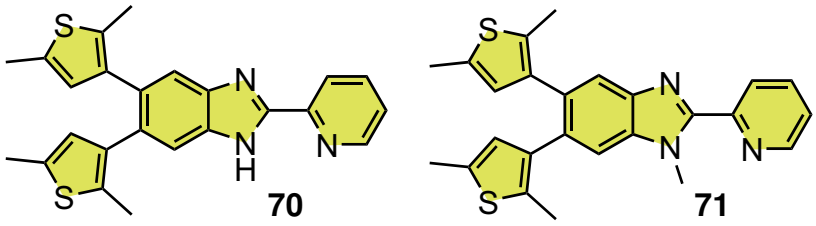

Scheme 4.21: Designed dithienylethenes **70** and **71** within this section.

Dithienylethene **70** will be synthesised in a convergent four-step synthesis starting from compound **76** and 2,5-dimethylthiophene (**107**) (Scheme 4.22). Compound **106** can be obtained by bromination of the starting material **76** and the boronic acid **109** by bromination followed by a borylation of 2,5-dimethylthiophene (**107**). In the end compounds **106** and **109** will be reacted in a Suzuki cross-coupling reaction to obtain the first dithienylethene **70**.

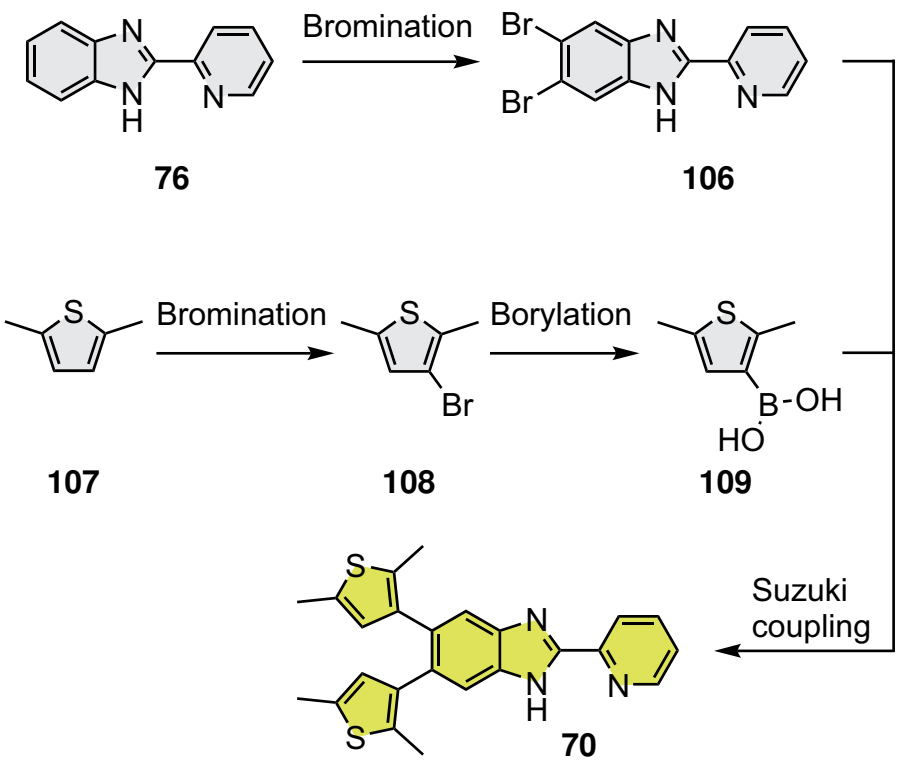

Scheme 4.22: Proposed synthesis of 5,6-di(2'',5''-dimethylthiophen-3''-yl)-2-(pyridin-2'-yl)-1*H*-benzo[*d*]imidazole (**70**).

Initally, compound **76** was brominated adapting a procedure from Kriete *et al.* to obtain the product **106** (Scheme 4.23).[20] The reaction was performed with *N*-bromosuccinimide as the bromination agent and glacial acetic acid as the solvent at 60 °C for 22 h. After flash chromatography the product **106** was obtained impure, however, after several recrystallisation attempts the impurity was removed and compound **106** was obtained in a yield of 32%. Product losses are attributed to the difficult purification since the product **106** and the starting material **76** had similar retention factors and both streak on silica gel leading to demanding flash chromatography. In addition, the recrystallsation from toluene was performed multiple times due to the simultaneous precipitation of product **106** and starting material **76** in some attempts.

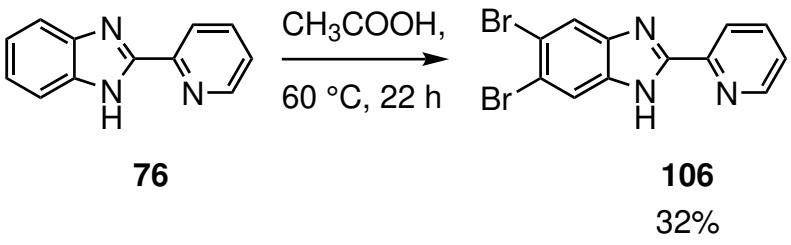

Scheme 4.23: Synthesis of 5,6-dibromo-2-(pyridin-2'-yl)-1*H*-benzo[*d*]imidazole (**106**).[20]

Subsequently, compound **108** was prepared from 2,5-dimethylthiophene (**107**) that was brominated with *N*-bromosuccinimide in glacial acetic acid at room temperature for 19-48.5 h adapting a procedure from Ando *et al.*[21] (Scheme 4.24). In initial attempts the obtained yield of the product **108** was 52% (with a reaction time of 19 h) after purification by flash chromatography. Based on the light sensitivity of *N*-bromosuccinimide the reaction was repeated in the dark and the reaction was stirred for 48.5 h instead of 19 h, increasing the yield up to 95%. The obtained yield is also higher than the reported value of 75%.[21]

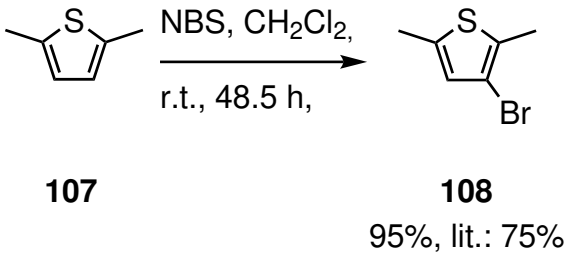

Scheme 4.24: Synthesis of 3-bromo-2,5-dimethylthiophene (**108**).[21]

Boronic acid **109** was then prepared adapting a procedure from Ko *et al.* (Scheme 4.25).[22] Compound **108** was lithiated with *n*-butyllithium in tetrahydrofuran at -78 °C and the lithiated species was trapped with tributyl borate. Hydrochloric acid was added to cleave the boronic ester and after work up compound **109** was obtained by precipitation in a yield of 70%.

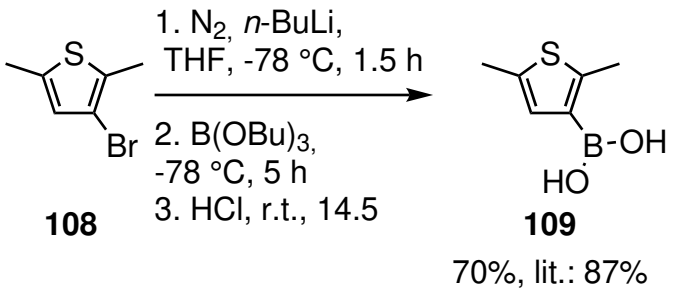

Scheme 4.25: Synthesis of (2,5-dimethylthiophen-3-yl)boronic acid (**109**)[22].

The last reaction step, a Suzuki cross-coupling reaction, was performed using adapted reaction conditions from Mörtel *et al.* (Scheme 4.26).[247] Compound **106** was reacted with boronic acid **109** using $Pd(PPh_3)_4$ as the catalyst, sodium carbonate as the base and a mixture of 1,4-dioxane and water as the solvents at 100 °C for 68 h. After work up the crude product was analysed by NMR spectroscopy. The ^{1}H NMR spectrum only indicated unconsumed starting material and catalyst derivatives (triphenylphosphine oxide). The desired product **70** did not form, potentially due the

free *N-H* group that could be deprotonated and inhibit the cross-coupling reaction to take place, as previously observed for Sonogashira cross-coupling reactions (see Section 3.2.1).[13]

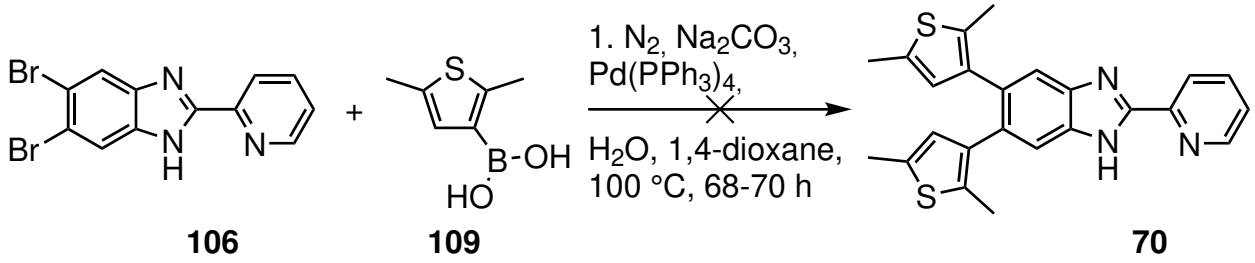

Scheme 4.26: Synthesis of 5,6-di(2",5"-dimethylthiophen-3"-yl)-2-(pyridin-2'-yl)-1*H*-benzo[*d*]imidazole (**70**).[247]

Based on this result a different approach was investigated by Niclas Grocholski during his Bachelor thesis.[248] The Bachelor thesis was supervised by the author, Tobias Paschelke. In this approach the Suzuki cross-coupling reaction to literature-known compound **111** was performed before the condensation reaction to compound **70** (Scheme 4.27).[170,248] After multiple attempts product **111** was not isolated, but was just poorly visible as an impurity in the ^{1}H NMR spectrum. Potassium phosphate heptahydrate was used by Milek *et al.*,[170] but unfortunately, the chemical was not commerically available during these studies. The attempts by Niclas Grocholski[248] also included varying the amounts of water to mimic the heptahydrate in the reaction mixture without success. The crystal water was assumed to play an important role in the reaction. In addition, using different Suzuki coupling reaction conditions did also not lead to the desired product **111** due to the unprotected amine.[248]

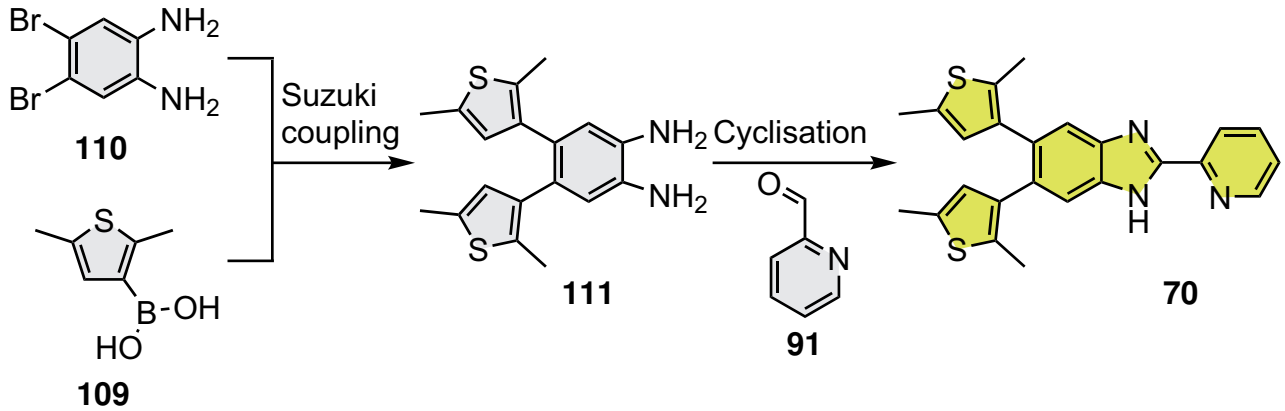

Scheme 4.27: Proposed synthesis of 5,6-di(2",5"-dimethylthiophen-3"-yl)-2-(pyridin-2'-yl)-1*H*-benzo[*d*]imidazole (**70**) during the Bachelor thesis of Niclas Grocholski.[248]

After the investigations by Niclas Grocholski,[248] a second approach was investigated using a protecting group for the free *N-H* group in the Suzuki cross-coupling reaction. Overall, starting from

the already prepared compound **106** three reaction steps would be necessary, including a protection, Suzuki coupling and a deprotection to obtain dithienylethene **70** (Scheme 4.28).

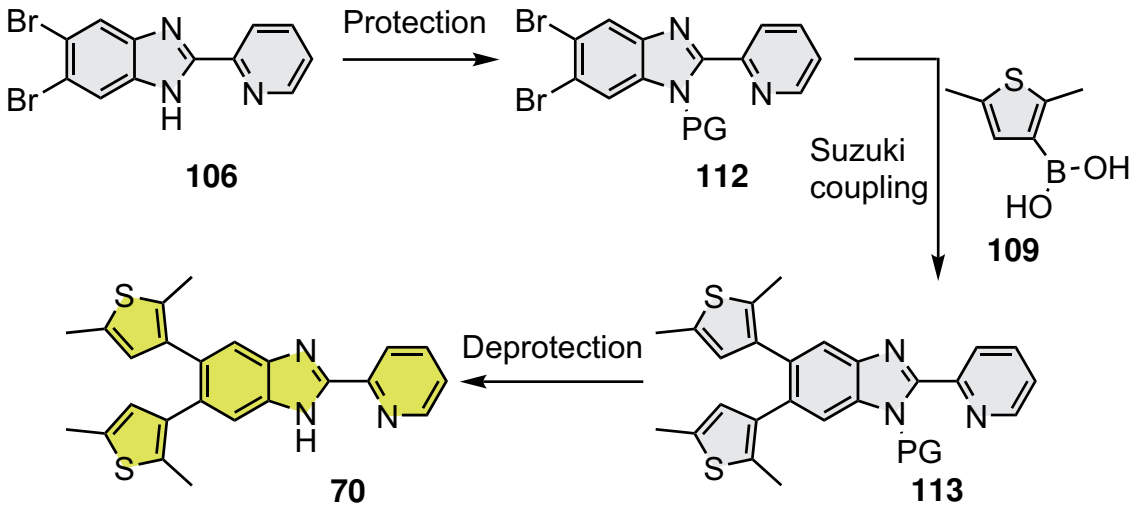

Scheme 4.28: Proposed synthesis of 5,6-di(2",5"-dimethylthiophen-3"-yl)-2-(pyridin-2'-yl)-1*H*-benzo[*d*]imidazole (**70**) using protecting groups (PG).

First of all, a Boc protecting group was introduced adapting a procedure from Taylor *et al.* (Scheme 4.29).[2] Compound **106** was reacted with di-*tert*-butyl dicarbonate and 4-dimethylaminopyridine in dichloromethane at room temperature for 21 h. Purification by flash chromatography yielded pure fractions of compound **114**. In addition, impure fractions were recrystallised from methanol to give product **114** in yield of 29%. Similar retention factors of the product **114** and starting material **106** as well as a slow crystallisation led to potential product losses, explaining the low yield.

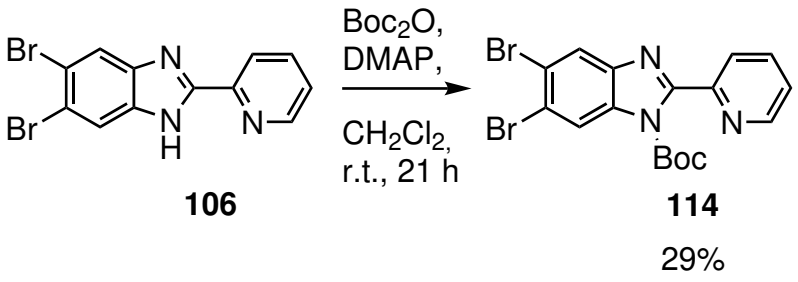

Scheme 4.29: Synthesis of *tert*-butyl 5',6'-dibromo-2'-(pyridin-2"-yl)-1*H*-benzo[*d*]imidazole-1-carboxylate (**114**).[2]

Suzuki cross-coupling reaction conditions adapted from Burke *et al.* were used for the synthesis of precursor **115**.[25] Compound **114** was reacted with boronic acid **109** with potassium carbonate as the base, $Pd(PPh_3)_4$ as the catalyst and a mixture of ethanol, *N*,*N*-dimethylformamide and water as

the solvent at 80 °C for 20 h (Scheme 4.30). After purification by flash chromatography the desired product **115** was not obtained, instead unprotected starting material **114** was isolated. Based on these findings a benzyl protecting group was used instead due to its more robust nature towards basic reaction conditions.[236]

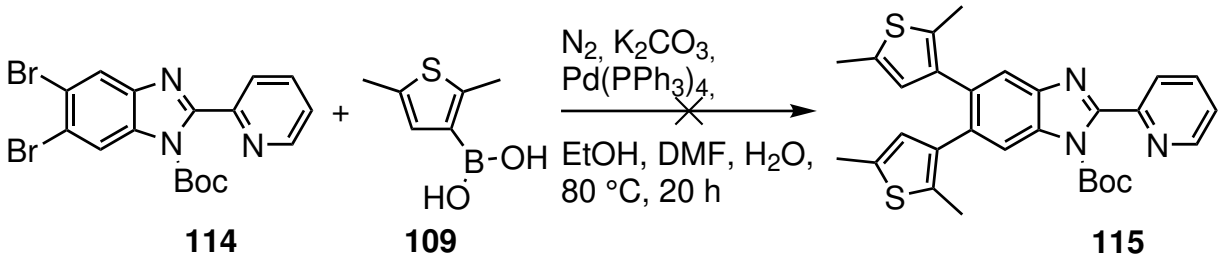

114 **109** **115**

Scheme 4.30: Synthesis of *tert*-butyl 5',6'-bis(2''',5'''-dimethylthiophen-3'''-yl)-2'-(pyridin-2''-yl)-1*H*-benzo[*d*]imidazole-1-carboxylate (**115**).[25]

In the first reaction a benzyl protecting group was introduced by applying adapted reaction conditions from Huang *et al.*.[23] Compound **76** was protected with benzyl bromide using potassium carbonate as the base in *N*,*N*-dimethylformamide at room temperature for 23.25 h. The product **116** was obtained after flash chromatography in a yield of 56%.

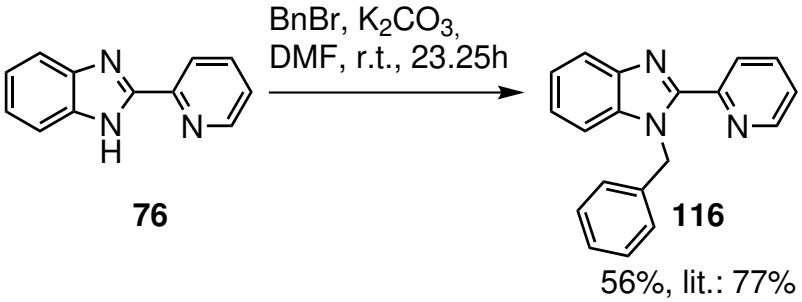

76 **116**

56%, lit.: 77%

Scheme 4.31: Synthesis of 1-benzyl-2-(pyridin-2'-yl)-1*H*-benzo[*d*]imidazole (**116**).[23]

Next, compound **116** was brominated adapting reaction conditions from Kriete *et al.* (Scheme 4.32),[20] similar to the synthesis of compound **106** (see Scheme 4.23). Although product **117** was identified it was not possible to purify it by recrystallisation since crystallisation conditions were not identified.

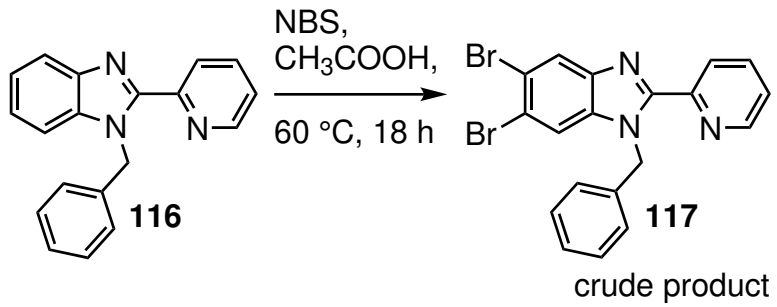

Scheme 4.32: Synthesis of 1-benzyl-5,6-dibromo-2-(pyridin-2'-yl)-1*H*-benzo[*d*]imidazole (**117**).[20]

Due to the difficult purification a different pathway was designed (Scheme 4.33). The previously synthesised compound **106** could be benzylated in order to obtain the product **117** using the same reaction conditions for the benzylation as for compound **116** (see Scheme 4.31).[23] After purification by flash chromatography product **117** was successfully isolated in a yield of 42%.

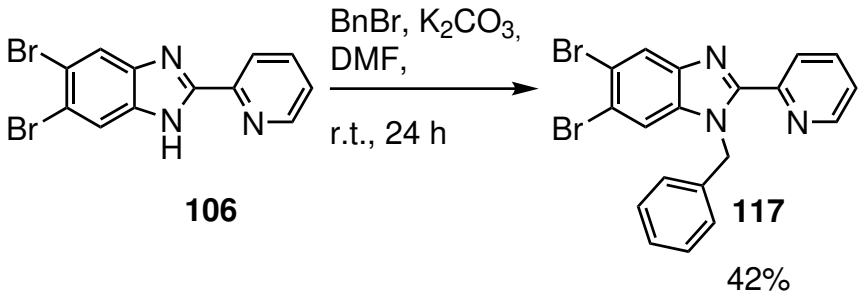

Scheme 4.33: Synthesis of 1-benzyl-2-(pyridin-2'-yl)-1*H*-benzo[*d*]imidazole (**116**) from compound **106**.[23]

In the next step compound **117** was reacted with boronic acid **109** under standard Suzuki cross-coupling reaction conditions at 80 °C for 21 h (Scheme 4.34).[25] Purification by flash chromatography gave a crude product. Analysis by ^{1}H NMR spectroscopy suggested the formation of the desired product **118** with an additional unidentified impurity. Purification by flash chromatography and recrystallisation was not successful. Based on the challenging purification no further attempts were investigated to obtain the target ligand **70**.

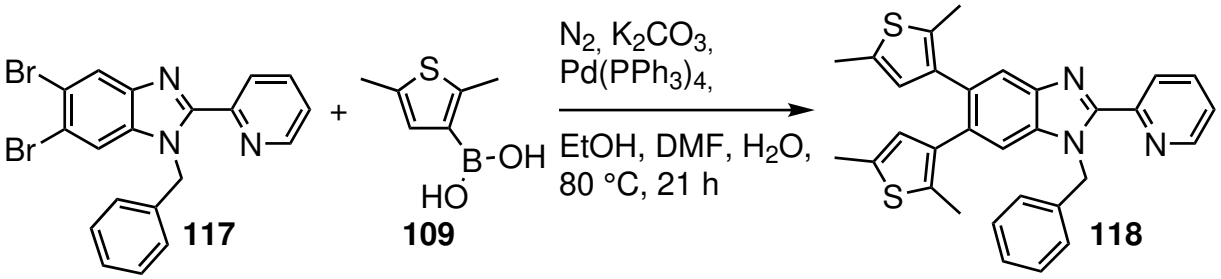

Scheme 4.34: Synthesis of 6,7-di(2",5"-dimethylthiophen-3"-yl)-1-benzyl-2-(pyridin-2'-yl)benzimidazole (**118**).

Consequently, the focus was changed towards the synthesis of the dithienylethene **71** due to the more simple synthetic access (Scheme 4.35). The synthesis consists of three additional steps from the already known compounds **76** and **109** (Scheme 4.35). Starting from substance **76** the desired ligand **71** will be obtained after a methylation, a bromination and a Suzuki cross-coupling reaction.

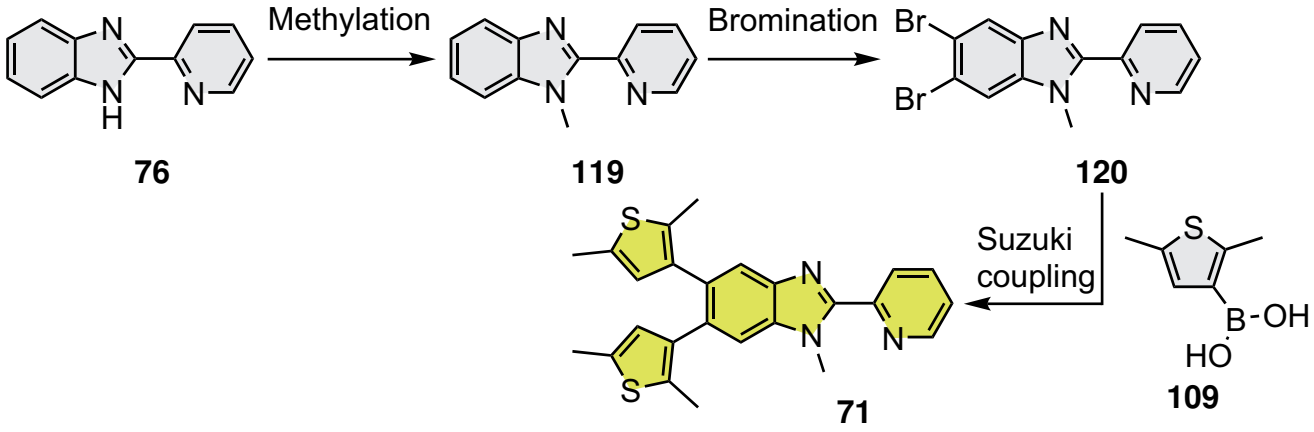

Scheme 4.35: Proposed synthesis of 6,7-di(2",5"-dimethylthiophen-3"-yl)-1-methyl-2-(pyridin-2'-yl)benzimidazole (**71**).

Initially, compound **76** was reacted with methyl iodide and potassium carbonate as the base in *N*,*N*-dimethylformamide at room temperature for 20 h adapting a procedure from Lin *et al.*.[12] After work up the product **119** was obtained in a good yield of 81%.

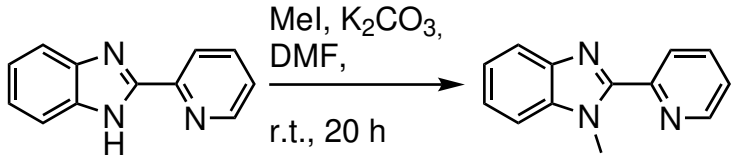

76 **119**
81%

Scheme 4.36: Synthesis of 1-methyl-2-(pyridin-2'-yl)-1*H*-benzo[*d*]imidazole (**119**).

Compound **119** was also brominated adapting the procedure from Kriete *et al.* (Scheme 4.37).[20] After stirring at 60 °C for 20 h the reaction mixture was worked up to obtain a crude product. The crude product was then recrystallised from toluene and the precipitated product collected by filtration to yield product **120** in a yield of 36%. In the recrystallisation attempts only small amounts of the product **120** crystallised and multiple recrystallisations of the crude product were required. Product losses are attributed to the challenging purification.

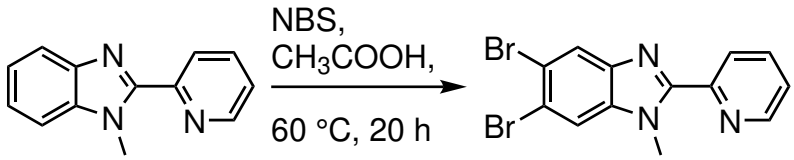

119 **120**
36%

Scheme 4.37: Synthesis of 5,6-dibromo-1-methyl-2-(pyridin-2'-yl)-benzimidazole (**120**).

The final Suzuki cross-coupling reaction was initially investigated during the Bachelor thesis of Niclas Grocholski. The product **71** was first synthesised by Niclas Grocholski and the reported reaction conditions applied to this attempt.[248] The product **120** was reacted with the boronic acid **109** under standard Suzuki cross-coupling conditions at 80 °C for 19 h (Scheme 4.38).[25] Purification by flash chromatography with an additional recrystallisation from methanol gave the desired dithienylethene **71** in a yield of 23%.

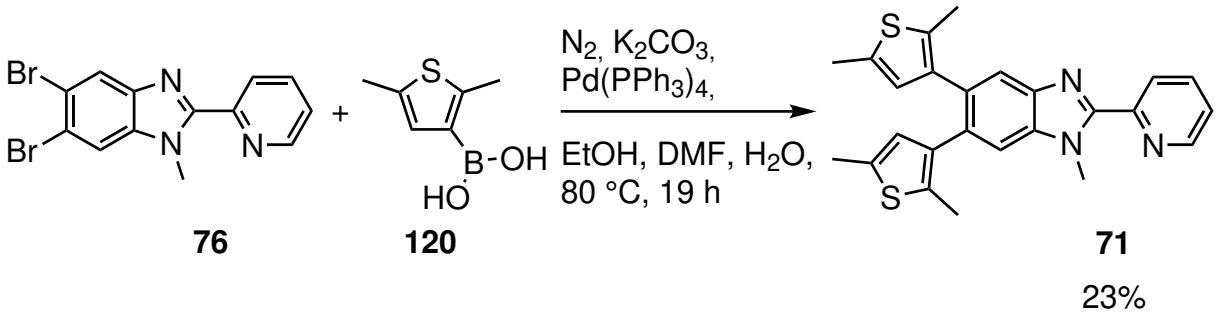

76 **120** **71**

23%

Scheme 4.38: Synthesis of 6,7-di(2",5"-dimethylthiophen-3"-yl)-1-methyl-2-(pyridin-2'-yl)benzimidazole (**71**).

4.2.1 Photochemical properties of dithienylethene 71

After the successful synthesis of dithienylethene **71** its switching behaviour in solution was investigated by NMR spectroscopy. Niclas Grocholski performed preliminary UV/Vis studies with dithienylethene **71**, thus the absorption profile of compound **71** is known.[248] In the first attempt the cyclisation process was investigated in three different deuterated solvents (acetonitrile, chloroform and toluene) since 2-(2'-pyridyl)-1*H*-benzimidazole-based dithienylethenes and their photochemical properties such as the switching behaviour in different solvents are not known yet. For this purpose the ligand was dissolved in the corresponding deuterated solvent ($1.63\text{-}1.96 \cdot 10^{-2}$ M) and a ^{1}H NMR spectrum was recorded as a reference (Figures 4.11, 4.11 and 4.11). Based on the ideal switching behaviour of other reported dithienylethenes,[249,250] only short irradiation times were expected to be necessary for the cyclisation process. All samples were irradiated with 325 nm for three seconds. Unexpectedly, changes in the ^{1}H NMR spectra were not visible. Furthermore, a characteristic colour change was also not observed. After repeated irradiation with 325 nm for one minute and further five minutes, no additional signals or chemical shift changes were visible in the ^{1}H NMR spectrum. By using an alternative light source of 310 nm based on the UV/Vis data of Niclas Grocholski,[248] irradiating for five minutes, changes were not observed as well.

Oruganti *et al.* investigated the switching behaviour of a thiophene *ortho*-substituted benzene derivative **121** (Scheme 4.39).[251] By switching the dithienylethene, the loss of aromaticitiy leads to a direct fast thermal backrelaxation, therefore, making it difficult to detect the cyclisation product **122** after irradiation on the NMR spectroscopy time scale.[251] Interestingly, the cyclisation product **122** was simply trapped by irradiation with 254 nm under atmospheric conditions causing oxidation to compound **123**. Based on these results of Oruganti *et al.*[251] the photocyclisation process of compound **71** by irradiation with 325-310 nm was assumed not to work due to the loss of aromaticity during the cyclisation leading to an nonaromatic system.

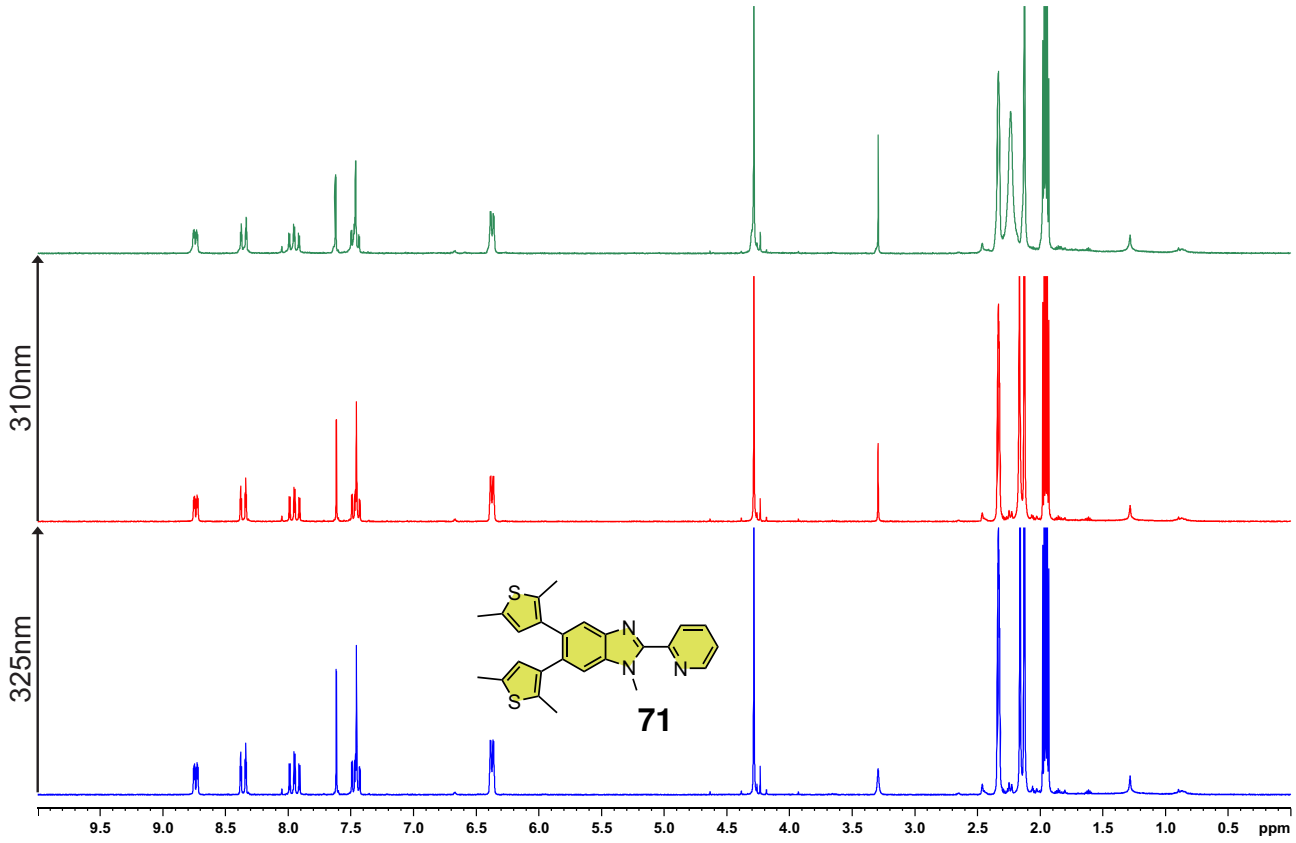

Figure 4.11: ^{1}H NMR spectra (200 MHz, CD_3CN, 298 K) of dithienylethene **71** before (blue) and after irradiation with 325 nm (red) for 6 min and 310 nm for 5 min (green).

Since Oruganti *et al.*[251] were able to find evidence for a fast thermal backrelaxation, the irradiation conditions were adapted to dithienylethene **71**. For this purpose ligand **71** was dissolved in deuterated acetonitrile and a ^{1}H NMR spectrum recorded as the reference. As a light source a 265 nm lamp was used since equipment with a shorter wavelength was not available. The irradiation experiment was again monitored by NMR spectroscopy.The sample was then irradiated with 265 nm for 30 min. A colour change from colourless to yellow was visible. Based on the reported results from Oruganti *et al.* an oxidised species was already detectable after 10 min of irradiation, however, in this case no changes within the ^{1}H NMR spectrum were observed. Further exposure to 265 nm for 60 min intensified the yellow colour and smaller signals appeared within the ^{1}H NMR spectrum, likely attributed to the degradation of dithienylethene **71** instead of an oxidised species since many smaller signals grew in. The oxidiation did not take place due to the assumed loss of aromaticity inhibiting the photocyclisation, completely.

Overall, dithienylethene **70** was not synthesised after multiple attempts. However, *N*-methylated derivative **71** was successfully synthesised within a few steps and moderate yields. The cyclisation of ligand **71** was analysed by NMR spectroscopy, but did not show any response to irradiation due to

the potential loss of aromaticity during the isomerisation. Future work will be shown in Section 5.2 using a modified octafluorocyclopentene backbone. The ligand was designed to prevent the loss of aromaticity.

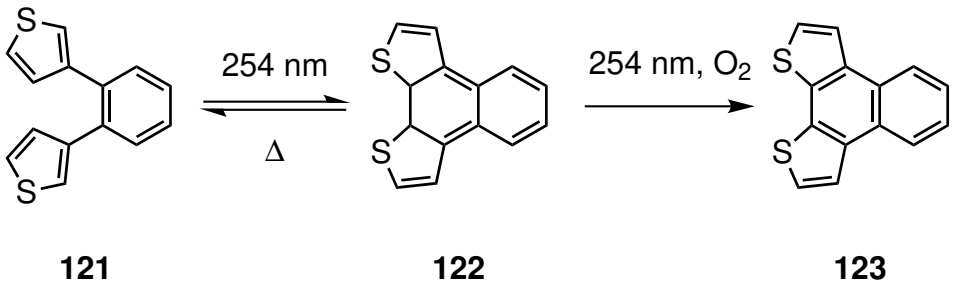

Scheme 4.39: Photocyclisation by irradiation with 265 nm and fast thermal backrelaxation as observed for dithienylethene **121** by Oruganti *et al.*.The cyclisation product **122** was trapped by oxidation with atmospheric oxygen under irradiation.[251]

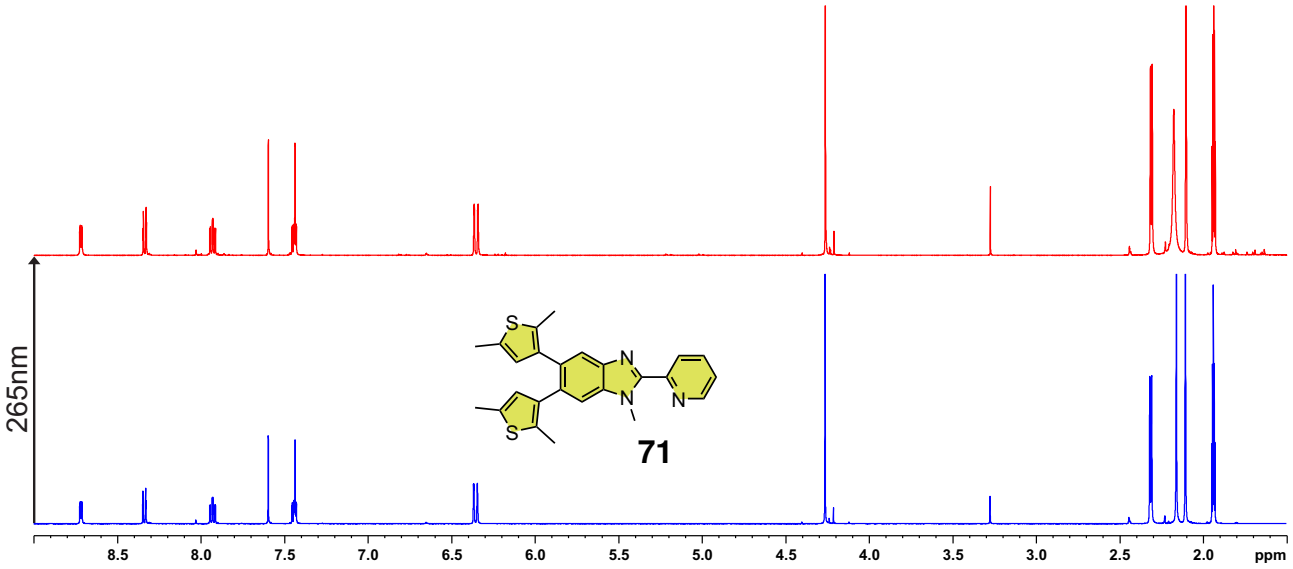

Figure 4.12: ^{1}H NMR spectra (500 MHz, CD_3CN, 298 K) of dithienylethene **71** before (blue) and after irradiation with 265 nm (red) for 90 min.

Chapter 5

5 Dual-Responsive Spin-Crossover Cages

In this chapter the knowledge gained about the spin-crossover properties of thermal spin-crossover cages as well as the LD-LISC model complexes will be used and combined to design a first generation of dual-responsive spin-crossover cages (Figure 5.1). For that reason, the chapter is divided into section 5.1, dealing with azobenzenes as photoswitchable groups that are attached to 2-(2'-pyridyl)-1*H*-benzimidazole binding motifs and section 5.2 that focuses on an improved dithienylethene system overcoming inhibited photoisomerisation by an octafluorocyclopentene backbone.

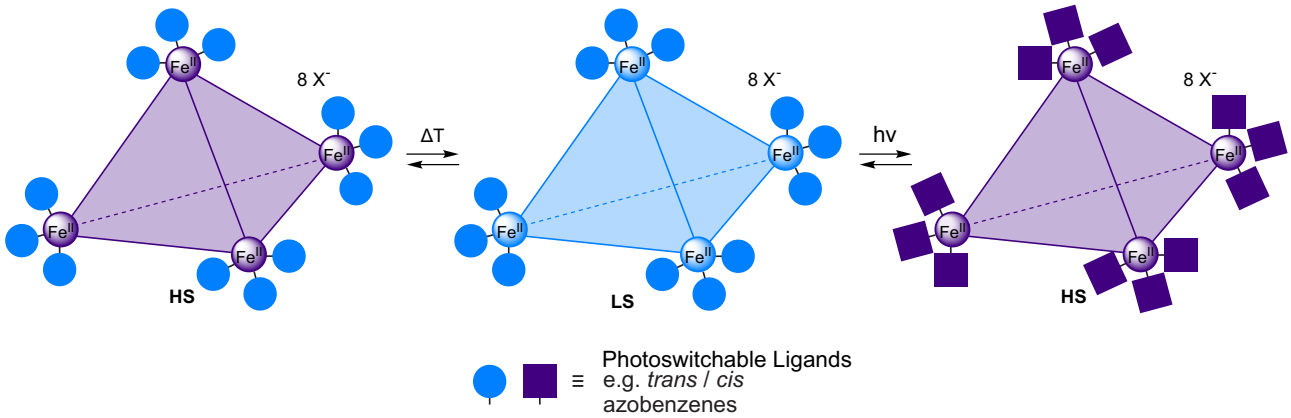

Figure 5.1: Dual-responsive spin-crossover cages with photoswitchable groups (blue spheres and purple squares). Temperature and light can induce spin-state transitions.

5.1 Azobenzene-based Metal-Organic Cages

In this section 2-(2'-pyridyl)-1*H*-benzimidazole compounds bearing two azobenzene units will be investigated. The designed ligands should undergo effective photoisomerisation upon irradiation with light as well as show long half-life times such as seen for the azobenzene derivative **68**. The synthetic knowledge gained from the ligand synthesis of azobenzenes **67**, **68** and **69** shall be used to develop strategies to obtain ligands functionalised with azobenzenes for metal-organic cages. The ligand design

is based on a 2-(2'-pyridyl)-1*H*-benzimidazole scaffold since the ligand motif has shown to have a ligand field strength suitable for spin-crossover investigations in previous studies (publication iii), section 3.1.3)[235] and by other groups.[16,214,215] In addition, an alkyne linker was chosen since the spin-crossover temperature was the closest to room temperature in comparison to a phenylene spacer or no spacer ((publication iii), section 3.1.3), cages **5**-**7**).[235] Furthermore, the characterisation of the self-assembled Fe^{II}-based metal-organic cages is expected to be facilitated since previous results from the research group McConnell using similar ligand scaffolds show the exclusive formation of the *fac* isomer within metal-organic cages,[13,231,232,235] although also other mixed cage species[98] or *mer* isomers[87] are known from other groups. The formation of one isomer might help to reduce the complexity of characterisation by NMR spectroscopy.

In section 3.2 the unsubstituted ligand **35** was synthesised, but obtained impure. Further self-assembly experiments did not indicate the formation of a discrete cage species (Section 3.2.3) Based on these results, an unsubstituted azobenzene-functionalised ligand was not designed in this section. Instead, the regioisomers **124** and **125** bearing two azobenzene units with a methylated 2-(2'-pyridyl)-1*H*-benzimidazole backbone were designed due to synthetic ease (Figure 5.2). The ligands will be methylated in order to increase the spin-crossover temperature.[215] Based on the results of section 4.1 the position of the azobenzene unit on the benzimidazole moiety is also expected change the photochemical properties such as the half-life time of the resulting ligands **124** and **125**.

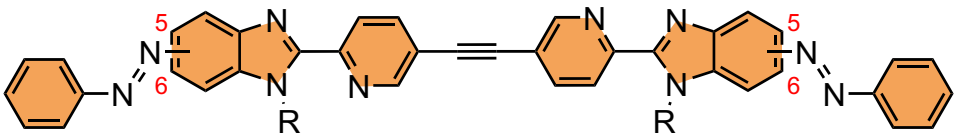

124 5-Azo R = Me
125 6-Azo R = Me

Figure 5.2: Designed azobenzenes as ligands for Fe^{II}-based dual-responsive spin-crossover metal-organic cages.

The two regioisomers can be synthesised in seven reaction steps (Scheme 5.1). Starting from 2-iodo-5-bromopyridine (**126**), an aldehyde function will be introduced with a Grignard reagent. After the introduction of an aldehyde protecting group multiple Sonogashira cross-coupling reactions will be performed and the protecting group be removed under acidic conditions. In comparison to the condensation reactions with polyphosphoric acid,[11,13] milder reaction conditions can be used for the synthesis of the isomers **132** and **133**. After an electrophilic aromatic substitution the products **124** and **125** will be obtained.

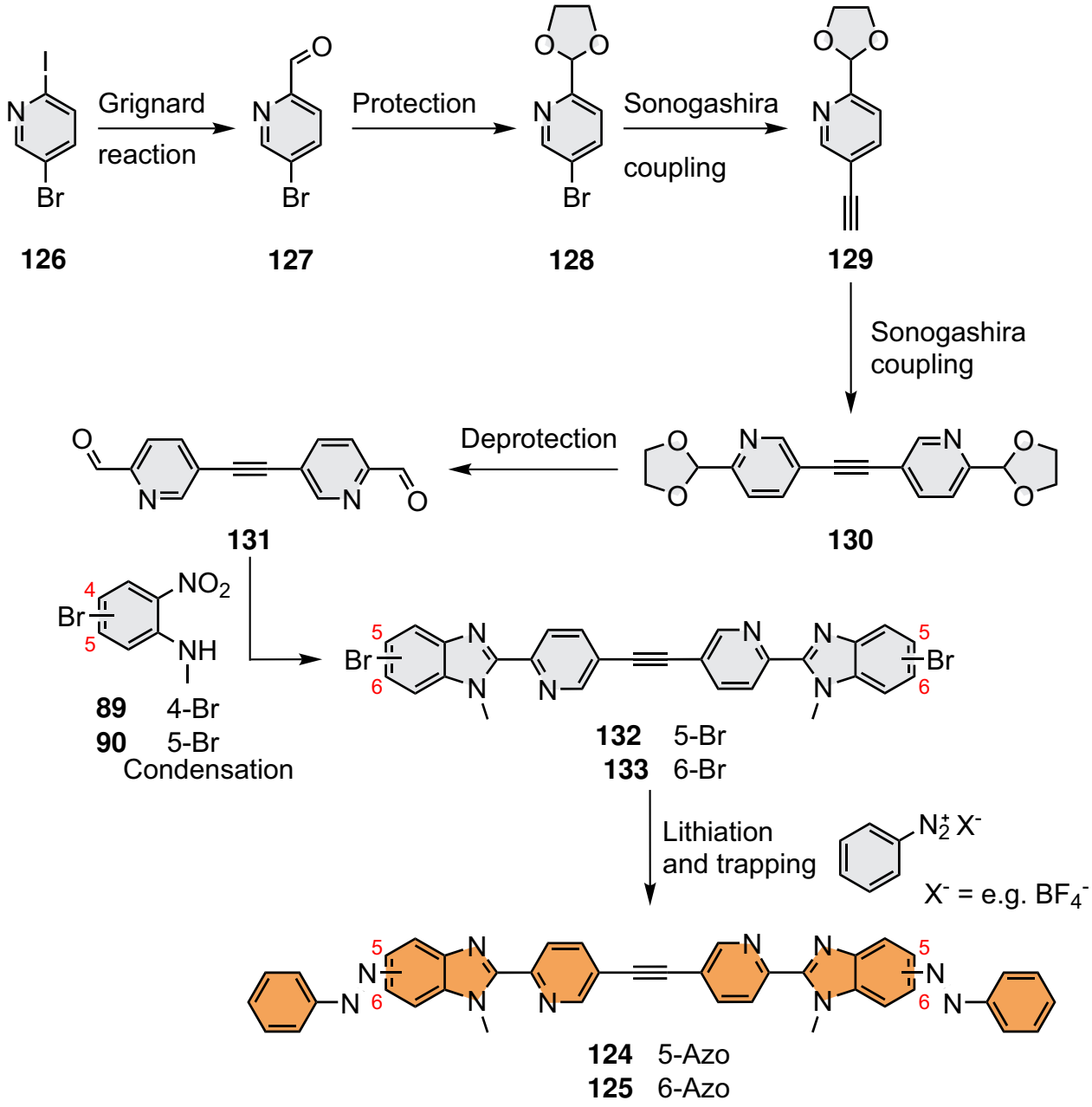

Scheme 5.1: Proposed synthesis of the methylated azobenzene derivatives **124** and **125**.

The first two reactions (Grignard reaction and protection) were performed according to adapted procedures from Roberts *et al.* (Scheme 5.2).[26] 2-Iodo-5-bromopyridine (**126**) was reacted with commercially available *iso*-propylmagnesium chloride in tetrahydrofuran solution at -30 °C for 1 h. The formed intermediate was trapped with *N*,*N*-dimethylformamide to obtain aldehyde **127** after a simple work up procedure in a yield of 84%. In comparison to the literature known procedure[26] the yield is lower (99% by Roberts *et al.*) due to losses during the work up since their scale was 13 times higher. Aldehyde **127** was then protected with ethylene glycol, catalysed by *p*-toluene sulfonic acid

monohydrate, in toluene at 135 °C for 22 h. Again, only a simple work up was necessary to obtain the pure product **128** in a yield of 94%. The yield is in good agreement to the 99% reported by Roberts *et al.*.[26]

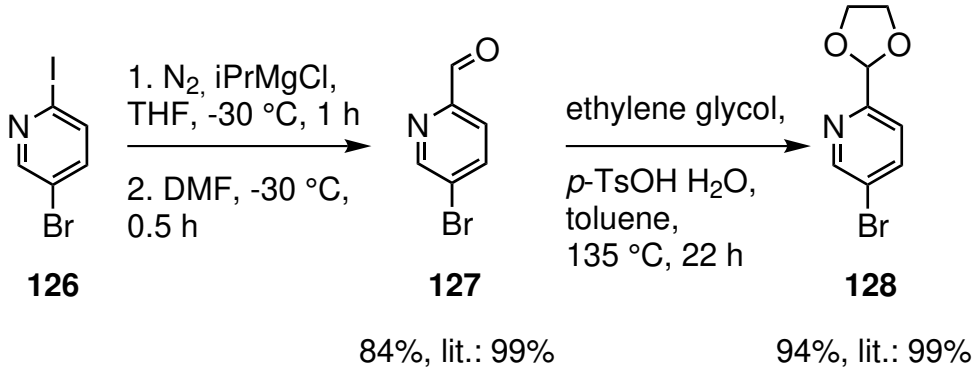

Scheme 5.2: Synthesis of 5'-bromopicolinaldehyde (**127**) and 5'-bromo-2'-(1,3-dioxolan-2-yl)pyridine (**128**).[26]

Compound **128** was then reacted with trimethylsilylacetylene in a standard Sonogashira cross-coupling with $Pd(PPh_3)_2Cl_2$ and CuI as catalysts, triethylamine as the base and tetrahydrofuran as the solvent at 60 °C for 23 h (Scheme 5.3). The procedure was adapted from Park *et al.*[7] After cooling to room temperature, purification of TMS protected alkyne **134** by flash chromatography was attempted. Thin-layer chromatography measurements indicated very similar retention factors for starting material **128** and product **134**. Flash chromatography was attempted but it did not lead to the separation of starting material **128** and **134**. Based on this result the TMS protected alkyne **134** was deprotected in the next step without further purification.

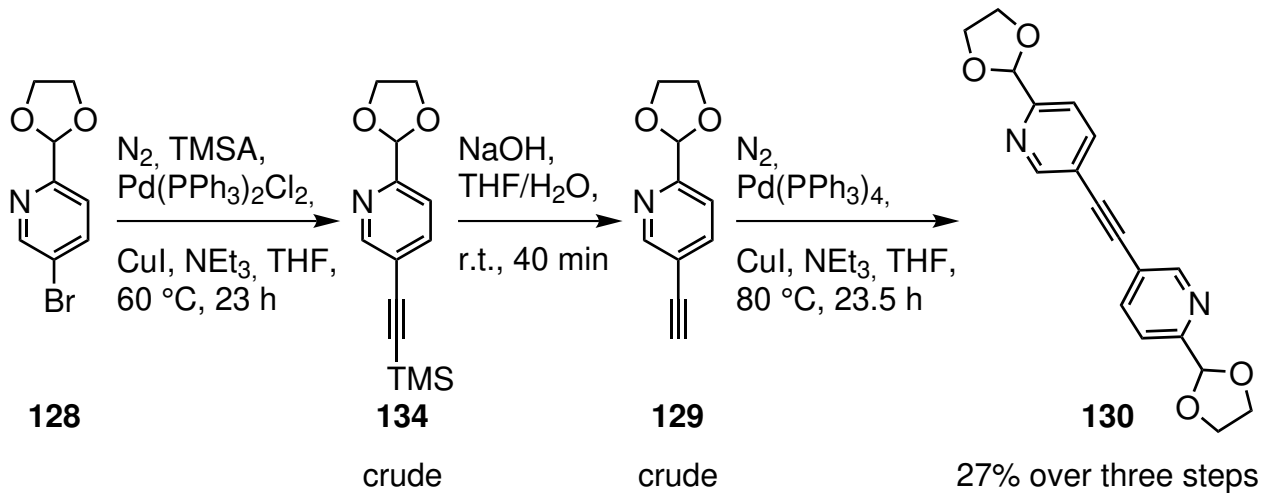

Figure 5.3: Synthesis of 1,2-bis(6'-(1'',3''-dioxolan-2''-yl)pyridin-3'-yl)ethyne (**130**) over three steps.[7,252]

Therefore, the crude product was dissolved in tetrahydrofuran and sodium hydroxide solution (1 M) was added. The mixture was stirred at room temperature, based on an adapted procedure from Borozdina *et al.*.[252] After 40 min thin-layer chromatography measurements indicated the complete conversion of compound **134** to **129**, however, again no separation by chromatography of compound **128** and **129** was possible due to similar retention factors. Based on integrals in the ^{1}H NMR spectrum a 1:1 mixture of product **129** and starting material **128** was suggested. Due to the challenging purification the crude product was used in the next step without further purification.
The crude mixture was again reacted in a Sonogashira cross-coupling reaction with $Pd(PPh_3)_4$ and CuI as the catalysts in a mixture of triethylamine and tetrahydrofuran at 80 °C for 23.5 h adapting reaction conditions from Park *et al.*[7] After purification by flash chromatography the pure product **130** was obtained in a yield of 27% over three steps (65% per step).

In a first attempt the deprotection of the aldehyde function was performed according to an adapted procedure from Borozdina *et al.* using *p*-toluenesulfonic acid monohydrate in a mixture of acetone and water at room temperature for 69 h (Scheme 5.4, upper arrow).[252] Afterwards, thin-layer chromatography measurements indicated no conversion of starting material **130**. The experiment was repeated, but using different reaction conditions from Giraldi *et al.* (Scheme 5.4, bottom arrow).[27] Compound **130** was dissolved in tetrahydrofuran and the protecting group was cleaved by the addition of hydrochloric acid (3 M) at 60 °C for 20.5 h. Product **131** was obtained after a simple work up in an excellent yield of 90%.

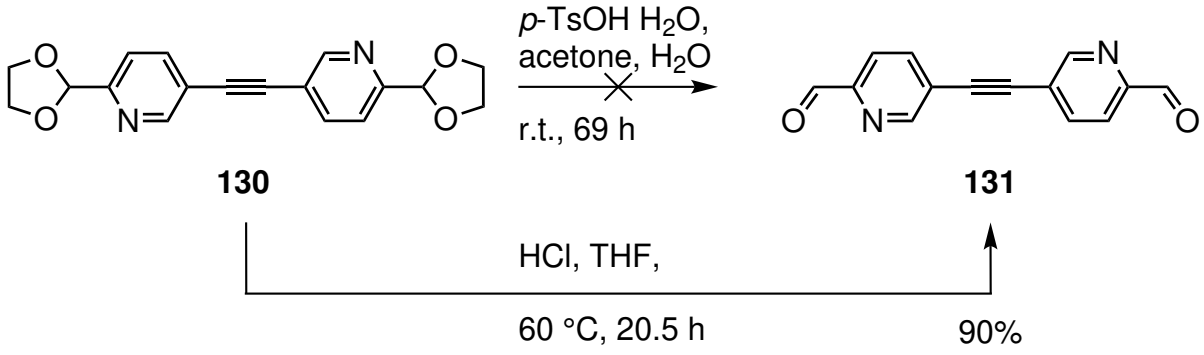

Figure 5.4: Synthesis of 5,5'-(ethyne-1,2-diyl)dipicolinaldehyde (**131**).[27,252]

The synthesis of compounds **132** and **133** was attempted using adapted reaction conditions from Yang *et al.* (Scheme 5.5).[18] Compound **131** was reacted with 4-bromo-*N*-methyl-2-nitroaniline (**89**) or 5-bromo-*N*-methyl-2-nitroaniline (**90**) with sodium dithionite in a mixture of ethanol, *N*,*N*-dimethylformamide and water at 80 °C for 21 h. After work up the desired isomer **132** was obtained as an impure mixture (4.31 mg). The impurity is still unidentified. In contrast, isomer **133** was

not obtained. The reactions were performed on a very small scale making filtering of the precipitate very challenging. Compound **132** was also found to be insoluble in organic solvents, thus ^{1}H NMR spectra were only recordable in deuterated trifluoroacetic acid. As a result, ligand precursor **132** is not suitable for further amination reactions in organic solvents. Further synthetic strategies were not designed or the reaction optimised due to the insolubility problem and time restraints.

During previous investigations by E. Trumpf precursor **132** was synthesised in optimised reaction conditions and obtained pure. Due to the same observed insolubility further reactions were not possible.[245] The same result was observed in the internship of R. Baier. The other precursor **133** was synthesised in a scaled-up reaction in 46%, but the isomer **133** was also insoluble in organic solvents.[253] These results indicate that a different synthetic strategy needs to be developed in order to access azobenzene-functionalised ligands for cages.

In future attempts the solubility of the azobenzene-based ligands should be improved by modifications such as more flexible spacer groups such as 1,4-dihydroxybenzene or the introduction of functional groups such as alkyl chains or polar groups. Afterwards, the synthesised ligands should be investigated in terms of their switching behaviour upon irradiation as well as the spin-crossover properties of their respective Fe^{II}-based metal-organic cages. Since the desired azobenzene derivatives **124** and **125** were not synthesised in this section, dithienylethenes were investigated as a class of photoswitchable groups (Section 5.2).

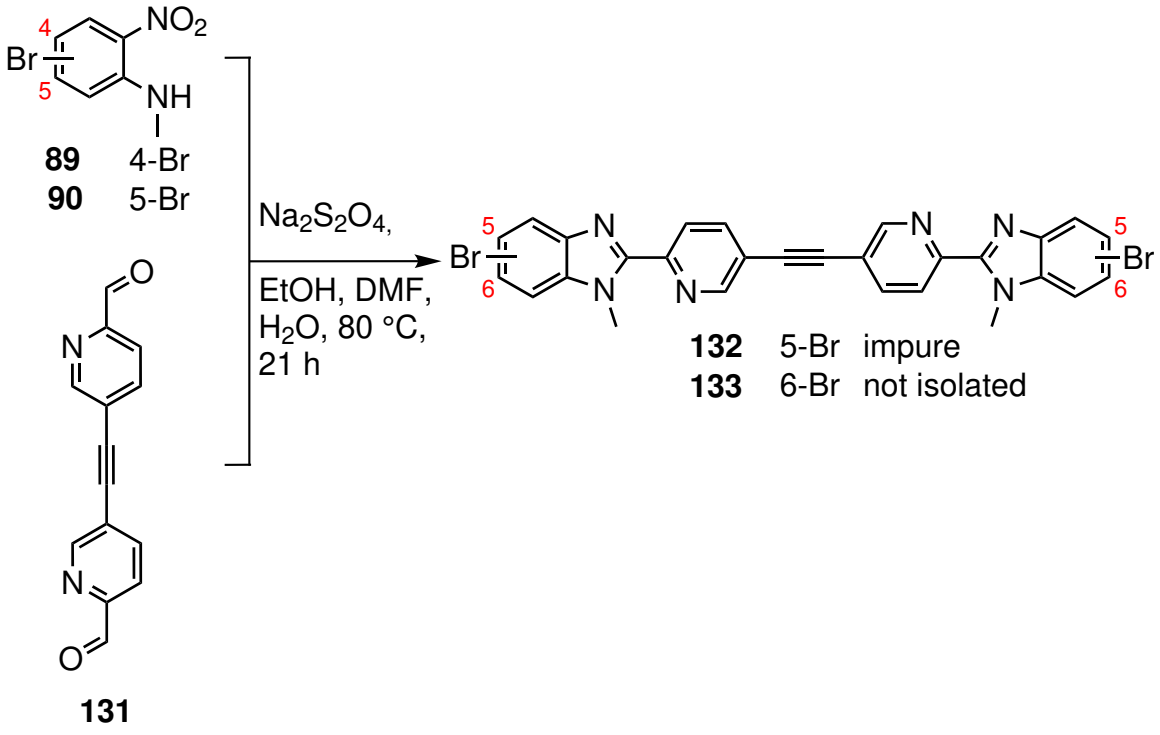

Figure 5.5: Synthesis of ligand isomers **132** and **133**.[18]

5.2 Diarylethene-based Metal-Organic Cages

In section 4.2 dithienylethene **71** was previously synthesised and the photoswitchable properties were investigated. By irradiation with different wavelengths isomerisation of dithienylethene **71** was not observed. Analysis of the ^{1}H NMR spectrum showed the occurance of smaller signals that are attributed to the potential degradation of compound **71**. Based on these results modification of ligand design was explored.

In 1992 Hanazawa *et al.* synthesised a dithienylethene with a perfluorocyclopentene bridge between both benzothiophene rings with a high thermal stability and fatigue-resistance over multiple thousand cycles (Scheme 5.3).[227] Later, in 1996 Irie showed evidence that the fatigue resistance of diarylethenes towards irradiation is higher when aryl groups such as a benzothiophene system are used.[228] Unfortunately, substituted benzothiophenes are challenging to access and are rarely commerically available. Therefore, dithienylethene **71** was modified and a ligand for metal-organic cages designed bearing a 1,2-bis(2'-methylthiophen-3'-yl)perfluorocyclopentene backbone (Scheme 5.4). Terminal 2-(2'pyridyl)benzimidazole binding sites will be introduced to the 5'-position of a 1,2-bis(2'-methylthiophen-3'-yl)perfluorocyclopentene backbone. Upon irradiation with UV light an isomerisation to the closed-ring isomer **138** is expected, whereas visible light irradiation should result in the cycloreversion back to ligand **137**.[227] In addition, during isomerisation the ligand's angle is expected to change with a loss of flexibility due to the enlargened aromatic system (Scheme 5.4, ligand **138**, black). After the synthesis of ligand **137** the self-assembly with multiple metal ions (Fe^{II}, Co^{II}, Zn^{II}) will be investigated in solution. In comparison to the dual-responsive spin-crossover illustration (see Scheme 5.1), the position of the photoswitchable groups is changed since the dithienylethene group is now centered on the axes of the expected cage structure. Furthermore, helicates instead of tetrahedral structures are expected due to the bent nature of ligands **137** and **138**.

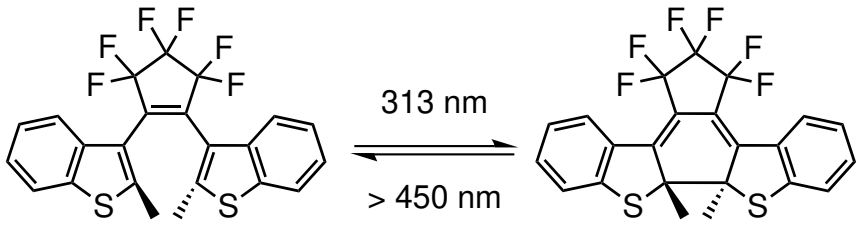

135 **136**

Scheme 5.3: Diarylethenes **135** and **136** were switched by irradiation with 313 nm or >450 nm over 12000 times.[227]

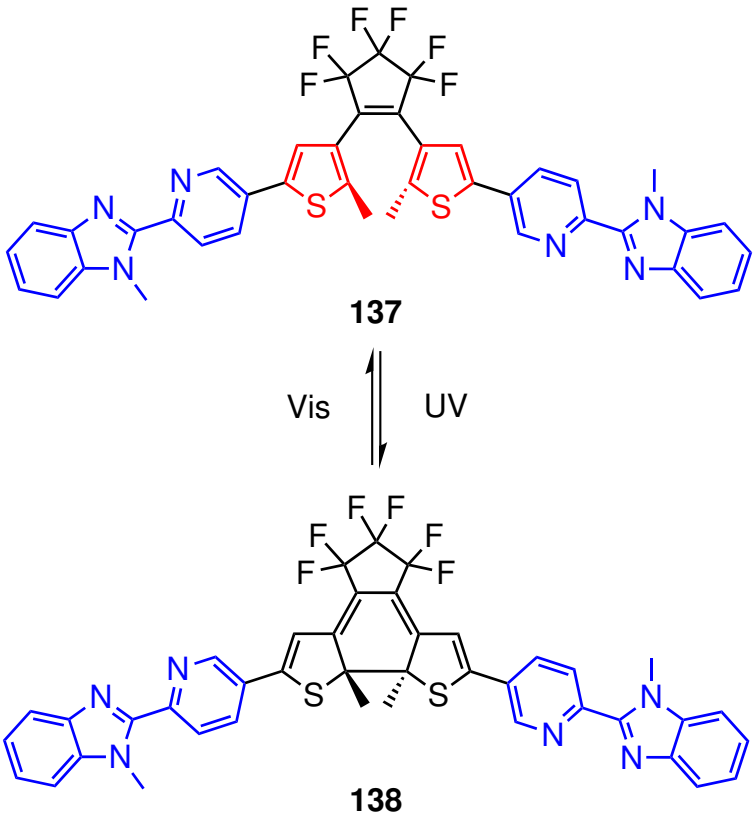

Scheme 5.4: Designed diarylethenes **137** and its closed isomer **138**, based on related diarylethenes.[227,228,254] The 2-(2'pyridyl)benzimidazole binding unit is highlighted in blue, the thiophenes in red and the perfluorocyclopentene backbone in black.

5.2.1 Synthesis of dithienylethene 137

The synthesis of dithienylethene **137** is a four step convergent synthetic route starting from 2-methylthiophene (**139**) and compound **142**. In the first steps 2-methylthiophene (**139**) will be brominated and borylated to obtain the boronic acid **141**. Afterwards, compound **141** will be used in a Suzuki cross-coupling with compound **142** (synthesised following a literature-known procedure).[13] Afterwards, precursor **143** will be lithiated and the intermediate trapped using octafluorocyclopentene to obtain the target dithienylethene **137**.

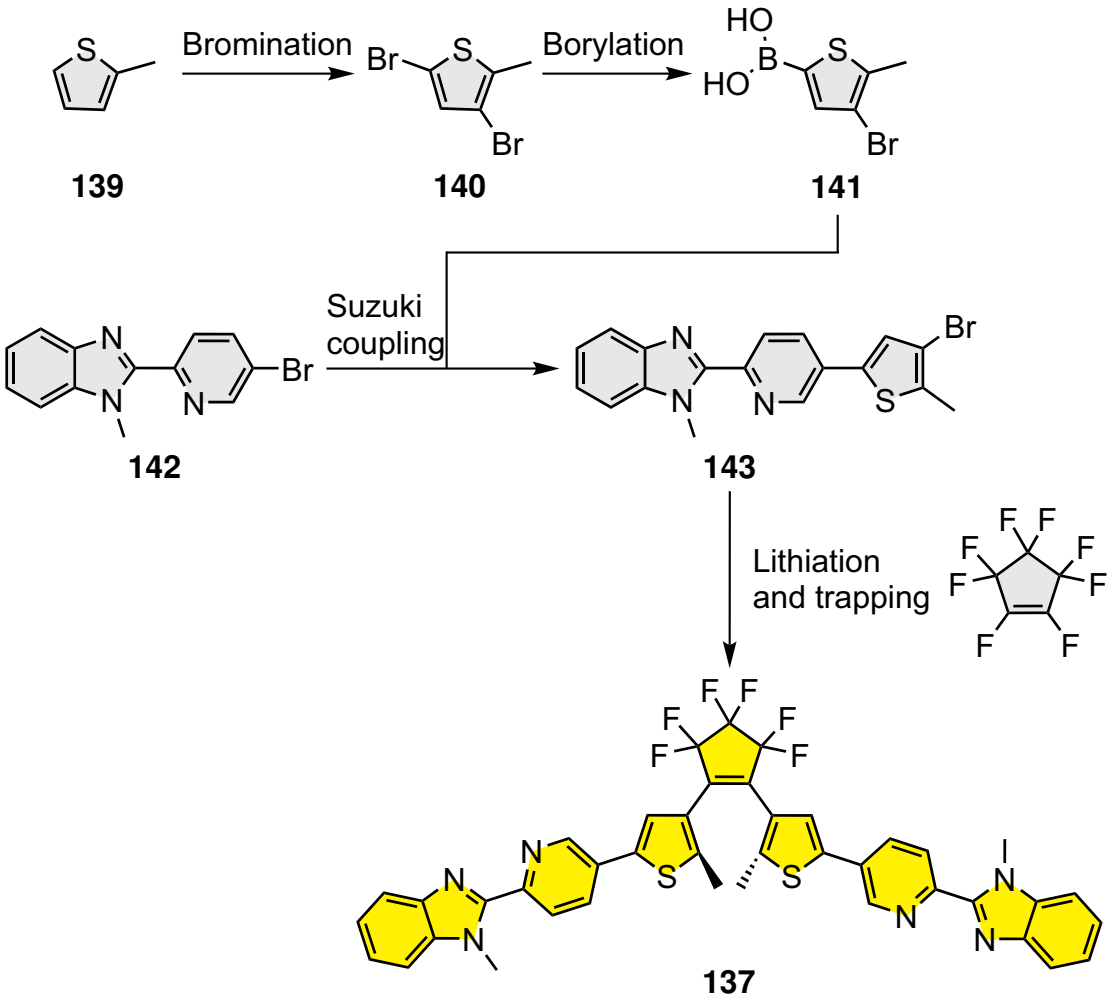

Scheme 5.5: Proposed synthesis of 2,2'-(((perfluorocyclopent-1"'-ene-1"',2"'-diyl)bis(5"-methylthiophene-4",2"-diyl))bis(pyridine-5',2'-diyl))bis(1-methyl-1*H*-benzo[*d*]imidazole) (**137**).

Based on an adapted procedure from Moreno *et al.*,[28] 2-methylthiophene (**139**) was reacted with *N*-bromosuccinimide in a mixture of chloroform and glacial acetic acid at room temperature for 23 h. After purification by column chromatography the product **140** was obtained in a yield of 51%. Losses of product can be attributed to the reaction conditions. Since *N*-bromosuccinimide is known to be light-sensitive the reaction should be performed in the absence of ambient light to increase the yield. The yield was not further improved since enough product **140** was obtained during this attempt.

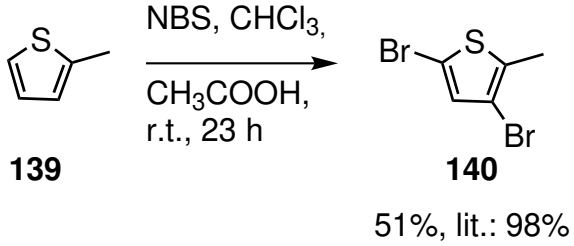

Figure 5.6: Synthesis of 3,5-dibromo-2-methylthiophene (**140**) according to a procedure from Moreno *et al.*.[28]

Subsequently, 3,5-dibromo-2-methylthiophene (**140**) was borylated according to an adapted procedure from von Irmer *et al.*.[29] Compound **140** was lithiated with *n*-butyllithium at -78 °C for 1 h and the lithiated intermediate was trapped using tributyl borate. After warming to room temperature the boronic ester was cleaved using hydrochloric acid and product **141** was obtained after precipitation in a yield of 72% as a mixture of the boronic acid **141** and the boroxine **144** in a ratio of 1:2.2, based on integrals in the ^{1}H NMR spectrum.

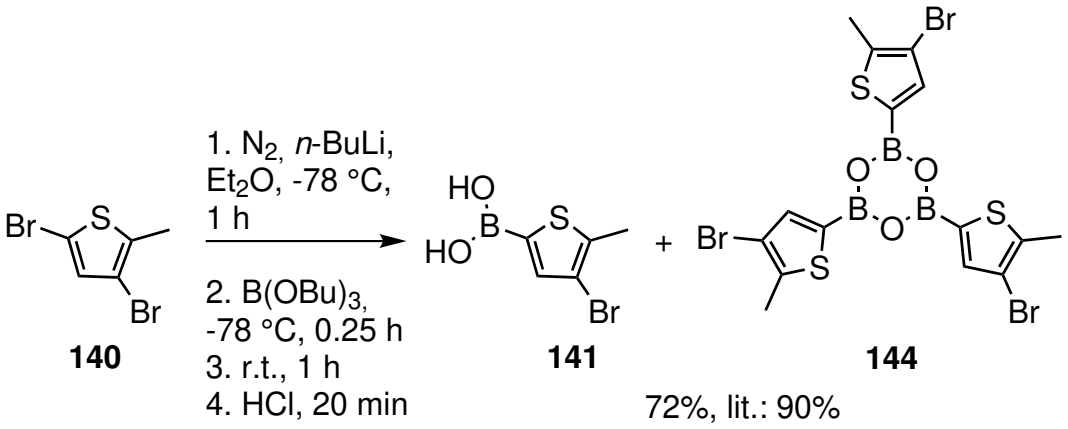

Figure 5.7: Synthesis of (4-bromo-5-methylthiophen-2-yl)boronic acid (**141**) according to a procedure from von Irmer *et al.*.[29]

Adapting a procedure from Burke *et al.*,[25] the boronic acid **141** and the precursor **142**[13] were reacted in a Suzuki cross-coupling with $Pd(PPh_3)_4$ as the catalyst and potassium carbonate as the base at

80 °C for 19 h. After purification by column chromatography with subsequent recrystallisation from methanol, the product **143** was obtained in a yield of 30%. In a second attempt the yield was further increased in a scaled up reaction (5.6x). After cooling to room temperature the product precipitated and the remaining filtrate was further purified by column chromatography to yield precursor **143** in 54%.

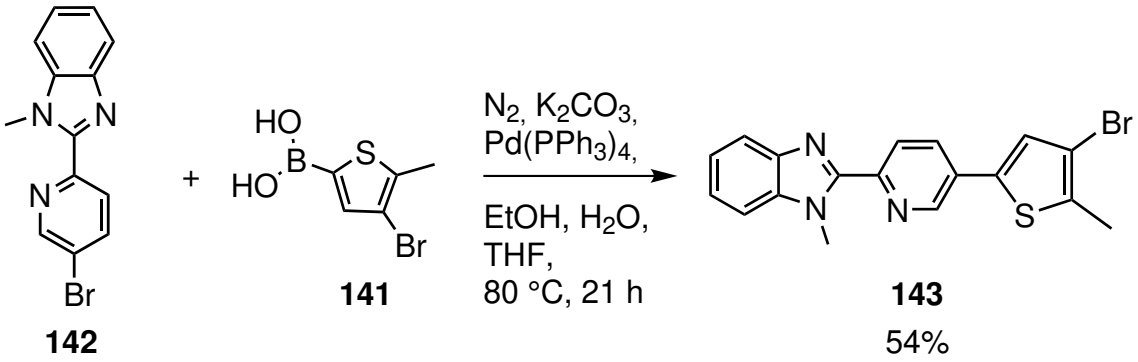

Figure 5.8: Synthesis of 2-(5'-(4"-bromo-5"-methylthiophen-2"-yl)pyridin-2'-yl)-1-methyl-1*H*-benzo[*d*]imidazole (**143**) adapting a procedure from Burke *et al.*.[25]

In the last step reaction conditions for the synthesis of dithienylethenes from Becker were adapted.[30] Precursor **143** was lithiated with *n*-butyllithium at -78 °C for 2 h. The lithiated species was then reacted with octafluorocyclopentene at -78 °C for 3 h and further at room temperature for 16.5 h. Purification by column chromatography gave the product **137** in a yield of 49%. During the purification process starting material **143** as well as two unknown side products were separated according to thin-layer chromatography measurements. The side products and recovered starting material **143** explain the incomplete conversion towards product **137**. Furthermore, separation of the side products and product **137** was difficult due to similar retention factors, thus the purification process is extremely time-consuming. However, the desired dithienylethene **137** was successfully synthesised in a good yield and can be further used for photochemical studies as well as self-assembly investigations.

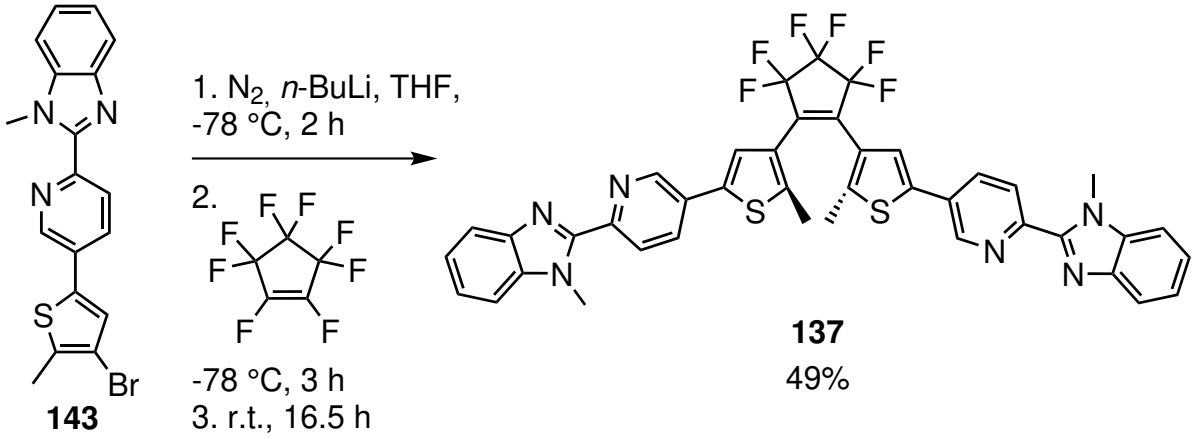

Figure 5.9: Synthesis of 2,2'-(((perfluorocyclopent-1"'-ene-1"',2"'-diyl)bis(5"-methylthiophene-4",2"-diyl))bis(pyridine-5',2'-diyl))bis(1-methyl-1*H*-benzo[*d*]imidazole) (**137**) adapting a procedure from Becker.[25]

5.2.2 Photochemical properties of dithienylethene 137

After the successful synthesis of dithienylethene **137** its photochemical properties were investigated in detail using NMR and UV/Vis spectroscopy. The switching process from the opened-ring isomer **137** to the closed-ring isomer **138** by irradiation with either UV light or visible light was examined using NMR spectroscopy (Scheme 5.10). Based on the poor solubility of dithienylethene **137** in CD_3CN the NMR spectroscopic measurements were performed in $CDCl_3$. The UV/Vis studies were performed in acetonitrile because small amounts of ligand **137** were dissolved.
Dithienylethene **137** ($5.1 \cdot 10^{-5}$ mol) was dissolved in deuterated chloroform (500 µL). Afterwards, the ratio of both isomers **137** and **138** was examined before and after irradiation by measuring ^{1}H and ^{19}F NMR spectra (Figure 5.6 & 8.11). After irradiation of the sample with 365 nm for 10 min the colour of the solution changes from yellow to blue, suggesting a conversion from the opened-ring isomer **137** to dithienylethene **138**. Further analysis of its ^{1}H NMR spectrum shows chemical shift changes that are attributed to the closed-ring isomer **138**. The PSS of the closed-ring isomer **138** was examined, being 98% based on integrals in the ^{19}F NMR spectra (Figure 8.11. Complete backisomerisation was observed after irradiation with 590 nm for 15 min to the opened-ring isomer **137**.

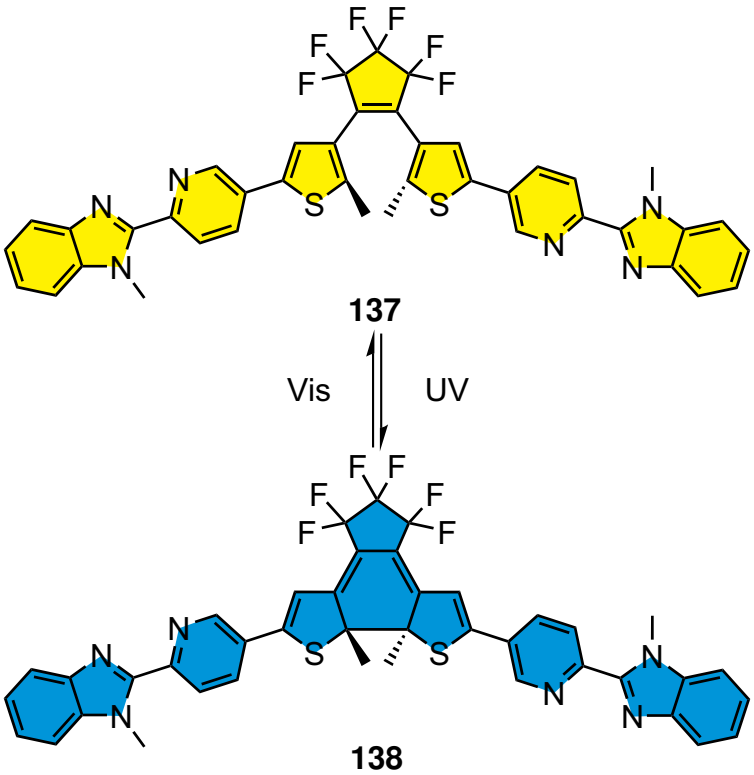

Figure 5.10: Switching between the opened-ring isomer **137** and **138** by UV/Vis irradiation.

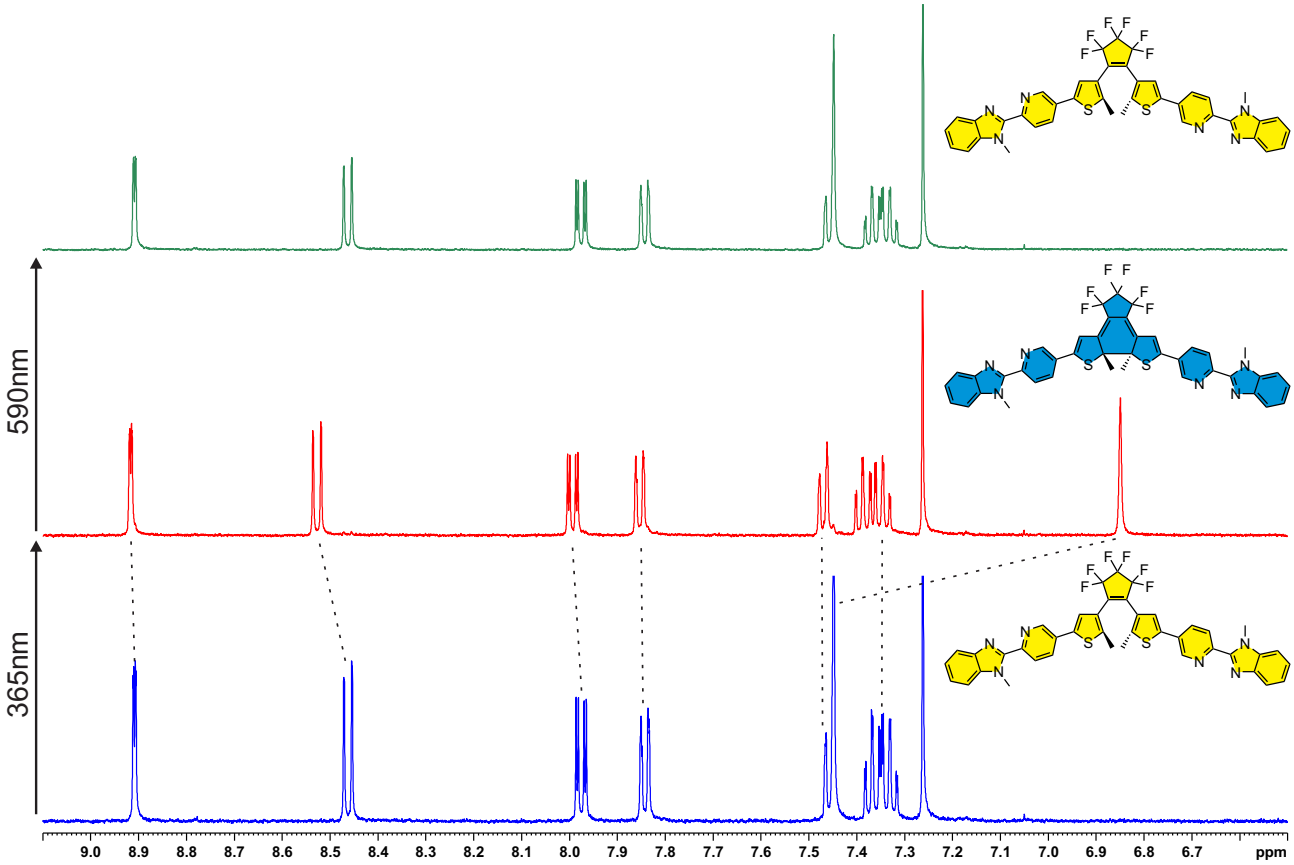

Figure 5.6: ^{1}H NMR spectra (500 MHz, $CDCl_3$, 298 K) of dithienylethene **137** before (blue) and after irradiation with 365 nm (red) or 590 nm (green). Chemical shift changes are illustrated with dotted lines.

After analysis of the photochemical properties of dithienylethene **137** by NMR spectroscopy, UV/Vis studies were performed. Ligand **137** ($1.18 \cdot 10^{-5}$ M) was dissolved in acetonitrile (HPLC grade, 100 mL) and UV/Vis spectra were recorded after certain time intervals (Figure 5.7, a) & c)). A characteristic maximum at 346 nm is observed attributed to the opened-ring isomer **137** (Figure 5.7, a)).[29,255–257] Upon irradiation with 365 nm for 1 s a bathochromic shift of the absorption band at 346 nm is visible and shifts towards 361 nm. Furthermore, a second band visible at 613 nm is attributed to an enlarged π-system resulting from the photocyclisation process and corresponds to the closed-ring isomer **138** in the photostationary state.[29,257] A colour change from light-yellow to blue is observed (Figure 5.7, b)). The cycloreversion process can be followed by irradiation with 590 nm for 180 seconds to obtain the original photostationary state of dithienylethene **137** (Figure 5.7, c)).

For the analysis of the fatigue resistance of both isomers the absorbance at 613 nm was plotted as a function of the cycle number (Figure 5.7, d)). However, after only 4.5 cycles the absorbance decreases gradually by about 5% based on the maximum absorption. In addition, increased absorbance after irradiation with 590 nm to the opened-ring isomer **137** was observed, suggesting an incomplete cycloreversion reaction.

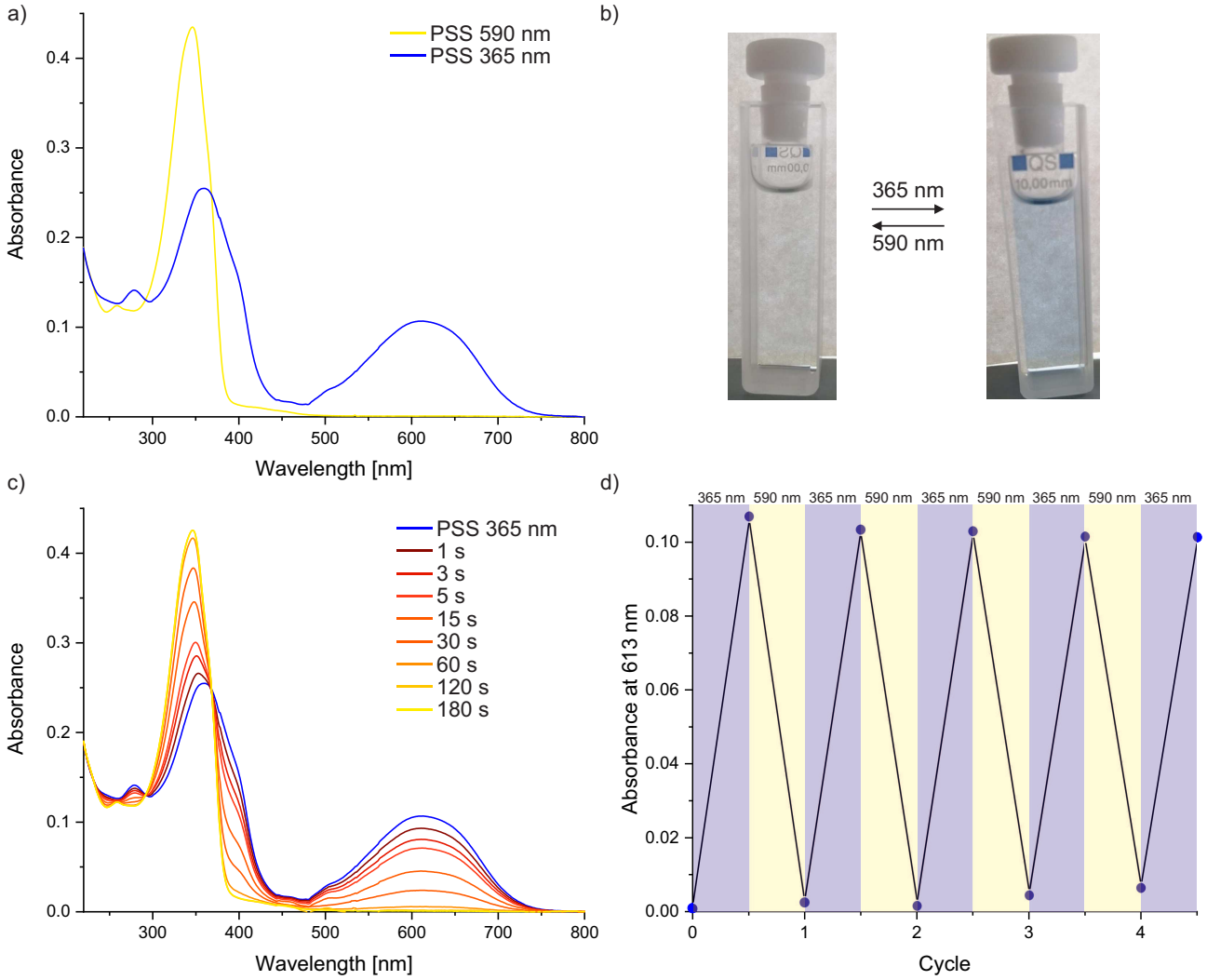

Figure 5.7: a) UV/Vis spectrum ($1.18 \cdot 10^{-5}$ M, acetonitrile, 293 K) of dithienylethene **137** in its photostationary states. b) Observed colour change of the photocyclisation by irradiation with 365 nm or 590 nm. c) UV/Vis spectra ($1.18 \cdot 10^{-5}$ M, acetone, 293 K) of dithienylethene **138** upon irradiation with 590 nm over the time course of overall 180 seconds. d) Fatigue resistance of dithienylethene **137** over 4.5 cycles.

5.2.3 Self-assembly of dithienylethene 137 with Zn^{II}, Co^{II} and Fe^{II}

In section 5.2.1 ligand **137** was successfully synthesised in a good yield and its photochemical properties were investigated by NMR and UV/Vis spectroscopy (Section 5.2.2). Upon irradiation with 365 nm a fast and almost quantitative (98%) photocyclisation of dithienylethene **137** was observed. Further irradiation with 590 nm led to a quantitative cycloreversion reaction to the open-ring isomer **137**. Based on these results this section focuses on the self-assembly of dithienylethene **137** and **138** with zinc(II)- and cobalt(II) bis(trifluoromethylsulfonyl)imide (Zn/Co$(NTf_2)_2$) and iron(II) trifluoromethanesulfonate (Fe$(OTf)_2$) to the expected M_2**137**$_3$ helicates (Scheme 5.8). The self-assembly with Zn^{II} ions will be investigated since the expected helicate could be used as the diamagnetic analogue of the Fe^{II}-based helicate for calculating the spin-crossover properties in future studies (for further details see Paschelke *et al.*[235]).[186] In addition, the self-assembly with Co^{II} is of great interest since the paramagnetism helps to characterise the expected helicate by larger chemical shifts. This data could be used as a comparison to characterise the self-assembly with Fe^{II}.[231,232,258] For all three self-assemblies M_2L_3-based helicates are expected and the self-assemblies will be analysed by NMR spectroscopy and ESI-MS. In addition, the photochemical properties of the self-assemblies will be analysed if discrete structures are obtained.

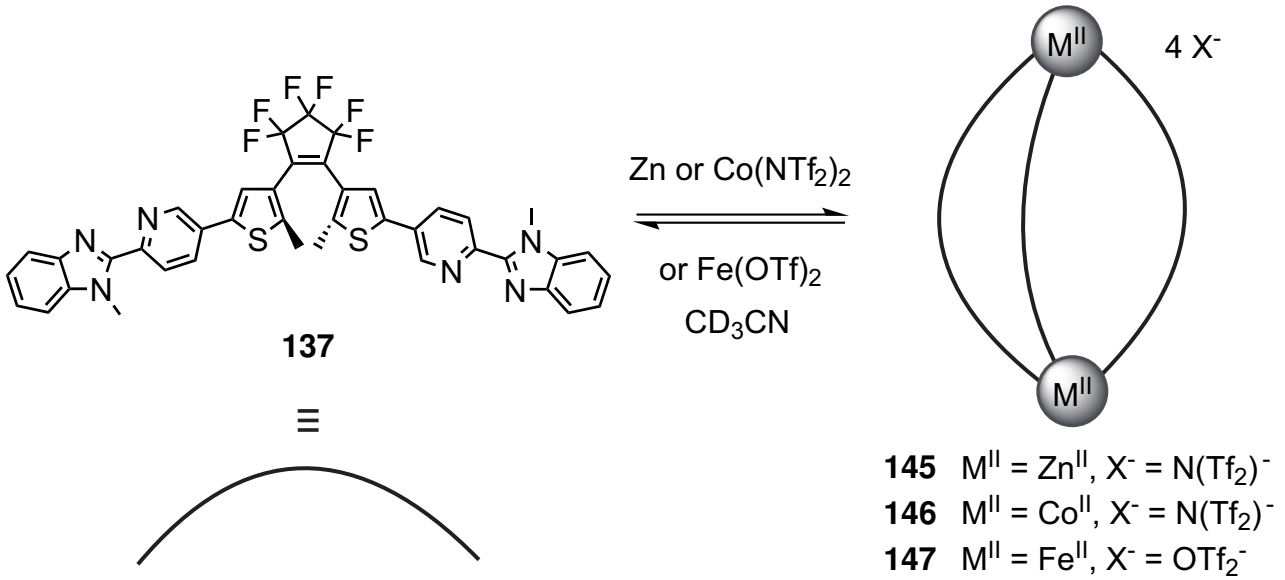

Scheme 5.8: Self-assembly of dithienylethene **137** with different metal salts in deuterated acetonitrile.

The proposed helicates were prepared *in situ* in deuterated acetonitrile (c = 1.31-1.53·10^{-5} M) using three equivalents of ligand **137** and two equivalents of the appropriate salt (Scheme 5.8). The preparation was performed in the dark to avoid possible switching of ligand **137**. Analysis of the ^{1}H

NMR spectra revealed in all three cases the formation of one discrete species having the expected 10 protons of the ligand **137** (Figure 5.9). This is also supported by the observation of two signals with an integral of 4:2 (based on one ligand) within the ^{19}F NMR spectra. The ^{19}F signals can be attributed to the perfluorocyclopentene backbone of one symmetrical species (Figure 8.12). Further analysis by ESI-MS showed three signals at *m/z* 619.5922, 919.0959 and 1519.6027 (Figure 5.11). By comparison of the experimental isotopic pattern to the theoretical pattern, the signals were assigned to the formation of the expected Zn_2**137**$_3(NTf_2)_4$ helicate. For the other two proposed helicates **146** (*m/z* 616.3460, 915.1003 and 1513.1106) and **147** (*m/z* 614.8467, 869.4462, 1378.6474) also three signals were observed and assigned to the respective helicates Co_2**137**$_3(NTf_2)_4$ (**146**) and Fe_2**137**$_3(OTf)_4$ (**147**) (Figures 8.13 and 8.14).

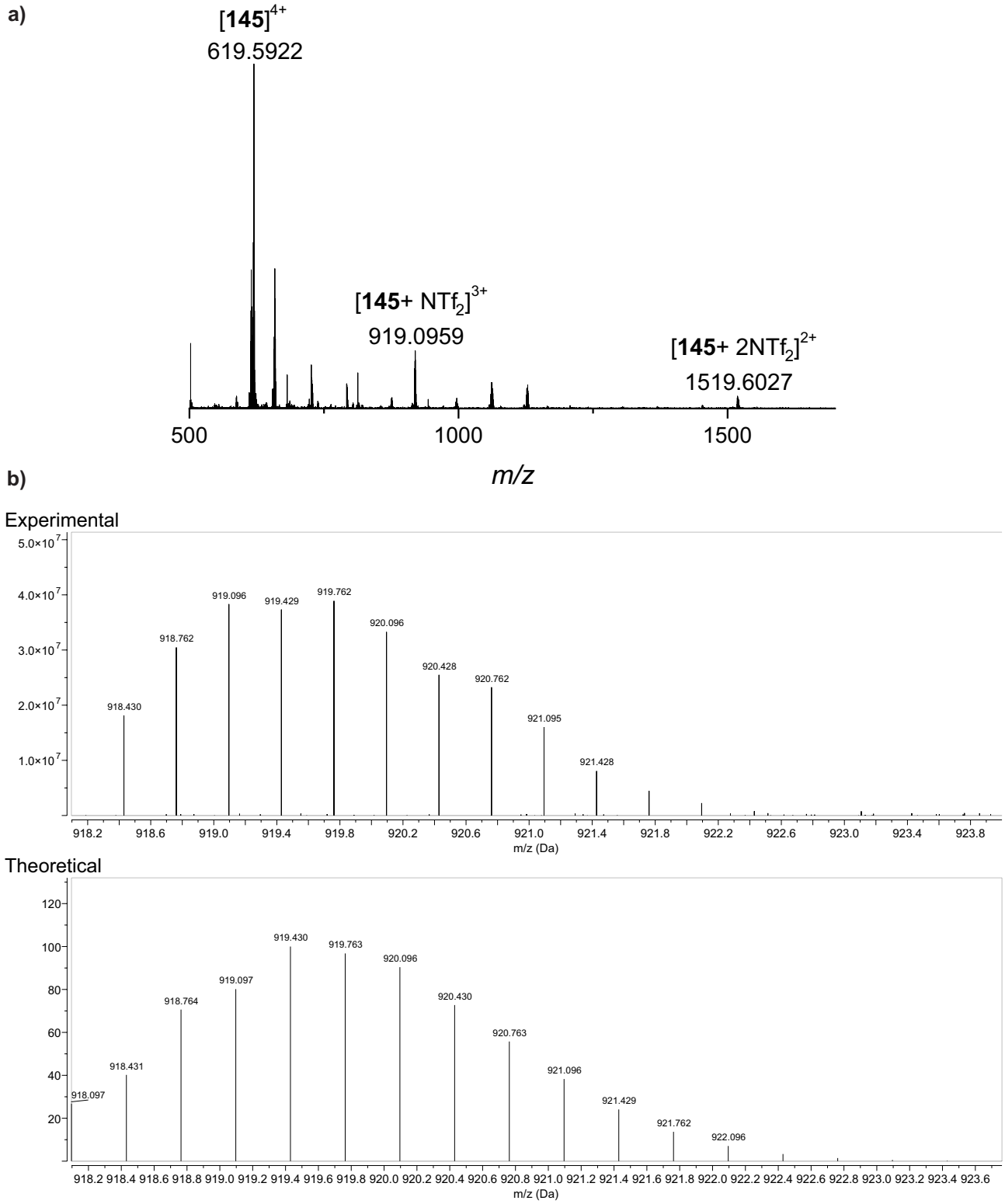

Figure 5.11: High resolution ESI mass spectrum of helicate **145** a) in the range of *m/z* 500-1700 and b) the experimental and theoretical isotopic patterns.

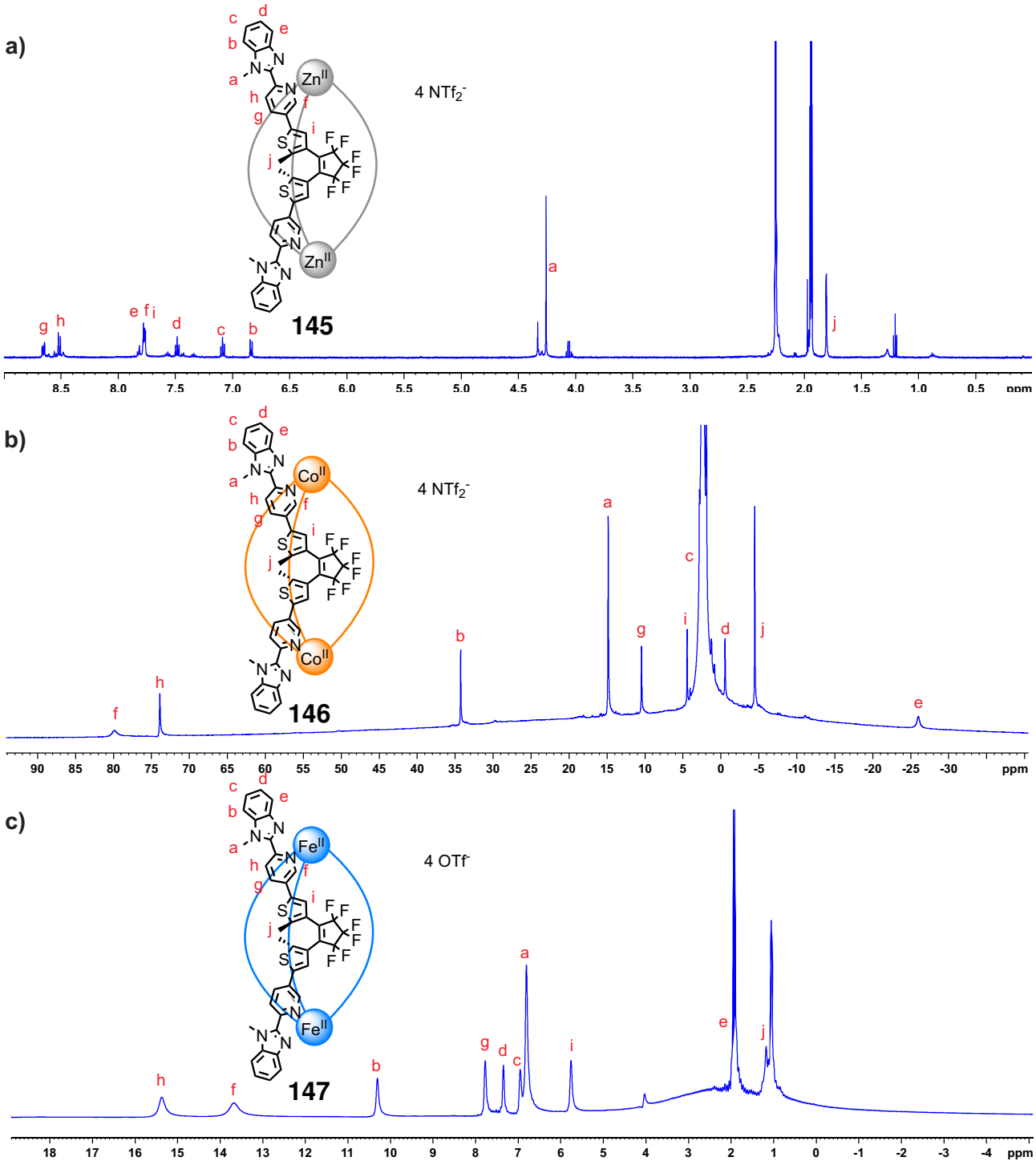

Figure 5.9: ^{1}H NMR spectra (500 MHz, CD_3CN, 298 K) of helicates a) **145**, b) **146** and c) **147**.

5.2.4 Photochemical investigations with helicates 145, 146 and 147

In all cases the expected helicates were formed *in situ*, as confirmed by ESI-MS and NMR spectroscopy. Furthermore, the photochemical properties are of great interest since the helicates can potentially be used as dual-responsive spin-crossover cages that are responsive to light and temperature. The wavelengths used for the cyclisation and cycloreversion are based on the UV/Vis studies in section 5.2.2. Starting with helicate **145**, a colour change from yellow to blue was observed after irradiation with 365 nm, indicating the possible formation of the closed-ring cage isomer **148** (Scheme 5.10). Analysis of the ^{1}H NMR and ^{19}F NMR spectra showed the formation of one symmetric species (Figures 5.12 and 5.13). However, complete characterisation of the blue-colored species was difficult due to ^{1}H signal overlap and broadness (Figure 5.12, red). Furthermore, insufficient cross-peaks were observed in the ^{1}H-^{1}H COSY spectrum making the assignment of protons challenging. However, the formed species was expected to be the closed-helicate isomer **148**. Upon irradiation with 590 nm cycloreversion reaction was observed, obtaining the initial helicate **145** as confirmed by ^{1}H NMR spectroscopy (Figure 5.12).

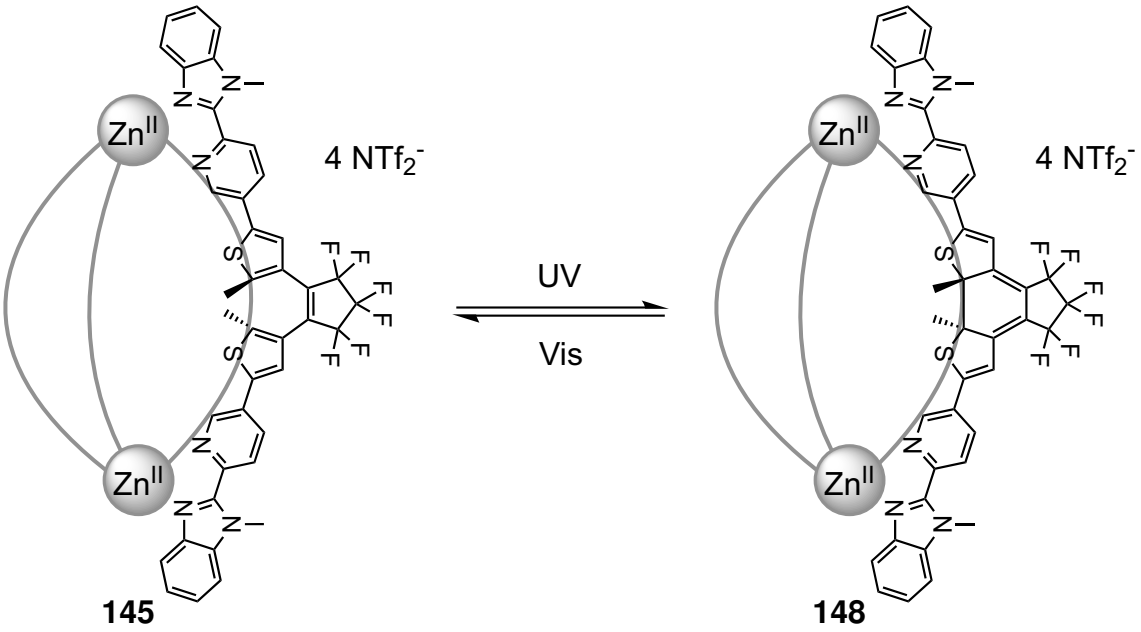

Scheme 5.10: Photocyclisation of helicate **145** (left) and cycloreversion reaction of the closed-isomer **148** (right) with either UV or Vis irradiation.

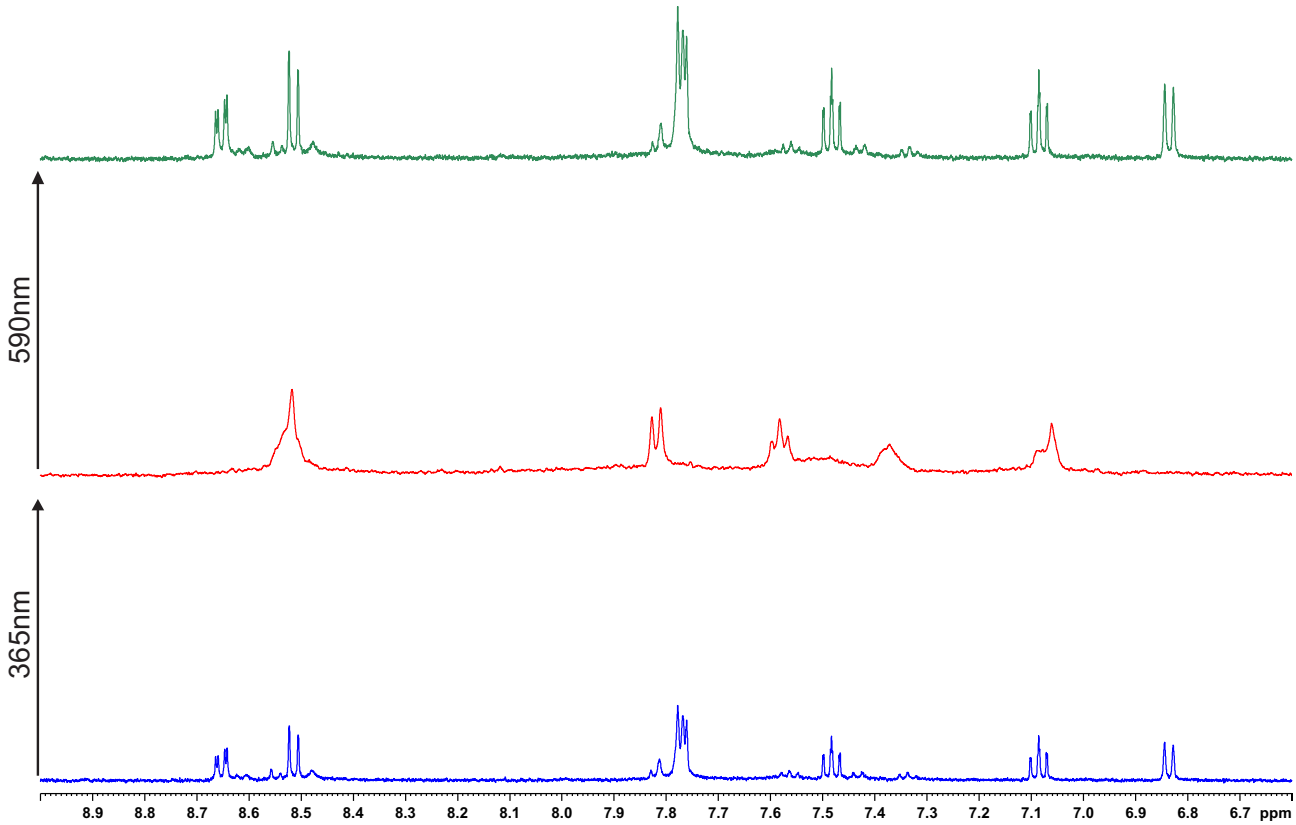

Figure 5.12: ^{1}H NMR spectra (500 MHz, CD_3CN, 298 K) of the photocyclisation process of helicate **145** (blue) to **148** upon irradiation with 365 nm (red) and the cycloreversion reaction by irradiation with 590 nm (green).

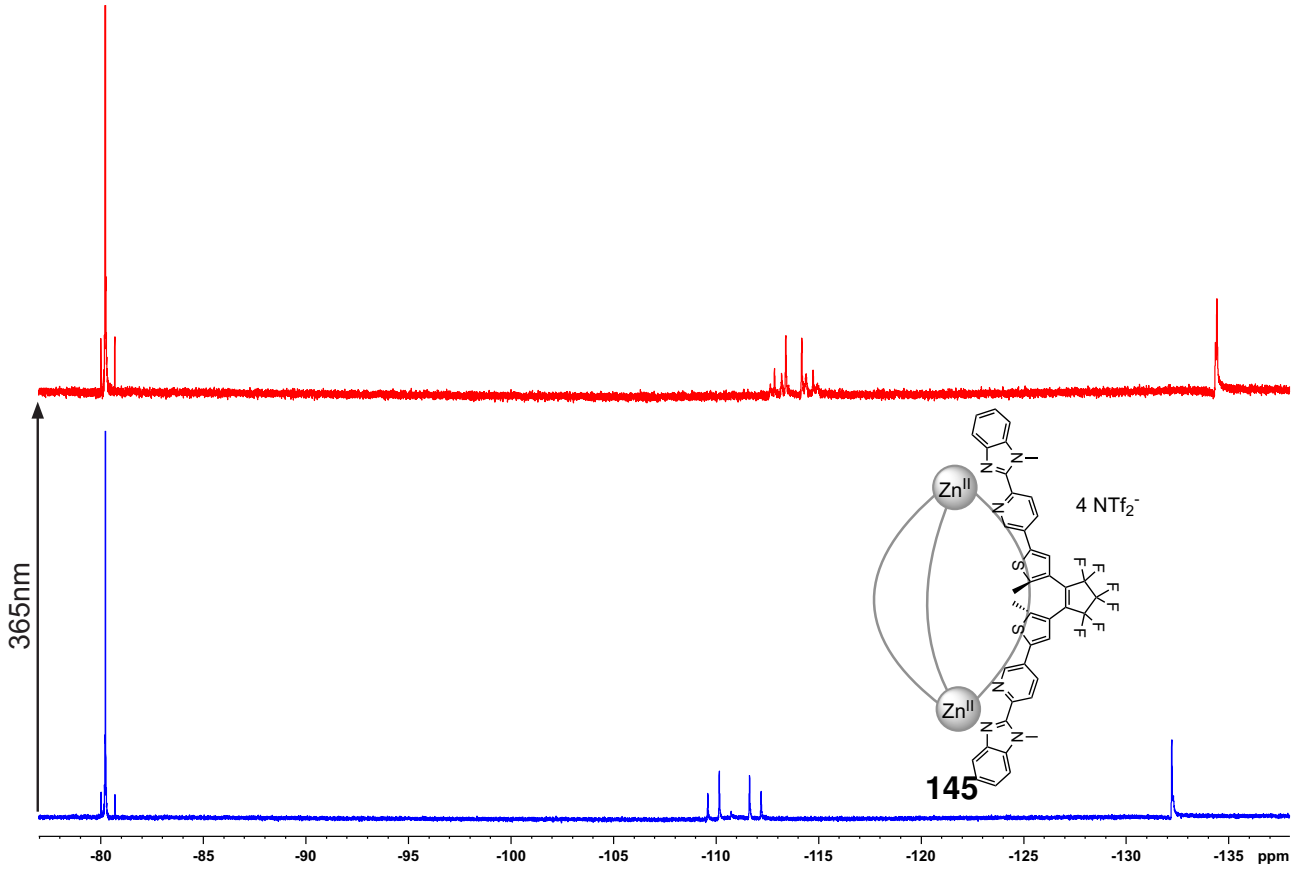

Figure 5.13: ^{19}F NMR spectra (471 MHz, CD_3CN, 298 K) of the photocyclisation process of helicate **145** to **148** upon irradiation with 365 nm.

The NMR irradiation experiments for helicate **145** with 365 nm and 590 nm (Figures 5.12 and 5.12) were repeated multiple times at the same concentration, however, the results obtained were not reproducible (Figure 5.11). Upon irradiation with 365 nm more signals appeared in the ^{1}H NMR spectrum than previously observed for the expected closed-ring helicate **148**. Shortening or lengthening the irradiation time did not improve the ^{1}H NMR spectra and results. Unexpectedly, upon irradiation with 590 nm for 45 min the initial spectrum of helicate **145** was obtained quantitatively. Unfortunately, ESI-MS measurements of the proposed closed-form helicate **148** were not measured since the initial results could not be reproduced. The reason for it is yet unknown. Further investigations should focus on the reason for the irreproducibility of the photocyclisation process to restore the photocyclisation process.

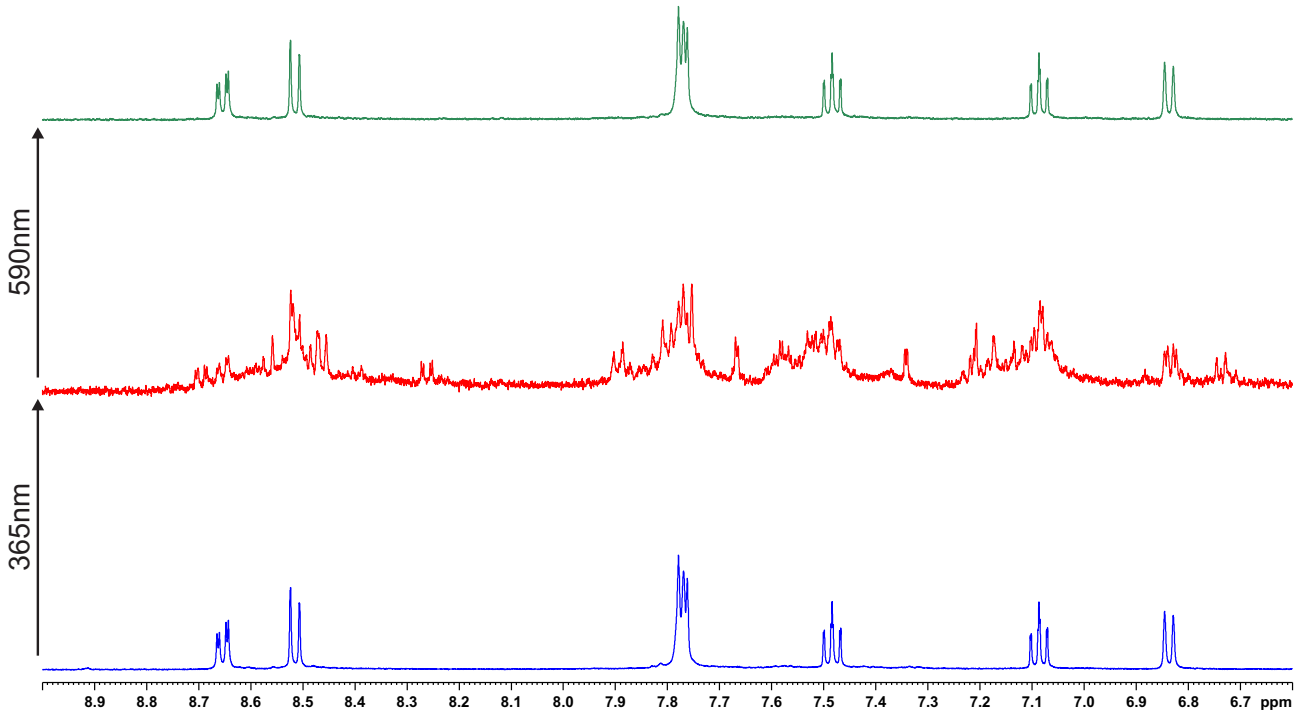

Figure 5.11: ^{1}H NMR spectra (500 MHz, CD_3CN, 298 K) of the attemped photocyclisation of helicate **145** upon irradiation with 365 nm. The initial state was restored after irradiation with 590 nm.

Afterwards, the photochemical properties of the Co^{II}-based helicate **146** were investigated. After its preparation *in situ* (see Figure 5.9) helicate **146** was irradiated with 365 nm for 15 min inducing a colour change from orange to green, suggesting possible photocyclisation. However, after recording a ^{1}H NMR spectrum no chemical shift changes of the protons or new signals growing in were visible (Figure 5.12). Moreover, the same result can be seen in the ^{19}F NMR spectra (Figure 8.15). Interestingly, by repeating the experiment with the Fe^{II}-based helicate **147** the same observation was made. Irradiation with 365 nm did not show any changes of the ^{1}H or ^{19}F chemical shifts (Figures 8.16 and 8.17). The poor efficiency could be attributed to an inappropriate spatial orientation of the ligand making the isomerisation sterically unfavored. Crystal growth experiments were conducted in order to provide evidence for this hypothesis, however, crystals were not obtained. Based on the poor photocyclisation efficiency no further irradiation experiments were performed with helicates **146** and **147** since an efficient photocyclisation process is desired for potential applications.

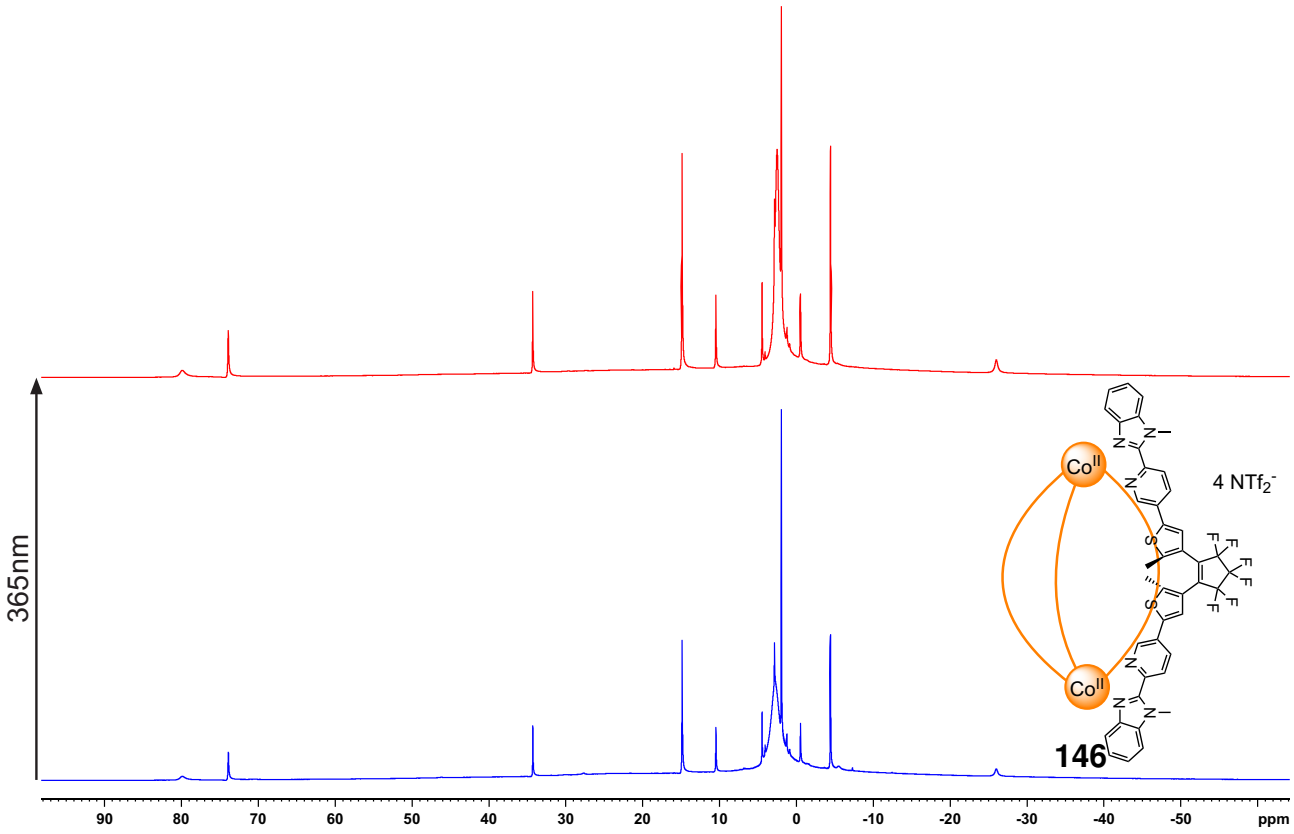

Figure 5.12: ^{1}H NMR spectra (500 MHz, CD_3CN, 298 K) of helicate **146** before (blue) and after (red) irradiation with 365 nm.

In 2019 Li *et al.*[254] investigated the photochemical properties of a similar ligand system bearing 2,2'-bipyridine binding units and a non-substituted cyclopentene backbone (Scheme 5.13). The conversion rate of the photocyclisation process by irradiation with 365 nm between the opened isomer **o-L** and the closed form **c-L** was determined to be 98-99% based on integrals in ^{1}H NMR spectra. By addition of $Fe(OTf)_2$ to the ligand the formed helicate Fe_2**o-L**$_3(OTf)_4$ was further investigated in relation to its photochemical properties. However, photocyclisation with UV light irradiation was poorly efficient and incomplete, taking several days, although the ligand adopted a photo-active conformation based on X-ray crystallography data. After this result, the helicate Fe_2**c-L**$_3(OTf)_4$ was self-assembled by mixing $Fe(OTf)_2$ with the closed and cyclised ligand **c-L** in a ratio of 2:3. Irradiation with visible light of Fe_2**c-L**$_3(OTf)_4$ yielded the initially prepared Fe_2**o-L**$_3(OTf)_4$ helicate within minutes (based on UV/Vis data) making this system a suitable one-way switch.

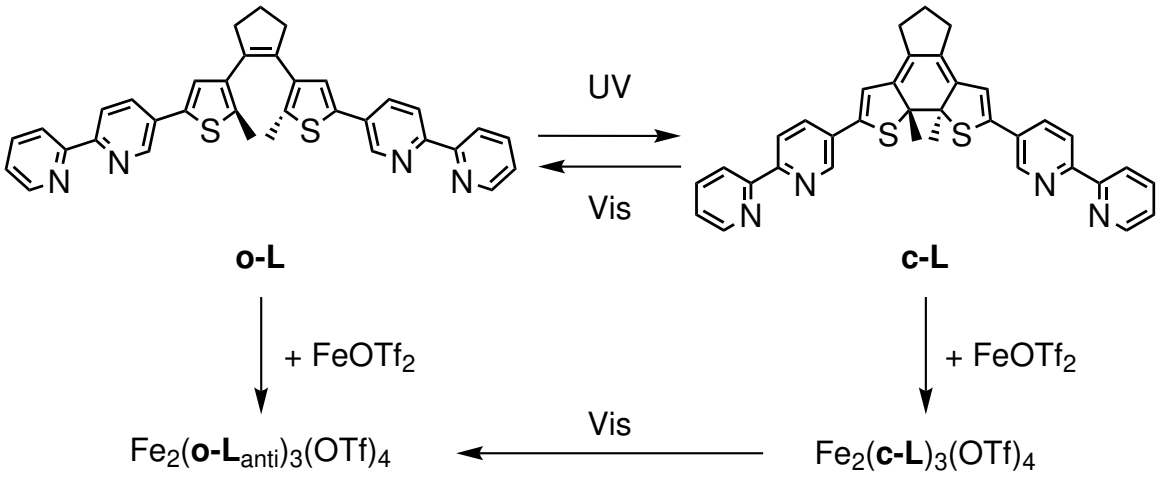

Scheme 5.13: Photocyclisation of the system of Li *et al.* upon irradiation with UV or Vis light.

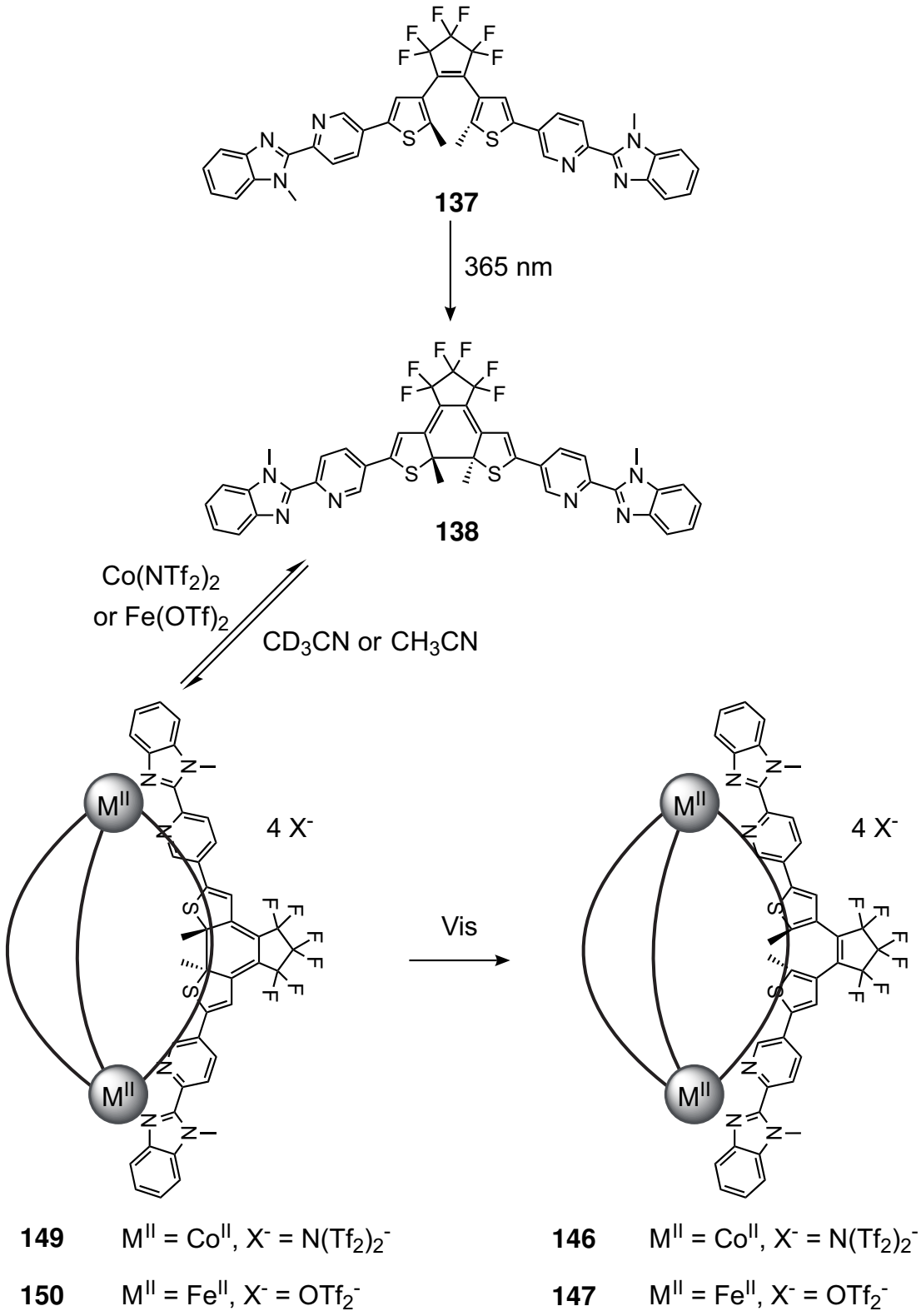

149 $M^{II} = Co^{II}$, $X^- = N(Tf_2)_2^-$ **146** $M^{II} = Co^{II}$, $X^- = N(Tf_2)_2^-$

150 $M^{II} = Fe^{II}$, $X^- = OTf_2^-$ **147** $M^{II} = Fe^{II}$, $X^- = OTf_2^-$

Scheme 5.14: Cycloreversion process between proposed helicates **149** and **150** by irradiation with visible light to obtain helicates **146** and **147**.

Based on the data of Li *et al.*[254] the same strategy was used to analyse if the closed-ring ligand **138** could be used in self-assemblies with Co^{II} and Fe^{II} as a one-way switch (Scheme 5.14). For that reason, ligand **137** was dissolved in deuterated chloroform ($1.13 \cdot 10^{-2}$ M) since ligand **137** is solubile in chloroform but has poor solubility in deuterated acetonitrile. The solution was then irradiated with 365 nm to obtain the target ligand **138**. At certain time intervals ^{1}H NMR spectra were recorded to monitor the photocyclisation process. Complete isomerisation to ligand **138** was observed after 18 min of irradiation with 365 nm. The solvent was removed *in vacuo* and self-assembly attempts to the closed-ring helicates **149** and **150** were performed based on the results of Li *et al.*[254] by mixing two equivalents of $Co(NTf_2)_2$ or $Fe(OTf)_2$ with three equivalents of ligand **138** in deuterated acetonitrile having the same concentrations as the open-ring helicates in section 5.2.3 ((c = $1.31\text{-}1.53 \cdot 10^{-5}$ M)). Both solutions were heated at 50 °C and the equilibrium was reached after 93 h (Co^{II}-based self-assembly) or 28 h (Fe^{II}-based self-assembly) as confirmed by ^{1}H NMR spectroscopy. More signals were observed upon heating suggesting the formation of multiple species being present in thermal equilibrium. Differentiation between the species or characterisation was not possible using 1D and 2D NMR spectroscopy techniques (Figure 5.15, a)). In addition, for the Fe^{II}-based self-assembly paramagnetic species were observed up to 73.1 ppm. Upon heating smaller signals disappeared, making analysis simpler. However, characterisation by NMR spectroscopy was unsuccessful due to broad ^{1}H signals (Figure 5.15). Based on the NMR data, it is assumed that more than one discrete structure was formed in the self-assembly attempts with ligand **138**. Based on these results ESI-MS measurements were performed to identify possible species at thermal equilibrium since assignment of ^{1}H signals by NMR spectroscopy was not possible.

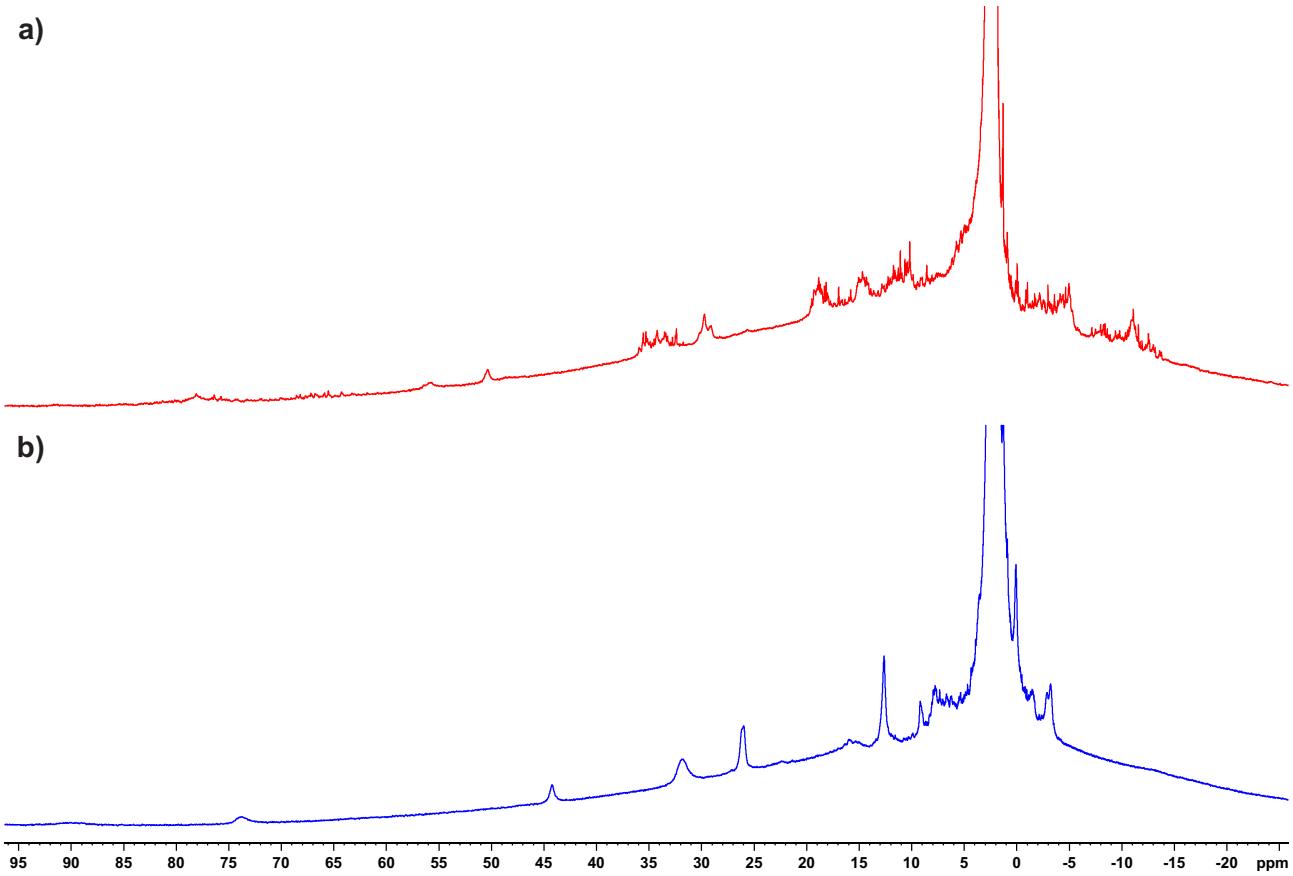

Figure 5.15: ^{1}H NMR spectra (500 MHz, CD_3CN, 298 K) of the self-assembly with ligand **138** with a) $Co(NTf_2)_2$ and b) $Fe(OTf)_2$.

ESI-MS data analysis for the self-assembly with $Co(NTf_2)_2$ was challenging since many signals were observed, however, *m/z* of 616.3455, 915.0997 and 1513.1095 were assigned to the proposed $Co_2\mathbf{138}_3(NTf_2)_2$ structure. Furthermore, *m/z* of 420.5517, 654.3757 and 1121.0219 were assigned to a $Co_2\mathbf{138}_2(NTf_2)_2$ species (Figure 5.14). Other signals could not be assigned. For the Fe^{II}-based self-assembly the expected $Fe_2\mathbf{138}_3(OTf)_4$ (*m/z* 614.8462, 869.4462 and 1379.1466) helicate was identified as well as a $Fe_2\mathbf{138}_2(OTf)_4$ species (*m/z* 608.7219, 987.0580 and 2124.0815) (Figure 8.18). Also other signals were visible in the ESI spectrum, but no further assignment to a specific species was possible. For further structural analysis crystal structure might help to identify certain products at the thermal equilibrium.

Although a discrete structure was not obtained, the cycloreversion process was investigated since this process was assumed to work more efficiently compared to the photocyclisation based on the results of Li *et al.*[254] Initially, the Co^{II}-based self-assembly was irradiated with visible light (590 nm) and the cycloreversion monitored by NMR spectroscopy (Figure 5.16). After irradiation with 590 nm for 30 min a colour change from blue to yellow was visible. Quantitative cycloreversion was observed as

visible in the ^{1}H NMR spectrum. The observed signals in the ^{1}H NMR spectrum were assigned to the open-ring helicate **146**. The same experiment was repeated for the Fe^{II}-based self-assembly and indeed, the cycloreversion was also observed with an extended irradiation time of 75 min instead of 55 min to ensure complete cycloreversion (Scheme 5.16). A colour change from blue to wine red was observed. The cycloreversion was suggested to be faster for compound **146** than for the Fe^{II}-based analogue **147**.

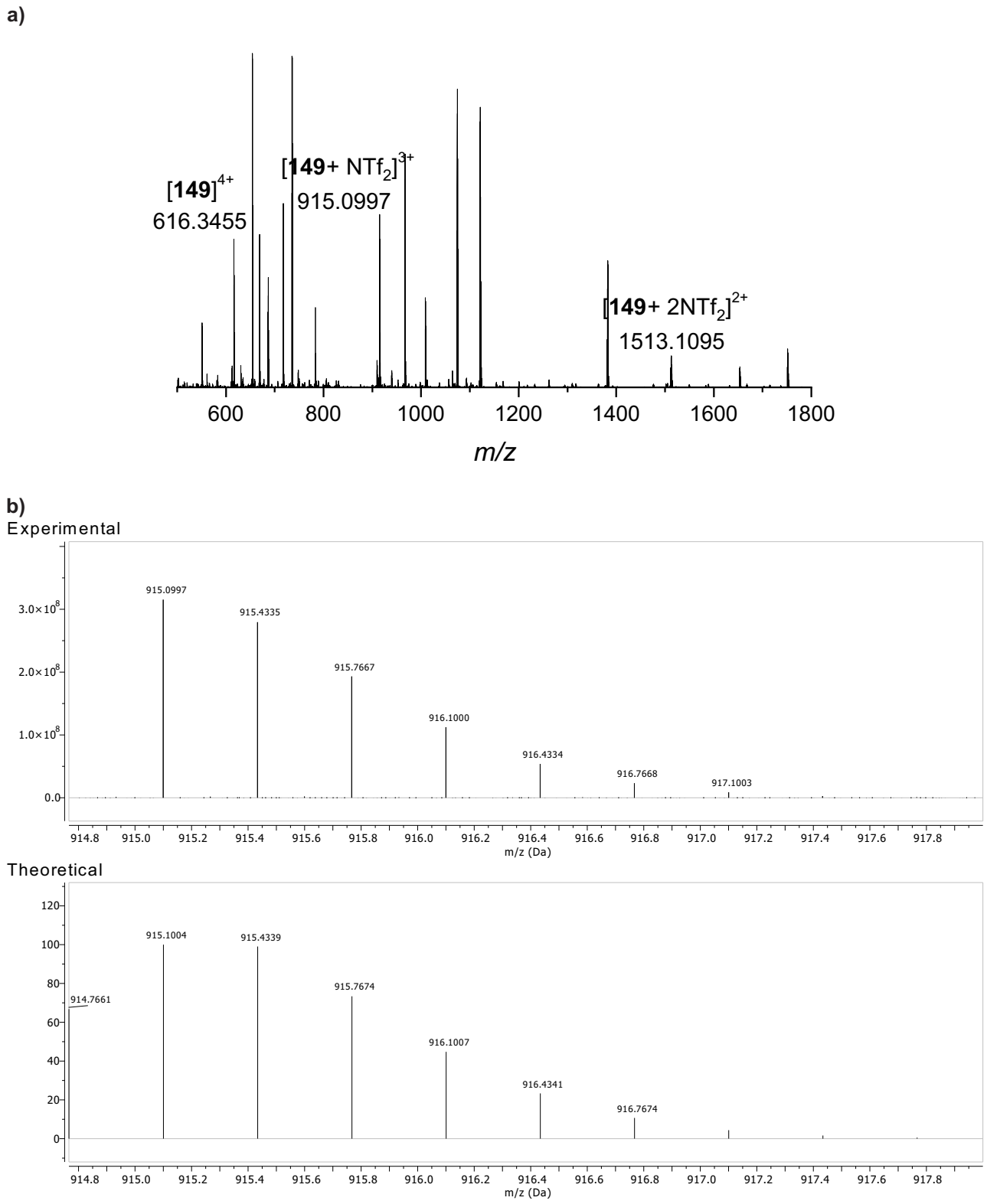

Figure 5.14: High resolution ESI mass spectrum of the Co^{II}-based self-assembly a) in the range of *m/z* 500-1800 and b) the experimental and theoretical isotopic patterns.

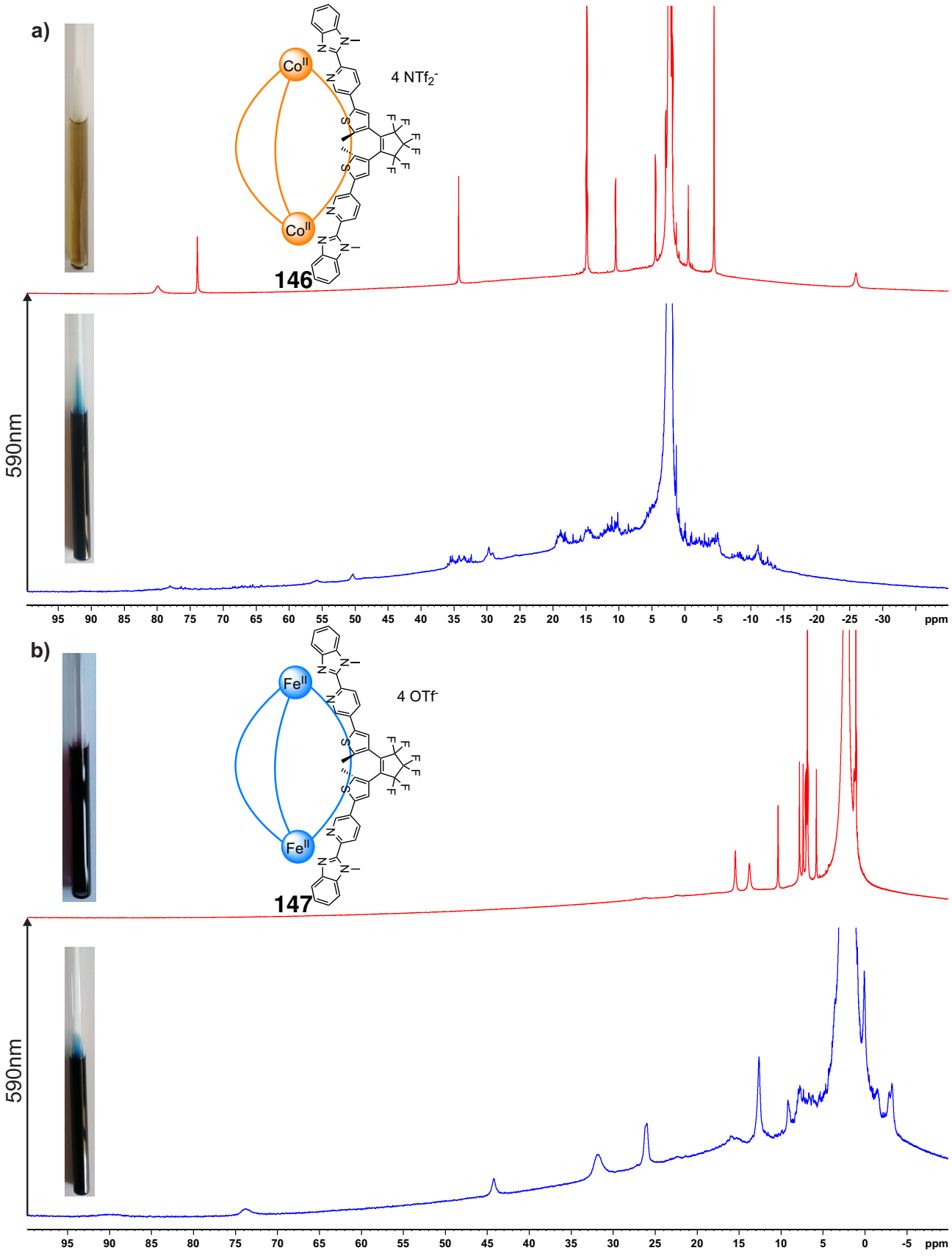

Figure 5.16: ^{1}H NMR spectra (500 MHz, CD_3CN, 298 K) of the cycloreversion upon irradiation with 590 nm for a) helicates **146** and the Co^{II}-based self-assembly and b) **147** and the Fe^{II}-based self-assembly.

Afterwards, the cycloreversion was investigated by UV/Vis spectroscopy. The self-assemblies with the closed-ring ligand **138** ($5 \cdot 10^{-6}$ M)) were freshly prepared *in situ* in acetonitrile (HPLC grade). The solutions were heated at 50 °C for 93 h (Co^{II}-based self-assembly) or 28 h (Fe^{II}-based self-assembly) to reach the thermal equilibrium. According to the NMR experiments (see Figure 5.15) in both cases discrete species were not obtained at thermal equilibrium, thus no specific absorption bands can be assigned to a specific species since multiple expected species might contribute to the observed absorbance. Upon irradiation of the Co^{II}-based self-assembly with 590 nm for 210 s a decrease of the absorption band at 360 nm is visible indicating the formation of the opened-ring helicate **146** with an absorption maxima at 359-360 nm. The UV/Vis data was compared to preliminary collected UV/Vis data for the helicate **146** to ensure correct assignment. The isosbestic point was measured at 399 nm. Furthermore, the decrease of the absorption band at 599 nm indicates opening of the extended π-system of the closed-isomer **138**. Irradiation with 365 nm supports very inefficient photocyclisation as also observed by Li *et al.*[254]; only a small decrease of the absorption band at 359-360 nm and an increase at 599 nm were visible, even after irradiation for 20 min. The same result was obtained for the irradiation experiment of the Fe^{II}-based self-assembly with 590 nm, but complete cycloreversion was observed after a longer reaction time of 20 min, compared to the 210 sec irradiation at 590 nm for the Co^{II}-based self-assembly of ligand **138**. A bathochromic shift in combination with an increased absorption of the band at 359-360 nm towards 365 nm is observed. The isosbestic point was also assigned at 399 nm. The cycloreversion also led to a decrease of the 599 nm absorption band attributed to the ring-opening reaction and shows after irradiation a band centered at 579 nm. Photocyclisation by irradiation of helicate **147** with 365 nm for 20 min showed only poor changes within the UV/Vis spectra, also supporting the poor photocyclisation efficiency observed in the NMR experiments and by Li *et al.* (Figure 5.15).[254]

In conclusion, the self-assembly of the opened-ring ligand **137** resulted in the formation of the three helicates **145** (Zn^{II}), **146** (Co^{II}) and **147** (Fe^{II}). In the first study the photocyclisation of helicate **145** was investigated. Upon irradiation with 365 nm a colour change and chemical shift changes in the ^{1}H NMR spectrum were visible assuming the formation of a closed-ring helicate (proposed structure is compound **148**). Cycloreversion with 590 nm was successful, but unfortunately, the results were not reproducible, thus ESI-MS data was not collected. The irreproducibility should be the main focus of future investigations to identify the cyclised species after irradiation with 365 nm. In comparison, the self-assembled helicates with Co^{II} and Fe^{II} (compounds **146** and **147**) did not isomerise upon irradiation with 365 nm. Utilising the results from Li *et al.*[254] the ligand was isomerised before the self-assembly to ligand **138** and then used for the self-assemblies with Co^{II} and Fe^{II}. In both cases multiple species such as M_2L_3 and M_2L_2 were observed according to ESI-MS data. Structural characterisation by NMR spectroscopy was not possible due to signal overlap and broadness. Upon irradiation with 590 nm both self-assembly attempts showed the quantitative formation of the opened-ring helicates **146** and **147**, proving to be very effective one-way switches. In this case crystal growth

experiments would be of great interest to identify possible structures at thermal equilibrium of the self-assemblies with the closed-ring ligand **138**. In addition, factors as e.g. templates could be used to influence the thermal equilibrium obtaining the desired helicates **149** and **150**.

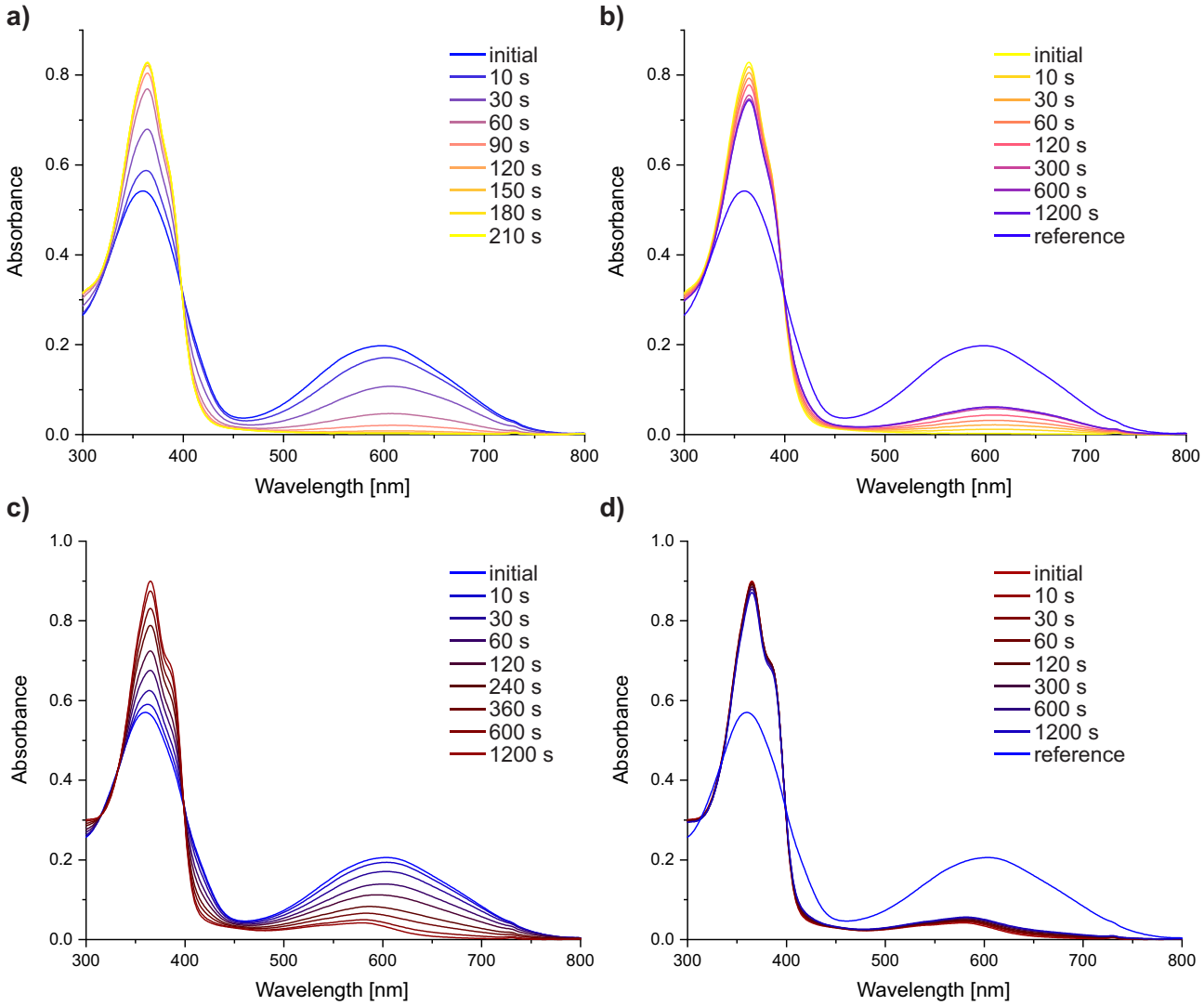

Figure 5.17: UV/Vis spectra ($5 \cdot 10^{-6}$ M, acetonitrile, 293 K) of the Co^{II}-based self-assembly with ligand **138** (a)) or the Fe^{II}-based self-assembly with ligand **138** (c)) upon irradiation with 590 nm and helicate **146** (b)) or **147** (d)) upon irradiation with 365 nm. The same sample was used to initially investigate the cycloreversion and afterwards the incomplete photocyclisation.

Chapter 6

6 Conclusion and Outlook

Metal-organic cages have attracted great attention due to the diversity of possible applications.[70,142–146] In 2013 Bilbeisi *et al.*[157] and Ferguson *et al.*[158] demonstrated the potential of metal-organic cages as thermal spin-crossover compounds. Although stimuli-responsive spin-crossover cages were reported utilising thermal energy[93,94,105,106,157,158,208,209,211] and irradiation[204], the number is limited. This dissertation was concered with the development of methods for synthesising, characterising and investigating new thermal- and light-responsive Fe^{II}-based spin-crossover metal-organic cages.

As a starting point for thermal spin-crossover cage investigations two methods were optimised. The first method focused on a characterisation toolbox for paramagnetic complexes and cages by NMR spectroscopy. A set of 1D and 2D NMR spectroscopic techniques were optimised for a Co^{II}-based mononuclear model complex bearing three 2-pyridylquinoline ligands since Co^{II} is paramagnetic. The optimised NMR spectroscopic techniques (^{1}H, ^{13}C, ^{1}H-^{1}H COSY/NOESY, ^{1}H-^{13}C HMQC) were further applied to demonstrate its applicability by the complete characterisation of six additional Co^{II}-based mononuclear complexes, one Co^{II}-based metal-organic cage and one Fe^{II}-based high-spin complex. The optimised NMR toolbox provides 1D and 2D NMR spectroscopic techniques utilisable for the complete characterisation of other paramagnetic compounds such as Fe^{II}-based cages and isomers (*fac*/*mer*).[231,232]

As the second method a Sonogashira cross-coupling reaction was optimised in order to access symmetric ligands for metal-organic cages. This aim was achieved by developing a Sonogashira cross-coupling reaction that enabled the synthesis of symmetric di((2,2'-bipyridine)alkyne and di(2-(2'-pyridyl)-1*H*-benzimidazole)alkyne ligands, combining three reaction steps in a one-pot procedure. The optimised reaction conditions (N_2 atmosphere, 1 eq. TMSA, 6 eq. degassed TBAF, 5 mol% $Pd(PPh_3)_4$, 70 °C, 3 h, pressure tube) were used to synthesise overall five ligands during this study, accessing di(2-(2'-pyridyl)-1*H*-benzimidazole)alkyne ligands in high-yields.[13] The optimised procedure was further applied to the synthesis of related di(2-(2'-pyridyl)-1*H*-benzimidazole)alkyne ligands accessing additional ligands for thermal spin-crossover cages (Sections 3.1.3 and 3.2).

Table 6.1: Studied thermal spin-crossover cages and the thermodynamic data in section 3.1.3.[235]

$[Fe_4L_6]OTf_8$ cage[1]	Cage Ligand (L)	$T_{1/2}$ [K][2]	ΔH (kJ/mol)	ΔS (J/mol·K)
1	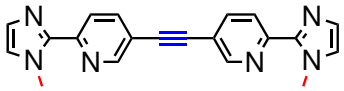	[-][3]	-	-
2	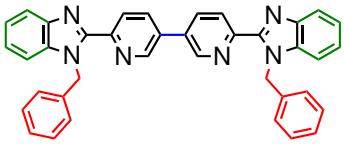	[-][3]	-	-
3	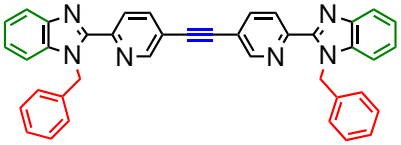	[-][3]	-	-
4	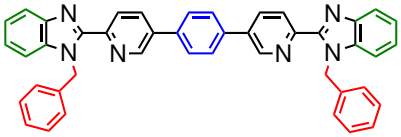	[-][3]	-	-
5	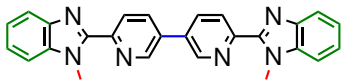	[-][3]	-	-
6	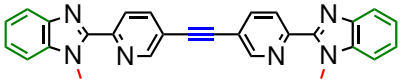	401	24.46 ± 0.58	60.94 ± 3.00
7	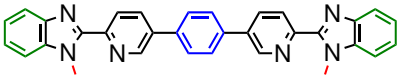	430	27.71 ± 0.91	64.48 ± 5.78
8	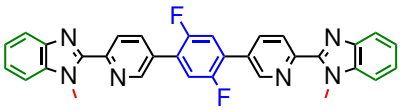	375	27.22 ± 0.93	72.61 ± 4.00
9	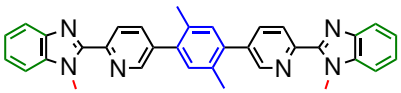	339	21.79 ± 0.48	64.32 ± 2.00
10	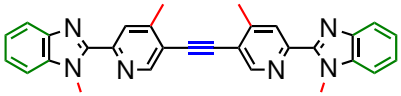	353	27.44 ± 1.12	77.65 ± 4.40
11	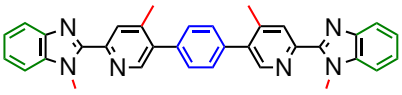	244	20.78 ± 0.22	85.05 ± 0.93

[1] Numbering of the cage is only identical to the numbering within the publication.[235]

[2] Spin-transition temperatures were calculated based on the ideal solution model.[186]

[3] Spin-transition temperature was not calculable due to insufficient chemical shift changes between 248 K and 348 K.

The spin-crossover properties of metal-organic cages bearing 2-(2'-pyridyl)-1*H*-benzimidazole or 2-(2'-pyridyl)-1*H*-imidazole ligands were extensively studied (Table 6.1). The ligands were synthesised

by standard Suzuki cross-coupling reactions[25,235] and the newly developed one-pot Sonogashira cross-coupling reaction.[13] The Fe^{II}-based cages **1**-**11** were fully characterised using diamagnetic and paramagnetic NMR spectroscopic techniques.[231,232] Changes to the spin-crossover temperature by modifications to the linker groups, substituents and steric bulk using the ideal solution model[186] were systematically investigated.

The low-spin state of cage **1** was destabilised by introduction of steric bulk changing the binding motif from 2-(2'-pyridyl)-1*H*-imidazole (cage **1**) to 2-(2'-pyridyl)-1*H*-benzimidazole (cage **6**). Counterion binding was observed for the smallest cages **2** and **5** as confirmed by X-ray crystal structures. However, the effect on the spin-crossover properties was not quantified due to the low-spin state of both cages. The introduction of an electron-donating group (CH_3) in the *p*-pyridine position led to a more stabilised high-spin state (cage **10**, $T_{1/2}$ = 353 K), attributed to the electron-donating character of the CH_3 group. Furthermore, phenyl linker modifications by substitution of H vs. F/CH_3 stabilised the high-spin state (cage **8**, $T_{1/2}$ = 375 K (H vs. F); cage **9**, $T_{1/2}$ = 339 K (H vs. CH_3)) assumed to be a result of increasing dihedral angles between the phenylene and pyridine rings based on the increasing steric bulk of the substituents. In a final study, two CH_3 groups were introduced in the *p*-pyridine positions with a phenyl spacer giving cage **11**. The combination of the CH_3 groups and the phenylene spacer gave the highest spin-crossover temperature change by small modifications (cage **11**, $T_{1/2}$ = 244 K)[235]
In future studies the focus should be on further modifications to tune the spin-crossover temperature towards room temperature for potential applications. This might be realisable by introduction of more electron-donating groups such as -OMe or -OH at the *p*-pyridine position or sterically bulkier groups at the phenylene spacer. Moreover, the effect of guest binding onto the spin-crossover properties would be also of great interest. Additional solid-state measurements could be part of a new study to investigate the influence of sample preparation (e.g. precipitation versus crystallisation), crystal solvent molecules and intermolecular interactions.

For the development of light-responsive cages LD-LISC mononuclear complexes as model systems for cages were studied and optimised. As the first LD-LISC model system azobenzene functionalised 2-(2'-pyridyl)-benzimidazoles were investigated. The synthesis of ligand **67** was reported and reproducible,[16] however, new synthetic strategies were conceptualised to successfully access the methylated isomeric azobenzenes **68** and **69** in good yield over five steps (Scheme 6.1, section 4). X-ray crystallography data was collected for both isomers confirming the expected structures (see Figure 8.130).

The photochemical properties of azobenzenes **67**, **68** and **69** were examined by NMR and UV/Vis spectroscopy (Table 6.2). Upon irradiation with 365 nm photostationary states of 8:92 (azobenzene **67**), 5:95 (azobenzene **68**) and 5:95 (azobenzene **69**) were obtained, in good agreement to the reported results of Hasegawa *et al* (PSS (365 nm) = 6:94).[16] After irradiation with 435 nm the same result was observed for the photostationary states (azobenzene **67**, **68** = 71:29, **69** = 70:30, Hasegawa *et al.* (ligand **67**) = 72:28).[16] However, the half-life times were different for the azobenzene derivatives

67, **68** and **69**. The half-life time of azobenzene **68** was found to be the highest with 180.4 h, being longer than azobenzene **69** ($\Delta\tau_{1/2}$ = 127.6 h) and **67** ($\Delta\tau_{1/2}$ = 95.6 h). The difference is attributed to an enlarged conjugated system in azobenzene **69** resulting in a more stabilised *trans* isomer and a shorter half-life time of the respective *cis* isomer **102**.

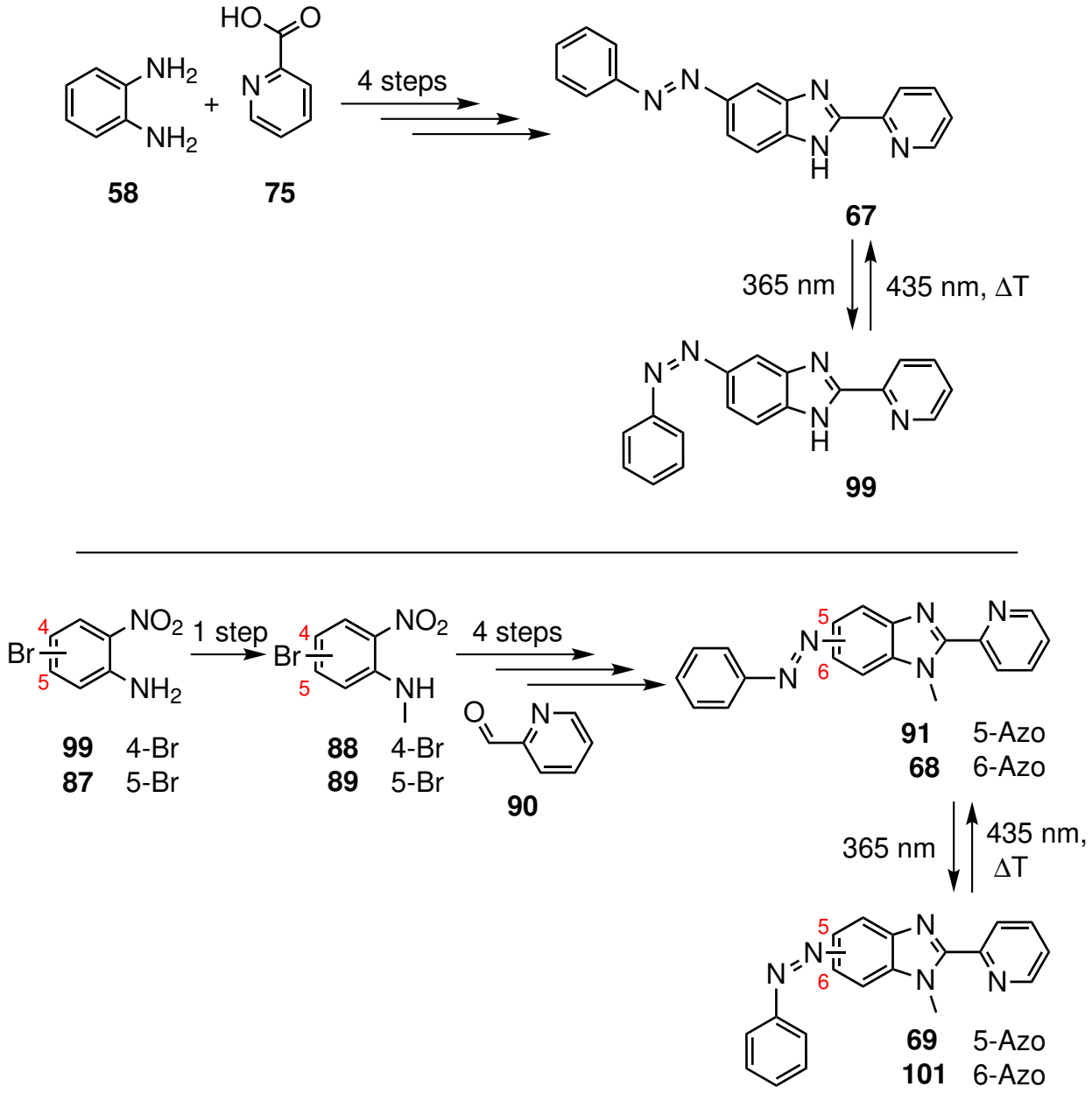

Scheme 6.1: Synthesised azobenzene derivatives **67**, **68** and **69** and the respective *cis* isomers in this dissertation.

Table 6.2: Azobenzenes **67**, **68** and **69** and their photochemical properties.

Compound	PSS 365 nm [%]	PSS 435 nm [%]	$\tau_{1/2}$ [h]
67	8:92	71:29	84.8±0.1
68	5:95	71:29	180.4±0.2
69	5:95	70:30	52.8±0.1

This result could indicate that azobenzene **68** is the most ideal ligand scaffold due to the high thermal stability of both isomers. Long half-life times are desired for LD-LISC systems since upon switching both spin-states are more stabilised. Subsequently, Fe^{II}-based LD-LISC model complexes were prepared with the synthesised azobenzenes **67**, **68** and **69**. Complex **103** (azobenzene **67**) was evidenced by ESI-MS, but structural analysis by paramagnetic NMR spectroscopy[231,232] was not possible due to signal overlap and broadness. Comparable results were obtained for the complex preparations with azobenzenes **68** and **69**. Only partial ^{1}H assignment to a certain ligand environment was possible by ^{1}H-^{1}H NOESY spectra due to missing cross-coupling information. In conclusion, the characterisation of the LD-LISC model complexes was challenging and as a result, the LD-LISC properties were not investigated. For the complex studies with azobenzenes **68** and **69** optimisation of the NMR spectroscopic experiments should be investigated using variable temperature NMR experiments to reduce signal overlap or sharpen signals. As a potential result, a higher number of cross-peaks could be obtained in the ^{1}H-^{1}H COSY and ^{1}H-^{1}H NOESY spectra leading to potential proton assignments. ESI-MS measurements should be used to confirm the structure of the observed species. Subsequent to complete characterisation the light- and thermal-induced spin-crossover properties of the potential complexes should be investigated to examine whether the methylation of azobenzene **67** to the isomers **68** and **69** improves the reported photoefficiency, spin-crossover temperature and switching fatigue of complex **103** by Hasegawa *et al.*[16]

Although the LD-LISC properties of the mononuclear model complexes were not investigated, a first generation of azobenzene-functionalised ligands for metal-organic cages was designed (Section 5). The synthesis of azobenzene functionalised ligands **124** and **125** was challenging since the necessary precursor **133** was not synthesised (Scheme 6.2, section 5.1), but precursor **132** for ligand **124** was isolated with an unknown impurity. The insolubility of the precursors **132** in organic solvents led to the conclusion that the synthetic strategy should be modified in future studies. Possible modifications could be the introduction of flexible spacer groups such as 1,4-dihydroxybenzene or substituents like alkyl chains or polar groups to increase the solubility. Otherwise, the synthetic strategy could be changed by using protecting groups for the amines in order to prepare the respective azobenzene functionalised 2-(5'-bromo-2'-pyridyl)-1*H*-benzimidazole **152** before the final Sonogashira cross-coupling reaction

is performed (Scheme 6.3).

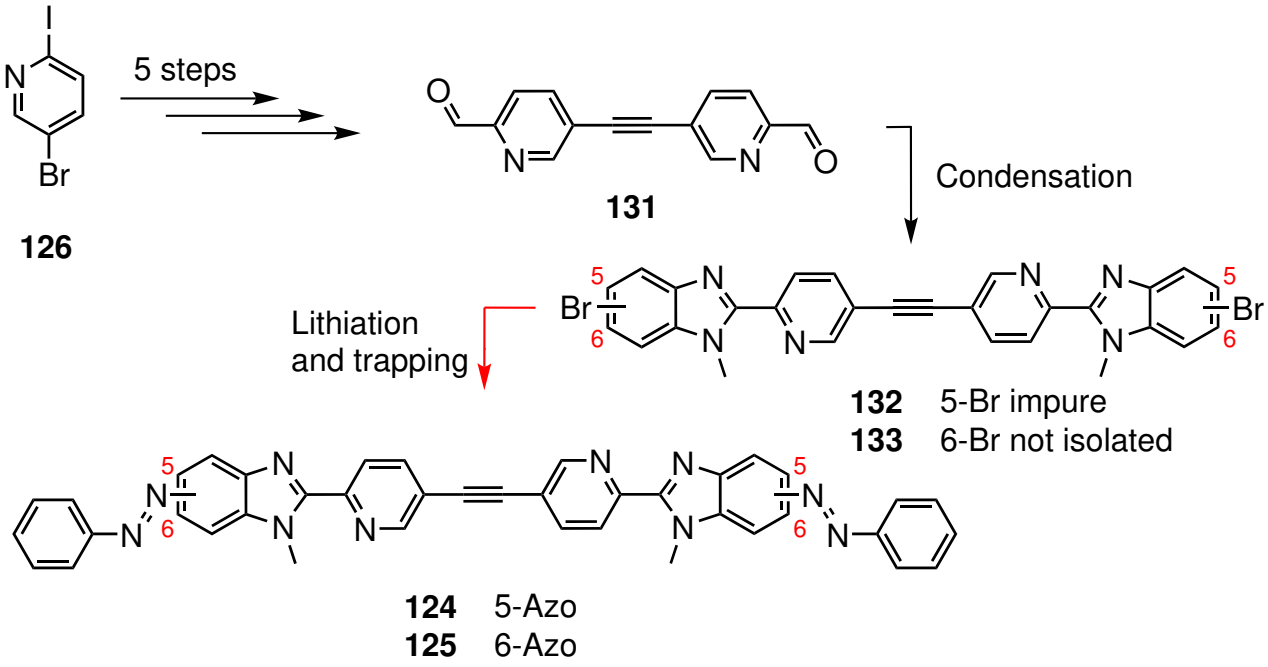

Scheme 6.2: Synthetic strategy to access the azobenzene functionalised ligands **124** and **125** in this dissertation. Red arrow indicates problematic reaction step. Precursor **132** was obtained as an impure mixture and precursor **133** was not isolated, but solubility investigations provide information about the insolubility in organic solvents. Hence the final step can not be performed.

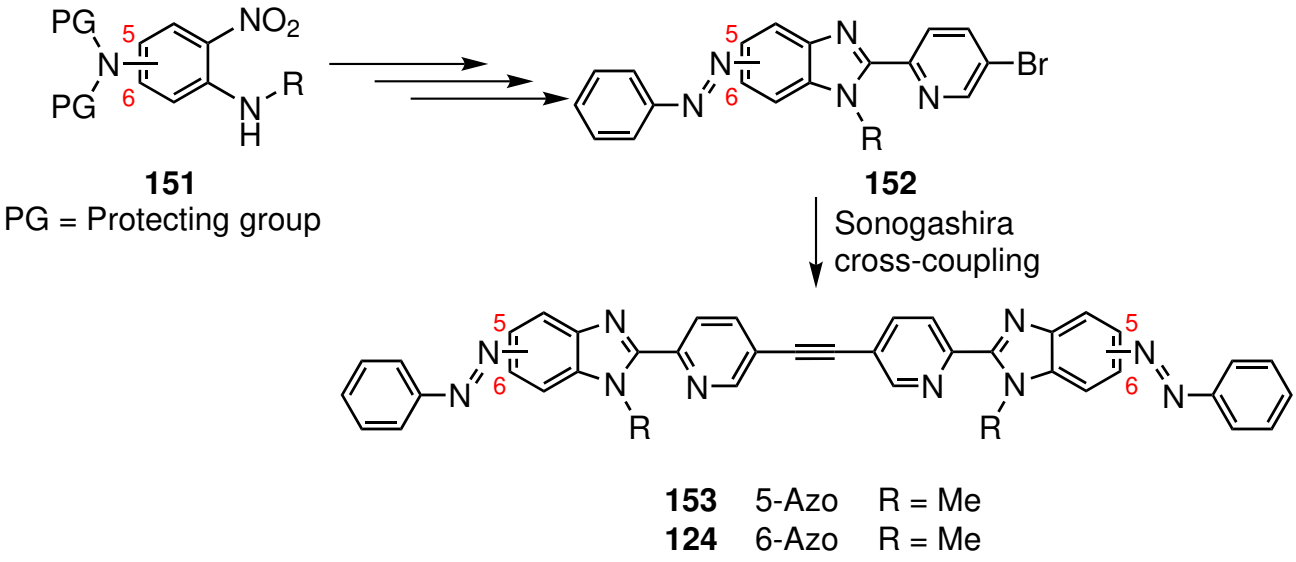

Scheme 6.3: Alternative synthetic strategy to access the azobenzene functionalised ligands **124** and **125**.

Dithienylethenes as potential photoswitchable groups for dual-responsive spin-crossover complexes and cages were also investigated. In total, dithienylethenes **70** and **71** were envisaged, but only dithienylethene **71** was successfully synthesised over in total five steps (Scheme 6.4, section 4.2). The isomerisation of compound **71** was investigated in different solvents using NMR spectroscopy (Section 4.2.1). Cyclisation to the closed-ring isomer of dithienylethene **71** was not observed. Instead, irradiation experiments resulted in degradation of dithienylethene **71** indicated by small signals appearing in the ^{1}H NMR spectrum. The photoinactivity of dithienylethene **71** is attributed to the loss of aromaticity associated with the isomerisation leading to an inhibited ring-closure reaction making dithienylethene **71** an unsuitable candidate for future LD-LISC model systems.

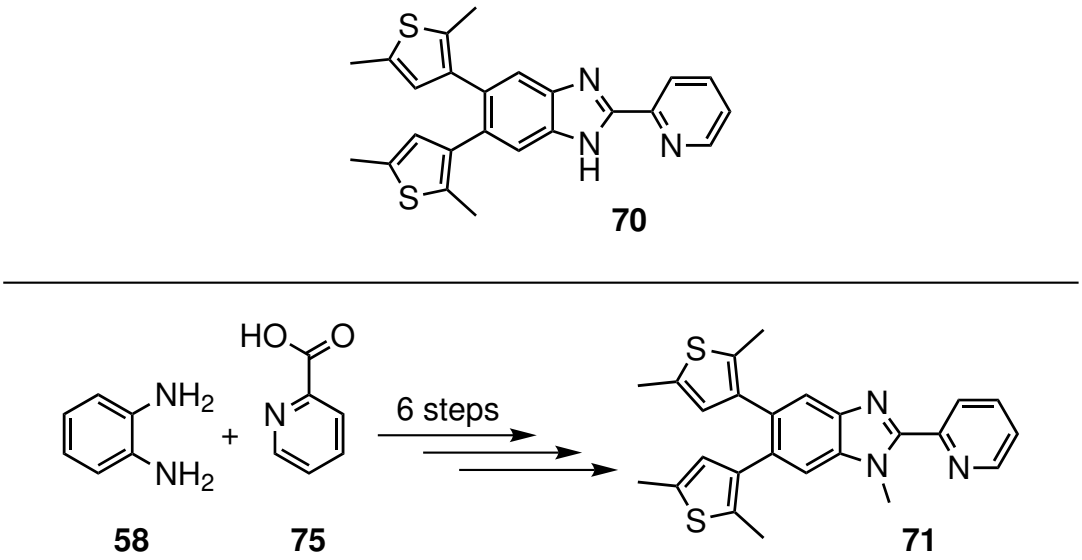

Scheme 6.4: The envisaged dithienylethenes as LD-LISC model systems in this dissertation. Dithienylethene **71** was successfully synthesised over six steps.

In order to overcome the photoinactivity of dithienylethene **71** and to design a cage ligand, an octafluorocyclopentene backbone was used to modify the previous dithienylethene design.[227,228] Dithienylethene **137** was synthesised over six steps in a good yield (Scheme 6.5). Excellent photochemical properties with almost quantitative photostationary states upon irradiation (PSS (365 nm) = 2:98, PSS (590 nm) = 100:0) of dithienylthene **137** were examined by NMR and UV/Vis spectroscopy.

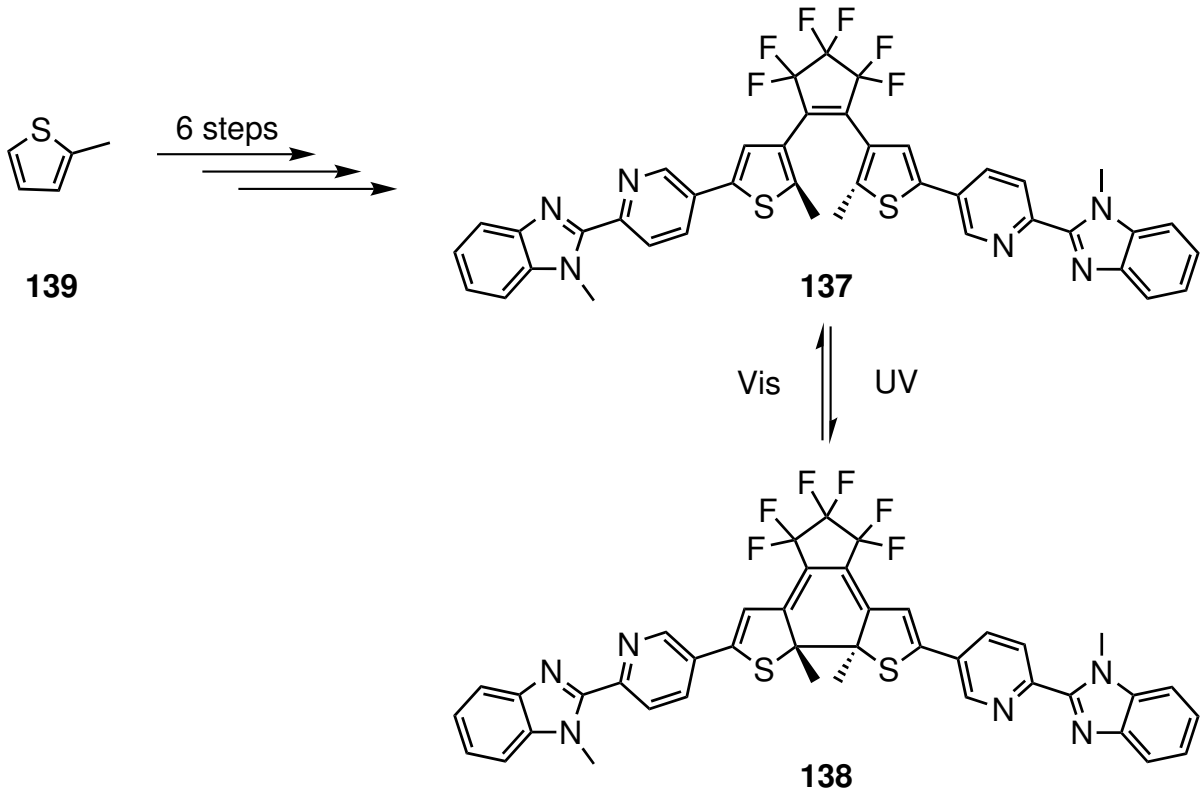

Scheme 6.5: The newly designed dithienylethene featuring a octafluorocyclopentene backbone was synthesised over six steps.

Afterwards, the self-assemblies with ligand **137** and Zn^{II}, Fe^{II} and Co^{II} were investigated (Section 5.2.3). The Co^{II}-based self-assembly was investigated since its complete characterisation could help to assign protons and carbons for the related Zn^{II} and Fe^{II}-based self-assemblies. The Fe^{II}- and Zn^{II}-based self-assemblies were investigated to identify in future studies the thermal spin-crossover properties based on the ideal solution model.[186,235] In all cases with ligand **137** the respective helicates M_2**137**$_3$ were confirmed by ESI-MS and the structures were characterised by NMR spectroscopy. Further irradiation experiments using wavelengths of 365 nm (cyclisation) and 590 nm (cycloreversion) investigated the photoefficiency and isomerisation of the helicates in comparison to the free ligand **137** by NMR spectroscopy. A successful cyclisation/cycloreversion was indicated in initial irradiation experiments with the self-assembled Zn^{II}-based helicate **145**. Unfortunately, the result was not reproducible, thus ESI-MS data for the potentially cyclised species **148** was not measured to identify the self-assembled structure after irradiation with 365 nm. In comparison, the cyclisation of the Fe^{II}- and Co^{II}-based helicates **147** and **146** was not observed by NMR spectroscopy (Section 5.2.4). Further analysis of UV/Vis data showed incomplete cyclisation. The ligand **137** is expected to adopt a spatial, twisted orientation making the cyclisation unfavourable. Crystal growth experiments should be part of future work to identify the three-dimensional orientation of ligand **137** in the helicates **147** and **146**.

The obtained results about the incomplete cyclisation were in good agreement with the results of Li *et al.*[254] about a similar Fe^{II}-based helicate. In addition, Li *et al.* reported that the self-assembly with their closed-ring ligand and $Fe(OTf)_2$ yielded a helicate that underwent cycloreversion upon visible light irradiation.[254] Based on these results, ligand **137** was isomerised upon irradiation with 365 nm. Self-assembly experiments with cyclised ligand **138** and the respective Fe^{II}- and Co^{II} salts were conducted. ^{1}H NMR assignment was not possible due to overlapping and broad signals. ESI-MS data suggested the formation of M_2L_2 and M_2L_3 species in the presence of other unidentified species. However, irradiation of the mixtures with 590 nm resulted in the quantitative self-assembly of the previously investigated helicates **147** and **146**, indicating the possibility to use the mixtures as one-way switches towards discrete helicates. Future work should investigate the cyclisation process for the Zn^{II}-based helicate **145** to identify whether the closed helicate **148** was self-assembled. Since discrete helicates were not obtained during the self-assembly experiments with the cyclised ligand **138**, guest binding experiments and solvent effects could be of great interest to change the equilibrium and selectively obtain one species by utilising guests as templates. In the final stages spin-crossover properties of the Fe^{II}-based self-assembled structure should be determined.

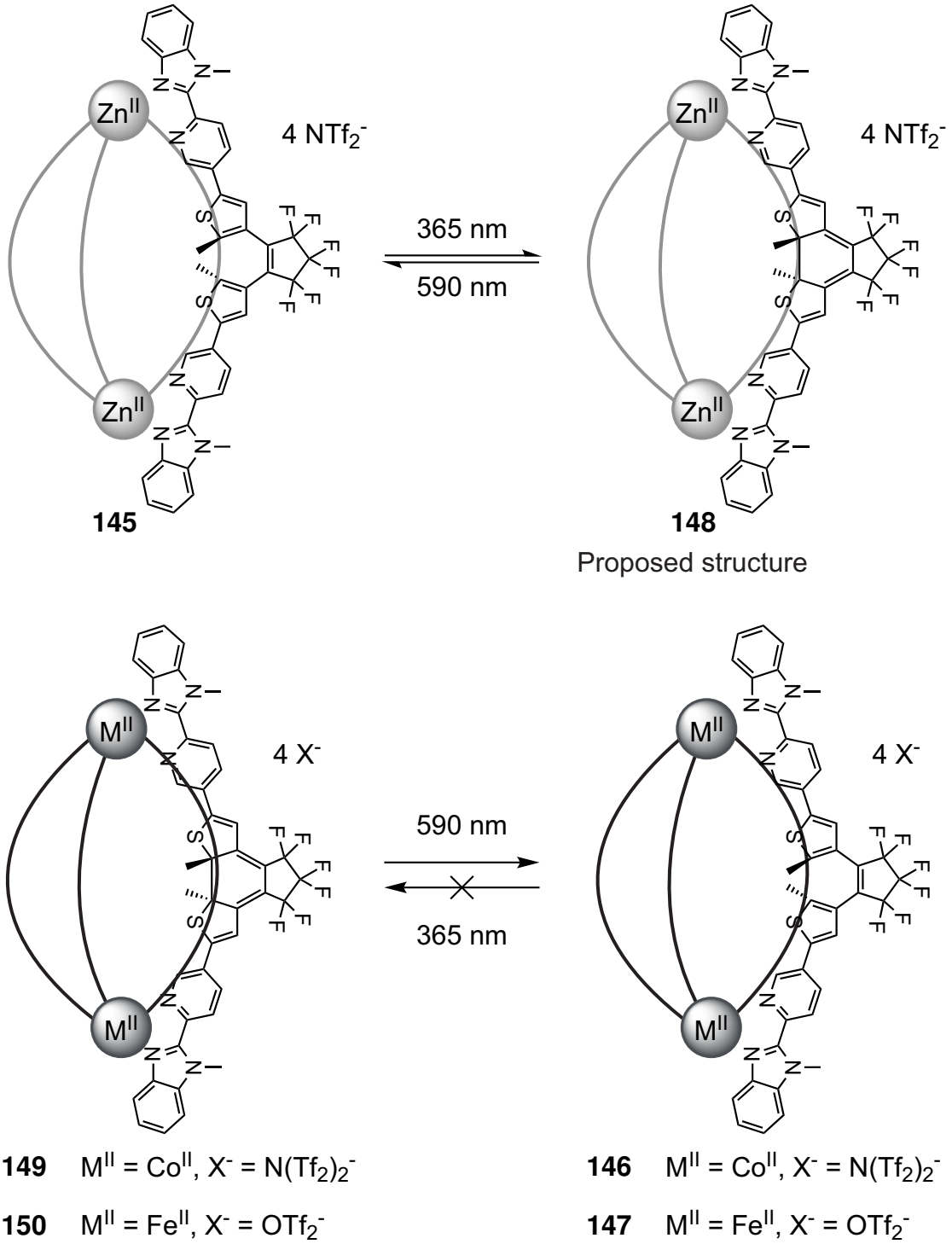

Scheme 6.6: The investigated self-assemblies with ligand **137** and **138** with Zn^{II}, Co^{II} and Fe^{II} salts in this dissertation.

Chapter 7

7 Experimental Section

7.1 Apparatus

NMR spectroscopy

For NMR measurements deuterated solvents from Deutero and Acros Organics were received and used without further purification. For spin-crossover studies deuterated acetonitrile was further dried as described by Paschelke *et al.*.[235] Depending on the synthesised compounds 1D (^{1}H, 13C, ^{19}F, ^{29}Si) and 2D (^{1}H-^{1}H COSY, ^{1}H-^{13}C HSQC, ^{1}H-^{13}C HMBC, ^{1}H-^{13}C HMQC, ^{1}H-^{1}H NOESY) techniques were used on Bruker instruments (Bruker Avance 200, Bruker Avance NEO and Bruker Avance 600) for complete characterisation. All NMR spectra were referenced to the chemical shift of the respective deuterated solvent as described by Fulmer *et al.*,[259] and in the case of ^{19}F NMR spectra to hexafluorobenzene. Abbreviations were used to assign the exhibited multiplicities.

Solvent	Degree of Deuteration [%]	Supplier
$CDCl_3$	99.8	Deutero
CD_3CN[1]	99.8	Deutero
$(CD_3)_2SO$	99.9	Sigma-Aldrich
CF_3COOD	99	ThermoFisher Scientific
$(CD_3)_2CO$	99.8	Deutero

[1] For spin-crossover studies dried over CaH_2.

Exhibited Multiplicity	Abbreviation used
Singlet	s
Doublet	d
Triplet	t
Doublet of Doublets	dd
Doublet of Doublets of Doublets	ddd
Doublet of Triplets	dt
Triplet of Doublets	td
Broad Signal	br
Multiplet	m
Unresolved	unres.

Mass spectrometry

The mass data was collected using an ACCUTOF from JEOL for HR-EI measurements (Acceleration voltage = 70 eV) or a Thermo Scientific™ Q Exactive™ with a resolution up to 280000 *m/z* for HR-ESI.

IR spectroscopy

IR spectra were measured using a Spectrum 100 FT-IR instrument from Perkin-Elmer. For simple probe preparaton the spectrometer is modified with a single reflection diamond ATR-Golden Gate unit from Specac Ltd Limited. The observed bands were divided based on their intensity into weak (w), medium (m) and strong (s).

Thin-layer and flash chromatography

Silica gel and aluminum oxide plates were purchased from Macherey-Nagel GmbH & Co. KG (POLYGRAM® SIL G/UV_{254}, ALUGRAM® Xtra SIL G/UV_{254} with 0.2 mm silica gel or POLYGRAM® ALOX N/UV_{254}, ALUGRAM® ALOX N/UV_{254} with 0.2 mm aluminum oxide) and were used for thin-layer chromatography measurements. Purification by flash chromatography was performed using Biotage® SNAP Ultra or Biotage® Sfär Silica D columns with 10 g, 25 g or 50 g of silica gel as the stationary phase on a Biotage® Isolera™ One. Racks were purchased from Biotage® and test tube (160 mm x 16 mm) from Hirschmann Laborgeräte GmbH & Co. KG (Hirschmann®).

UV/Vis spectroscopy

For UV/Vis spectroscopy measurements the UV/Vis Spectrometer Lambda 650 from Perkin Elmer or a UV-2600i UV-VIS Spectrophotometer from Shimadzu were used. UV/Vis measurement cells (High precision cells, quartz glass) were purchased from Hellma® Analytics with a pathlength of 10 mm.

Photostationary States

Photostationary states were examined using ^{1}H NMR spectroscopy. Therefore, azobenzenes **67**, **68** and **69** were dissolved in deuterated acetone or dithienylethene **137** in deuterated chloroform and a reference ^{1}H NMR spectrum was recorded. Isomerisation and backisomerisation were triggered by irradiation with suitable wavelengths and monitored by NMR spectroscopy. The photostationary state was examined based on ^{1}H integrals, when no further changes in the ^{1}H NMR spectra by irradiation were visible during the isomerisation/backisomerisation.

Half-Life Times

Half-life times were examined by UV/Vis spectroscopy for azobenzenes **67**, **68** and **69**. Therefore, the substances were dissolved in acetone and a reference UV/Vis spectrum was measured. Afterwards, the samples were irradiated with 365 nm and UV/Vis spectra were recorded after 30 min for overall 48 h. (in total 96 data points). The half-life times were calculated according to a kinetic first order.

Light sources

For irradiation experiments a LUMOS 43 apparatus (265 nm, 280 nm, 310 nm, 325 nm) from Atlas Photonics or home-made irradiation instruments equipped with LEDs (365 nm, 435 nm or 590 nm) were used.

X-ray crystallography

The crystals were measured and analysed using a XtaLAB Synergy, Dualflex, HyPix diffractometer (CuKα λ= 1.54184 Å) by Christian Näther at the University of Kiel.[260]

Compound **68**: The structure was solved using Olex2[261] (Program: SHELXT[262] structure solution) with intrinsic phasing. Further refinement was performed using the SHELXL[263] refinement package (Least Squares minimisation). Carbon and nitrogen atoms were refined anisotropic, whereas C-H H were refined isotropic (U_{iso} (H) = 1.2 U_{eq} (C), 1.5 for CH_3 hydrogen atoms) with a riding model by allowing rotation without tipping for CH_3 hydrogen atoms (idealised geometry).

Compound **69**: The structure was solved using SHELXT.[262] Further refinement was performed using the SHELXL[263] refinement package (Least Squares minimisation). Carbon and nitrogen atoms were refined anisotropic, whereas C-H H were refined isotropic (U_{iso} (H) = 1.2 U_{eq} (C), 1.5 for CH_3 hydrogen atoms) with a riding model.

7.2 Chemicals and Solvents

Standardly used chemicals (Acids, bases, silica gel, aluminum oxide, Celite®, salts and solvents) are part of the laboratory stock. Purchased compounds were used as purchased. The stabilizer in tetrahydrofuran and diethyl ether was removed by filtration over aluminum oxide and the purified solvents then dried with the PureSolv MD 5 Solvent Purification System from Inert Corporation.

Inorganic chemicals	Supplier	Purity / %
copper(I) iodide	Thermo Scientific	98
$Co(NTf_2)_2$	Thermo Scientific	-
$Fe(OTf)_2$	Sigma-Aldrich	85
$Fe(BF_4)_2$ 6 H_2O	Sigma-Aldrich	97
Iodine	Grüssing	$\geq$99.5
Lithium hydroxide monohydrate	Thermo Scientific	99.95
$Pd_2(dba)_3$	TCI	>75
$Pd(PPh_3)_2Cl_2$	TCI	98
$Pd(PPh_3)_4$	Thermo Scientific	99
Pd/C	Sigma-Aldrich	10% Pd on charcoal
Polyphosphoric acid	Thermo Scientific	115 (as H_3PO_4 eq.)
Sodium dithionite	BASF	$\geq$80
Sodium hydride	TCI	60% dispersion
Sodium *tert*-butoxide	ABCR	97
$Zn(NTf_2)_2$	Thermo Scientific	<100

Organic chemicals	Supplier	Purity / %
2-Aminothiophenol	Acros Organics	≥95
1*H*-Benzo[*d*]imidazole	AlfaAesar	98
Benzophenone imine	BLDpharm	97
Benzyl bromide	ABCR	≥98
R-BINAP	TCI	97
4-Bromo-2-nitroaniline	BLDpharm	98
5-Bromo-2-nitroaniline	BLDpharm	98
2-Bromo-5-iodopyridine	Fluorochem	97
5-Bromopicolinic acid	Fluorochem	98
5-Bromo-6-methylpicolinic acid	BLDpharm	95+
N-Bromosuccinimide	TCI	≥95
n-Butyllithium	Acros Organics	2.5 M in hexane
2,5-Dimethylthiophene	Acros Organics	≥98
Di-*tert*-butyl dicarbonate	Thermo Scientific	97
2-Iodo-5-bromopyridine	BLDpharm	97
N-Methyl-4-nitrobenzene-1,2-diamine	Fluorochem	96
Methyl iodide	Sigma-Aldrich	99.5
2-Methylthiophene	Sigma-Aldrich	98
Nitrosobenzene	TCI	97
o-Phenylenediamine	AlfaAesar	≥99
Picolinic acid	TCI	99
i-Propylmagnesium chloride	Sigma-Aldrich	2.0 M in tetrahydrofuran
2-Pyridinecarboxaldehyde	TCI	98
Tetrabutylammonium fluoride	TCI	1.0 M in tetrahydrofuran
p-Toluene sulfonic acid	Acros Organics	≥98.5
Tributyl borate	Sigma-Aldrich	≥99
Trimethylsilylacetylene	BLDpharm	≥98
Trityl chloride	TCI	98
Octafluorocyclopentene	TCI	>98

7.3 Synthetic Procedures for Chapter 1

7.3.1 Synthesis of 2-(5'-ethynylpyridin-2'-yl)-1*H*-benzo[*d*]imidazole (38)[1]

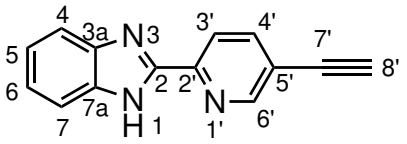

38

The reaction conditions were adapted from Pietsch.[1] The reaction was performed under a nitrogen atmosphere. In a three-neck flask compound **37** (250 mg, 912 μmol), $Pd(PPh_3)_2Cl_2$ (32.0 mg, 5 mol%) and copper(I) iodide (17.4 mg, 10 mol%) were dissolved in a mixture of tetrahydrofuran (dry, 30 ml) and triethylamine (250 μL). Trimethylsilylacetylene (190 μL, 1.37 mmol) was added and the reaction mixture was heated at 75 °C for 18 h. After cooling to room temperature, tetrabutylammonium fluoride (1 M in tetrahydrofuran, 2.00 mL, 2.00 mmol) was added and the solution was stirred at room temperature for further 3 h. Deion. water (30 mL) was added and the mixture was extracted with dichloromethane (3 x 30 mL). The org. layers were combined, dried over magnesium sulfate and the solvent was removed *in vacuo*. Purification by flash chromatography (silica gel, 5-20% ethyl acetate:cyclohexane) gave the product **38** as a colourless solid.

Yield: 12.0 mg (54.7 μmol, 6%) (Lit.:[1] 51%).

^{1}H NMR (500 MHz, DMSO–d_6, 298 K): δ = 13.2 (br, 1 H, *H*-1), 8.83 (dd, ^4J = 2.1 Hz, ^5J = 0.9 Hz, 1 H, *H*-6'), 8.32 (dd, ^3J = 8.3 Hz, ^5J = 0.9 Hz, 1 H, *H*-3'), 8.09 (dd, ^3J = 8.3 Hz, ^4J = 2.1 Hz, 1 H, *H*-4'), 7.74-7.67 (m, 1 H, *H*-4/7), 7.57-7.51 (m, 1 H, *H*-4/7), 7.29-7.19 (m, 2 H, *H*-5,6), 4.62 (s, 1 H, *H*-8') ppm.
^{13}C NMR (126 MHz, DMSO–d_6, 298 K): δ = 151.8 (*C*-6'), 149.8 (*C*-2), 147.7 (*C*-2'), 143.8 (*C*-3a/7a), 140.2 (*C*-4'), 134.9 (*C*-3a/7a), 123.4 (*C*-5/6), 122.0 (*C*-5/6), 120.8 (*C*-3'), 119.4 (*C*-4/7), 119.2 (*C*-5'), 112.1 (*C*-4/7), 85.5 (*C*-8'), 80.3 (*C*-7') ppm.
Mass spectrometry data was not collected due to the low isolated amount.

7.3.2 Synthesis of *tert*-butyl 2'-(5"-bromopyridin-2"-yl)-1*H*-benzo[*d*]imidazole-1'-carboxylate (41)[2]

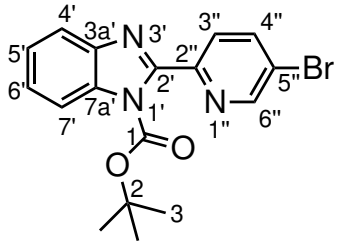

41

The reaction conditions were adapted from Taylor *et al.*.[2] In a three-neck flask compound **37** (800 mg, 2.92 mmol), di-*tert*-butyl dicarbonate (701 mg, 3.21 mmol) and 4-dimethylaminopyridine (35.7 mg, 292 µmol) were dissolved in dichloromethane (dry, 15 mL). The reaction mixture was stirred at room temperature for 17.5 h and the solvent was removed *in vacuo*. Purification by flash chromatography (silica gel, 20% ethyl acetate:cyclohexane) gave the colourless product **41**.

Yield: 1.03 g (2.76 mmol, 95%)

R_f (20% ethyl acetate:cyclohexane) = 0.29
^{1}H NMR (600 MHz, DMSO–d_6, 298 K): δ = 8.90 (dd, ^4J = 2.0 Hz, ^5J = 0.7 Hz, 1 H, *H*-6"), 8.30 (dd, ^3J = 8.4 Hz, ^4J = 2.0 Hz, 1 H, *H*-4"), 7.94 (ddd, ^3J = 8.1 Hz, ^4J = 1.3 Hz, ^5J = 0.8 Hz, 1 H, *H*-7'), 7.92 (dd, ^3J = 8.4 Hz, ^5J = 0.7 Hz, 1 H, *H*-3"), 7.82 (ddd, ^3J = 8.0 Hz, ^4J = 1.2 Hz, ^5J = 0.8 Hz, 1 H, *H*-4'), 7.51 (ddd, ^3J = 8.1 Hz, ^3J = 7.4 Hz, ^4J = 1.2 Hz, 1 H, *H*-6'), 7.44 (ddd, ^3J = 8.0 Hz, ^3J = 7.4 Hz, ^4J = 1.3 Hz, 1 H, *H*-5'), 1.36 (s, 9 H, *H*-3) ppm.
^{13}C NMR (151 MHz, DMSO–d_6, 298 K): δ = 150.6 (*C*-1), 149.8 (*C*-6"), 148.8 (*C*-2"), 147.8 (*C*-2'), 141.8 (*C*-3a'), 139.8 (*C*-4"), 133.3 (*C*-7a'), 125.8 (*C*-6'), 125.5 (*C*-3"), 124.6 (*C*-5'), 121.3 (*C*-5"), 120.3 (*C*-4'), 113.7 (*C*-7'), 85.4 (*C*-2), 27.0 (*C*-3) ppm.
MS (EI, 70 eV): *m/z* (%) = 373.04 (5) $[M]^+$.
HRMS (EI, 70 eV): *m/z* (%) ($C_{17}H_{16}{}^{79}Br_1N_3O_2$) =

	mass [*m/z*]	mass difference [ppm]	calc. formula
calculated	373.04259		
measured	373.04356	2.59	$C_{17}H_{16}{}^{79}Br_1N_3O_2$

FT-IR: $\tilde{\nu}$ = 2971.2 (w), 1746.9 (s), 1475.5 (w), 1447.1 (m), 1388.0 (m), 1366.0 (m), 1329.9 (s), 1291.1 (m), 1228.5 (s), 1148.8 (s), 1127.2 (m), 1109.4 (m), 1084.5 (m), 1061.5 (m), 1033.8 (w), 1007.3 (s), 940.0 (w), 929.1 (w), 849.6 (s) cm^{-1}.

7.3.3 Synthesis of 1-trityl-1*H*-benzo[*d*]imidazole (47)[3]

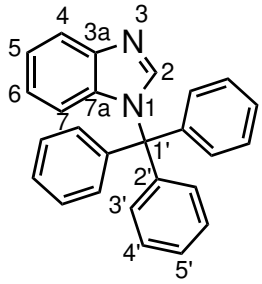

47

The reaction was performed following a procedure from Aldabbagh *et al.*.[3] The reaction was performed under a nitrogen atmosphere. In a three-neck flask 1*H*-benzo[*d*]imidazole (**46**) (1.51 g, 12.8 mmol) and trityl chloride (3.90 g, 14.0 mmol) were dissolved in a mixture of dichloromethane (dry, 20 mL) and triethylamine (3.50 mL) and the reaction mixture was stirred at room temperature for 19.5 h. The solvent was removed *in vacuo* and the crude product was recrystallised from ethanol. The product **47** was filtered and the filtrate was further purified by flash chromatography (silica gel, 80-85% ethyl acetate:cyclohexane) to give the product **47** as a colourless solid.

Yield: 4.58 g (12.7 mmol, 99%) (Lit.:[3] 67%).

^{1}H NMR (500 MHz, DMSO–d_6, 298 K): δ = 7.88 (s, 1 H, *H*-2), 7.66 (ddd, ^3J = 8.0 Hz, ^4J = 1.1 Hz, ^5J = 0.8 Hz, 1 H, *H*-7), 7.41-7.33 (m, 9 H, *H*-4',5'), 7.18-7.14 (m, 6 H, *H*-3'), 7.11 (ddd, ^3J = 8.0 Hz, ^3J = 7.2 Hz, ^4J = 1.1 Hz, 1 H, *H*-6), 6.91 (ddd, ^3J = 8.2 Hz, ^3J = 7.2 Hz, ^4J = 1.1 Hz, 1 H, *H*-5), 6.43 (ddd, ^3J = 8.2 Hz, ^4J = 1.1 Hz, ^5J = 0.8 Hz, 1 H, *H*-4) ppm.
^{13}C NMR (126 MHz, DMSO–d_6, 298 K): δ = 144.3 (*C*-7a), 143.6 (*C*-2), 140.8 (*C*-2'), 134.1 (*C*-3a), 129.3 (*C*-3'), 128.2 (*C*-4'), 127.9 (*C*-5'), 122.0 (*C*-5), 121.6 (*C*-6), 119.8 (*C*-7), 114.8 (*C*-4), 74.7 (*C*-1') ppm.
MS (EI, 70 eV): *m/z* (%) = 360.16 (1) $[M]^+$, 243.12 (100) $[C_{19}H_{15}]^+$, 117.05 (1) $[C_7H_5N_2]^+$.
HRMS (EI, 70 eV): *m/z* (%) ($C_{26}H_{20}N_2$) =

	mass [*m/z*]	mass difference [ppm]	calc. formula
calculated	360.16265		
measured	360.16205	-1.66	$C_{26}H_{20}N_2$

7.3.4 Synthesis of 2-iodo-1-trityl-1*H*-benzo[*d*]imidazole (48)[4]

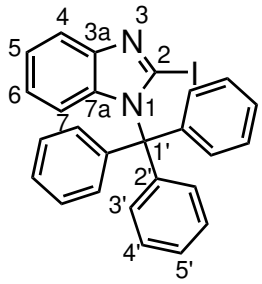

48

The reaction conditions were adapted from O'Connell *et al.*.[4] The reaction was performed under a nitrogen atmosphere. In a three-neck flask compound **47** (3.00 g, 8.32 mmol) was dissolved in tetrahydrofuran (dry, 90 mL). The solution was cooled to -78 °C and *n*-butyllithium (2.5 M in hexane, 3.40 mL, 8.50 mmol) was added and the temperature was kept for 10 min. The reaction mixture was warmed to room temperature over 1 h, iodine (2.11 g, 8.32 mmol) was added and the mixture was stirred for 20 h. Sat. sodium thiosulfate solution (300 mL) was added and the layers were separated. The aqueous layer was extracted with ethyl acetate (100 mL), the org. layers were combined and dried over magnesium sulfate. The solvent was removed *in vacuo*. Purification by flash chromatography (silica gel, 20-32% ethyl acetate:cyclohexane) gave the product **48** as a beige solid.

Yield: 792 mg (1.63 mmol, 19%) (Lit.:[4] 59%).

^{1}H NMR (500 MHz, $CDCl_3$, 298 K): δ = 7.69 (ddd, ^3J = 8.1 Hz, ^4J = 1.3 Hz, ^5J = 0.7 Hz, 1 H, *H*-7), 7.39-7.35 (m, 6 H, *H*-3',5'), 7.35-7.29 (m, 9 H, *H*-4'), 7.11 (ddd, ^3J = 8.1 Hz, ^3J = 7.3 Hz, ^4J = 0.9 Hz, 1 H, *H*-6), 6.77 (ddd, ^3J = 8.6 Hz, ^3J = 7.3 Hz, ^4J = 1.3 Hz, 1 H, *H*-5), 5.71 (ddd, ^3J = 8.6 Hz, ^4J = 0.9 Hz, ^5J = 0.7 Hz, 1 H, *H*-4) ppm.
^{13}C NMR (126 MHz, $CDCl_3$, 298 K): δ = 145.9 (*C*-7a), 142.0 (*C*-2'), 137.2 (*C*-3a), 131.1 (*C*-4'), 128.0 (*C*-5'), 127.9 (*C*-3'), 122.3 (*C*-5), 121.9 (*C*-6), 119.2 (*C*-7), 114.7 (*C*-4), 102.4 (*C*-2), 77.6 (*C*-1') ppm.

MS (EI, 70 eV): *m/z* (%) = 486.05 (0) $[M]^+$, 243.11 (100) $[C_{19}H_{15}]^+$, 242.94 (1) $[C_7H_4I_1N_2]^+$, 126.90 (3) $[I_1]^+$, 116.04 (1) $[C_7H_4N_2]^+$.
HRMS (EI, 70 eV): *m/z* (%) ($C_{26}H_{19}{}^{127}I_1N_2$) =

	mass [*m/z*]	mass difference [ppm]	calc. formula
calculated	486.05929		
measured	486.05828	-2.07	$C_{26}H_{19}{}^{127}I_1N_2$

FT-IR: $\tilde{\nu}$ = 3057.7 (w), 2938.6 (w), 1738.8 (w), 1598.7 (w), 1493.6 (m), 1446.1 (m), 1420.4 (s), 1395.7 (s), 1358.0 (m), 1343.9 (m), 1298.0 (w), 1262.7 (s), 1215.4 (m), 1205.6 (m), 1185.9 (m), 1148.1 (m), 1059.9 (w), 1002.2 (m), 968.8 (m), 946.0 (w), 932.4 (w), 888.3 (w), 861.6 (w), 849.2 (w) cm^{-1}.

7.3.5 Synthesis of 2-iodo-1*H*-benzo[*d*]imidazole (49)[4]

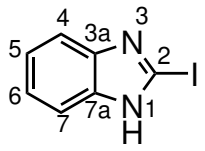

49

The reaction conditions were adapted from O'Connell *et al.*.[4] In a three-neck flask compound **48** (506 mg, 1.04 mmol) was dissolved in a mixture hydrochloric acid (12 M, 0.5 mL) and methanol (25 mL) and the reaction mixture was stirred at 75 °C for 3 h. After cooling to room temperature the solvent was removed *in vacuo*. The residue was redissolved in deion. water (20 mL) and the aqueous layer was extracted with dichloromethane (2 x 12.5 mL). The aqueous layer was filtered, the solvent was reduced and then neutralised with sodium carbonate. The solution was filtered, the filter cake was dissolved in ethyl acetate and the solvent was removed *in vacuo*.

Yield: 135 mg (553 µmol, 53%) (Lit.:[4] 75%).

^{1}H NMR (500 MHz, DMSO – d_6, 298 K): δ = 13.1 (br, 1 H, *H*-1), 7.53-7.48 (m, 2 H, *H*-4,7), 7.16-7.12 (m, 2 H, *H*-5,6) ppm.

^{13}C NMR (126 MHz, DMSO–d_6, 298 K): δ = 121.9 (*C*-5/6), 114.0 (*C*-4/7), 99.7 (*C*-2) ppm.
C-3a and 7a were not observed in the ^{13}C spectrum.
MS (EI, 70 eV): *m/z* (%) = 243.95 (100) $[M]^+$, 126.90 (6) $[I_1]^+$, 117.04 (18) $[C_7H_5N_2]^+$.
HRMS (EI, 70 eV): *m/z* (%) ($C_7H_5{}^{127}I_1N_2$) =

	mass [*m/z*]	mass difference [ppm]	calc. formula
calculated	243.94974		
measured	243.94976	0.07	$C_7H_5{}^{127}I_1N_2$

FT-IR: $\tilde{\nu}$ = 2924.2 (w), 2769.9 (w), 1618.0 (w), 1590.1 (w), 1495.3 (w), 1394.4 (s), 1357.0 (s), 1343.6 (s), 1288.7 (w), 1264.4 (s), 1214.5 (s), 1183.5 (m), 1144.5 (m), 1003.7 (w), 967.0 (s), 899.2 (w), 855.0 (w) cm^{-1}.

7.3.6 Synthesis of 1,2-bis(6'-bromopyridin-3'-yl)ethyne (51)[5]

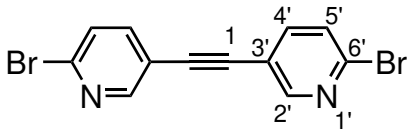

51

The reaction conditions were adapted from Mio *et al.*.[5] The reaction was performed under a nitrogen atmosphere. In a three-neck flask, wrapped into aluminum foil, 2-bromo-5-iodopyridine (**50**) (1.00 g, 3.52 mmol) was dissolved in a mixture of toluene (dry, 18 mL) and 1,8-diazabicyclo(5.4.0)undec-7-ene (3.15 mL, 21.1 mmol) and the solution was degassed using the freeze-pump thaw technique. Trimethylsilylacetylene (240 μmol, 1.73 mmol), $Pd(PPh_3)_2Cl_2$ (74.1 mg, 3 mol%), copper(I) iodide (67.0 mg, 10 mol%) and deion. water (25.0 μmol, 40 mol%) were added and the reaction mixture stirred vigorously at room temperature for 19.5 h. Deion. water (100 mL) was added, the mixture was extracted with diethyl ether (100 mL) and the layers were separated. The org. layer was washed with deion. water (3 x 100 mL) and brine (250 mL), dried over magnesium sulfate and the solvent was removed *in vacuo*. Purification by flash chromatography (silica gel, 20% ethyl acetate:cyclohexane) gave the product **51** as a brown solid.

Yield: 43.5 mg (132 μmol, 8%)

R_f (20% ethyl acetate:cyclohexane) = 0.57
^{1}H NMR (500 MHz, $CDCl_3$, 298 K): δ = 8.53 (dd, ^4J = 2.3 Hz, ^5J = 0.5 Hz, 2 H, *H*-2'), 7.66 (dd, ^3J = 8.2 Hz, ^4J = 2.4 Hz, 2 H, *H*-4'), 7.52 (dd, ^3J = 8.2 Hz, ^5J = 0.5 Hz, 2 H, *H*-5') ppm.
^{13}C NMR (126 MHz, $CDCl_3$, 298 K): δ = 152.4 (*C*-2'), 142.0 (*C*-6'), 140.6 (*C*-4'), 127.8 (*C*-5'), 118.7 (*C*-3'), 89.2 (*C*-1) ppm.
MS (EI, 70 eV): *m/z* (%) = 335.89 (50) $[M]^+$, 256.97 (34) $[C_{12}H_6Br_1N_2]^+$.
HRMS (EI, 70 eV): *m/z* (%) ($C_{12}H_6{}^{79}Br_2N_2$) =

	mass [*m/z*]	mass difference [ppm]	calc. formula
calculated	335.88977		
measured	335.88922	-1.66	$C_{12}H_6{}^{79}Br_2N_2$

7.3.7 Synthesis of methyl 5'-bromopicolinate (53)[6]

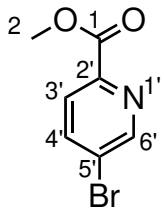

53

The reaction conditions were adapted from Andernach *et al.*.[6] In a round bottom flask compound **52** (5.12 g, 25.4 mmol) was added to a solution of methanol (200 mL) and sulfuric acid (1 mL). The mixture was heated at 70 °C for 89 h. The solution was cooled to room temperature. After removal of the solvent, the residue was dissolved in deion. water (10 mL) and the pH-value was adjusted to 9-10 using ammonia solution (25%). The aqueous layer was extracted with dichloromethane (200 mL), the layers were separated and the org. layer was dried over magnesium sulfate. The solvent was removed *in vacuo*.

Yield: 4.93 g (22.8 mmol, 90%) (Lit.:[6] 86%).

^{1}H NMR (500 MHz, $CDCl_3$, 298 K): δ = 8.80 (dd, ^4J = 2.3 Hz, ^5J = 0.8 Hz, 1 H, *H*-6'), 8.03 (dd, ^3J = 8.4 Hz, ^5J = 0.8 Hz, 1 H, *H*-3'), 7.99 (dd, ^3J = 8.4 Hz, ^4J = 2.3 Hz, 1 H, *H*-4'), 4.01 (s, 3 H, *H*-2)

ppm.
^{13}C NMR (126 MHz, $CDCl_3$, 298 K): δ = 165.1 (*C*-1), 151.1 (*C*-6'), 146.3 (*C*-2'), 139.8 (*C*-4'), 126.3 (*C*-3'), 125.1 (*C*-5'), 53.1 (*C*-2) ppm.
MS (EI, 70 eV): *m/z* (%) = 214.96 (11) $[M]^+$, 183.94 (11) $[C_6H_3Br_1N_1O_1]^+$, 155.94 (47) $[C_5H_3Br_1N_1]^+$.
HRMS (EI, 70 eV): *m/z* (%) ($C_7H_6{}^{79}Br_1N_1O_2$) =

	mass [*m/z*]	mass difference [ppm]	calc. formula
calculated	214.95819		
measured	214.95812	-0.34	$C_7H_6{}^{79}Br_1N_1O_2$

FT-IR: $\tilde{\nu}$ = 2154.3 (w), 1714.2 (s), 1436.0 (m), 1364.2 (s), 1306.0 (s), 1233.7 (s), 1194.7 (m), 1132.6 (s), 1115.1 (m), 1089.0 (m), 1006.3 (s), 954.4 (m), 863.8 (m), 837.9 (m) cm^{-1}.

7.3.8 Synthesis of methyl 5'-((trimethylsilyl)ethynyl)picolinate (54)[7]

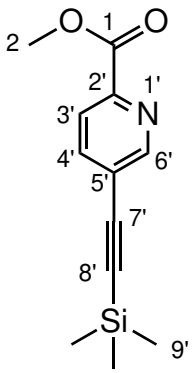

54

The reaction conditions were adapted from Park *et al.*[7] The reaction was performed under a nitrogen atmosphere. In a three-neck flask compound **53** (1.25 g, 5.79 mmol), $Pd(PPh_3)_2Cl_2$ (170 mg, 4 mol%) and copper(I) iodide (110 mg, 10 mol%) were dissolved in a mixture of tetrahydrofuran (dry, 50 mL) and triethylamine (12 mL). After the addition of trimethylsilylacetylene (1.28 mL, 9.26 mmol), the reaction was stirred at 60 °C for 22 h. The solution was cooled to room temperature, filtered through Celite® and the filter cake was washed with dichloromethane (50 mL). The solvent was removed *in*

vacuo. Purification by flash chromatography (silica gel, 10% ethyl acetate:cyclohexane) gave product **54** as a colourless solid.

Yield: 1.09 g (4.67 mmol, 81%) (Lit.:[7] 99%).

^{1}H NMR (500 MHz, $CDCl_3$, 298 K): δ = 8.77 (d, ^4J = 1.7 Hz, 1 H, *H*-6'), 8.08 (d, ^3J = 8.1 Hz, 1 H, *H*-3'), 7.88 (dd, ^3J = 8.1 Hz, ^4J = 1.7 Hz, 1 H, *H*-4'), 4.01 (s, 3 H, *H*-2), 0.28 (s, 9 H, *H*-9') ppm.
^{13}C NMR (126 MHz, $CDCl_3$, 298 K): δ = 165.3 (*C*-1), 152.6 (*C*-6'), 146.4 (*C*-2'), 140.0 (*C*-4'), 124.5 (*C*-3'), 123.9 (*C*-5'), 102.1 (*C*-8'), 100.7 (*C*-7'), 53.2 (*C*-2), -0.2 (*C*-9') ppm.
MS (EI, 70 eV): *m/z* (%) = 233.09 (8) $[M]^+$, 218.06 (100) $[C_{11}H_{12}N_1O_2Si_1]^+$, 174.97 (3) $[C_{10}H_{12}N_1Si_1]^+$, 145.03 (1) $[C_8H_3N_1O_2]^+$.
HRMS (EI, 70 eV): *m/z* (%) ($C_{12}H_{15}N_1O_2{}^{28}Si_1$) =

	mass [*m/z*]	mass difference [ppm]	calc. formula
calculated	233.08720		
measured	233.08729	0.37	$C_{12}H_{15}N_1O_2{}^{28}Si_1$

FT-IR: $\tilde{\nu}$ = 3225.9 (w), 3048.1 (w), 2954.8 (w), 2899.4 (w), 2162.6 (w), 1713.3 (s), 1583.9 (w), 1554.4 (w), 1469.3 (w), 1442.6 (m), 1367.6 (m), 1309.8 (s), 1243.4 (m), 1221.7 (s), 1193.5 (m), 1132.1 (s), 1116.5 (m), 1017.3 (m), 962.5 (w), 930.4 (w), 858.5 (s), 839.6 (s), 811.2 () cm^{-1}.

7.3.9 Synthesis of methyl 5'-ethynylpicolinate (55)[8]

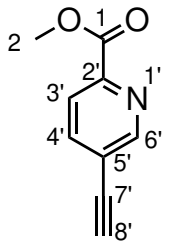

55

The reaction conditions were adapted from Soliman *et al.*.[8] In a round-bottom flask compound **54** (1.09 g, 4.67 mmol) and potassium carbonate (15.0 mg, 2.3 mol%) were added to methanol (12 mL)

and the reaction mixture was stirred at room temperature for 0.5 h. The solution was filtered and the solvent was removed *in vacuo*. The residue was redissolved in deion. water (10 mL) and the aqueous layer was extracted with dichloromethane (3 x 70 mL). The org. layers were combined, dried over magnesium sulfate and the solvent was removed *in vacuo*.

Yield: 688 mg (4.27 mmol, 92%)

^{1}H NMR (500 MHz, $CDCl_3$, 298 K): δ = 8.77 (dd, ^4J = 2.1 Hz, ^5J = 0.8 Hz, 1 H, *H*-6'), 8.11 (dd, ^3J = 8.1 Hz, ^5J = 0.8 Hz, 1 H, *H*-3'), 7.92 (dd, ^3J = 8.1 Hz, ^4J = 2.1 Hz, 1 H, *H*-4'), 4.02 (s, 3 H, *H*-2), 3.39 (s, 1 H, *H*-8') ppm.
^{13}C NMR (126 MHz, $CDCl_3$, 298 K): δ = 165.1 (*C*-1), 152.6 (*C*-6'), 146.8 (*C*-2'), 140.1 (*C*-4'), 124.4 (*C*-3'), 122.7 (*C*-5'), 83.5 (*C*-8'), 79.7 (*C*-7'), 53.1 (*C*-2) ppm.
MS (EI, 70 eV): *m/z* (%) = 161.05 (3) $[M]^+$, 102.03 (55) $[C_7H_4N_1]^+$.
HRMS (EI, 70 eV): *m/z* (%) ($C_9H_7N_1O_2$) =

	mass [*m/z*]	mass difference [ppm]	calc. formula
calculated	161.04768		
measured	161.04778	0.64	$C_9H_7N_1O_2$

FT-IR: $\tilde{\nu}$ = 3250.9 (m), 3100.0 (w), 3068.5 (w), 3018.7 (w), 2952.8 (w), 2848.2 (w), 2107.1 (w), 1725.1 (s), 1581.0 (w), 1557.5 (m), 1436.2 (m), 1363.4 (m), 1310.2 (s), 1273.8 (s), 1240.5 (s), 1205.5 (s), 1144.5 (m), 1120.4 (s), 1017.5 (m), 1000.0 (w), 974.8 (m), 932.5 (m), 877.9 (s), 842.1 (m) cm^{-1}.

7.3.10 Synthesis of dimethyl 5,5'-(ethyne-1",2"-diyl)dipicolinate (56) [9]

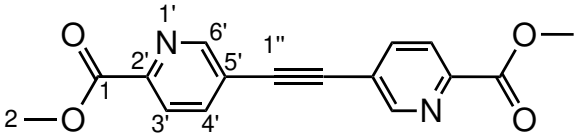

56

The reaction conditions were adapted from Jornet-Mollá *et al.*.[9] The reaction was performed under a nitrogen atmosphere. In a three-neck flask compound **53** (233 mg, 1.08 mmol), **55** (174 mg, 1.08 mmol) and $Pd(PPh_3)_4$ (37.4 mg, 3 mol%) were dissolved in a mixture of tetrahydrofuran (dry, 8 mL) and triethylamine (400 μL) and the reaction was stirred at 75 °C for 44 h. After cooling to room temperature, the solvent was removed *in vacuo* and the residue was further purified by flash chromatography (silica gel, 7% methanol:dichloromethane) to obtain product **56** as a brown solid.

Yield: 257 mg (867 μmol, 80%) (Lit.:[9] 80%).

^{1}H NMR (500 MHz, $CDCl_3$, 298 K): δ = 8.90 (dd, ^4J = 2.1 Hz, ^5J = 0.8 Hz, 2 H, *H*-6'), 8.17 (dd, ^3J = 8.1 Hz, ^5J = 0.8 Hz, 2 H, *H*-3'), 8.00 (dd, ^3J = 8.1 Hz, ^4J = 2.1 Hz, 2 H, *H*-4'), 4.03 (s, 6 H, *H*-2) ppm.
^{13}C NMR (126 MHz, $CDCl_3$, 298 K): δ = 165.1 (*C*-1), 152.1 (*C*-6'), 147.0 (*C*-2'), 139.7 (*C*-4'), 124.6 (*C*-3'), 122.6 (*C*-5'), 91.1 (*C*-1"), 53.2 (*C*-2) ppm.
MS (EI, 70 eV): *m/z* (%) = 296.08 (15) $[M]^+$, 265.06 (3) $[C_{15}H_9N_2O_3]^+$, 237.07 (5) $[C_{14}H_9N_2O_2]^+$, 178.05 (5) $[C_{12}H_6N_2]^+$.
HRMS (EI, 70 eV): *m/z* (%) ($C_{16}H_{12}N_2O_4$) =

	mass [*m/z*]	mass difference [ppm]	calc. formula
calculated	296.07971		
measured	296.07950	-0.69	$C_{16}H_{12}N_2O_4$

FT-IR: $\tilde{\nu}$ = 2962.1 (w), 1713.3 (s), 1589.9 (w), 1484.3 (w), 1439.4 (s), 1369.7 (m), 1319.2 (s), 1303.2 (m), 1238.0 (s), 1197.0 (m), 1135.9 (s), 1017.4 (s), 957.3 (m), 921.3 (m), 864.9 (s), 822.5 (m), 793.8 (m), 695.6 (s) cm^{-1}.

7.3.11 Synthesis of 5,5'-(ethyne-1",2"-diyl)dipicolinic acid (57)[9]

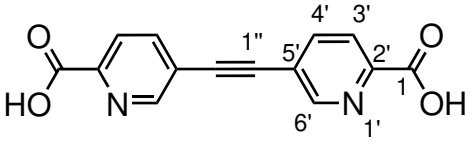

57

The reaction conditions were adapted from Jornet-Mollá *et al.*.[9] In a round-bottom flask compound **56** (726 mg, 2.45 mmol) was dissolved in a mixture of tetrahydrofuran (60 mL) and deion. water (32 mL). Lithium hydroxide monohydrate (206 mg, 4.91 mmol) was added and the reaction mixture was stirred at room temperature for 4 h. Tetrahydrofuran was removed *in vacuo* and the pH-value of the aqueous layer was adjusted to 2 with hydrochloric acid (1 M). The precipitate was filtered and was washed with deion. water (-4 °C, 80 mL) to obtain the product **57** as a colourless solid.

Yield: 643 mg (2.40 mmol, 98%) (Lit.:[9] 96%).

^{1}H NMR (500 MHz, DMSO–d_6, 298 K): δ = 8.94 (dd, ^4J = 2.0 Hz, ^5J = 1.0 Hz, 2 H, *H*-6'), 8.22 (dd, ^3J = 8.2 Hz, ^4J = 2.0 Hz, 2 H, *H*-4'), 8.11 (dt, ^3J = 8.2 Hz, ^5J = 1.0 Hz, 2 H, *H*-3') ppm.
^{13}C NMR (126 MHz, DMSO–d_6, 298 K): δ = 165.5 (*C*-1), 151.6 (*C*-6'), 147.8 (*C*-2'), 140.0 (*C*-4'), 124.3 (*C*-3'), 121.4 (*C*-5') ppm.
FT-IR: $\tilde{\nu}$ = 3459.9 (w), 1693.0 (s), 1593.2 (w), 1322.5 (s), 1240.9 (s), 1158.5 (m), 1027.0 (m), 932.8 (w), 858.2 (m) cm^{-1}.
Mass spectrometry data was attempted, but unsuccessful.

7.3.12 Synthesis of 1,2-bis(6"-(1*H*-benzo[*d*]imidazol-2'-yl)pyridin-3"-yl)ethyne (35)[10]

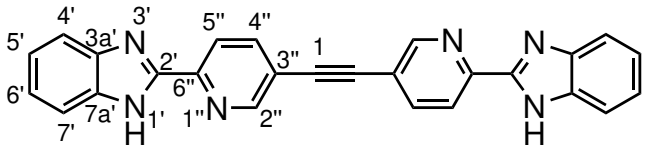

35

The reaction conditions were adapted from Turnbull *et al.*.[10] The reaction was performed under a nitrogen atmosphere. In a three-neck flask *o*-phenylenediamine (**58**) (443 mg, 4.10 mmol) and compound **57** (550 mg, 2.05 mmol) were dissolved in polyphosphoric acid (20 mL) and the reaction mixture stirred at 180 °C for 22 h. The mixture was cooled to 100 °C and deion. water (200 mL) was added. The solution was cooled to room temperature and was stirred for 1 h. The pH-value was adjusted to 8-9 using ammonia solution (25%), the suspension was stirred for further 1 h and was filtered. The crude product was dried *in vacuo*. Purification attempts were unsuccessful.

Yield: 718 mg (crude product)

MS (EI, 70 eV): *m/z* (%) = 412.14 (92) $[M]^+$, 218.07 (1) $[C_{14}H_8N_3]^+$, 194.07 (17) $[C_{12}H_8N_3]^+$.
HRMS (EI, 70 eV): *m/z* (%) ($C_{26}H_{16}N_6$) =

	mass [*m/z*]	mass difference [ppm]	calc. formula
calculated	412.14364		
measured	412.14341	-0.57	$C_{26}H_{16}N_6$

7.3.13 Synthesis of 2-(5'-bromo-6'-methylpyridin-2'-yl)-1*H*-benzo[*d*]imidazole (60)[11]

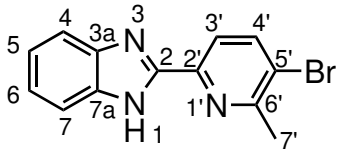

60

The reaction conditions were adapted from Jia *et al.*.[11] In a three-neck flask polyphosphoric acid (40 mL) was added and preheated to 140 °C. *o*-Phenylenediamine (**58**) (536 mg, 4.96 mmol) and 5-bromo-6-methylpicolinic acid (**59**) (1.07 g, 4.95 mmol) were added and the reaction mixture was stirred at 180 °C for 21.75 h. The mixture was cooled to 140 °C, poured into deion. water (100 mL) and the pH-value was adjusted to 7 using ammonia solution (25%). The precipitated grey product **60** was collected by filtration.

Yield: 1.06 g (3.68 mmol, 74%)

^{1}H NMR (500 MHz, DMSO–d_6, 298 K): δ = 12.9 (br, 1 H, *H*-1), 8.18 (d, ^3J = 8.4 Hz, 1 H, *H*-4'), 8.05 (dd, ^3J = 8.4 Hz, ^5J = 0.6 Hz, 1 H, *H*-3'), 7.69 (dt, ^3J = 7.8 Hz, ^4J = 1.0 Hz, 1 H, *H*-4/7), 7.56 (dt, ^3J = 7.9 Hz, ^4J = 1.0 Hz, 1 H, *H*-4/7), 7.28-7.23 (m, 1 H, *H*-5/6), 7.23-7.19 (m, 1 H, *H*-5/6), 2.73 (s, 3 H, *H*-7') ppm.
^{13}C NMR (126 MHz, DMSO–d_6, 298 K): δ = 156.4 (*C*-2'), 149.8 (*C*-2), 146.8 (*C*-6'), 143.8 (*C*-3a/7a), 141.0 (*C*-4'), 134.8 (*C*-3a/7a), 123.2 (*C*-5/6), 121.9 (*C*-5/6), 121.4 (*C*-5'), 120.5 (*C*-3'), 119.2

(*C*-4/7), 112.1 (*C*-4/7), 24.6 (*C*-7') ppm.
MS (EI, 70 eV): *m/z* (%) = 287.01 (100) $[M]^+$, 271.99 (3) $[C_{12}H_7Br_1N_3]^+$, 208.09 (12) $[C_{13}H_{10}N_3]^+$.
HRMS (EI, 70 eV): *m/z* (%) ($C_{13}H_{10}{}^{79}Br_1N_3$) =

	mass [*m/z*]	mass difference [ppm]	calc. formula
calculated	287.00581		
measured	287.00580	-0.02	$C_{13}H_{10}{}^{79}Br_1N_3$

FT-IR: $\tilde{\nu}$ = 1739.13 (s), 1439.5 (w), 1365.7 (m), 1217.0 (m), 835.2 (w) cm^{-1}.

7.3.14 Synthesis of 2-(5'-bromo-6'-methylpyridin-2'-yl)-1-methyl-1*H*-benzo[*d*]imidazole (61)[12]

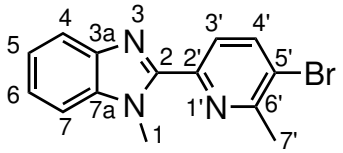

61

The reaction conditions were adapted from Lin *et al.*.[12] In a round-bottom flask compound **60** (670 mg, 2.33 mmol) and potassium carbonate (998 mg, 7.22 mmol) were dissolved in *N*,*N*-dimethylformamide (20 mL). Methyl iodide (200 µL, 3.21 mmol) was added and the reaction was stirred at room temperature for 20.5 h. The solution was poured into deion. water (100 mL) and the aqueous layer was extracted with ethyl acetate (2 x 100 mL). The org. layers were combined, washed with brine (200 mL) and sodium hydroxide solution (10%, w/w, 100 mL). The org. layer was dried over magnesium sulfate and the solvent was removed *in vacuo*. The product **61** was obtained as a brown solid.

Yield: 530 mg (1.75 mmol, 75%)

^{1}H NMR (600 MHz, DMSO–d_6, 298 K): δ = 8.19 (d, ^3J = 8.4 Hz, 1 H, *H*-4'), 8.05 (d, ^3J = 8.4 Hz, 1 H, *H*-3'), 7.71 (unres. dt, ^3J = 8.1 Hz, 1 H, *H*-4), 7.65 (unres. dt, ^3J = 8.1 Hz, 1 H, *H*-7), 7.34 (ddd,

^3J = 8.1 Hz, ^3J = 7.2 Hz, ^4J = 1.0 Hz, 1 H, *H*-6), 7.28 (ddd, ^3J = 8.1 Hz, ^3J = 7.2 Hz, ^4J = 1.0 Hz, 1 H, *H*-5), 4.23 (s, 3 H, *H*-1), 2.71 (s, 3 H, *H*-7') ppm.
^{13}C NMR (151 MHz, DMSO – d_6, 298 K): δ = 155.7 (*C*-2'), 148.8 (*C*-2), 148.4 (*C*-6'), 142.0 (*C*-3a), 141.1 (*C*-4'), 137.2 (*C*-7a), 123.4 (*C*-3'), 123.3 (*C*-6), 122.5 (*C*-5), 121.3 (*C*-5'), 119.5 (*C*-4), 110.9 (*C*-7), 32.7 (*C*-1), 24.8 (*C*-7') ppm.
HRMS (ESI): *m/z* (%) ($C_{14}H_{13}{}^{79}Br_1N_3$ ([M+H]$^+$)) =

	mass [*m/z*]	mass difference [ppm]	calc. formula
calculated	302.02874		
measured	302.02835	-1.28	$C_{14}H_{13}{}^{79}Br_1N_3$ ([M+H]$^+$)

FT-IR: $\tilde{\nu}$ = 1742.0 (m), 1561.4 (w), 1416.9 (m), 1228.1 (m), 1028.6 (m), 849.0 (m), 731.1 (s) cm^{-1}.

7.3.15 Synthesis of 1,2-bis(2"-methyl-6"-(1'-methyl-1*H*-benzo[*d*]imidazol-2'-yl)pyridin-3"-yl)ethyne (36)[13]

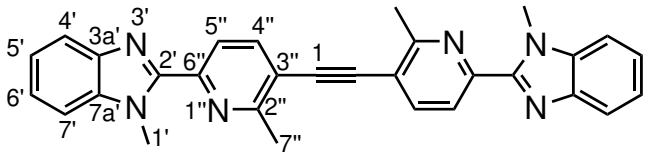

36

The reaction conditions were adapted from Lehr *et al.*.[13] The reaction was performed under a nitrogen atmosphere. In a pressure tube compound **61** (218 mg, 721 μmol) and $Pd(PPh_3)_4$ (41.8 mg, 5 mol%) were dissolved in tetrabutylammonium fluoride (1 M in tetrahydrofuran, 4.30 mL, 4.30 mmol). Trimethylsilylacetylene (100 μL, 723 μmol) was added, the tube was closed and the reaction mixture was heated at 70 °C for 19.5 h. The solution was cooled to room temperature and was filtered. The precipitated product was washed with tetrahydrofuran (-4 °C, 200 mL) and was obtained as a yellow solid.

Yield: 118 mg (252 μmol, 70%)

^{1}H NMR (500 MHz, $CDCl_3$, 298 K): δ = 8.30 (d, ^3J = 8.1 Hz, 1 H, *H*-5"), 7.95 (d, ^3J = 8.1 Hz, 1 H, *H*-4"), 7.84 (ddd, ^3J = 8.0 Hz, ^4J = 1.1 Hz, ^5J = 0.8 Hz, 1 H, *H*-4'), 7.46 (unres. ddd, 1 H, *H*-7'), 7.36 (ddd, ^3J = 8.0 Hz, ^3J = 7.1 Hz, ^4J = 1.2 Hz, 1 H, *H*-6'), 7.33 (ddd, ^3J = 7.6 Hz, ^3J = 7.2 Hz, ^4J = 1.5 Hz, 1 H, *H*-5'), 4.34 (s, 6 H, *H*-1'), 2.88 (s, 6 H, *H*-7") ppm.
^{13}C NMR (126 MHz, $CDCl_3$, 298 K): δ = 159.1 (*C*-2"), 149.7 (*C*-2'), 149.0 (*C*-6"), 142.6 (*C*-3a'), 139.7 (*C*-4"), 137.4 (*C*-7a'), 123.6 (*C*-6'), 122.8 (*C*-5'), 121.5 (*C*-5"), 120.1 (*C*-4'), 118.5 (*C*-3"), 109.9 (*C*-7'), 93.7 (*C*-1), 33.0 (*C*-1'), 24.0 (*C*-7") ppm.
MS (EI, 70 eV): *m/z* (%) = 468.22 (100) $[M]^+$, 337.16 (2) $[C_{22}H_{17}N_4]^+$, 246.11 (1) $[C_{16}H_{12}N_3]^+$, 222.11 (0) $[C_{14}H_{12}N_3]^+$.
HRMS (EI, 70 eV): *m/z* (%) ($C_{30}H_{24}N_6$) =

	mass [*m/z*]	mass difference [ppm]	calc. formula
calculated	468.20624		
measured	468.20614	-0.22	$C_{30}H_{24}N_6$

FT-IR: $\tilde{\nu}$ = 3048.8 (w), 1589.3 (m), 1548.1 (w), 1507.5 (w), 1484.2 (w), 1462.7 (m), 1439.9 (s), 1423.5 (m), 1392.5 (w), 1351.6 (w), 1329.0 (m), 1250.4 (w), 1224.7 (w), 1153.3 (w), 1125.7 (w), 1081.6 (w), 1008.7 (w), 984.7 (w), 922.2 (w), 848.8 (s), 727.2 (s) cm^{-1}.

7.3.16 Synthesis of 2-(5'-bromopyridin-2'-yl)benzo[*d*]thiazole (63)[11]

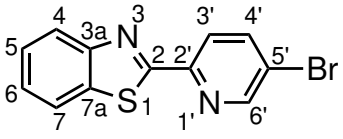

63

The reaction conditions were adapted from Jia *et al.*.[11] In a three-neck flask polyphosphoric acid (20 mL) was added and preheated to 140 °C. 2-Aminothiophenol (**62**) (680 μL, 6.30 mmol) and 5-bromopicolinic acid (**52**) (1.27 g, 6.29 mmol) were added and the reaction mixture stirred at 180 °C for 18.5 h. The mixture was cooled to 140 °C, poured into deion. water (200 mL) and the pH-value

was adjusted to 7 using ammonia solution (25%). The crude product was collected by filtration and was further purified by flash chromatography (silica gel, 10% ethyl acetate:cyclohexane) to obtain the product **63** as a mauve colored solid.

Yield: 467 mg (1.60 mmol, 26%)

R_f (10% ethyl acetate:cyclohexane) = 0.55
^{1}H NMR (600 MHz, DMSO–d_6, 298 K): δ = 8.90 (dd, ^4J = 2.2 Hz, ^5J = 0.8 Hz, 1 H, *H*-6'), 8.32 (dd, ^3J = 8.5 Hz, ^4J = 2.2 Hz, 1 H, *H*-4'), 8.28 (dd, ^3J = 8.5 Hz, ^5J = 0.8 Hz, 1 H, *H*-3'), 8.20 (ddd, ^3J = 8.4 Hz, ^4J = 1.2 Hz, ^5J = 0.6 Hz, 1 H, *H*-4/7), 8.13 (ddd, ^3J = 8.4 Hz, ^4J = 1.2 Hz, ^5J = 0.6 Hz, 1 H, *H*-4/7), 7.60 (ddd, ^3J = 8.2 Hz, ^3J = 7.3 Hz, ^4J = 1.2 Hz, 1 H, *H*-5/6), 7.53 (ddd, ^3J = 7.9 Hz, ^3J = 7.3 Hz, ^4J = 1.2 Hz, 1 H, *H*-5/6) ppm.
^{13}C NMR (151 MHz, DMSO–d_6, 298 K): δ = 167.6 (*C*-2), 153.6 (*C*-3a/7a), 150.7 (*C*-6'), 149.0 (*C*-2), 140.5 (*C*-4'), 135.3 (*C*-3a/7a), 126.7 (*C*-5/6), 126.2 (*C*-5/6), 123.3 (*C*-4/7), 122.6 (*C*-4/7), 121.8 (*C*-3'), 121.1 (*C*-5') ppm.
MS (EI, 70 eV): *m/z* (%) = 289.95 (97) $[M]^+$, 211.03 (13) $[C_{12}H_7N_2S_1]^+$.
HRMS (EI, 70 eV): *m/z* (%) ($C_{12}H_7{}^{79}Br_1N_2{}^{32}S_1$) =

	mass [*m/z*]	mass difference [ppm]	calc. formula
calculated	289.95133		
measured	289.95092	-1.43	$C_{12}H_7{}^{79}Br_1N_2{}^{32}S_1$

FT-IR: $\tilde{\nu}$ = 2365.6 (m), 1740.4 (s), 1365.6 (m), 1216.9 (m) cm^{-1}.

7.3.17 Synthesis of 1,2-bis(2'-(benzo[*d*]thiazol-2''-yl)pyridin-5'-yl)ethyne (34)[13]

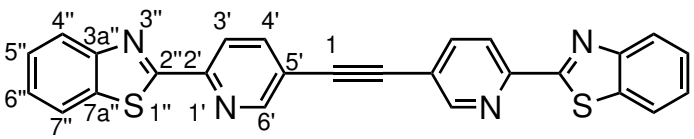

34

The reaction was followed according to reaction conditions from Lehr *et al.*.[13] The reaction was performed under a nitrogen atmosphere. In a pressure tube compound **63** (211 mg, 725 µmol) and $Pd(PPh_3)_4$ (41.8 mg, 5 mol%) were dissolved in tetrabutylammonium fluoride (degassed, 4.30 mL, 4.30 mL). Trimethylsilylacetylene (100 µL, 723 µmol) was added, the tube was closed and was stirred at 70 °C for 3 h. The solution was cooled to room temperature and was filtered. The solid was washed with tetrahydrofuran (-4 °C, 200 mL) to obtain product **34** as a yellow solid.

Yield: 86.6 mg (194 µmol, 54%)

^{1}H NMR (500 MHz, TFA–d_1, 298 K): δ = 9.38 (d, ^4J = 1.7 Hz, 2 H, *H*-6'), 8.81 (dd, ^3J = 8.4 Hz, ^4J = 1.7 Hz, 2 H, *H*-4'), 8.72 (d, ^3J = 8.4 Hz, 2 H, *H*-3'), 8.54 (unres. dt, ^3J = 8.3 Hz, 2 H, *H*-4"/7"), 8.45 (unres. dt, ^3J = 8.3 Hz, 2 H, *H*-4"/7"), 8.16 (ddd, ^3J = 8.3 Hz, ^3J = 7.3 Hz, ^4J = 0.9 Hz, 2 H, *H*-5"/6"), 8.09 (ddd, ^3J = 8.3 Hz, ^3J = 7.3 Hz, ^4J = 0.9 Hz, 2 H, *H*-5"/6") ppm.
^{13}C NMR (126 MHz, TFA–d_1, 298 K): δ = 167.1 (*C*-2"), 152.7 (*C*-6'), 147.4 (*C*-4'), 147.1 (*C*-3a"/7a"), 145.0 (*C*-2'), 135.3 (*C*-3a"/7a"), 133.2 (*C*-5"/6"), 132.5 (*C*-5"/6"), 127.2 (*C*-3'), 126.9 (*C*-5"), 125.4 (*C*-4"/7"), 122.8 (*C*-4"/7"), 93.7 (*C*-1) ppm.
MS (EI, 70 eV): *m/z* (%) = 446.06 (100) $[M]^+$, 235.03 (1) $[C_{14}H_7N_2S_1]^+$, 211.03 (1) $[C_{12}H_7N_2S_1]^+$.
HRMS (EI, 70 eV): *m/z* (%) ($C_{26}H_{14}N_4{}^{32}S_2$) =

	mass [*m/z*]	mass difference [ppm]	calc. formula
calculated	446.06599		
measured	446.06527	-1.62	$C_{26}H_{14}N_4{}^{32}S_2$

7.4 Synthetic Procedures for Chapter 2

7.4.1 Synthesis of 2-(pyridin-2'-yl)-1*H*-benzo[*d*]imidazole (76)[11]

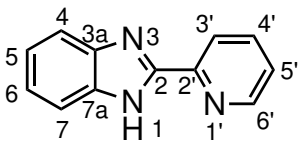

76

The reaction conditions were adapted from Jia *et al.*.[11] In a three-neck flask polyphosphoric acid (30 mL) was added and was preheated to 140 °C. *o*-Phenylenediamine (**58**) (1.88 g, 17.4 mmol) and picolinic acid (**75**) (2.14 g, 17.4 mmol) were added and the reaction mixture was stirred at 170 °C for 20 h. The mixture was cooled to 140 °C, was poured into deion. water (200 mL) and the pH-value was adjusted to 7 using ammonia solution (25%). The precipitated pink product **76** was collected by filtration.

Yield: 2.85 g (14.6 mmol, 84%) (Lit.:[11] 60-80%).

^{1}H NMR (500 MHz, DMSO–d_6, 298 K): δ = 13.1 (br, 1 H, *H*-1), 8.73 (ddd, ^3J = 4.8 Hz, ^4J = 1.8 Hz, ^5J = 1.0 Hz, 1 H, *H*-6'), 8.32 (dt, ^3J = 7.8 Hz, ^5J = 1.0 Hz, 1 H, *H*-3'), 8.00 (td, ^3J = 7.8 Hz, ^4J = 1.8 Hz, 1 H, *H*-4'), 7.71-7.69 (m, 1 H, *H*-4/7), 7.55-7.53 (m, 1 H, *H*-5'), 7.52 (ddd, ^3J = 7.5 Hz, ^3J = 4.8 Hz, ^4J = 1.2 Hz, 1 H, *H*-4/7), 7.25 (unres. ddd, ^3J = 7.1 Hz, ^4J = 1.2 Hz, 1 H, *H*-5/6), 7.21 (unres. ddd, ^3J = 7.2 Hz, ^4J = 1.5 Hz, 1 H, *H*-5/6) ppm.
^{13}C NMR (126 MHz, DMSO–d_6, 298 K): δ = 150.6 (*C*-2), 149.3 (*C*-6'), 148.4 (*C*-2'), 143.8 (*C*-3a/7a), 137.5 (*C*-4'), 134.8 (*C*-3a/7a), 124.6 (*C*-4/7), 123.0 (*C*-5/6), 121.8 (*C*-5/6), 121.3 (*C*-3'), 119.2 (*C*-4/7), 112.0 (*C*-5') ppm.
MS (EI, 70 eV): *m/z* (%) = 195.08 (100) $[M]^+$.
HRMS (EI, 70 eV): *m/z* (%) ($C_{12}H_9N_3$) =

	mass [*m/z*]	mass difference [ppm]	calc. formula
calculated	195.07965		
measured	195.08048	4.26	$C_{12}H_9N_3$

FT-IR: $\tilde{\nu}$ = 2970.4 (w), 1737.7 (s), 1365.3 (s), 1216.9 (s) cm^{-1}.

7.4.2 Synthesis of 5-nitro-2-(pyridin-2'-yl)-1*H*-benzo[*d*]imidazole (77)[14]

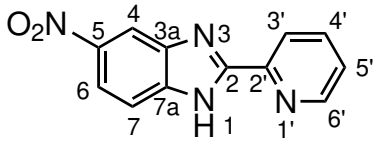

77

The reaction conditions were adapted from Ambacheu *et al.*.[14] In a three-neck flask compound **76** (1.00 g, 5.12 mmol) was dissolved in sulfuric acid (2 mL). The solution was cooled to 0 °C, a mixture of nitric acid and sulfuric acid (4 ml:5 mL) was slowly added and the reaction mixture was stirred first at 0 °C for 1 h and then at room temperature for 1 h. The solution was poured into crushed ice, the pH-value was adjusted to 7-9 using ammonia solution (25%) and the precipitated product **77** was collected by filtration as an orange solid.

Yield: 1.23 g (5.12 mmol, 100%) (Lit.:[14] 99.6%).

^{1}H NMR (500 MHz, DMSO–d_6, 298 K): δ = 13.1 (br, 1 H, *H*-1), 8.80 (ddd, ^3J = 4.8 Hz, ^4J = 1.7 Hz, ^5J = 1.0 Hz, 1 H, *H*-6'), 8.51 (d, ^5J = 2.2 Hz, 1 H, *H*-4), 8.39 (dt, ^3J = 7.7 Hz, ^5J = 1.0 Hz, 1 H, *H*-3'), 8.16 (dd, ^3J = 8.9 Hz, ^4J = 2.2 Hz, 1 H, *H*-6), 8.06 (td, ^3J = 7.7 Hz, ^4J = 1.7 Hz, 1 H, *H*-4'), 7.79 (d, ^3J = 8.9 Hz, 1 H, *H*-7), 7.61 (ddd, ^3J = 7.7 Hz, ^3J = 4.8 Hz, ^4J = 1.0 Hz, 1 H, *H*-5') ppm.
^{13}C NMR (126 MHz, DMSO–d_6, 298 K): δ = 155.2 (*C*-2), 149.6 (*C*-6'), 147.3 (*C*-2'), 142.9 (*C*-5), 137.8 (*C*-4'), 125.7 (*C*-5'), 122.1 (*C*-3'), 118.2 (*C*-6) ppm.
C-3a and *C*-7a were not observed in ^{13}C, HMQC or HMBC spectra.
MS (EI, 70 eV): *m/z* (%) = 240.06 (100) $[M]^+$, 194.07 (50) $[C_{12}H_8N_3]^+$.
HRMS (EI, 70 eV): *m/z* (%) ($C_{12}H_8N_4O_2$) =

	mass [*m/z*]	mass difference [ppm]	calc. formula
calculated	240.06473		
measured	240.06464	-0.37	$C_{12}H_8N_4O_2$

FT-IR: $\tilde{\nu}$ = 2251.4 (m), 1739.5 (s), 1366.1 (m), 1217.0 (m) cm^{-1}.

7.4.3 Synthesis of 5-amino-2-(pyridin-2'-yl)-1*H*-benzo[*d*]imidazole (78)[15]

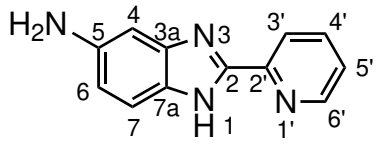

78

The reaction conditions were adapted from Schiffmann *et al.*.[15] The reaction was performed under a hydrogen atmosphere. In a three-neck flask compound **77** (503 mg, 2.09 mmol) and Pd/C (250 mg) were dissolved in ethanol (dry, 50 mL). A first balloon, filled with hydrogen gas, was bubbled through the solution for 30 min to create a hydrogen gas atmosphere. Afterwards, the balloon was refilled and the gas was bubbled through the solution at room temperature for 21.5 h. The solution was filtered over Celite®, washed with ethanol (150 mL) and the solvent was removed *in vacuo*. Purification by flash chromatography (silica gel, 5% methanol:ethyl acetate) gave the product **78** in an impure mixture. Further purification by recrystallisation from ethanol was unsuccessful.

Yield: 207 mg (crude product) (Lit.:[15] 80%).

^{1}H NMR (500 MHz, DMSO – d_6, 298 K): δ = 12.5 (br, 1 H, *H*-1), 8.65 (ddd, ^3J = 4.8 Hz, ^4J = 1.7 Hz, ^5J = 1.0 Hz, 1 H, *H*-6'), 8.19 (dt, ^3J = 7.7 Hz, ^5J = 1.0 Hz, 1 H, *H*-3'), 7.91 (td, ^3J = 7.7 Hz, ^4J = 1.4 Hz, 1 H, *H*-4'), 7.41 (ddd, ^3J = 7.7 Hz, ^3J = 4.8 Hz, ^4J = 1.4 Hz, 1 H, *H*-5'), 7.33 (d, ^3J = 8.6 Hz, 1 H, *H*-7), 6.66 (d, ^4J = 2.1 Hz, 1 H, *H*-4), 6.54 (dd, ^3J = 8.6 Hz, ^4J = 2.1 Hz, 1 H, *H*-6), 5.05 (s, 1 H, N-*H*) ppm.
^{13}C NMR (126 MHz, DMSO – d_6, 298 K): δ = 149.1 (*C*-2), 149.0 (*C*-2'), 148.9 (*C*-6'), 147.9 (*C*-2), 145.6 (*C*-5), 137.1 (*C*-4'), 136.2 (*C*-3a, 7a), 123.5 (*C*-5'), 120.4 (*C*-3'), 119.3 (*C*-7), 112.0 (*C*-6), 94.4 (*C*-4) ppm.
MS (EI, 70 eV): *m/z* (%) = 210.09 (100) $[M]^+$, 195.07 (0) $[C_{12}H_9N_3]^+$.
HRMS (EI, 70 eV): *m/z* (%) ($C_{12}H_{10}N_4$) =

	mass [*m/z*]	mass difference [ppm]	calc. formula
calculated	210.09055		
measured	210.09021	-1.60	$C_{12}H_{10}N_4$

7.4.4 Synthesis of (*E*/*Z*)-2-(5'-bromopyridin-2'-yl)-5-(phenyldiazenyl)-1*H*-benzo[*d*]imidazole (*E*:67, *Z*:99)[16]

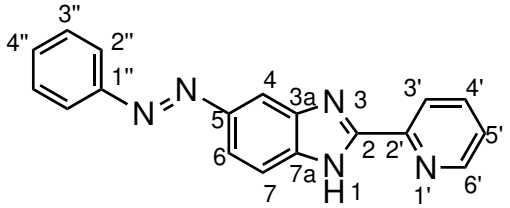

67

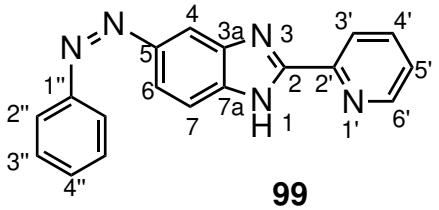

99

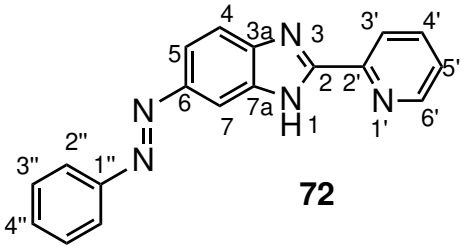

72

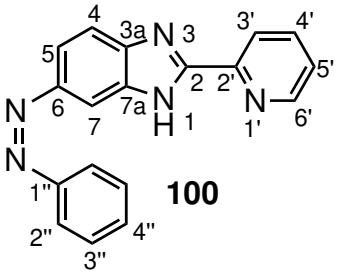

100

The reaction was performed according to the reaction conditions of Hasegawa *et al.*.[16] In a two-neck flask, wrapped into aluminum foil, nitrosobenzene (**79**) (177 mg, 1.65 mmol) and compound **78** (314 mg crude product) were dissolved in a mixture of chloroform (8 mL) and glacial acetic acid (5.5 ml) and the reaction mixture was stirred at room temperature for 19 h. The solvent was removed *in vacuo*. Purification by flash chromatography (aluminum oxide, neutral, 70% chloroform:cyclohexane) gave the product **67** as a red solid. The *cis* isomer **99** was obtained after irradiation of azobenzene **67** with 435 nm in deuterated acetone.

Yield: 81.4 mg (272 μmol, 5% over two steps) (Lit.:[16] 42%).

Note: The *trans* and *cis* isomers were obtained as a mixture of both tautomeric forms.

Compound **67**/**72** (*E* isomer):
^{1}H NMR (500 MHz, acetone–d_6, 298 K): δ = 12.4 (br, 2 H, *H*-1), 8.73 (ddd, ^3J = 4.9 Hz, ^4J = 1.7 Hz, ^5J = 1.0 Hz, 1 H, *H*-6'), 8.72 (ddd, ^3J = 5.0 Hz, ^4J = 1.7 Hz, ^5J = 1.0 Hz, 1 H, *H*-6'), 8.46 (dt, ^3J = 7.9 Hz, ^5J = 1.0 Hz, 1 H, *H*-3'), 8.45 (dt, ^3J = 7.9 Hz, ^5J = 1.0 Hz, 1 H, *H*-3'), 8.34 (dd, ^4J = 1.8 Hz, ^5J = 0.4 Hz, 1 H, *H*-4), 8.26 (dd, ^4J = 1.9 Hz, ^5J = 0.5 Hz, 1 H, *H*-4), 8.05-8.01 (m, 2 H, *H*-4'), 8.01-

7.95 (m, 6 H, *H*-2",6), 7.88 (dd, ^3J = 8.7 Hz, ^5J = 0.4 Hz, 1 H, *H*-7), 7.81 (dd, ^3J = 8.7 Hz, ^5J = 0.4 Hz, 1 H, *H*-7), 7.62-7.58 (m, 4 H, *H*-3"), 7.56-7.51 (m, 4 H, *H*-4",5') ppm.
^{13}C NMR (126 MHz, acetone – d_6, 298 K): δ = 152.7 (*C*-1"), 153.7 (*C*-6'), 150.4 (*C*-6'), 138.3 (*C*-4'), 131.7 (*C*-4"), 131.5 (*C*-4"), 130.2 (*C*-3"), 130.1 (*C*-3"), 125.9 (*C*-5'), 125.8 (*C*-5'), 123.4 (*C*-2"), 123.4 (*C*-2"), 122.6 (*C*-3'), 122.5 (*C*-3'), 120.9 (*C*-7), 118.7 (*C*-6), 118.4 (*C*-7a), 117.1 (*C*-4), 113.2 (*C*-7), 108.4 (*C*-4) ppm.
MS (EI, 70 eV): *m/z* (%) = 299.11 (32) $[M]^+$, 194.07 (100) $[C_{12}H_8N_3]^+$.
HRMS (EI, 70 eV): *m/z* (%) ($C_{18}H_{13}N_5$) =

	mass [*m/z*]	mass difference [ppm]	calc. formula
calculated	299.11710		
measured	299.11677	-1.10	$C_{18}H_{13}N_5$

FT-IR: $\tilde{\nu}$ = 2971.1 (w), 2365.0 (w), 1737.5 (s), 1365.9 (m), 1217.0 (m) cm^{-1}.

Compound **99/100** (*Z* isomer):
^{1}H NMR (600 MHz, acetone – d_6, 298 K): δ = 12.2 (br, 2 H, *H*-1), 8.67-8.65 (m, 2 H, *H*-6'), 8.36 (dt, ^3J = 8.0 Hz, ^5J = 1.0 Hz, 1 H, *H*-3'), 8.34 (dt, ^3J = 8.0 Hz, ^5J = 1.1 Hz, 1 H, *H*-3'), 7.99-7.95 (m, 2 H, *H*-4'), 7.60 (dd, ^3J = 8.5 Hz, ^5J = 0.5 Hz, 1 H, *H*-7), 7.55 (dd, ^3J = 8.5 Hz, ^5J = 0.5 Hz, 1 H, *H*-7), 7.48 (dt, ^3J = 4.9 Hz, ^5J = 1.0 Hz, 1 H, *H*-5'), 7.47 (dt, ^3J = 4.9 Hz, ^5J = 1.1 Hz, 1 H, *H*-5'), 7.32-7.27 (m, 4 H, *H*-3"), 7.22 (dd, ^4J = 1.7 Hz, ^5J = 0.5 Hz, 1 H, *H*-4), 7.17 (dd, ^4J = 1.9 Hz, ^5J = 0.5 Hz, 1 H, *H*-4), 7.17-7.13 (m, 2 H, *H*-4"), 6.91-6.88 (m, 5 H, *H*-4",6), 6.81 (dd, ^3J = 8.5 Hz, ^4J = 1.9 Hz, 1 H, *H*-6), ppm.
^{13}C NMR (151 MHz, acetone – d_6, 298 K): δ = 150.4 (*C*-6'), 150.3 (*C*-6'), 138.2 (*C*-4'), 129.8 (*C*-3"), 129.7 (*C*-3"), 127.7 (*C*-4"), 127.5 (*C*-4"), 125.7 (*C*-5'), 125.7 (*C*-5'), 122.4 (*C*-3'), 122.3 (*C*-3'), 120.8 (*C*-4"), 120.7 (*C*-4"), 120.4 (*C*-7), 118.5 (*C*-6), 116.9 (*C*-6), 122.8 (*C*-4), 112.7 (*C*-7), 105.6 (*C*-4) ppm.
Mass spectrometry data was not collected.

7.4.5 Synthesis of 2-(pyridin-2'-yl)-1-methyl-5-nitro-1*H*-benzo[*d*]imidazole (85)[11]

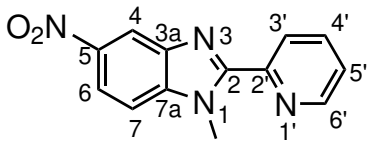

85

The reaction conditions were adapted from Jia *et al.*.[11] In a three-neck flask polyphosphoric acid (25 mL) was added and was preheated to 140 °C. *N*-Methyl-4-nitrobenzene-1,2-diamine (**84**) (1.45 g, 8.70 mmol) and picolinic acid (**75**) (1.07 g, 8.70 mmol) were added and the reaction mixture was stirred at 180 °C for 28 h. The mixture was cooled to 140 °C, poured into deion. water (200 mL) and the pH-value was adjusted to 7 using ammonia solution (25%). The crude product was filtered and purification by flash chromatography (silica gel, 20% ethyl acetate:cyclohexane) gave the product **85** as a colourless solid.

Yield: 113 mg (339 μmol, 5%)

R_f (20% ethyl acetate:cyclohexane) = 0.68
^{1}H NMR (600 MHz, DMSO – d_6, 298 K): δ = 8.80 (ddd, ^3J = 4.8 Hz, ^4J = 1.6 Hz, ^5J = 1.0 Hz, 1 H, *H*-6'), 8.62 (d, ^5J = 2.2 Hz, 1 H, *H*-4), 8.35 (dt, ^3J = 7.7 Hz, ^5J = 1.0 Hz, 1 H, *H*-3'), 8.25 (dd, ^3J = 9.0 Hz, ^4J = 2.2 Hz, 1 H, *H*-6), 8.06 (td, ^3J = 7.7 Hz, ^4J = 1.6 Hz, 1 H, *H*-4'), 7.92 (d, ^3J = 9.0 Hz, 1 H, *H*-7), 7.61 (ddd, ^3J = 7.7 Hz, ^3J = 4.8 Hz, ^4J = 1.0 Hz, 1 H, *H*-5'), 4.30 (s, 3 H, *H*-1) ppm.
^{13}C NMR (151 MHz, DMSO – d_6, 298 K): δ = 153.6 (*C*-2), 149.1 (*C*-2'), 149.0 (*C*-6'), 143.2 (*C*-5), 141.4 (*C*-7a), 141.1 (*C*-3a), 137.7 (*C*-4'), 125.1 (*C*-5'), 125.0 (*C*-3'), 118.5 (*C*-6), 115.6 (*C*-4), 111.7 (*C*-7), 33.4 (*C*-1) ppm.
MS (EI, 70 eV): *m/z* (%) = 254.10 (100) $[M]^+$.
HRMS (EI, 70 eV): *m/z* (%) ($C_{13}H_{10}N_4O_2$) =

	mass [*m/z*]	mass difference [ppm]	calc. formula
calculated	254.08038		
measured	254.07955	-3.24	$C_{13}H_{10}N_4O_2$

FT-IR: $\tilde{\nu}$ = 2946.56 (w), 1738.84 (m), 1615.24 (w), 1586.09 (w), 1523.51 (s), 1472.93 (m), 1444.2 (s), 1421.8 (m), 1368.4 (m), 1339.3 (s), 1282.8 (m), 1269.9 (w), 1216.6 (m), 1135.2 (m), 1091.9 (m), 1057.2 (m), 994.2 (m), 887.8 (m), 869.6 (m), 825.7 (s), 813.4 (m) cm^{-1}.

7.4.6 Synthesis of 4-bromo-*N*-methyl-2-nitroaniline (89)[17]

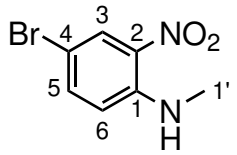

89

The reaction conditions were adapted from Zhegalova *et al.*.[17] The reaction was performed under a nitrogen atmosphere. In a three-neck flask 4-bromo-2-nitroaniline (**87**) (2.33 g, 10.7 mmol) was dissolved in tetrahydrofuran (dry, 12 mL) and the mixture was cooled to 0 °C. Sodium hydride (504 mg, 12.6 mmol) was slowly added, the reaction mixture was stirred at 0 °C for 5 min and methyl iodide (660 μL, 10.6 mmol) was added. The solution was warmed up to room temperature and was stirred for 18.5 h. Ethyl acetate (200 mL) was added and the org. layer was washed with brine (200 mL). The layers were separated, the org. layer was dried over magnesium sulfate and the solvent was removed *in vacuo*. The product **89** was obtained as an orange solid.

Yield: 2.29 g (9.91 mmol, 94%) (Lit.:[17] 99%).

^{1}H NMR (500 MHz, $CDCl_3$, 298 K): δ = 8.31 (d, ^4J = 2.4 Hz, 1 H, *H*-3), 8.02 (br, 1 H, N-*H*), 7.52 (dd, ^3J = 9.1 Hz, ^4J = 2.4 Hz, ^5J = 0.7 Hz, 1 H, *H*-5), 6.76 (d, ^3J = 9.1 Hz, 2 H, *H*-6), 3.02 (d, ^3J = 5.1 Hz, 3 H, *H*-1') ppm.
^{13}C NMR (126 MHz, $CDCl_3$, 298 K): δ = 145.2 (*C*-1), 139.0 (*C*-5), 132.2 (*C*-2), 128.9 (*C*-3), 115.1 (*C*-6), 106.4 (*C*-4), 29.8 (*C*-1') ppm.
HRMS (ESI): *m/z* (%) ($C_7H_8{}^{79}Br_1N_2O_2$ ($[M+H]^+$)) =

	mass [*m/z*]	mass difference [ppm]	calc. formula
calculated	230.97637		
measured	230.97613	-1.01	$C_7H_8{}^{79}Br_1N_2O_2$ ($[M+H]^+$)

FT-IR: $\tilde{\nu}$ = 2921.8 (s), 2853.1 (s), 2252.0 (w), 1612.8 (w), 1560.2 (m), 1458.6 (m), 1376.8 (m), 1344.1 (m), 1248.4 (m), 1173.9 (m), 875.2 (m), 810.4 (m), 667.7 (m) cm^{-1}.

7.4.7 Synthesis of 5-bromo-*N*-methyl-2-nitroaniline (90)[17]

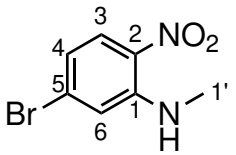

90

The reaction conditions were adapted from Zhegalova *et al.*.[17] The reaction was performed under a nitrogen atmosphere. In a three-neck flask 5-bromo-2-nitroaniline (**88**) (1.99 g, 9.17mmol) was dissolved in tetrahydrofuran (dry, 12 mL) and the mixture cooled to 0 °C. Sodium hydride (433 mg, 10.8 mmol) was slowly added, the reaction mixture was stirred at 0 °C for 5 min and methyl iodide (570 μL, 9.16 mmol) was added. The solution was warmed up to room temperature and was stirred for 18.5 h. Ethyl acetate (200 mL) was added and the org. layer was washed with brine (200 mL). The layers were separated, the org. layer was dried over magnesium sulfate and the solvent was removed *in vacuo*. The product **90** was obtained as an orange solid.

Yield: 2.03 g (8.79 mmol, 96%)

^{1}H NMR (500 MHz, $CDCl_3$, 298 K): δ = 8.03 (br, 1 H, N-*H*), 8.02 (d, ^3J = 9.1 Hz , 2 H, *H*-3), 7.00 (d, ^4J = 2.0 Hz, 1 H, *H*-6), 6.76 (dd, ^3J = 9.1 Hz, ^4J = 2.0 Hz, 1 H, *H*-4), 3.02 (d, ^3J = 5.1 Hz, 3 H, *H*-1') ppm.
^{13}C NMR (126 MHz, $CDCl_3$, 298 K): δ = 146.6 (*C*-1), 131.8 (*C*-5), 130.9 (*C*-2) 128.1 (*C*-3), 118.6 (*C*-4), 116.1 (*C*-6), 29.8 (*C*-1') ppm.
MS (EI, 70 eV): *m/z* (%) = 229.97 (38) $[M]^+$, 214.96 (3) $[C_6H_4Br_{79}N_2O_2]^+$, 183.96 (9) $[C_7H_7Br_1N_1]^+$.

7.4.8 Synthesis of 5-bromo-1-methyl-2-(pyridin-2'-yl)-1*H*-benzo[*d*]imidazole (92)[18]

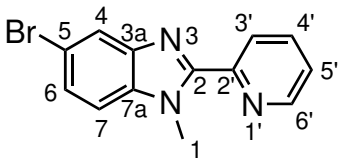

92

The reaction conditions were adapted from Yang *et al.*.[18] In a three-neck flask compound **89** (442 mg, 1.91 mmol) and 2-pyridinecarboxaldehyde (**91**) (200 µL, 2.10 mmol) were dissolved in a mixture of ethanol (12 mL) and *N*,*N*-dimethylformamide (6 mL). Sodium dithionite (1.25 g, 5.74 mmol) was dissolved in deion. water (5.7 mL) and both solutions were combined. The reaction mixture was stirred at 80 °C for 20 h. After cooling to room temperature, ammonia solution (25%, 4 mL), ethyl acetate (50 mL) and deion. water (50 mL) were added, the layers were separated and the aqueous layer was further extracted with ethyl acetate (200 mL). The org. layers were combined, washed with brine (200 mL), dried over magnesium sulfate and the solvent was removed *in vacuo* to obtain product **92** as a yellow solid.

Yield: 405 mg (1.41 mmol, 74%)

^{1}H NMR (600 MHz, DMSO–d_6, 298 K): δ = 8.76 (ddd, ^3J = 4.8 Hz, ^4J = 1.8 Hz, ^5J = 1.0 Hz, 1 H, *H*-6'), 8.29 (dt, ^3J = 7.7 Hz, ^5J = 1.0 Hz, 1 H, *H*-3'), 8.02 (td, ^3J = 7.7 Hz, ^4J = 1.8 Hz, 1 H, *H*-4'), 7.92 (d, ^4J = 1.8 Hz, 1 H, *H*-4), 7.65 (d, ^3J = 8.6 Hz, 1 H, *H*-7), 7.55 (ddd, ^3J = 7.7 Hz, ^3J = 4.8 Hz, ^4J = 1.0 Hz, 1 H, *H*-5'), 7.47 (dd, ^3J = 8.6 Hz, ^4J = 1.8 Hz, 1 H, *H*-6), 4.22 (s, 3 H, *H*-1) ppm.
^{13}C NMR (151 MHz, DMSO–d_6, 298 K): δ = 150.9 (*C*-2), 149.6 (*C*-2'), 148.9 (*C*-6'), 143.3 (*C*-3a), 137.5 (*C*-4'), 136.3 (*C*-7a), 125.8 (*C*-6), 124.6 (*C*-3'), 124.5 (*C*-5'), 121.7 (*C*-4), 114.6 (*C*-5), 112.8 (*C*-7), 32.9 (*C*-1) ppm.
HRMS (ESI): *m/z* (%) ($C_{13}H_{11}{}^{79}Br_1N_3$ ([M+H]$^+$)) =

	mass [*m/z*]	mass difference [ppm]	calc. formula
calculated	288.01309		
measured	288.01268	-1.40	$C_{13}H_{11}{}^{79}Br_1N_3$ ([M+H]$^+$)

7.4.9 Synthesis of 6-bromo-1-methyl-2-(pyridin-2'-yl)-1*H*-benzo[*d*]imidazole (93)[18]

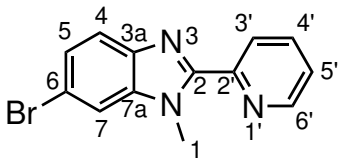

93

The reaction conditions were adapted from Yang *et al.*.[18] In a three-neck flask compound **90** (442 mg, 1.91 mmol) and 2-pyridinecarboxaldehyde (**91**) (200 µL, 2.10 mmol) were dissolved in a mixture of ethanol (12 mL) and *N*,*N*-dimethylformamide (6 mL). Sodium dithionite (1.25 g, 5.74 mmol) was dissolved in deion. water (6 mL) and both solutions were combined. The reaction mixture was stirred at 80 °C for 26 h. After cooling to room temperature, ammonia solution (25%, 4 mL), ethyl acetate (50 mL) and deion. water (50 mL) were added, the layers were separated and the aqueous layer was further extracted with ethyl acetate (150 mL). The org. layers were combined, dried over magnesium sulfate and the solvent was removed *in vacuo* to obtain product **92** as a yellow solid.

Yield: 394 mg (1.37 mmol, 72%)

^{1}H NMR (500 MHz, DMSO – d_6, 298 K): δ = 8.76 (ddd, ^3J = 4.8 Hz, ^4J = 1.8 Hz, ^5J = 1.1 Hz, 1 H, *H*-6'), 8.30 (dt, ^3J = 7.8 Hz, ^5J = 1.1 Hz, 1 H, *H*-3'), 8.01 (td, ^3J = 7.8 Hz, ^4J = 1.8 Hz, 1 H, *H*-4'), 7.96 (dd, ^4J = 1.9 Hz, ^5J = 0.4 Hz, 1 H, *H*-7), 7.67 (dd, ^3J = 8.6 Hz, ^5J = 0.4 Hz, 1 H, *H*-4), 7.54 (ddd, ^3J = 7.8 Hz, ^3J = 4.8 Hz, ^4J = 1.1 Hz, 1 H, *H*-5'), 7.41 (dd, ^3J = 8.6 Hz, ^4J = 1.9 Hz, 1 H, *H*-5), 4.22 (s, 3 H, *H*-1) ppm.
^{13}C NMR (126 MHz, DMSO – d_6, 298 K): δ = 150.5 (*C*-2), 149.6 (*C*-2'), 148.8 (*C*-6'), 140.9 (*C*-3a), 138.2 (*C*-7a), 137.4 (*C*-4'), 125.3 (*C*-5), 124.4 (*C*-3'), 124.3 (*C*-5'), 121.0 (*C*-4), 115.4 (*C*-), 113.8 (*C*-7), 32.8 (*C*-1) ppm.
HRMS (ESI): *m/z* (%) ($C_{13}H_{11}{}^{79}Br_1N_3$ ([M+H]$^+$)) =

	mass [*m/z*]	mass difference [ppm]	calc. formula
calculated	288.01309		
measured	288.01269	-1.40	$C_{13}H_{11}{}^{79}Br_1N_3$ ([M+H]$^+$)

FT-IR: $\tilde{\nu}$ = 2920.2 (m), 2851.9 (m), 1584.0 (w), 1566.4 (w), 1468.7 (m), 1443.9 (m), 1421.5 (m), 1375.3 (m), 1325.8 (m), 1276.8 (m), 1125.8 (m), 1089.0 (m), 1065.1 (m), 1042.5 (m), 992.3 (m), 907.3 (m), 825.9 (s), 799.5 (m), 788.92 (s), 757.8 (m), 739.9 (s), 696.3 (s) cm^{-1}.

7.4.10 Synthesis of *N*-(1'-methyl-2'-(pyridin-2"-yl)-1*H*-benzo[*d*]imidazol-5'-yl)-1,1-diphenylmethanimine (94)[19]

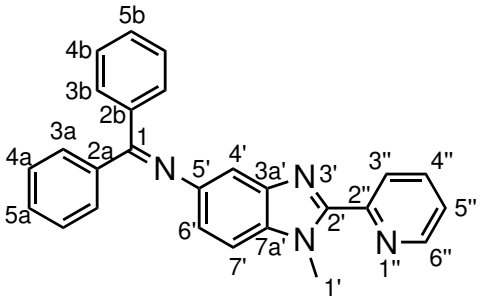

94

The reaction conditions were adapted from Wolfe *et al.*.[19] The reaction was performed under a nitrogen atmosphere. In a three-neck flask compound **92** (696 mg, 2.42 mmol), sodium *tert*-butoxide (349 mg, 3.63 mmol), *R*-BINAP (45.2 mg, 3.0 mol%) and $Pd_2(dba)_3$ (33.2 mg, 1.5 mol%) were dissolved in toluene (dry, 10 mL). Benzophenone imine (**96**) (432 mg, 2.38 mmol) was added and the reaction was stirred at 90 °C for 24 h. After cooling to room temperature diethyl ether (100 mL) was added, filtered and the solvent of the filtrate was removed *in vacuo*. Recrystallisation from methanol gave the product **94** as a yellow solid.

Yield: 607 mg (1.56 mmol, 66%)

^{1}H NMR (600 MHz, DMSO–d_6, 298 K): δ = 8.72 (ddd, ^3J = 4.8 Hz, ^4J = 1.6 Hz, ^5J = 0.8 Hz, 1 H, *H*-6"), 8.23 (dt, ^3J = 7.9 Hz, ^5J = 0.8 Hz, 1 H, *H*-3"), 7.96 (td, ^3J = 7.9 Hz, ^4J = 1.6 Hz, 1 H, *H*-4"), 7.68 (unres. dt, ^3J = 7.6 Hz, 2 H, *H*-3a), 7.55-7.45 (m, 4 H, *H*-4a,5a,5"), 7.42 (d, ^3J = 8.6 Hz, 1 H, *H*-7'), 7.33-7.26 (m, 3 H, *H*-4b,5b), 7.21-7.18 (m, 2 H, *H*-3b), 6.98-6.97 (m, 1 H, *H*-4'), 6.76 (dd, ^3J = 8.6 Hz, ^4J = 1.8 Hz, 1 H, *H*-6'), 4.14 (s, 3 H, *H*-1') ppm.
^{13}C NMR (151 MHz, DMSO–d_6, 298 K): δ = 167.4 (*C*-1), 150.1 (*C*-2"), 149.8 (*C*-2'), 148.8 (*C*-6"), 146.6 (*C*-5'), 142.1 (*C*-3a'), 139.1 (*C*-2a), 137.3 (*C*-4"), 136.3 (*C*-2b), 133.7 (*C*-7a'), 130.8 (*C*-5a), 128.9 (*C*-3b), 128.7 (*C*-3a), 128.4 (*C*-5b), 128.3 (*C*-4a), 128.1 (*C*-4b), 124.2 (*C*-3"), 124.1 (*C*-7.49), 117.8 (*C*-6'), 110.4 (*C*-7'), 110.1 (*C*-4'), 32.6 (*C*-1') ppm.

MS (EI, 70 eV): *m/z* (%) = 388.18 (100) $[M]^+$, 311.14 (44) $[C_{20}H_{15}N_4]^+$, 208.09 (10) $[C_{13}H_{10}N_3]^+$.
HRMS (EI, 70 eV): *m/z* (%) ($C_{26}H_{20}N_4$) =

	mass [*m/z*]	mass difference [ppm]	calc. formula
calculated	388.16880		
measured	388.16892	0.31	$C_{26}H_{20}N_4$

FT-IR: $\tilde{\nu}$ = 2923.6 (m), 2852.9 (m), 2252.8 (w), 1586.2 (m), 1569.0 (m), 1463.4 (m), 1442.4 (m), 1421.2 (m), 1381.1 (m), 1315.0 (m), 1276.7 (m), 1251.4 (m), 1125.4 (m), 1042.9 (w), 971.7 (m), 857.8 (m), 809.8 (m), 785.9 (m), 772.2 (m), 750.6 (m), 730.5 (m), 694.4 (s), 678.7 (m), 656.1 (m) cm^{-1}.

7.4.11 Synthesis of 1-methyl-2-(pyridin-2'-yl)-1*H*-benzo[*d*]imidazol-5-amine (86)[19]

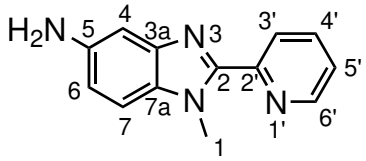

86

The reaction conditions were adapted from Wolfe *et al.*.[19] In a round-bottom flask compound **94** (389 mg, 1.00 mmol) was dissolved in tetrahydrofuran (10 mL). Hydrochloric acid (2 M, 150 µL) was added and the solution was stirred at room temperature for 25 min. Ethyl acetate (50 mL) and hydrochloric acid (0.5 M, 50 mL) were added, the phases were separated and the pH-value of the aqueous layer was adjusted to 13 using sodium hydroxide solution (2 M). The aqueous layer was extracted with ethyl acetate (100 mL), dried over magnesium sulfate and the solvent was removed *in vacuo*.

Yield: 162 mg (722 µmol, 72%)

^{1}H NMR (600 MHz, DMSO–d_6, 298 K): δ = 8.70 (ddd, ^3J = 4.8 Hz, ^4J = 1.7 Hz, ^5J = 1.0 Hz, 1 H, *H*-6'), 8.24 (dt, ^3J = 7.7 Hz, ^5J = 1.0 Hz, 1 H, *H*-3'), 7.95 (td, ^3J = 7.7 Hz, ^4J = 1.7 Hz, 1 H, *H*-4'),

7.46 (ddd, ^3J = 7.7 Hz, ^3J = 4.8 Hz, ^4J = 1.0 Hz, 1 H, *H*-5'), 7.30 (d, ^3J = 8.5 Hz, 1 H, *H*-7), 6.82 (d, ^4J = 1.7 Hz, 1 H, *H*-4), 6.70 (dd, ^3J = 8.5 Hz, ^4J = 1.7 Hz, 1 H, *H*-6), 4.88 (br, 2 H, N-*H*), 4.14 (s, 3 H, *H*-1) ppm.
^{13}C NMR (151 MHz, DMSO–d_6, 298 K): δ = 150.5 (*C*-2'), 148.7 (*C*-6'), 148.6 (*C*-2), 144.7 (*C*-3a), 143.4 (*C*-5), 137.2 (*C*-4'), 130.0 (*C*-7a), 124.0 (*C*-3'), 123.6 (*C*-5'), 113.4 (*C*-6), 110.5 (*C*-7), 101.9 (*C*-4), 32.4 (*C*-1) ppm.
MS (EI, 70 eV): *m/z* (%) = 224.11 (100) $[M]^+$, 208.09 (2) $[C_{13}H_{10}N_3]^+$, 146.08 (39) $[C_8H_8N_3]^+$.
HRMS (EI, 70 eV): *m/z* (%) ($C_{13}H_{12}N_4$) =

	mass [*m/z*]	mass difference [ppm]	calc. formula
calculated	224.10620		
measured	224.10607	-0.56	$C_{13}H_{12}N_4$

7.4.12 Synthesis of 1-methyl-2-(pyridin-2'-yl)-1*H*-benzo[*d*]imidazol-6-amine (98)[19]

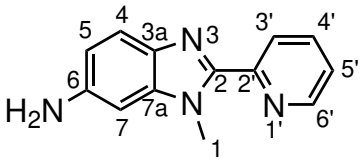

98

Method A: The reaction conditions were adapted from Wolfe *et al.*.[19] The reaction was performed under a nitrogen atmosphere. In a three-neck flask compound **93** (348 mg, 1.21 mmol), sodium *tert*-butoxide (174 mg, 1.81 mmol), *R*-BINAP (22.5 mg, 3.0 mol%) and $Pd_2(dba)_3$ (16.6 mg, 1.5 mol%) were dissolved in toluene (dry, 5 mL). Benzophenone imine (**96**) (203 µL, 1.21 mmol) was added and the reaction was stirred at 90 °C for 21.25 h. After cooling to room temperature ethyl acetate (50 mL) and deion. water (50 mL) were added, the phases were separated, the org. layer was dried over magnesium sulfate and the solvent was removed *in vacuo*. Hydrochloric acid (2 M, 0.5 mL) was added and the reaction was stirred at room temperature for 1.5 h. Afterwards, hydrochloric acid (0.5 M, 50 mL) and ethyl acetate (100 mL) were added, the layers were separated and the pH-value of the aqueous layer was adjusted to >7 using sodium hydroxide solution (2 M). The aqueous layer was

extracted with ethyl acetate (200 mL), the org. layer was dried over magnesium sulfate and the solvent was removed *in vacuo*. The crude product **98** was used in the next step without further purification.

Yield: 200 mg (crude product)

Method B: The reaction conditions were adapted from Wolfe *et al.*.[19] The reaction was performed under a nitrogen atmosphere. In a three-neck flask compound **93** (348 mg, 1.21 mmol), sodium *tert*-butoxide (174 mg, 1.81 mmol), *R*-BINAP (22.5 mg, 3.0 mol%) and $Pd_2(dba)_3$ (16.6 mg, 1.5 mol%) were dissolved in toluene (dry, 5 mL). Benzophenone imine (**96**) (203 µL, 1.21 mmol) was added and the reaction was stirred at 90 °C for 22.5 h. After cooling to room temperature ethyl acetate (50 mL) and deion. water (50 mL) were added, the phases were separated, the org. layer was dried over magnesium sulfate and the solvent was removed *in vacuo*. Hydrochloric acid (1.5 M, 1 mL) was added and the reaction was stirred at room temperature for 1.5 h. Afterwards, hydrochloric acid (0.75 M, 50 mL) and ethyl acetate (50 mL) were added, the layers were separated and the pH-value of the aqueous layer was adjusted to 9 using sodium hydroxide solution (2 M). The aqueous layer was extracted with ethyl acetate (50 mL), the org. layer was dried over magnesium sulfate and the solvent was removed *in vacuo*. The product **98** was obtained as a yellow syrup-oilish solid.

Yield: 183 mg (816 µmol, 68%)

^{1}H NMR (500 MHz, DMSO – d_6, 298 K): δ = 6.95 (dd, ^3J = 8.0 Hz, ^4J = 1.6 Hz, 1 H, *H*-4'), 6.89 (d, ^4J = 1.6 Hz , 2 H, *H*-6'), 6.62 (d, ^3J = 8.0 Hz, 1 H, *H*-3'), 4.63 (s, 2 H, *H*-1), 3.13 (br, 2 H, N-*H*), 2.23 (s, 3 H, *H*-7') ppm.
^{13}C NMR (126 MHz, DMSO – d_6, 298 K): δ = 143.4 (*C*-2'), 129.8 (*C*-6'), 129.7 (*C*-4'), 127.5 (*C*-5'), 125.0 (*C*-1'), 116.2 (*C*-3'), 64.3 (*C*-1), 20.3 (*C*-7') ppm.
MS (EI, 70 eV): *m/z* (%) = 224.11 (100) $[M]^+$, 208.09 (1) $[C_{13}H_{10}N_3]^+$, 146.07 (34) $[C_8H_8N_3]^+$.
HRMS (EI, 70 eV): *m/z* (%) ($C_{13}H_{12}N_4$) =

	mass [*m/z*]	mass difference [ppm]	calc. formula
calculated	224.10620		
measured	224.10627	0.32	$C_{13}H_{12}N_4$

7.4.13 Synthesis of (*E*/*Z*)-1-methyl-5-(phenyldiazenyl)-2-(pyridin-2'-yl)-1*H*-benzo[*d*]imidazole (*E*: 68, *Z*: 101)[16]

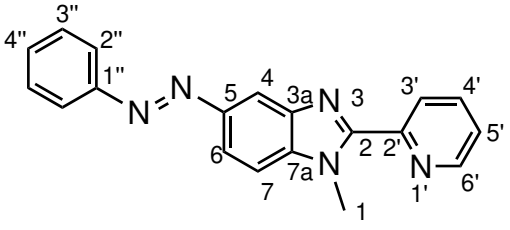

68

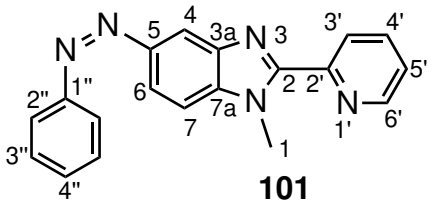

101

The reaction conditions were adapted from Hasegawa *et al.*.[16] In a three-neck flask, wrapped into aluminum foil, nitrosobenzene (**79**) (59.3 mg, 554 µmol) and compound **86** (113 mg, 504 µmol) were dissolved in a mixture of chloroform (3 mL) and glacial acetic acid (2 ml) and the reaction mixture was stirred at room temperature for 23 h. The solvent was removed *in vacuo*. Purification by flash chromatography (silica gel, acetone) and recrystallisation from hexane, with small amounts of dichloromethane, gave the product **68** as red crystals, suitable for X-ray crystallography.

Yield: 40.2 mg (128 µmol, 25%)

Compound **68** (*E* isomer):
^{1}H NMR (600 MHz, acetone–d_6, 298 K): δ = 8.78 (ddd, ^3J = 4.8 Hz, ^4J = 1.7 Hz, ^5J = 1.0 Hz, 1 H, *H*-6'), 8.47 (dt, ^3J = 8.0 Hz, ^5J = 1.0 Hz, 1 H, *H*-3'), 8.31 (unres. dd, ^4J = 1.7 Hz, 1 H, *H*-4), 8.04-8.01 (m, 2 H, *H*-6,4'), 7.98-7.95 (m, 2 H, *H*-2"), 7.76 (d, ^3J = 8.7 Hz, 1 H, *H*-7), 7.62-7.58 (m, 2 H, *H*-3"), 7.54 (unres. dt, ^4J = 1.1 Hz, 1 H, *H*-4"), 7.53 (unres. ddd, ^3J = 4.8 Hz, ^4J = 1.0 Hz, 1 H, *H*-5'), 4.39 (s, 3 H, *H*-1) ppm.
^{13}C NMR (151 MHz, acetone–d_6, 298 K): δ = 153.6 (*C*-1"), 152.9 (*C*-2), 151.5 (*C*-2'), 149.8 (*C*-5), 149.6 (*C*-6'), 143.8 (*C*-3a), 140.8 (*C*-7a), 138.0 (*C*-4'), 131.6 (*C*-4"), 130.1 (*C*-3"), 125.6 (*C*-3'), 125.1 (*C*-5'), 123.4 (*C*-2"), 118.3 (*C*-6), 117.1 (*C*-4), 111.7 (*C*-7), 33.6 (*C*-1) ppm.
HRMS (ESI): *m/z* (%) ($C_{19}H_{16}N_5$ ($[M+H]^+$)) =

	mass [*m/z*]	mass difference [ppm]	calc. formula
calculated	314.14002		
measured	314.13939	-2.01	$C_{19}H_{16}N_5$ ($[M+H]^+$)

FT-IR: $\tilde{\nu}$ = 2970.7 (w), 2025.0 (m), 1755.5 (m), 1738.0 (s), 1444.4 (w), 1365.6 (m), 1217.0 (s), 1060.0 (w) cm^{-1}.

Compound **101** (*Z* isomer):
^{1}H NMR (600 MHz, acetone–d_6, 298 K): δ = 8.73 (ddd, ^3J = 4.8 Hz, ^4J = 1.8 Hz, ^5J = 1.0 Hz, 1 H, *H*-6'), 8.35 (dt, ^3J = 7.8 Hz, ^5J = 1.0 Hz, 1 H, *H*-3'), 7.97 (td, ^3J = 7.8 Hz, ^4J = 1.8 Hz, 1 H, *H*-4'), 7.51 (d, ^3J = 8.6 Hz, ^5J = 0.4 Hz, 1 H, *H*-7), 7.48 (ddd, ^3J = 7.8 Hz, ^3J = 4.8 Hz, ^4J = 1.0 Hz, 1 H, *H*-5'), 7.32-7.28 (m, 2 H, *H*-3"), 7.20 (dd, ^4J = 1.9 Hz, ^5J = 0.4 Hz, 1 H, *H*-4), 7.16-7.13 (m, 1 H, *H*-4"), 6.94 (dd, ^3J = 8.6 Hz, ^4J = 1.9 Hz, 1 H, *H*-6), 6.91-6.88 (m, 2 H, *H*-2"), 4.28 (s, 3 H, *H*-1) ppm.
^{13}C NMR (151 MHz, acetone–d_6, 298 K): δ = 155.7 (*C*-1"), 152.5 (*C*-2), 151.5 (*C*-2'), 150.2 (*C*-5), 149.7 (*C*-6'), 143.3 (*C*-3a), 138.0 (*C*-4'), 137.6 (*C*-7a), 129.9 (*C*-3"), 127.6 (*C*-4"), 125.5 (*C*-3'), 125.1 (*C*-5'), 120.8 (*C*-2"), 118.3 (*C*-6), 112.9 (*C*-4), 111.4 (*C*-7), 33.5 (*C*-1) ppm.
Mass spectrometry data was not collected.

7.4.14 Synthesis of (*E*/*Z*)-1-methyl-6-(phenyldiazenyl)-2-(pyridin-2'-yl)-1*H*-benzo[*d*]imidazole (*E*: 69, *Z*: 102)[16]

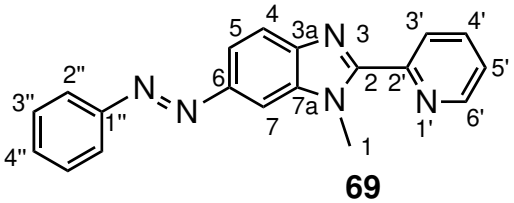

69

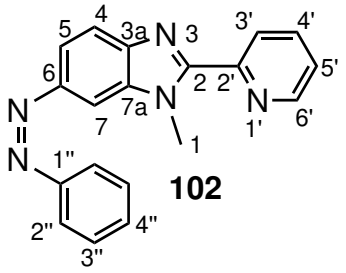

102

The reaction conditions were adapted from Hasegawa *et al.*.[16] In a three-neck flask, wrapped into aluminum foil, nitrosobenzene (**79**) (105 mg, 980 μmol) and compound **98** (200 mg, crude product) were dissolved in a mixture of chloroform (5.4 mL) and glacial acetic acid (3.6 ml) and the reaction mixture was stirred at room temperature for 22 h. The solvent was removed *in vacuo*. Purification by flash chromatography (silica gel, acetone) and recrystallisation from hexane, with small amounts of dichloromethane, gave the product **69** as a red solid. Single crystals were obtained by repeating the procedure with pure amine **98** following the same purification process.

Yield: 79.0 mg (252 μmol, 21% over three steps).

Compound **69** (*E* isomer):

^{1}H NMR (600 MHz, acetone–d_6, 298 K): δ = 8.79 (ddd, ^{3}J = 4.7 Hz, ^{4}J = 1.7 Hz, ^{5}J = 1.0 Hz, 1 H, *H*-6'), 8.47 (dt, ^{3}J = 7.8 Hz, ^{5}J = 1.0 Hz, 1 H, *H*-3'), 8.20 (unres. dd, ^{4}J = 1.8 Hz, 1 H, *H*-7), 8.03 (td, ^{3}J = 7.8 Hz, ^{4}J = 1.7 Hz, 1 H, *H*-4'), 7.99-7.96 (m, 3 H, *H*-2",5), 7.85 (dd, ^{3}J = 8.6 Hz, ^{5}J = 0.4 Hz, 1 H, *H*-4), 7.62-7.59 (m, 2 H, *H*-3"), 7.56-7.52 (m, 2 H, *H*-4",5'), 4.46 (s, 3 H, *H*-1) ppm.

^{13}C NMR (151 MHz, acetone–d_6, 298 K): δ = 153.6 (*C*-1"), 153.4 (*C*-2), 151.4 (*C*-2'), 149.8 (*C*-6), 149.7 (*C*-6'), 146.2 (*C*-3a), 139.0 (*C*-7a), 138.0 (*C*-4'), 131.7 (*C*-4"), 130.2 (*C*-3"), 125.6 (*C*-3'), 125.2 (*C*-5'), 123.4 (*C*-2"), 120.9 (*C*-4), 118.3 (*C*-5), 107.3 (*C*-7), 33.6 (*C*-1) ppm.

HRMS (ESI): *m/z* (%) ($C_{19}H_{16}N_5$ ($[M+H]^+$)) =

	mass [*m/z*]	mass difference [ppm]	calc. formula
calculated	314.14002		
measured	314.13945	-1.81	$C_{19}H_{16}N_5$ ($[M+H]^+$)

Compound **102** (*Z* isomer):

^{1}H NMR (500 MHz, acetone–d_6, 298 K): δ = 8.74 (ddd, ^{3}J = 4.8 Hz, ^{4}J = 1.9 Hz, ^{5}J = 1.0 Hz, 1 H, *H*-6'), 8.37 (dt, ^{3}J = 7.6 Hz, ^{5}J = 1.0 Hz, 1 H, *H*-3'), 7.98 (td, ^{3}J = 7.6 Hz, ^{4}J = 1.9 Hz, 1 H, *H*-4'), 7.54 (dd, ^{3}J = 8.5 Hz, ^{5}J = 0.6 Hz, 1 H, *H*-4), 7.49 (ddd, ^{3}J = 7.6 Hz, ^{3}J = 4.8 Hz, ^{4}J = 1.0 Hz, 1 H, *H*-5'), 7.31-7.27 (m, 2 H, *H*-3"), 7.24 (dd, ^{4}J = 1.9 Hz, ^{5}J = 0.6 Hz, 1 H, *H*-7), 7.17-7.14 (m, 1 H, *H*-4"), 6.92-6.89 (m, 2 H, *H*-2"), 6.73 (dd, ^{3}J = 8.5 Hz, ^{4}J = 1.9 Hz, 1 H, *H*-5), 4.22 (s, 3 H, *H*-1) ppm.

^{13}C NMR (125 MHz, acetone–d_6, 298 K): δ = 155.5 (*C*-1"), 152.6 (*C*-2), 150.6 (*C*-6), 149.6 (*C*-6'), 142.7 (*C*-3a), 138.3 (*C*-7a), 137.9 (*C*-2'), 129.7 (*C*-3"), 127.7 (*C*-4"), 125.4 (*C*-3'), 125.0 (*C*-5'), 123.5 (*C*-4'), 120.9 (*C*-2"), 120.4 (*C*-4), 116.5 (*C*-5), 104.9 (*C*-7), 33.3 (*C*-1) ppm.

Mass spectrometry data was not collected.

7.4.15 Synthesis of complex 103[16]

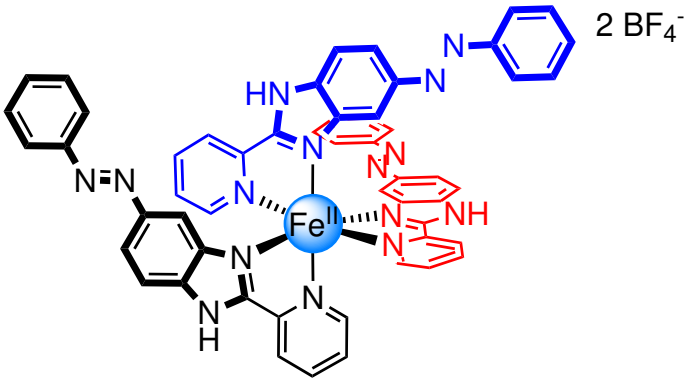

103

In a test tube azobenzene **67** (53.3 mg, 178 μmol) and iron tetrafluoroborate hexahydrate (20.0 mg, 59.4 μmol) were dissolved in CD_3CN (6 mL). The solution was split into two 3 mL portions and and each portion was added to diethyl ether (20 mL). The mixtures were centrifuged, washed with diethyl ether (10 mL) and were again centrifuged before dried on air.

Note: Nishihara and co-workers used a different procedure, which was also attempted, but unsuccessful.[16] Therefore, the procedure from McConnell and co-workers for metal-organic cages was adapted.[13]

Yield: 25.0 mg (21.9 μmol, 37%)

MS (ESI): *m/z* (%) = 476.6423 [**103**]$^{2+}$.

7.4.16 Synthesis of 5,6-dibromo-2-(pyridin-2'-yl)-1*H*-benzo[*d*]imidazole (106)[20]

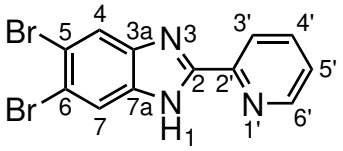

106

The reaction conditions were adapted from Kriete *et al.*.[20] In a three-neck flask compound **76** (500 mg, 2.56 mmol) was dissolved in glacial acetic acid (3.7 mL), was heated to 60 °C and *N*-bromosuccinimide (957 mg, 5.38 mmol) was added. The reaction mixture was stirred at 60 °C for 22 h before cooled to room temperature and the solution was filtered. Ammonia solution (25%) was added to the filtrate to adjust the pH-value to 7 and the solution was again filtered and the solvent of the filtrate was removed *in vacuo*. Purification by flash chromatography (silica gel, 20% ethyl acetate:cyclohexane) and recrystallisation from toluene gave the product **106** as a beige solid.

Yield: 293 mg (830 µmol, 32%)

^{1}H NMR (500 MHz, DMSO – d_6, 298 K): δ = 13.4 (s, 1 H, *H*-1) 8.76 (ddd, ^3J = 4.7 Hz, ^4J = 1.7 Hz, ^5J = 1.0 Hz, 1 H, *H*-6'), 8.32 (dt, ^3J = 7.7 Hz, ^5J = 1.0 Hz, 1 H, *H*-3'), 8.14 (br, 1 H, *H*-4), 8.04 (td, ^3J = 7.7 Hz, ^4J = 1.7 Hz, 1 H, *H*-4'), 7.87 (br, 1 H, *H*-7), 7.58 (ddd, ^3J = 7.7 Hz, ^3J = 4.7 Hz, ^4J = 1.0 Hz, 1 H, *H*-5') ppm.
^{13}C NMR (126 MHz, DMSO – d_6, 298 K): δ = 152.8 (*C*-2), 149.5 (*C*-6'), 147.5 (*C*-2'), 144.3 (*C*-3a), 137.7 (*C*-4'), 135.2 (*C*-7a), 125.3 (*C*-5'), 123.6 (*C*-4), 121.8 (*C*-3'), 117.1 (*C*-6), 116.3 (*C*-7), 116.1 (*C*-5) ppm.
MS (EI, 70 eV): *m/z* (%) = 350.93 (51) $[M]^+$, 272.00 (4) $[C_{12}H_7Br_1N_3]^+$, 193.08 (39) $[C_{12}H_7N_3]^+$.
HRMS (EI, 70 eV): *m/z* (%) ($C_{12}H_7{}^{79}Br_2N_3$) =

	mass [*m/z*]	mass difference [ppm]	calc. formula
calculated	350.90067		
measured	350.90024	-1.22	$C_{12}H_7{}^{79}Br_2N_3$

FT-IR: $\tilde{\nu}$ = 3562.9 (w), 3087.8 (m), 1770.6 (w), 1699.7 (w), 1650.8 (w), 1592.9 (m), 1570.8 (w), 1464.8 (m), 1436.3 (s), 1420.9 (s), 1384.4 (s), 1284.4 (s), 1078.0 (m), 994.5 (m), 967.7 (m), 927.0 (m), 857.1 (s) cm^{-1}.

7.4.17 Synthesis of 3-bromo-2,5-dimethylthiophene (108)[21]

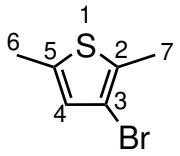

108

The reaction conditions were adapted from Ando *et al.*.[21] In a round-bottom flask, wrapped into aluminum foil, 2,5-dimethylthiophene (**107**) (3.03 g, 27.0 mmol) was dissolved in dichloromethane (200 mL). *N*-Bromosuccinimide (4.81 g, 27.0 mmol) was added and the reaction mixture was stirred at room temperature for 48.5 h. The solvent was removed *in vacuo* and purification by flash chromatography (silica gel, cyclohexane) gave the product **108** as a colourless oil.

Yield: 4.89 g (25.6 mmol, 95%) (Lit.:[21] 75%).

^{1}H NMR (500 MHz, $CDCl_3$, 298 K): $\delta =$ 6.55 (d, $^4J = 0.8$ Hz, 1 H, *H*-4), 2.39 (d, $^4J = 0.8$ Hz, 3 H, *H*-6), 2.32 (s, 3 H, *H*-7) ppm.
^{13}C NMR (126 MHz, $CDCl_3$, 298 K): δ = 136.9 (*C*-5), 131.6 (*C*-2), 127.6 (*C*-4), 108.0 (*C*-3), 15.3 (*C*-6), 14.5 (*C*-7) ppm.
Mass spectrometry data was not collected.

7.4.18 Synthesis of (2,5-dimethylthiophen-3-yl)boronic acid (109)[22]

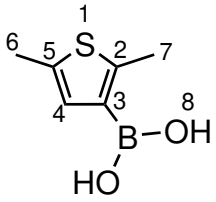

109

The reaction conditions were adapted from Ko *et al.*.[22] The reaction was performed under a nitrogen atmosphere. In a three-neck flask compound **108** (1.49 g, 7.80 mmol) was dissolved in tetrahydrofuran (dry, 25 mL). The solution was cooled to -78 °C and *n*-butyllithium (2.5 M in hexane, 3.80 mL,

9.50 mmol) was added and stirring was continued for 1.5 h. Tributyl borate (2.10 mL, 7.82 mmol) was added and the mixture was stirred at -78 °C for 5 h before the addition of hydrochloric acid (2 M, 20 mL). The reaction mixture was warmed to room temperature and was stirred for 14.5 h. The layers were separated and the aqueous layer was extracted with diethyl ether (50 mL). The org. layers were combined, extracted with sodium hydroxide solution (2 M, 80 mL), the layers were separated and the pH-value of the aqueous layer was adjusted to 7 using hydrochloric acid (12 M). The product **109** was collected by filtration as a colourless solid as the boroxine.

Yield: 855 mg (5.48 mmol, 70%) (Lit.:[22] 87%).

^{1}H NMR (500 MHz, $CDCl_3$, 298 K): δ = 7.08 (d, ^{4}J = 1.0 Hz, 3 H, *H*-4), 2.82 (s, 9 H, *H*-7), 2.46 (d, ^{4}J = 1.0 Hz, 9 H, *H*-6) ppm.
^{13}C NMR (126 MHz, $CDCl_3$, 298 K): δ = 153.7 (*C*-2), 135.9 (*C*-5), 131.5 (*C*-4), 129.7 (*C*-3), 16.1 (*C*-7), 14.9 (*C*-6) ppm.
MS (EI, 70 eV): *m/z* (%) = 156.04 (30) $[M]^+$.
HRMS (EI, 70 eV): *m/z* (%) ($C_6H_9{}^{11}B_1O_2{}^{32}S_1$) =

	mass [*m/z*]	mass difference [ppm]	calc. formula
calculated	156.04163		
measured	156.04143	-0.21	$C_6H_9{}^{11}B_1O_2{}^{32}S_1$

FT-IR: $\tilde{\nu}$ = 3221.0 (m), 2915.1 (w), 1551.2 (m), 1482.3 (s), 1367.7 (s), 1305.0 (s), 1241.8 (s), 1147.9 (m), 1131.9 (m), 846.1 (m) cm^{-1}.

7.4.19 Synthesis of *tert*-butyl 5',6'-dibromo-2'-(pyridin-2''-yl)-1*H*-benzo[*d*]imidazole-1-carboxylate (114)[2]

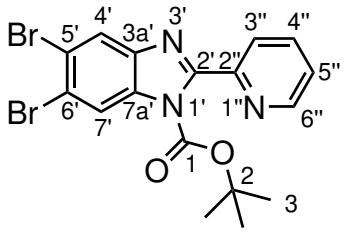

114

The reaction conditions were adapted from Taylor *et al.*.[2] In a round-bottom flask compound **106** (353 mg, 1.00 mmol), di-*tert*-butyl dicarbonate (240 mg, 1.10 mmol) and 4-dimethylaminopyridine (12.2 mg, 99.9 µmol) were dissolved in dichloromethane (dry, 10 mL) and the reaction was stirred at room temperature for 21 h. The solvent was removed *in vacuo* and the crude product was purified by flash chromatography (silica gel, 20% ethyl acetate:cyclohexane) to obtain the product **114** as a colourless solid. Impure fractions were further purified by recrystallisation from methanol.

Yield: 133 mg (294 µmol, 29%)

^{1}H NMR (500 MHz, DMSO–d_6, 298 K): δ = 8.76 (ddd, ^3J = 4.9 Hz, ^4J = 1.6 Hz, ^5J = 0.9 Hz, 1 H, *H*-6''), 8.29 (s, 1 H, *H*-4'), 8.26 (s, 1 H, *H*-7'), 8.05 (ddd, ^3J = 8.3 Hz, ^3J = 7.8 Hz, ^4J = 1.6 Hz, 1 H, *H*-4''), 7.96-7.93 (m, 1 H, *H*-3''), 7.62 (ddd, ^3J = 7.8 Hz, ^3J = 4.9 Hz, ^4J = 1.1 Hz, 1 H, *H*-5''), 1.32 (s, 9 H, *H*-3) ppm.
^{13}C NMR (126 MHz, DMSO–d_6, 298 K): δ = 153.2 (*C*-1), 149.2 (*C*-2''), 149.0 (*C*-6''), 147.2 (*C*-2'), 142.1 (*C*-3a'), 137.2 (*C*-4''), 133.5 (*C*-7a'), 125.0 (*C*-5''), 124.6 (*C*-4'), 123.9 (*C*-3''), 119.9 (*C*-6'), 118.8 (*C*-5'), 118.0 (*C*-7'), 86.0 (*C*-2), 26.7 (*C*-3) ppm.
MS (EI, 70 eV): *m/z* (%) = 450.95 (2) $[M]^+$, 349.89 (1) $[C_{12}H_6Br_2N_3]^+$, 270.97 (3) $[C_{12}H_6Br_3N_3]^+$, 192.05 (4) $[C_{12}H_6N_3]^+$.
HRMS (ESI): *m/z* (%) ($C_{17}H_{15}{}^{79}Br_2N_3O_2$) =

	mass [*m/z*]	mass difference [ppm]	calc. formula
calculated	450.95310		
measured	450.95277	-0.73	$C_{17}H_{15}{}^{79}Br_2N_3O_2$

FT-IR: $\tilde{\nu}$ = 3748.7 (w), 2924.3 (w), 1741.3 (s), 1591.1 (w), 1568.8 (w), 1534.6 (w), 1455.7 (w), 1433.6 (s), 1394.9 (w), 1370.8 (m), 1331.8 (s), 1291.9 (w), 1249.5 (w), 1227.8 (s), 1141.4 (s), 1091.1 (w), 1063.6 (m), 1046.8 (w), 992.8 (w), 947.6 (w), 872.4 (m), 859.7 (m), 848.2 (s), 833.6 (m) cm^{-1}.

7.4.20 Synthesis of 1-benzyl-2-(pyridin-2'-yl)-1*H*-benzo[*d*]imidazole 116[23]

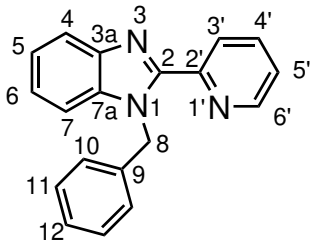

116

The reaction conditions were adapted from Huang *et al.*.[23] In a three-neck flask compound **76** (437 mg, 2.24 mmol) was dissolved in *N*,*N*-dimethylformamide (dry, 5 mL). Afterwards, potassium carbonate (496 mg, 3.59 mmol) and benzyl bromide (350 µL, 2.94 mmol) were added. The reaction mixture was stirred at room temperature for 23.25 h and the solvent was removed *in vacuo* (55 °C, 16-20 mbar). The residue was redissolved in ethyl acetate (75 mL), was washed with deion. water (50 mL), brine (200 mL) and sodium hydroxide solution (10%, w/w, 50 mL). The org. layer was dried over magnesium sulfate and the solvent was removed *in vacuo*. Purification by flash chromatography (silica gel, 20% ethyl acetate:cyclohexane) gave the product **116** as a beige solid.

Yield: 360 mg (1.26 mmol, 56%) (Lit.:[23] 77%).

^{1}H NMR (500 MHz, DMSO–d_6, 298 K): δ = 8.71 (ddd, ^3J = 4.8 Hz, ^4J = 1.8 Hz, ^5J = 1.0 Hz, 1 H, *H*-6'), 8.38 (dt, ^3J = 8.0 Hz, ^5J = 1.0 Hz, 1 H, *H*-3'), 8.02 (ddd, ^3J = 8.0 Hz, ^3J = 7.6 Hz, ^4J = 1.8 Hz, 1 H, *H*-4'), 7.79-7.75 (m, 1 H, *H*-4), 7.61-7.56 (m, 1 H, *H*-7), 7.52 (ddd, ^3J = 7.6 Hz, ^3J = 4.8 Hz, ^4J = 1.2 Hz, 1 H, *H*-5'), 7.31-7.22 (m, 4 H, *H*-5,6,11), 7.22-7.17 (m, 1 H, *H*-12), 7.15-7.12 (m, 2 H, *H*-10), 6.24 (s, 2 H, *H*-8) ppm.
^{13}C NMR (126 MHz, DMSO–d_6, 298 K): δ = 149.9 (*C*-2), 149.2 (*C*-2'), 148.7 (*C*-6'), 142.1 (*C*-3a), 137.6 (*C*-9), 137.4 (*C*-4'), 136.4 (*C*-7a), 128.4 (*C*-11), 127.1 (*C*-12), 126.6 (*C*-10), 124.3 (*C*-5'), 124.2 (*C*-3'), 123.3 (*C*-5/6), 122.5 (*C*-5/6), 119.5 (*C*-4), 111.2 (*C*-7), 47.8 (*C*-8) ppm.

MS (EI, 70 eV): *m/z* (%) = 285.13 (84) $[M]^+$, 194.07 (1) $[C_{12}H_8N_3]^+$.
HRMS (EI, 70 eV): *m/z* (%) ($C_{19}H_{15}N_3$) =

	mass [*m/z*]	mass difference [ppm]	calc. formula
calculated	285.12660		
measured	285.12645	-0.53	$C_{19}H_{15}N_3$

FT-IR: $\tilde{\nu}$ = 1736.5 (s), 1439.5 (s), 1368.5 (s), 1217.1 (m) cm^{-1}.

7.4.21 Synthesis of 1-benzyl-5,6-dibromo-2-(pyridin-2'-yl)-1*H*-benzo[*d*]imidazole (117)[24]

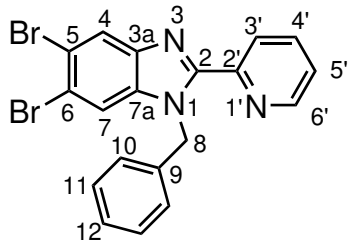

117

The reaction conditions were adapted from Kriete *et al.*.[20] In a three-neck flask compound **106** (791 mg, 2.24 mmol) was dissolved in *N*,*N*-dimethylformamide (dry, 7 mL). Afterwards, potassium carbonate (496 mg, 3.59 mmol) and benzyl bromide (350 µL, 2.94 mmol) were added. The reaction mixture was stirred at room temperature for 24 h and *N*,*N*-dimethylformamide was removed *in vacuo* (55 °C, 16 mbar). The residue was redissolved in ethyl acetate (200 mL), was washed with deion. water (200 mL), brine (200 mL) and sodium hydroxide solution (10%, w/w, 50 mL). The org. layer was dried over magnesium sulfate and the solvent was removed *in vacuo*. Purification by flash chromatography (silica gel, 20% ethyl acetate:cyclohexane) gave the product **116** as a colourless solid.

Yield: 421 mg (1.19 mmol, 42%)

^{1}H NMR (600 MHz, DMSO – d_6, 298 K): δ = 8.70 (ddd, ^3J = 4.8 Hz, ^4J = 1.8 Hz, ^5J = 1.1 Hz, 1 H, *H*-6'), 8.32 (dt, ^3J = 7.8 Hz, ^5J = 1.1 Hz, 1 H, *H*-3'), 8.18 (s, 1 H, *H*-4), 8.10 (s, 1 H, *H*-7), 8.01 (td, ^3J = 7.8 Hz, ^4J = 1.8 Hz, 1 H, *H*-4'), 7.54 (ddd, ^3J = 7.8 Hz, ^3J = 4.8 Hz, ^4J = 1.1 Hz, 1 H, *H*-5'), 7.26-7.22 (m, 2 H, *H*-11), 7.21-7.18 (m, 1 H, *H*-12), 7.09-7.06 (m, 2 H, *H*-10), 6.21 (s, 2 H, *H*-8) ppm.
^{13}C NMR (151 MHz, DMSO – d_6, 298 K): δ = 151.4 (*C*-2), 149.2 (*C*-2'), 149.1 (*C*-6'), 142.7 (*C*-3a), 137.9 (*C*-4'), 137.3 (*C*-9), 137.0 (*C*-7a), 128.8 (*C*-11), 127.5 (*C*-12), 126.7 (*C*-10), 125.1 (*C*-5'), 124.8 (*C*-3'), 124.0 (*C*-4), 117.9 (*C*-6), 117.2 (*C*-5), 116.2 (*C*-7), 48.3 (*C*-8) ppm.
HRMS (ESI): *m/z* (%) ($C_{19}H_{14}{}^{79}Br_2N_3$ ([M+H]$^+$)) =

	mass [*m/z*]	mass difference [ppm]	calc. formula
calculated	441.95490		
measured	441.95420	-1.59	$C_{19}H_{14}{}^{79}Br_2N_3$ ([M+H]$^+$)

FT-IR: $\tilde{\nu}$ = 2931.2 (w), 2250.8 (w), 1589.0 (m), 1567.9 (w), 1495.3 (w), 1440.2 (s), 1426.0 (m), 1382.4 (m), 1350.3 (m), 1306.0 (m), 1282.3 (m), 1149.7 (w), 1096.4 (w), 1073.8 (w), 1046.8 (w), 994.2 (w), 924.5 (w), 889.9 (m), 830.9 (s) cm^{-1}.

7.4.22 Synthesis of 1-methyl-2-(pyridin-2'-yl)-1*H*-benzo[*d*]imidazole (119)[12]

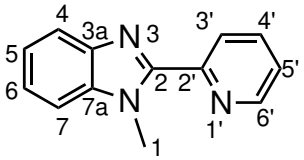

119

The reaction conditions were adapted from Lin *et al.*.[12] In a round-bottom flask compound **76** (1.14 g, 5.84 mmol) and potassium carbonate (milled, 2.50 g, 18.1 mmol) were dissolved in *N*,*N*-dimethylformamide (25 mL). Methyl iodide (500 μL, 8.04 mmol) was added and the reaction was stirred at room temperature for 20 h. The solution was poured into deion. water (100 mL) and the aqueous layer was extracted with ethyl acetate (3 x 50 mL). The org. layers were combined, washed with brine (200 mL) and sodium hydroxide solution (10%, w/w, 120 mL). The org. layer was dried over magnesium sulfate and the solvent was removed *in vacuo*.

Yield: 989 mg (4.73 mmol, 81%)

^{1}H NMR (500 MHz, DMSO–d_6, 298 K): δ = 8.76 (ddd, ^3J = 4.8 Hz, ^4J = 1.8 Hz, ^5J = 0.9 Hz, 1 H, *H*-6'), 8.31 (dt, ^3J = 8.0 Hz, ^4J = 1.2 Hz , 2 H, *H*-3'), 8.01 (ddd, ^3J = 8.0 Hz, ^3J = 7.7 Hz, ^4J = 1.8 Hz, 1 H, *H*-4'), 7.73 (ddd, ^3J = 8.1 Hz, ^4J = 1.2 Hz, ^5J = 0.8 Hz, 1 H, *H*-4), 7.65 (ddd, ^3J = 8.2 Hz, ^4J = 1.2 Hz, ^5J = 0.8 Hz, 1 H, *H*-7), 7.53 (ddd, ^3J = 7.7 Hz, ^3J = 4.8 Hz, ^4J = 1.2 Hz, 1 H, *H*-5'), 7.34 (ddd, ^3J = 8.1 Hz, ^3J = 7.2 Hz, ^4J = 1.2 Hz, 1 H, *H*-6), 7.28 (ddd, ^3J = 8.2 Hz, ^3J = 7.2 Hz, ^4J = 1.2 Hz, 1 H, *H*-5), 4.24 (s, 3 H, *H*-1) ppm.
^{13}C NMR (126 MHz, DMSO–d_6, 298 K): δ = 150.0 (*C*-2'), 149.6 (*C*-2), 148.7 (*C*-6'), 141.9 (*C*-3a), 137.3 (*C*-4'), 137.0 (*C*-7a), 124.3 (*C*-3'), 124.1 (*C*-5'), 123.0 (*C*-6), 122.2 (*C*-5), 119.3 (*C*-4), 110.7 (*C*-7), 32.5 (*C*-1) ppm.
MS (EI, 70 eV): *m/z* (%) = 209.10 (63) $[M+H]^+$, 208.09 (100) $[M]^+$, 131.06 (16) $[C_8H_7N_2]^+$.
HRMS (EI, 70 eV): *m/z* (%) ($C_{13}H_{10}N_3$) =

	mass [*m/z*]	mass difference [ppm]	calc. formula
calculated	208.08747		
measured	208.08740	-0.34	$C_{13}H_{10}N_3$

FT-IR: $\tilde{\nu}$ = 3047.9 (w), 2946.0 (w), 1739.4 (w), 1668.3 (w), 1589.2 (m), 1564.9 (m), 1212.3 (w), 1470.1 (m), 1445.0 (s), 1423.3 (s), 1382.2 (s), 1328.4 (m), 1293.5 (w), 1279.3 (m), 1254.8 (m), 1216.2 (w), 1147.2 (m), 1090.3 (m), 1067.6 (w), 1043.7 (m), 1008.6 (w), 991.8 (m), 929.5 (w), 903.2 (w), 823.7 (m) cm^{-1}.

7.4.23 Synthesis of 5,6-dibromo-1-methyl-2-(pyridin-2'-yl)-benzimidazole (120)[20]

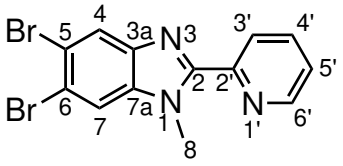

120

The reaction conditions were adapted from Kriete *et al.*.[20] Compound **119** (1.31 g, 6.26 mmol) was dissolved in glacial acetic acid (9 mL), heated to 60 °C and *N*-bromosuccinimide (2.23 g, 12.5 mmol) was added. The reaction mixture was stirred at 60 °C for 20 h before cooled to room temperature. Ammonia solution (25%) was added to adjust the pH-value to 10-13 and the aqueous layer extracted with dichloromethane (3 x 100 mL). The organic layers were combined, dried over magnesium sulfate and the solvent removed *in vacuo*. After recrystallisation from toluene the product **120** was obtained as a brown solid.

Yield: 820 mg (2.23 mmol, 36%)

^{1}H NMR (500 MHz, $CDCl_3$, 298 K): δ = 8.77 (unres. ddd, ^{3}J = 4.7 Hz, 1 H, *H*-6'), 8.29 (dt, ^{3}J = 7.8 Hz, ^{5}J = 0.9 Hz, 1 H, *H*-3'), 8.21 (s, 1 H, *H*-7), 8.14 (s, 1 H, *H*-4), 8.03 (td, ^{3}J = 7.8 Hz, ^{4}J = 1.7 Hz, 1 H, *H*-4'), 7.56 (ddd, ^{3}J = 7.8 Hz, ^{3}J = 4.7 Hz, ^{4}J = 0.9 Hz, 1 H, *H*-5'), 4.22 (s, 3 H, *H*-8) ppm.
^{13}C NMR (126 MHz, $CDCl_3$, 298 K): δ = 151.6 (*C*-2), 149.2 (*C*-2'), 148.9 (*C*-6'), 142.3 (*C*-3a), 137.5 (*C*-4'), 137.4 (*C*-7a), 124.7 (*C*-5'), 124.6 (*C*-3'), 123.5 (*C*-4), 117.2 (*C*-5/6), 116.5 (*C*-5/6), 115.8 (*C*-7), 33.0 (*C*-8) ppm.
MS (EI, 70 eV): *m/z* (%) = 364.91 (44) $[M]^+$.
HRMS (EI, 70 eV): *m/z* (%) ($C_{13}H_9{}^{79}Br_2N_3$) =

	mass [*m/z*]	mass difference [ppm]	calc. formula
calculated	364.91632		
measured	364.91641	0.25	$C_{13}H_9{}^{79}Br_2N_3$

7.4.24 Synthesis of 6,7-di(2",5"-dimethylthiophen-3"-yl)-1-methyl-2-(pyridin-2'-yl)benzimidazole (71)[25]

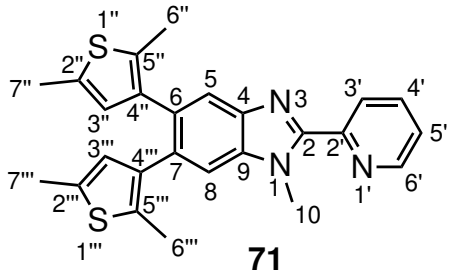

71

The reaction conditions were adapted from Burke *et al.*.[25] The reaction was performed under a nitrogen atmosphere. Compound **120** (268 mg, 730 μmol), potassium carbonate (milled, 252 mg, 1.83 mmol) and $Pd(PPh_3)_4$ (42.2 mg, 5 mol%) were dissolved in ethanol (dry, 12 mL), deion. water (degassed, 12 mL) and tetrahydrofuran (dry, 24 mL). The reaction mixture was degassed using freeze-pump-thaw cycling before the addition of thiophene **109** (228 mg, 1.46 mmol). The reaction mixture was heated at 80 °C for 19 h. Dichloromethane (100 mL) was added, the organic layer was washed with deion. water (1 x 90 mL), half-concentrated potassium carbonate solution (1 x 100 mL), again deion. water (1 x 90 mL) and the last aqueous layer extracted with dichloromethane (2 x 50 mL). The organic layers were combined, dried over magnesium sulfate and the solvent removed *in vacuo*. Purification by flash chromatography (silica gel, 50% ethyl acetate:cyclohexane) and recrystallisation from methanol gave the product **71** as a colourless solid.

Yield: 72.2 mg (168 μmol, 23%)

^{1}H NMR (500 MHz, CD_3CN, 298 K): δ = 8.72 (ddd, ^3J = 4.8 Hz, ^4J = 1.8 Hz, ^5J = 1.1 Hz, 1 H, *H*-6'), 8.34 (dt, ^3J = 7.8 Hz, ^4J = 1.1 Hz, 1 H, *H*-3'), 7.93 (td, ^3J = 7.8 Hz, ^4J = 1.8 Hz, 1 H, *H*-4'), 7.59 (d, ^5J = 0.6 Hz, 1 H, *H*-5), 7.44 (ddd, ^3J = 7.8 Hz, ^3J = 4.8 Hz, ^4J = 1.1 Hz, 1 H, *H*-5'), 7.43 (d, ^5J = 0.6 Hz, 1 H, *H*-8), 6.37-6.36 (m, 1 H, *H*-3"), 6.36-6.34 (m, 1 H, *H*-3"'), 4.26 (s, 3 H, *H*-10), 2.32-2.31 (m, 3 H, *H*-7"), 2.31-2.30 (m, 3 H, *H*-7"'), 2.11-2.10 (m, 6 H, *H*-6",6"') ppm.
^{13}C NMR (126 MHz, CD_3CN, 298 K): δ = 152.3 (*C*-2), 151.8 (*C*-2'), 149.8 (*C*-6'), 142.9 (*C*-6), 139.6 (*C*-4"), 139.6 (*C*-4"'), 138.2 (*C*-4'), 137.9 (*C*-4), 135.3 (*C*-2"), 135.1 (*C*-2"'), 133.4 (*C*-5"), 133.2 (*C*-5"'), 133.1 (*C*-7), 132.4 (*C*-9), 129.6 (*C*-3"'), 129.5 (*C*-3"), 125.5 (*C*-3'), 125.1 (*C*-5'), 121.9 (*C*-5), 113.0 (*C*-8), 33.6 (*C*-10), 15.1 (*C*-7",7"'), 14.0 (*C*-6",6"') ppm.

MS (EI, 70 eV): *m/z* (%) = 429.13 (100) $[M]^+$.
HRMS (EI, 70 eV): *m/z* (%) ($C_{25}H_{23}{}^{32}S_2N_3$) =

	mass [*m/z*]	mass difference [ppm]	calc. formula
calculated	429.13334		
measured	429.13314	-0.46	$C_{25}H_{23}{}^{32}S_2N_3$

7.5 Synthetic Procedures for Chapter 3

7.5.1 Synthesis of 5'-bromopicolinaldehyde (127)[26]

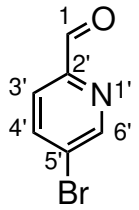

127

The reaction conditions were adapted from Roberts *et al.*.[26] The reaction was performed under a nitrogen atmosphere. In a three-neck flask 2-iodo-5-bromopyridine (**126**) (7.63 g, 27.0 mmol) was dissolved in tetrahydrofuran (dry, 60 mL) and the reaction was cooled to -20 °C. *i*-Propylmagnesium chloride (2 M in tetrahydrofuran, 15.0 mL, 30.0 mmol) was slowly added and the reaction mixture was stirred at -30 °C for 1 h. Afterwards, *N*,*N*-dimethylformamide (3.10 mL, 40.3 mmol) was added and stirring was continud for further 0.5 h. The solution was warmed up to room temperature over 1 h and hydrochloric acid (2 M, 30 mL) was added while keeping the temperature below 20 °C. The pH-value of the solution was adjusted to 9 with sodium hydroxide solution (2 M), the layers were separated and the aqueous layer was extracted with dichloromethane (3 x 75 mL). The org. layers were combined, washed with brine (125 mL), deion. water (25 mL), dried over magnesium sulfate and the solvent was removed *in vacuo*.

Yield: 4.23 g (22.7 mmol, 84%) (Lit.:[26] 99%).

^{1}H NMR (600 MHz, $CDCl_3$, 298 K): δ = 10.0 (s, 1 H, *H*-1), 8.86 (d, ^4J = 1.9 Hz, 1 H, *H*-6'), 8.03 (dd, ^3J = 8.3 Hz, ^4J = 1.9 Hz, 1 H, *H*-4'), 7.86 (d, ^3J = 8.3 Hz, 1 H, *H*-3') ppm.
^{13}C NMR (151 MHz, $CDCl_3$, 298 K): δ = 192.4 (*C*-1), 151.6 (*C*-6'), 151.1 (*C*-2'), 139.9 (*C*-4'), 126.2 (*C*-5'), 122.6 (*C*-3') ppm.
HRMS (ESI): *m/z* (%) ($C_6H_5{}^{79}Br_1N_1O_1$) =

	mass [*m/z*]	mass difference [ppm]	calc. formula
calculated	185.95490		
measured	185.95479	-0.61	$C_6H_5{}^{79}Br_1N_1O_1$

FT-IR: $\tilde{\nu}$ = 2169.8 (m), 2137.4 (m), 1963.0 (m), 1751.2 (s), 1365.2 (w), 1203.4 (w), 837.8 (m), 692.0 (m) cm^{-1}.

7.5.2 Synthesis of 5'-bromo-2'-(1,3-dioxolan-2-yl)pyridine (128)[26]

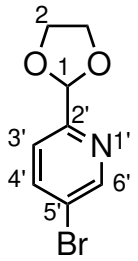

128

The reaction conditions were adapted from Roberts *et al.*.[26] In a round-bottom flask compound **127** (4.00 g, 21.5 mmol), *p*-toluene sulfonic acid (205 mg, 1.08 mmol) and ethylene glycol (4.00 g, 64.4 mmol) were dissolved in toluene (72 mL) and the solution was heated at 135 °C for 22 h in a dean-stark apparatus. After cooling to room temperature sat. sodium hydrogen carbonate (70 mL) was added, the layers were separated and the aqueous layer was extracted with diethyl ether (2 x 75 mL). The org. layers were combined, dried over magnesium sulfate and the solvent was removed *in vacuo* to obtain a brown solid.

Yield: 4.63 g (20.1 mmol, 94%) (Lit.:[26] 99%).

^{1}H NMR (500 MHz, $CDCl_3$, 298 K): δ = 8.68 (dd, ^4J = 2.3 Hz, ^5J = 0.7 Hz, 1 H, *H*-6'), 7.87 (ddd, ^3J = 8.3 Hz, ^4J = 2.3 Hz, ^5J = 0.3 Hz, 2 H, *H*-4'), 7.45-7.43 (m, 1 H, *H*-3'), 5.82 (br, 1 H, *H*-1), 4.19-4.12 (m, 2 H, *H*-2), 4.12-4.05 (m, 2 H, *H*-2) ppm.
^{13}C NMR (126 MHz, $CDCl_3$, 298 K): δ = 155.6 (*C*-2'), 150.5 (*C*-6'), 139.4 (*C*-4'), 122.0 (*C*-3'), 121.1 (*C*-5'), 103.0 (*C*-1), 65.6 (*C*-2) ppm.
MS (ESI,): *m/z* (%) = 229.98 (100) $[M+H]^+$.
HRMS (ESI): *m/z* (%) ($C_8H_9{}^{79}Br_1N_1O_2$) =

	mass [*m/z*]	mass difference [ppm]	calc. formula
calculated	229.98112		
measured	229.98082	-1.29	$C_8H_9{}^{79}Br_1N_1O_2$

FT-IR: $\tilde{\nu}$ = 1089.6 (s), 1008.0 (m), 826.2 (m) cm^{-1}.

7.5.3 Synthesis of 1,2-bis(6'-(1",3"-dioxolan-2"-yl)pyridin-3'-yl)ethyne (130)[7]

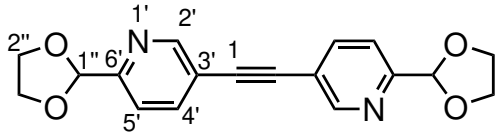

130

Preparation of the 1:1 mixture of compound **128** and **129**: The reaction conditions were adapted from Park *et al.* and Borozdina *et al.*.[7,252] The reaction was performed under a nitrogen atmosphere. In a three-neck flask compound **128** (2.78 g, 12.1 mmol), $Pd(PPh_3)_2Cl_2$ (340 mg, 4 mol%) and copper(I) iodide (230 mg,10 mol%) were dissolved in tetrahydrofuran (dry, 40 mL) and triethylamine (12 mL). Trimethylsilylacetylene (2.73 mL, 19.3 mmol) was added and the reaction mixture stirred at 60 °C for 23 h. The solution was cooled to room temperature, filtered and the residue washed with dichloromethane (100 mL). The solvent was removed *in vacuo*. Purification by flash chromatography (silica gel, 60% dichloromethane:cyclohexane) was unsuccessful. The crude product was dissolved in tetrahydrofuran (20 mL) and sodium hydroxide solution (1 M, 50 mL) was added. The reaction was stirred at room temperature for 40 min. Brine (200 ml) was added, the phases were separated and

the aqueous layer extracted with ethyl acetate (200 mL). The org. layers were combined, dried over magnesium sulfate and the solvent removed *in vacuo*. The crude 1:1 mixture of compound **128** and **129** was used in the next step without further purification.

Synthesis of compound **130**: The reaction conditions were adapted from Park *et al.*.[7] The reaction was performed under a nitrogen atmosphere. In a three-neck flask the 1:1 mixed crude product of compound **128** and **129** (1.65 g, crude product), $Pd(PPh_3)_2Cl_2$ (272 mg, 5 mol%) and copper(I) iodide (44.9 mg, 5 mol%) were dissolved in a mixture of tetrahydrofuran (dry, 22 mL) and triethylamine (6 mL). The reaction was stirred at 80 °C for 23.5 h. After cooling to room temperature the precipitate was collected by filtration and was redissolved in ethyl acetate (10 mL). The solvent of both org. layers was removed *in vacuo*. Purification by flash chromatography (silica gel, ethyl acetate) gave the product **130** as a colourless solid.

Yield: 538 mg (1.66 mmol, 27% over three steps).

^{1}H NMR (600 MHz, $CDCl_3$, 298 K): $\delta =$ 8.78 (dd, $^4J = 2.0$ Hz, $^5J = 0.8$ Hz, 2 H, *H*-2'), 7.88 (dd, $^3J = 8.1$ Hz, $^4J = 2.0$ Hz, 2 H, *H*-4'), 7.56 (dd, $^3J = 8.1$ Hz, $^5J = 0.8$ Hz, 2 H, *H*-5'), 5.88 (s, 2 H, *H*-1"), 4.21-4.08 (m, 8 H, *H*-2") ppm.
^{13}C NMR (151 MHz, $CDCl_3$, 298 K): $\delta =$ 156.6 (*C*-6'), 151.9 (*C*-2'), 139.4 (*C*-4'), 120.2 (*C*-5'), 120.0 (*C*-3'), 103.3 (*C*-1"), 89.4 (*C*-1), 65.7 (*C*-2") ppm.
MS (EI, 70 eV): *m/z* (%) = 324.12 (5) $[M]^+$, 251.09 (4) $[C_{15}H_{11}N_2O_2]^+$.
HRMS (EI, 70 eV): *m/z* (%) ($C_{18}H_{16}N_2O_4$) =

	mass [*m/z*]	mass difference [ppm]	calc. formula
calculated	324.11101		
measured	324.11112	0.34	$C_{18}H_{16}N_2O_4$

FT-IR: $\tilde{\nu} =$ 859.4 (m), 750.4 (s), 695.3 (m) cm^{-1}.

7.5.4 Synthesis of 5,5'-(ethyne-1,2-diyl)dipicolinaldehyde (131)[27]

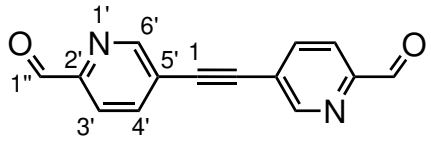

131

The reaction conditions were adapted from Giraldi *et al.*.[27] In a round-bottom flask compound **130** (100 mg, 308 µmol) was dissolved in a mixture of tetrahydrofuran (2 mL) and hydrochloric acid (3 M, 2 mL) and the solution was stirred at 60 °C for 20.5 h. After cooling to room temperature sat. sodium hydrogen carbonate solution was added to adjust the pH-value to 8. After 1 h the solution was filtered, the precipitate was washed with deion. water (10 mL) and the product **131** obtained as a beige solid.

Yield: 65.3 mg (276 µmol, 90%)

^{1}H NMR (500 MHz, $CDCl_3$, 298 K): δ = 10.11 (d, ^5J = 0.8 Hz, 2 H, *H*-1") 8.96 (dd, ^4J = 2.0 Hz, ^5J = 0.9 Hz, 2 H, *H*-6'), 8.04 (ddd, ^3J = 8.1 Hz, ^4J = 2.0 Hz, ^5J = 0.8 Hz, 2 H, *H*-4'), 8.01 (dd, ^3J = 8.1 Hz, ^5J = 0.9 Hz, 2 H, *H*-3') ppm.
^{13}C NMR (126 MHz, $CDCl_3$, 298 K): δ = 192.4 (*C*-1"), 152.6 (*C*-6'), 151.7 (*C*-2'), 139.7 (*C*-4'), 123.4 (*C*-5'), 121.1 (*C*-3'), 91.6 (*C*-1) ppm.
MS (EI, 70 eV): *m/z* (%) = 236.06 (96) $[M]^+$, 207.06 (17) $[C_{13}H_7N_2O_1]^+$, 146.08 (39) $[C_8H_8N_3]^+$.
HRMS (EI, 70 eV): *m/z* (%) ($C_{14}H_8N_2O_2$) =

	mass [*m/z*]	mass difference [ppm]	calc. formula
calculated	236.05858		
measured	236.05851	-0.29	$C_{14}H_8N_2O_2$

FT-IR: $\tilde{\nu}$ = 1718.9 (s), 1584.2 (w), 1361.9 (w), 1205.8 (m), 1021.5 (w), 861.9 (s), 798.1 (m), 735.4 (w) cm^{-1}.

7.5.5 Synthesis of 1,2-bis(6'-(6"-bromo-1"-methyl-1*H*-benzo[*d*]imidazol-2"-yl)pyridin-3'-yl)ethyne (132)[18]

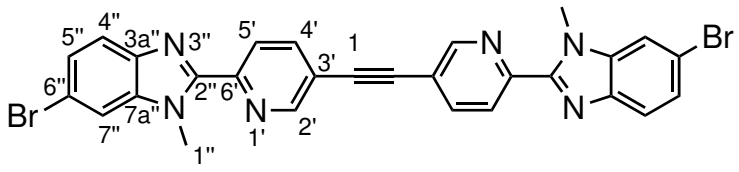

132

The reaction conditions were adapted from Yang *et al.*.[18] In a microwave vial compounds **89** (64.7 mg, 280 μmol) and **131** (33.0 mg, 140 μmol) were dissolved in a mixture of ethanol (1.8 mL) and *N*,*N*-dimethylformamide (0.9 mL). Sodium dithionite (183 mg, 840 μmol) was dissolved in deion. water (0.9 mL) and both solutions were combined. The reaction mixture was stirred at 80 °C for 21 h. After cooling to room temperature, ammonia solution (25%, 0.5 mL) was added and the precipitate was collected by filtration. After washing with tetrahydrofuran (-4 °C, 100 mL) product **132** was obtained an impure solid. Further purification attempts were not performed due to the small scale.

Yield: 4.31 mg (crude product)

^{1}H NMR (500 MHz, TFA – d_1, 298 K): δ = 9.39 (dd, ^4J = 2.0 Hz, ^5J = 0.7 Hz, 2 H, *H*-2'), 8.67 (dd, ^3J = 8.2 Hz, ^4J = 2.0 Hz, 2 H, *H*-4'), 8.51 (dd, ^3J = 8.2 Hz, ^5J = 0.7 Hz, 2 H, *H*-5'), 8.24 (dd, ^4J = 1.5 Hz, ^5J = 0.4 Hz, 2 H, *H*-7"), 8.09 (dd, ^3J = 8.8 Hz, ^4J = 1.5 Hz, 2 H, *H*-5"), 7.95 (dd, ^3J = 8.8 Hz, ^4J = 0.4 Hz, 2 H, *H*-4"), 4.53 (s, 6 H, *H*-1") ppm.
^{13}C NMR (125 MHz, TFA – d_1, 298 K): δ = 155.0 (*C*-2'), 147.8 (*C*-2"), 145.1 (*C*-4'), 141.3 (*C*-6'), 136.8 (*C*-7a"), 135.2 (*C*-5"), 131.2 (*C*-3a"), 128.8 (*C*-5'), 126.8 (*C*-3'), 124.9 (*C*-6"), 118.0 (*C*-7"), 117.8 (*C*-4"), 93.4 (*C*-1), 35.1 (*C*-1") ppm.
Mass spectrometry data was not collected due to insolubility problems.

7.5.6 Synthesis of 3,5-dibromo-2-methylthiophene (140)[28]

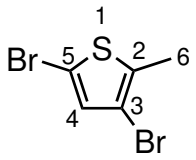

140

The reaction conditions were adapted from Moreno *et al.*.[28] In a round-bottom flask mixtures of *N*-bromosuccinimide (10.2 g, 57.5 mmol) in chloroform (70 mL) and glacial acetic acid (70 mL) and 2-methylthiophene (**139**) (2.82 g, 28.7 mmol) in glacial acetic acid (28 mL) were combined. The reaction was stirred at room temperature for 23 h, poured into cyclohexane (150 mL) and deion. water (150 mL) was added. The layers were separated and the org. layer was washed with sodium hydroxide solution (2 M, 200 mL), brine (250 mL) and dried over magnesium sulfate. The solvent was removed *in vacuo*. Purification by flash chromatography (silica gel, cyclohexane) gave the product **140** as a colourless oil.

Yield: 3.74 g (14.6 mmol, 51%) (Lit.:[28] 98%).

^{1}H NMR (500 MHz, $CDCl_3$, 298 K): δ = 6.86 (s, 1 H, *H*-4), 2.34 (s, 1 H, *H*-6) ppm.
HRMS (ESI): *m/z* (%) ($C_5H_3{}^{79}Br_2{}^{32}S_1$) =

	mass [*m/z*]	mass difference [ppm]	calc. formula
calculated	252.83222		
measured	252.83215	-0.29	$C_5H_3{}^{79}Br_2{}^{32}S_1$

7.5.7 Synthesis of (4-bromo-5-methylthiophen-2-yl)boronic acid (141)[29]

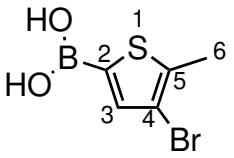

141

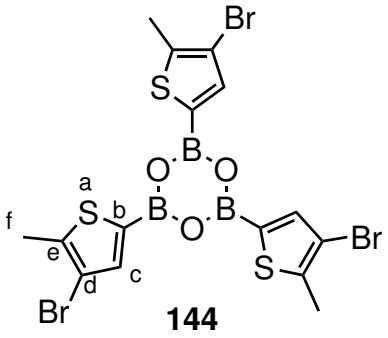

144

The reaction conditions were adapted from von Irmer *et al.*.[29] The reaction was performed under a nitrogen atmosphere. In a three-neck flask compound **140** (3.39 g, 13.2 mmol) was dissolved in diethyl ether (dry, 35 mL) and the mixture was cooled to -78 °C. *n*-Butyllithium (2.5 M in hexane, 5.60 mL, 14.0 mmol) was slowly added and the mixture was stirred at -78 °C for 1 h. Tributyl borate (3.80 mL, 14.1 mmol) was added and the stirring was continued for further 0.25 h. The reaction mixture was warmed to room temperature and was stirred for 1 h. Hydrochloric acid (2 M, 12 mL) was added and stirring was continued for 20 min. The layers were separated, the org. layer was extracted with sodium hydroxide solution (2 M, 150 mL) and the aqueous layers were combined and washed with cyclohexane (150 mL). The layers were separated, the aqueous layer was acidified with hydrochloric acid (12 M) and the precipitate was collected by filtration. The precipitate was washed with deion. water (200 mL) and the product **141** was obtained as a colourless solid.

Yield: 2.09 g (9.46 mmol, 72%) (Lit.:[29] 90%).

^{1}H NMR (600 MHz, $CDCl_3$, 298 K): δ = 7.75 (s, 3 H, *H*-c), 7.33 (s, 1 H, *H*-3), 4.52 (s, 2 H, O-*H*), 2.51 (s, 9 H, *H*-f), 2.45 (s, 3 H, *H*-6) ppm.
^{13}C NMR (151 MHz, $CDCl_3$, 298 K): δ = 144.9 (*C*-e), 142.1 (*C*-c), 141.7 (*C*-5), 138.4 (*C*-3), 128.1 (*C*-b), 122.7 (*C*-), 111.7 (*C*-d), 111.0 (*C*-4), 15.5 (*C*-f), 15.1 (*C*-6) ppm.
MS (EI, 70 eV): *m/z* (%) = 219.93 (21) $[M]^+$, 174.92 (24) $[C_5H_4Br_1S_1]^+$, 141.02 (35) $[C_5H_6B_1O_2S_1]^+$.
FT-IR: $\tilde{\nu}$ = 3192.0 (s), 2260.7 (w), 1738.6 (w), 1399.9 (s), 1378.3 (s), 1190.3 (s), 1084.5 (m), 1002.0 (w), 883.7 (w), 850.8 (m) cm^{-1}.

7.5.8 Synthesis of 2-(5'-(4"-bromo-5"-methylthiophen-2"-yl)pyridin-2'-yl)-1-methyl-1*H*-benzo[*d*]imidazole (143)[25]

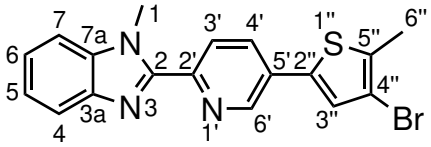

143

The reaction conditions were adapted from Burke *et al.*.[25] The reaction was performed under a nitrogen atmosphere. In a three-neck flask compound **142** (1.96 g, 6.79 mmol), potassium carbonate (2.36 mg, 17.1 mmol) and $Pd(PPh_3)_4$ (392 mg, 5 mol%) were dissolved in a mixture of ethanol (dry, 23 mL), deion. water (degassed, 23 mL) and tetrahydrofuran (dry, 50 mL) and the solution was degassed using the freeze-pump-thaw technique. Afterwards, compound **141** (1.50 g, 6.79 mmol) was added and the reaction mixture was stirred at 80 °C for 21 h. The solution was cooled to room temperature and the precipitated pure product **143** was collected by filtration. The filtrate was further purified by extraction of the aqueous layer with dichloromethane (100 mL), the org. layers were combined, dried and the solvent was removed *in vacuo*. Purification by flash chromatography (silica gel, 50% ethyl acetate:cyclohexane) gave the product **143** as a yellow solid.

Yield: 1.40 g (3.65 mmol, 54%)

^{1}H NMR (600 MHz, $CDCl_3$, 298 K): δ = 8.86 (dd, ^4J = 2.4 Hz, ^5J = 0.7 Hz, 1 H, *H*-6'), 8.43 (dd, ^3J = 8.3 Hz, ^5J = 0.7 Hz, 1 H, *H*-3'), 7.93 (dd, ^3J = 8.3 Hz, ^4J = 2.4 Hz, 1 H, *H*-4'), 7.83 (ddd, ^3J = 7.8 Hz, ^4J = 1.1 Hz, ^5J = 0.8 Hz, 1 H, *H*-4), 7.45 (ddd, ^3J = 7.8 Hz, ^4J = 1.4 Hz, ^5J = 0.7 Hz, 1 H, *H*-7), 7.36 (ddd, ^3J = 7.8 Hz, ^3J = 7.1 Hz, ^4J = 1.2 Hz, 1 H, *H*-6), 7.32 (ddd, ^3J = 7.7 Hz, ^3J = 7.2 Hz, ^4J = 1.4 Hz, 1 H, *H*-5), 7.26 (s, 1 H, *H*-3"), 4.31 (s, 3 H, *H*-1), 2.47 (s, 3 H, *H*-6") ppm.
^{13}C NMR (151 MHz, $CDCl_3$, 298 K): δ = 149.8 (*C*-2), 149.4 (*C*-2'), 145.0 (*C*-6'), 142.6 (*C*-3a), 137.4 (*C*-7a), 136.9 (*C*-2"), 135.7 (*C*-4"), 132.9 (*C*-4'), 129.3 (*C*-5'), 127.2 (*C*-3"), 124.7 (*C*-3'), 123.5 (*C*-6), 122.7 (*C*-5), 120.1 (*C*-4), 110.6 (*C*-5"), 109.9 (*C*-7), 68.0 (*C*-), 32.9 (*C*-1), 15.0 (*C*-6") ppm.
MS (EI, 70 eV): *m/z* (%) = 383.01 (66) $[M]^+$, 251.96 (1) $[C_{10}H_7Br_1N_1S_1]^+$, 208.10 (1) $[C_{13}H_{10}N_3]^+$, 131.07 (14) $[C_8H_7N_2]^+$.
HRMS (ESI): *m/z* (%) ($C_{18}H_{15}{}^{79}Br_1N_3{}^{32}S_1$ ($[M^+H]^+$)) =

	mass [*m/z*]	mass difference [ppm]	calc. formula
calculated	384.01646		
measured	384.01604	-1.09	$C_{18}H_{15}{}^{79}Br_1N_3{}^{32}S_1$ ($[M^+H]^+$)

FT-IR: $\tilde{\nu}$ = 1737.4 (s), 1365.5 (m), 1217.1 (m), 822.8 (m) cm^{-1}.

7.5.9 Synthesis of 2,2'-(((perfluorocyclopent-1"'-ene-1"',2"'-diyl)bis(5"-methylthiophene-4",2"-diyl))bis(pyridine-5',2'-diyl))bis(1-methyl-1*H*-benzo[*d*]imidazole) (137)[30]

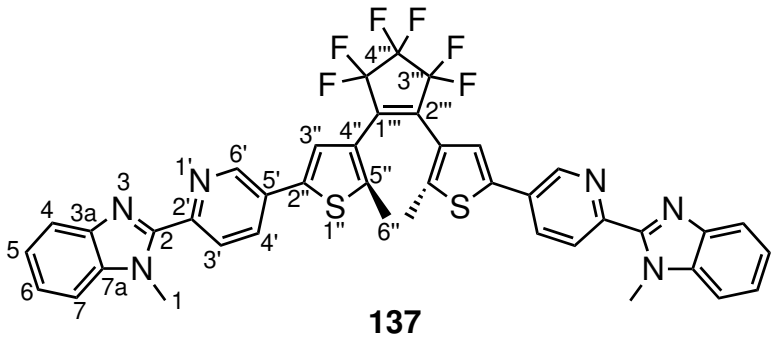

137

The reaction conditions were adapted from Becker.[30] The reaction was performed under a nitrogen atmosphere. In a three-neck flask compound **143** (1.03 g, 2.68 mmol) was dissolved in tetrahydrofuran (dry, 127 mL) and the solution was cooled to -78 °C. *n*-Butyllithium (2.5 M in hexane, 1.10 mL, 2.75 mmol) was slowly added and the reaction mixture was stirred at -78 °C for 2 h. Afterwards, octafluorocyclopentene (180 µL, 1.34 mmol) was added and stirring was continued at -78 °C for further 3 h. The solution was warmed up to room temperature and was stirred for 16.5 h. The solvent was removed *in vacuo* and purification by flash chromatography (silica gel, 20-100% ethyl acetate:cyclohexane) gave the product **137** as a yellow solid. Impure fractions were further purified by recrystallisation from acetone.

Note: Due to the low boiling point of octafluorocyclopentene the apparatus, used syringes and the chemical itself need to be cooled prior to uses. The flash chromatography is time consuming since

multiple side products and remaining starting material need to be removed. The reaction as well as the work up / purification were performed in the absence of light.

Yield: 512 mg (654 μmol, 49%)

^{1}H NMR (500 MHz, $CDCl_3$, 298 K): δ = 8.91 (dd, ^{4}J = 2.4 Hz, ^{5}J = 0.8 Hz, 2 H, *H*-6'), 8.46 (dd, ^{3}J = 8.3 Hz, ^{5}J = 0.8 Hz, 2 H, *H*-3'), 7.97 (dd, ^{3}J = 8.3 Hz, ^{4}J = 2.4 Hz, 2 H, *H*-4'), 7.84 (ddd, ^{3}J = 7.7 Hz, ^{4}J = 1.2 Hz, ^{5}J = 0.7 Hz, 2 H, *H*-4), 7.46-7.45 (m, 2 H, *H*-7), 7.44 (s, 2 H, *H*-3"), 7.37 (ddd, ^{3}J = 7.7 Hz, ^{3}J = 7.2 Hz, ^{4}J = 1.2 Hz, 2 H, *H*-6), 7.33 (ddd, ^{3}J = 7.7 Hz, ^{3}J = 7.2 Hz, ^{4}J = 1.2 Hz, 2 H, *H*-5), 4.32 (s, 6 H, *H*-1), 2.06 (s, 6 H, *H*-6") ppm.
^{13}C NMR (126 MHz, $CDCl_3$, 298 K): δ = 149.7 (*C*-2'), 149.6 (*C*-2), 145.2 (*C*-6'), 143.0 (*C*-4"), 142.6 (*C*-3a), 138.3 (*C*-2"), 137.4 (*C*-7a), 133.2 (*C*-4'), 129.0 (*C*-5'), 126.3 (*C*-5"), 124.7 (*C*-3'), 124.0 (*C*-3"), 123.6 (*C*-6), 122.8 (*C*-5), 120.1 (*C*-4), 110.0 (*C*-7), 32.9 (*C*-1), 14.8 (*C*-6") ppm.
C-1"',3"' and *C*-4"' were not observed in the ^{13}C (^{1}H decoupled) spectrum.[264]
^{19}F NMR (471 MHz, $CDCl_3$, 298 K, C_6F_6): δ = -111.2 (t, ^{3}J = 4.9 Hz, 4 H, *F*-3"'), -132.9-(-132.95) (m, 2 H, *F*-4"') ppm.
MS (EI, 70 eV): *m/z* (%) = 782.17 (100) $[M]^+$, 651.11 (5) $[C_{33}H_{21}F_6N_4S_S]^+$.
HRMS (EI, 70 eV): *m/z* (%) ($C_{41}H_{28}F_{19}N_6{}^{32}S_2$) =

	mass [*m/z*]	mass difference [ppm]	calc. formula
calculated	782.17210		
measured	782.17224	0.18	$C_{41}H_{28}F_{19}N_6{}^{32}S_2$

FT-IR: $\tilde{\nu}$ = 3255.0 (w), 2253.5 (m), 2042.8 (m), 1742.9 (s), 1729.5 (s), 1271.0 (s), 1116.2 (s), 988.2 (s), 843.6 (m), 822.4 (m), 739.5 (s) cm^{-1}.

7.5.10 Synthesis of 2,2'-((4",4",5",5",6",6"-hexafluoro-9a",9b"-dimethyl-5",6",9a",9b"-tetrahydro-4*H*-indeno[5,4-b:6,7-b']dithiophene-2",8"-diyl)bis(pyridine-5',2'-diyl))bis(1-methyl-1*H*-benzo[*d*]imidazole) (138)

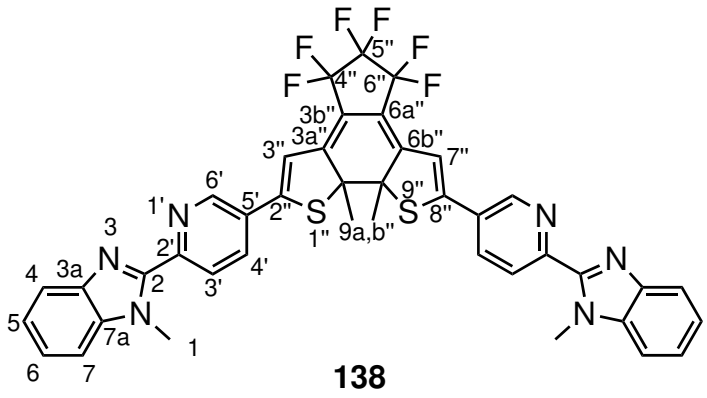

138

In a test tube compound **137** (4.00 mg, 5.11 μmol) was dissolved in deuterated chloroform (500 μL) and was irradiated with 365 nm for 10 min.

^{1}H NMR (600 MHz, $CDCl_3$, 298 K): δ = 8.92 (dd, ^4J = 2.4 Hz, ^5J = 0.6 Hz, 1 H, *H*-6'), 8.53 (dd, ^3J = 8.4 Hz, ^5J = 0.6 Hz, 1 H, *H*-3'), 7.99 (dd, ^3J = 8.4 Hz, ^4J = 2.4 Hz, 1 H, *H*-4'), 7.84 (ddd, ^3J = 8.0 Hz, ^4J = 1.1 Hz, ^5J = 0.7 Hz, 1 H, *H*-4), 7.47 (unres. ddd, 1 H, *H*-7), 7.39 (ddd, ^3J = 8.0 Hz, ^3J = 7.0 Hz, ^4J = 1.1 Hz, 1 H, *H*-6), 7.35 (ddd, ^3J = 8.1 Hz, ^3J = 7.2 Hz, ^4J = 1.2 Hz, 1 H, *H*-5), 6.85 (s, 1 H, *H*-3"), 4.34 (s, 3 H, *H*-1), 2.26 (s, 3 H, *H*-9a",9b") ppm.
^{13}C NMR (151 MHz, $CDCl_3$, 298 K): δ = 154.2 (*C*-2"), 151.8 (*C*-2'), 149.1 (*C*-2), 149.0 (*C*-3a"), 146.6 (*C*-6'), 142.7 (*C*-3a), 137.6 (*C*-7a), 134.4 (*C*-4'), 128.5 (*C*-5'), 124.3 (*C*-3'), 124.0 (*C*-6), 123.0 (*C*-5), 120.2 (*C*-4), 115.5 (*C*-3"), 110.1 (*C*-7), 33.1 (*C*-1), 25.4 (*C*-9a",9b") ppm.
C-3b", 4" and *C*-5" were not observed in the ^{13}C (^{1}H decoupled) spectrum.[264]
^{19}F NMR (471 MHz, $CDCl_3$, 298 K, C_6F_6): δ = -113.1-(-115.1) (m, 4 H, *F*-6"), -134.8-(-134.9) (m, 2 H, *F*-5") ppm.
Mass spectrometry data was not collected.

7.5.11 Synthesis of cages 145 and the proposed helicate 148

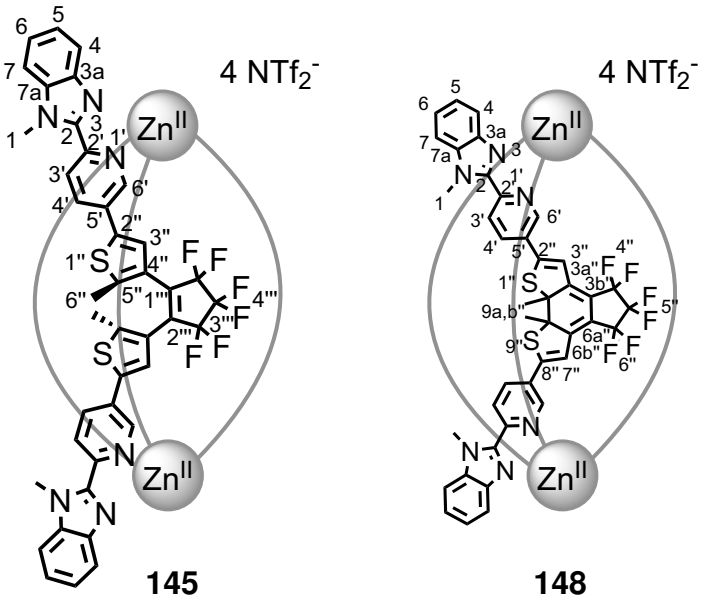

Compound **137** (3.58 mg, 4.58 μmol) and $Zn(NTf_2)_2$ (1.91 mg, 3.05 μmol) were dissolved in CD_3CN (500 μL) to self-assemble cage **145**. Irradiation with 365 nm for 20 min yielded the supposed ring-closed isomer **148**.

Compound **145**:

^{1}H NMR (500 MHz, CD_3CN, 298 K): δ = 8.65 (dd, ^3J = 8.7 Hz, ^4J = 2.4 Hz, 3 H, *H*-4'), 8.51 (d, ^3J = 8.7 Hz, ^5J = 0.7 Hz, 3 H, *H*-3'), 7.78-7.75 (m, 9 H, *H*-4,6',3"), 7.48 (ddd, ^3J = 8.4 Hz, ^3J = 7.3 Hz, ^4J = 1.0 Hz, 3 H, *H*-5), 7.09 (ddd, ^3J = 8.4 Hz, ^3J = 7.3 Hz, ^4J = 0.9 Hz, 3 H, *H*-6), 6.84 (unres. dt, ^3J = 8.3 Hz, 3 H, *H*-7), 4.26 (s, 18 H, *H*-1), 1.80 (br, 18 H, *H*-6") ppm.

^{13}C NMR (126 MHz, CD_3CN, 298 K): δ = 149.4 (*C*-2), 145.8 (*C*-6'), 145.4 (*C*-4"/5"), 143.4 (*C*-2'), 138.8 (*C*-3a), 138.7 (*C*-7a), 137.7 (*C*-4'), 136.8 (*C*-5'/2"), 133.0 (*C*-5'), 128.0 (*C*-3"), 127.4 (*C*-4"/5"), 126.9 (*C*-5), 126.5 (*C*-6), 125.9 (*C*-3'), 122.2 (*C*-5'/2"), 118.3 (*C*-7), 113.3 (*C*-4), 34.8 (*C*-1), 15.2 (*C*-6") ppm.

MS (ESI): *m/z* (%) = 1519.6027 [**145** + 2 NTf_2]$^{2+}$, 919.0959 [**145** + NTf_2]$^{3+}$, 619.5922 [**145**]$^{4+}$.

Proposed compound **148**:

^{1}H NMR (600 MHz, CD_3CN, 298 K): δ = 8.58-8.48 (m, 2 H, *H*-3',4'), 7.82 (d, ^3J = 8.4 Hz, 1 H, *H*-4), 7.58 (t, ^3J = 7.2 Hz, 1 H, *H*-5), 7.51 (br, 1 H, *H*-6'), 7.41-7.33 (m, 1 H, *H*-6), 7.10-7.04 (m, 1 H, *H*-7), 4.31 (s, 3 H, *H*-1), 2.24 (s, 3 H, *H*-9a,b") ppm.

H-3" was not observed in the ^{1}H spectrum.

^{13}C NMR (151 MHz, CD_3CN, 298 K): δ = 148.7 (*C*-2), 144.7 (*C*-2'), 139.8 (*C*-3'/4'), 138.7 (*C*-7a),

127.1 (*C*-5), 126.6 (*C*-6), 125.2 (*C*-3'/4'), 119.5 (*C*-7), 119.0 (*C*-3a), 113.2 (*C*-4), 34.6 (*C*-1), 25.8 (*C*-9a,b") ppm.
Carbon signals at 122.0 and 119.9 ppm were not assigned and listed due to missing cross-peaks in the HSQC and HMBC spectra.

7.5.12 Synthesis of cage 146

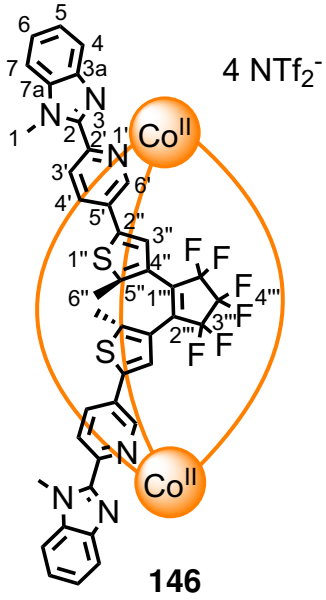

Compound **137** (3.32 mg, 4.24 μmol) and $Co(NTf_2)_2$ (1.75 mg, 2.83 μmol) were dissolved in CD_3CN (500 μL).

Note: ^{13}C NMR signals were assigned based on cross-peaks within ^{1}H-^{13}C HMQC spectra.

^{1}H NMR (600 MHz, CD_3CN, 298 K): δ = 80.0 (br, 6 H, *H*-6'), 73.9 (s, 6 H, *H*-3'), 34.3 (s, 6 H, *H*-7), 14.9 (s, 6 H, *H*-1), 10.5 (s, 6 H, *H*-4'), 4.47 (s, 6 H, *H*-3"), 2.85 (s, 6 H, *H*-6), -0.53 (s, 6 H, *H*-5), -4.44 (s, 18 H, *H*-6"), -26.0 (s, 18 H, *H*-4) ppm.
^{13}C NMR (151 MHz, CD_3CN, 298 K): δ = 407.8 (*C*-3'), 227.9 (*C*-7), 159.2 (*C*-4'), 155.4 (*C*-3"), 141.8 (*C*-1), 136.4 (*C*-6), 88.2 (*C*-5), 3.7 (*C*-6") ppm.
^{19}F NMR (471 MHz, CD_3CN, 298 K, C_6F_6): δ = -80.5 (NTf_2^-), -112.2 (q, ^{1}J = 262.7 Hz, 4 H, *F*-3"'), -133.3 (s, 2 H, *F*-4"') ppm.
MS (ESI): *m/z* (%) = 1513.1106 [**146** + 2 NTf_2]$^{2+}$, 915.1003 [**146** + NTf_2]$^{3+}$, 616.3460 [**146**]$^{4+}$.

7.5.13 Synthesis of cage 147

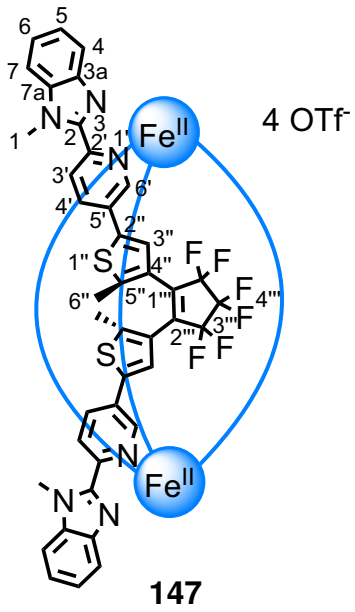

147

Compound **137** (3.09 mg, 3.95 μmol) and $Fe(OTf)_2$ (1.10 mg, 2.63 μmol) were dissolved in CD_3CN (500 μL).

Note: ^{13}C NMR signals were assigned based on cross-peaks within ^{1}H-^{13}C HMQC spectra.

^{1}H NMR (600 MHz, CD_3CN, 298 K): δ = 15.4 (s, 6 H, *H*-3'), 13.7 (br, 6 H, *H*-6'), 10.3 (s, 6 H, *H*-7), 7.81 (s, 6 H, *H*-4'), 7.37 (s, 6 H, *H*-5), 6.98 (s, 6 H, *H*-6), 6.84 (s, 18 H, *H*-1), 5.79 (s, 6 H, *H*-3"), 1.97 (s, 6 H, *H*-4), 1.08 (s, 18 H, *H*-6") ppm.
^{13}C NMR (151 MHz, CD_3CN, 298 K): δ = 140.0 (*C*-4'), 130.1 (*C*-5), 126.1 (*C*-6), 125.9 (*C*-7), 122.5 (*C*-3"), 44.7 (*C*-1), 13.4 (*C*-6") ppm.
^{19}F NMR (471 MHz, CD_3CN, 298 K, C_6F_6): δ = -76.3 (*OTf*$^-$), -111.5 (q, ^{1}J = 264.8 Hz, 4 H, *F*-3"'), -132.7 (s, 2 H, *F*-4"') ppm.
MS (ESI): *m/z* (%) = 1378.6474 [**147** + 2 OTf]$^{2+}$, 869.4462 [**147** + OTf]$^{3+}$, 614.8467 [**147**]$^{4+}$.

Chapter 8

8 Appendix

8.1 Abbreviation list

NMR Nuclear magnetic resonance

COSY Correlation spectroscopy

HSQC Heteronuclear single quantum coherence spectroscopy

HMQC Heteronuclear multiple quantum correlation

HMBC Heteronuclear multiple bond correlation

NOESY Nuclear overhauser effect spectroscopy

EXSY Exchange spectroscopy

MS Mass spectrometry

EI Electron ionization

ESI Electrospray ionization

HR High-resolution

HRMS High-resolution mass spectrometry

TOF Time of Flight

IR Infrared

UV/Vis Ultraviolet/Visible

VT Variable temperature

deion. Deionised

sat. Saturated

Lit. Literature

org. Organic

TLC Thin-layer chromatography

LS Low-spin

HS High-spin

LIESST Light-induced excited spin-state trapping

LD-CISSS Light-driven coordination-induced spin-state switching

LD-LISC Ligand-driven light-induced spin-state change

8.2 ^{1}H NMR spectra of the photostationary states for azobenzenes 67, 68 and 69

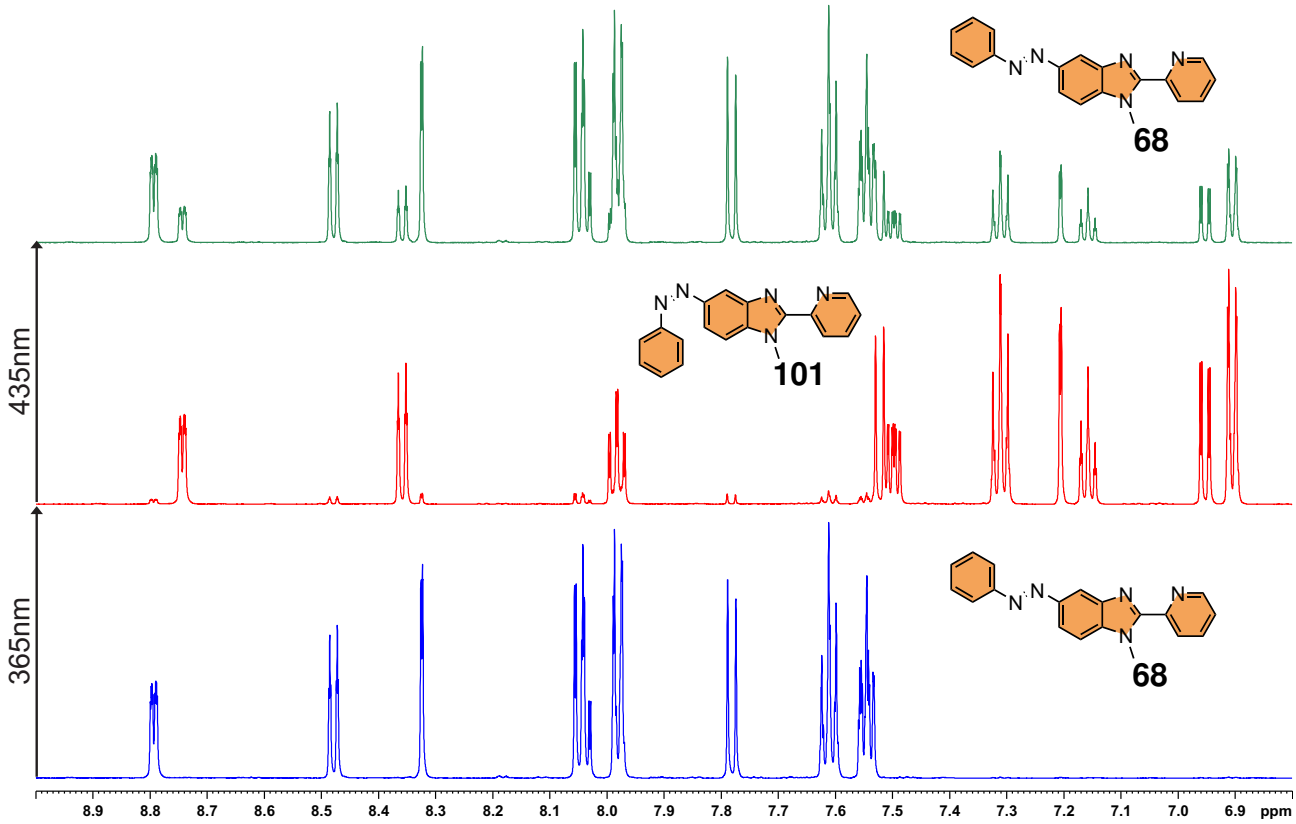

Figure 8.1: ^{1}H NMR spectra (500 MHz, acetone-d_6, 298 K) of azobenzene **68** before (blue) and after irradiation with 365 nm (red) and 435 nm (green).

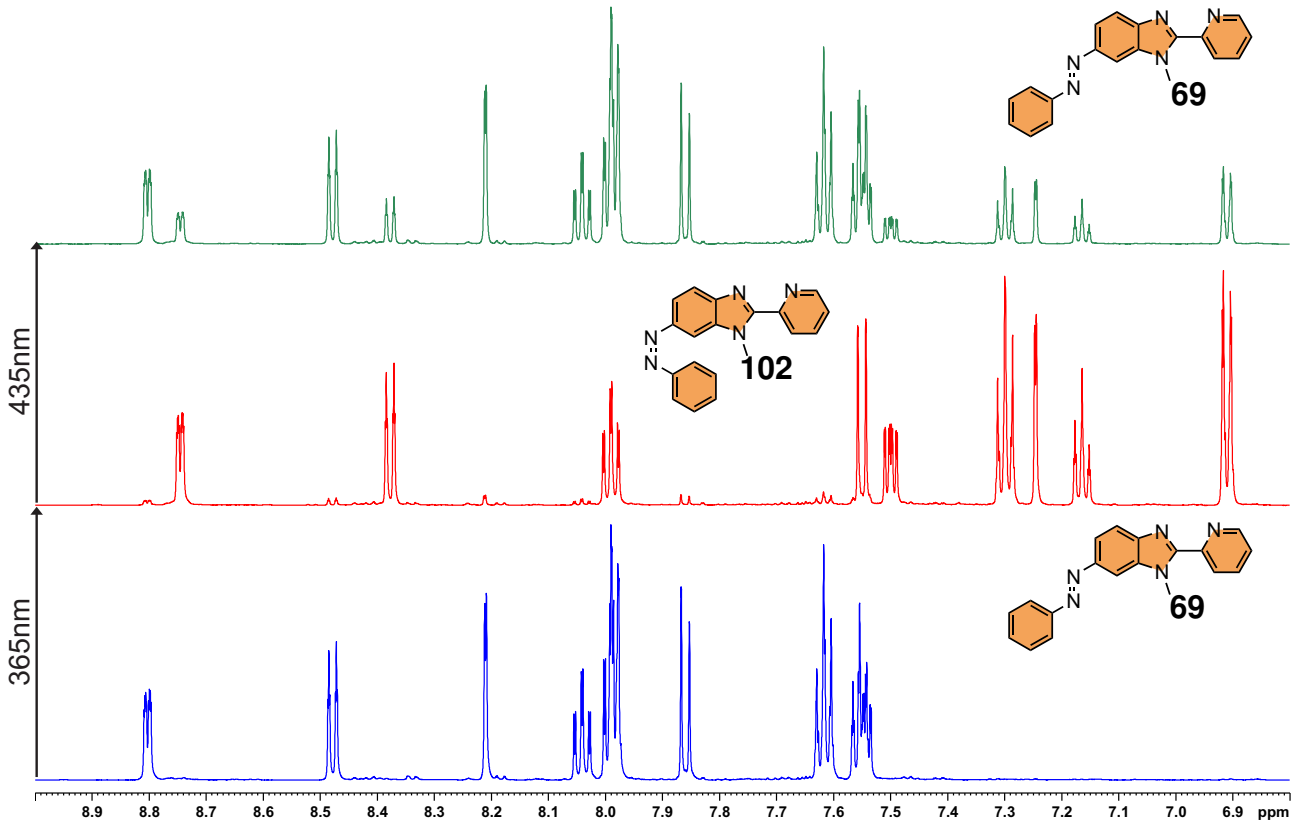

Figure 8.2: ^{1}H NMR spectra (500 MHz, acetone-d_6, 298 K) of azobenzene **69** before (blue) and after irradiation with 365 nm (red) and 435 nm (green).

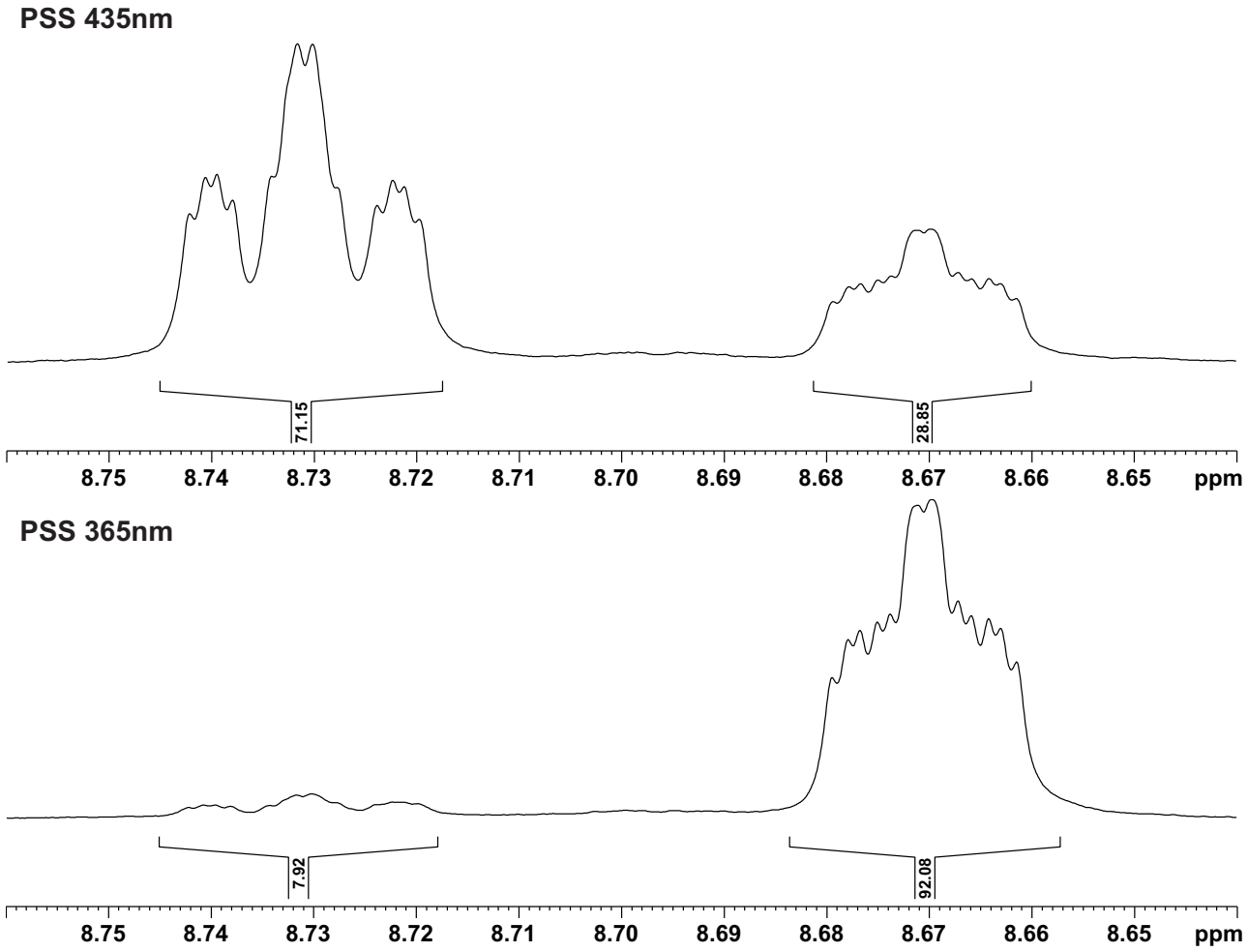

Figure 8.3: Photostationary states of azobenzene **67** based on the ^{1}H NMR spectra (500 MHz, acetone-d_6, 298 K).

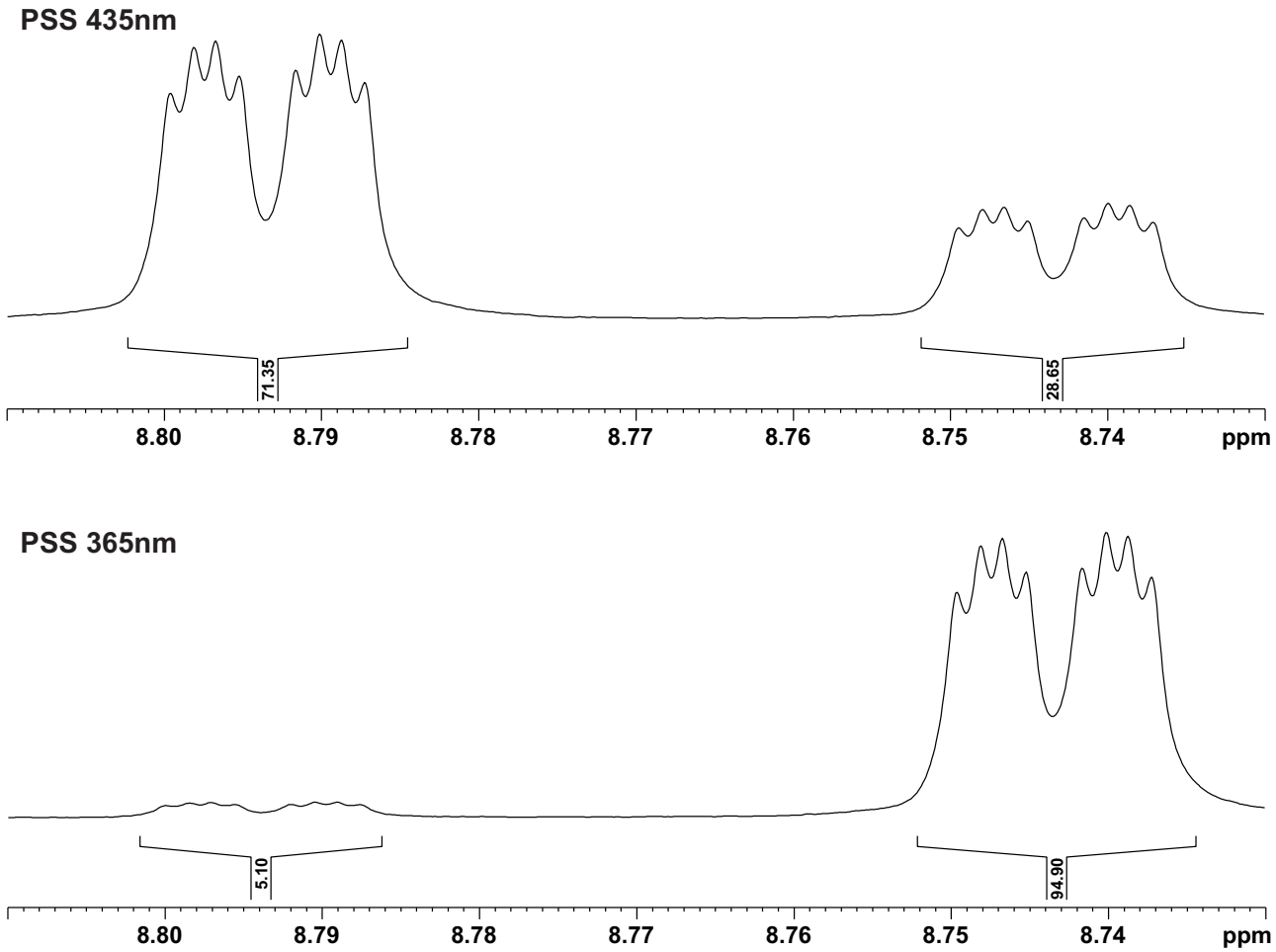

Figure 8.4: Photostationary states of azobenzene **68** based on the ^{1}H NMR spectra (500 MHz, acetone-d_6, 298 K).

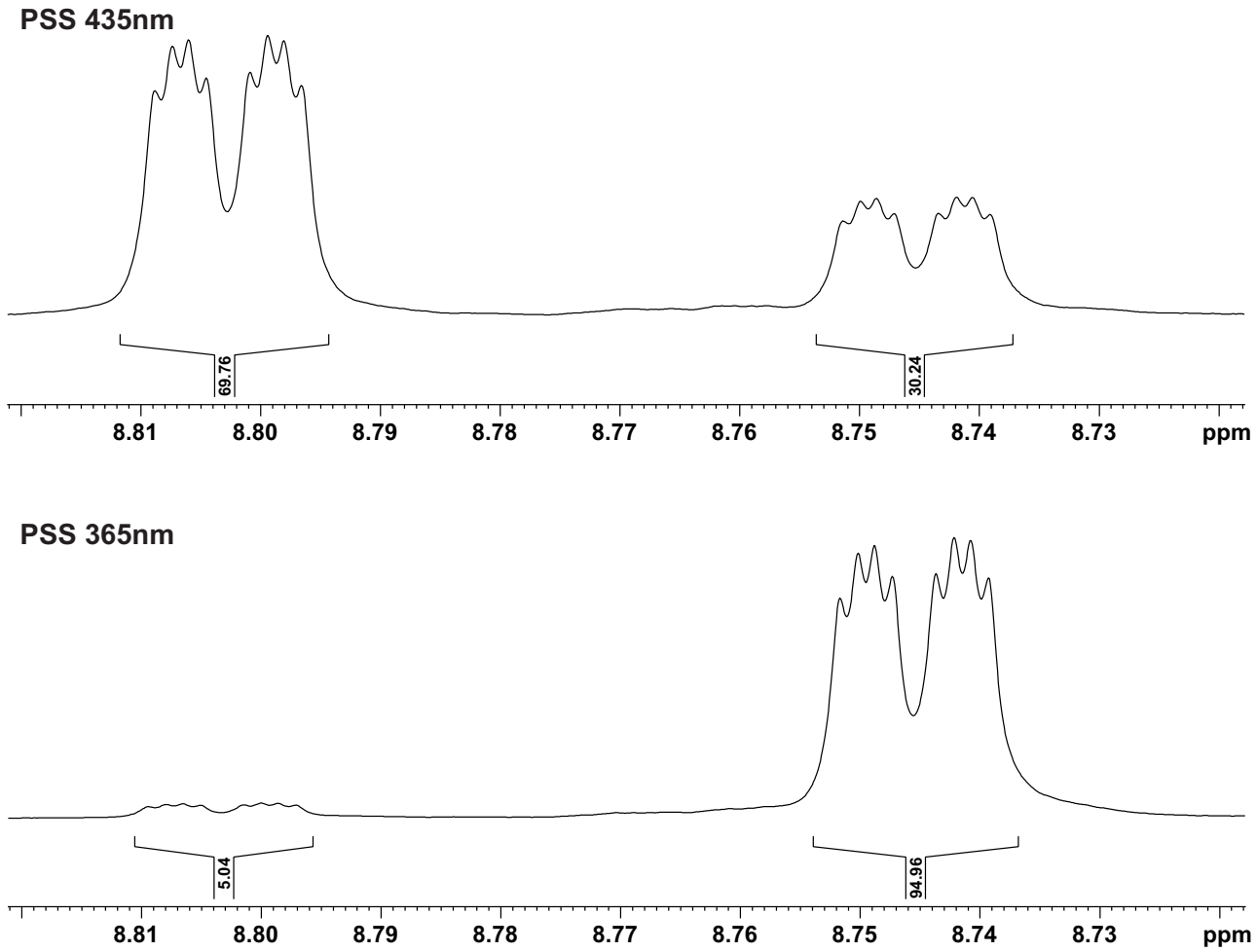

Figure 8.5: Photostationary states of azobenzene **69** based on the ^{1}H NMR spectra (500 MHz, acetone-d_6, 298 K).

8.3 Half-life time measurements for azobenzenes 99/100, 101 and 102

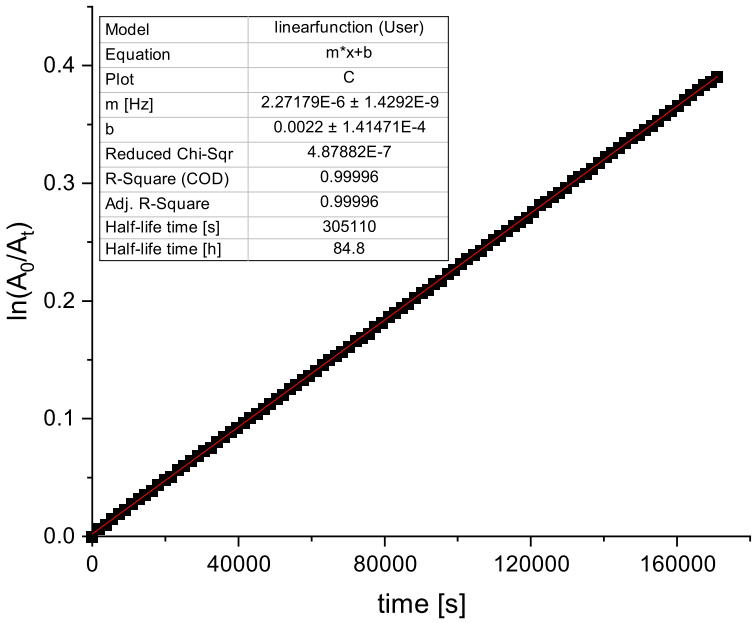

Figure 8.6: Graphical representation of the backisomerisation of azobenzenes **99** and **100** at 355 nm.

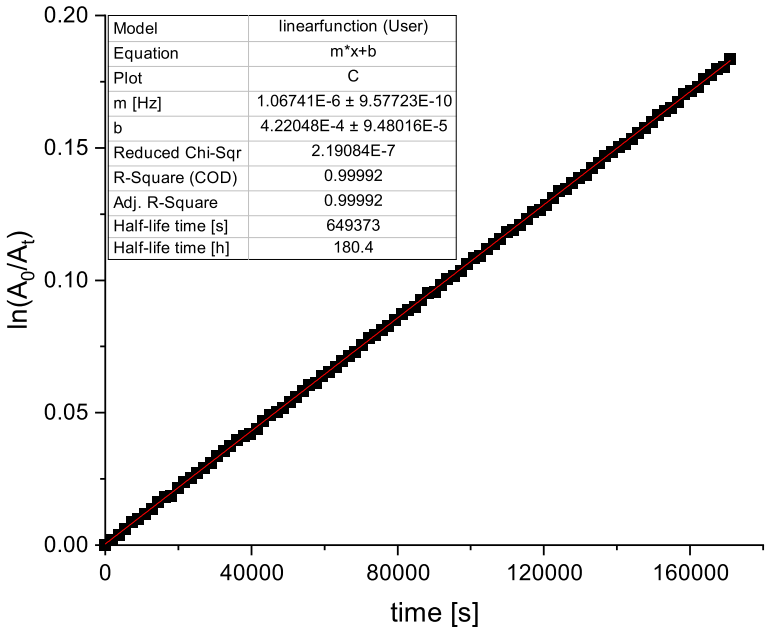

Figure 8.7: Graphical representation of the backisomerisation of azobenzene **101** at 350 nm.

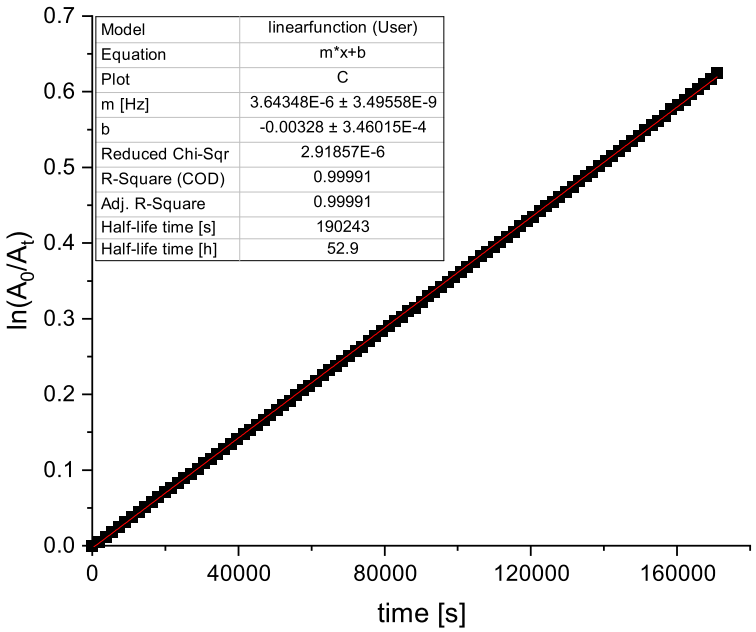

Figure 8.8: Graphical representation of the backisomerisation of azobenzene **102** at 363 nm.

8.4 ^{1}H NMR spectra for dithienylethene 71

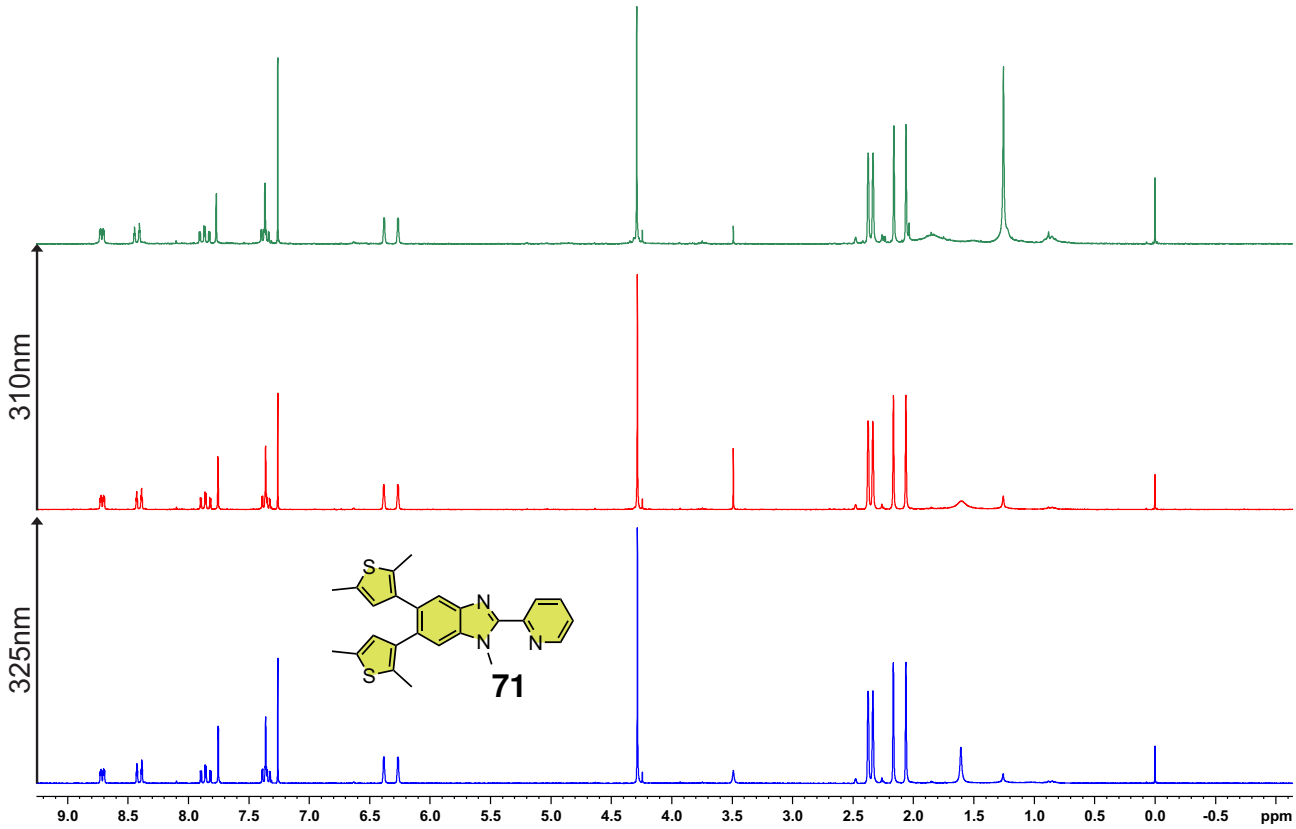

Figure 8.9: ^{1}H NMR spectra (200 MHz, $CDCl_3$, 298 K) of dithienylethene **71** before (blue) and after irradiation with 325 nm (red) for 6 min and 310 nm for 5 min (green).

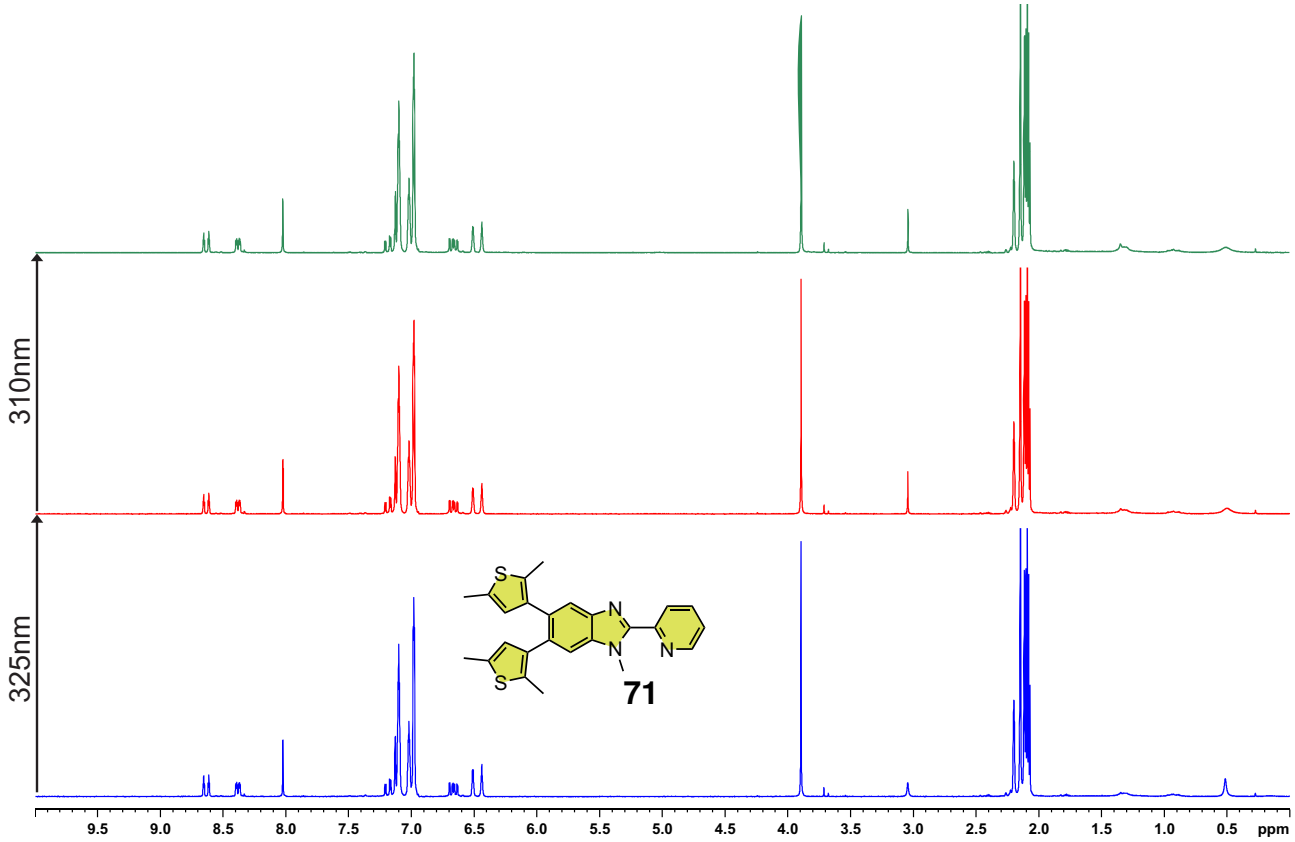

Figure 8.10: ^{1}H NMR spectra (200 MHz, toluene-d_8, 298 K) of dithienylethene **71** before (blue) and after irradiation with 325 nm (red) for 6 min and 310 nm for 5 min (green).

8.5 ^{19}F NMR spectra for dithienylethene 137 and 138

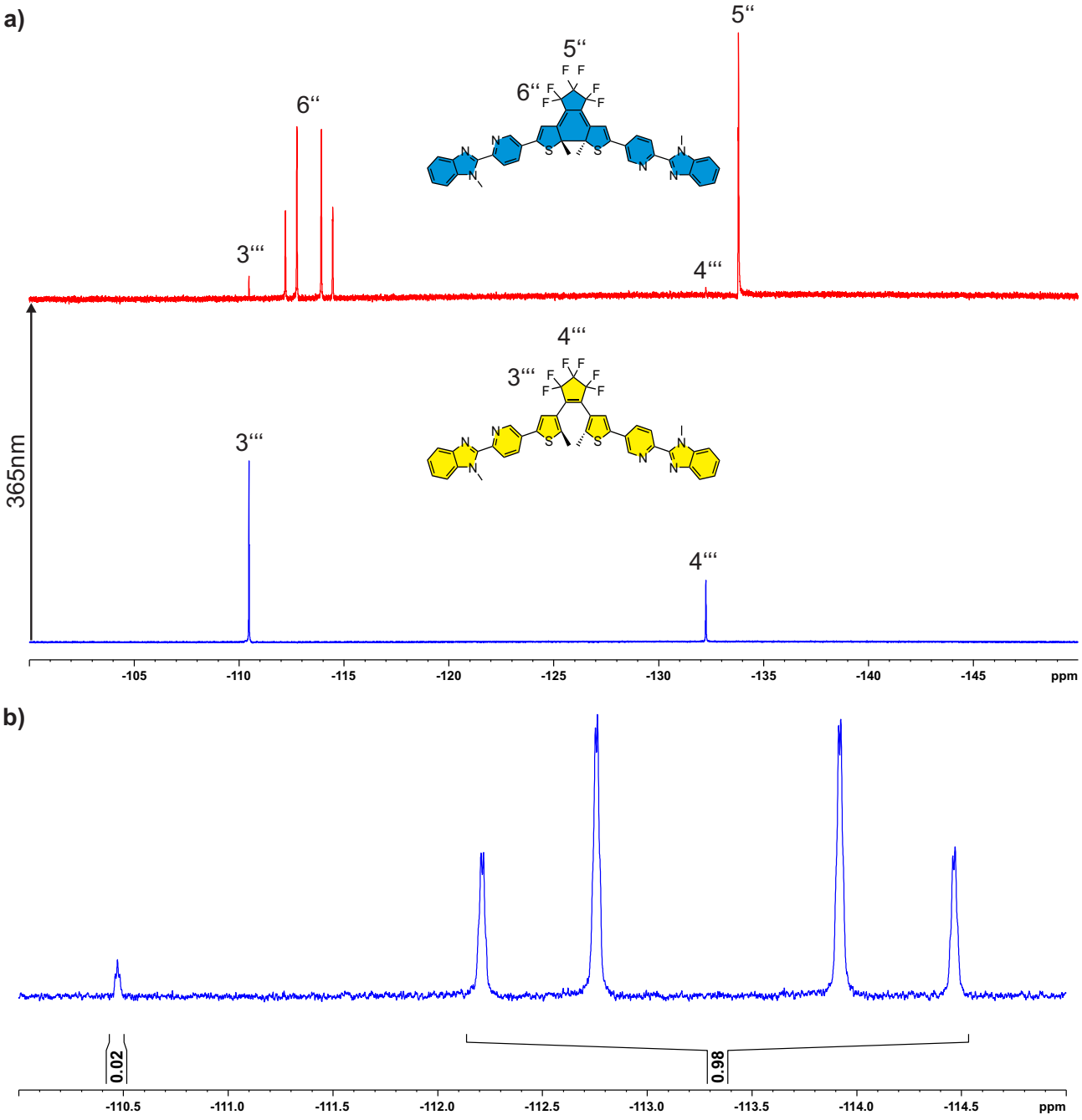

Figure 8.11: ^{19}F NMR spectra (471 MHz, $CDCl_3$, 298 K) of dithienylethene **137**. a) Before (blue) and after irradiation with 365 nm (red) and b) cutout of the irradiated ^{19}F NMR spectrum in the PSS within the range of -110 ppm and -115 ppm (a), red).

8.6 ^{1}H and ^{19}F NMR spectra and mass data for helicates 145, 146 and 147

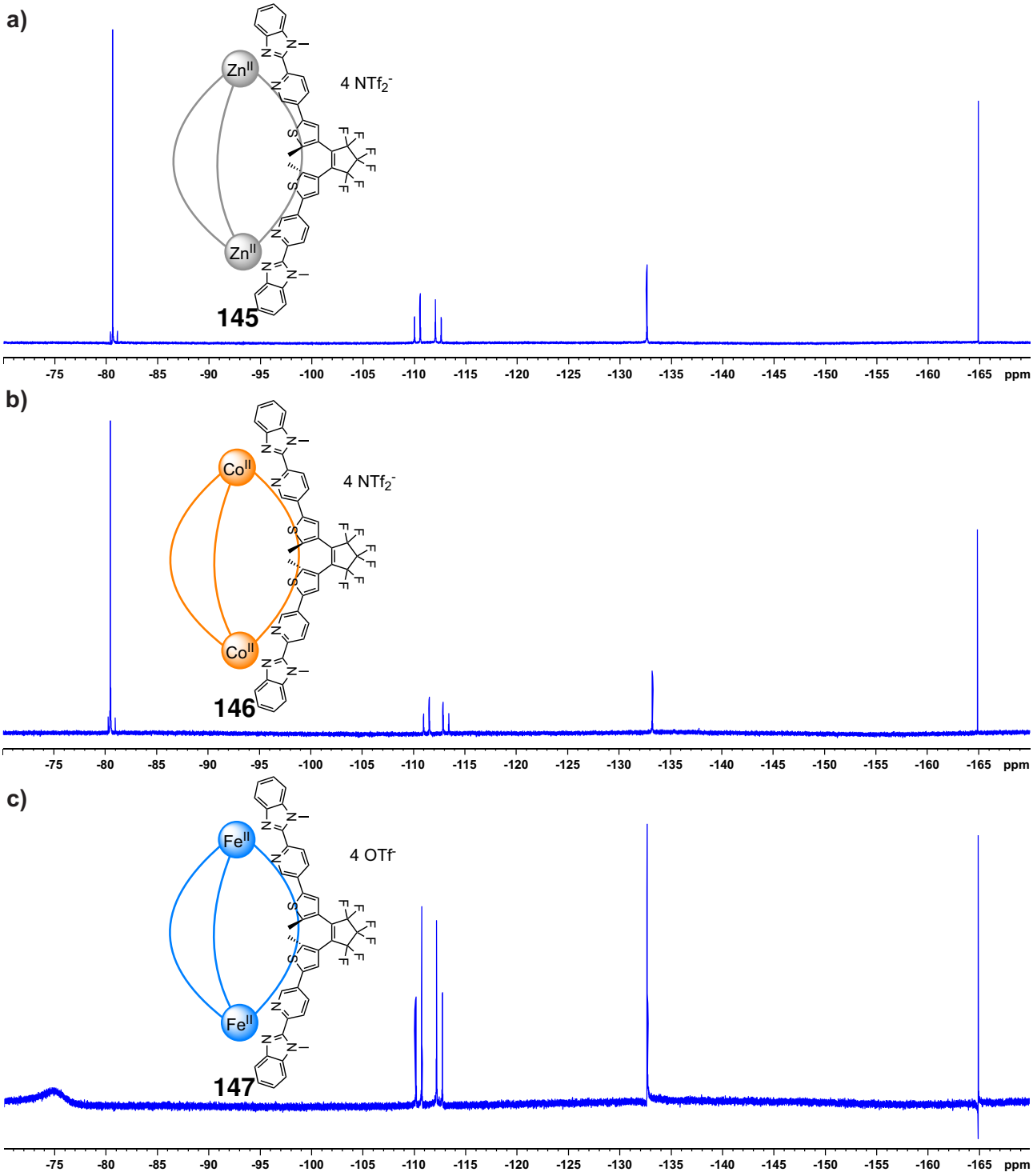

Figure 8.12: ^{19}F NMR spectra (471 MHz, CD_3CN, 298 K, C_6F_6) of cages a) **145**, b) **146** and c) **147**.

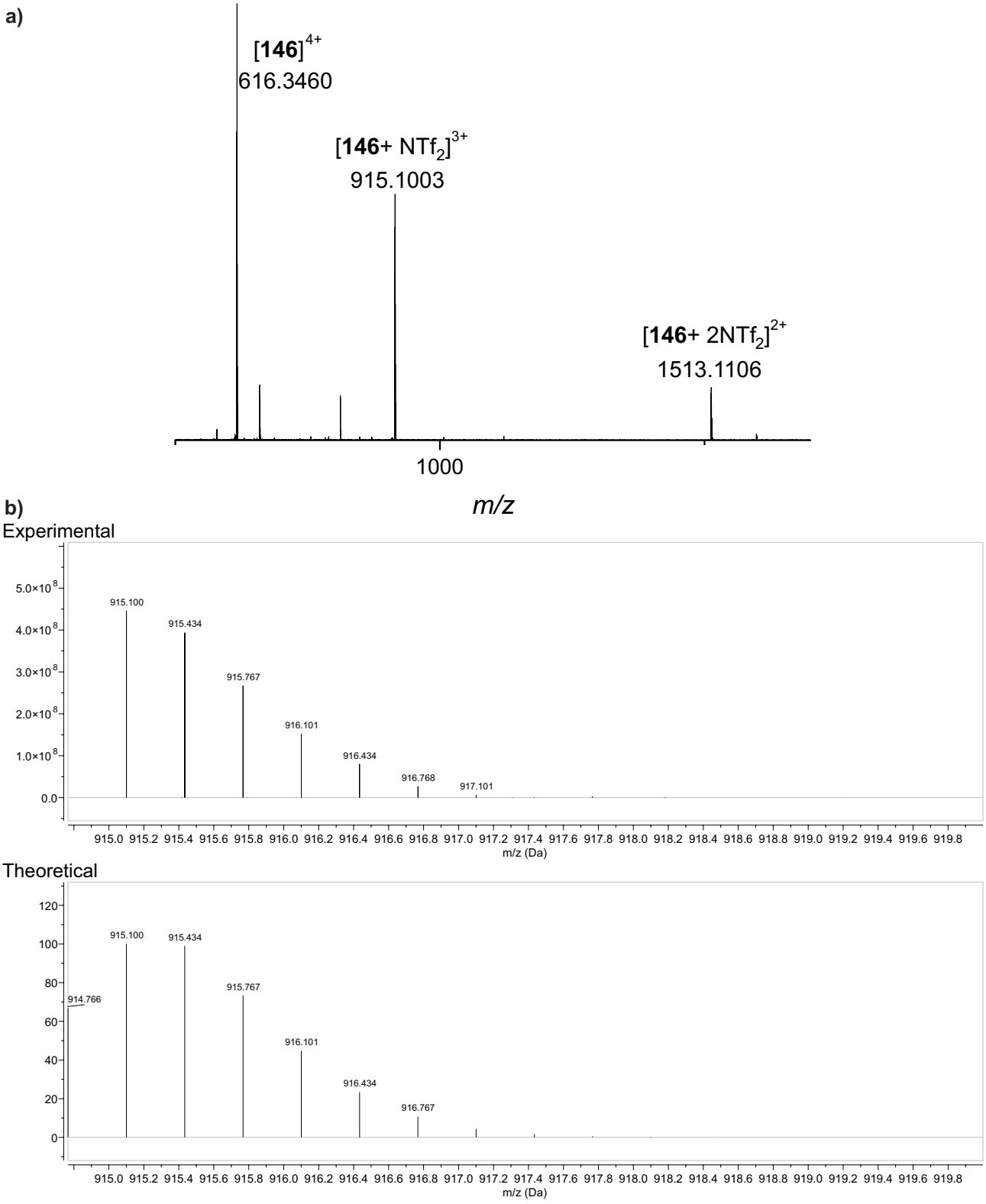

Figure 8.13: High resolution ESI mass spectrum of helicate **146** a) in the range of *m/z* 500-1700 and b) the experimental and theoretical isotopic patterns.

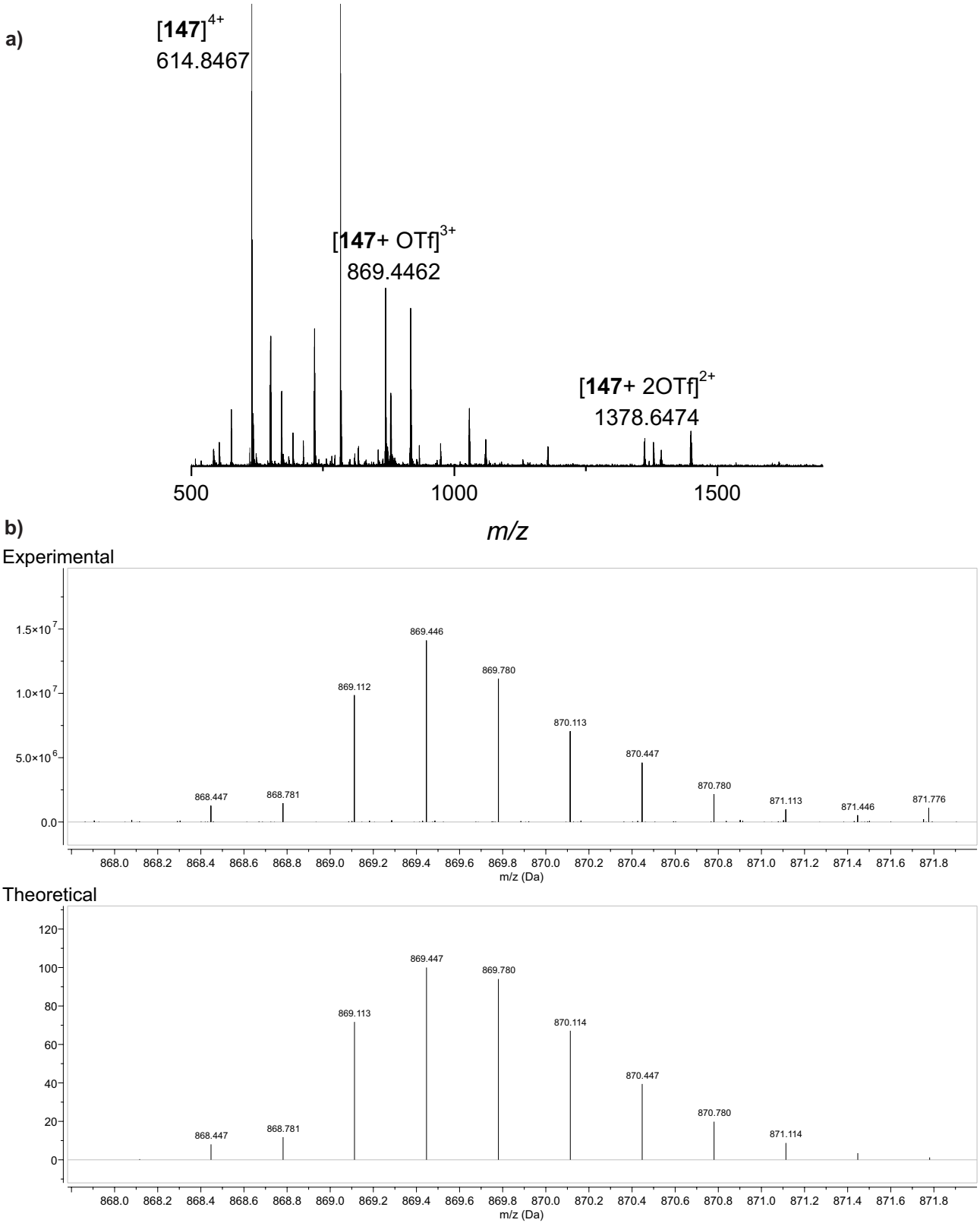

Figure 8.14: High resolution ESI mass spectrum of helicate **147** a) in the range of *m/z* 500-1700 and b) the experimental and theoretical isotopic patterns.

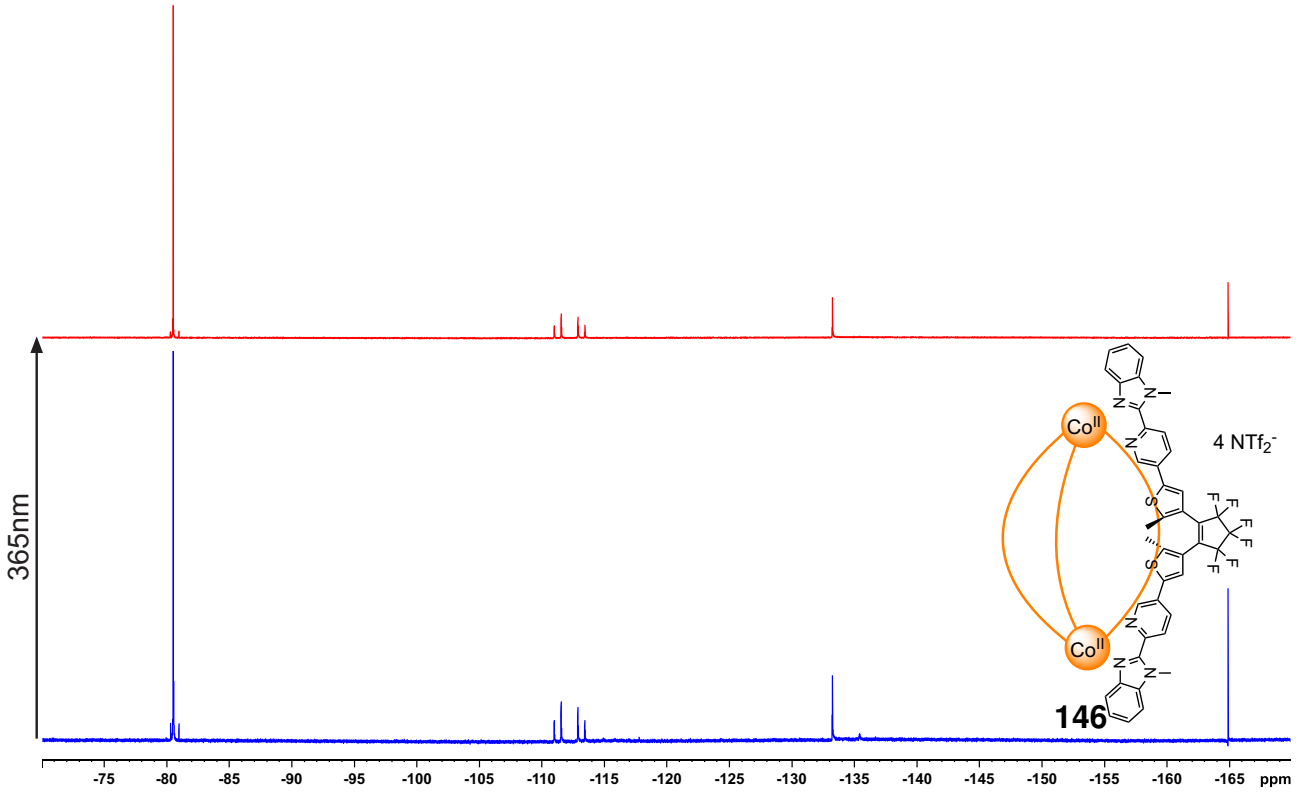

Figure 8.15: ^{19}F NMR spectra (471 MHz, CD_3CN, 298 K, C_6F_6) of helicate **146** before (blue) and after (red) irradiation with 365 nm.

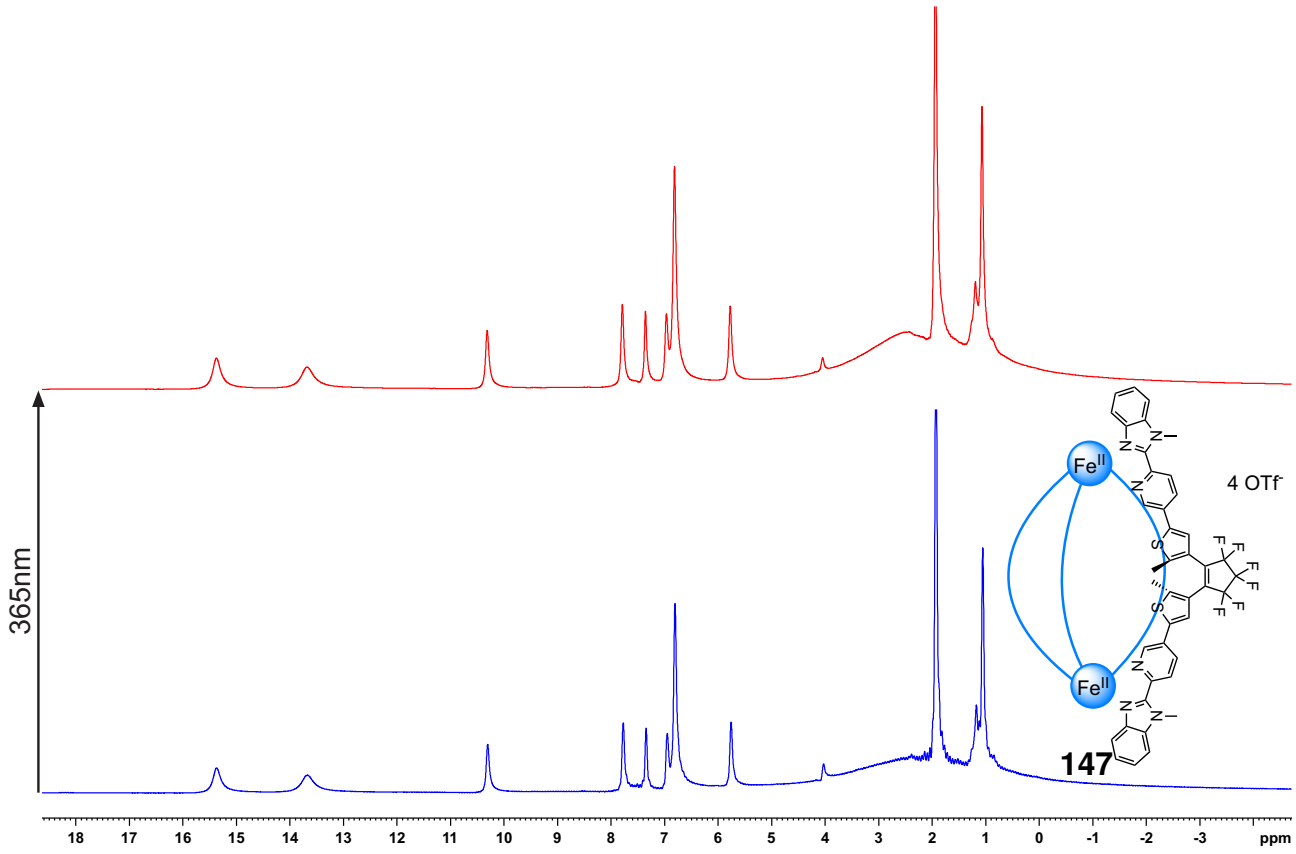

Figure 8.16: ^{1}H NMR spectra (500 MHz, CD_3CN, 298 K) of helicate **147** before (blue) and after (red) irradiation with 365 nm.

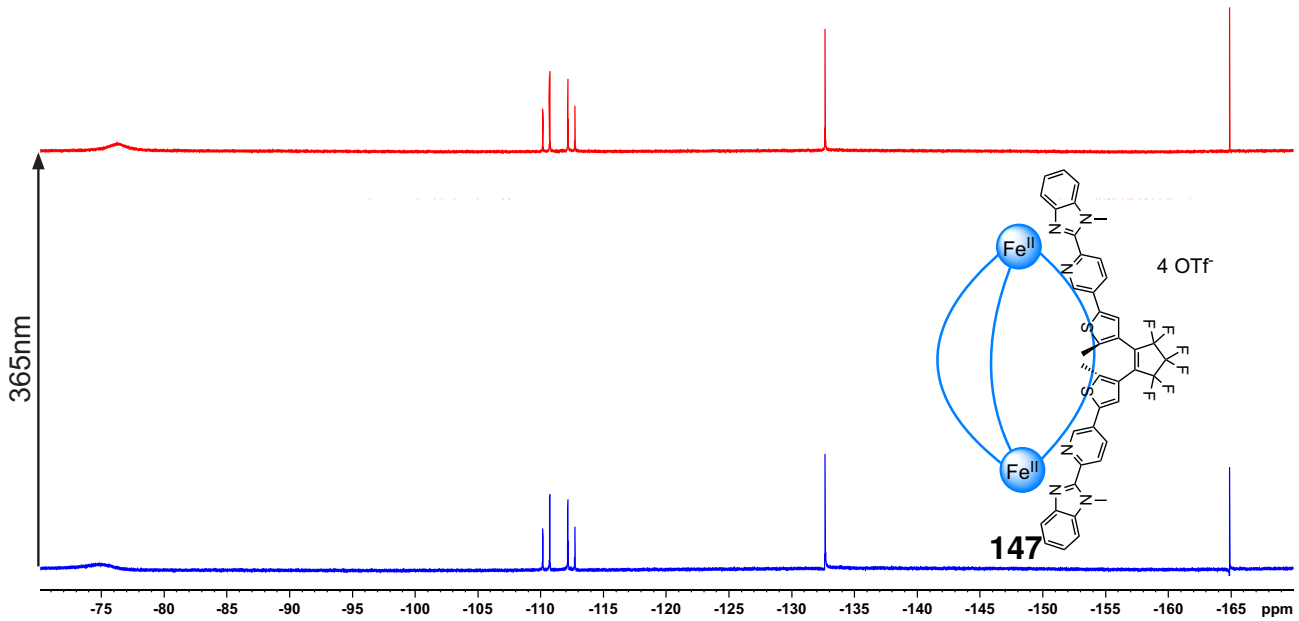

Figure 8.17: ^{19}F NMR spectra (471 MHz, CD_3CN, 298 K, C_6F_6) of helicate **147** before (blue) and after (red) irradiation with 365 nm.

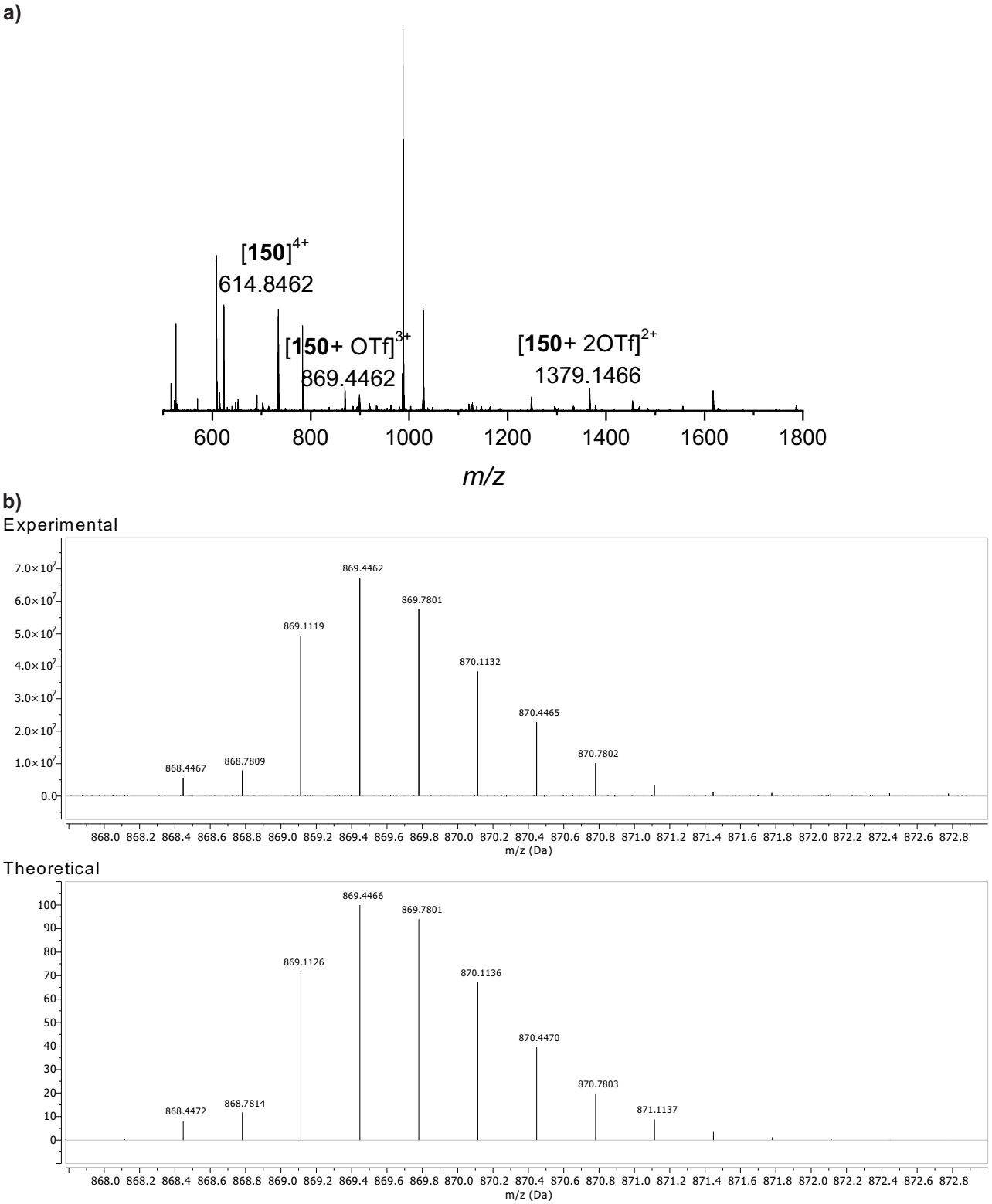

Figure 8.18: High resolution ESI mass spectrum of the Fe^{II}-based self-assembly with ligand **138** a) in the range of *m/z* 500-1800 and b) the experimental and theoretical isotopic patterns.

8.7 ^{1}H, ^{13}C NMR spectra for Chapter 3

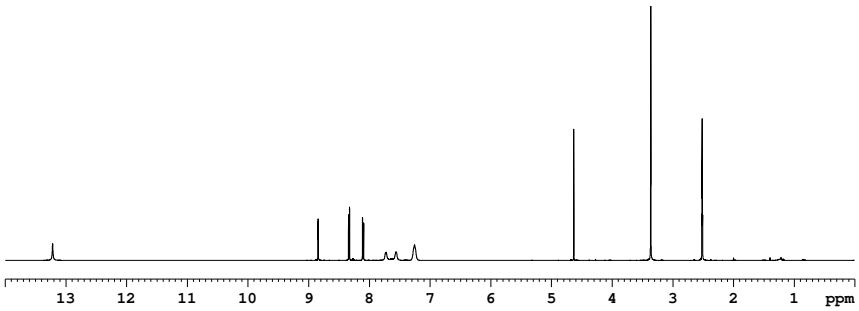

Figure 8.19: 500 MHz ^{1}H NMR spectrum (DMSO-d_6, 298 K) of 2-(5'-ethynylpyridin-2'-yl)-1*H*-benzo[*d*]imidazole (**38**).

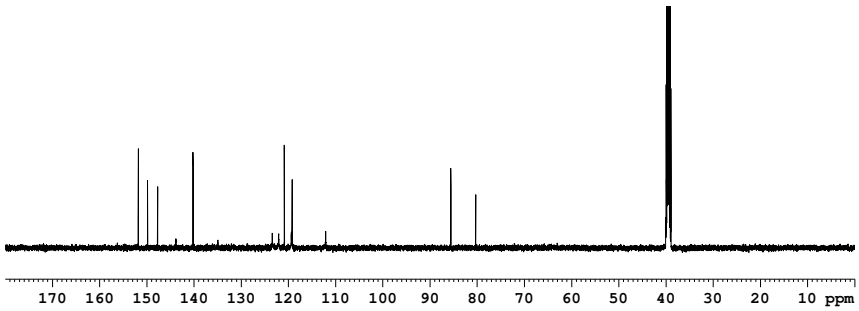

Figure 8.20: 126 MHz ^{13}C NMR spectrum (DMSO-d_6, 298 K) of 2-(5'-ethynylpyridin-2'-yl)-1*H*-benzo[*d*]imidazole (**38**).

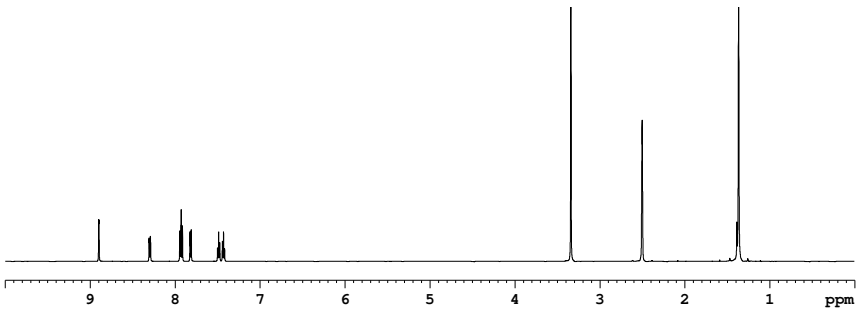

Figure 8.21: 600 MHz ^{1}H NMR spectrum (DMSO-d_6, 298 K) of *tert*-butyl 2'-(5"-bromopyridin-2"-yl)-1*H*-benzo[*d*]imidazole-1'-carboxylate (**41**).

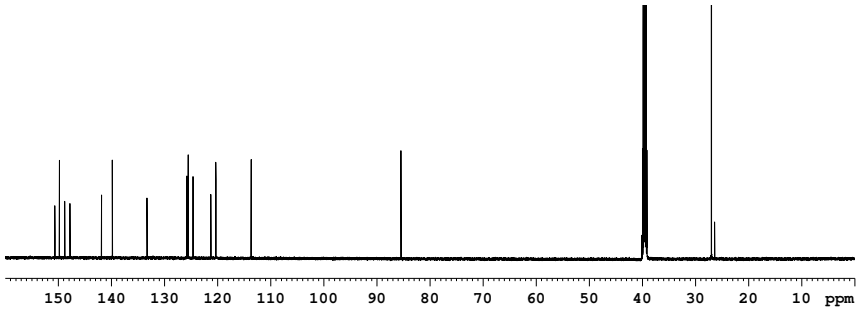

Figure 8.22: 151 MHz ^{13}C NMR spectrum (DMSO-d_6, 298 K) of *tert*-butyl 2'-(5"-bromopyridin-2"-yl)-1*H*-benzo[*d*]imidazole-1'-carboxylate (**41**).

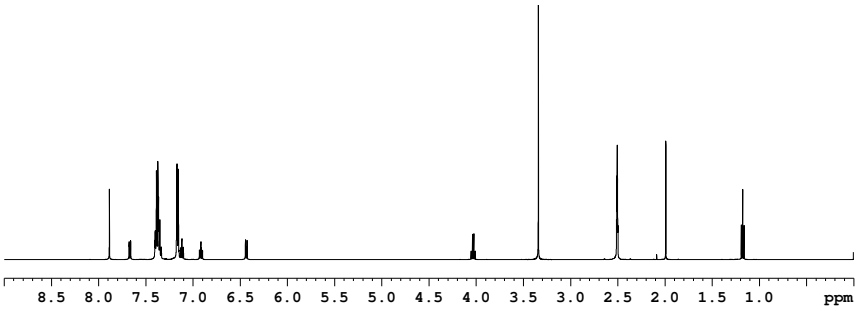

Figure 8.23: 500 MHz ^{1}H NMR spectrum (DMSO-d_6, 298 K) of 1-trityl-1*H*-benzo[*d*]imidazole (**47**).

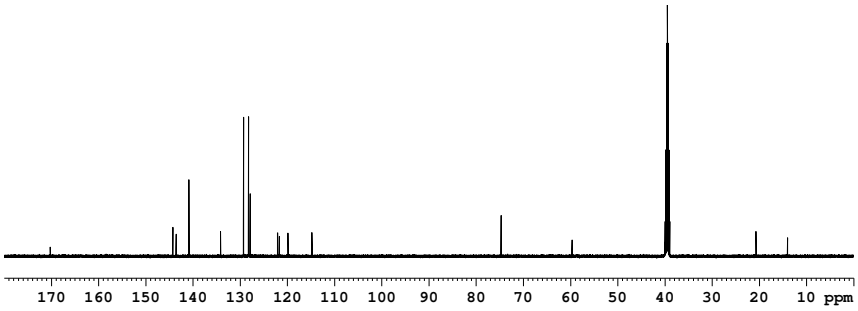

Figure 8.24: 126 MHz ^{13}C NMR spectrum (DMSO-d_6, 298 K) of 1-trityl-1*H*-benzo[*d*]imidazole (**47**).

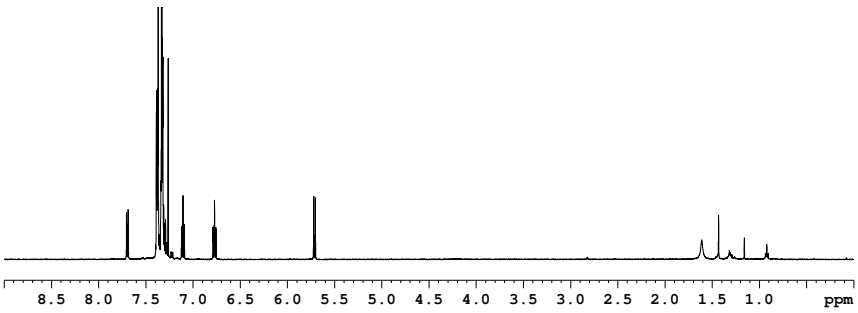

Figure 8.25: 500 MHz ^{1}H NMR spectrum ($CDCl_3$, 298 K) of 2-iodo-1-trityl-1*H*-benzo[*d*]imidazole (**48**).

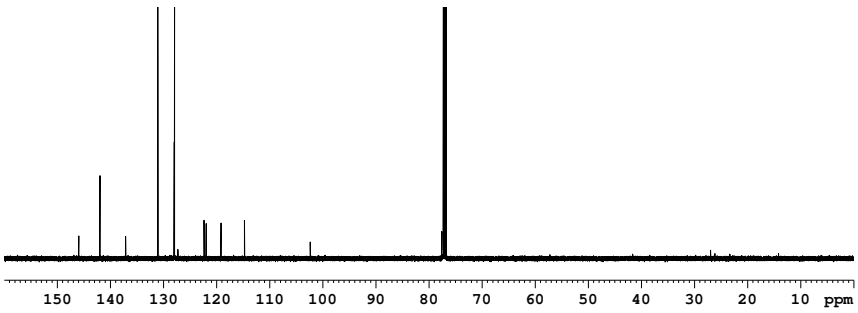

Figure 8.26: 126 MHz ^{13}C NMR spectrum ($CDCl_3$, 298 K) of 2-iodo-1-trityl-1*H*-benzo[*d*]imidazole (**48**).

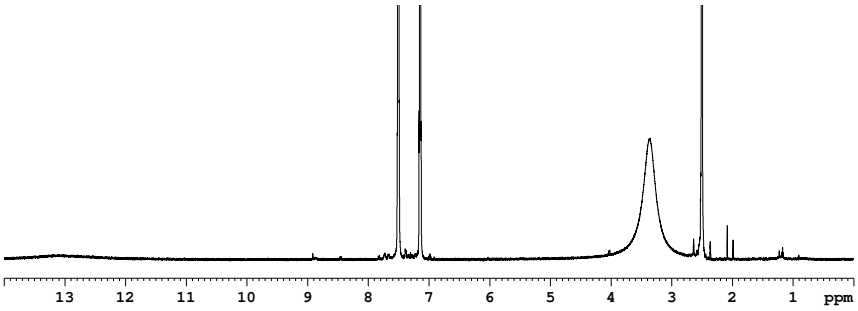

Figure 8.27: 500 MHz ^{1}H NMR spectrum (DMSO-d_6, 298 K) of 2-iodo-1*H*-benzo[*d*]imidazole (**49**).

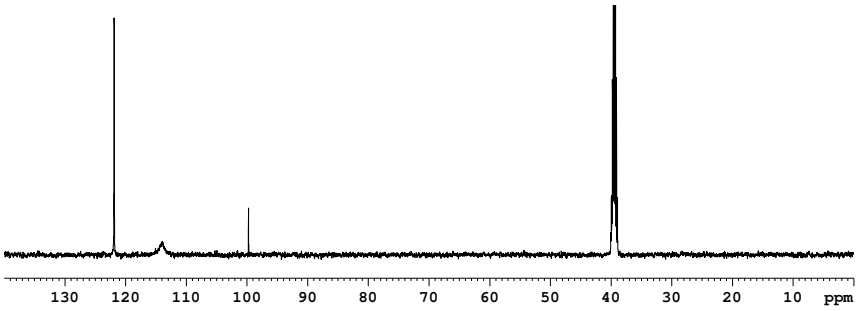

Figure 8.28: 126 MHz ^{13}C NMR spectrum (DMSO-d_6, 298 K) of 2-iodo-1*H*-benzo[*d*]imidazole (**49**).

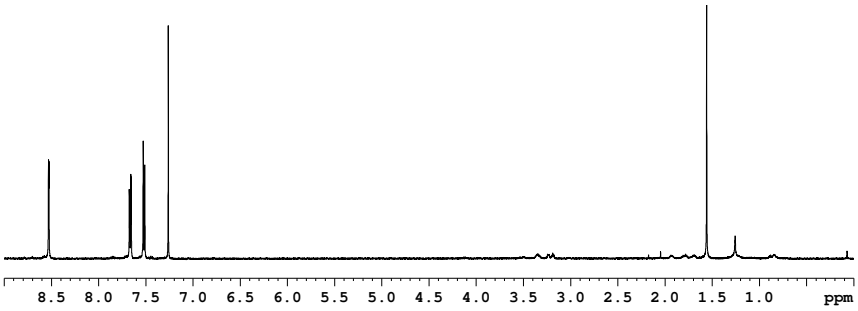

Figure 8.29: 500 MHz ^{1}H NMR spectrum ($CDCl_3$, 298 K) of 1,2-bis(6'-bromopyridin-3'-yl)ethyne (**51**).

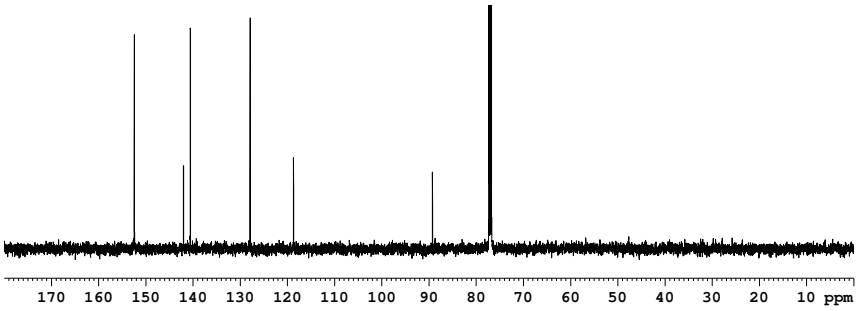

Figure 8.30: 126 MHz ^{13}C NMR spectrum ($CDCl_3$, 298 K) of 1,2-bis(6'-bromopyridin-3'-yl)ethyne (**51**).

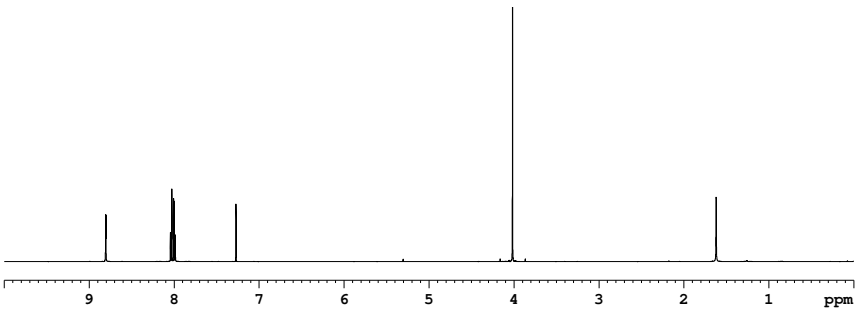

Figure 8.31: 500 MHz ^{1}H NMR spectrum ($CDCl_3$, 298 K) of methyl 5'-bromopicolinate (**53**).

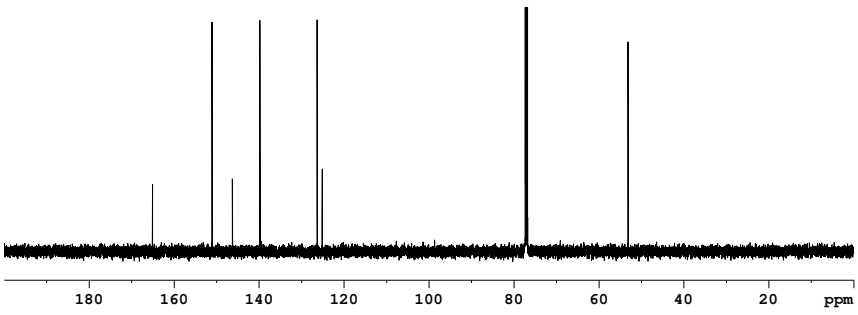

Figure 8.32: 126 MHz ^{13}C NMR spectrum ($CDCl_3$, 298 K) of methyl 5'-bromopicolinate (**53**).

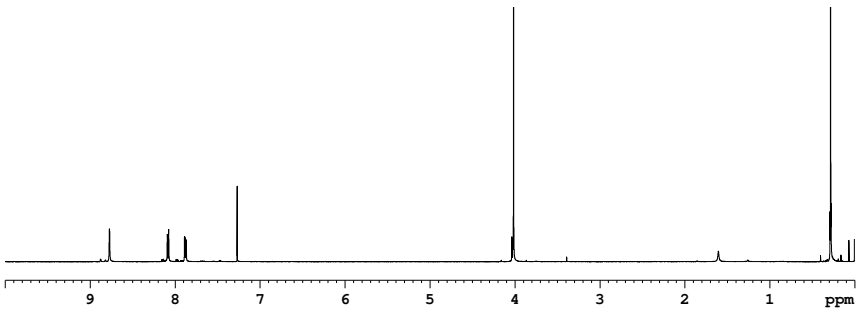

Figure 8.33: 500 MHz ^{1}H NMR spectrum ($CDCl_3$, 298 K) of methyl 5'-((trimethylsilyl)ethynyl)picolinate (**54**).

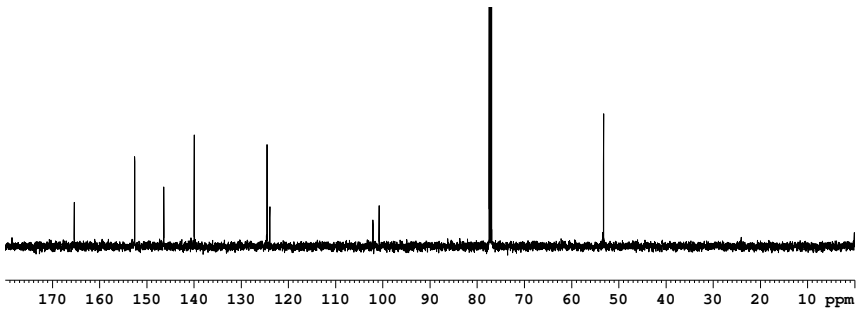

Figure 8.34: 126 MHz ^{13}C NMR spectrum ($CDCl_3$, 298 K) of methyl 5'-((trimethylsilyl)ethynyl)picolinate (**54**).

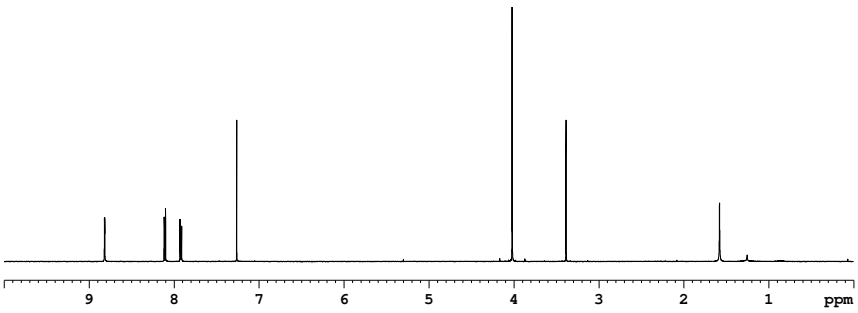

Figure 8.35: 500 MHz ^{1}H NMR spectrum ($CDCl_3$, 298 K) of methyl 5'-ethynylpicolinate (**55**).

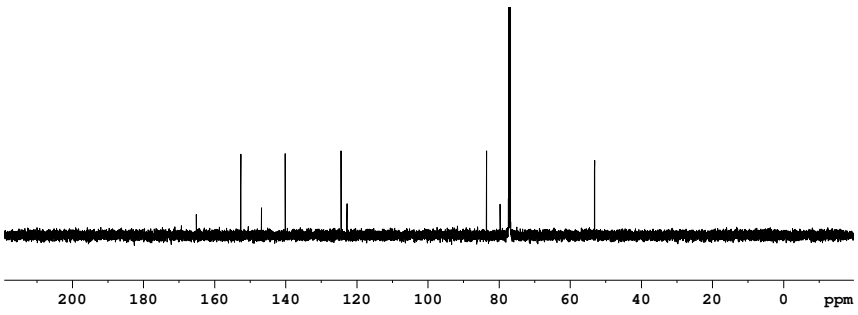

Figure 8.36: 126 MHz ^{13}C NMR spectrum ($CDCl_3$, 298 K) of methyl 5'-ethynylpicolinate (**55**).

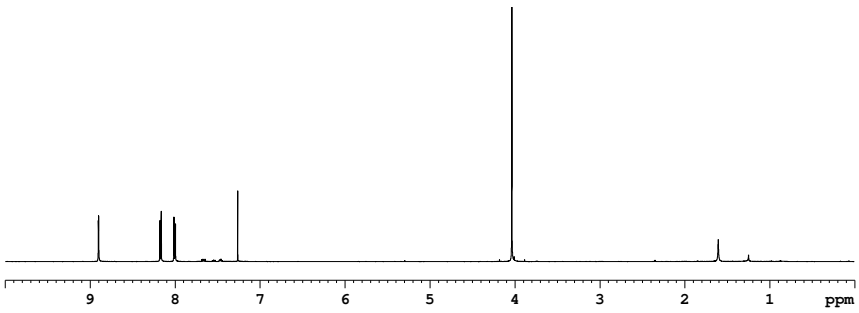

Figure 8.37: 500 MHz ^{1}H NMR spectrum ($CDCl_3$, 298 K) of dimethyl 5,5'-(ethyne-1",2"-diyl)dipicolinate (**56**).

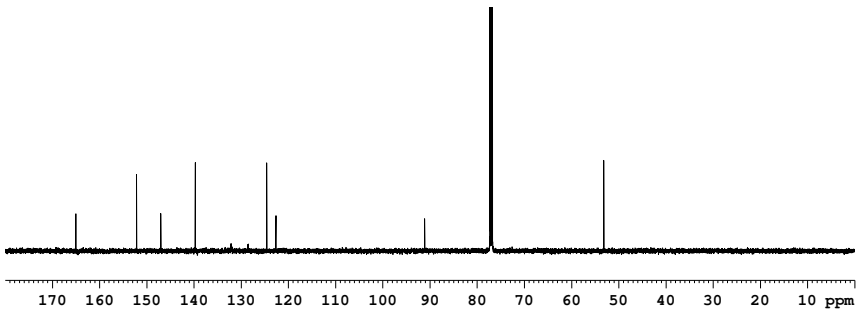

Figure 8.38: 126 MHz ^{13}C NMR spectrum ($CDCl_3$, 298 K) of dimethyl 5,5'-(ethyne-1",2"-diyl)dipicolinate (**56**).

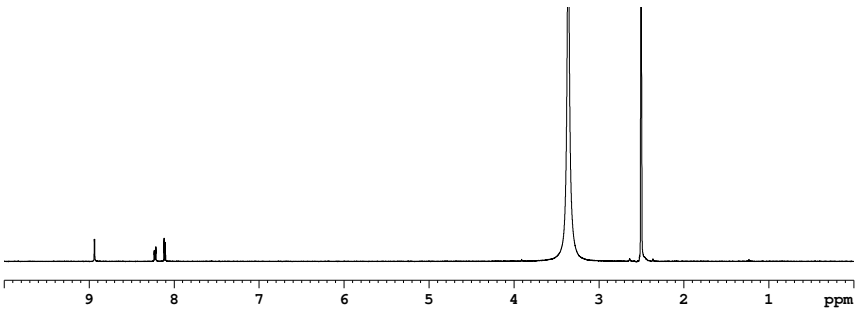

Figure 8.39: 500 MHz ^{1}H NMR spectrum (DMSO-d_6, 298 K) of 5,5'-(ethyne-1",2"-diyl)dipicolinic acid (**57**).

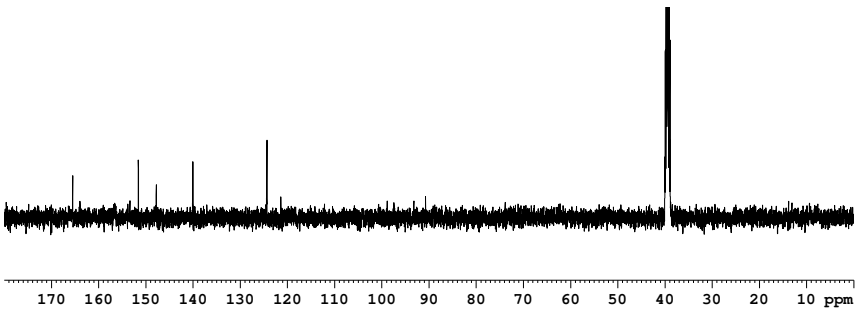

Figure 8.40: 126 MHz ^{13}C NMR spectrum (DMSO-d_6, 298 K) of 5,5'-(ethyne-1",2"-diyl)dipicolinic acid (**57**).

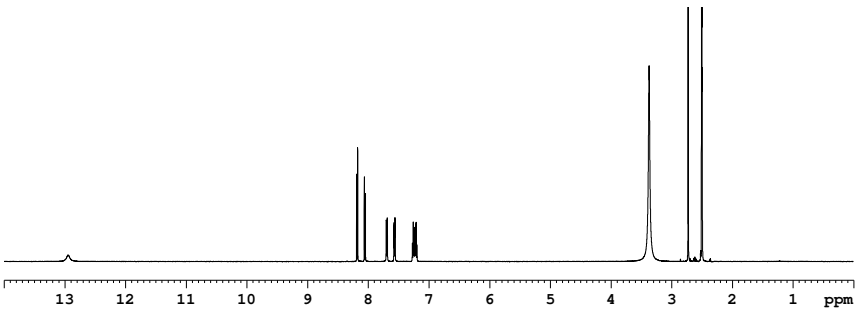

Figure 8.41: 500 MHz ^{1}H NMR spectrum (DMSO-d_6, 298 K) of 2-(5'-bromo-6'-methylpyridin-2'-yl)-1*H*-benzo[*d*]imidazole (**60**).

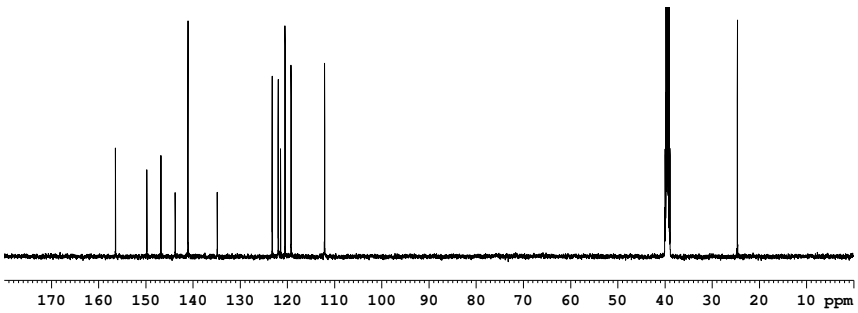

Figure 8.42: 126 MHz ^{13}C NMR spectrum (DMSO-d_6, 298 K) of 2-(5'-bromo-6'-methylpyridin-2'-yl)-1*H*-benzo[*d*]imidazole (**60**).

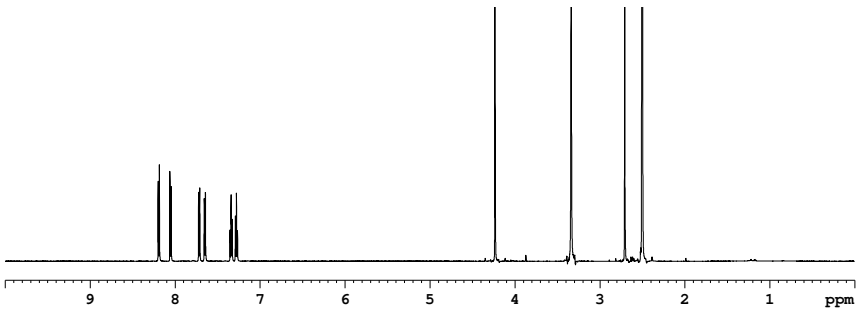

Figure 8.43: 600 MHz ^{1}H NMR spectrum (DMSO-d_6, 298 K) of 2-(5'-bromo-6'-methylpyridin-2'-yl)-1-methyl-1*H*-benzo[*d*]imidazole (**61**).

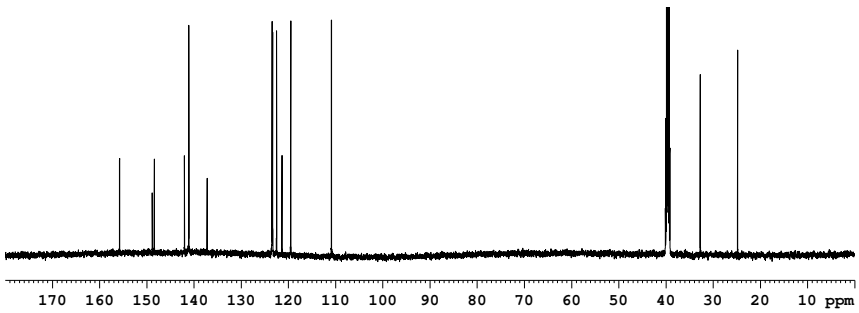

Figure 8.44: 151 MHz ^{13}C NMR spectrum (DMSO-d_6, 298 K) of 2-(5'-bromo-6'-methylpyridin-2'-yl)-1-methyl-1*H*-benzo[*d*]imidazole (**61**).

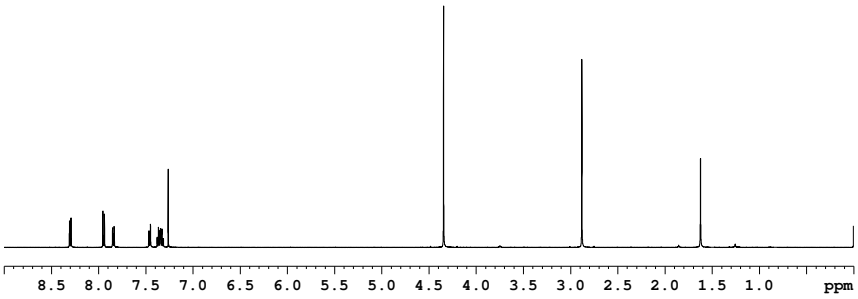

Figure 8.45: 500 MHz ^{1}H NMR spectrum ($CDCl_3$, 298 K) of 1,2-bis(2”-methyl-6”-(1’-methyl-1*H*-benzo[*d*]imidazol-2’-yl)pyridin-3”-yl)ethyne (**36**).

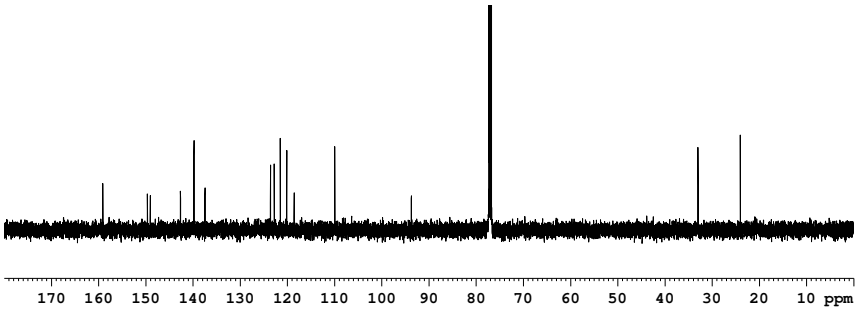

Figure 8.46: 126 MHz ^{13}C NMR spectrum ($CDCl_3$, 298 K) of 1,2-bis(2”-methyl-6”-(1’-methyl-1*H*-benzo[*d*]imidazol-2’-yl)pyridin-3”-yl)ethyne (**36**).

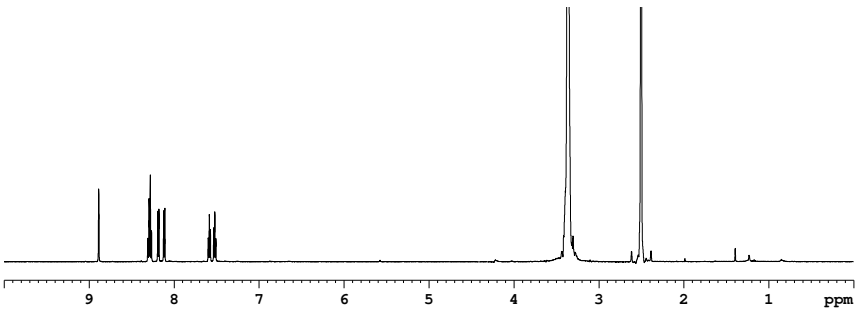

Figure 8.47: 500 MHz ^{1}H NMR spectrum (DMSO-d_6, 298 K) of 2-(5'-bromopyridin-2'-yl)benzo[*d*]thiazole (**63**).

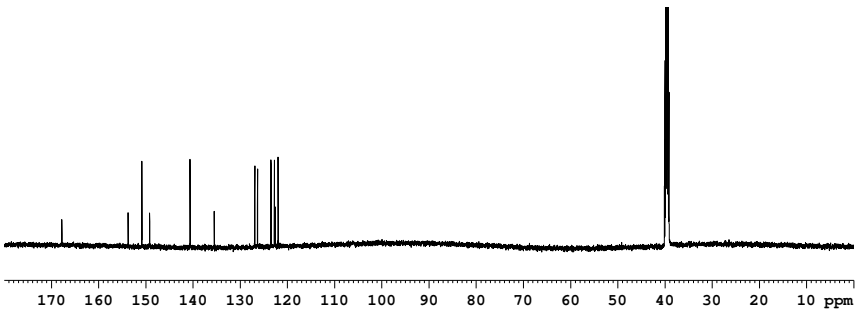

Figure 8.48: 126 MHz ^{13}C NMR spectrum (DMSO-d_6, 298 K) of 2-(5'-bromopyridin-2'-yl)benzo[*d*]thiazole (**63**).

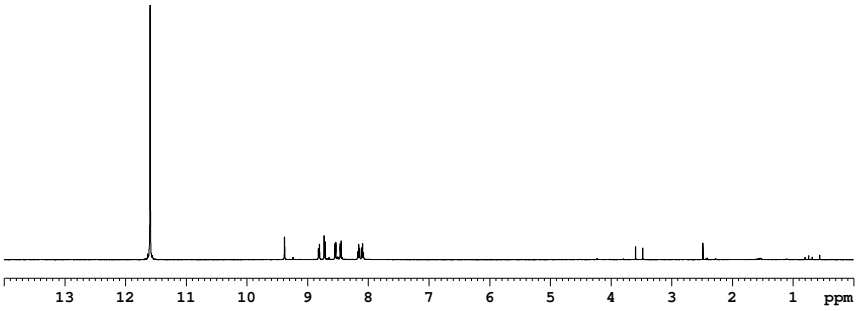

Figure 8.49: 500 MHz ^{1}H NMR spectrum (TFA-d_1, 298 K) of 1,2-bis(2'-(benzo[*d*]thiazol-2''-yl)pyridin-5'-yl)ethyne (**34**).

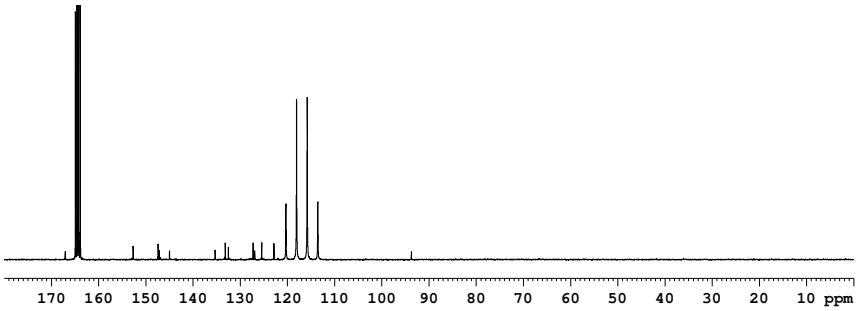

Figure 8.50: 126 MHz ^{13}C NMR spectrum (TFA-d_1, 298 K) of 1,2-bis(2'-(benzo[*d*]thiazol-2''-yl)pyridin-5'-yl)ethyne (**34**).

8.8 ^{1}H, ^{13}C NMR spectra for Chapter 4

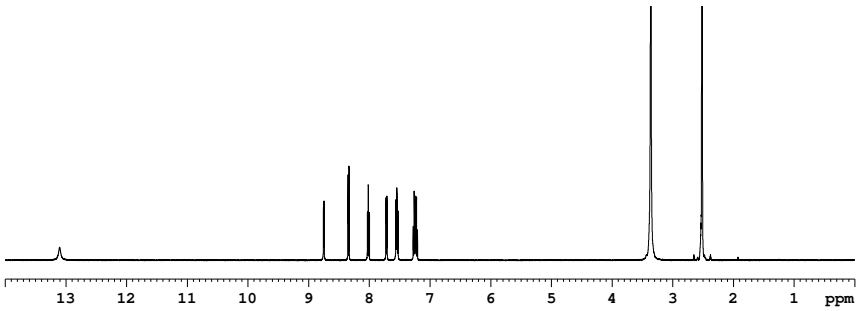

Figure 8.51: 500 MHz ^{1}H NMR spectrum (DMSO-d_6, 298 K) of 2-(pyridin-2'-yl)-1*H*-benzo[*d*]imidazole (**76**).

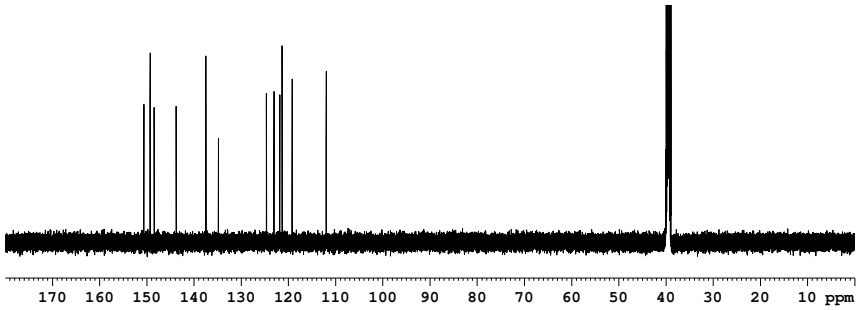

Figure 8.52: 126 MHz ^{13}C NMR spectrum (DMSO-d_6, 298 K) of 2-(pyridin-2'-yl)-1*H*-benzo[*d*]imidazole (**76**).

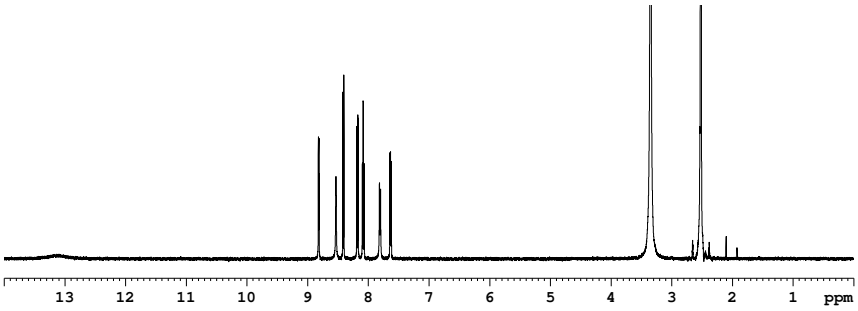

Figure 8.53: 500 MHz ^{1}H NMR spectrum (DMSO-d_6, 298 K) of 5-nitro-2-(pyridin-2'-yl)-1*H*-benzo[*d*]imidazole (**77**).

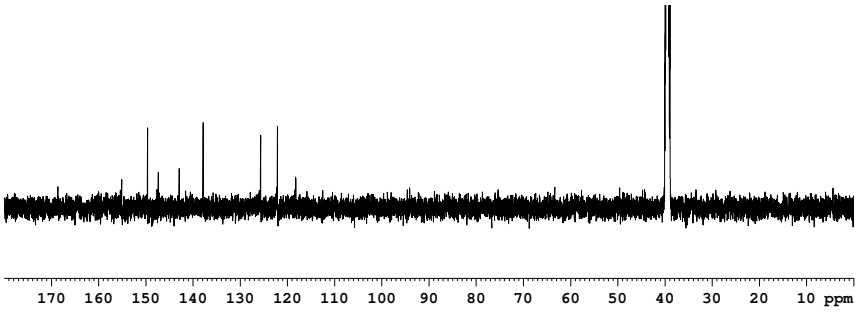

Figure 8.54: 126 MHz ^{13}C NMR spectrum (DMSO-d_6, 298 K) of 5-nitro-2-(pyridin-2'-yl)-1*H*-benzo[*d*]imidazole (**77**).

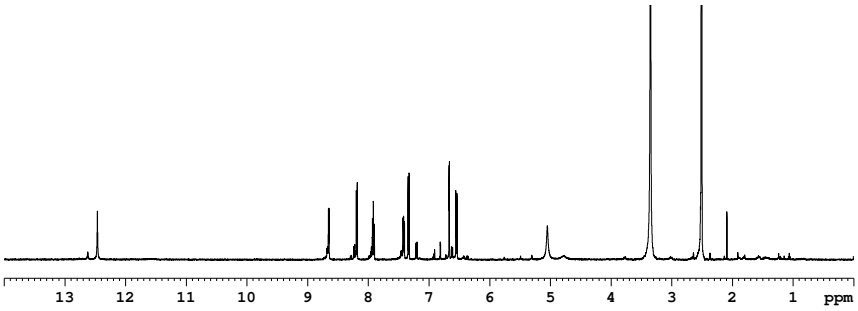

Figure 8.55: 500 MHz ^{1}H NMR spectrum (DMSO-d_6, 298 K) of 5-amino-2-(pyridin-2'-yl)-1*H*-benzo[*d*]imidazole (**78**).

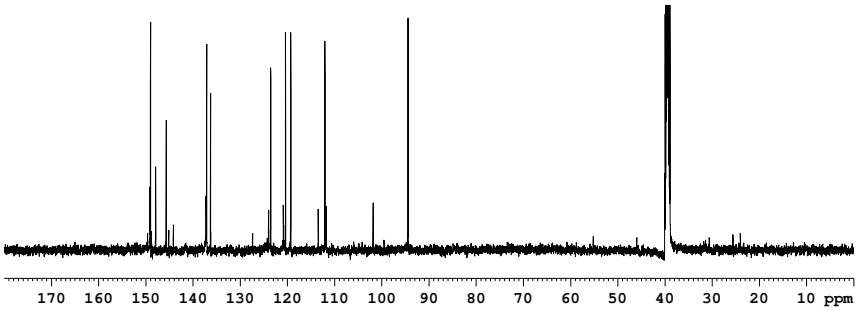

Figure 8.56: 126 MHz ^{13}C NMR spectrum (DMSO-d_6, 298 K) of 5-amino-2-(pyridin-2'-yl)-1*H*-benzo[*d*]imidazole (**78**).

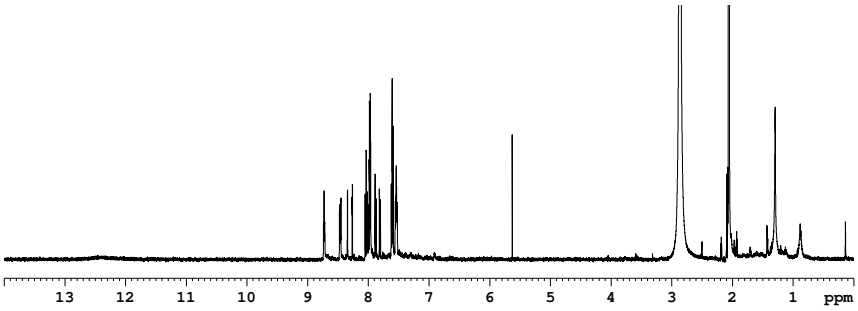

Figure 8.57: 500 MHz ^{1}H NMR spectrum (acetone-d_6, 298 K) of (*E*)-2-(5'-bromopyridin-2'-yl)-5-(phenyldiazenyl)-1*H*-benzo[*d*]imidazole (**67**).

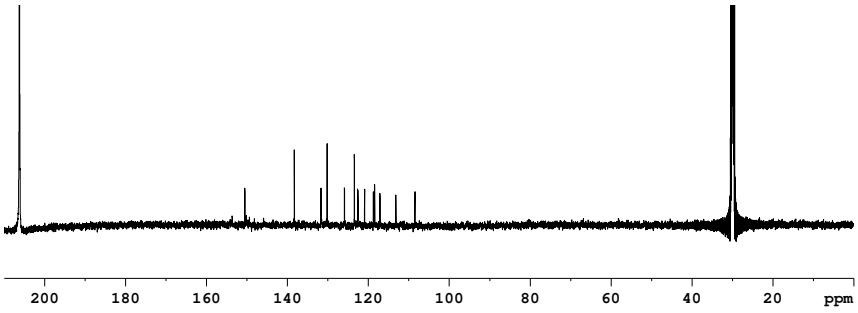

Figure 8.58: 126 MHz ^{13}C NMR spectrum (acetone-d_6, 298 K) of (*E*)-2-(5'-bromopyridin-2'-yl)-5-(phenyldiazenyl)-1*H*-benzo[*d*]imidazole (**67**).

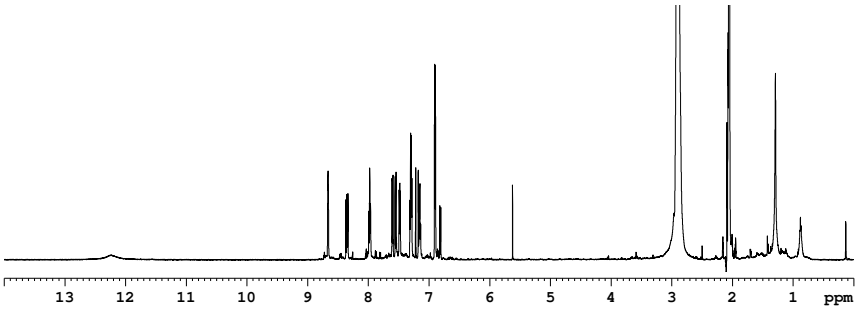

Figure 8.59: 600 MHz ^{1}H NMR spectrum (acetone-d_6, 298 K) of (*Z*)-2-(5'-bromopyridin-2'-yl)-5-(phenyldiazenyl)-1*H*-benzo[*d*]imidazole (**99**).

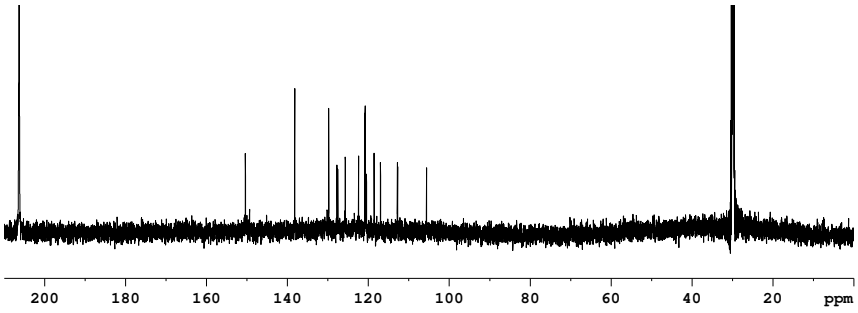

Figure 8.60: 151 MHz ^{13}C NMR spectrum (acetone-d_6, 298 K) of (*Z*)-2-(5'-bromopyridin-2'-yl)-5-(phenyldiazenyl)-1*H*-benzo[*d*]imidazole (**99**).

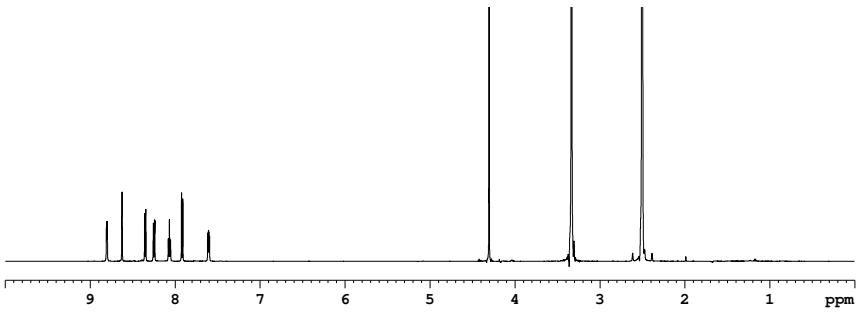

Figure 8.61: 600 MHz ^{1}H NMR spectrum (DMSO-d_6, 298 K) of 2-(pyridin-2'-yl)-1-methyl-5-nitro-1*H*-benzo[*d*]imidazole (**85**).

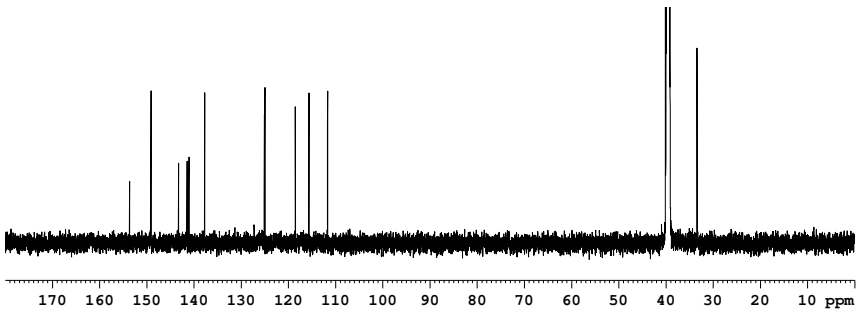

Figure 8.62: 151 MHz ^{13}C NMR spectrum (DMSO-d_6, 298 K) of 2-(pyridin-2'-yl)-1-methyl-5-nitro-1*H*-benzo[*d*]imidazole (**85**).

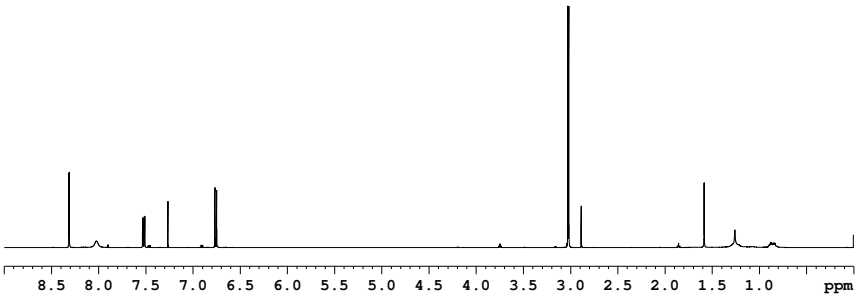

Figure 8.63: 500 MHz ^{1}H NMR spectrum ($CDCl_3$, 298 K) of 4-bromo-*N*-methyl-2-nitroaniline (**89**).

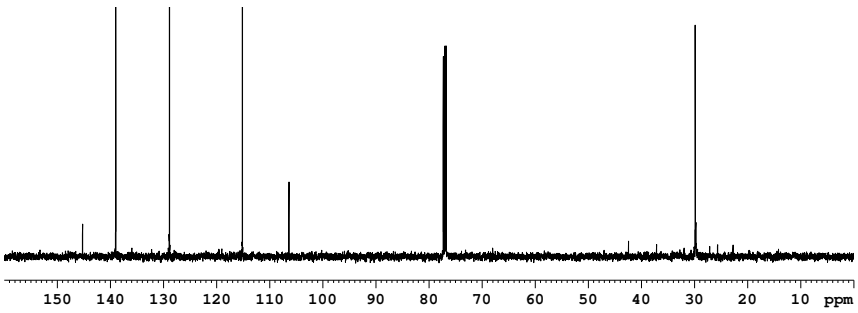

Figure 8.64: 126 MHz ^{13}C NMR spectrum ($CDCl_3$, 298 K) of 4-bromo-*N*-methyl-2-nitroaniline (**89**).

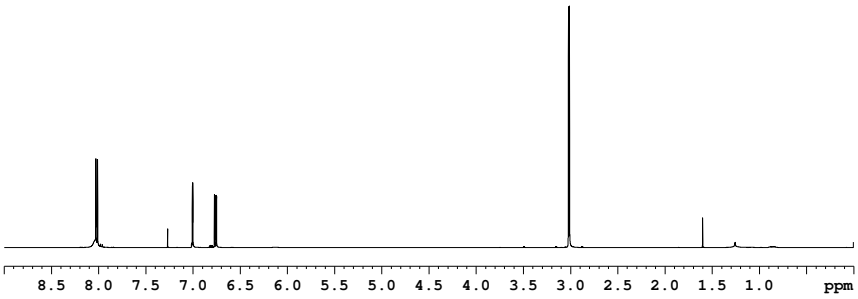

Figure 8.65: 500 MHz ^{1}H NMR spectrum ($CDCl_3$, 298 K) of 5-bromo-*N*-methyl-2-nitroaniline (**90**).

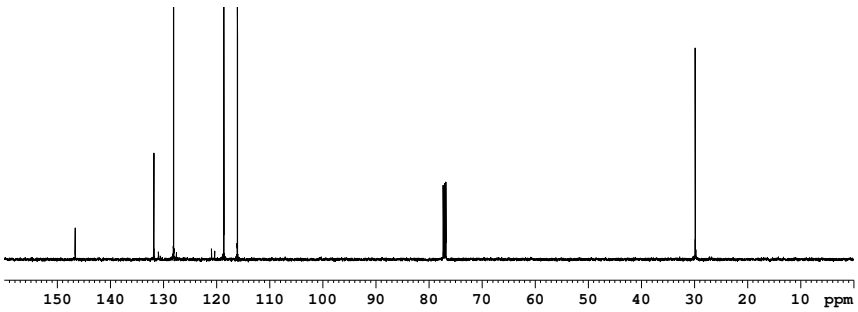

Figure 8.66: 126 MHz ^{13}C NMR spectrum ($CDCl_3$, 298 K) of 5-bromo-*N*-methyl-2-nitroaniline (**90**).

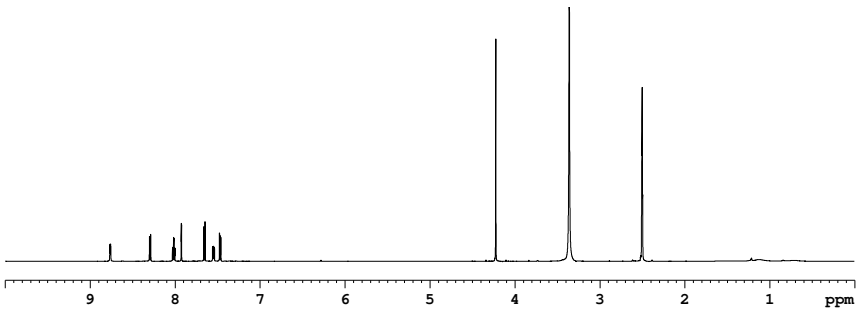

Figure 8.67: 600 MHz ^{1}H NMR spectrum (DMSO-d_6, 298 K) of 5-bromo-1-methyl-2-(pyridin-2'-yl)-1*H*-benzo[*d*]imidazole (**92**).

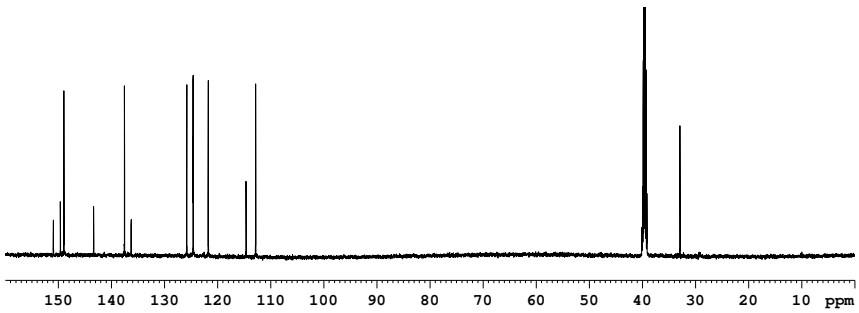

Figure 8.68: 151 MHz ^{13}C NMR spectrum (DMSO-d_6, 298 K) of 5-bromo-1-methyl-2-(pyridin-2'-yl)-1*H*-benzo[*d*]imidazole (**92**).

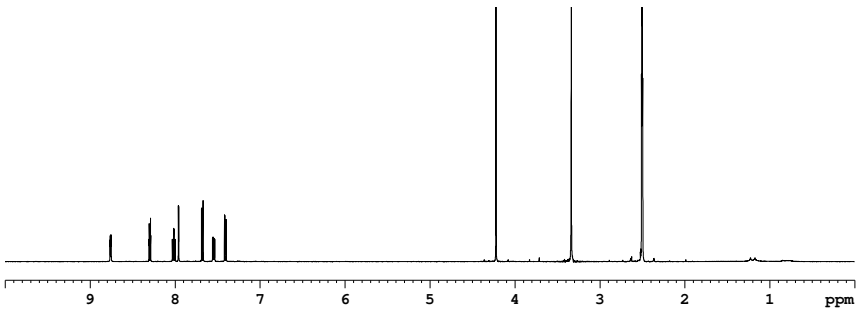

Figure 8.69: 500 MHz ^{1}H NMR spectrum (DMSO-d_6, 298 K) of 6-bromo-1-methyl-2-(pyridin-2'-yl)-1*H*-benzo[*d*]imidazole (**93**).

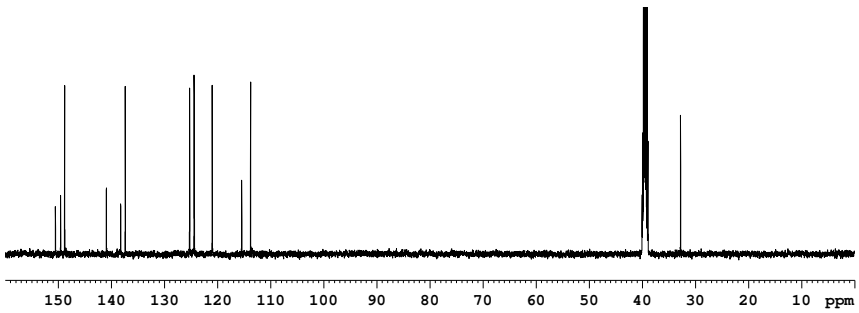

Figure 8.70: 126 MHz ^{13}C NMR spectrum (DMSO-d_6, 298 K) of 6-bromo-1-methyl-2-(pyridin-2'-yl)-1*H*-benzo[*d*]imidazole (**93**).

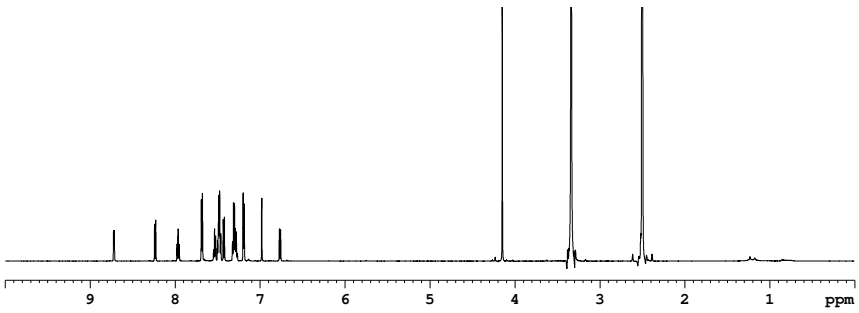

Figure 8.71: 500 MHz ^{1}H NMR spectrum (DMSO-d_6, 298 K) of *N*-(1'-methyl-2'-(pyridin-2"-yl)-1*H*-benzo[*d*]imidazol-5'-yl)-1,1-diphenylmethanimine (**94**).

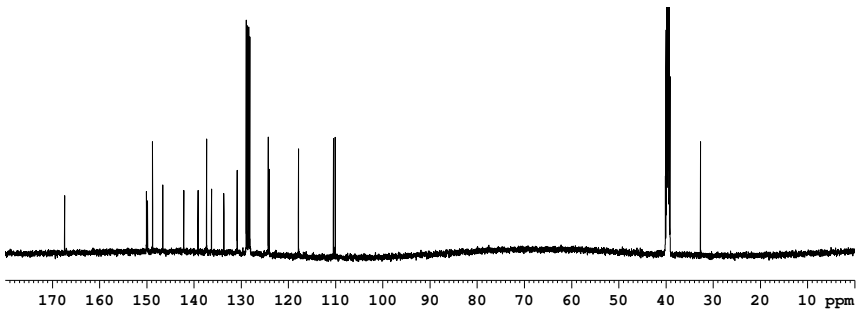

Figure 8.72: 126 MHz ^{13}C NMR spectrum (DMSO-d_6, 298 K) of *N*-(1'-methyl-2'-(pyridin-2"-yl)-1*H*-benzo[*d*]imidazol-5'-yl)-1,1-diphenylmethanimine (**94**).

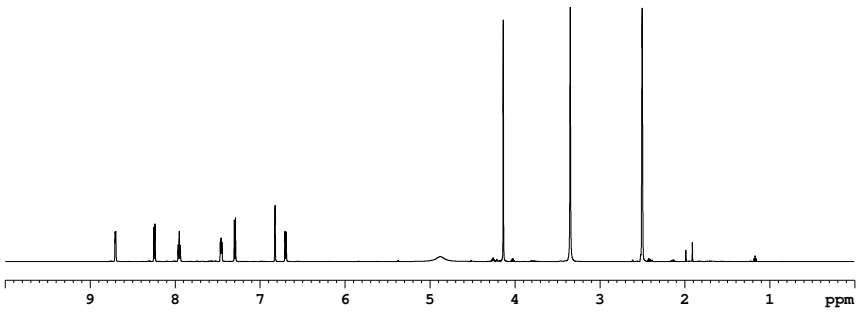

Figure 8.73: 600 MHz ^{1}H NMR spectrum (DMSO-d_6, 298 K) of 1-methyl-2-(pyridin-2'-yl)-1*H*-benzo[*d*]imidazol-5-amine (**86**).

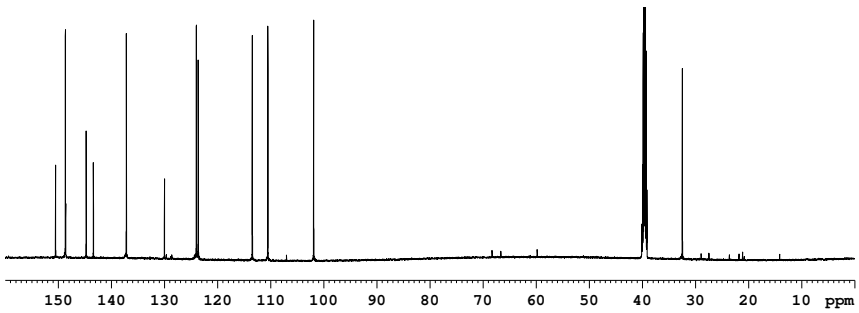

Figure 8.74: 151 MHz ^{13}C NMR spectrum (DMSO-d_6, 298 K) of 1-methyl-2-(pyridin-2'-yl)-1*H*-benzo[*d*]imidazol-5-amine (**86**).

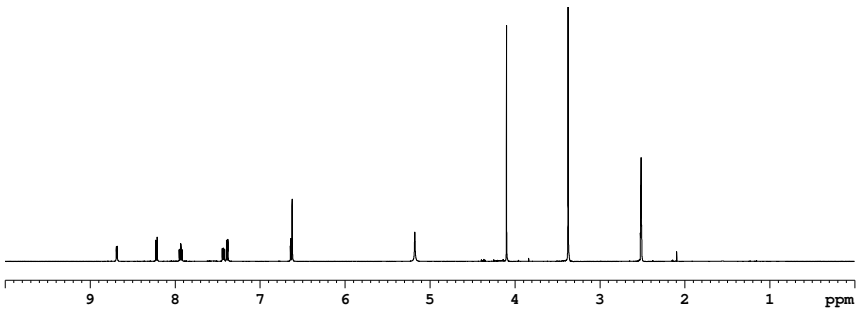

Figure 8.75: 500 MHz ^{1}H NMR spectrum ($CDCl_3$, 298 K) of 1-methyl-2-(pyridin-2'-yl)-1*H*-benzo[*d*]imidazol-6-amine (**98**).

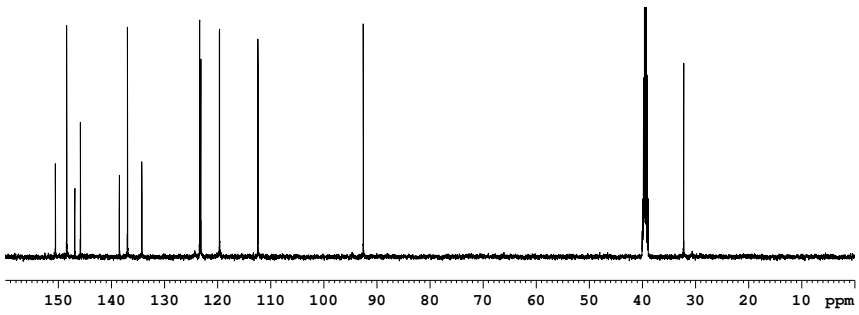

Figure 8.76: 126 MHz ^{13}C NMR spectrum ($CDCl_3$, 298 K) of 1-methyl-2-(pyridin-2'-yl)-1*H*-benzo[*d*]imidazol-6-amine (**98**).

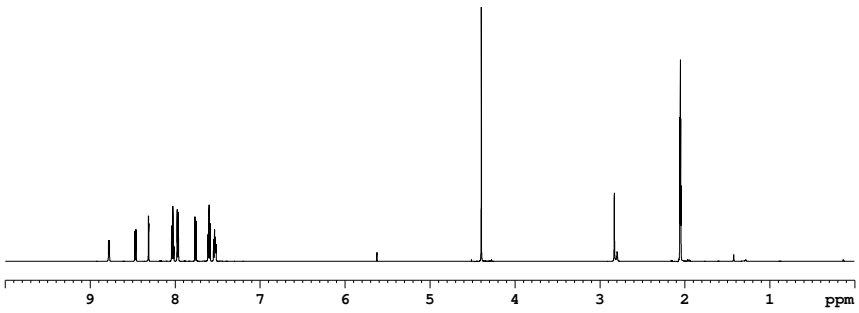

Figure 8.77: 600 MHz ^{1}H NMR spectrum (acetone-d_6, 298 K) of (*E*)-1-methyl-5-(phenyldiazenyl)-2-(pyridin-2'-yl)-1*H*-benzo[*d*]imidazole (**68**).

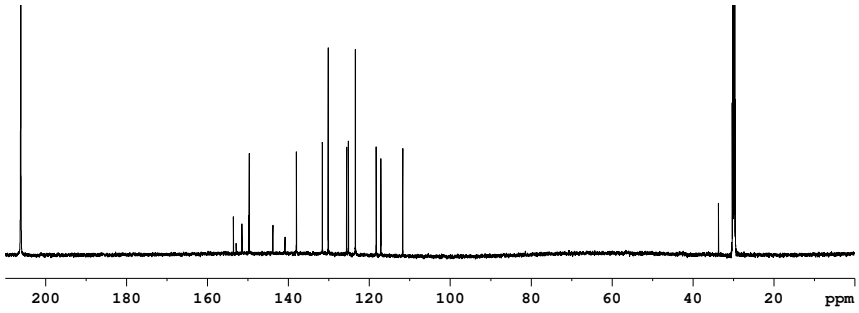

Figure 8.78: 151 MHz ^{13}C NMR spectrum (acetone-d_6, 298 K) of (*E*)-1-methyl-5-(phenyldiazenyl)-2-(pyridin-2'-yl)-1*H*-benzo[*d*]imidazole (**68**).

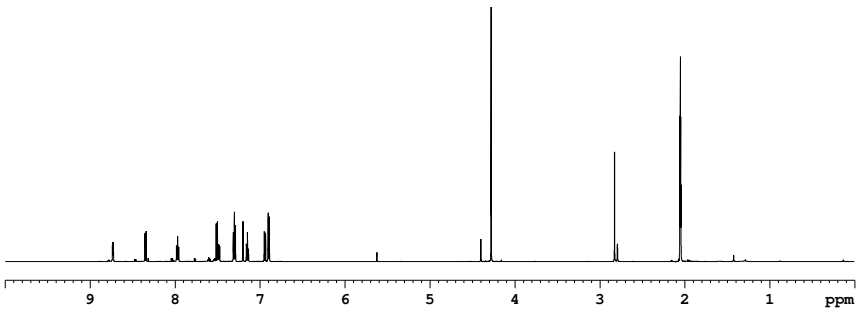

Figure 8.79: 600 MHz ^{1}H NMR spectrum (acetone-d_6, 298 K) of (*Z*)-1-methyl-5-(phenyldiazenyl)-2-(pyridin-2'-yl)-1*H*-benzo[*d*]imidazole (**101**).

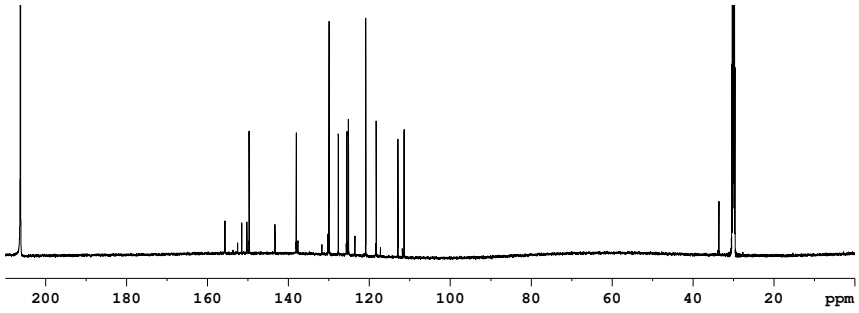

Figure 8.80: 151 MHz ^{13}C NMR spectrum (acetone-d_6, 298 K) of (*Z*)-1-methyl-5-(phenyldiazenyl)-2-(pyridin-2'-yl)-1*H*-benzo[*d*]imidazole (**101**).

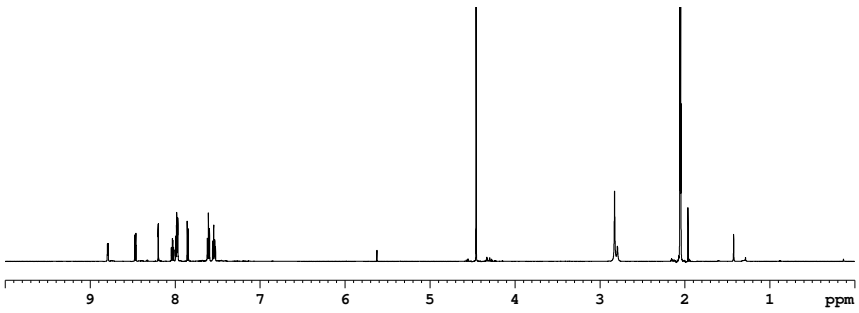

Figure 8.81: 600 MHz ^{1}H NMR spectrum (acetone-d_6, 298 K) of (*E*)-1-methyl-6-(phenyldiazenyl)-2-(pyridin-2'-yl)-1*H*-benzo[*d*]imidazole (**69**).

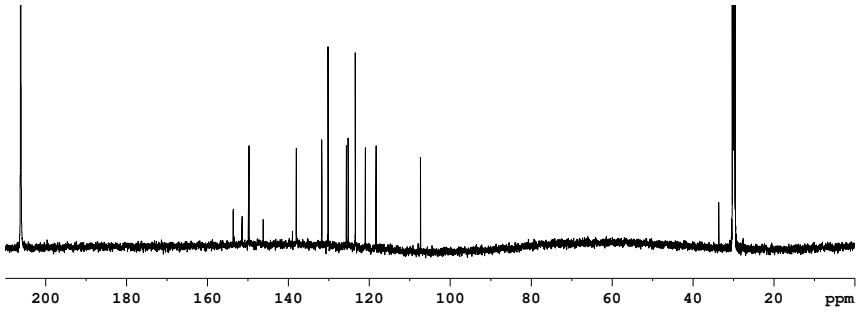

Figure 8.82: 151 MHz ^{13}C NMR spectrum (acetone-d_6, 298 K) of (*E*)-1-methyl-6-(phenyldiazenyl)-2-(pyridin-2'-yl)-1*H*-benzo[*d*]imidazole (**69**).

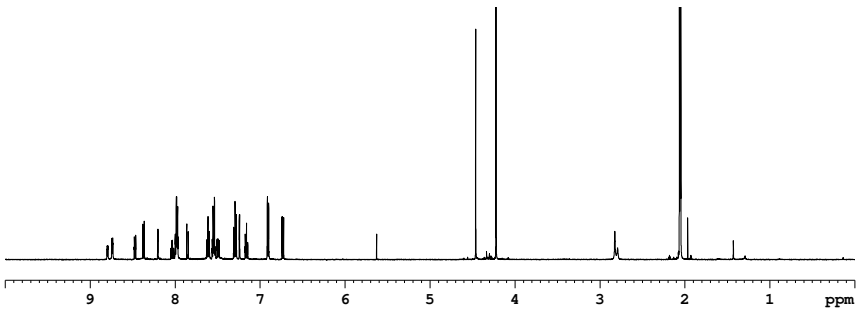

Figure 8.83: 500 MHz ^{1}H NMR spectrum (acetone-d_6, 298 K) of (*Z*)-1-methyl-6-(phenyldiazenyl)-2-(pyridin-2'-yl)-1*H*-benzo[*d*]imidazole (**102**).

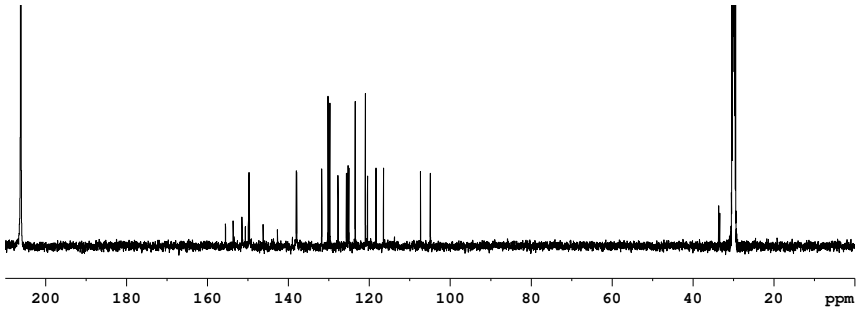

Figure 8.84: 126 MHz ^{13}C NMR spectrum (acetone-d_6, 298 K) of (*Z*)-1-methyl-6-(phenyldiazenyl)-2-(pyridin-2'-yl)-1*H*-benzo[*d*]imidazole (**102**).

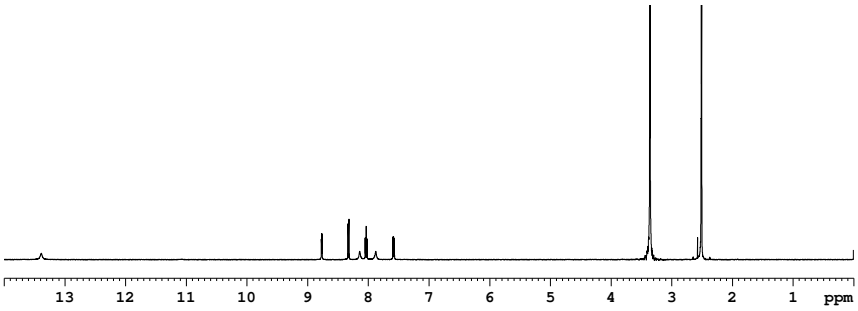

Figure 8.85: 500 MHz ^{1}H NMR spectrum (DMSO-d_6, 298 K) of 5,6-dibromo-2-(pyridin-2'-yl)-1*H*-benzo[*d*]imidazole (**106**).

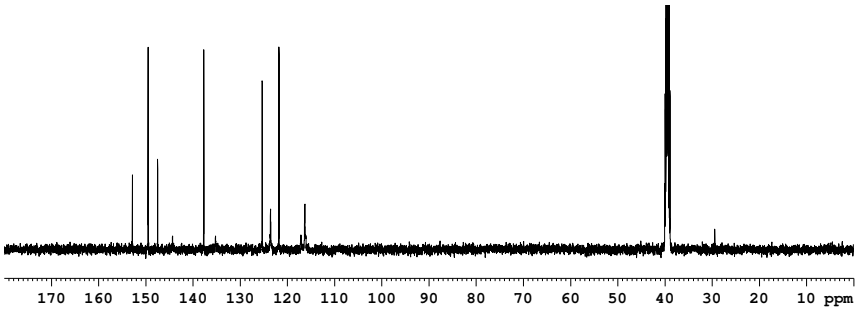

Figure 8.86: 126 MHz ^{13}C NMR spectrum (DMSO-d_6, 298 K) of 5,6-dibromo-2-(pyridin-2'-yl)-1*H*-benzo[*d*]imidazole (**106**).

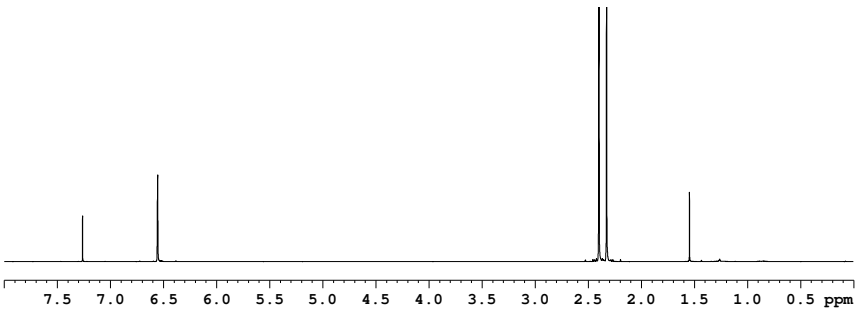

Figure 8.87: 500 MHz ^{1}H NMR spectrum ($CDCl_3$, 298 K) of 3-bromo-2,5-dimethylthiophene (**108**).

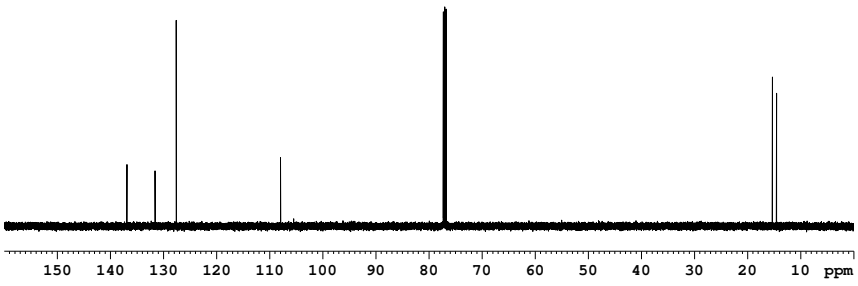

Figure 8.88: 126 MHz ^{13}C NMR spectrum ($CDCl_3$, 298 K) of 3-bromo-2,5-dimethylthiophene (**108**).

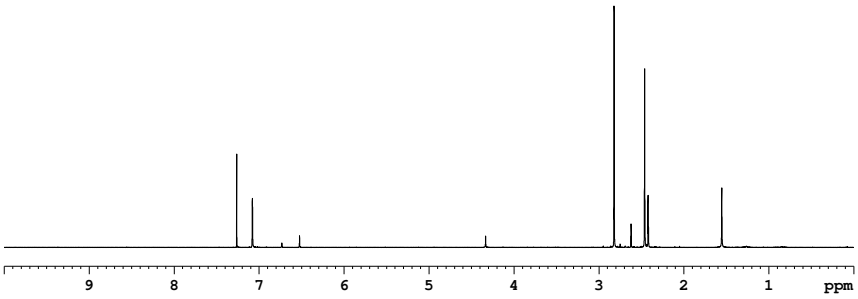

Figure 8.89: 500 MHz ^{1}H NMR spectrum ($CDCl_3$, 298 K) of (2,5-dimethylthiophen-3-yl)boronic acid (**109**).

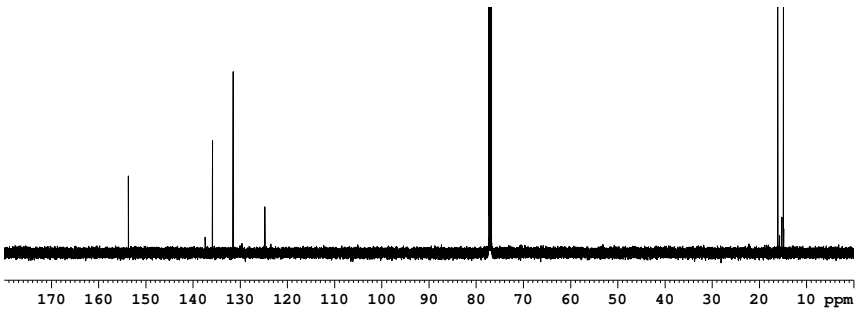

Figure 8.90: 126 MHz ^{13}C NMR spectrum ($CDCl_3$, 298 K) of (2,5-dimethylthiophen-3-yl)boronic acid (**109**).

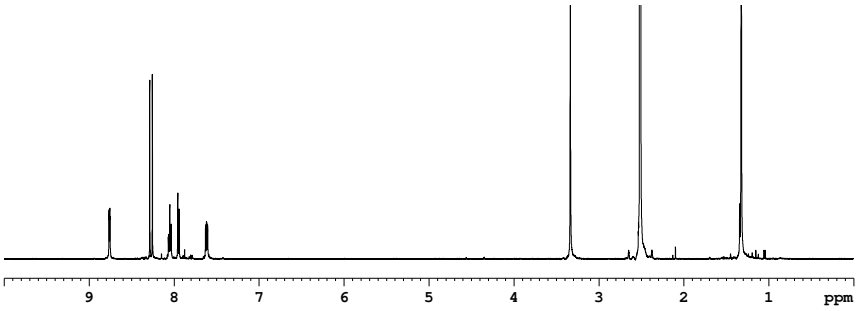

Figure 8.91: 500 MHz ^{1}H NMR spectrum (DMSO-d_6, 298 K) of 5',6'-dibromo-2'-(pyridin-2"-yl)-1*H*-benzo[*d*]imidazole-1-carboxylate (**114**).

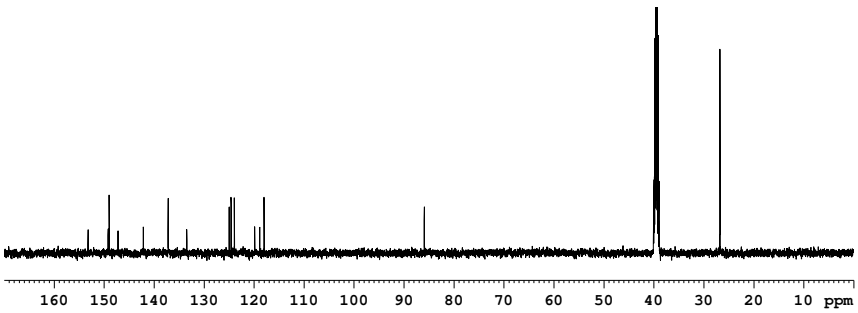

Figure 8.92: 126 MHz ^{13}C NMR spectrum (DMSO-d_6, 298 K) of 5',6'-dibromo-2'-(pyridin-2"-yl)-1*H*-benzo[*d*]imidazole-1-carboxylate (**114**).

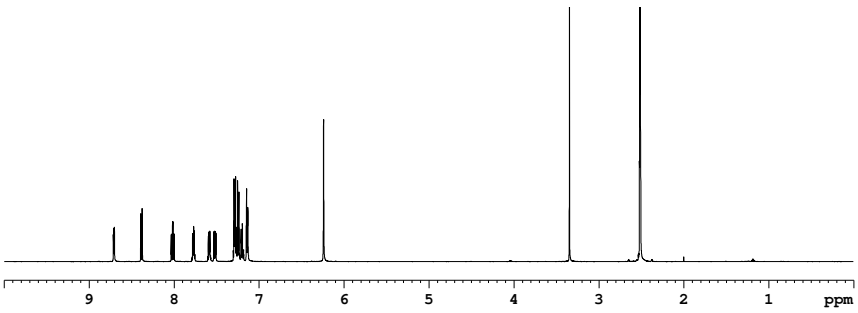

Figure 8.93: 500 MHz ^{1}H NMR spectrum (DMSO-d_6, 298 K) of 1-benzyl-2-(pyridin-2'-yl)-1*H*-benzo[*d*]imidazole (**116**).

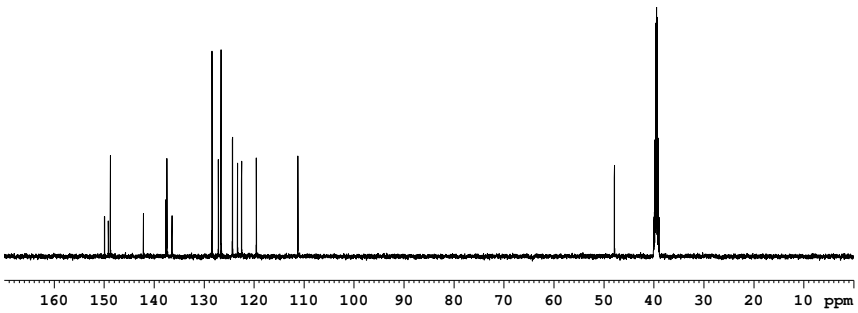

Figure 8.94: 126 MHz ^{13}C NMR spectrum (DMSO-d_6, 298 K) of 1-benzyl-2-(pyridin-2'-yl)-1*H*-benzo[*d*]imidazole (**116**).

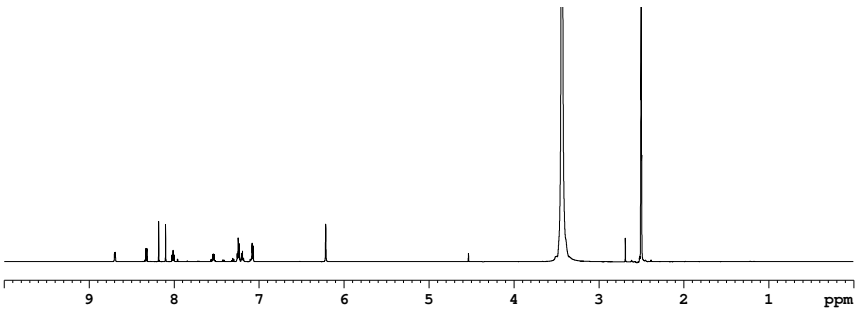

Figure 8.95: 600 MHz ^{1}H NMR spectrum (DMSO-d_6, 298 K) of 1-benzyl-5,6-dibromo-2-(pyridin-2'-yl)-1*H*-benzo[*d*]imidazole (**117**).

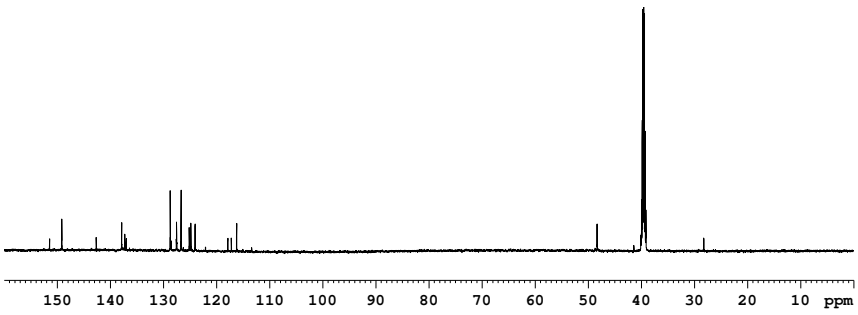

Figure 8.96: 151 MHz ^{13}C NMR spectrum (DMSO-d_6, 298 K) of 1-benzyl-5,6-dibromo-2-(pyridin-2'-yl)-1*H*-benzo[*d*]imidazole (**117**).

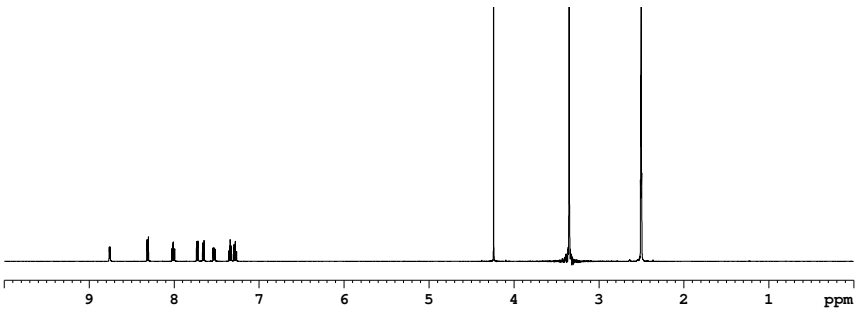

Figure 8.97: 500 MHz ^{1}H NMR spectrum (DMSO-d_6, 298 K) of 1-methyl-2-(pyridin-2'-yl)-1*H*-benzo[*d*]imidazole (**119**).

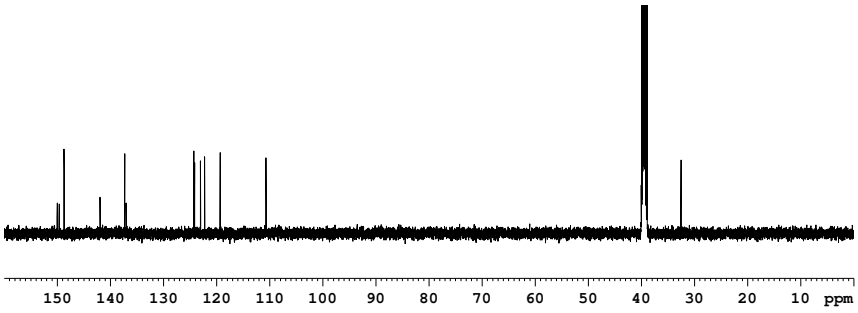

Figure 8.98: 126 MHz ^{13}C NMR spectrum (DMSO-d_6, 298 K) of 1-methyl-2-(pyridin-2'-yl)-1*H*-benzo[*d*]imidazole (**119**).

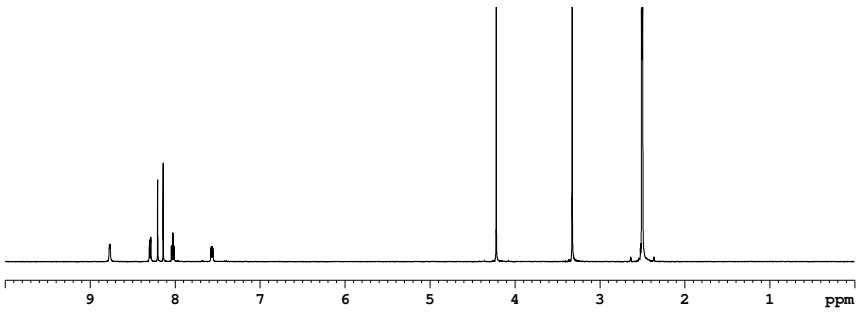

Figure 8.99: 500 MHz ^{1}H NMR spectrum ($CDCl_3$, 298 K) of 5,6-dibromo-1-methyl-2-(pyridin-2'-yl)-benzimidazole (**120**).

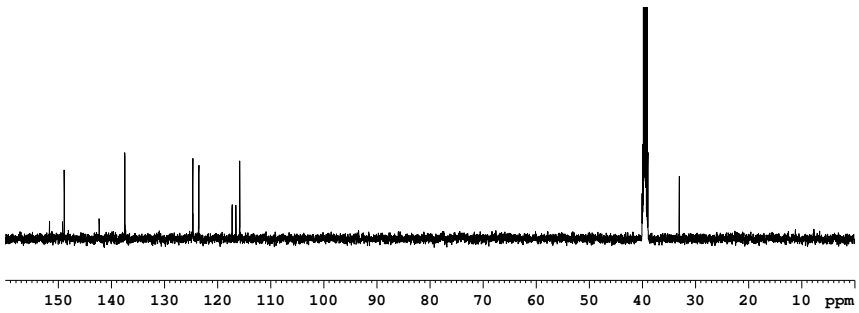

Figure 8.100: 126 MHz ^{13}C NMR spectrum ($CDCl_3$, 298 K) of 5,6-dibromo-1-methyl-2-(pyridin-2'-yl)-benzimidazole (**120**).

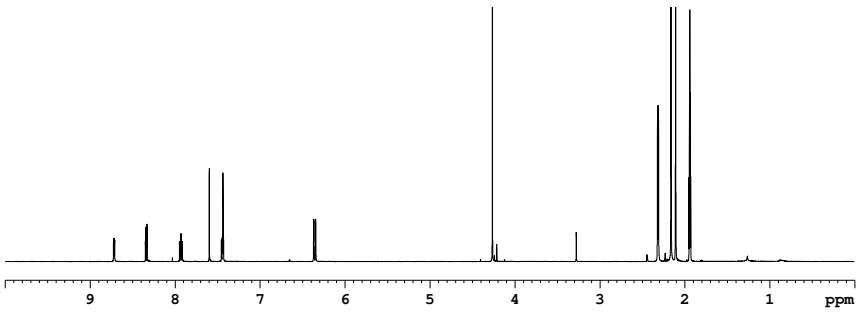

Figure 8.101: 500 MHz ^{1}H NMR spectrum (CD3CN, 298 K) of 6,7-di(2",5"-dimethylthiophen-3"-yl)-1-methyl-2-(pyridin-2'-yl)benzimidazole (**71**).

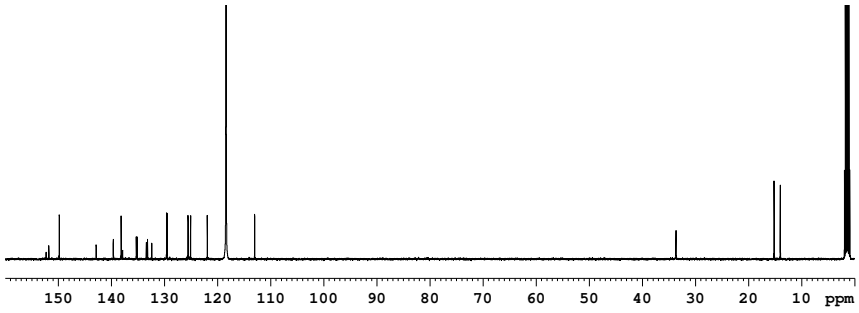

Figure 8.102: 126 MHz ^{13}C NMR spectrum (CD3CN, 298 K) of 6,7-di(2",5"-dimethylthiophen-3"-yl)-1-methyl-2-(pyridin-2'-yl)benzimidazole (**71**).

8.9 ^{1}H, ^{13}C and ^{19}F NMR spectra for Chapter 5

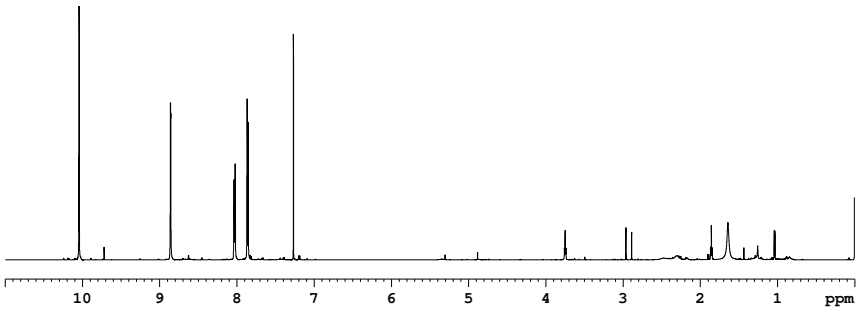

Figure 8.103: 600 MHz ^{1}H NMR spectrum ($CDCl_3$, 298 K) of 5'-bromopicolinaldehyde (**127**).

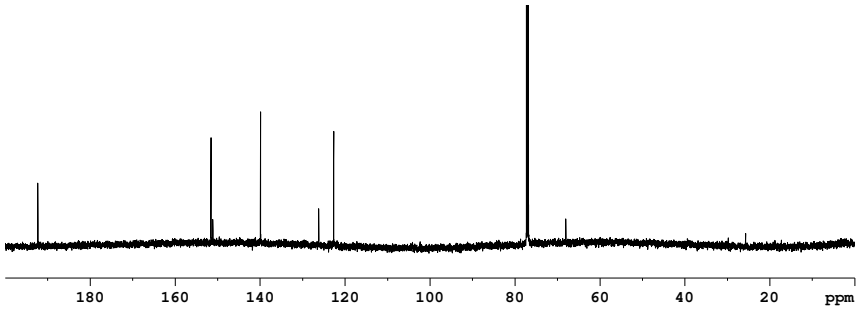

Figure 8.104: 151 MHz ^{13}C NMR spectrum ($CDCl_3$, 298 K) of 5'-bromopicolinaldehyde (**127**).

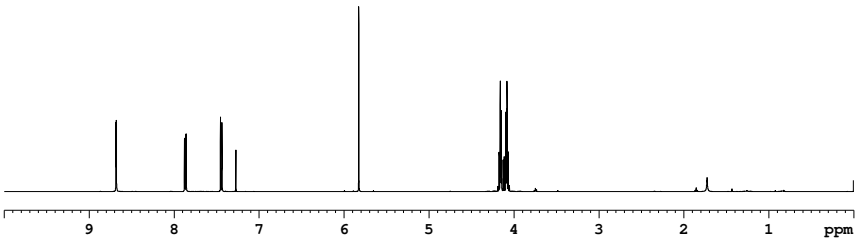

Figure 8.105: 500 MHz ^{1}H NMR spectrum ($CDCl_3$, 298 K) of 5'-bromo-2'-(1,3-dioxolan-2-yl)pyridine (**128**).

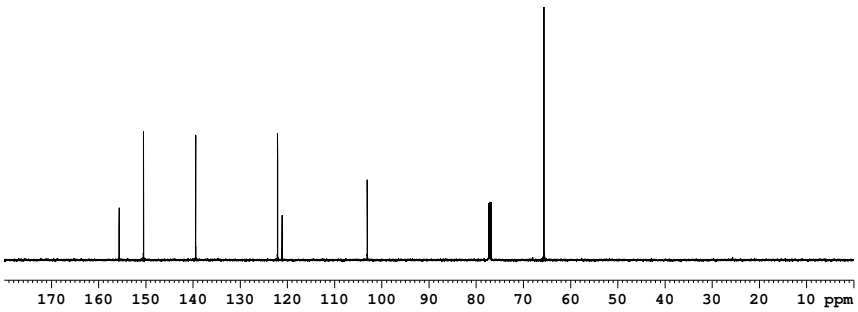

Figure 8.106: 126 MHz ^{13}C NMR spectrum ($CDCl_3$, 298 K) of 5'-bromo-2'-(1,3-dioxolan-2-yl)pyridine (**128**).

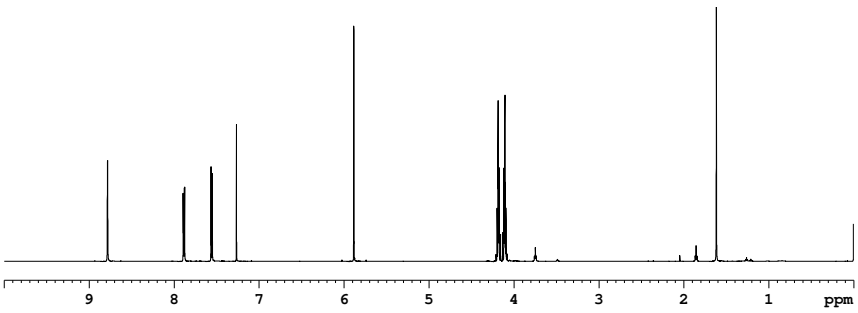

Figure 8.107: 600 MHz ^{1}H NMR spectrum ($CDCl_3$, 298 K) of 1,2-bis(6'-(1",3"-dioxolan-2"-yl)pyridin-3'-yl)ethyne (**130**).

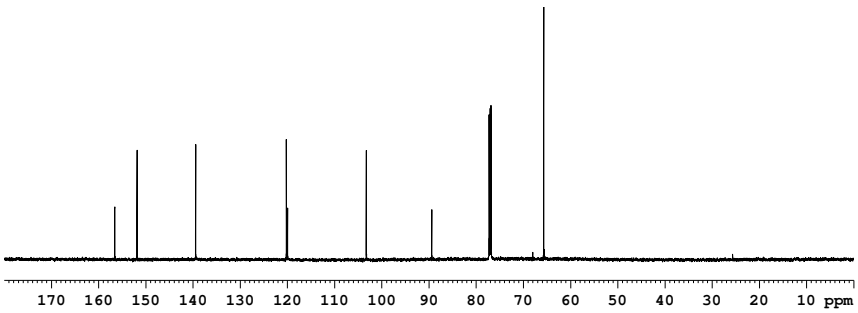

Figure 8.108: 151 MHz ^{13}C NMR spectrum ($CDCl_3$, 298 K) of 1,2-bis(6'-(1",3"-dioxolan-2"-yl)pyridin-3'-yl)ethyne (**130**).

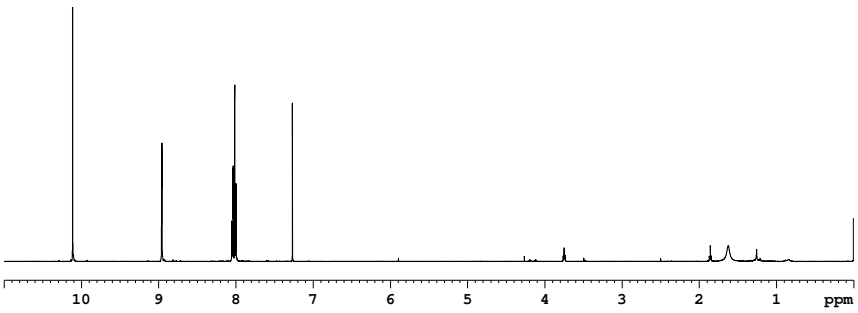

Figure 8.109: 500 MHz ^{1}H NMR spectrum ($CDCl_3$, 298 K) of 5,5'-(ethyne-1,2-diyl)dipicolinaldehyde (**131**).

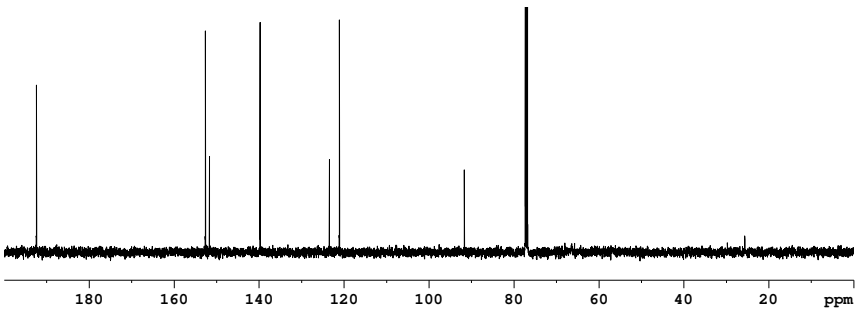

Figure 8.110: 126 MHz ^{13}C NMR spectrum ($CDCl_3$, 298 K) of 5,5'-(ethyne-1,2-diyl)dipicolinaldehyde (**131**).

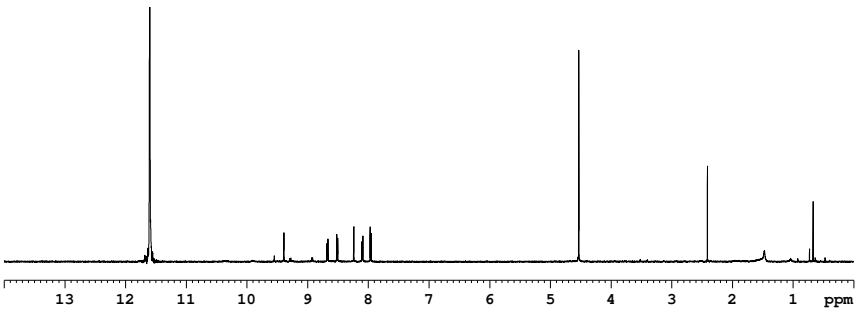

Figure 8.111: 500 MHz ^{1}H NMR spectrum (TFA-d_1, 298 K) of 1,2-bis(6'-(6"-bromo-1"-methyl-1*H*-benzo[*d*]imidazol-2"-yl)pyridin-3'-yl)ethyne (**132**).

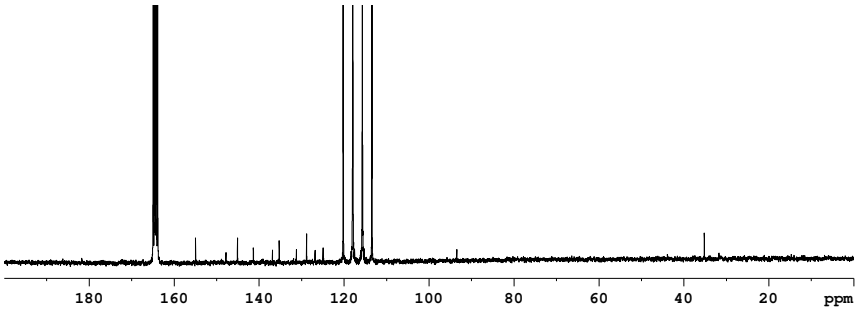

Figure 8.112: 126 MHz ^{13}C NMR spectrum (TFA-d_1, 298 K) of 1,2-bis(6'-(6"-bromo-1"-methyl-1*H*-benzo[*d*]imidazol-2"-yl)pyridin-3'-yl)ethyne (**132**).

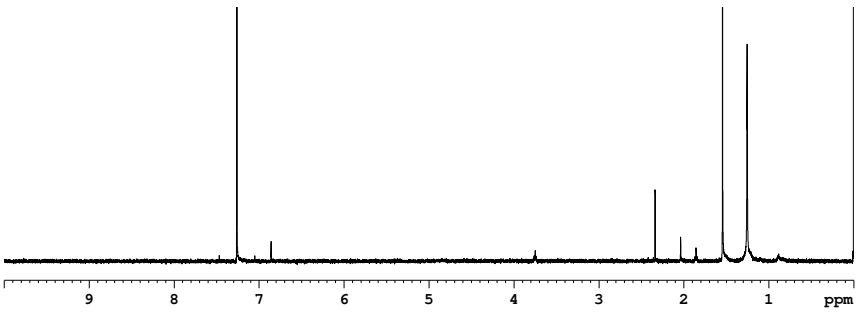

Figure 8.113: 500 MHz ^{1}H NMR spectrum ($CDCl_3$, 298 K) of 3,5-dibromo-2-methylthiophene (**140**).

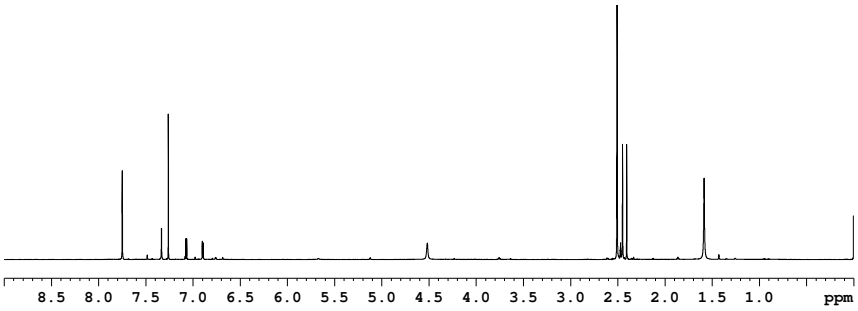

Figure 8.114: 600 MHz ^{1}H NMR spectrum ($CDCl_3$, 298 K) of (4-bromo-5-methylthiophen-2-yl)boronic acid (**141**).

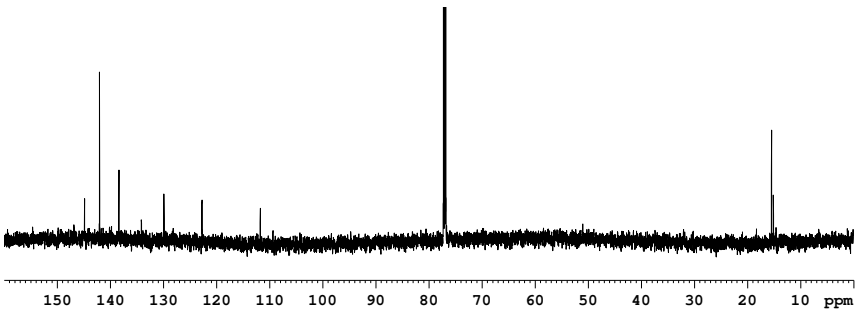

Figure 8.115: 151 MHz ^{13}C NMR spectrum ($CDCl_3$, 298 K) of (4-bromo-5-methylthiophen-2-yl)boronic acid (**141**).

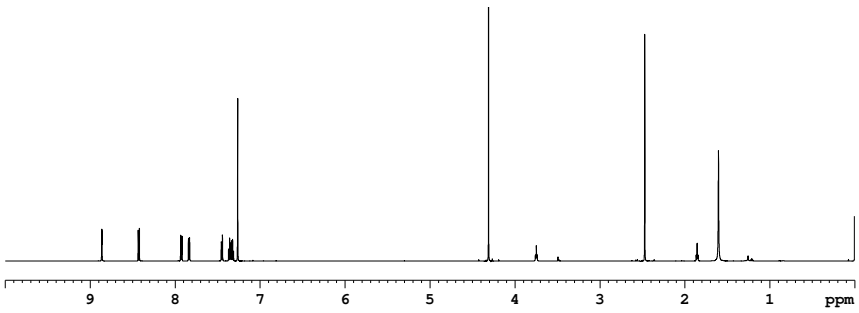

Figure 8.116: 600 MHz ^{1}H NMR spectrum ($CDCl_3$, 298 K) of 2-(5'-(4''-bromo-5''-methylthiophen-2''-yl)pyridin-2'-yl)-1-methyl-1*H*-benzo[*d*]imidazole (**143**).

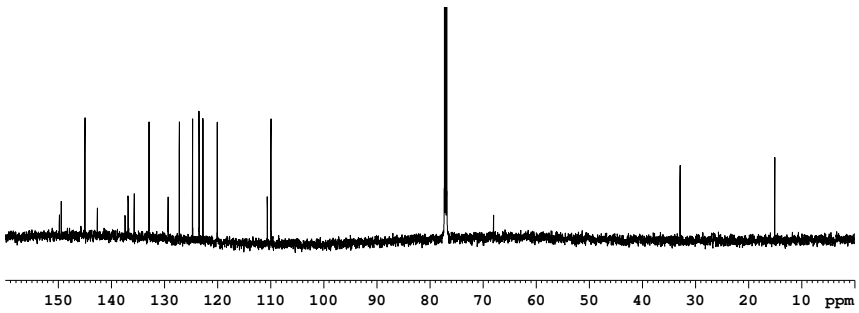

Figure 8.117: 151 MHz ^{13}C NMR spectrum ($CDCl_3$, 298 K) of 2-(5'-(4''-bromo-5''-methylthiophen-2''-yl)pyridin-2'-yl)-1-methyl-1*H*-benzo[*d*]imidazole (**143**).

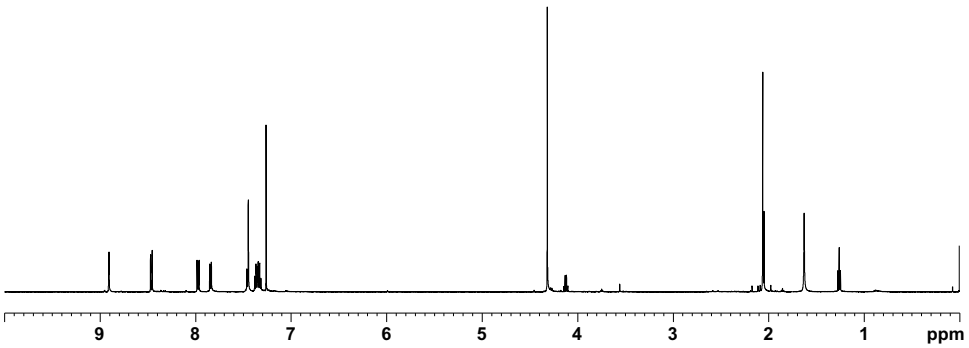

Figure 8.118: 500 MHz ^{1}H NMR spectrum ($CDCl_3$, 298 K) of 2,2'-(((perfluorocyclopent-1"'-ene-1"',2"'-diyl)bis(5"-methylthiophene-4",2"-diyl))bis(pyridine-5',2'-diyl))bis(1-methyl-1*H*-benzo[*d*]imidazole) (**137**).

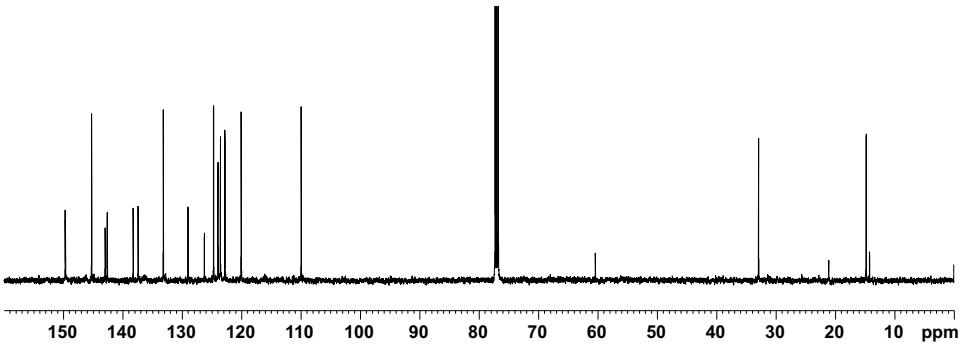

Figure 8.119: 126 MHz ^{13}C NMR spectrum ($CDCl_3$, 298 K) of 2,2'-(((perfluorocyclopent-1"'-ene-1"',2"'-diyl)bis(5"-methylthiophene-4",2"-diyl))bis(pyridine-5',2'-diyl))bis(1-methyl-1*H*-benzo[*d*]imidazole) (**137**).

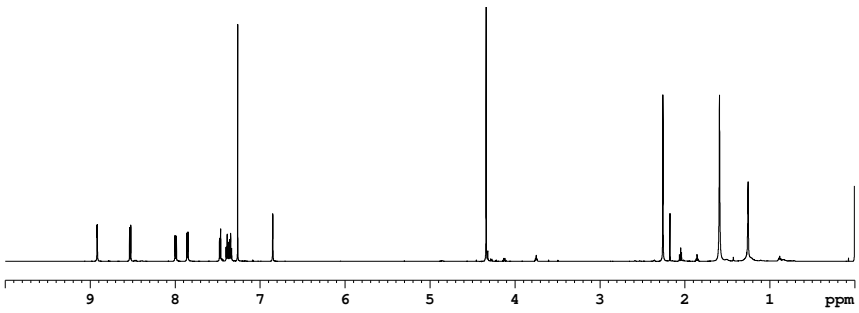

Figure 8.120: 600 MHz ^{1}H NMR spectrum ($CDCl_3$, 298 K) of 2,2'-((4",4",5",5",6",6"-hexafluoro-9a",9b"-dimethyl-5",6",9a",9b"-tetrahydro-4*H*-indeno[5,4-b:6,7-b']dithiophene-2",8"-diyl)bis(pyridine-5',2'-diyl))bis(1-methyl-1*H*-benzo[*d*]imidazole (**138**).

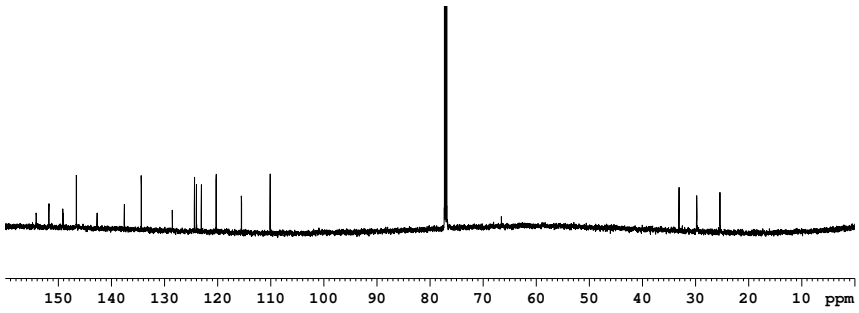

Figure 8.121: 151 MHz ^{13}C NMR spectrum ($CDCl_3$, 298 K) of 2,2'-((4",4",5",5",6",6"-hexafluoro-9a",9b"-dimethyl-5",6",9a",9b"-tetrahydro-4*H*-indeno[5,4-b:6,7-b']dithiophene-2",8"-diyl)bis(pyridine-5',2'-diyl))bis(1-methyl-1*H*-benzo[*d*]imidazole (**138**).

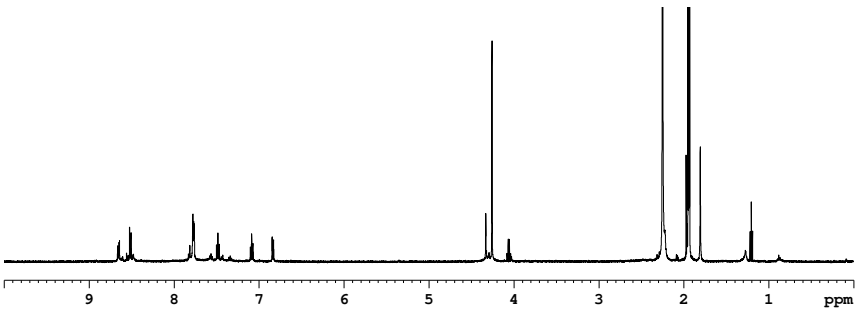

Figure 8.122: 500 MHz ^{1}H NMR spectrum (CD3CN, 298 K) of cage **145**.

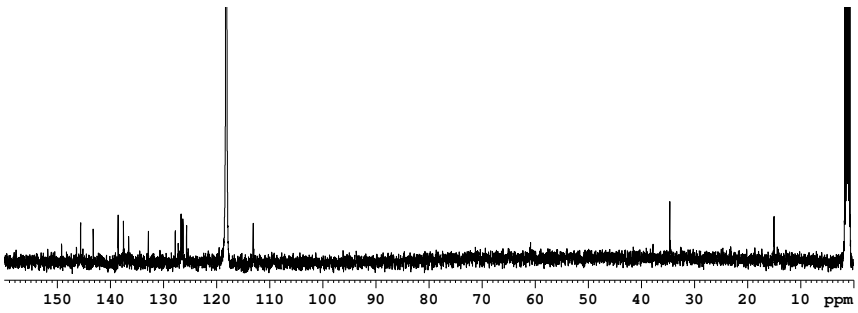

Figure 8.123: 126 MHz ^{13}C NMR spectrum (CD3CN, 298 K) of cage **145**.

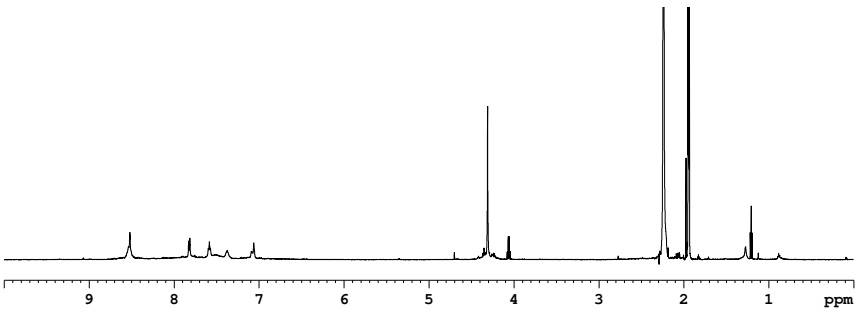

Figure 8.124: 600 MHz ^{1}H NMR spectrum (CD3CN, 298 K) of the proposed cage **148**.

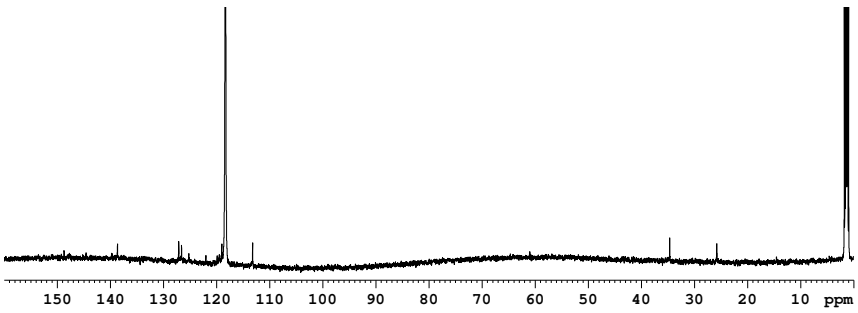

Figure 8.125: 151 MHz ^{13}C NMR spectrum (CD3CN, 298 K) of the proposed cage **148**.

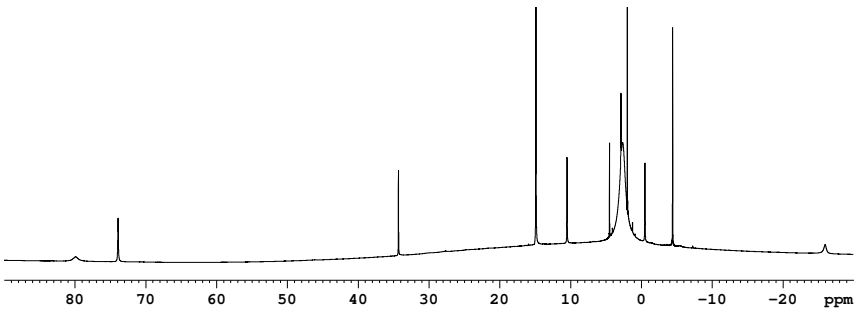

Figure 8.126: 600 MHz ^{1}H NMR spectrum (CD3CN, 298 K) of cage **146**.

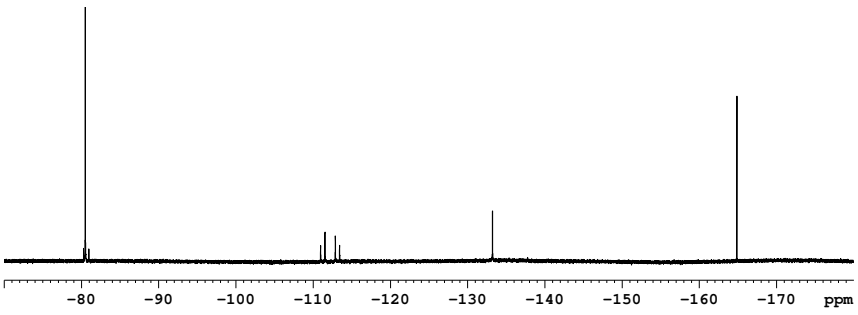

Figure 8.127: 471 MHz ^{19}F NMR spectrum (CD3CN, 298 K, C_6F_6) of cage **146**.

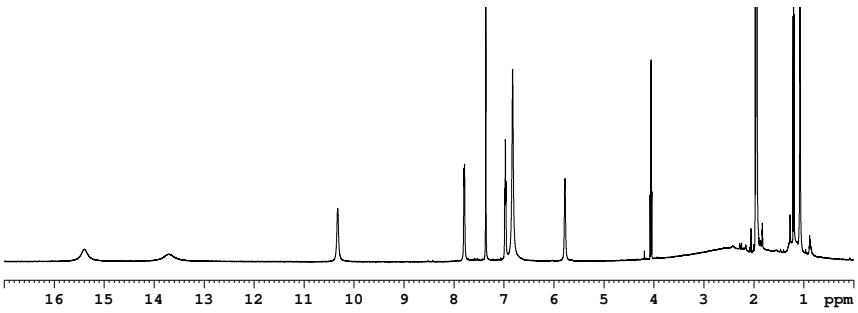

Figure 8.128: 600 MHz ^{1}H NMR spectrum (CD3CN, 298 K) of cage **147**.

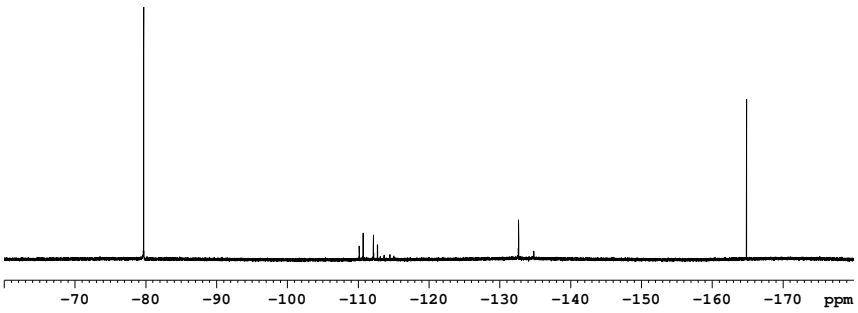

Figure 8.129: 471 MHz ^{19}F NMR spectrum (CD3CN, 298 K, C_6F_6) of cage **147**.

8.10 Crystallographic Data

Substances	Azobenzene **68**	Azobenzene **69**
Chemical Formula	$C_{19}H_{15}N_5$	$C_{19}H_{15}N_5$
Molecular weight [g/mol]	313.36	313.36
Temperature [K]	100.00(10)	150.00(10)
Crystal system	orthorhombic	orthorhombic
Space group	*Pbca*	*Pbca*
Cell parameters		
a [Å]	13.00596(5)	12.4326(2)
b [Å]	20.36890(10)	8.64610(10)
c [Å]	23.11940(10)	28.5530(4)
α [°]	90	90
β [°]	90	90
γ [°]	90	90
Volume [Å^3]	6124.72(5)	3069.26(7)
Z	16	8
Density [g/cm^3]	1.359	1.356
μ [mm]	0.675	0.673
Crystal size [mm^3]	0.22x0.16x0.03	0.25x0.22x0.20
Data collection 2θ range [°]	7.648-159.842	6.19-148.936
Measured reflections	61907	25788
Unique reflections	6636	3134
R_{int}	0.0163	0.0401
R_{sigma}	0.0072	0.0144
Reflections F_0>4$\sigma(F_0)$	6246	3037
Parameter	436	218
R_1 (F_0>4$\sigma(F_0)$)	0.0348	0.0486
wR_2 [all data]	0.1013	0.1399
Goodness-of-fit on F^2	1.060	1.083
Largest diff. peak/hole [eÅ^{-3}]	0.30/-0.17	0.31/-0.21

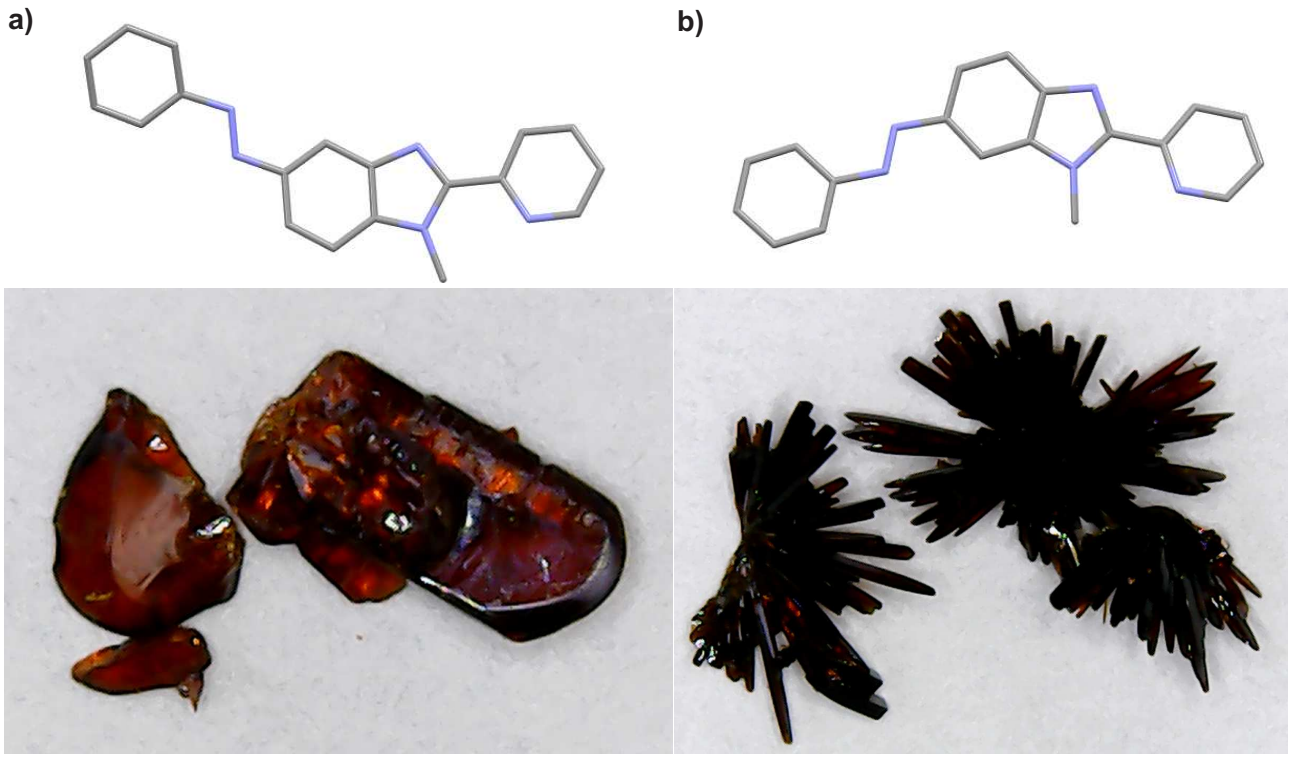

Figure 8.130: X-ray structures and crystals of azobenzenes a) **68** and b) **69**.

Bibliography

[1] L. Pietsch, *Bachelor Thesis*, Christian-Albrechts-Universität of Kiel **2018**.

[2] N. J. Taylor, E. Emer, S. Preshlock, M. Schedler, M. Tredwell, S. Verhoog, J. Mercier, C. Genicot, V. Gouverneur, *J. Am. Chem. Soc.* **2017**, *139*, 8267–8276.

[3] F. Aldabbagh, W. R. Bowman, *Tetrahedron* **1999**, *55*, 4109–4122.

[4] J. M. O'Connell, E. Moriarty, F. Aldabbagh, *Synthesis* **2012**, *44*, 3371–3377.

[5] M. J. Mio, L. C. Kopel, J. B. Braun, T. L. Gadzikwa, K. L. Hull, R. G. Brisbois, C. J. Markworth, P. A. Grieco, *Org. Lett.* **2002**, *4*, 3199–3202.

[6] L. Andernach, T. Opatz, *Eur. J. Org. Chem.* **2014**, 4780–4784.

[7] B. G. Park, M. Pink, D. Lee, *J. Organomet. Chem.* **2011**, *696*, 4039–4045.

[8] A. M. Soliman, D. Fortin, P. D. Harvey, E. Zysman-Colman, *Chem. Commun.* **2012**, *48*, 1120–1122.

[9] V. Jornet-Mollá, F. M. Romero, *Tetrahedron Lett.* **2015**, *56*, 6120–6122.

[10] W. L. Turnbull, L. G. Luyt, *Chem. Eur. J.* **2018**, *24*, 14539–14546.

[11] J. Jia, C. Jiang, X. Zhang, Y. Jiang, D. Ma, *Tetrahedron Lett.* **2011**, *52*, 5593–5595.

[12] M. Lin, Q. Tang, H. Zeng, G. Xing, Q. Ling, *Russ. J. Gen. Chem.* **2016**, *86*, 1747–1752.

[13] M. Lehr, T. Paschelke, V. Bendt, A. Petersen, L. Pietsch, P. Harders, A. J. McConnell, *Eur. J. Org. Chem.* **2021**, 2728–2735, Creative Commons — Attribution 4.0 International — CC BY 4.0 (https://creativecommons.org/licenses/by/4.0/), no changes were made.

[14] K. D. Ambacheu, V. G. Pleshakov, B. S. Baatkh, V. P. Zvolinskii, M. D. Kharlamova, A. A. Obynochnyi, N. S. Prostakov, *Chem. Heterocycl. Com.* **2000**, *36*, 421–428.

[15] R. Schiffmann, A. Neugebauer, C. D. Klein, *J. Med. Chem.* **2006**, *49*, 511–522.

[16] Y. Hasegawa, S. Kume, H. Nishihara, *Dalton Trans.* **2009**, 280–284.

[17] N. G. Zhegalova, G. Gonzales, M. Y. Berezin, *Org. Biomol. Chem.* **2013**, *11*, 8228–8234.

[18] D. Yang, D. Fokas, J. Li, L. Yu, C. M. Baldino, *Synthesis* **2005**, 47–56.

[19] J. P. Wolfe, J. Åhman, J. P. Sadighi, R. A. Singer, S. L. Buchwald, *Tetrahedron Lett.* **1997**, *38*, 6367–6370.

[20] B. Kriete, A. S. Bondarenko, V. R. Jumde, L. E. Franken, A. J. Minnaard, T. L. C. Jansen, J. Knoester, M. S. Pshenichnikov, *J. Phys. Chem. Lett.* **2017**, *8*, 2895–2901.

[21] N. Ando, A. Fukazawa, T. Kushida, Y. Shiota, S. Itoyama, K. Yoshizawa, Y. Matsui, Y. Kuramoto, H. Ikeda, S. Yamaguchi, *Angew. Chem. Int. Ed.* **2017**, *56*, 12210–12214.

[22] C.-C. Ko, W.-M. Kwok, V. W.-W. Yam, D. L. Phillips, *Chem. Eur. J.* **2006**, *12*, 5840–5848.

[23] W.-K. Huang, C.-W. Cheng, S.-M. Chang, Y.-P. Lee, E. W.-G. Diau, *Chem. Commun.* **2010**, *46*, 8992–8994.

[24] Q. Cao, D. S. Bailie, R. Fu, M. J. Muldoon, *Green Chem.* **2015**, *17*, 2750–2757.

[25] M. J. Burke, G. S. Nichol, P. J. Lusby, *J. Am. Chem. Soc.* **2016**, *138*, 9308–9315.

[26] D. A. Roberts, B. S. Pilgrim, J. D. Cooper, T. K. Ronson, S. Zarra, J. R. Nitschke, *J. Am. Chem. Soc.* **2015**, *137*, 10068–10071.

[27] E. Giraldi, A. B. Depallens, D. Ortiz, F. Fadaei-Tirani, R. Scopelliti, K. Severin, *Chem. Eur. J.* **2020**, *26*, 7578–7582.

[28] J. Moreno, F. Schweighöfer, J. Wachtveitl, S. Hecht, *Chem. Eur. J.* **2016**, *22*, 1070–1075.

[29] J. von Irmer, F. Frieß, D. Herold, J. Kind, C. M. Thiele, M. Gallei, *J. Mater. Chem. C* **2019**, *7*, 14088–14097.

[30] D. Becker, *dissertation*, Technische Universität Berlin **2017**.

[31] S. H. Davy, *Philos. Trans. R. Soc. London* **1811**, *101*, 1–35.

[32] M. R. Prado, A. Pham, R. E. Ferazzi, K. Edwards, K. C. Janda, *J. Chem. Educ.* **2007**, *84*, 1790–1791.

[33] E. D. S. Jr., C. A. Koh, *Clathrate Hydrates of Natural Gases, Third Edition (Chemical Industries Series)*, CRC Press, Boca Raton **2007**, 752.

[34] J.-M. Lehn, *Acc. Chem. Res.* **1978**, *11*, 49–57.

[35] J.-M. Lehn, *Angew. Chem. Int. Ed.* **1988**, *27*, 89–112.

[36] J.-M. Lehn, *Angew. Chem.* **1988**, *100*, 91–116.

[37] J.-M. Lehn, *Science* **1985**, *227*, 849–856.

[38] F. D. Toste, *Acc. Chem. Res.* **2018**, *51*, 2980–2981.

[39] *https://www.nobelprize.org/prizes/chemistry/1987/summary/ (24.04.2023, 12:28).*

[40] *https://www.nobelprize.org/prizes/chemistry/2016/summary/ (24.04.2023, 12:29).*

[41] X. Ji, Y. Yao, X. Yan, F. Huang, *J. Am. Chem. Soc.* **2013**, *135*, 74–77.

[42] A. M. Pettiwala, P. K. Singh, *ACS Omega* **2017**, *2*, 8779–8787.

[43] J. Chen, Y. Zhang, L. Zhao, Y. Zhang, L. Chen, M. Ma, X. Du, Z. Meng, C. Li, Q. Meng, *ACS Appl. Mater. Interfaces* **2021**, *13*, 53564–53573.

[44] L. R. Hart, J. L. Harries, B. W. Greenland, H. M. Colquhoun, W. Hayes, *ACS Appl. Mater. Interfaces* **2015**, *7*, 8906–8914.

[45] F. Herbst, S. Seiffert, W. H. Binder, *Polym. Chem.* **2012**, *3*, 3084–3092.

[46] C. J. Hastings, M. D. Pluth, R. G. Bergman, K. N. Raymond, *J. Am. Chem. Soc.* **2010**, *132*, 6938–6940.

[47] M. Kuil, T. Soltner, P. W. N. M. van Leeuwen, J. N. H. Reek, *J. Am. Chem. Soc.* **2006**, *128*, 11344–11345.

[48] J. D. Watson, F. H. C. Crick, *Nature* **1953**, *171*, 737–738.

[49] J. D. Watson, *Biochim. Biophys. Acta* **1954**, *13*, 10–19.

[50] P. J. G. Butler, *Phil. Trans. R. Soc. Lond. B* **1999**, *354*, 537–550.

[51] R. E. Gillard, F. M. Raymo, J. F. Stoddart, *Chem. Eur. J.* **1997**, *3*, 1933–1940.

[52] J. P. Hill, L. K. Shrestha, S. Ishihara, Q. Ji, K. Ariga, *Molecules* **2014**, *19*, 8589–8609.

[53] E. Mattia, S. Otto, *Nat. Nanotechnol.* **2015**, *10*, 111–119.

[54] J.-M. Lehn, *Chemical Synthesis Gnosis to Prognosis*, Springer Netherlands, Dordrecht **1996**.

[55] M. Crego-Calama, D. N. Reinhoudt, J. J. García-López, J. M. C. A. Kerckhoffs, *Nanostructure Science and Technologie*, Springer Science+Business Media, Inc, Boston **2005**.

[56] A. P. Minton, *J. Mol. Recognit.* **1993**, *6*, 211–214.

[57] Y.-H. Luo, S.-W. Ge, W.-T. Song, B.-W. Sun, *New J. Chem.* **2014**, *38*, 723–729.

[58] S. Dong, L. Wang, J. Wu, L. Jin, Y. Ge, Z. Qi, C. Wu, *Langmuir* **2017**, *33*, 13861–13866.

[59] N. Fu, J. J. Gassensmith, B. D. Smith, *Supramol. Chem.* **2009**, *21*, 118–124.

[60] A. Coskun, M. Hmadeh, G. Barin, F. Gándara, Q. Li, E. Choi, N. L. Strutt, D. B. Cordes, A. M. Z. Slawin, J. F. Stoddart, J.-P. Sauvage, O. M. Yaghi, *Angew. Chem. Int. Ed.* **2012**, *51*, 2160–2163.

[61] A. Coskun, M. Hmadeh, G. Barin, F. Gándara, Q. Li, E. Choi, N. L. Strutt, D. B. Cordes, A. M. Z. Slawin, J. F. Stoddart, J.-P. Sauvage, O. M. Yaghi, *Angew. Chem.* **2012**, *124*, 2202–2205.

[62] S.-T. Luo, F.-Y. Qiu, H.-T. Shi, W. Yu, *ChemistrySelect* **2021**, *6*, 11994–12000.

[63] D. Zhang, T. K. Ronson, J. Mosquera, A. Martinez, J. R. Nitschke, *Angew. Chem. Int. Ed.* **2018**, *57*, 3717–3721.

[64] D. Zhang, T. K. Ronson, J. Mosquera, A. Martinez, J. R. Nitschke, *Angew. Chem.* **2018**, *130*, 3779–3783.

[65] R. W. Saalfrank, A. Stark, K. Peters, H. G. von Schnering, *Angew. Chem. Int. Ed. Engl.* **1988**, *27*, 851–853.

[66] R. W. Saalfrank, A. Stark, K. Peters, H. G. von Schnering, *Angew. Chem.* **1988**, *100*, 878–880.

[67] E.-S. M. El-Sayed, Y. D. Yuan, D. Zhao, D. Yuan, *Acc. Chem. Res.* **2022**, *55*, 1546–1560.

[68] A. E. M. Díaz, J. E. M. Lewis, *Front. Chem.* **2021**, *9:706462.*

[69] T. Tateishi, M. Yoshimura, S. Tokuda, F. Matsuda, D. Fujita, S. Furukawa, *Coord. Chem. Rev.* **2022**, *467*, 214612.

[70] M. Yoshizawa, M. Tamura, M. Fujita, *Science* **2006**, *312*, 251–254.

[71] J. Jiao, C. Tan, Z. Li, X. Han, Y. Cui, *J. Am. Chem. Soc.* **2018**, *140*, 2251–2259.

[72] E. Benchimol, B.-N. T. Nguyen, T. K. Ronson, J. R. Nitschke, *Chem. Soc. Rev.* **2022**, *51*, 5101–5135.

[73] B. S. Pilgrim, N. R. Champness, *ChemPlusChem* **2020**, *85*, 1842–1856.

[74] T. K. Ronson, W. Meng, J. R. Nitschke, *J. Am. Chem. Soc.* **2017**, *139*, 9698–9707.

[75] L. R. Holloway, P. M. Bogie, Y. Lyon, C. Ngai, T. F. Miller, R. R. Julian, R. J. Hooley, *J. Am. Chem. Soc.* **2018**, *140*, 8078–8081.

[76] Z. Lu, R. Lavendomme, O. Burghaus, J. R. Nitschke, *Angew. Chem. Int. Ed.* **2019**, *58*, 9073–9077.

[77] Z. Lu, R. Lavendomme, O. Burghaus, J. R. Nitschke, *Angew. Chem.* **2019**, *131*, 9171–9175.

[78] A. J. McConnell, *Chem. Soc. Rev.* **2022**, *51*, 2957–2971.

[79] S.-J. Hu, X.-Q. Guo, L.-P. Zhou, D.-N. Yan, P.-M. Cheng, L.-X. Cai, X.-Z. Li, Q.-F. Sun, *J. Am. Chem. Soc.* **2022**, *144*, 4244–4253.

[80] Y. Zhou, H. Li, T. Zhu, T. Gao, P. Yan, *J. Am. Chem. Soc.* **2019**, *141*, 19634–19643.

[81] P. Mal, D. Schultz, K. Beyeh, K. Rissanen, J. R. Nitschke, *Angew. Chem. Int. Ed.* **2008**, *47*, 8297–8301.

[82] P. Mal, D. Schultz, K. Beyeh, K. Rissanen, J. R. Nitschke, *Angew. Chem.* **2008**, *120*, 8421–8425.

[83] D. Hugenbusch, M. Lehr, J.-S. von Glasenapp, A. J. McConnell, R. Herges, *Angew. Chem. Int. Ed.* **2023**, *62*, e202212571.

[84] D. Hugenbusch, M. Lehr, J.-S. von Glasenapp, A. J. McConnell, R. Herges, *Angew. Chem.* **2023**, *135*, e202212571.

[85] W. Cullen, C. A. Hunter, M. D. Ward, *Inorg. Chem.* **2015**, *54*, 2626–2637.

[86] D. Samanta, P. S. Mukherjee, *Chem. Eur. J.* **2014**, *20*, 12483–12492.

[87] M. Kieffer, B. S. Pilgrim, T. K. Ronson, D. A. Roberts, M. Aleksanyan, J. R. Nitschke, *J. Am. Chem. Soc.* **2016**, *138*, 6813–6821.

[88] Q.-F. Sun, J. Iwasa, D. Ogawa, Y. Ishido, S. Sato, T. Ozeki, Y. Sei, K. Yamaguchi, M. Fujita, *Science* **2010**, *328*, 1144–1147.

[89] D. Fujita, Y. Ueda, S. Sato, H. Yokoyama, N. Mizuno, T. Kumasaka, M. Fujita, *Chem* **2016**, *1*, 91–101.

[90] S. R. Seidel, P. J. Stang, *Acc. Chem. Res.* **2002**, *35*, 972–983.

[91] I. S. Tidmarsh, T. B. Faust, H. Adams, L. P. Harding, L. Russo, W. Clegg, M. D. Ward, *J. Am. Chem. Soc.* **2008**, *130*, 15167–15175.

[92] Z. R. Bell, L. P. Harding, M. D. Ward, *Chem. Commun.* **2003**, 2432–2433.

[93] N. Struch, C. Bannwarth, T. K. Ronson, Y. Lorenz, B. Mienert, N. Wagner, M. Engeser, E. Bill, R. Puttreddy, K. Rissanen, J. Beck, S. Grimme, J. R. Nitschke, A. Lützen, *Angew. Chem. Int. Ed.* **2017**, *56*, 4930–4935.

[94] N. Struch, C. Bannwarth, T. K. Ronson, Y. Lorenz, B. Mienert, N. Wagner, M. Engeser, E. Bill, R. Puttreddy, K. Rissanen, J. Beck, S. Grimme, J. R. Nitschke, A. Lützen, *Angew. Chem.* **2017**, *129*, 5012–5017.

[95] C. Provent, E. Rivara-Minten, S. Hewage, G. Brunner, A. F. Williams, *Chem. Eur. J.* **1999**, *5*, 3487–3494.

[96] S. Zarra, J. K. Clegg, J. R. Nitschke, *Angew. Chem. Int. Ed.* **2013**, *52*, 4837–4840.

[97] S. Zarra, J. K. Clegg, J. R. Nitschke, *Angew. Chem.* **2013**, *125*, 4937–4940.

[98] J. A. Davies, T. K. Ronson, J. R. Nitschke, *Chem* **2022**, *8*, 1099–1106.

[99] T. Zhang, L.-P. Zhou, X.-Q. Guo, L.-X. Cai, Q.-F. Sun, *Nat. Commun.* **2017**, *8*, 15898.

[100] I. A. Riddell, Y. R. Hristova, J. K. Clegg, C. S. Wood, B. Breiner, J. R. Nitschke, *J. Am. Chem. Soc.* **2013**, *135*, 2723–2733.

[101] M. Tominaga, K. Suzuki, M. Kawano, T. Kusukawa, T. Ozeki, S. Sakamoto, K. Yamaguchi, M. Fujita, *Angew. Chem. Int. Ed.* **2004**, *43*, 5621–5625.

[102] M. Tominaga, K. Suzuki, M. Kawano, T. Kusukawa, T. Ozeki, S. Sakamoto, K. Yamaguchi, M. Fujita, *Angew. Chem.* **2004**, *116*, 5739–5743.

[103] J. Zheng, L. K. S. von Krbek, T. K. Ronson, J. R. Nitschke, *Angew. Chem. Int. Ed.* **2022**, *61*, e202212634.

[104] J. Zheng, L. K. S. von Krbek, T. K. Ronson, J. R. Nitschke, *Angew. Chem.* **2022**, *134*, e202212634.

[105] M. Hardy, J. Tessarolo, J. J. Holstein, N. Struch, N. Wagner, R. Weisbarth, M. Engeser, J. Beck, S. Horiuchi, G. H. Clever, A. Lützen, *Angew. Chem. Int. Ed.* **2021**, *60*, 22562–22569.

[106] M. Hardy, J. Tessarolo, J. J. Holstein, N. Struch, N. Wagner, R. Weisbarth, M. Engeser, J. Beck, S. Horiuchi, G. H. Clever, A. Lützen, *Angew. Chem.* **2021**, *133*, 22736–22743.

[107] R.-J. Li, M. Han, J. Tessarolo, J. J. Holstein, J. Lübben, B. Dittrich, C. Volkmann, M. Finze, C. Jenne, G. H. Clever, *ChemPhotoChem* **2019**, *3*, 378–383.

[108] R.-J. Li, J. J. Holstein, W. G. Hiller, J. Andréasson, G. H. Clever, *J. Am. Chem. Soc.* **2019**, *141*, 2097–2103.

[109] D. Luo, X.-Z. Wang, C. Yang, X.-P. Zhou, D. Li, *J. Am. Chem. Soc.* **2018**, *140*, 118–121.

[110] L. Li, L. Yang, X. Li, J. Wang, X. Liu, C. He, *Inorg. Chem.* **2021**, *60*, 8802–8810.

[111] V. Brega, M. Zeller, Y. He, H. P. Lu, J. K. Klosterman, *Chem. Commun.* **2015**, *51*, 5077–5080.

[112] H.-T. Shi, S.-T. Luo, H.-R. Ma, W. Yu, X. Wei, *ChemistrySelect* **2022**, *7*, e202202940.

[113] X. Zhu, C. He, D. Dong, Y. Liu, C. Duan, *Dalton Trans.* **2010**, *39*, 10051–10055.

[114] C.-L. Liu, R.-L. Zhang, C.-S. Lin, L.-P. Zhou, L.-X. Cai, J.-T. Kong, S.-Q. Yang, K.-L. Han, Q.-F. Sun, *J. Am. Chem. Soc.* **2017**, *139*, 12474–12479.

[115] R. W. Layer, *Chem. Rev.* **1963**, *63*, 489–510.

[116] H. Schiff, *Liebigs Ann. Chem.* **1864**, *131*, 118–119.

[117] S. J. Rowan, S. J. Cantrill, G. R. L. Cousins, J. K. M. Sanders, J. F. Stoddart, *Angew. Chem. Int. Ed.* **2002**, *41*, 898–952.

[118] S. J. Rowan, S. J. Cantrill, G. R. L. Cousins, J. K. M. Sanders, J. F. Stoddart, *Angew. Chem.* **2002**, *114*, 938–993.

[119] V. E. Campbell, J. R. Nitschke, *Synlett* **2008**, 3077–3090.

[120] I. Langmuir, *J. Am. Chem. Soc.* **1919**, *41*, 868–934.

[121] C. R. K. Glasson, G. V. Meehan, J. K. Clegg, L. F. Lindoy, P. Turner, M. B. Duriska, R. Willis, *Chem. Commun.* **2008**, 1190–1192.

[122] S. Borsley, M. M. Haugland, S. Oldknow, J. A. Cooper, M. J. Burke, A. Scott, W. Grantham, J. Vallejo, E. K. Brechin, P. J. Lusby, S. L. Cockroft, *Chem* **2019**, *5*, 1275–1292.

[123] A. J. McConnell, C. M. Aitchison, A. B. Grommet, J. R. Nitschke, *J. Am. Chem. Soc.* **2017**, *139*, 6294–6297.

[124] K. Acharyya, S. Mukherjee, P. S. Mukherjee, *J. Am. Chem. Soc.* **2013**, *135*, 554–557.

[125] C. D. Meyer, C. S. Joiner, J. F. Stoddart, *Chem. Soc. Rev.* **2007**, *36*, 1705–1723.

[126] M. Whitehead, S. Turega, A. Stephenson, C. A. Hunter, M. D. Ward, *Chem. Sci.* **2013**, *4*, 2744–2751.

[127] Y.-L. Lu, J.-Q. Song, Y.-H. Qin, J. Guo, Y.-H. Huang, X.-D. Zhang, M. Pan, C.-Y. Su, *J. Am. Chem. Soc.* **2022**, *144*, 8778–8788.

[128] M. Darari, A. Francés-Monerris, B. Marekha, A. Doudouh, E. Wenger, A. Monari, S. Haacke, P. C. Gros, *Molecules* **2020**, *25*, 5991.

[129] I. S. Jahro, D. Onggo, Ismunandar, S. I. Rahayu, M. C. Muñoz, A. B. Gaspar, M. Seredyuk, P. Gütlich, J. A. Real, *Inorg. Chim. Acta* **2008**, *361*, 4047–4054.

[130] Y. Marcus, *Chem. Rev.* **1988**, *88*, 1475–1498.

[131] T. Dudev, C. Lim, *J. Am. Chem. Soc.* **2000**, *122*, 11146–11153.

[132] J. Miller, A. D. McLachlan, A. Klug, *EMBO J.* **1985**, *4*, 1609–1614.

[133] U. Carrillo, A. Francés-Monerris, A. R. Marri, C. Cebrián, P. C. Gros, *ACS Org. Inorg. Au* **2022**, *2*, 525–536.

[134] M. Schmid, K. Harms, C. Degitz, T. Morgenstern, A. Hofmann, P. Friederich, H.-H. Johannes, W. Wenzel, W. Kowalsky, W. Brütting, *ACS Appl. Mater. Interfaces* **2020**, *12*, 51709–51718.

[135] A. J. Metherell, W. Cullen, A. Stephenson, C. A. Hunter, M. D. Ward, *Dalton Trans.* **2014**, *43*, 71–84.

[136] S. L. Dabb, N. C. Fletcher, *Dalton Trans.* **2015**, *44*, 4406–4422.

[137] A. Francés-Monerris, K. Magra, M. Darari, C. Cebrián, M. Beley, E. Domenichini, S. Haacke, M. Pastore, X. Assfeld, P. C. Gros, A. Monari, *Inorg. Chem.* **2018**, *57*, 10431–10441.

[138] C. P. Sebli, S. E. Howson, G. J. Clarkson, P. Scott, *Dalton Trans.* **2010**, *39*, 4447–4454.

[139] S. E. Howson, L. E. N. Allan, N. P. Chmel, G. J. Clarkson, R. J. Deeth, A. D. Faulkner, D. H. Simpson, P. Scott, *Dalton Trans.* **2011**, *40*, 10416–10433.

[140] T. Morozumi, R. Matsuoka, T. Nakamura, T. Nabeshima, *Chem. Sci.* **2021**, *12*, 7720–7726.

[141] S. Ma, M. M. J. Smulders, Y. R. Hristova, J. K. Clegg, T. K. Ronson, S. Zarra, J. R. Nitschke, *J. Am. Chem. Soc.* **2013**, *135*, 5678–5684.

[142] S. Pullen, S. Löffler, A. Platzek, J. J. Holstein, G. H. Clever, *Dalton Trans.* **2020**, *49*, 9404–9410.

[143] Y. Wang, Y. Gu, E. G. Keeler, J. V. Park, R. G. Griffin, J. A. Johnson, *Angew. Chem. Int. Ed.* **2017**, *56*, 188–192.

[144] Y. Wang, Y. Gu, E. G. Keeler, J. V. Park, R. G. Griffin, J. A. Johnson, *Angew. Chem.* **2017**, *129*, 194–198.

[145] Z. Meng, F. Yang, X. Wang, W.-L. Shan, D. Liu, L. Zhang, G. Yuan, *Inorg. Chem.* **2023**, *62*, 1297–1305.

[146] N. Xu, Y.-X. Tan, E.-S. M. El-Sayed, D. Yuan, *Cryst. Growth Des.* **2022**, *22*, 2768–2773.

[147] I. A. Riddell, M. M. J. Smulders, J. K. Clegg, J. R. Nitschke, *Chem. Commun.* **2011**, *47*, 457–459.

[148] T. Jiao, L. Chen, D. Yang, X. Li, G. Wu, P. Zeng, A. Zhou, Q. Yin, Y. Pan, B. Wu, X. Hong, X. Kong, V. M. Lynch, J. L. Sessler, H. Li, *Angew. Chem. Int. Ed.* **2017**, *56*, 14545–14550.

[149] T. Jiao, L. Chen, D. Yang, X. Li, G. Wu, P. Zeng, A. Zhou, Q. Yin, Y. Pan, B. Wu, X. Hong, X. Kong, V. M. Lynch, J. L. Sessler, H. Li, *Angew. Chem.* **2017**, *129*, 14737–14742.

[150] S. Chen, K. Li, F. Zhao, L. Zhang, M. Pan, Y.-Z. Fan, J. Guo, J. Shi, C.-Y. Su, *Nat. Commun.* **2016**, *7*, 13169.

[151] A. Ahmedova, R. Mihaylova, D. Momekova, P. Shestakova, S. Stoykova, J. Zaharieva, M. Yamashina, G. Momekov, M. Akita, M. Yoshizawa, *Dalton Trans.* **2016**, *45*, 13214–13221.

[152] M. Han, R. Michel, B. He, Y.-S. Chen, D. Stalke, M. John, G. H. Clever, *Angew. Chem. Int. Ed.* **2013**, *52*, 1319–1323.

[153] M. Han, R. Michel, B. He, Y.-S. Chen, D. Stalke, M. John, G. H. Clever, *Angew. Chem.* **2013**, *125*, 1358–1362.

[154] H.-J. Yu, Z.-M. Liu, M. Pan, K. Wu, Z.-W. Wei, Y.-W. Xu, Y.-N. Fan, H.-P. Wang, C.-Y. Su, *Eur. J. Inorg. Chem.* **2018**, 80–85.

[155] X.-Q. Guo, L.-P. Zhou, S.-J. Hu, L.-X. Cai, P.-M. Cheng, Q.-F. Sun, *J. Am. Chem. Soc.* **2021**, *143*, 6202–6210.

[156] T.-Z. Xie, K. J. Endres, Z. Guo, J. M. Ludlow, C. N. Moorefield, M. J. Saunders, C. Wesdemiotis, G. R. Newkome, *J. Am. Chem. Soc.* **2016**, *138*, 12344–12347.

[157] R. A. Bilbeisi, S. Zarra, H. L. C. Feltham, G. N. L. Jameson, J. K. Clegg, S. Brooker, J. R. Nitschke, *Chem. Eur. J.* **2013**, *19*, 8058–8062.

[158] A. Ferguson, M. A. Squire, D. Siretanu, D. Mitcov, C. Mathonière, R. Clérac, P. E. Kruger, *Chem. Commun.* **2013**, *49*, 1597–1599.

[159] F. A. Cotton, *J. Chem. Educ.* **1964**, *41*, 466–476.

[160] E. Riedel, *Anorganische Chemie*, Bd. 2nd Edition, Walter de Gruyter Berlin New York **1990**.

[161] A. Hauser, *Top. Curr. Chem.* **2004**, *233*, 49–58.

[162] Y. Tokura, N. Nagaosa, *Science* **2000**, *288*, 462–468.

[163] P. W. Atkins, *Physikalische Chemie*, Bd. 1st Edition (2nd corrected reprint), VCH Verlagsgesellschaft mbH Weinheim, Weinheim **1990**.

[164] P. Gütlich, Y. Garcia, H. A. Goodwin, *Chem. Soc. Rev.* **2000**, *29*, 419–427.

[165] R. W. Hogue, S. Singh, S. Brooker, *Chem. Soc. Rev.* **2018**, *47*, 7303–7338.

[166] R. Tsuchida, *Bull. Chem. Soc. Jpn.* **1938**, *13*, 388–400.

[167] T. Ishii, S. Tsuboi, G. Sakane, M. Yamashita, B. K. Breedlove, *Dalton Trans.* **2009**, 680–687.

[168] C. Lochenie, K. Schötz, F. Panzer, H. Kurz, B. Maier, F. Puchtler, S. Agarwal, A. Köhler, B. Weber, *J. Am. Chem. Soc.* **2018**, *140*, 700–709.

[169] M. Enamullah, W. Linert, V. Gutmann, R. F. Jameson, *Monatsh. Chem.* **1994**, *125*, 1301–1309.

[170] M. Milek, A. Witt, C. Streb, F. W. Heinemann, M. M. Khusniyarov, *Dalton Trans.* **2013**, *42*, 5237–5241.

[171] L. Zhang, Y. Tong, M. Kelai, A. Bellec, J. Lagoute, C. Chacon, Y. Girard, S. Rousset, M.-L. Boillot, E. Rivière, T. Mallah, E. Otero, M.-A. Arrio, P. Sainctavit, V. Repain, *Angew. Chem. Int. Ed.* **2020**, *59*, 13341–13346.

[172] L. Zhang, Y. Tong, M. Kelai, A. Bellec, J. Lagoute, C. Chacon, Y. Girard, S. Rousset, M.-L. Boillot, E. Rivière, T. Mallah, E. Otero, M.-A. Arrio, P. Sainctavit, V. Repain, *Angew. Chem.* **2020**, *132*, 13443–13448.

[173] S. Thies, H. Sell, C. Schütt, C. Bornholdt, C. Näther, F. Tuczek, R. Herges, *J. Am. Chem. Soc.* **2011**, *133*, 16243–16250.

[174] T. Delgado, M. Villard, *J. Chem. Educ.* **2022**, *99*, 1026–1035.

[175] S. Decurtins, P. Gütlich, C. P. Köhler, H. Spiering, A. Hauser, *Chem. Phys. Lett.* **1984**, *105*, 1–4.

[176] M. M. Khusniyarov, *Chem. Eur. J.* **2016**, *22*, 15178–15191.

[177] H. E. Mason, W. Li, M. A. Carpenter, M. L. Hamilton, J. A. K. Howard, H. A. Sparkes, *New J. Chem.* **2016**, *40*, 2466–2478.

[178] J.-P. Tuchagues, A. Bousseksou, G. Molnár, J. J. McGarvey, F. Varret, *Spin-Crossover in Transition Metal Compounds III*, Kap. The Role of Molecular Vibrations in the Spin Crossover Phenomenon, Springer Berlin Heidelberg **2004**, 84–103.

[179] M. Nadeem, J. Cruddas, G. Ruzzi, B. J. Powell, *J. Am. Chem. Soc.* **2022**, *144*, 9138–9148.

[180] D. F. Evans, *J. Chem. Soc.* **1959**, 2003–2005.

[181] C. Yi, Y.-S. Meng, L. Zhao, N.-T. Yao, Q. Liu, W. Wen, R.-X. Li, Y.-Y. Zhu, H. Oshio, T. Liu, *CCS Chem.* **2023**, *5*, 915–924.

[182] T. K. Ekanayaka, H. Kurz, A. S. Dale, G. Hao, A. Mosey, E. Mishra, A. T. N'Diaye, R. Cheng, B. Weber, P. A. Dowben, *Mater. Adv.* **2021**, *2*, 760–768.

[183] Ökten Üngör, E. S. Choi, M. Shatruk, *Chem. Sci.* **2021**, *12*, 10765–10779.

[184] B. N. Livesay, M. P. Shores, *Inorg. Chem.* **2021**, *60*, 15445–15455.

[185] S. Rodríguez-Jiménez, S. Brooker, *Inorg. Chem.* **2017**, *56*, 13697–13708.

[186] W. Kläui, W. Eberspach, P. Gütlich, *Inorg. Chem.* **1987**, *26*, 3977–3982.

[187] A. Bousseksou, K. Boukheddaden, M. Goiran, C. Consejo, M.-L. Boillot, J.-P. Tuchagues, *Phys. Rev. B* **2002**, *65*, 172412.

[188] P. N. Martinho, F. F. Martins, N. A. G. Bandeira, M. J. Calhorda, *Sustainability* **2020**, *12*, 2512.

[189] K. Dankhoff, C. Lochenie, B. Weber, *Molecules* **2020**, *25*, 581.

[190] D. Savard, C. Cook, G. D. Enright, I. Korobkov, T. J. Burchell, M. Murugesu, *CrystEngComm* **2011**, *13*, 5190–5197.

[191] S. E. Lazaro, A. Alkas, S. J. Lee, S. G. Telfer, K. S. Murray, W. Phonsri, P. Harding, D. J. Harding, *Dalton Trans.* **2019**, *48*, 15515–15520.

[192] B. Weber, R. Tandon, D. Himsl, *Z. Anorg. Allg. Chem.* **2007**, *633*, 1159–1162.

[193] J. Kröber, J.-P. Andière, R. Claude, E. Codjovi, O. Kahn, *Chem. Mater.* **1994**, *6*, 1404–1412.

[194] R. Boča, P. Baran, M. Boča, L. Dlháň, H. Fuess, W. Haase, W. Linert, B. Papánková, R. Werner, *Inorg. Chim.* **1998**, *278*, 190–196.

[195] S. Decurtins, P. Gütlich, K. M. Hasselbach, A. Hauser, H. Spiering, *Inorg. Chem.* **1985**, *24*, 2174–2178.

[196] A. Hauser, *Coord. Chem. Rev.* **1991**, *111*, 275–290.

[197] O. Sato, T. Iyoda, A. Fujishima, K. Hashimoto, *Science* **1996**, *272*, 704–705.

[198] S. Venkataramani, U. Jana, M. Dommaschk, F. D. Sönnichsen, F. Tuczek, R. Herges, *Science* **2011**, *331*, 445–448.

[199] C. Roux, J. Zarembowitch, B. Gallois, T. Granier, R. Claude, *Inorg. Chem.* **1994**, *33*, 2273–2279.

[200] M.-L. Boillot, C. Roux, J.-P. Audière, A. Dausse, J. Zarembowitch, *Inorg. Chem.* **1996**, *35*, 3975–3980.

[201] D. J. van Dijken, P. Kovaříček, S. P. Ihrig, S. Hecht, *J. Am. Chem. Soc.* **2015**, *137*, 14982–14991.

[202] M. Irie, *Proc. Jpn. Acad., Ser. B.* **2010**, *86*, 472–483.

[203] M. Milek, F. W. Heinemann, M. M. Khusniyarov, *Inorg. Chem.* **2013**, *52*, 11585–11592.

[204] D. Pelleteret, R. Clérac, C. Mathonière, E. Harté, W. Schmitt, P. E. Kruger, *Chem. Commun.* **2009**, 221–223.

[205] R.-J. Li, J. Holstein, W. G. Hiller, J. Andréasson, G. H. Clever, *J. Am. Chem. Soc.* **2019**, *141*, 2097–2103.

[206] S. Fu, Q. Luo, M. Zang, J. Tian, Z. Zhang, M. Zeng, Y. Ji, J. Xu, J. Liu, *Mater. Chem. Front.* **2019**, *3*, 1238–1243.

[207] P. Cecot, A. Walczak, G. Markiewicz, A. R. Stefankiewicz, *Inorg. Chem. Front.* **2021**, *8*, 5195–5200.

[208] L. Li, N. Saigo, Y. Zhang, D. J. Fanna, N. D. Shephard, J. K. Clegg, R. Zheng, S. Hayami, L. F. Lindoy, J. R. Aldrich-Wright, C.-G. Li, J. K. Reynolds, D. G. Harman, F. Li, *J. Mater. Chem. C* **2015**, *3*, 7878–7882.

[209] L. Li, A. R. Craze, O. Mustonen, H. Zenno, J. J. Whittaker, S. Hayami, L. F. Lindoy, C. E. Marjo, J. K. Clegg, J. R. Aldrich-Wright, F. Li, *Dalton Trans.* **2019**, *48*, 9935–9938.

[210] W. Li, C. Liu, J. Kfoury, J. Oláh, K. Robeyns, M. L. Singleton, S. Demeshko, F. Meyer, Y. Garcia, *Chem. Commun.* **2022**, *58*, 11653–11656.

[211] D.-H. Ren, D. Qiu, C.-Y. Pang, Z. Li, Z.-G. Gu, *Chem. Commun.* **2015**, *51*, 788–791.

[212] W.-K. Han, H.-X. Zhang, Y. Wang, W. Liu, X. Yan, T. Li, Z.-G. Gu, *Chem. Commun.* **2018**, *54*, 12646–12649.

[213] Q.-Q. Wang, S. Gonell, S. H. A. M. Leenders, M. Dürr, I. Ivanović-Burmazović, J. N. H. Reek, *Nat. Chem.* **2016**, *8*, 225–230.

[214] B. Brachňaková, J. A. Kožíšková, J. Kožíšek, E. Melníková, M. Gál, R. Herchel, T. Dubaj, I. Šalitroš, *Dalton Trans.* **2020**, *49*, 17786–17795.

[215] A. W. Addison, S. Burman, C. G. Wahlgren, O. A. Rajan, T. M. Rowe, E. Sinn, *J. Chem. Soc., Dalton Trans.* **1987**, 2621–2630.

[216] C. Bartual-Murgui, S. Vela, M. Darawsheh, R. Diego, S. J. Teat, O. Roubeau, G. Aromí, *Inorg. Chem. Front.* **2017**, *4*, 1374–1383.

[217] L. J. K. Cook, R. Kulmaczewski, R. Mohammed, S. Dudley, S. A. Barrett, M. A. Little, R. J. Deeth, M. A. Halcrow, *Angew. Chem. Int. Ed.* **2016**, *55*, 4327–4331.

[218] L. J. K. Cook, R. Kulmaczewski, R. Mohammed, S. Dudley, S. A. Barrett, M. A. Little, R. J. Deeth, M. A. Halcrow, *Angew. Chem.* **2016**, *128*, 4399–4403.

[219] S. Singh, S. Brooker, *Inorg. Chem.* **2020**, *59*, 1265–1273.

[220] G. Auböck, M. Chergui, *Nat. Chem.* **2015**, *7*, 629–633.

[221] J. R. Sams, T. B. Tsin, *Inorg. Chem.* **1976**, *15*, 1544–1550.

[222] R. Boča, F. Renz, M. Boča, H. Fuess, W. Haase, G. Kickelbick, W. Linert, M. Vrbová-Schikora, *Inorg. Chem. Commun.* **2005**, *8*, 227–230.

[223] M. Enamullah, M. N. Uddin, D. Hossain, M. Kabir, A. Awwal, W. Linert, *J. Coord. Chem.* **2000**, *49*, 171–180.

[224] S. Singh, S. Brooker, *Chem. Sci.* **2021**, *12*, 10919–10929.

[225] N. Struch, N. Wagner, G. Schnakenburg, R. Weisbarth, S. Klos, J. Beck, A. Lützen, *Dalton Trans.* **2016**, *45*, 14023–14029.

[226] H.-J. Lin, D. Siretanu, D. A. Dickie, D. Subedi, J. J. Scepaniak, D. Mitcov, R. Clérac, J. M. Smith, *J. Am. Chem. Soc.* **2014**, *136*, 13326–13332.

[227] M. Hanazawa, R. Sumiya, Y. Horikawa, M. Irie, *J. Chem. Soc., Chem. Commun.* **1992**, 206–207.

[228] M. Irie, *Pure & Appl. Chem.* **1996**, *68*, 1367–1371.

[229] N. Deorukhkar, C. Besnard, L. Guénée, C. Piguet, *Dalton Trans.* **2021**, *50*, 1206–1223.

[230] T. Paschelke, *Masterarbeit*, Christian-Albrechts-Universität zu Kiel **2020**.

[231] M. Lehr, T. Paschelke, E. Trumpf, A.-M. Vogt, C. Näther, F. D. Sönnichsen, A. J. McConnell, *Angew. Chem. Int. Ed.* **2020**, *59*, 19344–19351, Creative Commons — Attribution 4.0 International — CC BY 4.0 (https://creativecommons.org/licenses/by/4.0/), no changes were made.

[232] M. Lehr, T. Paschelke, E. Trumpf, A.-M. Vogt, C. Näther, F. D. Sönnichsen, A. J. McConnell, *Angew. Chem.* **2020**, *132*, 19508–19516, Creative Commons — Attribution 4.0 International — CC BY 4.0 (https://creativecommons.org/licenses/by/4.0/), no changes were made.

[233] Y. Liang, Y.-X. Xie, J.-H. Li, *J. Org. Chem.* **2006**, *71*, 379–381.

[234] A. Mori, J. Kawashima, T. Shimada, M. Suguro, K. Hirabayashi, Y. Nishihara, *Org. Lett.* **2000**, *2*, 2935–2937.

[235] T. Paschelke, E. Trumpf, D. Grantz, M. Pankau, N. Grocholski, C. Näther, F. D. Sönnichsen, A. J. McConnell, *Dalton Trans.* **2023**, *52*, 12789–12795, Creative Commons — Attribution 3.0 Unported — CC BY 3.0 (https://creativecommons.org/licenses/by/3.0/), no changes were made.

[236] T. W. Green, P. G. M. Wuts, *Protective Groups in Organic Synthesis*, 3. Aufl., Wiley-Interscience, New York **1999**.

[237] S. Routier, L. Saugé, N. Ayerbe, G. Coudert, J.-Y. Mérour, *Tetrahedron Lett.* **2002**, *43*, 589–591.

[238] M. Liu, M. Ye, Y. Xue, G. Yin, D. Wang, J. Huang, *Tetrahedron Lett.* **2016**, *57*, 3137–3139.

[239] J. Huang, J. Chan, Y. Chen, C. J. Borths, K. D. Baucom, R. D. Larsen, M. M. Faul, *J. Am. Chem. Soc.* **2010**, *132*, 3674–3675.

[240] U. E. Hille, C. Zimmer, C. A. Vock, R. W. Hartmann, *ACS Med. Chem. Lett.* **2011**, *2*, 2–6.

[241] K. B. Abdireimov, N. S. Mukhamedov, M. Z. Aiymbetov, K. M. Shakhidoyatov, *Chem. Heterocycl. Com.* **2010**, *46*, 941–946.

[242] P. H.-M. Lee, C.-C. Ko, N. Zhu, V. W.-W. Yam, *J. Am. Chem. Soc.* **2007**, *129*, 6058–6059.

[243] R. D. Haugwitz, B. V. Maurer, G. A. Jacobs, V. L. Narayanan, *J. Med. Chem.* **1979**, *22*, 1113–1118.

[244] M. H. Jung, J. M. Park, I.-Y. C. Lee, M. Ahn, *J. Heterocycl. Chem.* **2003**, *40*, 37–44.

[245] E. Trumpf, *unpublished results*, Christian-Albrechts-Universität of Kiel **2021-2023**.

[246] E. N. Cho, D. Zhitomirsky, G. G. D. Han, Y. Liu, J. C. Grossman, *ACS Appl. Mater. Interfaces* **2017**, *9*, 8679–8687.

[247] M. Mörtel, T. Lindner, A. Scheurer, F. W. Heinemann, M. M. Khusniyarov, *Inorg. Chem.* **2020**, *59*, 2659–2666.

[248] N. Grocholski, *Bachelor Thesis*, Christian-Albrechts-Universität of Kiel **2021**.

[249] H.-H. Liu, Y. Chen, *J. Phys. Chem. A* **2009**, *113*, 5550–5553.

[250] R.-J. Li, M. Han, J. Tessarolo, J. J. Holstein, J. Lübben, B. Dittrich, C. Volkmann, M. Finze, C. Jenne, G. H. Clever, *ChemPhotoChem* **2019**, *3*, 378–383.

[251] B. Oruganti, P. P. Kalapos, V. Bhargav, G. London, B. Durbeej, *J. Am. Chem. Soc.* **2020**, *142*, 13941–13953.

[252] Y. B. Borozdina, E. A. Mostovich, P. T. Cong, L. Postulka, B. Wolf, M. Lang, M. Baumgarten, *J. Mater. Chem. C* **2017**, *5*, 9053–9065.

[253] R. Baier, *unpublished results*, Christian-Albrechts-Universität of Kiel **2021-2022**.

[254] Z.-Y. Li, J.-W. Dai, M. Damjanović, T. Shiga, J.-H. Wang, J. Zhao, H. Oshio, M. Yamashita, X.-H. Bu, *Angew. Chem. Int. Ed.* **2019**, *58*, 4339–4344.

[255] Z.-X. Li, L.-Y. Liao, W. Sun, C.-H. Xu, C. Zhang, C.-J. Fang, C.-H. Yan, *J. Phys. Chem. C* **2008**, *112*, 5190–5196.

[256] F. Hu, L. Jiang, M. Cao, Z. Xu, J. Huang, D. Wu, W. Yang, S. H. Liu, J. Yin, *RSC Adv.* **2015**, *5*, 5982–5987.

[257] S.-C. Wei, M. Pan, Y.-Z. Fan, H. Liu, J. Zhang, C.-Y. Su, *Chem. Eur. J.* **2015**, *21*, 7418–7427.

[258] S. Turega, M. Whitehead, B. R. Hall, A. J. H. M. Meijer, C. A. Hunter, M. D. Ward, *Inorg. Chem.* **2013**, *52*, 1122–1132.

[259] G. R. Fulmer, A. J. M. Miller, N. H. Sherden, H. E. Gottlieb, A. Nudelman, B. M. Stoltz, J. E. Bercaw, K. I. Goldberg, *Organometallics* **2010**, *29*, 2176–2179.

[260] C. Näther, Christian-Albrechts-Universität of Kiel, Institute of Inorganic Chemistry **2021/2023**.

[261] O. V. Dolomanov, L. J. Bourhis, R. J. Gildea, J. A. K. Howard, H. Puschmann, *J. Appl. Cryst.* **2009**, *42*, 339–341.

[262] G. M. Sheldrick, *Acta Cryst. A* **2015**, *71*, 3–8.

[263] G. M. Sheldrick, *Acta Cryst. C* **2015**, *71*, 3–8.

[264] R.-J. Li, J. J. Holstein, W. G. Hiller, J. Andréasson, G. H. Clever, *J. Am. Chem. Soc.* **2019**, *141*, 2097–2103.